



ULPGC
Universidad de
Las Palmas de
Gran Canaria

Escuela de
Doctorado

Programa de Doctorado en Ingenierías
Química, Mecánica y de Fabricación

Tesis Doctoral

Estudio de la reciclabilidad de materiales compuestos
poliméricos con carga de caña común (*Arundo donax* L.)

Autor: Luis Adargoma Suárez García
Directora: Zaida Cristina Ortega Medina

Las Palmas de Gran Canaria
Julio de 2025



ULPGC
Universidad de
Las Palmas de
Gran Canaria

Escuela de
Doctorado

Programa de Doctorado en Ingenierías
Química, Mecánica y de Fabricación

Estudio de la reciclabilidad de materiales compuestos poliméricos
con carga de caña común (*Arundo donax* L.)

*Study of the recyclability of polymeric composite materials
loaded with giant reed (Arundo donax L.)*

Autor:

Directora:

Luis Adargoma Suárez García

Zaida Cristina Ortega Medina

Las Palmas de Gran Canaria, a 21 de julio de 2025

AGRADECIMIENTOS / ACKNOWLEDGEMENTS

Esta tesis doctoral ha sido cofinanciada por la Agencia Canaria de Investigación, Innovación y Sociedad de la Información y por el Fondo Social Europeo (FSE), mediante contrato predoctoral (TESIS2021010008). Además, se ha recibido el apoyo para el desarrollo de la investigación del proyecto Inv2Mac (MAC2/4.6d/229) financiado por el Fondo Europeo para el Desarrollo Regional (FEDER), programa INTERREG MAC 2014-2020; así como financiación para la realización de estancias de investigación a través de los programas de movilidad Erasmus+ SMT y STT.

Quiero agradecer al Grupo de investigación en Fabricación Integrada y Avanzada por haber confiado en mí y haberme permitido desarrollar mi carrera profesional en el ámbito de la investigación durante todos estos años. Gracias a todos los compañeros que de una u otra manera me han ayudado y acompañado en este camino para llegar hasta aquí. Gracias, Mario, Mariola, Nizardo, Pedro, Rubén, Pablo, Fran, Sara, Jérica, Aday, Raquel, Gisela, Joshua, Ricardo, Joserra, Ana, Yamilet, Iván, Alfonso, Pepe, Estil, Heriberto. Gracias también a Fernando, Noelia, David y María Elena. Thanks to Timo and Jakob, who also contributed to this work during their stay in Gran Canaria.

I would like to thank the Polymer Processing Research Centre and Queen's University of Belfast for the opportunity to work with you and for sharing with me all your expertise. Thank you for making possible what I had never imagined before, to spend the best year of my life living abroad. Thanks to all PPRC staff, for making me feel at home. Thanks, Eoin, Bronagh, Paula, Graham, Billham, Paul, Alan, McCourt, Ife. Thanks also to all the guys I met at QUB and who made everything easier for me. Thanks, Jake, Aoife, Jude, Jordan, Jonny, Troy, Connor, Paul, John, Richard, Hannah, Chris, Mohamad...

Thanks to the colleagues from Poznan University of Technology for sharing with me not only your knowledge and such a fruitful collaboration, but also for your friendship and joy. Thanks, Mateusz, Joanna, Jacek. Thanks as well to Paula from Arcada University of Applied Sciences.

Gracias a mi familia por su apoyo, cariño y comprensión. Y, sobre todo,

Gracias, Zaida. Gracias por todo.

RESUMEN

El creciente reconocimiento a nivel mundial sobre el proceso de cambio climático y la degradación del medio ambiente demanda la exploración urgente de materiales alternativos que minimicen la huella ecológica, garanticen la sostenibilidad del consumo de los recursos naturales y, al mismo tiempo, cumplan los requisitos industriales. Un aspecto fundamental de esta investigación es entender que la transición hacia materiales más sostenibles implica un cambio de paradigma, no solo en la elección de las materias primas, sino también en las metodologías que se utilizan para evaluar su rendimiento a lo largo de su ciclo de vida.

La hipótesis planteada en este compendio de investigación se enfocó hacia la exploración exhaustiva de los materiales compuestos de base natural y, particularmente, de los compuestos termoplásticos que incorporan refuerzos lignocelulósicos procedentes de la especie vegetal *Arundo donax* L., conocida como caña común. Mediante la determinación de sus propiedades, comportamiento y aplicaciones prácticas, esta tesis pretende abordar las lagunas críticas de la literatura existente en relación con la sostenibilidad de los compuestos de fibras naturales, centrándose en el estudio de la biomasa de caña común para la obtención de recursos sostenibles de alto valor añadido. La literatura indica que, si bien numerosos estudios alaban las ventajas de los materiales compuestos de origen natural, avaladas por sus propiedades físico-químicas, su rendimiento mecánico, sus características de aislamiento térmico y acústico, o consideraciones económicas, entre otras, a menudo descuidan evaluaciones esenciales relativas a sus escenarios de fin de vida útil, en particular en lo que respecta a la reciclabilidad y la biodegradabilidad de los mismos. Esta investigación tiene como objetivo abordar un vacío importante proporcionando un análisis empírico sólido que ponga de relieve no sólo las ventajas de estos materiales, sino también los retos que plantean en un contexto de sostenibilidad.

Para comprender la relevancia de este trabajo de investigación es fundamental situar los compuestos biobasados dentro del panorama más amplio de la ciencia de los materiales. Los materiales compuestos se caracterizan por ofrecer unas propiedades mejoradas gracias a la combinación sinérgica de dos o más materiales de distinta naturaleza, físicamente diferenciables y mecánicamente separables. Los materiales compuestos o *composites* habitualmente están constituidos por una fase continua o matriz, que actúa como aglutinante, y una fase dispersa o discontinua, que se incorpora a la misma como refuerzo o relleno; de esta forma, cada una de las fases aporta sus propiedades para crear un material final con características únicas y superiores. Sin embargo, las implicaciones medioambientales de los materiales sintéticos tradicionales, empleados como matriz o como refuerzo, han impulsado un cambio hacia el desarrollo de materiales compuestos basados en recursos renovables: biopolímeros y fibras naturales, entre otros. Esta transición se alinea con los Objetivos de Desarrollo Sostenible en lo relativo a la conservación de los recursos y reducción de los residuos.

Desde la declaración del 2009 como "Año Internacional de las Fibras Naturales" por la FAO, ha habido un creciente interés en el uso de las fibras naturales como refuerzo de materiales compuestos en múltiples sectores, incluidas las industrias del transporte y la construcción. Los estudios evidencian, cada vez más, la importancia de desarrollar materiales biodegradables y considerar la viabilidad del reciclaje como alternativas para una producción y consumo más sostenibles. Además, la investigación se está dirigiendo hacia fibras vegetales menos convencionales, que no compitan con la producción alimentaria en términos de consumo de recursos (agua y suelo) y que sean más accesibles y rentables. En este sentido, la caña común (*Arundo donax* L.) emerge como una opción prometedora en regiones como las Islas Canarias, donde está considerada como especie vegetal invasora, no solo por su rápido crecimiento y disponibilidad, sino también como un recurso valioso para la biorrefinería y la remediación de suelos, potenciando así su uso en un contexto productivo más sostenible.

Teniendo en cuenta los antecedentes y la hipótesis de trabajo presentados, el objetivo principal de esta tesis doctoral fue determinar el potencial de utilización de la biomasa de *Arundo donax* L. para la obtención de fibras naturales y su posterior incorporación como fase dispersa en la producción de materiales compuestos de matriz polimérica. Se emplearon procesos de *compounding*, mediante extrusión de doble husillo, y moldeo por inyección, compresión y rotomoldeo, para la obtención de muestras y piezas finales con objeto de abordar su caracterización. En la investigación se consideró la utilización de diferentes matrices termoplásticas, como polietileno de alta densidad (HDPE) o ácido poliláctico (PLA), para determinar sus propiedades y procesabilidad mediante la incorporación de diferentes proporciones de material vegetal de caña. A continuación, se analizó la capacidad de reprocesado de los compuestos basados en matriz de origen fósil, y se realizaron pruebas de biodegradabilidad para determinar su efecto sobre aquellos producidos con termoplástico biobasado.

Para alcanzar los objetivos planteados, se planificaron varias etapas:

- Preparación del material vegetal. Se evaluó la necesidad de extracción de fibras, procedentes de las partes aéreas de los especímenes de caña (tallos y hojas), y la posibilidad de utilización de todo el material vegetal (plantas enteras). Se realizaron pruebas de extracción de fibras, siguiendo procesos de degradación natural mediante enriado y procesamiento mecánico, y aprovechamiento integral mediante el triturado de toda la biomasa. Se llevaron a cabo ensayos de caracterización de los materiales lignocelulósicos obtenidos, determinando sus constituyentes principales (celulosa, hemicelulosa y lignina), su estabilidad térmica, su morfología, resistencia mecánica y características físico-químicas.
- Obtención de materiales compuestos utilizando matrices termoplásticas con diferentes proporciones del material vegetal. Se produjeron composites con hasta un 40 % (en peso) de *Arundo donax*, mediante procesos de extrusión, inyección, moldeo por compresión y rotomoldeo. El objetivo fue determinar la procesabilidad de los compuestos a base de caña mediante diferentes técnicas de transformación y caracterizarlos con el fin de encontrar posibles aplicaciones para dichos biocomposites.

- Evaluación de la biodegradación y reciclabilidad de los materiales compuestos. Los compuestos de caña con matriz de polietileno fueron reprocesados varias veces con el fin de determinar su potencial reciclabilidad, mientras que los basados en ácido poliláctico fueron sometidos a ensayos de biodesintegración y degradación en agua, con el fin de determinar el efecto de la biomasa sobre la durabilidad y rendimiento de los materiales a lo largo de su vida útil.

Además de varias comunicaciones en congresos internacionales de reconocido prestigio, esta tesis doctoral ha dado lugar a dos artículos de revisión y ocho trabajos de investigación, publicados en revistas científicas de alto impacto, que abordan diferentes aspectos sobre el aprovechamiento de la caña común y su utilización para la elaboración de materiales compuestos.

En el primer artículo de revisión se analiza la especie vegetal *Arundo donax* L. y su interés para la explotación en biorrefinerías, mientras que el segundo se centra en el uso de la caña común para la producción de compuestos poliméricos. Los artículos de revisión producidos durante la fase inicial de la investigación doctoral son:

1. A review on the use of giant reed (*Arundo donax* L.) in the biorefineries context. Reviews in Chemical Engineering, 40(3), 2024. DOI: [10.1515/revce-2022-0069](https://doi.org/10.1515/revce-2022-0069)
2. Use of giant reed (*Arundo donax* L.) for polymer composites obtaining: a mapping review. Cellulose, 30, 2023. DOI: [10.1007/s10570-023-05176-x](https://doi.org/10.1007/s10570-023-05176-x)

A continuación, se analizó, en otra publicación, la caracterización de la planta en términos de su composición y procesado para la obtención de fibras a partir de los tallos y las hojas, así como su aprovechamiento integral. También se incluyó allí la caracterización de los materiales lignocelulósicos obtenidos en términos de comportamiento mecánico, estabilidad térmica, composición, índice de cristalinidad y características físicas. Los datos del citado artículo son los siguientes:

3. Giant Reed (*Arundo donax* L.) Fibre Extraction and Characterization for Its Use in Polymer Composites. Journal of Natural Fibres, 20:1, 2023. DOI: [10.1080/15440478.2022.2131687](https://doi.org/10.1080/15440478.2022.2131687)

Una vez obtenidas y analizadas las fibras y materiales lignocelulósicos de caña común, se prepararon materiales compuestos con diferentes matrices poliméricas (polietileno de alta densidad, HDPE; ácido poliláctico, PLA) bajo diferentes tecnologías de procesado, a saber, extrusión, inyección, rotomoldeo y moldeo por compresión. Los materiales compuestos se caracterizaron para determinar sus propiedades físico-químicas, reológicas y termomecánicas. También se evaluó la influencia de la longitud de la fibra durante la alimentación, la elaboración del *compound*, el proceso de inyección y el reprocesado de las piezas moldeadas, analizando el cambio en los parámetros morfológicos (diámetro y longitud) de las partículas de relleno que determinan las propiedades finales de los composites. Por último, también se evaluó el comportamiento de desintegración de los compuestos basados en PLA, así como el efecto de la degradación en agua sobre el comportamiento de los mismos. Las publicaciones derivadas de la investigación sobre los materiales compuestos de *Arundo donax* son:

4. A New Image Analysis Assisted Semi-Automatic Geometrical Measurement of Fibres in Thermoplastic Composites: A Case Study on Giant Reed Fibres. Journal of Composites Science, 7(8), 2023. DOI: [10.3390/jcs7080326](https://doi.org/10.3390/jcs7080326)
5. Influence of Giant Reed (*Arundo Donax* L.) Culms Processing Procedure on Physicochemical, Rheological, and Thermomechanical Properties of Polyethylene Composites. Journal of Natural Fibres, 21(1), 2024. DOI: [10.1080/15440478.2023.2296909](https://doi.org/10.1080/15440478.2023.2296909)
6. Relationship Between the Shape of Giant Reed-Based Fillers and Thermal Properties of Polyethylene Composites: Structural Related Thermal Expansion and Diffusivity Studies. Waste and Biomass Valorization, 15(12), 2024. DOI: [10.1007/s12649-024-02626-w](https://doi.org/10.1007/s12649-024-02626-w)
7. Recyclability Assessment of Lignocellulosic Fibre Composites: Reprocessing of Giant Reed/HDPE Composites by Compression Molding. Lecture Notes in Mechanical Engineering IV, 3, 2024. DOI: [10.1007/978-3-031-56474-1_15](https://doi.org/10.1007/978-3-031-56474-1_15)
8. Recycling of HDPE-giant reed composites: Processability and performance. Green Processing and Synthesis, 14(1), 2025. DOI: [10.1515/gps-2024-0229](https://doi.org/10.1515/gps-2024-0229)
9. Influence of Giant Reed Fibres on Mechanical, Thermal, and Disintegration Behavior of Rotomolded PLA and PE Composites. Journal of Polymers and the Environment, 30(11), 2022. DOI: [10.1007/s10924-022-02542-x](https://doi.org/10.1007/s10924-022-02542-x)
10. Giant reed (*Arundo donax* L.) enhanced polylactic acid composites: processing, characterization, and performance of injection moulded and water degraded samples. Submitted to Composites Part A: Applied Science and Manufacturing (enviado el 08/07/2025; pendiente de revisión)

Las publicaciones anteriormente enumeradas, se encuentran incluidas en este documento de tesis, después de tres secciones (capítulos 2, 3 y 4) en los que se resumen los métodos y conclusiones de cada trabajo y se acredita la unidad temática del trabajo de investigación.

A continuación, se presenta un sumario con las conclusiones finales de la tesis para, posteriormente, concluir este resumen con una serie de potenciales líneas de investigación futura.

- Esta tesis presenta el primer análisis en profundidad de materiales compuestos de *Arundo donax* con matrices termoplásticas de HDPE y PLA procesados mediante extrusión, moldeo por inyección, moldeo rotacional y moldeo por compresión, que incluye no sólo su análisis mecánico, térmico o reológico, sino que también analiza sus opciones de reciclabilidad y biodegradabilidad.
- *Arundo donax* ha demostrado ser un prometedor refuerzo sostenible para la producción de compuestos poliméricos. La caña común es una fuente de biomasa de rápido crecimiento, renovable y ampliamente disponible, especialmente en climas templados y regiones áridas como las Islas Canarias, debido a sus bajos requerimientos y buena adaptabilidad. El trabajo realizado aporta nuevos datos para apoyar el uso de biomasa de plantas invasoras en un contexto de economía circular.

- Se ha propuesto un procedimiento específico para la obtención de fibras de buena calidad y alta relación de aspecto a partir de los tallos y hojas de caña común, basado en un procedimiento químico-mecánico. Con este proceso se obtienen fibras vegetales con un alto contenido en celulosa (hasta el 70 %), una estabilidad térmica favorable ($>230\text{ }^{\circ}\text{C}$) y propiedades mecánicas competitivas (resistencia a la tracción $\sim 900\text{ MPa}$, módulo elástico $\sim 45\text{ GPa}$), comparables a las de otras fibras naturales comerciales como el yute o el lino.
- Se ha demostrado que la morfología y el procesamiento de las fibras desempeñan un papel fundamental en el rendimiento de los materiales compuestos. El comportamiento reológico, la estabilidad térmica, la cristalinidad y la adhesión interfacial se ven influidos por el tipo y la proporción de la biomasa empleada como refuerzo o relleno.
- A partir del análisis de las longitudes de las fibras desde la obtención inicial y hasta el reprocesado, se confirmó que el procesamiento mecánico (extrusión de doble husillo) reduce significativamente la longitud de las fibras, especialmente en las primeras zonas de amasado en el interior del barril de extrusión. A pesar de ello, las fibras procesadas mantienen relaciones de aspecto suficientes para actuar como refuerzos eficaces, incluso tras varios ciclos de reprocesado mediante triturado, extrusión y moldeo por inyección.
- Los compuestos basados en fibras de caña superan sistemáticamente a los que utilizan material vegetal triturado de esta especie, sobre todo en rigidez y propiedades térmicas, debido a su mejor estabilidad térmica, por el menor contenido de hemicelulosa, y también a su elevada relación de aspecto (longitud/diámetro).
- Los compuestos de *Arundo* a base de HDPE muestran mejores propiedades mecánicas y térmicas que la matriz de polietileno puro. Por ejemplo, el módulo de tracción aumentó hasta un 78 % con una proporción de fibra del 20 % (en peso). Del mismo modo, los materiales compuestos mostraron una mejor estabilidad dimensional y térmica, evidenciada por el aumento de la temperatura de deflexión térmica y la disminución de los coeficientes de expansión térmica. Estas mejoras sugieren aplicaciones en envases técnicos, interiores de automóviles y paneles estructurales.
- Los compuestos *Arundo*-HDPE demuestran su aptitud para el reciclaje con una pérdida de rendimiento mínima. Los compuestos fibrosos de HDPE conservaron más del 80 % de su resistencia original a la tracción tras múltiples ciclos de reciclado. Mostraron una mayor rigidez y mantuvieron la estabilidad térmica tras cinco ciclos de reprocesado. El uso de *Arundo* puede aportar propiedades antioxidantes, mejorando la resistencia a la oxidación y en escenarios de reciclaje en circuito cerrado.
- Los compuestos *Arundo*-PLA ofrecen alternativas totalmente biodegradables y de base biológica. Los materiales compuestos moldeados por inyección con un contenido de fibra de entre el 10 y el 20 % mostraron un equilibrio óptimo entre rigidez y tenacidad.

- La biodesintegración de los materiales compuestos de caña común en condiciones de compostaje fue más rápida y eficaz que la del PLA puro, especialmente en condiciones de compostaje doméstico, debido a la mayor absorción de agua de los *biocomposites*, que favorece la ruta de degradación hidrolítica del biopolímero.
- La absorción de agua es mayor en los compuestos de PLA reforzados con fibras de caña, debido a la mayor superficie de las fibras en comparación con las partículas de *Arundo* triturado. La absorción de agua provoca una reducción del rendimiento mecánico, aunque éste puede recuperarse parcialmente tras el resecado.
- El rendimiento de los composites de PLA depende del tipo de relleno (fibras o material vegetal triturado), el contenido y los parámetros de procesado: los composites con fibras superan a los rellenos de partículas debido a una mayor relación de aspecto y una mejor transferencia de tensiones.
- Por último, el potencial industrial de los compuestos producidos resulta evidente por el comportamiento que presentan, aunque aún es necesario realizar más estudios. Las aplicaciones podrían incluir la producción de diferentes productos en los sectores del envasado, agricultura, bienes de consumo y materiales de construcción.

Como resultado del trabajo realizado hasta la fecha, surgen algunas nuevas vías de investigación que permitirían seguir contribuyendo a un mayor conocimiento de los compuestos basados en caña común, así como en el estudio de diferentes posibilidades de aprovechamiento para maximizar el uso de este recurso natural, *Arundo donax* L., como fuente de material sostenible.

- Preparación de materiales compuestos con otras matrices de base biológica, como PHA/PHB o PBS. Debería llevarse a cabo una exploración de estos materiales en sistemas de extrusión-soplado y termoconformado, con el objetivo de producir materiales para aplicaciones de envasado.
- Modificación de las fibras y de la biomasa derivada de la caña, con el fin de mejorar su compatibilidad con la matriz polimérica y obtener prestaciones mejoradas y adaptadas a diferentes aplicaciones. En este punto, es interesante aclarar que en este trabajo no se realizaron modificaciones para reducir la huella medioambiental de los composites, debido a la enorme cantidad de agua necesaria para dichas modificaciones. Sin embargo, debería realizarse un análisis de ciclo de vida (ACV) exhaustivo para establecer los beneficios reales del uso de dicha biomasa en el sector de los composites.
- Completar el análisis del rendimiento de los materiales compuestos analizando sus propiedades acústicas y su comportamiento frente al fuego, factores cruciales para el uso de estos materiales en el diseño de mobiliario y la ecologización de espacios interiores, siguiendo los principios de la ingeniería Kansei.
- Explorar otras alternativas al uso de la biomasa, como la separación de la lignina para producir la llamada madera transparente o aditivos retardantes del fuego.
- Establecimiento de un enfoque integrado en cascada para maximizar el uso de la biomasa derivada de la caña, incluida la producción potencial de bioplásticos a partir de los carbohidratos (azúcar y almidón) presentes en la planta de forma natural.

- Ampliar el alcance de los ensayos de reciclabilidad para garantizar su viabilidad en ciclos de larga duración. Esto debería incluir el estudio del comportamiento de envejecimiento de los composites en comparación con las matrices puras; la incorporación de la caña sin procesar, con extractivos y polifenoles podría proporcionar un efecto estabilizador en el material compuesto frente al reprocesado y también frente a la radiación UV.
- Ensayos completos de envejecimiento de los materiales producidos, tanto con la matriz de HDPE como con la de PLA, bajo radiación UV y ciclos hidrotérmicos, con el fin de definir la durabilidad de los mismos en condiciones de servicio. De particular interés sería el análisis del comportamiento de degradación bajo atmósfera salina, así como el análisis de biodegradación de los compuestos de PLA en ambientes marinos.
- Establecer una cadena de valor a través de la valorización de la biomasa derivada de *Arundo*, que considere los impactos ambientales, sociales y económicos de todo el procesamiento, desde la cosecha hasta el final de la vida útil de los productos, estableciendo una gama de diferentes aplicaciones.

INDEX

1. Introduction	1
1.1. Context.....	1
1.2. Objectives	3
1.3. Publications arising from the work	4
2. State of the art.....	5
3. Fibre extraction and characterization	9
4. Preparation and characterization of composites	11
4.1. Influence of the compounding stage in fibre morphology	11
4.2. HDPE-based composites.....	13
4.3. Recyclability assessment of HDPE-based composites.....	15
4.4. PLA-based composites.....	17
Rotomolded composites and biodegradation assays.....	17
Injection-molded composites and water ageing assays.....	18
5. References	23
6. Published works	29
6.1. A review on the use of giant reed (<i>Arundo donax</i> L.) in the biorefineries context	31
6.2. Use of giant reed (<i>Arundo donax</i> L.) for polymer composites obtaining: a mapping review	57
6.3. Giant reed (<i>Arundo donax</i> L.) fibre extraction and characterization for its use in polymer composites	79
6.4. A New Image Analysis Assisted Semi-Automatic Geometrical Measurement of Fibres in Thermoplastic Composites: A Case Study on Giant Reed Fibres.....	95
6.5. Influence of Giant Reed (<i>Arundo Donax</i> L.) Culms Processing Procedure on Physicochemical, Rheological, and Thermomechanical Properties of Polyethylene Composites	111
6.6. Relationship between the shape of giant reed-based fillers and thermal properties of polyethylene composites: structural related thermal expansion and diffusivity studies .	145

6.7. Recyclability assessment of lignocellulosic fibre composites: reprocessing of giant reed/HDPE composites by compression moulding.....	157
6.8. Recycling of HDPE-giant reed composites: Processability and performance.....	175
6.9. Influence of giant reed fibres on mechanical, thermal, and disintegration behaviour of rotomolded PLA and PE composites.....	201
6.10. Giant reed (<i>Arundo donax</i> L.) enhanced polylactic acid composites: processing, characterization, and performance of injection moulded and water degraded samples	219
7. Outlook.....	245
7.1. Conclusions	245
7.2. Future research lines	247

1. INTRODUCTION

This introductory chapter is the basis of this doctoral thesis, which brings together a series of publications focused on the advancement of sustainable materials science, particularly emphasizing natural-based composites consisting of a polymer matrix and lignocellulosic materials derived from *Arundo donax* L. (giant reed). The increasing global recognition of climate change and environmental degradation necessitates urgent explorations into alternative materials that minimize ecological footprints while fulfilling industrial requirements. Central to this research is the understanding that the transition to sustainable materials involves a paradigm shift not only in material selection but also in the methodologies employed to evaluate their performance throughout their life cycles.

The principal aim of this research compendium is to comprehensively explore the performance, properties, and practical applications of natural-based composites. This thesis seeks to address critical gaps in the existing literature concerning the sustainability of composite materials, particularly in those based on giant reed. The literature indicates that while numerous studies highlight the mechanical advantages of natural-based composites, they often neglect essential evaluations regarding their end-of-life scenarios, particularly concerning recyclability and biodegradability. This research, therefore, fills a significant gap by providing robust empirical analyses that emphasize not only the benefits of such materials but also the challenges they pose in a sustainability context.

To accurately understand the relevance of this research work, it is critical to situate bio-based composites within the broader landscape of materials science. Composites are characterized by providing enhanced properties through the synergistic combination of two or more individual materials; however, the environmental implications of traditional synthetic materials have driven a shift toward the development of composites based on renewable resources, such as biopolymer matrices and natural fillers and reinforcing materials. This transition aligns with the philosophy of sustainability, resource conservation and waste reduction.

1.1. CONTEXT

The main objective of this doctoral thesis was to determine the potential for utilizing the biomass produced by giant reed (*Arundo donax* L.) for the production of polymer-matrix composite materials. The environmental impact generated by the excessive consumption of plastic materials and their disposal, generally after a short product lifespan, makes necessary to study alternative materials with good properties, versatility, and a lower environmental impact. One strategy to achieve this is the use of biodegradable polymer matrices or the incorporation of natural fibres, thereby obtaining biocomposites that reduce the environmental footprint generated by the widespread use of plastics.

The application of composite materials in several sectors has been growing unceasingly in the last decades, as they offer a combination of properties impossible to obtain with conventional metals, ceramics, and polymers. A composite material is defined as the one obtained by combining two or more materials of different nature, physically distinguishable and mechanically separable, with chemically distinct phases, insoluble in each other, and separated by an interface, and whose properties are superior to the simple addition of the properties of the individual components. Regarding materials used as fillers or reinforcements, concerns about sustainability and climate change, combined with the economic and environmental costs of producing synthetic fibres, have motivated the search for alternative fibres, with plant fibres emerging as a low-cost, low-density, biodegradable option with high specific properties [1,2].

Since the FAO declared 2009 as the "International Year of Natural Fibres", numerous studies have focused on the use of such fibres as reinforcement in composite materials, analysing different combinations of polymer matrices and plant-based reinforcements and finding applications in different sectors ranging from transportation to construction. The focus is increasingly on achieving composite materials that can be biodegraded at the end of their useful life [3], although recycling also presents an interesting alternative for the reuse of the material. In addition, there is a need to evaluate less common plant-based fibres that offer a lower cost and greater availability [4] than those that have already been studied and used, such as jute, hemp, flax, sisal, or kenaf fibres, and that, in addition, do not compete with food production in terms of resources (water and soil). In this context, the use of the giant reed plant as a source of reinforcement or filler material has been proposed, given the widespread use of this plant in the Canary Islands, where it is considered as an invasive plant species, due to its rapid growth under unfavourable conditions. This feature makes it to have been pointed out as a promising plant species for the biorefinery sector, with the focus on producing carbohydrate-rich products and fibres, as well as a strategy for soil remediation and to avoid soil erosion.

Few works were found to use *Arundo* fibres to obtain composite material, which is the focus of this doctoral thesis. For instance, Ghalehno [5] proposed the incorporation of 20 - 40 % ground reed in a urea formaldehyde resin and the compression moulding process, obtaining a composite material with improved mechanical properties compared to the neat resin. Similarly, Baquero-Basto and collaborators [6] introduced 30 - 40 % of ground reed to a vegetable polyurethane resin, increasing the rigidity and tensile strength of the resin, although with a decrease in the flexural properties. Fernández-García [7], on the other hand, obtained a composite material using only *Arundo donax* plant material and citric acid as a natural binder, obtaining boards with mechanical and thermal properties good enough to be used as insulating materials in construction. These same authors also obtained a composite material using urea formaldehyde resin as a matrix and ground reed, in three different sizes, obtaining good results for use as acoustic insulation [8]. However, these first works are mainly working with the ground plant, without any plant processing. Fiore and collaborators proposed the preparation of fibres from the giant reed stems, starting with a manual procedure, consisting on peeling the stems with a blade [9]. In a subsequent study, this same group obtained a compression-moulded composite material with a polylactic acid

(PLA) matrix, using ground stems as a reinforcement material [10] at 10 and 20 % ratios. The study concluded that increasing the *Arundo* content also increased the tensile and flexural elastic moduli, while the tensile and flexural strength decreased. Another study by the same authors shows similar behaviour (improved tensile elastic modulus and reduced strength) when the composite material is obtained using an epoxy resin as a matrix; the results show that these composites could be useful in semi-structural applications [11], when used in proportions between 5 and 15 %.

On the other hand, several authors emphasize the complexity and cost of the recycling processes for composite materials [12–14]. These studies, among others, conclude with the need to study the recyclability of these materials in greater depth to address the existing lack of knowledge in this field.

1.2. OBJECTIVES

Considering the background and working hypothesis presented above, the general objective of this thesis is to assess the eco-sustainable use of *Arundo donax* L. biomass as a reinforcing material, with special emphasis on the recyclability of the resulting biocomposites. The potential end of life of giant reed composites was also considered in this work, as neither the actual recyclability nor their biodegradability has yet been studied in detail. The aim was therefore to obtain a polymer composite material using a thermoplastic matrix (such as polyethylene (PE) or polylactic acid (PLA)) and determine their properties and processability with different proportions of plant fillers from giant reed. The obtained composite materials based on conventional polyolefin were then reprocessed several times, determining the extent to which the composite material is recyclable compared to the virgin polyethylene. While, for the PLA-based ones, biodegradability tests were also performed, determining the effect of the giant reed fibres in the disintegrability of the PLA matrix.

The literature review conducted did not revealed the use of this type of fibre in thermoplastic matrices using injection moulding, nor has it revealed any studies on the recyclability and biodegradability of these materials, which demonstrates the novelty and interest of the proposed work. In order to achieve this main objective, several stages were planned:

- Preparation of the plant material, assessing the need for fibre extraction and the possibility of utilizing the entire plant material. Fibre extraction tests were performed, following natural degradation processes (retting) and mechanical processes. Fibres characterization tests were conducted, determining main constituents (cellulose, hemicellulose and lignin), thermal stability, morphological features, strength and physico-chemical characteristics.
- Obtaining the composite material using thermoplastic matrices with different proportions of the plant material. Composites with up to 40 % biomass were produced (by weight), using injection, rotational, compression and extrusion processes. The aim was determining the processability of reed-based composites on

different processing techniques and characterizing them in order to find possible applications for such materials.

- Disintegration and recyclability assessment of lignocellulose-based composites. Composites with a PE matrix were reprocessed several times in order to determine their potential recyclability, while those based on PLA were subjected to biodisintegration and water degradation assays, in order to determine the effect of the biomass upon such process, as well as the impact on the biobased composites' durability and lifetime performance.

1.3. PUBLICATIONS ARISING FROM THE WORK

Apart of several communications into international well-reputed conferences, this doctoral thesis resulted in two review papers and eight research works dealing with different aspects of giant reed composites. In the first review paper the plant species and its interest for biorefineries are analysed while the second one focuses on the use of *Arundo* for the production of composite materials. Next, the characterization of the plant in terms of composition and its processing to obtain fibres from the stems and the leaves were analysed in a different publication; the characterization of obtained fibres in terms of mechanical behaviour, thermal stability, composition, crystallinity index and physical features was also included there.

Once the fibres were obtained and analysed, composite materials were prepared with different polymer matrices (high-density polyethylene (HDPE); polylactic acid (PLA)) under different processing technologies, namely, twin-screw extrusion, injection, rotational, and compression moulding. The composites were characterized to determine their mechanical and thermal properties. The influence of fibre length at the feeding, compounding parameters and reprocessing in the final properties were also assessed, determining the change in the morphological parameters (diameter, length and aspect ratio) and in properties. Finally, disintegration and water degradation behaviour were also determined for PLA-based composites.

The publications arising from this research work can be found in this document, after three sections, which summarize the methods and findings from each work. Each publication is later included as a different section of the document, which finishes with a summary of the conclusions obtained and a series of potential research lines to continue contributing to a further understanding of the reed-based composites.

2. STATE OF THE ART

This section summarizes the state of the art about the use of natural fibres for composites obtaining and, particularly, for giant reed. For this specific plant species, two different approaches were followed: the entire use of the plant as a raw material for biorefinery processes, with a later focus on the obtaining of fibres and polymer composites.

Two review papers about the use of *Arundo donax* have been published during this thesis preparation (Figure 1):

- P1. A review on the use of giant reed (*Arundo donax* L.) in the biorefineries context. Reviews in Chemical Engineering, 40(3), 2024. DOI: [10.1515/revce-2022-0069](https://doi.org/10.1515/revce-2022-0069)
- P2. Use of giant reed (*Arundo donax* L.) for polymer composites obtaining: a mapping review. Cellulose, 30, 2023. DOI: [10.1007/s10570-023-05176-x](https://doi.org/10.1007/s10570-023-05176-x)

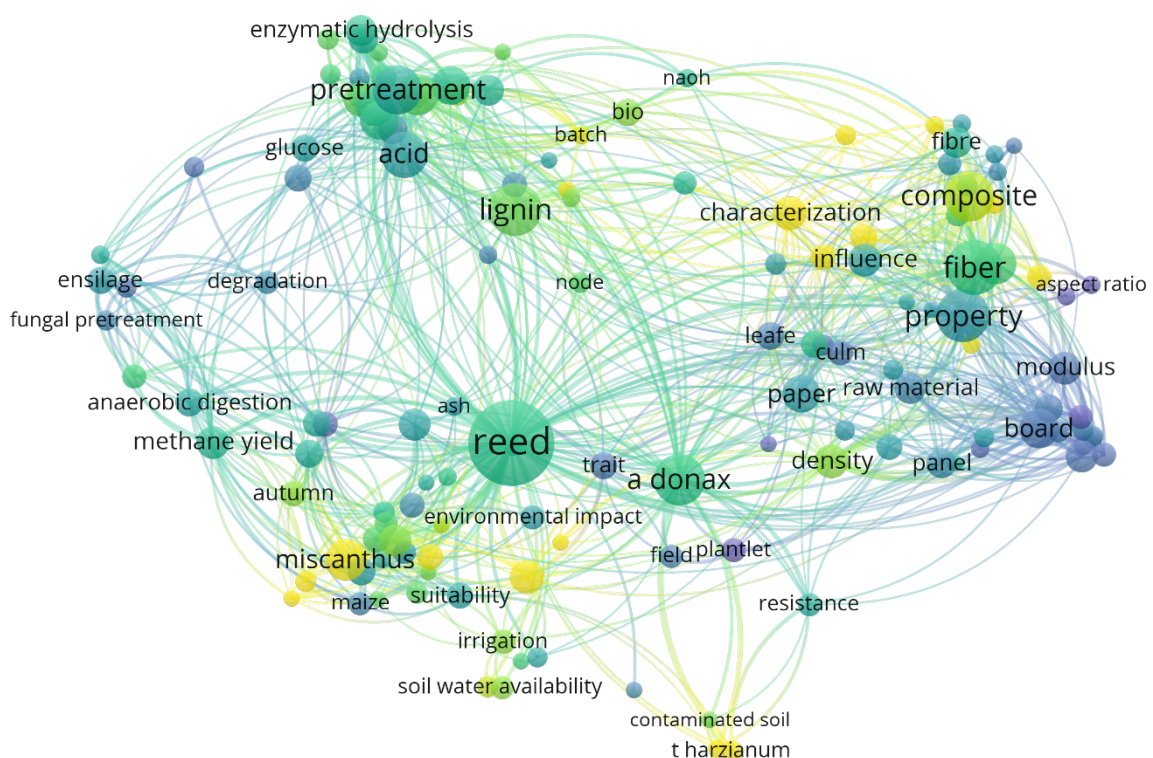


Figure 1. Overlay visualisation of keywords from both review papers dealing with *Arundo donax* L. in the context of biorefineries and polymer composites. (Obtained using the VOSviewer tool).

The first review paper focuses on the potential of this plant species as a sustainable biomass resource for biorefineries [15]. A discussion on agronomic practices, environmental impacts, and techno-economic considerations is performed, concluding with the need for more research to optimize its integration into the bioeconomy. Several aspects of the giant reed, such as its high yield, chemical composition, and viability for biofuels (bioethanol, biogas),

thermochemical processes (pyrolysis, gasification), and for materials like paper or composites, are included.

The massive availability of biomass generated by the giant reed (*Arundo donax* L.) motivates the search for its possible industrial use for the generation of high added-value products through implementing a biorefinery approach. The literature demonstrates the potential of this plant species to obtain different high-value compounds, such as levulinic acid, oligosaccharides, fermentable sugars, highly digestible fibre for animal feed, polyphenols, and natural fibres for composite materials, among others. The data shows the upward trend in Europe toward the generation of new green industries, grouped under the biorefinery concept. *Arundo donax* L. is a perennial grass from the *Gramineae* family, with an uncertain origin, although many authors place its origin in East Asia [16]. The rapid spread of this plant and its poor genetic diversity is explained by its reproduction method, mainly happening through the rhizomes or by producing roots on the nodes [17]. Figure 2 shows two specimens of *Arundo* and the main parts of the plant: leaves, culm or stem, and rhizome. Stems or culms are hollow and have diameters around 2-3 cm, reaching up to 6 m in height, with stem-clasping leaves along the entire stem [18].



Figure 2. Different parts of giant reed plant.

The rapid growth and adaptability of *Arundo donax* L. to various environmental conditions, including drought and salinity [19–21], have supported its widespread naturalization. This is particularly evident in Mediterranean countries, where it has also become invasive [22,23], being even classified among the world's most invasive species by the International Union for the Conservation of Nature (IUCN) [24,25]. Despite this, it is not listed as an invasive alien species of Union concern (European Union, 2017), but is instead recognized as a valuable lignocellulosic feedstock [26]. Furthermore, in Spain it was listed as invasive plant in 2013 [27] being removed in 2019 [28], when it was included in the National bioeconomy strategy [29], which reflects the international trend toward supporting its industrial use. However, concerns remain regarding its environmental impact, and the need of manage the plant

adequately to reduce the danger is highlighted; in fact, long-term studies on the environmental impacts of the cultivation of this plant are still ongoing [30]. Apart of its high potential as a lignocellulosic feedstock for biorefineries due to its high biomass yields, low water and fertilizer needs, and ability to thrive in poor soils [31–33], its cultivation can also offer some environmental benefits, such as soil remediation and erosion prevention [34,35].

Once defined the great interest of this plant species for the bioeconomy industrial sector, a deeper analysis on the possibilities of using it for the obtaining of fibres for composites was performed in the second review paper arising from this thesis [36]. Compared to the extensive research on biofuels and biomolecules, little attention has been paid to obtaining reed composites, and therefore this review has the objective of understand the potential of using this plant species as reinforcement or filler of composites. In this work, a mapping review on the incorporation of giant reed fibres in the production of polymer composites was performed. The work was organized into distinct sections that address the processes involved in fibre extraction (primarily mechanical procedures), as well as the characterization of the fibres. Key properties discussed include the chemical composition, thermal degradation, mechanical properties, and crystallinity of the fibres, all of which are crucial for assessing their suitability in composite applications. The findings indicate that most research to date has concentrated on the production of board panels featuring insulating properties, alongside integrating reed fibres into thermoset resins. However, there exists a notable gap in the literature regarding the exploration of thermoplastic composites created from *Arundo donax*, which is the main aim of this doctoral thesis.

The different methodologies employed for obtaining fibres from *Arundo donax*, which can include mechanical, chemical, or hybrid approaches, are assessed; finding that mechanical processes such as chopping and grinding are prevalent. Fibres obtained from mechanical procedures are mainly used for composites production, while the use of chemical methods provide purified cellulose for diverse applications. One aspect highlighted in the review is the variation in chemical composition and physical properties of giant reed fibres resulting from different extraction methods. For instance, fibres obtained chemically often exhibit lower lignin content and higher cellulose percentages [9]. Specifically, fibres derived mechanically tend to have lignin content ranging from 17 – 25 %, whereas those extracted via chemical methods can drop to as low as 5.3 %. Degradation temperatures and mechanical properties are also affected by the extraction method, which is mainly correlated with the hemicellulose content. Another work derived from this thesis [37], which will be discussed later, provides cellulose contents ranging from 43 – 68 %, with degradation temperature around 275 °C, suitable to be used as reinforcement of polymeric matrices, with a tensile strength of 905 ± 300 MPa, an elastic modulus of 45 ± 12 GPa and a crystallinity index over 65 %. These properties are within the range of commercial lignocellulose fibres, such as jute, flax, abaca or sisal.

In terms of applications, this review summarizes the various uses of *Arundo donax*-reinforced composites in sectors like construction, packaging, and automotive, demonstrating their versatility [10,11,38]. Not much information on the behaviour of polymer-based composites was found in the literature; results on the composites obtained within this thesis will be shown in the next sections of this document.

P1

P2

P3

P4

P5

P6

P7

P8

P9

P10

Although the invasive potential of *Arundo donax* is well-documented, implementing an effective management strategy could yield significant environmental benefits, particularly in regions susceptible to soil erosion and drought. An effective management plan should encompass not only methods aimed at maximizing bioproduct yields with minimal energy input but also strategic crop management practices. This includes cultivating *Arundo donax* exclusively in marginal or degraded lands, utilizing low-quality water resources, or even treating wastewater to reduce the need of nitrogen fertilizers. Consequently, the cultivation of giant reed can serve as a viable solution to mitigate soil erosion, particularly in areas with high risk of desertification, such as the Mediterranean region.

Several valorisation strategies for reed can be followed, depending on the desired final products. Among these, the sugar platform emerges as particularly promising due to the wide range of bioproducts it can generate. These include biopolymers such as polylactic acid (PLA), polyhydroxyalkanoates (PHA), and polybutylene succinate (PBS), as well as fats suitable for biodiesel production, bioethanol, and other chemically significant compounds like xylose and levulinic acid. Following the production of sugars, the remaining solid biomass can be integrated into subsequent processes for the extraction of lignin and cellulose fibres, or further processed to enhance sugar yield. Given the high yields achievable under relatively mild processing conditions, direct energy conversion through combustion is pointed out as an inefficient and undesirable option, turning biorefining into a more sustainable and effective alternative.

On the other hand, before turning this plant species into a valuable and viable raw material, some advancements must be made to scale up infrastructure, bridging the gap between pilot demonstration facilities and large-scale production operations, as highlighted in the Global Bioeconomy Summit in 2020. This presents a fertile area for research, aligned with the European Union's Green Deal strategy and the Sustainable Development Goals, aiming to optimize both the technical viability of biorefineries and the environmental, economic, and social benefits of such initiatives.

3. FIBRE EXTRACTION AND CHARACTERIZATION

For the production of the composites, two approaches were followed: the use of the aerial parts of the plant, with a simple grinding process, and the obtaining of fibres either from the culms or from the leaves. The characterization and extraction trials were performed following this classification: shredded plant, fibres from leaves, and fibres from culms. The procedures and complete results can be found in:

- P3.** Giant Reed (*Arundo donax* L.) Fibre Extraction and Characterization for Its Use in Polymer Composites. Journal of Natural Fibres, 20:1, 2023. DOI: [10.1080/15440478.2022.2131687](https://doi.org/10.1080/15440478.2022.2131687)



Figure 3. Fibres obtained from *Arundo donax* L. culms, leaves and whole plants (from left to right).

This paper explores the extraction and characterization of giant reed fibres to assess their potential as reinforcement materials in polymer composites [37]. Given the growing interest in sustainable materials, the study provides insights into the mechanical properties and chemical composition of *Arundo donax* fibres as a strategy for the development of green composites.

The research incorporates both mechanical and chemical methods for extracting the reed fibres, using separately the aerial parts of the plant, namely stems and leaves. The mechanical extraction process involves chopping and grinding the whole reed specimens to obtain fibres suitable for composite production. For the chemical and hybrid chemical-

mechanical hybrid procedures, *Arundo* leaves and stems were retted in a sodium hydroxide (NaOH) solution to remove lignin and hemicellulose, enhancing cellulose content. The fibres were characterized to determine their structure, chemical properties, and thermal stability, by means of Fourier transform infrared (FTIR) spectroscopy, scanning electron microscopy (SEM), crystallinity index, from X-ray diffraction (XRD) and thermogravimetric analysis (TGA).

The mechanical extraction method yielded fibres containing approximately 35 – 45 % cellulose, while the chemical treatment increased the cellulose content up to 70 %, significantly decreasing lignin content to around 5.3 %. These results align with existing literature, highlighting the effectiveness of chemical treatments in enhancing lignocellulosic fibre quality. Similarly, the thermal analysis revealed a thermal degradation temperature suitable for polymers processing, and in the range, of other commercial natural fibres, such as flax or jute, exceeding 230 °C.

Finally, in terms of mechanical properties, the study reported that the tensile strength of *Arundo donax* fibres slightly varied depending on the part of the plant from which they originate. The fibres obtained through chemical treatment from the reed culms exhibited tensile strength values approaching 900 MPa and an elastic modulus around 45 GPa. This performance compares favourably to other natural fibres such as kenaf (approximately 600 MPa) and jute (around 300 MPa), establishing reed fibres as a competitive option for composites reinforcement.

In conclusion, this research work demonstrates the viability of *Arundo donax* fibres as sustainable reinforcement materials for composites. The combination of high cellulose yield, enhanced mechanical properties, and good thermal stability makes *Arundo* a compelling alternative to conventional synthetic fibres. It has been shown that fibres from leaves are thinner (diameter around 70 µm) and show higher crystallinity than fibres from stems, which are thicker (around 150 µm). Future research directions may include evaluating the environmental impacts of giant reed cultivation and scaling up fibre extraction processes to foster commercial applications.

4. PREPARATION AND CHARACTERIZATION OF COMPOSITES

This section includes a summary of the different papers published (or under review) showing the procedures and results from the preparation and characterization of composites using different polymer matrices and processing techniques:

- P4. A New Image Analysis Assisted Semi-Automatic Geometrical Measurement of Fibres in Thermoplastic Composites: A Case Study on Giant Reed Fibres. Journal of Composites Science, 7(8), 2023. DOI: [10.3390/jcs7080326](https://doi.org/10.3390/jcs7080326)
- P5. Influence of Giant Reed (*Arundo Donax* L.) Culms Processing Procedure on Physicochemical, Rheological, and Thermomechanical Properties of Polyethylene Composites. Journal of Natural Fibres, 21(1), 2024. DOI: [10.1080/15440478.2023.2296909](https://doi.org/10.1080/15440478.2023.2296909)
- P6. Relationship Between the Shape of Giant Reed-Based Fillers and Thermal Properties of Polyethylene Composites: Structural Related Thermal Expansion and Diffusivity Studies. Waste and Biomass Valorization, 15(12), 2024. DOI: [10.1007/s12649-024-02626-w](https://doi.org/10.1007/s12649-024-02626-w)
- P7. Recyclability Assessment of Lignocellulosic Fibre Composites: Reprocessing of Giant Reed/HDPE Composites by Compression Molding. Lecture Notes in Mechanical Engineering IV, 3, 2024. DOI: [10.1007/978-3-031-56474-1_15](https://doi.org/10.1007/978-3-031-56474-1_15)
- P8. Recycling of HDPE-giant reed composites: Processability and performance. Green Processing and Synthesis, 14(1), 2025. DOI: [10.1515/gps-2024-0229](https://doi.org/10.1515/gps-2024-0229)
- P9. Influence of Giant Reed Fibres on Mechanical, Thermal, and Disintegration Behavior of Rotomolded PLA and PE Composites. Journal of Polymers and the Environment, 30(11), 2022. DOI: [10.1007/s10924-022-02542-x](https://doi.org/10.1007/s10924-022-02542-x)
- P10. Giant reed (*Arundo donax* L.) enhanced polylactic acid composites: processing, characterization, and performance of injection moulded and water degraded samples. Submitted to Composites Part A: Applied Science and Manufacturing (04/07/2025, pending review)

4.1. INFLUENCE OF THE COMPOUNDING STAGE IN FIBRE MORPHOLOGY

The paper entitled "A New Image Analysis Assisted Semi-Automatic Geometrical Measurement of Fibres in Thermoplastic Composites: A Case Study on Giant Reed Fibres" [39] presents an innovative low-cost approach for evaluating the geometrical properties of natural fibres embedded in thermoplastic composites (Figure 4).

P1

P2

P3

P4

P5

P6

P7

P8

P9

P10

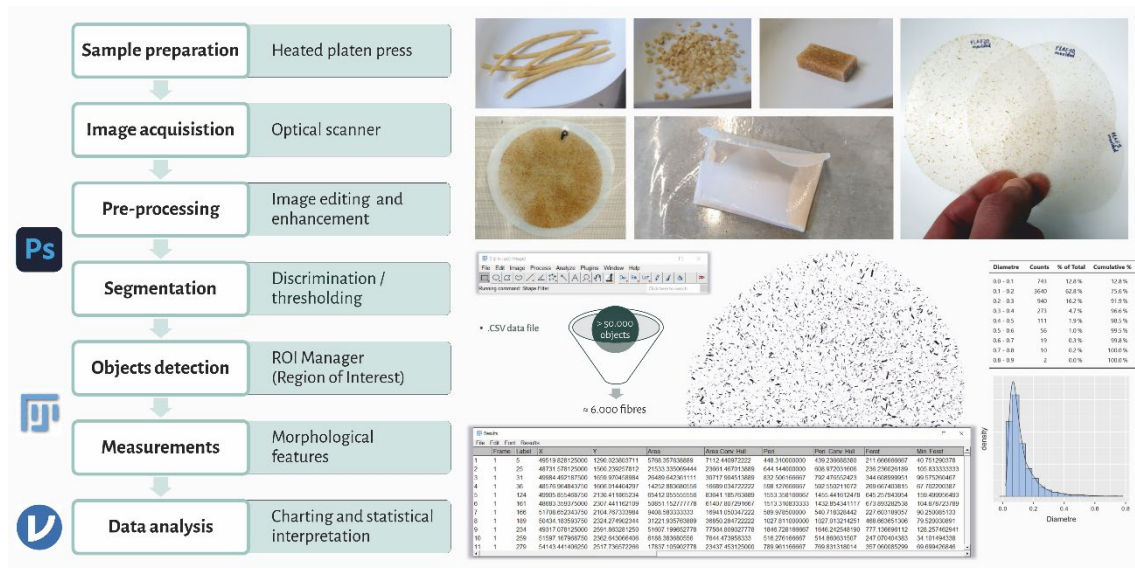


Figure 4. Graphical abstract showing the workflow for fibre morphometric analysis.

This work aims at enhancing the efficiency of measuring fibre characteristics, which are crucial for optimizing the manufacturing and performance of composite materials in various applications. The physical degradation of lignocellulosic fibres during the compounding process is affected by parameters such as the feed and shear rate, as well as the rotation speed and geometric configuration of the extruder screws [40]. During the compounding process, the fibres suffer severe stresses, which cause their breakage [41]. It is well-known that the length and diameter of the fibres (their aspect ratio) is a key parameter, together with the fibre strength and the quality of the adhesion between the fibre and the matrix in the final performance of the composite [39,41]. Fibres in extruded thermoplastic composites usually exhibit lengths of a few millimetres, becoming even smaller after injection moulding processing [42]. Diameters are also affected by attrition processes of the fibre bundles [40,41], and therefore, the aspect ratio of the fibres is also modified during processing.

The study conducted establishes a systematic methodology integrating image analysis for the characterization of fibrous composites, using giant reed fibres as part of the research. The key procedures include the capture of images by affordable scanning techniques, instead of high cost equipment (such as micro-CT) or complicated processes, involving the use of solvents to remove the matrix. The images obtained were analysed using open-source software, namely ImageJ, carrying out semi-automated measurements of various geometrical parameters: fibre length, diameter and aspect ratio. Finally, in order to validate the reliability of the proposed method, the results obtained by this procedure were compared against traditional measurement data (manual measurement of fibres using an optical microscope), finding that this is a practical, efficient, reliable and affordable technique for characterizing fibres in composite materials.

Once determined that the method proposed provides reliable results, different analyses were performed, varying the polymer matrix, the fibre length at the feeding and the extruder parameters, using two different twin-screw extruders to produce the compound. This was done in order to determine the effect of this first processing stage in the length and diameter of the reed fibres and particles in the final compound. It was found that the fibre size

distributions were very similar in the compound produced, regardless of the size of the input fibres or the type of polymer matrix. However, the processing is affected by the fibre size input, being more complicated for longer fibres, which tend to entangle and clog the feeding zone.

An analysis of fibre lengths was performed along the extruder length, determining that the most significant changes happen in the first kneading zone of the extrusion process, where more than 85 % of the fibres for HDPE and 90 % for the PLA compound were reduced to less than 1 mm in length. This high reduction during compounding results in the injection moulding process not significantly affecting the fibres morphology.

4.2. HDPE-BASED COMPOSITES

This section summarizes the findings and conclusions of the composites prepared with *Arundo* derived materials introduced into a HDPE matrix. In order to determine the properties of injection-moulded *Arundo*-based composites, the compound was prepared in a ThermoScientific Process11 twin screw-extruder, using HDPE as matrix, and 20 or 40 % (by weight) fibres or shredded reed, as explained in section 3 of this document about Fibre extraction and characterization. The increasing interest in natural fibres for composite materials due to their sustainability, cost-effectiveness, and potential for reducing environmental impact, together with the lack of information on *Arundo donax* composites, justify the interest of this approach.

The composites prepared were characterized to determine the morphology of the biomass, the thermal stability, and the rheological and physicochemical properties. Injection-moulded samples were used to assess the mechanical performance (tensile, flexural and impact behaviour), together with dynamic mechanical thermal analysis (DMTA) [43]. In a later work [44] the characterization of the composites were completed by a comprehensive assessment of the influence of filler shape derived from giant reed on the thermal properties (thermal expansion and diffusivity) of polyethylene composites. Understanding these properties can enhance the performance and applicability of biocomposites in thermal management applications.

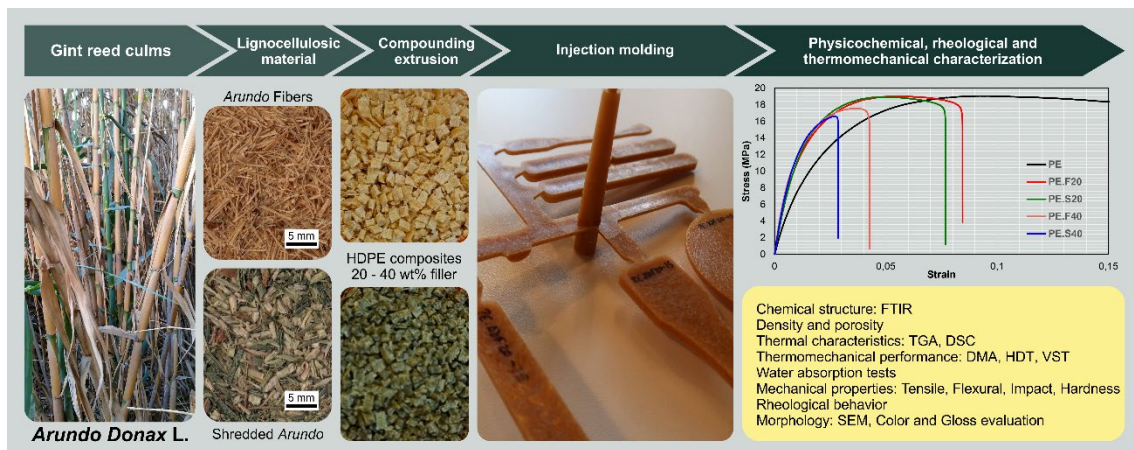


Figure 5. Graphical abstract about the preparation and characterization of giant reed – HDPE composites.

From the first work, it was found that injection-moulded HDPE composites reinforced with 20 % and 40 % of either *Arundo* fibres or shredded aerial plant parts demonstrated improvements in mechanical properties. For instance, the tensile modulus increased significantly with fibre reinforcement: by 78 % for composites with 20 % fibres (reaching up to 1900 MPa), and by 50 % for composites with 20 % shredded reed (up to 1560 MPa), compared to the ≈ 1000 MPa exhibited by the neat HDPE. Flexural modulus also increased for both filler types, though the enhancement was more pronounced in fibre-based composites.

Fibre-reinforced composites exhibited higher heat deflection temperature (HDT) and Vicat softening temperature (VST), with increases up to 78 % compared to neat polyethylene. This indicates superior thermomechanical stability, attributable to the high aspect ratio and directional alignment of the fibres within the matrix. These improvements are essential for applications requiring dimensional and structural integrity at elevated temperatures. These findings correlate with the results from the second paper discussed in this section, where it was determined that the coefficient of thermal expansion (CTE) was significantly reduced in fibre-reinforced composites: from $1.6 \times 10^{-4} \text{ K}^{-1}$ for neat HDPE to $6.1 \times 10^{-5} \text{ K}^{-1}$ and $3.5 \times 10^{-5} \text{ K}^{-1}$ for composites with 20 and 40 % fibres, respectively. The lower thermal expansion coefficients suggest an improved dimensional stability of the fibrous-composites compared to the matrix or the composites with shredded biomass. This enhanced dimensional stability supports potential use in automotive interior components and technical packaging.

Thermal diffusivity also increased with filler content, with the most significant rise (60 %) found for composites with 40 % reed fibres. The orientation of fibres during injection moulding likely improved heat transfer within the composite, compensating for the slight decrease in thermal conductivity due to increased porosity.

These studies collectively validate the incorporation of *Arundo donax* L. derived materials as a multifunctional, sustainable reinforcement for HDPE composites. Fibre-based reinforcements exhibit a better mechanical, thermal, and dimensional performance than shredded filler composites, although the results for those samples also show improvements compared to the neat HDPE matrix. Further analysis, including the study of the environmental footprint of both options by means of life cycle assessment (LCA), would be needed to complete the characterization of these materials. In any case, the obtained results support the feasibility of incorporating giant reed into industrial biocomposites as a way to align material innovation with sustainability principles. It is therefore clear that material design can significantly impact thermal management capabilities, which might constitute a future research path to obtain high-performance, environmentally-friendly materials in industrial applications.

4.3. RECYCLABILITY ASSESSMENT OF HDPE-BASED COMPOSITES

A further step in the research about composites was the assessment of the recyclability of lignocellulose-based composites. In line with circular economy principles, the recyclability of such composites is crucial for reducing environmental impacts and maximizing resource efficiency. These composites would ensure a better environmental behaviour if, apart of consisting of a certain ratio of biobased renewable material, they could also be effectively recycled. Therefore, these studies investigate the mechanical and thermal stability of high-density polyethylene (HDPE) composites reinforced with *Arundo donax* L. fibres or shredded plant material, with a focus on performance retention across recycling cycles. Using compression and injection moulding techniques, the work (Figure 6) complements previous research on injection-moulded composites, providing new insights into the end-of-life behaviour of these materials.

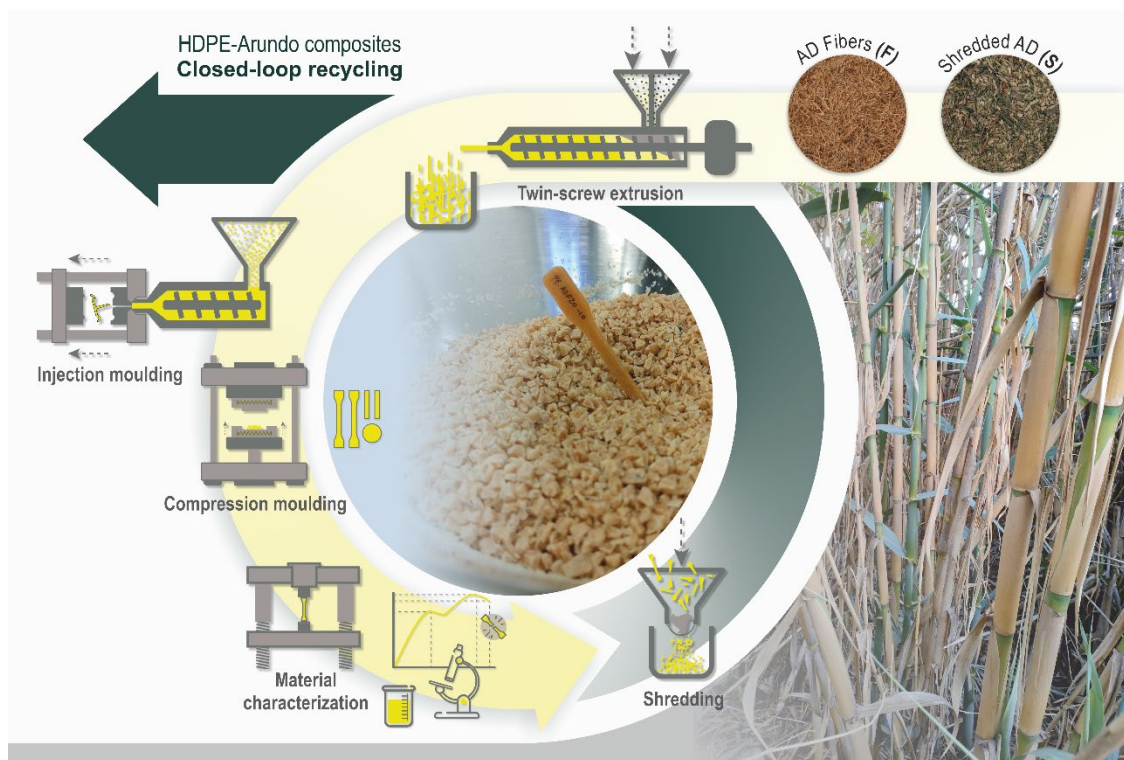


Figure 6. Graphical abstract about the closed-loop recycling of compression and injection-moulded giant reed – HDPE composites.

Composites were manufactured via compression or injection moulding using HDPE matrices filled with 20 % or 40 % of either *Arundo donax* fibres or shredded biomass. After initial processing and obtaining of the raw composite properties, samples were subjected to mechanical grinding, drying, and reprocessing through a next compounding and processing (compression or injection moulding) cycle to simulate recycling.

In a first step, compression moulding was performed to reduce degradative phenomena related to shear stress in injection moulding [45]. The results revealed that all composites experienced some mechanical degradation after recycling, though the extent varied with

filler type and content. Fibrous composites retained over 80 % of their original tensile strength after recycling, while shredded composites showed decreases that are more significant; flexural properties followed the same trend, demonstrating improved structural resilience during reprocessing for fibre-based composites. The reduction in particles size after reprocessing explains this different behaviour, with fibres enabling a better load transfer capacity. Thermal analysis confirmed the stability of composites, ensuring their safe reprocessing.

Next, injection-moulded composites were also subjected to five recycling stages [46], assessing the structural evolution and material integrity over successive processing cycles, and concluding that the reprocessing of HDPE-*Arundo* composites reveals some controllable structural and thermal changes. As also observed for compression-moulded samples, fibre-reinforced materials provide a higher stability and performance than ground-based composites. In any case, both families of composites can be effectively recycled on closed loops to support the development of bio-based recyclable composites contributing that way to circular material systems. It is important to remind that no additives, i.e. adhesion promoters, were used in the compounding phase, which seems to improve processability and some aspects of mechanical performance rather than degrading the materials throughout the recycling process.

Fourier Transform Infrared (FTIR) analysis did not show significant formation of carbonyl groups, indicating a limited oxidative degradation of the HDPE matrix. The changes observed on FTIR spectra primarily affected the lignocellulosic phase, contributing to homogenization and reduced filler visibility on sample surfaces.

Reprocessed composites showed an increase in melt flow index (MFI), providing improved processability. The increase was most evident in shredded-filled composites due to filler size reduction and increased flow homogeneity. Similarly, oscillatory rheology showed that fibrous composites maintained or slightly increased viscosity and storage modulus after reprocessing, while shredded composites exhibited a decrease. This suggests that fibre-filled systems retained better structural integrity. All composites remained thermally stable in a wide temperature range, with main degradation events found on thermogravimetric analysis (TGA) at about 30 °C over processing temperatures.

Oxidation Induction Time (OIT) analyses showed significant stabilization in composites, particularly for those with 40 % fibre loading, nearly doubling the induction time compared to neat HDPE (first processing). After recycling, OIT dropped across all samples, while the composites still showed an enhanced stability, likely due to antioxidant phenolic compounds from lignin in the biomass.

Finally, regarding mechanical behaviour, recycled composites showed increased stiffness under tensile and flexural testing, with the PE.S40-r series reaching up to 50 % and 200 % increases, respectively. Recycled composites with 40 % fibre exhibited the highest modulus values. In the same line, DMTA results revealed higher storage moduli in recycled composites, increasing up to 64 % at -60 °C. Fibrous materials had better modulus retention and stress transfer post-reprocessing. Loss moduli also increased, reflecting a more viscous material response.

In conclusion, the possibility of recycling HDPE-*Arundo donax* composites without drastic loss of performance supports their application in industrial sectors prioritizing sustainability, such as automotive interiors, construction panels, and consumer goods. The higher performance retention of fibre-based composites highlights the importance of filler processing and morphology in designing recyclable bio-based materials. Nonetheless, further investigation into long-term durability and full life cycle assessment (LCA) remains essential to validate these environmental benefits. The reprocessing performed within this research work is done in a closed loop, and their effective recyclability is still constrained by the lack of standardized recycling pathways, particularly in post-consumer waste streams. The absence of efficient sorting systems and separated recycling pathways result in cross-contamination, diminishing the recycle quality and limiting high-value reuse [47]. Future development of infrared or chemical marker-based sorting technologies could help address this limitation and enable industrial-scale recyclability of such composite materials.

4.4. PLA-BASED COMPOSITES

The giant reed fillers were combined with a PLA matrix in order to get a fully biobased composite. A first work to this approach was performed by rotational moulding (Figure 7), which focused on understanding how the introduction of these fibres affects not only the mechanical and thermal properties of these materials but also their behaviour during biodegradation [48]. A second work (under review) produced PLA-composites with up to 40 % giant reed derived materials by injection moulding, deeply assessing their structure and properties, and assessing their performance after their saturation with water.

ROTOMOLDED COMPOSITES AND BIODEGRADATION ASSAYS

Due to the particularities of the rotomoulding process, low ratios of fibres were used (10 %), by dry-blending the fibres with the PLA in powder form before their introduction into the cube-shaped mould for its processing. During the rotomoulding cycle the maximum internal air temperature was controlled to ensure an adequate melting and densification and to avoid any over-cooking, which would result in the polymer degradation.

After obtaining the cube-shaped test items, these were cut and machined to produce the test samples, which were analysed to elucidate the mechanical performance, thermal characteristics and morphological details in addition to disintegration behaviour of the resulting composites. Mechanical properties are greatly influenced by the incorporation of the reed fibres, as otherwise expected due to the sensitiveness of this process to the incorporation of foreign materials; particularly, impact strength drastically dropped for the composites, while flexural and tensile properties were reduced in a lower extent. This reduced strength is related to the higher porosity of the composites, as a consequence of the hindered movement of the polymer particles inside the mould and the difficulties for the sintering among them to happen by the incorporation of a non-molten material. Glass transition and melting temperatures increased with the incorporation of *Arundo* fibres due

to hindering PLA chains' mobility, with composites exhibiting a lower crystallinity than neat PLA, reflecting the complex interaction between the fibres and the matrix.

The most significant contribution of this work relies in the biodisintegration assays conducted over these composites in order to assess the environmental sustainability of the PLA composites. PE-based composites were produced and analysed following the same procedure as a way to ensure the validity of the experiment. These assays are critical in evaluating how these materials break down in natural conditions, thereby providing insights into their lifecycle impacts.

The biodisintegration tests performed were designed to simulate composting conditions, a common environment for the degradation of biodegradable polymers. In these assays, samples of the developed composites were subjected to controlled compost environments, allowing for a structured assessment of microbial action on the materials. Different time intervals were monitored to evaluate the rate and extent of disintegration.

The samples were assessed after the disintegration process by differential scanning calorimetry (DSC) in order to determine the extent of the degradation, finding a significant reduction in glass transition and melting temperatures. Besides, FTIR analysis also confirmed the degradation of the matrix, visible at naked eye, with an increase of the intensity of the bands associated to carbonyl and ester groups. Mechanical testing was not performed due to the fragility of the specimens after such procedure. In conclusion, these assays indicate the higher extent of the biodegradation of the composite samples, demonstrating that the composites could effectively disintegrate under composting conditions in a more effective and fast way than neat PLA, particularly when home composting conditions are used (at low temperatures).

The key conclusions from these biodisintegration assays support the viability of giant reed fibres as reinforcements in eco-friendly composite materials. The effective disintegration under composting conditions effectively places these composites as viable alternative to synthetic composites, confirming their role in reducing environmental impact through sustainable design practices. This research contributed significantly to the literature on biodegradable composites, not so developed by that time, showing that the incorporation of natural fibres can lead to enhancements in both performance and environmental safety.

INJECTION-MOLDED COMPOSITES AND WATER AGEING ASSAYS

Another part of the study comprised the processing of the reed materials into a PLA matrix through conventional twin-screw extrusion and injection moulding processes. The results of this part of the work have been submitted to a JCR-indexed journal for publication (Composites Part A: Applied Science and Manufacturing, on July 8th 2025) and are still under review at the moment of preparation of this document. Therefore, the main procedures, results and conclusions are summarized below in order to complete the results of this doctoral thesis, although also including the manuscript as annex to this document, together with the published works.

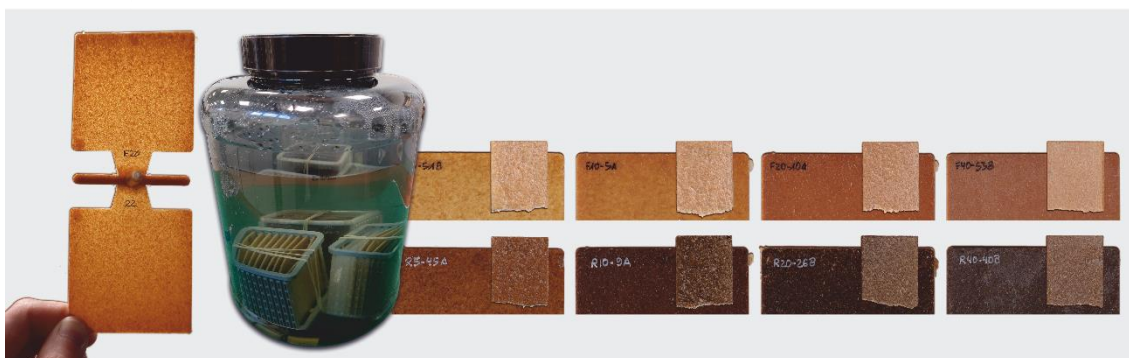


Figure 7. Injection-moulded and water-degraded PLA – based giant reed composites.

In this study, the two types of *Arundo*-derived fillers used for HDPE composites, namely fibres and shredded reed, were introduced in different ratios, from 5 to 40 % into the PLA matrix (Luminy L105® from TotalEnergies Corbion), via twin-screw compounding, obtaining injection-moulded samples for later characterization. A comprehensive analysis of the properties of the composites was performed, including FTIR, TGA, DSC, WAXS, DMTA, hydrophilicity, roughness and rheological analysis, therefore assessing their structure and performance. A set of samples for each composition were water soaked until saturation, determining their water uptake parameters. Besides, the saturated samples were subjected to further characterization, namely DMTA, mechanical testing (tensile and flexural) and rheology, in order to determine the effect of the water ageing in the samples performance, investigating the durability and usability of such composites in moisture-prone environments, such as those related to food contact applications or agricultural products.

The results indicate that the incorporation of *Arundo donax* fillers has minimal impact on the chemical structure of the PLA matrix, evidencing no specific interactions between the filler and the matrix, or these being overlapped on the fingerprint of both constituents. However, it significantly influences the rheological behaviour, with different performances observed as a consequence of the filler type (shredded particles vs. fibres) and loading ratio. Both types of fillers promote shear-thinning characteristics typical of non-Newtonian polymer melts. Given the uneven viscous behaviour, several measurements were made in order to determine if this was an unexpected trend or measurement artifacts, however, the trend followed in all cases was similar in all tests. Fibre morphology played a key role in determining flow behaviour, with fibrous fillers enhancing alignment and network formation under shear, while shredded particles showed less predictable responses. Conducted MFI analysis confirms that 40 % filler content drastically reduces flowability, impacting processing conditions.

Thermal analyses revealed that while the addition of lignocellulosic materials reduced the degradation onset temperature compared to neat PLA, as expected considering the lower thermal stability of the biomass compared to the biopolymer; in any case, all composites exhibited thermal stability suitable for injection moulding processes. Wide-angle X-ray scattering (WAXS) patterns allowed concluding that the PLA and its composites exhibit a mostly amorphous structure, resulting from rapid cooling during moulding. Overall, filler ratios play a more influential role than the specific type of filler, fibres or shredded biomass, on the thermal properties of composites. From DSC analysis, it was found that the

P1

P2

P3

P4

P5

P6

P7

P8

P9

P10

incorporation of the reed fractions has no influence on either T_m or T_g values, with these parameters barely varying from 173 °C and 66 °C for all formulations, respectively. This behaviour is similar to that obtained in PLA composites where other plant or animal fibres have been used [49–51]. Comparison of thermograms from the first and second heating shows that during the second heating, the endothermic glass transition peak and the exothermic cold crystallisation peak are significantly reduced; this results from the material's relaxation following the injection moulding process and the removal of its thermal history. The decrease in crystallization temperature for all composite materials evidenced that the plant fillers act as nucleating agent for the Poly-L-lactide (PLLA) matrix, altering the mobility of the polymer chains and improving the crystallization behaviour [52,53]. Finally, it was also observed that neat PLA exhibits cold crystallization at 97.4 °C, which disappears for the second heating in all composite samples. Other authors have reported a similar behaviour, with a decrease in crystallization temperature for composites, with the filler increasing the ratio of disordered alpha phase in PLA, more related to the amount of the filler than to its size [53]. This lack of cold crystallization in the second heating explains the high levels of crystallinity index calculated from melting enthalpies, while the first heating cycle refers to the injection-moulded material, which shows that it is mostly amorphous, as also found from WAXD analysis. The fibres seem to hinder the crystallization of the matrix during processing, as also do the shredded filler, although to a lower extent; for both cases, an increase in the ratio of the biomass result in higher crystallinity indexes.

Regarding the mechanical efficiency of the different series of composites prepared, it was determined that composites containing 10 % and 20 % fibres provided optimal performance, combining enhanced stiffness with good strength and impact resistance. These formulations exhibited improved stress transfer between the matrix and the filler, indicating good interfacial adhesion [54–56]. At higher filler loadings (40 %), stiffness increased further, but at the cost of reduced elongation at break and overall brittleness, suggesting a trade-off between reinforcement and ductility. Shredded particle composites showed less pronounced improvements, likely due to lower aspect ratios and a greater tendency for agglomeration [39,57,58]. To finish, interfacial adhesion, determined from the adhesion factor, which considers the relationship between the damping factor of the neat polymer and the composite, and the volume fraction of the biofiller, increased significantly at 40 % filler content (meaning a lower adhesion occurs), consistent with the reduced tensile strength in this series. These findings suggest that intermediate filler loadings (i.e. 10 and 20 %) provide the best balance between mechanical performance and structural cohesion.

MicroCT imaging confirmed the obtaining of a homogeneous distribution of filler particles in the matrix, achieving acceptable porosity levels in the composites, under 1 % in all cases. On the other hand, the present work highlights the critical impact of filler type on moisture absorption, where higher lignocellulosic loading, especially fibres (needle-like and higher aspect ratio), leads to higher water absorption, reaching up to 14 % uptake for composites with 40 % fibres, and about 10 % moisture weight increase for 40 % shredded composites. The influence of surface morphology on water uptake was also evident, as increased surface roughness associated with higher filler content resulted in reduced wettability. Contact angle measurements showed a slight increase in surface hydrophobicity with higher filler contents,

due to increased surface roughness, as also found previously [59], as these parameters increasing with increased filler content. These findings underscore the complex interplay between filler characteristics, composite structure, and their effects on mechanical properties and durability, which are crucial for evaluating the suitability of PLA composites in various applications.

The water uptake led to significant reductions in mechanical performance, as found from DMTA analysis conducted over saturated samples. However, partial recovery of properties was observed after re-drying, indicating some resilience of the PLA-*Arundo* composites to cyclic wet-dry exposure; in some cases, though, some samples resulted in lowered mechanical properties, evidencing the hydrolytic degradation of the PLA matrix. As a conclusion, PLA-*Arundo* composites show their potential applicability across various industries, suggesting their resilience under moderate loads after water-saturation. Future studies should explore long-term aging and cyclic wetting and drying effects for a comprehensive understanding of material performance.

Finally, surface analysis confirmed that the increase in roughness and filler content resulted in increased opacity and reduced gloss. Composites with fibrous fillers exhibited lighter colours, while those with shredded biomass showed darker, less translucent finishes. Additionally, water degradation leads to lighter coloured materials with increased opacity, attributed to structural changes in the polymer matrix and bonding interface. These changes in surface and aesthetic properties may influence the suitability of the composites for specific applications, particularly where visual appearance and tactile qualities are important.

In conclusion, the incorporation of giant reed derived materials into PLA matrices offers a promising pathway to enhance the mechanical and thermal properties of biodegradable composites while making use of an abundant, renewable, fast growing natural resource. Composites containing 10 to 20 % fibres yield optimal results, demonstrating improved stiffness, acceptable durability, and manageable moisture sensitivity. These findings highlight the potential of PLA-*Arundo* composites for use in moderately demanding applications, such as packaging, agriculture, and consumer goods, where ecological sustainability must align with material performance.

The comprehensive analysis of giant reed fibre effects provides a critical perspective on their reinforcing efficiency and ecological benefits, emphasizing the need to balance material properties, processing techniques, and biodegradation behaviour. The study also underscores the complex interplay between filler morphology, dispersion, interfacial bonding, and environmental durability, offering valuable insights for the future design of biocomposites and promoting more sustainable practices in materials engineering within a circular economy.

P1

P2

P3

P4

P5

P6

P7

P8

P9

P10

5. REFERENCES

*Each published work, included in next chapters, accounts with its own references section, being this list only referred to the introduction chapter (sections 1 to 4 in the document).

1. Yashas Gowda, T.G.; Sanjay, M.R.; Subrahmanya Bhat, K.; Madhu, P.; Senthamaraikannan, P.; Yogesha, B. Polymer Matrix-Natural Fibre Composites: An Overview. *Cogent Eng.* 2018, *5*, 1446667.
2. Ahmad, F.; Choi, H.S.; Park, M.K. A Review: Natural Fibre Composites Selection in View of Mechanical, Light Weight, and Economic Properties. *Macromol. Mater. Eng.* **2015**, *300*, 10–24, doi:10.1002/mame.201400089.
3. Gurunathan, T.; Mohanty, S.; Nayak, S.K. A Review of the Recent Developments in Biocomposites Based on Natural Fibres and Their Application Perspectives. *Compos. Part A Appl. Sci. Manuf.* 2015, *77*, 1–25.
4. Sarasini, F.; Fiore, V. A Systematic Literature Review on Less Common Natural Fibres and Their Biocomposites. *J. Clean. Prod.* **2018**, *195*, 240–267, doi:10.1016/j.jclepro.2018.05.197.
5. Dahmardeh Ghalehno, M.; Madhoushi, M.; Tabarsa, T.; Nazerian, M. The Manufacture of Particleboards Using Mixture of Reed (Surface Layer) and Commercial Species (Middle Layer). *Eur. J. Wood Wood Prod.* **2011**, *69*, 341–344, doi:10.1007/S00107-010-0437-7/TABLES/2.
6. Baquero Basto, D.; Monsalve Alarcón, J.; Sánchez Cruz, M.; Alarcón, J.M.; Sánchez Cruz, M.; Monsalve Alarcón, J.; Sánchez Cruz, M. Experimental Characterization of Composite Panels Made with Arundo Donax Fibres and Vegetable Resin. *Sci. Tech. Año XXII* **2018**, *23*, 119–125.
7. Ferrandez-Garcia, M.T.; Ferrandez-Garcia, C.E.; Garcia-Ortuño, T.; Ferrandez-Garcia, A.; Ferrandez-Villena, M. Experimental Evaluation of a New Giant Reed (Arundo Donax L.) Composite Using Citric Acid as a Natural Binder. *Agronomy* **2019**, *9*, 882, doi:10.3390/agronomy9120882.
8. Ferrandez-García, M.T.; Ferrandez-Garcia, A.; Garcia-Ortuño, T.; Ferrandez-Garcia, C.E.; Ferrandez-Villena, M. Assessment of the Physical, Mechanical and Acoustic Properties of Arundo Donax L. Biomass in Low Pressure and Temperature Particleboards. *Polymers (Basel)*. **2020**, *12*, 1361, doi:10.3390/polym12061361.
9. Fiore, V.; Scalici, T.; Valenza, A. Characterization of a New Natural Fibre from Arundo Donax L. as Potential Reinforcement of Polymer Composites. *Carbohydr. Polym.* **2014**, *106*, 77–83, doi:10.1016/j.carbpol.2014.02.016.

10. Fiore, V.; Botta, L.; Scaffaro, R.; Valenza, A.; Pirrotta, A. PLA Based Biocomposites Reinforced with Arundo Donax Fillers. *Compos. Sci. Technol.* **2014**, *105*, 110–117, doi:10.1016/j.compscitech.2014.10.005.
11. Fiore, V.; Scalici, T.; Vitale, G.; Valenza, A. Static and Dynamic Mechanical Properties of Arundo Donax Fillers-Epoxy Composites. *Mater. Des.* **2014**, *57*, 456–464, doi:10.1016/j.matdes.2014.01.025.
12. Ramzy, A. Recycling Aspects of Natural Fibre Reinforced Polypropylene Composites, Clausthal University of Technology: Clausthal, 2018.
13. Suárez, L.; Castellano, J.; Díaz, S.; Tcharkhtchi, A.; Ortega, Z. Are Natural-Based Composites Sustainable? *Polymers (Basel)*. **2021**, *13*, 2326, doi:10.3390/polym13142326.
14. Cestari, S.P.; da Silva Freitas, D. de F.; Rodrigues, D.C.; Mendes, L.C. Recycling Processes and Issues in Natural Fibre-Reinforced Polymer Composites. In *Green Composites for Automotive Applications*; Elsevier, 2019; pp. 285–299.
15. Ortega, Z.; Bolaji, I.; Suárez, L.; Cunningham, E. A Review of the Use of Giant Reed (*Arundo Donax* L.) in the Biorefineries Context. *Rev. Chem. Eng.* **2023**, *0*, doi:10.1515/revce-2022-0069.
16. Jensen, E.F.; Casler, M.D.; Farrar, K.; Finnan, J.M.; Lord, R.; Palmborg, C.; Valentine, J.; Donnison, I.S. Giant Reed: From Production to End Use. In *Perennial Grasses for Bioenergy and Bioproducts*; Alexopoulou, E., Ed.; Academic Press Inc. Elsevier: London, 2018; pp. 107–150 ISBN 9780128129005.
17. Corno, L.; Pilu, R.; Adani, F. Arundo Donax L.: A Non-Food Crop for Bioenergy and Bio-Compound Production. *Biotechnol. Adv.* **2014**, *32*, 1535–1549, doi:10.1016/j.biotechadv.2014.10.006.
18. Csurhes, S. Invasive Weed Risk Assessment: Giant Reed Arundo Donax; 2016;
19. Romero-Munar, A.; Baraza, E.; Cifre, J.; Achir, C.; Gulías, J. Leaf Plasticity and Stomatal Regulation Determines the Ability of Arundo Donax Plantlets to Cope with Water Stress. *Photosynthetica* **2018**, *56*, 698–706, doi:10.1007/s11099-017-0719-y.
20. Romero-Munar, A.; Tauler, M.; Gulías, J.; Baraza, E. Nursery Preconditioning of Arundo Donax L. Plantlets Determines Biomass Harvest in the First Two Years. *Ind. Crops Prod.* **2018**, *119*, 33–40, doi:10.1016/j.indcrop.2018.03.065.
21. Sánchez, E.; Scordia, D.; Lino, G.; Arias, C.; Cosentino, S.L.; Nogués, S. Salinity and Water Stress Effects on Biomass Production in Different Arundo Donax L. Clones. *BioEnergy Res.* **2015**, *8*, 1461–1479, doi:10.1007/s12155-015-9652-8.
22. Lambertini, C. Why Are Tall-Statured Energy Grasses of Polyploid Species Complexes Potentially Invasive? A Review of Their Genetic Variation Patterns and Evolutionary Plasticity. *Biol. Invasions* **2019**, *21*, 3019–3041, doi:10.1007/S10530-019-02053-2.

23. Shtein, I.; Baruchim, P.; Lev-Yadun, S. Division of Labour among Culms in the Clonal Reed *Arundo Donax* (Poaceae) Is Underlain by Their Pre-Determined Hydraulic Structure. *Bot. J. Linn. Soc.* **2021**, *195*, 348–356, doi:10.1093/botlinnean/boaa062.
24. Jiménez-Ruiz, J.; Hardion, L.; Del Monte, J.P.; Vila, B.; Santín-Montanyá, M.I. Monographs on Invasive Plants in Europe N° 4: *Arundo Donax* L. *Bot. Lett.* **2021**, *168*, 131–151, doi:10.1080/23818107.2020.1864470.
25. Group, I.S.S. *Arundo Donax* - Global Invasive Species Database Available online: <https://www.iucngisd.org/gisd/speciesname/Arundo+donax> (accessed on 12 April 2025).
26. Mantziaris, S.; Iliopoulos, C.; Theodorakopoulou, I.; Petropoulou, E. Perennial Energy Crops vs. Durum Wheat in Low Input Lands: Economic Analysis of a Greek Case Study. *Renew. Sustain. Energy Rev.* **2017**, *80*, 789–800, doi:10.1016/J.RSER.2017.05.263.
27. Ministerio de Agricultura Alimentación y Medioambiente *Disposición 8565 Del BOE Núm. 185 de 2013*, 2013;
28. Ministerio para la Transición Ecológica Real Decreto 216/2019, de 29 de Marzo, Por El Que Se Aprueba La Lista de Especies Exóticas Invasoras Preocupantes Para La Región Ultraperiférica de Las Islas Canarias y Por El Que Se Modifica El Real Decreto 630/2013, de 2 de Agosto, Por El Que Se Regula ; Ministerio para la Transición Ecológica, 2019; pp. 32902–32921;.
29. Ministerio de Economía Industria y Competitividad; España, G. de *Biorrefinerías En España*, 2017;
30. Schmidt, T.; Fernando, A.L.; Monti, A.; Rettenmaier, N. Life Cycle Assessment of Bioenergy and Bio-Based Products from Perennial Grasses Cultivated on Marginal Land in the Mediterranean Region. *BioEnergy Res.* **2015**, *8*, 1548–1561, doi:10.1007/s12155-015-9691-1.
31. Amaducci, S.; Perego, A. Field Evaluation of *Arundo Donax* Clones for Bioenergy Production. *Ind. Crops Prod.* **2015**, *75*, 122–128, doi:10.1016/j.indcrop.2015.04.044.
32. Bonfante, A.; Impagliazzo, A.; Fiorentino, N.; Langella, G.; Mori, M.; Fagnano, M. Supporting Local Farming Communities and Crop Production Resilience to Climate Change through Giant Reed (*Arundo Donax* L.) Cultivation: An Italian Case Study. *Sci. Total Environ.* **2017**, *601–602*, 603–613, doi:10.1016/j.scitotenv.2017.05.214.
33. Forte, A.; Zucaro, A.; Fagnano, M.; Bastianoni, S.; Basosi, R.; Fierro, A. LCA of *Arundo Donax* L. Lignocellulosic Feedstock Production under Mediterranean Conditions. *Biomass and Bioenergy* **2015**, *73*, 32–47, doi:10.1016/j.biombioe.2014.12.005.
34. Bernal, M.P.; Grippi, D.; Clemente, R. Potential of the Biomass of Plants Grown in Trace Element-Contaminated Soils under Mediterranean Climatic Conditions for Bioenergy Production. *Agronomy* **2021**, *11*, doi:10.3390/AGRONOMY11091750.

35. Garau, M.; Castaldi, P.; Diquattro, S.; Pinna, M.V.; Senette, C.; Roggero, P.P.; Garau, G. Combining Grass and Legume Species with Compost for Assisted Phytostabilization of Contaminated Soils. *Environ. Technol. Innov.* **2021**, *22*, doi:10.1016/J.ETI.2021.101387.
36. Suárez, L.; Ortega, Z.; Barczewski, M.; Cunningham, E. Use of Giant Reed (*Arundo Donax* L.) for Polymer Composites Obtaining: A Mapping Review. *Cellulose* **2023**, *30*, 4793–4812, doi:10.1007/s10570-023-05176-x.
37. Suárez, L.; Barczewski, M.; Kosmela, P.; Marrero, M.D.; Ortega, Z. Giant Reed (*Arundo Donax* L.) Fibre Extraction and Characterization for Its Use in Polymer Composites. *J. Nat. Fibres* **2023**, *20*, 1–14, doi:10.1080/15440478.2022.2131687.
38. Fiore, V.; Piperopoulos, E.; Calabrese, L. Assessment of *Arundo Donax* Fibres for Oil Spill Recovery Applications. *Fibres* **2019**, *7*, 75, doi:10.3390/fib7090075.
39. Suárez, L.; Billham, M.; Garrett, G.; Cunningham, E.; Marrero, M.D.; Ortega, Z. A New Image Analysis Assisted Semi-Automatic Geometrical Measurement of Fibres in Thermoplastic Composites: A Case Study on Giant Reed Fibres. *J. Compos. Sci.* **2023**, *7*, 326, doi:10.3390/jcs7080326.
40. Dickson, A.; Teuber, L.; Gaugler, M.; Sandquist, D. Effect of Processing Conditions on Wood and Glass Fibre Length Attrition during Twin Screw Composite Compounding. *J. Appl. Polym. Sci.* **2020**, *137*, 48551, doi:10.1002/app.48551.
41. Bourmaud, A.; Shah, D.U.; Beaugrand, J.; Dhakal, H.N. Property Changes in Plant Fibres during the Processing of Bio-Based Composites. *Ind. Crops Prod.* **2020**, *154*, 112705, doi:10.1016/j.indcrop.2020.112705.
42. Mallick, P.K. Thermoplastics and Thermoplastic–Matrix Composites for Lightweight Automotive Structures. In *Materials, Design and Manufacturing for Lightweight Vehicles*; Elsevier, 2021; pp. 187–228.
43. Suárez, L.; Hanna, P.R.; Ortega, Z.; Barczewski, M.; Kosmela, P.; Millar, B.; Cunningham, E. Influence of Giant Reed (*Arundo Donax* L.) Culms Processing Procedure on Physicochemical, Rheological, and Thermomechanical Properties of Polyethylene Composites. *J. Nat. Fibres* **2024**, *21*, doi:10.1080/15440478.2023.2296909.
44. Barczewski, M.; Suárez, L.; Mietliński, P.; Kloziński, A.; Ortega, Z. Relationship Between the Shape of Giant Reed-Based Fillers and Thermal Properties of Polyethylene Composites: Structural Related Thermal Expansion and Diffusivity Studies. *Waste and Biomass Valorization* **2024**, doi:10.1007/s12649-024-02626-w.
45. Suárez, L.; Ní Mhuirí, A.; Millar, B.; McCourt, M.; Cunningham, E.; Ortega, Z. Recyclability Assessment of Lignocellulosic Fibre Composites: Reprocessing of Giant Reed/HDPE Composites by Compression Molding. In *Manufacturing 2024*; Hamrol, A., Grabowska, M., Hinz, M., Eds.; Springer Nature, 2024; pp. 198–212.
46. Suárez, L.; Barczewski, M.; Billham, M.; Miklaszewski, A.; Mietliński, P.; Ortega, Z. Recycling of HDPE-Giant Reed Composites: Processability and Performance. *Green Process. Synth.* **2025**, *14*, doi:10.1515/gps-2024-0229.

47. Zhao, X.; Copenhaver, K.; Wang, L.; Korey, M.; Gardner, D.J.; Li, K.; Lamm, M.E.; Kishore, V.; Bhagia, S.; Tajvidi, M.; et al. Recycling of Natural Fibre Composites: Challenges and Opportunities. *Resour. Conserv. Recycl.* **2022**, *177*, 105962, doi:10.1016/j.resconrec.2021.105962.
48. Suárez, L.; Ortega, Z.; Romero, F.; Paz, R.; Marrero, M.D. Influence of Giant Reed Fibres on Mechanical, Thermal, and Disintegration Behavior of Rotomolded PLA and PE Composites. *J. Polym. Environ.* **2022**, *30*, 4848–4862, doi:10.1007/s10924-022-02542-x.
49. Szczepanik, E.; Szatkowski, P.; Molik, E.; Pielichowska, K. The Effect of Natural Plant and Animal Fibres on PLA Composites Degradation Process. *Appl. Sci.* **2024**, *Vol. 14*, Page 5600 **2024**, *14*, 5600, doi:10.3390/APP14135600.
50. Awad, S.; Siakeng, R.; Khalaf, E.M.; Mahmoud, M.H.; Fouad, H.; Jawaaid, M.; Sain, M. Evaluation of Characterisation Efficiency of Natural Fibre-Reinforced Polylactic Acid Biocomposites for 3D Printing Applications. *Sustain. Mater. Technol.* **2023**, *36*, e00620, doi:10.1016/J.SUSMAT.2023.E00620.
51. Cheng, S.; Lau, K. tak; Liu, T.; Zhao, Y.; Lam, P.M.; Yin, Y. Mechanical and Thermal Properties of Chicken Feather Fibre/PLA Green Composites. *Compos. Part B Eng.* **2009**, *40*, 650–654, doi:10.1016/J.COMPOSITESB.2009.04.011.
52. Nurazzi, N.M.; Abdullah, N.; Norrrahim, M.N.F.; Kamarudin, S.H.; Ahmad, S.; Shazleen, S.S.; Rayung, M.; Asyraf, M.R.M.; Ilyas, R.A.; Kuzmin, M. Thermogravimetric Analysis (TGA) and Differential Scanning Calorimetry (DSC) of PLA/Cellulose Composites. In *Polylactic Acid-Based Nanocellulose and Cellulose Composites*; CRC Press, 2022; pp. 145–164 ISBN 9781003160458.
53. Fiore, V.; Botta, L.; Scaffaro, R.; Valenza, A.; Pirrotta, A. PLA Based Biocomposites Reinforced with Arundo Donax Fillers. *Compos. Sci. Technol.* **2014**, *105*, 110–117, doi:10.1016/j.compscitech.2014.10.005.
54. Fendler, A.; Villanueva, M.P.; Gimenez, E.; Lagarón, J.M. Characterization of the Barrier Properties of Composites of HDPE and Purified Cellulose Fibres. *Cellulose* **2007**, *14*, 427–438, doi:10.1007/s10570-007-9136-x.
55. Qiu, W.; Endo, T.; Hirotsu, T. Interfacial Interactions of a Novel Mechanochemical Composite of Cellulose with Maleated Polypropylene. *J. Appl. Polym. Sci.* **2004**, *94*, 1326–1335, doi:10.1002/app.21123.
56. Moreno, G.; Ramirez, K.; Esquivel, M.; Jimenez, G. Biocomposite Films of Polylactic Acid Reinforced with Microcrystalline Cellulose from Pineapple Leaf Fibres. *J. Renew. Mater.* **2019**, *7*, 9–20, doi:10.32604/jrm.2019.00017.
57. Aliotta, L.; Gigante, V.; Coltelli, M.-B.; Cinelli, P.; Lazzeri, A.; Seggiani, M. Thermo-Mechanical Properties of PLA/Short Flax Fibre Biocomposites. *Appl. Sci.* **2019**, *9*, 3797, doi:10.3390/app9183797.

58. Wang, X.; Li, S.-C.; Xiang, D.-W.; Gao, M.; Zuo, H.-M.; Li, D.-S. Flexural Properties and Failure Mechanisms of Short-Carbon-Fibre-Reinforced Polylactic Acid Composite Modified with MXene and GO. *Materials (Basel)*. **2024**, *17*, 1389, doi:10.3390/ma17061389.
59. de Bomfim, A.S.C.; de Oliveira, D.M.; Benini, K.C.C. de C.; Cioffi, M.O.H.; Voorwald, H.J.C.; Rodrigue, D. Effect of Spent Coffee Grounds on the Crystallinity and Viscoelastic Behavior of Polylactic Acid Composites. *Polym. 2023, Vol. 15, Page 2719* **2023**, *15*, 2719, doi:10.3390/POLYM15122719.

6. PUBLISHED WORKS

- A review on the use of giant reed (*Arundo donax* L.) in the biorefineries context. Reviews in Chemical Engineering, 40(3), 2024. DOI: [10.1515/revce-2022-0069](https://doi.org/10.1515/revce-2022-0069)
- Use of giant reed (*Arundo donax* L.) for polymer composites obtaining: a mapping review. Cellulose, 30, 2023. DOI: [10.1007/s10570-023-05176-x](https://doi.org/10.1007/s10570-023-05176-x)
- Giant Reed (*Arundo donax* L.) Fibre Extraction and Characterization for Its Use in Polymer Composites. Journal of Natural Fibres, 20:1, 2023. DOI: [10.1080/15440478.2022.2131687](https://doi.org/10.1080/15440478.2022.2131687)
- A New Image Analysis Assisted Semi-Automatic Geometrical Measurement of Fibres in Thermoplastic Composites: A Case Study on Giant Reed Fibres. Journal of Composites Science, 7(8), 2023. DOI: [10.3390/jcs7080326](https://doi.org/10.3390/jcs7080326)
- Influence of Giant Reed (*Arundo Donax* L.) Culms Processing Procedure on Physicochemical, Rheological, and Thermomechanical Properties of Polyethylene Composites. Journal of Natural Fibres, 21(1), 2024. DOI: [10.1080/15440478.2023.2296909](https://doi.org/10.1080/15440478.2023.2296909)
- Relationship Between the Shape of Giant Reed-Based Fillers and Thermal Properties of Polyethylene Composites: Structural Related Thermal Expansion and Diffusivity Studies. Waste and Biomass Valorization, 15(12), 2024. DOI: [10.1007/s12649-024-02626-w](https://doi.org/10.1007/s12649-024-02626-w)
- Recyclability Assessment of Lignocellulosic Fibre Composites: Reprocessing of Giant Reed/HDPE Composites by Compression Molding. Lecture Notes in Mechanical Engineering IV, 3, 2024. DOI: [10.1007/978-3-031-56474-1_15](https://doi.org/10.1007/978-3-031-56474-1_15)
- Recycling of HDPE-giant reed composites: Processability and performance. Green Processing and Synthesis, 14(1), 2025. DOI: [10.1515/gps-2024-0229](https://doi.org/10.1515/gps-2024-0229)
- Influence of Giant Reed Fibres on Mechanical, Thermal, and Disintegration Behavior of Rotomolded PLA and PE Composites. Journal of Polymers and the Environment, 30(11), 2022. DOI: [10.1007/s10924-022-02542-x](https://doi.org/10.1007/s10924-022-02542-x)
- Giant reed (*Arundo donax* L.) enhanced polylactic acid composites: processing, characterization, and performance of injection moulded and water degraded samples. Submitted to Compos. Part A: Appl. Sci. Manuf., July 2025: [pending review](#)

P1

P2

P3

P4

P5

P6

P7

P8

P9

P10

6.1. A REVIEW ON THE USE OF GIANT REED (*ARUNDO DONAX* L.) IN THE BIOREFINERIES CONTEXT

P1

P2

P3

P4

P5

P6

P7

P8

P9

P10

Review

Zaida Ortega*, Ife Bolaji, Luis Suárez and Eoin Cunningham

A review of the use of giant reed (*Arundo donax* L.) in the biorefineries context

<https://doi.org/10.1515/revce-2022-0069>

Received November 16, 2022; accepted April 3, 2023;

published online May 10, 2023

Abstract: The massive availability of biomass generated by the common giant reed (*Arundo donax* L.) motivates the search for its possible industrial use for the generation of high added-value products through implementing a biorefinery approach. The literature demonstrates the potential of common cane to obtain different high-value compounds, such as levulinic acid, oligosaccharides, fermentable sugars, highly digestible fiber for animal feed, polyphenols, and natural fibers for composite materials, among others. The data shows the upward trend in Europe toward the generation of new green industries, grouped under the biorefinery concept. Therefore, this review summarizes the current knowledge on the use of *Arundo* to produce materials, fibers, and chemicals. Major environmental concerns related to this plant are also reviewed. Special attention has been paid to the potential use of *Arundo* to produce chemicals using green chemistry approaches, as a way to contribute to and advance the achievement of Sustainable Development Goals. Recommendations for future research are also outlined.

Keywords: *Arundo donax*; biomass; biorefinery; giant reed; green chemistry.

1 Introduction

Biorefineries are facilities aimed at transforming biomass into biobased products (Ministerio de Economía Industria y

Competitividad 2017). A biorefinery integrates different processes, which can be chemical, physical, thermal, or biological, and allows the production of various high-value products. The variety of products is extensive, depending on the raw material used and the processes employed. These can range from energy products (biofuels such as biodiesel, bioethanol, or biogas) to fertilizers, animal feed, or bioplastics.

Certain plant species, such as *Arundo donax* L., also known as common cane, giant reed, or reed, have an impressive growth rate, are abundant around the globe during all year, and can be cultivated on marginal lands using low-quality waters (Licursi et al. 2018; Scordia and Cosentino 2019). These characteristics make these plants of high interest in the biorefineries sector, especially for producing ethanol and bioenergy products (Accardi et al. 2015; Jensen et al. 2018).

Reed has also gained attention in the production of some biomolecules, such as furfural or levulinic acid, among others (Antonetti et al. 2015; Di Fidio et al. 2020; Raspolli Galletti et al. 2013). Other uses of *Arundo* have been investigated, such as paper and pulp (Raposo Oliveira Garcez et al. 2022; Shatalov and Pereira 2006), biochar production (Ahmed 2016), or oil spill recovery (Fiore et al. 2019; Piperopoulos et al. 2021). Some other uses proposed for *Arundo* are found in the restoration of traditional architecture (Malheiro et al. 2021), also serving as insulation material (Barreca et al. 2019). Its cultivation is also a strategy for soil bioremediation (Alshaal et al. 2015; Fernando et al. 2016), with biomass's ulterior valorization for methane or biochar production.

The use of ground material or fibers from *Arundo* as filler or reinforcement in different matrices has also been studied in the literature, as these have similar properties to other widely studied vegetal fibers (Fiore et al. 2014b; Suárez et al. 2023). Most studies focus on particleboard production, using natural-derived binders or no binders (Andreu-Rodríguez et al. 2013; Barreca et al. 2019; Ferrández-García et al. 2012, 2019, 2020; Ferrández Villena et al. 2020; García-Ortuño et al. 2011). Other polymer composites studied consist of urea-formaldehyde, epoxy, or polyester (Dahmardeh

*Corresponding author: Zaida Ortega, Departamento de Ingeniería de Procesos, Universidad de Las Palmas de Gran Canaria, Campus Universitario de Tafira Baja, 35017, Las Palmas de Gran Canaria, Spain, E-mail: zaida.ortega@ulpgc.es. <https://orcid.org/0000-0002-7112-1067>

Ife Bolaji and Eoin Cunningham, School of Mechanical and Aerospace Engineering, Queen's University Belfast, Stranmillis Road, BT9 5AH Belfast, UK. <https://orcid.org/0000-0003-4322-6002> (I. Bolaji). <https://orcid.org/0000-0003-2555-7705> (E. Cunningham)

Luis Suárez, Departamento de Ingeniería Mecánica, Universidad de Las Palmas de Gran Canaria, Campus Universitario de Tafira Baja, 35017, Las Palmas de Gran Canaria, Spain. <https://orcid.org/0000-0002-6709-1555>

Ghalehno et al. 2011), as well as polyethylene, polypropylene (Ortega et al. 2021; Suárez et al. 2021, 2022) or polylactic acid (Fiore et al. 2014a). Other authors also have proposed the production of composites for building applications, using concrete and plaster (Badagliacco et al. 2020; Manniello et al. 2022a,b; Martínez Gabarrón et al. 2014) or asphalt (Sargin Karahancer et al. 2016) as matrixes.

This paper aims to comprehensively review *Arundo*'s potential for its exploitation as biomass feedstock in a biorefinery context, including the potential benefits of its cultivation on the conservation and restoration of harmed riparian ecosystems. Special attention is paid to cascade processes to maximize the use of this lignocellulosic material.

Sustainable Development Goals (SDGs) are a set of 17 objectives, settled by the United Nations and adopted by most countries, to commit to the advancement of sustainable development, the reduction of inequalities, and the construction and consolidation of peaceful and fair societies. Some of these objectives relate to the sustainable production and consumption of goods, access to quality education, or the protection of earth and water ecosystems. There is a clear relationship between the bioeconomy, developed through the biorefineries, and SDGs, especially when it comes to the use (or reuse) of wastes or side-products from other processes. It is a clear way to make more efficient use of resources, reduce the amount of waste going to landfill, and produce valuable compounds under the principles of Green Chemistry (Leong et al. 2021; Solarte-Toro and Cardona Alzate 2021).

2 Methods

The literature review has assessed several papers related to *Arundo* and sustainable development. Although this paper focuses on evaluating the potential of this species for a biorefinery approach, different terms were used in the bibliographic search to have an idea of the potential applications of these plants in several contexts. The bibliographic search was performed in several databases (Scopus, Science Direct, Taylor & Francis, and Google Scholar), using the combination of the following keywords, plus the term "*Arundo*": *biorefinery*, *fiber*, *composite*, *ethanol*, *energy*, *invasive*, *environment*, *LCA* (*life cycle assessment*), *sustainable*, *renewable*, *value chain*, *green chemistry*, *fermentation*, *hydrolysis*, *valorization*, *polymer*, *profit*, *feed*, *soil*, *preservation*, *remediation*.

A remarkable number of papers have been published in the last decade (Figure 1); there has been an evident rise until 2019, with a decrease in the current year in the total number of published papers. Regarding the different topics, composites and invasive species are the least frequent. The trend in publications during this decade for the keywords used in the search is relatively stable.

From Scopus, the search performed using only "*Arundo*" led to 1475 publications, while 442 documents were downloaded using the list of keywords above. All papers were organized and compiled in the Mendeley software, classifying them by relevance for this paper and specific topic. To the authors' knowledge, only one review on *A. donax* L. and its potential in biorefinery has been found in the literature, dating back to 2014 (Corno et al. 2014).

From these 442 documents, considering the last 10 years and removing conference papers or sources not included in JCR, the list of documents decreased to 217. The next step was to analyze the authors' keywords from the retrieved articles, finding around 50 keywords repeated more than 5 times in the different works. These were reduced to 18 categories by grouping them by similarity; i.e., "toxic metals" includes "heavy metals" or "cadmium," "saccharification" includes "sugars," "oligosaccharides," "glucose," or "farming" also contains "crop" and "harvest"; the levels of appearance of these concepts are shown in Figure 2: (note that "*Arundo*," "*A. donax*," "reed," "giant reed," and "lignocellulosic biomass" were excluded from the list, as they appear in most documents).

Biorefinery, bioenergy, and chemical synthesis account for over a third of the total author keywords. In contrast, the remaining keywords appeared less frequently, with a slight prevalence of "composites" and "thermal processing". These five keywords appear in half of the studied papers, so this review focuses on these terms. The first section of this document focuses on plant characteristics, abundance, cultivation, invasive character, and environmental applications, such as soil remediation. The paper then reviews *Arundo*'s use for obtaining chemicals in a biorefinery context, including thermal and biobased processes for producing chemicals (sugars, levulinic, succinic acid, etc.), bioenergy, and biobased composites, thus covering most of the categories mentioned above.

The online tool Inciteful XYZ (Literature connector) has been used to refine the search and reduce the number of papers from the over 400 retrieved. This open-source tool produces graphs with connections among different papers related to a specific field. A chart showing the relationships between various studies on the use of *Arundo* in biorefineries is obtained (Figure 3). The tool also provides the most important papers in the field, refining the search by the number of citations and closeness to the papers used as seeds, which in this case were the ones listed in Figure 3a. The interconnections in Figure 3b were obtained by refining the search to show papers on *Arundo*. With all this, 50 papers were selected as the most relevant to the topic. The list of references contains more bibliography apart from these 50 studies, as Inciteful has only been applied to the use of *Arundo* and not its cultivation or environmental behavior.

3 Giant reed (*A. donax* L.)

A. donax L. is a perennial grass from the *Gramineae* family, with an uncertain origin due to its small size and the high number of chromosomes, although many authors place its origin in East Asia (Jensen et al. 2018). Giant reed produces flowers, although its seeds are not usually viable, at least out of Asia (Jiménez-Ruiz et al. 2021); this plant reproduces through the rhizome or by producing roots on the nodes

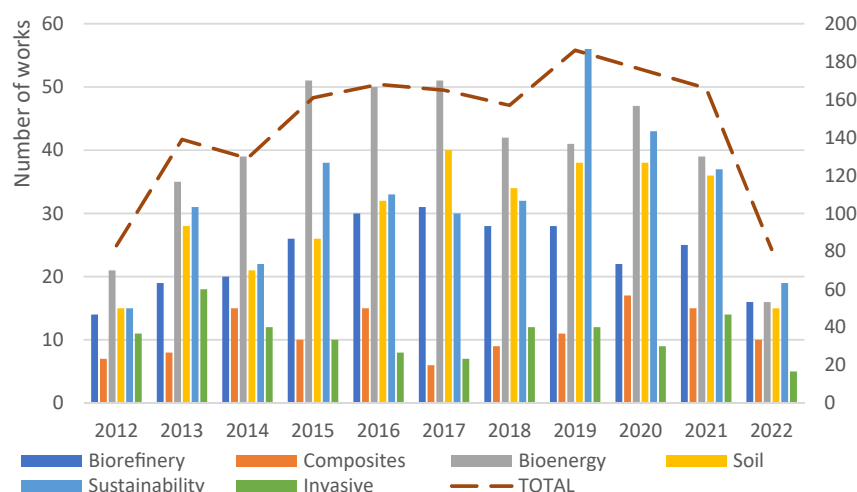


Figure 1: Evolution of publications in Scopus related to different keywords and *Arundo* in the last decade.

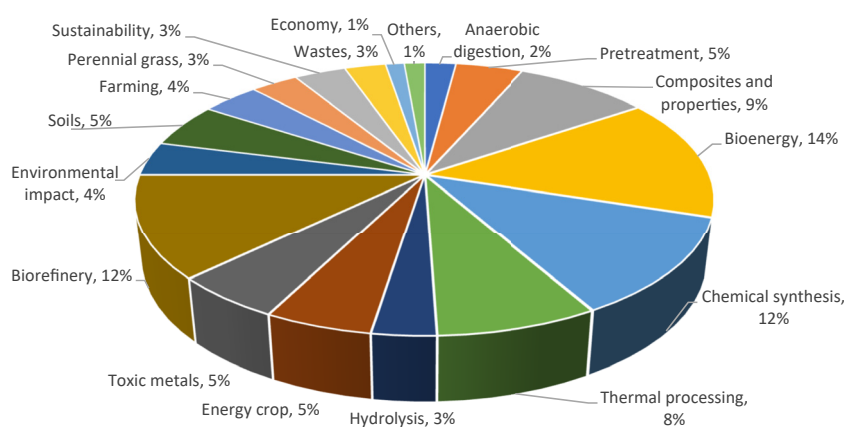


Figure 2: Frequencies of appearance of authors' keywords.

(Corno et al. 2014), which explains its rapid spread and poor genetic diversity (Pilu et al. 2014; Sicilia et al. 2020). When intended to be used as an energy crop, the clonal selection is needed to increase the characteristics of the plant, namely the number of culms and culm diameter and height (Amaducci and Perego 2015; Danelli et al. 2019, 2020; Fabbrini et al. 2019). Figure 4 shows two specimens of *Arundo* and the main parts of the plant: leaves, culm or stem, and rhizome.

Stems or culms are hollow and have diameters around 2–3 cm, reaching up to 6 m in height, with stem-clasping leaves along the entire stem (Csurhes 2016). Giant reed is generally recognized as an interesting source of biomass due to its high productivity and low requirements (Jensen et al. 2018), as it can be grown on almost any type of soil and with a minimal amount of water (Ahmed 2016), with high thermal and pathogens resistance (Accardi et al. 2015; Amaducci and Perego 2015; Lewandowski et al. 2003).

The rapid growth of this species and its quick adaption to a wide range of environmental conditions, even drought or high salinity (Romero-Munar et al. 2018a,b; Sánchez et al. 2015), which point them as a promising source of

lignocellulosic feedstock, have contributed to its great spread and naturalization, especially in Mediterranean countries, where it has also become invasive (Lambertini 2019; Shtein et al. 2021). *Arundo* is considered one of the worst invasive plants in the world (Jiménez-Ruiz et al. 2021), and several actions take place periodically to try to control their spread in many parts of the world. Of particular concern is the distribution of *Arundo* in the Mediterranean or subtropical climate areas, such as Algeria, Morocco, Brazil, France, Portugal, Spain, Italy, and Australia, among others (Ministerio de Agricultura Alimentación y Medioambiente 2013). This is due to the rapid growth of this specie, of up to 10 cm per day (You et al. 2013), its pyrophyte nature, and its contribution to the spread of fires.

However, this species is not included in Europe's list of invasive alien species of Union concern (European Union 2017), but instead has been pointed out as a promising source of lignocellulose materials and has been included as an energy crop in the European Union (EU) (Eurostat 2020). For example, in 2013, Italy accounted for around 4000 ha of *Arundo* cultivation lands (Mantziaris et al. 2017), being the

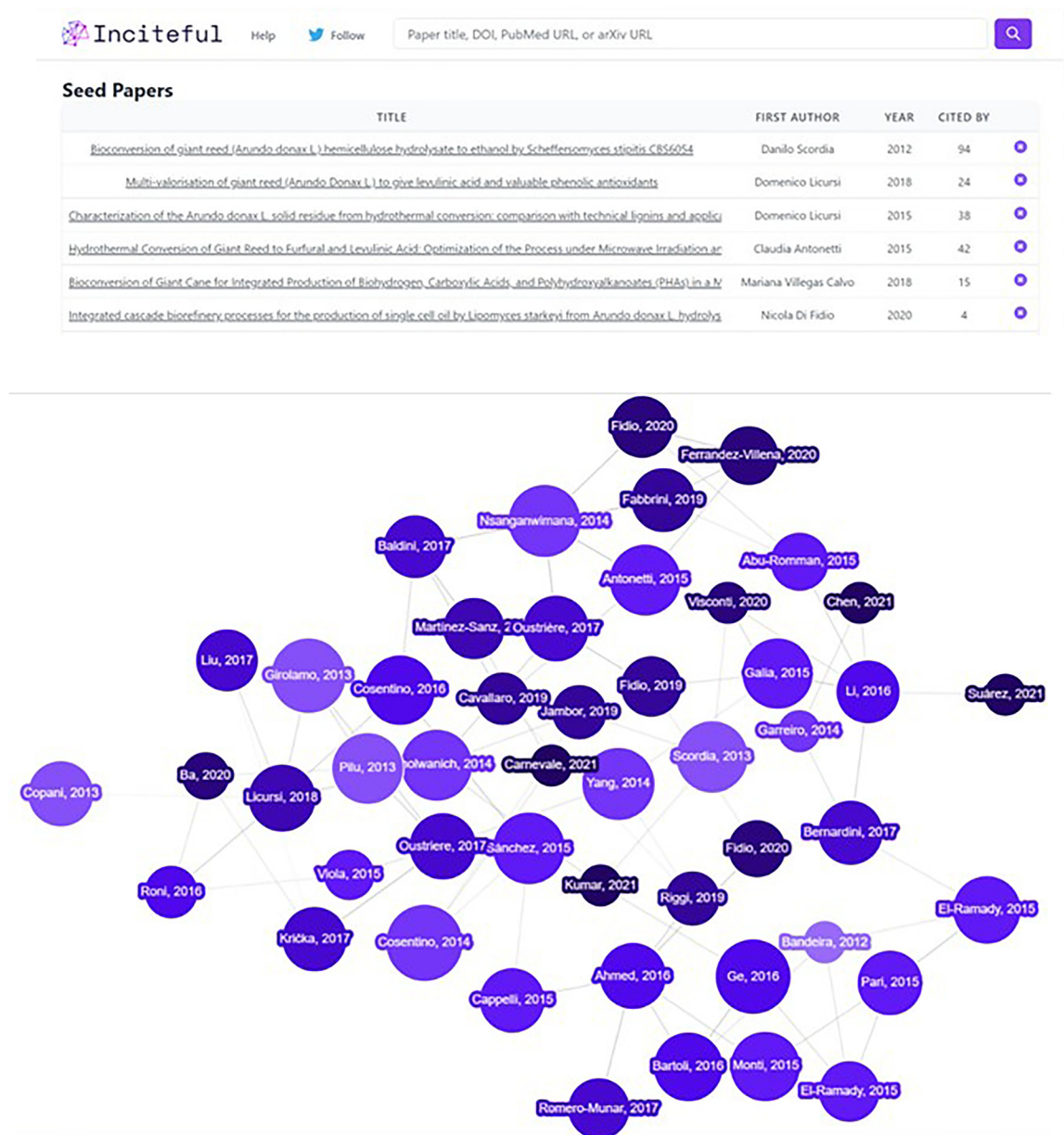


Figure 3: (a) Seed papers used in Inciteful XYZ and (b) graph showing the connections between the most important papers in the literature search.

most extensive area in Europe (no further data are published to date). Another example is found in Spain, where *Arundo* was considered an invasive plant in the 2013 catalogue (Ministerio de Agricultura Alimentación y Medioambiente 2013; Jiménez-Ruiz et al. 2021), being removed in a later revision of the document in 2019 (Ministerio para la Transición Ecológica 2019), after being included in a governmental document about biorefineries in Spain and interest crops (Ministerio de Economía Industria y Competitividad 2017), launched in 2017.

This change allows for the industrial use of *Arundo* in Spain, aligned with most countries worldwide. It then

seems there is still a controversy between those authors considering *Arundo* as a resource to exploit and those concerned by the invasive character of the plant. In any case, most studies agree in stating that the invasive character of this plant should not be neglected, even if it is considered naturalized. It should not be forgotten that an uncontrolled spread can lead to biodiversity loss and increase fire events' periodicity and susceptibility (Jiménez-Ruiz et al. 2021). Issues associated with the end of the crop cycle should also be considered, as plants and rhizomes need to be removed (Corno et al. 2014). Corno et al. (2014) and Jiménez-Ruiz et al. (2021) suggest using



Figure 4: Different parts of *Arundo donax* L. plants.

glyphosate solution to damage new canes and inhibit the germination of new plants; this is apparently the most cost-effective solution for *Arundo* control.

Figure 5 summarizes the main environmental drawbacks and potential benefits of *Arundo* as raw material for industrial purposes, as discussed in Sections 3.1 and 3.2.

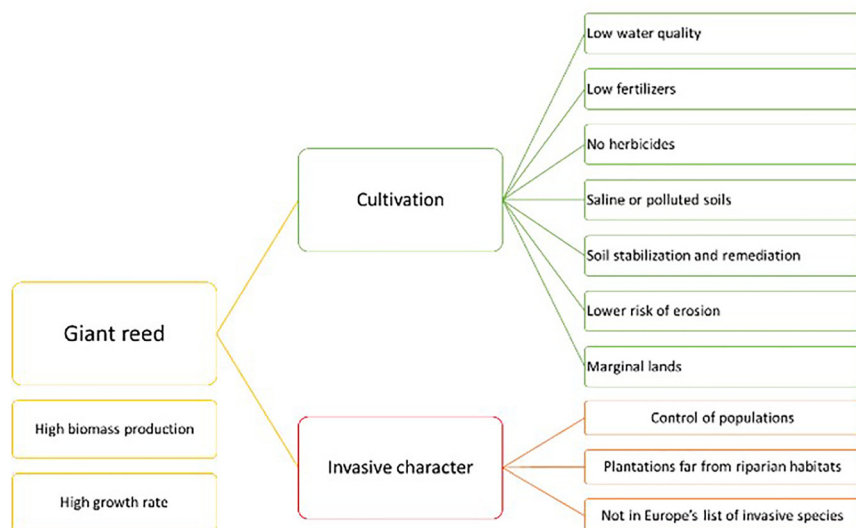


Figure 5: Potential environmental benefits and drawbacks of *Arundo donax* L. use in an industrial context.

3.1 Cultivation

The cultivation of *Arundo* has been proven attractive as a lignocellulosic feedstock material (Amaducci and Perego 2015; Bonfante et al. 2017; D'Imporzano et al. 2018; Lewandowski et al. 2003). It is considered a promising crop for the biorefineries sector, with good environmental behavior (due to the low need for water and fertilizer) and resistance to salinity and polluted soils. It is generally recognized that this crop is highly water-demanding, although some authors point out that low-quality water can be used (Amaducci and Perego 2015). Other authors also state that other energy crops, such as *Miscanthus giganteus* or *Cynara cardunculus* provide lower yields in dry mass with higher water requirements, which also gives a positive point to *Arundo* (Fazio and Barbanti 2014; Ge et al. 2016; Monti et al. 2009; Singh et al. 2018). In this sense, Angelini et al. (2009) compared *Arundo* and *Miscanthus* over a 10-year period and found a higher yield in dry biomass for *Arundo* as well as a higher calorific value and energy yields. On the other hand, the work by Krička et al. (2017) reveals that, due to its higher lignin and ash content, *Arundo* has better performance than *Miscanthus* as solid fuel, while *Miscanthus* can also be used for obtaining liquid fuel. Other studies have also shown that *Arundo* is less affected by harvesting time or weather conditions compared to *Miscanthus* or switchgrass, which is a further advantage for reed cultivation (Alexopoulou et al. 2015; Monti et al. 2015; Nassi o Di Nasso et al. 2011).

Despite its invasive potential, several papers dealing with its cultivation and crop optimization can be found in the literature (Cosentino et al. 2006; Dragoni et al. 2015a). Some studies have assessed the storage of *Arundo* to avoid energy losses or material degradation prior to its use

(Pari et al. 2015, 2021). Besides, some authors consider its cultivation of interest in the Mediterranean basin and other arid regions with possible soil losses due to its growth potential in unfavorable conditions (Forte et al. 2015).

Regarding cultivation, the crucial step is the first year, the planting (Corno et al. 2014; Romero-Munar et al. 2018a,b). Corno et al. (2014) indicate that 5000 to 10,000 plants/ha, or 10,000–20,000 in warm climates, are required to obtain good production in years 1–2, and the overall duration of the plantation is around 15 years. Once the plants are settled, they usually don't require watering, fertilization, or herbicide treatment, as *Arundo* suppresses weeds (Curt et al. 2017; Gazoulis et al. 2021). However, using fertilizers generally results in higher biomass yields; especially when using nitrogen, better development of rhizomes and new sprouts are obtained, thus increasing the yields. Biomass yields are highly variable and dependent on climate, year of cultivation, and crop management and vary from 1.3 to 45.2 t/ha (Corno et al. 2014), with a more common yield of 30 t/ha (Corno et al. 2014; Dragoni et al. 2015b; Siri-Prieto et al. 2021). Some studies have also indicated that lower plantation densities could lead to higher biomass yields due to lower resource competition (Corno et al. 2014; Lewandowski et al. 2003). The studies performed by Christou in the framework of the EuroBioRef project (from the 7th EU framework) arrived at similar conclusions, that is, similar dry mass yields for *Arundo* cultivation versus *Miscanthus* (15–35 t/ha vs. 10–30, respectively), with similar needs of nitrogen fertilization, although reed cultivation was limited to the Mediterranean area (Christou 2011). The potential economic benefits for these cultivations were also assessed in such project, concluding that *Miscanthus* cultivation could produce around 250 €/ha, while *Arundo* could reach up to 400 €/ha, considering a plantation for 20-year period in both cases.

Although most studies on the crop optimization are performed in the Mediterranean basin, the Giant Reed Network project (FAIR-CT-96-2028) performed in the European Union (Bacher et al. 2001) studied the cultivation of giant reed in Germany, finding that it is possible to produce giant reed in cold climatic conditions, although at lower yields, with a maximum of 25 t/ha, which was, in any case, a similar yield to *Miscanthus* grown in similar conditions.

The excessive pressure on soils and the lack of regulation on their recovery and preservation have brought about huge areas of degraded or polluted soils, where cultivation of food or plant species sensitive to metals or high salinity levels is not possible. The lack of vegetation contributes to further erosion and soil loss, with negative consequences for the environment. In Europe, over 400,000 km² are in high

risk of desertification and soil loss, especially in the Mediterranean basin (Ferreira et al. 2022). The cultivation of plant species, such as *Arundo*, might help reduce the effects of the unsustainable management practices performed decades ago. The soils restoring would reduce the negative impacts associated with such degradation, which lead to the loss of ecosystems service and affects biodiversity. Besides, the cultivation of such species, with high biomass rate production, would provide a second benefit: the stable availability of biomass useful as raw material for green chemical industries, which is one of the main factors affecting the biorefinery growth, without any displacement in food production.

3.2 Potential environmental benefits of *Arundo* cultivation

The invasive potential of this species and the controversy about its cultivation and use have already been mentioned. However, there are also some studies on the potential environmental benefits of giant reed cultivation, which goes beyond its use to produce bio-chemicals or bio-energy products. Several studies have shown the potential of energy crops for the remediation of polluted soils. For example, Bernal et al. (2021) reported soil phytostabilization as a result of cultivating *Arundo* and other perennial grass on soils with mining trace elements (Cd, Cu, Zn, As, etc.). Similarly, Garau et al. (2021) achieved soil stabilization and increased metals uptake with municipal solid waste compost. Zeng et al. (2022) also achieved high levels of Cu removal (over 75 %) in *Arundo* plantations, with higher efficiencies when alternated with other species cultivated together. Furthermore, Cristaldi et al. (2020) found a high bioaccumulation ratio of several metals in the giant reed, especially for As, Hg, and Cd, apart from Cu.

Besides soil remediation, reed can also be used to treat industrial wastes, such as red mud from alumina production (Zhang et al. 2021). According to Buss and collaborators, the biomass obtained from plants growing in polluted soils cannot be used as raw material for any application. They found that biochar produced in heavily polluted soils led to high concentrations of such metals, which exceed the permitted values (Buss et al. 2016). However, a good yield in methane production could still be obtained from such biomass (Bernal et al. 2021). Giant reed can also be used to set up wetlands for wastewater purification in isolated regions with good performance (Liu et al. 2019, 2021a; Otter et al. 2020). Other authors highlight the benefits of this plant for the soil, as organic carbon content in the soil is increased while total nitrogen is kept stable (Fagnano et al. 2015; Siri-

Prieto et al. 2021). These authors also emphasize the potential of *Arundo* to reduce soil erosion; Hong and Lee (2016) reached a similar conclusion regarding soil erosion in coastal environments.

Several authors have studied the sustainability of growing cane as a resource for the implementation of biorefineries, concluding that the fertilization stages are essential to the life cycle and the impact generated by this crop (Bosco et al. 2016; Fagnano et al. 2015; Forte et al. 2015). Some authors point out that the use of wild plants supports a better state of conservation of natural spaces due to the control of its excessive growth; this, together with the non-fertilization or irrigation of the plants, also results in better environmental performance. Most of the studies on the environmental performance of *Arundo* crops found in the literature do not provide clear results. For example, Forte et al. (2015) concluded that the ecological load related to nitrogen fertilization and the harvesting operations provide the highest environmental impacts. Despite pointing out that further studies are required, the study seems to arrive at a positive environmental behavior of such crops, as also found by Zucaro et al. (2018), stating that giant reed crops can act as greenhouse gases sink.

Monti et al. (2009) performed a life cycle assessment (LCA) to compare the environmental and yield performance of reed cultivation versus rotation of maize-wheat, finding reductions over 50 % in environmental impact for reed, as also concluded by Dragoni et al. (2015b). However, Schmidt et al. (2015) indicate that giant reed cultivation should only occur in marginal lands, avoiding watering and fertilization and adapting the processing chain to the plant properties. Abreu et al. (2022) make the same recommendation and signal the potential benefits of *Arundo* and other perennial grasses cultivations on marginal lands, especially for biofuel production. These authors highlight the low research performed to date in transforming reed biomass into biofuels, anticipating a high rise in the interest of this plant for this purpose.

Furthermore, Solinas et al. (2019) have calculated that reed cultivation provides a 20 % reduction of the environmental impact caused by sorghum, as water and nitrogen inputs are the factors with the highest weights, and these could have been optimized. In this sense, sludge from wastewaters can be used as fertilizer, achieving similar yields to N-fertilized crops (Cano-Ruiz et al. 2021). Other authors proposed the irrigation of these crops with wastewaters; for example, Costa et al. (2016) have determined no changes in the dry mass production when using piggery wastewaters, while Shilpi et al. have obtained higher yields in dry biomass and methane production when the crop is irrigated with municipal or abattoir wastewaters (Shilpi

et al. 2019). Besides, *Arundo* crops have been proposed to treat wastewaters (Zhang et al. 2021), reducing the risk of nitrate pollution, thus increasing the options to use cattle slurry as fertilizer (Ceotto et al. 2018).

Other authors propose using indigenous plants as an alternative to these invasive species. For example, *Arundo micrantha*, native to the Mediterranean region, has been compared in terms of yield to *A. donax*, leading to the obtaining of dry matter in high proportions, while also being able to grow on marginal lands with wastewater use (Tomàs et al. 2020).

All studies on LCA of giant reed crops agree on the lack of a tool measuring environmental impacts capable of considering the case and site-specific analysis and the difficulty in considering watering needs in that tool, and that further efforts are needed to get a more realistic and defined picture. In any case, *Arundo* has been considered to meet the sustainability criteria to produce biomass suitable for biofuels or other compounds production (Cappelli et al. 2015; Gazoulis et al. 2021). Furthermore, some studies highlight the potential of *Arundo* as an industrial crop in polluted soils as a strategy to increase the sustainability of the industry by increasing the amount of soil cultivated without any displacement in food production (Nsanganwimana et al. 2014).

Even if there is no absolute consensus on the use of *Arundo* as feedstock and its environmental benefits, most authors agree on the benefits of using this species, based on its rapid growth, good yields on dry matter, and low-quality water use, although measures should be taken to avoid its dispersion in the natural environment, especially in riparian habitats.

The availability of marginal and degraded soils, especially with high salinity in the Mediterranean area, and the ability of *Arundo* to grow in such conditions make it interesting to conduct long-term studies on the production of biomass and evolution of soils quality using no fertilizers and low-quality waters, as this is also a scarce resource in this area. The studies performed to date do not take place over a long period, enough to assess the associated changes that occur in the ground (organic matter, nitrogen content, permeability, etc.). Even if the production of biomass is not maximized by optimized cultivation conditions (watering and fertilization), the potential benefits on soil remediation and preservation with low inputs, together with the production of bioproducts of high-added value through a biorefinery scheme, would favorably tip the balance through the exploitation of such degraded soils, both at economic and environmental levels.

The LCA tools and the biorefineries are relatively recent, and there are not still appropriate methods to consider the

huge number of factors involved in determining the environmental impact of such industries, especially when the raw material is not obtained from conventional agricultural processes. Even if the need of inorganic fertilizers, which pose adverse impacts, was demonstrated as necessary, the influence on the potential soil recovery would need to also be introduced in the analysis. Soils are still rather unknown and there is a lack of accurate systematic and comparable data about their environmental, societal, and economic implications, especially when they are degraded (Ferreira et al. 2022). Hence, there is still massive work to undertake before such data can be accurately introduced into environmental assessments to determine the potential effects of *Arundo* (or any other species) cultivation for biorefinery use.

4 Use of giant reed as raw material in biorefineries

Giant reed has been investigated for producing different bio-based products: chemicals, fibers for composite materials, polymers, or bioenergy products. This section is divided into three, discussing the application of *A. donax* L. in chemicals and bioenergy production. The first section gives an overview of the major components of giant reed. The production of chemicals such as bioethanol, levulinic, lactic, or succinic acid is covered in the second section, while the production of biogas and hydrogen as well as direct pyrolysis of the lignocellulosic material is discussed in the third section.

4.1 Composition of giant reed

Table 1 summarizes the composition of different parts of *Arundo* obtained from various references. Ash content is higher in the leaves than in the stems: 12 % versus about 3 %, respectively; the value for the entire plant is around 4 %, closer to the ash content in the culms, as most of the weight of the plant is due to the stem. As observed, the three major constituents of plant species (lignin, hemicellulose, and cellulose) are in similar proportions, with slightly higher values for hemicellulose (up to 42 %).

The chemical composition of this plant would allow a cascade approach for the solubilization and valorization of these three fractions. Other crops or residues widely studied in the biorefineries sector have similar compositional values to giant reed. For example, sugarcane bagasse has about 40 % cellulose, 24 % hemicellulose, and 24 % lignin (Chen et al. 2021; Jeon et al. 2010), wheat straw about 24 %

cellulose and 25 % hemicellulose (Jeon et al. 2010), giant *miscanthus* about 35 % cellulose and 28 % hemicellulose (Baldini et al. 2017; Ge et al. 2011). These are widely studied raw materials for sugars or energy production, which shows the potential of *Arundo* to become raw materials for such products.

The higher lignin content of reed compared to other materials such as maize or *Miscanthus* might imply a higher recalcitrance of the material, and so that pre-treatment is probably needed to allow its further processing. However, as discussed later, these are performed in order to obtain a more selective fractioning of its components. The relatively mild conditions used for *Arundo* hydrolysis are indicative of the low recalcitrance of this biomass, which eases its processing. Such pre-treatments have been explored in literature and allow the release of sugars, mainly xylans, coming from the degradation of hemicellulose, but also the production of phenolic compounds with antioxidant activity, as discussed later in this paper.

On the other hand, the rhizome has the lowest content of structural carbohydrates due to its high concentration of free sugars and starch, around 30 % (Proietti et al. 2017). The variation in lignin has been attributed to the age of the plant, with more mature plants having a higher lignin content (Neto et al. 1997); Klason lignin contents reported for stems vary from 18 to 26 %, with lower values (10–15 %) for leaves. In any case, it is worth noting that the characterization method used can influence the results obtained and may lead to the over-quantification of some components. The use of wild or cultivated biomass, the climate, or the soil conditions, do not seem to provide any significant trend regarding the composition. As observed in Table 1, the plant composition data reported by the different papers are not always fully comparable, although the values provided might indicate that the vegetal material is quite stable, in terms of composition, which poses an indubitable advantage for its exploitation, as the processes followed wouldn't need to be adapted for different origins or growth conditions on the plant, or season of harvesting.

4.2 Giant reed for chemical synthesis

Levulinic acid, succinic acid, furfural, or xylitol are essential precursors in chemical synthesis and are considered some of the most important renewable molecules today, among others. These molecules, known as building blocks, are widely used in various industries to produce bioplastics, biofuels, phytosanitary products, or fertilizers (Antonetti et al. 2016). These are some of the main compounds obtained in biorefineries, and hence, the focus of this review.

Table 1: Composition (in % of dry mass) of different fractions of *Arundo donax* L.

Material	Origin	Lignin (%)			Holocellulose (%)		Extractives			Ashes (%)	References
		Klason (%)	Acid soluble (%)	Total (%)	Cellulose (%)	Hemicellulose (%)	Water	Ethanol	Total		
Stems	Spain; wild	21.1 ± 0.9	–	–	38.0 ± 4.6	34.0 ± 1.5	–	–	–	–	(Suárez et al. 2021)
	China; crop	18.4	1.24	19.7	42.2	30.5	–	–	–	3.0	(You et al. 2013)
	Portugal; wild	24.3	1.8	–	–	–	–	4.4	–	3.4	(Pinto et al. 2015)
	China; crop	20.2 ± 0.8	1.3 ± 0.0	21.5 ± 0.8	35.6 ± 1.6	24.0 ± 1.4	–	–	–	–	(You et al. 2018)
Leaves	Spain; wild	15.5 ± 2.0	–	–	27.7 ± 3.5	34.1 ± 3.3	–	–	–	–	(Suárez et al. 2021)
	China; crop	10.1	2.3	12.5	24.4	20.4	–	–	–	12.9	(You et al. 2013)
Plant	Spain; wild	24.9 ± 0.3	8.2 ± 1.0	32.4 ± 2.7	38.0 ± 3.7	42.4 ± 1.3	1.2 ± 0.3	1.8 ± 1.8	3.0 ± 2.2	4.9 ± 1.1	(Suárez et al. 2022)
	Italy; crop	24.3	1.8	26.1	39.5	25.8	–	–	4.2	4.4	(Licursi et al. 2015)
	Italy; crop	22.0 ± 0.0	0.9 ± 1.0	22.9 ± 1.0	36.3 ± 0.4	23.4 ± 0.4	–	–	15.4 ± 0.8	2.0 ± 0.0	(Di Fidio et al. 2019)
	Italy; crop	–	–	29.9	–	65.4	–	–	–	4.7	(Barana et al. 2016)
Rhizome	Spain; wild	19.1 ± 2.1	–	–	21.0 ± 1.0	29.6 ± 2.9	–	–	–	–	(Suárez et al. 2021)
	Italy; crop	19.1 ± 0.3	1.2 ± 0.0	20.3 ± 0.3	28.0 ± 0.7	13.9 ± 0.2	29.0 ± 1.8	3.6 ± 0.2	32.6 ± 2.0	7.4 ± 0.1	(Proietti et al. 2017)
	Italy; crop	17.8 ± 0.3	1.4 ± 0.3	19.2 ± 0.3	23.5 ± 0.3	11.9 ± 0.3	33.5 ± 1.8	3.2 ± 0.3	36.6 ± 1.7	5.9 ± 0.2	(Proietti et al. 2017)
	Italy; crop	17.1 ± 0.7	1.6 ± 0.0	18.7 ± 0.7	22.4 ± 0.3	11.1 ± 0.4	31.6 ± 0.6	3.0 ± 0.2	34.6 ± 0.4	5.0 ± 0.2	(Proietti et al. 2017)

Different parts of the plant have been used as raw material in hydrolysis reactions to break down the lignocellulosic material into fractions of interest. Table 2 summarizes the main pre-treatments applied to *Arundo* to increase digestibility and to obtain valuable products directly from this first step.

4.2.1 Pre-treatments: hemicellulose solubilization

As summarized in Table 1, hemicellulose accounts for 20–40 % of the aerial part of the reed. So, most studies focus on the solubilization of this fraction to produce xylose, xylo-oligomers, furfural, and levulinic acid. Besides, hemicellulose is the most accessible compound to break. In addition, the digestibility and accessibility of cellulose for enzymatic digestion are increased during pre-treatment and consequently higher product yields.

In this sense, Shatalov and Pereira (2012) recovered 94 % of the xylose present in *Arundo* through acid hydrolysis,

using a low concentration of sulfuric acid (1.27 %) and temperatures of 140 °C; the liquor obtained had a low content of glucose and degradation products, and the digestibility of the material increased from 9 to 70 % due to the treatment. This conversion means that 22 g of xylose/100 g of dry biomass was obtained and transformed to 0.54 g of xylitol/g of xylose (Shatalov et al. 2013). Other studies agree that the acid hydrolysis of common cane, under mild conditions, allows selective hydrolysis of hemicellulose, so liquors with more than 90 % xylose content are obtained (Torrado et al. 2014).

The particle size does not seem to significantly affect the yields obtained nor the selectivity of the hydrolysis reaction, which is an advantage when processing the material (Torrado et al. 2014). Di Fidio et al. (2019) conducted a similar study, using ferric chloride instead of acid and heating by microwaves. They achieved a xylose production yield of 98.2 % in the first stage. These authors proposed a cascade process so that the resulting solid after the first hydrolysis stage was used in a second hydrolysis stage (under similar

Table 2: Most common pre-treatments applied to giant reed.

Material	Pre-treatment	Conditions	Results	Objective	References
Plant	Autohydrolysis	200 °C 20 min SLR: 50 g/l water Semi-continuous system	Complete hemicellulose degradation: 4.6 % xylose + 24 % xylo-oligomers	Sugars	(Galia et al. 2015)
Plant	Autohydrolysis	185 °C Non-isothermal SLR: 1/8	Partial degradation of hemicellulose: 2.4–3.0 % xylo-oligomers, 0.6–0.7 % xylose, 0.9–1.1 % glucose Organosolv process to the solid	Cellulose pulp	(Caparrós et al. 2006; López et al. 2010)
Plant	Autohydrolysis	150 °C; 10 min SLR: 1/5	Increased solid digestibility: CH ₄ yield 10 % higher than for untreated material (300 ml/g VS)	Methane	(di Girolamo et al. 2013)
Plant	Catalyzed hydrolysis	Amberlyst70 20 % 100 g biomass/500 g solution 160 °C, 20 min	Hemicellulose hydrolysis: 18.9 g xylose/100 g biomass + 4.1 g glucose/100 g biomass Solid further enzymatic hydrolyzation: 18.9 g/glucose/100 g biomass + lignin-rich solid	Sugars	(Di Fidio et al. 2020)
Plant	Catalyst hydrolysis	HCl 0.4 M 100 °C, 2 h 5 % Ru/C 70 °C; 2 h	Direct obtaining of valerolactone: 16.3 g/100 g biomass	Chemicals: γ-valerolactone	(Raspolli Galletti et al. 2013)
Plant	Acid hydrolysis	5 % H ₂ SO ₄ SLR: 1/10 121 °C, 20 min	Hemicellulose and cellulose degradation: 80 g/l sugars Hydrolysate fermentations: up to 180 g lipids/l	Lipids (biofuel)	(Pirozzi et al. 2015)
Plant	Acid hydrolysis	Autoclave 150–190 °C 15 min 1.68 % wt HCl 0.35 g biomass/5 g solution	Low temperature: high yield in furfural and moderate in levulinic acid: 8–9 % wt each High temperature: only traces of furfural and up to 22 % levulinic acid	Chemicals: levulinic acid, furfural	(Antonetti et al. 2015)
Plant	Acid hydrolysis	HCl 0.4 M 100 °C, 2 h 9 % biomass	Complete conversion of hemicellulose and cellulose: 23.3 g levulinic acid/100 g biomass Partial depolymerization of lignin	Chemicals: levulinic acid	(Raspolli Galletti et al. 2013)
Stems	Acid hydrolysis	1.27 % H ₂ SO ₄ 5 g biomass/75 ml solution 141.6 °C, 36.4 min	Complete hemicellulose conversion: 94 % xylose recovery Increased solid digestibility (70 %): fermentation for sugars production	Chemicals: xylose, sugars	(Shatalov and Pereira 2012)
Plant	Acid hydrolysis	40.7 g biomass/605 ml solution 1.7 % HCl 190 °C, 1 h	Hemicellulose fractionation Solid liquified with glycerol and PEG: 50 °C for 2 min and used as polyol for PU obtaining	Chemicals: levulinic acid, polyol for PU	(Bernardini et al. 2017)
Plant	Acid hydrolysis	1 kg biomass/30 l solution H ₂ SO ₄ 1.4 % wt 200 °C, 5 min	Liquid fraction: converted to fur-aldehyde with Amberlyst 15: 33.5 % furfural (10 min, 157 °C) Solid fraction suitable for enzymatic hydrolysis and fermentation: 43–51 g ethanol/l	Ethanol	(De Bari et al. 2020)
Plant	Acid + alkaline hydrolysis (plus precipitation)	HCl 0.1 M, 2 h, 100 °C NaOH 0.1 M, 2 h, 100 °C Acidification and precipitation	48 % Lignin recovery, with high purity (98 %) A further step of bleaching with H ₂ O ₂ and acid hydrolysis allows obtaining cellulose nanocrystals	Lignin	(Barana et al. 2016)

Table 2: (continued)

Material	Pre-treatment	Conditions	Results	Objective	References
Plant	Alkaline pulping (plus precipitation)	18 % alkali SLR: 1:4 160 °C, 210 min	0.5 kg pulp/kg biomass + 128 lignin/kg biomass	Cellulose pulp Chemicals: poly-phenols from lignin	(Pinto et al. 2015)
Plant	Autohydrolysis assisted with microwaves	200 °C 20 min SLR: 50 g/l water	55 % hemicellulose + 16 % cellulose degradation: 9.8 % xylose + 4.5 % xylo-oligomers + 1.8 % glucose	Chemicals: xylose	(Galia et al. 2015)
Plant	Alkaline assisted with microwaves	0.5 % w/v NaOH Liquid to solid ratio: 15:1 (ml/g biomass) 120 °C, 5 min	Maximum sugars yield: 4.5 g sugars/100 g biomass	Sugars	(Komolwanich et al. 2014)
Plant	Acid assisted with microwaves	Autoclave 190 °C 1 h 0.1 % HCl 41 g biomass/580 g solution	20–23 % levulinic acid 30 % lignin: reactive hydrochar	Chemicals: levulinic acid	(Licursi et al. 2015)
Plant	Acid assisted with microwaves	1.66 % HCl LSR: 15 g/g 190 °C, 20 min	21.3 % levulinic acid 28.9 % hydrochar	Chemicals: levulinic acid	(Licursi et al. 2018)
Plant	Catalyzed hydrolysis assisted with microwaves	1.6 wt % FeCl ₃ 9 % biomass 150 °C, 2.5 min	Hemicellulose solubilization: 98.2 % xylose obtained 14.1 % glucose also obtained	Chemicals: xylose	(Di Fidio et al. 2019)
Plant	Acid+catalyst hydrolysis assisted with microwaves	2.8 wt% FeCl ₃ 9 % biomass 150 °C, 2.5 min	Hemicellulose solubilization: 19.4 g xylose/l, 5.6 g glucose/l Enzymatic digestion of the solid: 12.6 g glucose/l Glucose fermentation: 7.8 g single cell oil/l (15–25 % lipids)	Lipids (biofuel)	(Di Fidio et al. 2021)
Plant	Catalyzed hydrolysis assisted with microwaves	2.4 wt % FeCl ₃ 9 % biomass 190 °C, 30 min	Levulinic acid yield: 57.6 % Formic acid: 65 %	Chemicals: levulinic acid, formic acid	(Di Fidio et al. 2019)
Plant	Two steps assisted with microwaves: alkaline + acid hydrolysis	0.5 % NaOH + 0.5 % w/v H ₂ SO ₄ Liquid to solid ratio: 15:1 (ml/g biomass) 180 °C, 30 min	Final sugars yield: 31.9 g/100 g biomass	Sugars	(Komolwanich et al. 2014)
Plant	Ionic liquid	[C4mim]Cl + Amberlyst™ 35DRY 5 g biomass/95 g solvent 160 °C, 1.5 h	Hemicellulose content reduction Higher digestibility of the solid: higher glucose yields (10.4 g vs. 1.2 glucose/l)	Sugars	(You et al. 2016)
Plant	Ionic liquid	[C2C1im][OAc] 160 °C, 3 h	Solids with increased digestibility: glucan conversion to glucose: 40.8–76.2 %	Sugars	(Corno et al. 2016)
Plant	Ionic liquid	[Bmim]HSO ₄ 16 g/l SLR: 20 g biomass/200 ml 80 °C, 3 h	Higher digestibility of solids: 7.9 g glucose/L Photofermentation of liquors: 101.6 ml H ₂ /g TS (35 % higher than for untreated biomass)	Hydrogen	(Chen et al. 2022)
Plant	Ionic liquid	[C2C1im][OAc] 160 °C, 3 h	Increased solids digestibility: 71 % cellulose converted to glucose Dark fermentation: 70.5 N ml/g biomass + 100 mg/l organic acids Fermentation of OA: 100g PHA/kg biomass	Chemicals: ethanol, PHA	(Villegas Calvo et al. 2018)
Plant	Switchable ionic liquid	DBU/MEA/SO ₂	67 % lignin extraction		(Gavilá et al. 2018)

Table 2: (continued)

Material	Pre-treatment	Conditions	Results	Objective	References
Plant	White rot fungi	2 g biomass/10 g SIL + 6 ml water	Digestible solid: 5.7 g glucose/l, fully transformed in 5.6 g lactic acid/l by fermentation	Chemicals: lactic acid	(Piccitto et al. 2022)
		120 °C, 2 h Pleurotus ostreatus 30 % solid loading in water 26 °C, 30 days	High D-lactic acid purity (>97 %) 30 % lignin degradation: increased anaerobic digestion: 130.9 N mL/g VS	Methane	
Plant	Mechanical	Hammer + pin mill	Reduction in lignin content: 137 % increase in CH ₄ production versus untreated biomass (212 N mL/g VS)	Methane	(Dell'Omo and Spena 2020)

conditions). In addition to the lignin-rich solid obtained after the second hydrolysis stage, levulinic acid (with a yield of 57.6 %) and formic acid (up to 65 % yields) were also produced.

The milder conditions favored furfural production, while more severe conditions generated levulinic acid (Antonetti et al. 2015). These authors also used an acid catalyzer (Amberlyst-70), obtaining similar xylose yields (about 96 %) with high selectivity. The cellulose-rich solid was further hydrolyzed using the same catalyzer, resulting in glucose yields of over 30 %, although enzymatic hydrolysis provided higher conversion values, higher than 55 %. In this study, Di Fidio et al. (2020) successfully recovered xylose and glucose without the pre-treatment of the *Arundo*. Komolwanich et al. (2014) hydrolyzed *Arundo* with microwave heating in an alkali solution followed by dilute acid hydrolysis; this two-step process increased the sugar release, reaching up to 31.9 g glucose/100 g.

Likewise, Galia et al. (2015) performed the hydrolysis of reed biomass (stalks and leaves) in pure water under microwave irradiation in batches and compared it with continuous processing by hot water. The work proposed this strategy to ease the scaling-up of the autohydrolysis process and also as an approach to Green Chemistry principles, as no reagents were used. Authors found that, although hemicellulose degradation was similar, microwaves are most effective in depolymerizing cellulose, which increases the possibilities for the later use of the solid fraction. Given the high amount of biochar produced, its exploitation must be considered; this by-product is a valuable source of simple phenolic compounds with good antioxidant properties (Licursi et al. 2015, 2018).

Raspolli-Galleti et al. (2013) reported for the first time the production of levulinic acid with yields above 23 %, which corresponds to almost 83 % of the theoretical yield, using HCl

as a catalyzer and working at 190 °C. These authors also used a ruthenium-based catalyst to directly obtain γ -valerolactone, a compound of great interest for biofuel production, at 70 °C, getting yields close to 17 %, with almost complete conversion of the levulinic acid. Under similar conditions to those used for xylose production, Licursi et al. (2018) proposed using microwaves and very diluted hydrochloric acid (1.66 %), reaching temperatures of 190 °C, and the use of an autoclave (under the same conditions) as possible treatments for plant material. They reported similar yields of levulinic acid and carbon, 22 % and 30 % respectively (Licursi et al. 2015, 2018).

In a different work, Licursi et al. (2015) obtained yields of around 8–10 % furfural and 23–25 % levulinic acid under these mild conditions and low concentrations of HCl; these conditions also allow for the recycling of most water and acid. In a one-step process, levulinic acid is the only product obtained, with similar yields. It then appears that a two-step mild process could be more advantageous than a single step, in terms of yields, although a lifecycle assessment would be needed to balance obtained yields, with regard to the inputs and their respective impacts. The solid fraction obtained in both cases is rich in lignin and shows higher thermal stability than commercial lignin, with some reactivity due to the presence of free carbonyl and hydroxyl groups, which makes them classified as reactive hydrochar, with low solubility, similar to Brown coal.

Most studies emphasize the need for pre-treatment for producing sugars (or directly to obtain interesting final products) and for improving the digestibility of the solid material under mild conditions (low acid concentration, low temperatures, and low processing time). This allows the operation with low or moderate severity factors (temperatures under 150 °C), consequently resulting in energy savings, of great importance under real industrial

processing (Shatalov et al. 2017). In this sense, You et al. (2016, 2018) have proposed the use of ionic liquids to pretreat the reed biomass, obtaining up to 50 % hemicellulose removal and increased digestibility of the resulting material (5 g glucose/kg h for untreated material, increasing to 93 g glucose/kg h of initial enzymatic hydrolysis rate, also increasing the total digestibility by twofold). These studies generated glucose concentrations over 10 g/l in 34 min for the pre-treated material and less than 1 g/l for the untreated raw material.

Gavilá et al. (2018) have also proposed using ionic liquids for sugar production, in this case for lactic acid production. This research has found that the use of a switching ionic liquid heated with microwaves can hydrolyze over 60 % of giant reed lignin within 1 h, with minimal amounts of degradation products. More importantly, the solvent can be recovered by precipitation of the remaining pulp. Despite the higher costs of the ionic liquid used in this study, the authors highlight its potential, due to the excellent results obtained and the possibility of reusing the solvent.

4.2.2 Further processing: sugars, cellulose, bioplastics, and lignin production

The products obtained after the fractionation treatment of the reed can also be used to obtain other compounds through biological processes. This cascade approach allows for maximizing the yield and potential of the lignocellulosic biomass.

For example, Ventorino et al. (2017) obtained succinic acid, with a yield of 0.69 g acid/g hydrolyzed material (9.4 g/l succinic acid), through bacterial fermentation using the hydrolysate obtained from the steam explosion of reed and bacteria from the rumen of cows and steers. When reed biomass was supplemented with nitrogen, the same authors found a significant increase in acids recovery, getting up to 12.1, 1.7, and 5.2 g/l of lactate, succinate, and acetate, respectively, using *Cosenzaea myxofaciens* bacterial strain (Ventorino et al. 2016).

For their part, Shatalov et al. (2013) have proposed using the solid residue from acid hydrolysis in an enzymatic hydrolysis process. They obtained a cellulose conversion of 75 % to glucose (26.4 g/100 g dry biomass). Some studies performed by Scordia et al. (2011) used oxalic acid as pre-treatment for ethanol production; 5 % of oxalic acid solution at 180 °C produced maximum glucan conversion, close to 70 %, and enough for ulterior fermentation. Giacobbe et al. (2016) proposed a different approach for biomass pre-treatment, performing an ammonia expansion pre-treatment before enzymatic saccharification using various enzyme cocktails. However, these authors did not

run a control saccharification test without pre-treatment, so it is impossible to know the benefits of such a process in terms of enzymatic yields. The production of sugars for bioethanol production is discussed in more detail in the next section, as it is mainly used for energy purposes.

Reed can also be used to obtain cellulosic fibers, for use in different applications. Shatalov and Pereira (2013) suggest conducting an initial hydrolysis step, to remove hemicellulose and lignin, to produce high-purity cellulosic fibers; this method resulted in pulps with around 94 % α -cellulose. Barana et al. (2016) proposed a sequential approach for obtaining lignin, hemicellulose, and cellulose nanocrystals, following a chemical procedure consisting of an alkaline treatment followed by bleaching and acid hydrolysis. These authors recovered around 50 % of the cellulose, hemicellulose, and lignin. Martínez-Sanz et al. (2018) prepared lignocellulosic films by selective removal of lignin and hemicellulose by chemical methods. The films, especially those obtained after hemicellulose removal, showed good mechanical and water barrier properties and high transparency, comparable to thermoplastic starch films, making them interesting for the packaging industry.

Some studies have also used giant reed in biopolymer development, following a multistage approach (Corneli et al. 2016; Calvo et al. 2018). After a chemical pre-treatment and enzymatic hydrolysis, Villegas Calvo et al. (2018) proposed conducting a first fermentation step in dark conditions to produce hydrogen. After this first step, the resulting liquid fraction is transferred into a reactor with the inoculum (solids from the secondary treatment of a Wastewater Treatment Plant) for the production of PHA (poly-hydroxyalkanoate). They obtained similar results to those given by other lignocellulosic materials, around 100 g PHA/kg volatile suspended solids (biomass + polymer).

On the other hand, the study by Corneli et al. (2016) proposed using different lignocellulosic materials, including reed, to obtain the biopolymer through a silage pre-treatment. Polylactic acid (PLA) can also be obtained from reed hydrolysis and fermentation to yield lactic acid (Gavilá et al. 2018). Finally, the char recovered from acid hydrolysis for levulinic acid production has been used to synthesize flexible polyurethane (Bernardini et al. 2017). To obtain this, the solid was liquefied by microwaves at low temperatures, using glycerol and PEG as solvents, and water as a foaming agent. The obtained polyol was used at a concentration of 7 wt % of the final foam, which showed properties suitable for packaging applications.

Sterols, lipids, and fatty acids have been produced from the rhizome, along with other compounds such as terpenoids, alkaloids, xanthones, xanthene, and phenolic compounds (Liu et al. 2021b; Pansuksan et al. 2020).

As summarized in Figure 6, the reed is an excellent source of lignin (contains about 20–25 % Klason lignin), made up of p-hydroxyphenyl, guaiacyl, and syringyl phenylpropanoid units linked predominantly by β -O-4' aryl ether linkages (~70–80 %), with the remainder being β - β' , β -5', β -1', γ α , β -diaryl ether bonds (You et al. 2013). Different authors have investigated composites based on this complex compound (Thakur et al. 2014; Vaidya et al. 2019) due to its excellent mechanical, antioxidant, and biodegradable properties. Besides, lignin can be used to produce polymers, carbon fibers, or phenolic compounds (Savy and Piccolo 2014; Licursi et al. 2015) with antioxidant properties, such as vanillin or syringaldehyde (Pinto et al. 2015). Other authors highlight the importance of lignin valorization for improving biorefineries' economic and ecological performance; the final aim is the production of green molecules and biofuels (Cotana et al. 2014; Molino et al. 2018).

For example, Cotana et al. (2014) have proposed three routes for getting lignin from the residues of bioethanol production from giant reed. They found that a rich-lignin material (around 73 %) with high thermal stability, suitable for composites manufacturing, can be obtained with a simple NaOH treatment, followed by an acid step to precipitate the lignin.

Savy and Piccolo (2014) characterized lignin fractions from *Arundo* stem obtained by acid hydrolysis and alkaline oxidation. These authors obtained higher lignin recovery from sulfuric acid hydrolysis, although the lignin obtained from the alkaline process showed higher oxidized lignin, which is also water-soluble.

Also, Pinto et al. (2015) proposed pulping *Arundo* stalks in an alkali solution at a moderate temperature (160 °C) to obtain cellulose pulp and being able to recover lignin from the black liquor, thus allowing for its further valorization. Around 100 g lignin/kg of dry matter was obtained by this method. These authors consider giant reed a good option for producing low molecular weight phenolics, favorable for aldehydes production, as the ones already mentioned.

4.3 Bioenergy production from giant reed

Regarding energy production from the lignocellulosic materials derived from giant reed, Krička et al. (2017) obtained the heat value from direct burning of the dry plant, obtaining higher and lower heating values (17.5 and 16.1 MJ/kg, respectively) similar to those obtained for other widely used crops for energy production, such as *Miscanthus* (18.2 and 16.8 MJ/kg). These authors state that the high lignin content of this plant makes them more suitable for direct burning instead of transformation into other energy products. However, this

option should be discouraged, due to the low recalcitrance of this biomass and the good yields obtained for biochemicals and bioenergy production, as demonstrated by other authors and discussed below. Biomass direct burning should only be contemplated in those cases where the obtaining of bioderived products would need energy consumption higher than the value to be obtained from such bioproducts.

Several authors have evaluated the potential of reed for ethanol production. The process proposed begins with acid hydrolysis, as mentioned in the previous section, followed by alkaline treatment. Lemons e Silva et al. (2015) performed simultaneous saccharification with cellulase and fermentation with *Saccharomyces cerevisiae*, obtaining 42 g glucose/l in 30 h which was thereafter transformed into 39 g ethanol/l in 70 h. These authors worked with relatively high enzyme loadings (25 FPU g/solids) and supplemented the medium with urea, potassium dihydrogen phosphate, yeast extract, and a salt solution. The biomass was added in five batches every 12 h.

Loaces et al. (2017) followed a similar approach and compared the sugars and ethanol yields obtained in simultaneous and separate saccharification and fermentation. These authors used liquid hot water treatment (or autohydrolysis) and dilute acid as pre-treatment and obtained up to 33 g glucose/l and 24 g ethanol/l in the separate process and a similar value (35 g/l) for the simultaneous process. This research used *Escherichia coli* in the fermentation process, and the ethanol yields were higher than those obtained for other strains, such as *S. cerevisiae*, *Scheffersomyces stipites*, or *Saccharomyces carlsbergensis*, which led to 19.0, 18.0, and 16 g ethanol/l, respectively (Ask et al. 2012; Scordia et al. 2011, 2012, 2013).

A different study (Sidana et al. 2022) that used *Meyerozyma guilliermondii* yeast on reed hydrolysates following a two-step acid/alkali hydrolysis process, obtained ethanol yields of 33 g/l in 72 h. The *Arundo* biomass has been signaled as a valuable source of pentosans as its xylose content is similar, or even higher, than glucose. Moreover, it has higher xylose content than other biomasses, such as sugar cane bagasse (Neto et al. 1997). Both *E. coli* and *M. guilliermondii* can metabolize pentoses during fermentation. Viola et al. (Viola et al. 2015) reported higher ethanol yields, using *S. cerevisiae*, on hydrolysates obtained by autohydrolysis of fresh ripe reed (no prior drying step). Other authors have also studied the rhizome as a raw material for potentially obtaining green energy, in the form of ethanol, as this part of the plant contains over 30 % sugar (Proietti et al. 2017). The use of reed provides higher bioethanol yields than those obtained from other energy crops, such as cassava, *Miscanthus*, sugar cane, or beet, with the additional advantage of not being a food crop (Corno et al. 2014).

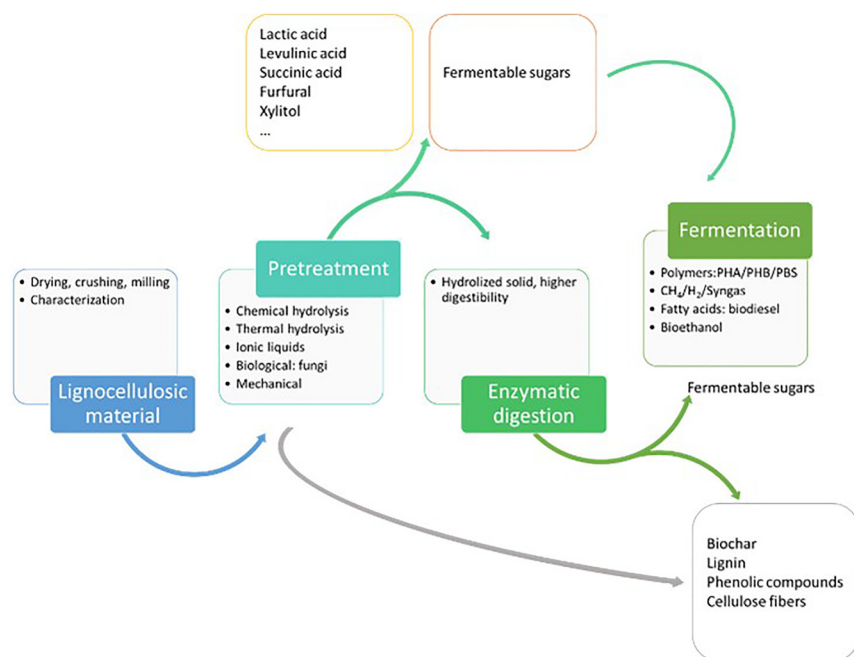


Figure 6: Different biorefinery processes combined to produce several compounds of interest, starting from *Arundo donax*. L. PHA, polyhydroxyalkanoate; PHB, polyhydroxybutyrate; PBS, polybutylene succinate.

The pyrolysis of reed to obtain biogas and phenol-rich chars has also been assessed in the literature. Bartoli et al. (Bartoli et al. 2016) produced biochar and bio-oil by microwave-assisted pyrolysis. They found that rhizomes and leaves provided large bio-char quantities (up to 60 %), due to the different ash contents in the three fractions, which would catalyze the biochar formation. In comparison, stems produced a larger amount of bio-oil (around 40 %). The pyrolysis reactions are quick for the three materials (about 20 min for 100 g of biomass). The bio-chars showed a calorific value of about 31 MJ/kg, similar to other solid fuels. The obtained bio-chars showed a very low hydrogen content, demonstrating the extent of the thermal process; they also had an important amount of volatile organic compounds (around 25 %), attributed by authors to the batch processing and the low temperatures reached in the pyrolysis process (lower than 700 °C). Moreover, the bio-oils consisted significant amount of aromatic compounds (over 200 g/l) and acetic acid (around 120 g/l). Slow pyrolysis at lower temperatures (300–400 °C for 60–90 min) of *Arundo* stems revealed carbon contents over 80 %, with a similar composition to the biochar obtained by Bartoli and collaborators (2016), although with higher content in volatiles (over 50 %) (Carnevale et al. 2022). Zheng et al. (2018) obtained biochar as by-product of pyrolysis vinegar (mainly acetic acid and phenol-derived compounds) production by *Arundo* stems at different temperatures, finding that higher temperatures led to lower biochar and similar vinegar yields. These authors did not further characterize the char. Ribechini et al. (2012) have found that pyrolysis at 150 and 190 °C results in the total

conversion of hemicellulose and cellulose, with partial depolymerization of lignin. The result of their solid analysis suggests the potential of the char as an antioxidant source instead of fuel, as it is mainly derived from the lignin fraction, thus getting a high-added value product. As mentioned in Section 4.2.1, the solubilization of hemicellulose produces an important amount of biochar, rich in phenolic compounds and with antioxidant properties, which can be further valorized (Licursi et al. 2015, 2018).

A different approach consists of the anaerobic digestion of giant reed biomass. For example, Amaducci and Perego (2015) obtained a biochemical biogas potential ranging from 345 to 506 ml/g volatile solids (VS), with a methane content of about 50 %, highly influenced by the lignin and ash content of the raw material. Yang and Li (2014) obtained similar methane production values with fresh *Arundo* (150.8 ml/g VS); methane production yields were lower with dried *Arundo*, particularly with solid contents by 20 %. However, other authors have reported the need for pre-treatment to get acceptable yields of methane production; for example, Baldini et al. (2017) applied ensilage as pre-treatment, before the anaerobic digestion, with biochemical biogas potential similar to the results of Amaducci and Perego (Amaducci and Perego 2015), which equates to approximately 50 % of the theoretical biomethane production.

Di Girolamo et al. (2014) reported an increase in methane production yield (up to 30 %) when reed was treated with a low concentration NaOH solution (0.15 N); these same authors also used maleic anhydride as pre-treatment, which led to higher methane yields (Di Girolamo

et al. 2016). Methane production values were similar between the silage and the NaOH pre-treatments, while maleic anhydride ones reached higher values, comparable to those of *sorghum* or barley straw. Liu et al. (2015, 2016a,b) performed similar studies, comparing methane production yields for giant reed pre-treated by ensilage, fungus, and urea application. Urea pre-treatment yielded 173 ml/g VS in 30 days (production took place in the first 5 days), which indicates an increase of 18 % when compared to the untreated raw material (Liu et al. 2015).

The effect of fungus was opposite to that expected due to the degradation of cellulose and solid contents reduction (Liu et al. 2016b); the ensilage pre-treatment resulted in a 15 % increase in the methane yield, while fungal pre-treatment resulted in a 30 % decrease. In addition to the effect of pre-treatment on the methane yields, these authors also found some differences with regard to the harvest time. *Arundo* harvested in December contained higher water cellulose carbohydrates while the ones harvested in August had a higher lignin content, which resulted in lower biomass digestibility (Liu et al. 2016b; Ragaglini et al. 2014). The results from these authors suggest that urea pre-treatment provided higher yields than the ensilage pre-treatment (173 ml/g vs. 165 ml/g, respectively).

Lignin from giant reed stems, separated after the steam explosion and alkaline hydrolysis, has been used to obtain syngas via supercritical water gasification (Molino et al. 2018). Operating at 550 °C and 250 bar, Molino et al. (2018) generated a gas rich in syngas (>90 %) with no carbon dioxide, a hydrogen content of 65 %, and a higher heating value of 43 MJ/kg, similar to conventional methane. Besides, an organic-rich liquor with valuable chemicals, such as glucose, xylose, formic acid, acetic acid, and syringaldehyde, was also obtained.

Yang et al. (2020) also evaluated the pyrolysis of residual lignin from *Arundo* hydrolysis and fermentation for ethanol production, obtaining biochar and biogas. They obtained 7.5 % of biogas and 16.7 % of ethanol for the fermentation plus pyrolysis route versus 26.6 % of biogas production for direct pyrolysis. This approach increases the overall process yield and provides a more valuable utilization of the lignocellulosic materials compared to direct pyrolysis.

Reed hydrolysates rich in xylose and glucose can also serve as a substrate for the growth of oily yeasts (*Lipomyces starkeyi*) to obtain fats at a concentration of 30 %, with a good yield of transformation of sugars to lipids (15–24 %) (Di Fidio et al. 2021). In this approach, the hydrolysates are first obtained using microwaves or acid/enzymatic hydrolysis processes; afterward, a yeast strain capable of transforming the obtained xylose into fats is used. These authors follow a cascade approach, using both the hydrolysate and solid

residue. For the solid, enzymatic hydrolysis is proposed, followed by a process where the same yeast strain is used to transform glucose into single-cell oils. Other authors followed a similar strategy, starting from acid hydrolysis of the reed to obtain the hydrolysate (Pirozzi et al. 2014) and getting yields that are comparable to those obtained in biodiesel production plants. Also, Pirozzi et al. (2013) performed different studies using the hydrolysates from *Arundo* to grow oil yeasts. They obtained 110 g lipids/l, with oleic acid as the major component. However, if a two-step process was applied to the biomass (steam explosion followed by enzymatic hydrolysis), the oil yield could increase up to 150 g/l (Pirozzi et al. 2014).

4.4 *Arundo donax* biorefinery: current limitations and future opportunities

From the literature review performed, it can be concluded that *A. donax* L. has great potential as biorefinery feedstock, due to its composition, year-round availability, and fast growth rate. As summarized in Figure 6, there are several paths for the transformation of reed biomass into building blocks, energy products or cellulose fibers. The relatively high content in hemicellulose, around 25–30 % for the aerial parts of the plant (stems and leaves), suggests performing a first hydrolysis step, under mild conditions (140 °C and low acid concentration) for the recovery of xylans, also degrading the amorphous part of cellulose into glucose. More severe conditions are not recommended, due to the degradation of these monomers into furfural or HMF, which means the hydrolysates would need of further purification stages. The obtained solid, with improved digestibility, could be later processed by enzymatic means to increase the glucose yields. This is a procedure commonly followed in literature, although assays are usually performed at small scale. The cost of enzymes on a large scale would reduce the economic profitability of such installations, so other options, such as further chemical treatments or pyrolysis, should be considered. Something similar happens for the thermochemical treatments; it is generally considered that moderate temperatures are required for biomass fractionation, although there are several paths to achieve so, from pressurized reactors, conventional heating, or microwaves. Again, assays are mainly performed at lab-scale, and some of these procedures might not be fully scalable. On the other hand, the use of ultrasounds and cavitation has not been fully explored and might also provide good yields. Energy efficiency should be considered, and cavitation is one of the techniques with higher energy efficiency and shorter processing times (Poddar et al. 2022).

Despite the wide availability of studies on the potential use of giant reed, scalability assays have not been found. The cultivation of fungi that produce enzymes for the ulterior processing of the reed biomass would be an exciting option although, again, this needs to be further assessed. So, the alternative is the use of chemicals, in the lower proportion possible, to allow the separation of the original biomass into profitable products. This is, in the authors' opinion, the next steps to undertake: shifting from the grams scale used in the lab to a pilot-scale plant, working with at least kilograms, and optimizing the procedures to maximize yields. The comparison between lab and pilot-scale plant conditions and yields would allow for a later design of appropriate industrial facilities for the processing of such biomass.

On the other hand, only 7 % of the arable land in the EU is devoted to industrial crops (Eurostat 2019), most of it being occupied with cereals. It is important to note that, despite the interest of the scientific community and the strategies settled by different organisms to increase the availability of raw materials for biorefinery development and reduce the oil dependence, food production is prioritized, and energy or industrial crops cannot displace it. The use of by-products or residues from food production are undeniably a valuable resource and they should be reintroduced into the industrial value chain to maximize the use of resources.

Based on *Arundo*'s specific resistance to salinity, droughts, pathogens, etc. a strategy to increase the cultivated lands for industrial purposes could be the use of marginal or degraded soils, using low-quality waters. This would allow for reducing soil loss and restoring their quality while, at the same time, getting valuable lignocellulose material for further industrial use. It is estimated that about 60–70 % of European soils are degraded, while over 25 % are identified as with a high or very high risk of desertification, especially in southern Europe. The Mediterranean basin is particularly sensitive to soil loss, also having low levels of organic matter and high salinization (Ferreira et al. 2022). Even if the yields obtained in such conditions are not optimal, the low requirements of such plant species could provide additional environmental benefits, regarding soil restoration and preservation. Besides, not only degraded soils could be used; a recent study has estimated that over 8 million hectares of EU agricultural soil are not used due to non-optimized conditions and is considered marginal agricultural land (Reinhardt et al. 2022), while about 40 % of such surface can be considered as profitable land (Sallustio et al. 2022). An assessment performed in China for a plant processing 2000 t/day would lead to 28 MW power, plus over 50 t/day of bio-oil, 555 t/day of vinegar and similar values of biochar (Abreu et al. 2022), showing the potential of *Arundo* for producing several fractions at high-scale. Considering the use of only

1 % of such area, and the estimated yields for this plant of 30 t/ha, about 2.4 million tons of *Arundo* biomass could be obtained yearly, which can be translated into over 70 MW energy, over 125 t of bio-oil and almost 1500 t of biochar and pyrolysis vinegar. The use of unused soil for the obtaining of biomass feedstock would also help reduce the dependence on external sources to produce chemicals or energy, advancing the SDGs objectives on sustainable and responsible consumption, green energy, soils preservation, etc. while, at the same time, would not have any impact on food production, as no crop substitution would be required.

The European Strategy for Bioeconomy has as its main aim the production and commercialization of food, forestry products, bio-products and bioenergy obtained from environmentally friendly competitive processes. The commitment to the achievement of SDGs and the advancement toward more sustainable and efficient processes and products can be reflected in the growing number of biorefineries installed, among other factors. In Europe alone, over 2300 installations are identified, mainly located in central Europe (Germany, France, Sweden, and Italy) (Parisi 2022). Most of them are devoted to bioenergy products (biomethane in particular), although chemical production has gained importance in the last years. Most of these installations in Europe is one platform biorefinery, focusing on oil products, while the non-EU ones (led by China and the USA) are mostly devoted to sugars platform, starting from sugar and starch crops (Baldoni et al. 2021). Most of these plants operate with a commercial purpose, although at different scales (Parisi 2022), from a few to hundreds of thousands of tons of input raw material. The casuistic is so wide (type of raw materials, main product, type of process) that there is no guide on the potential scale to reach a certain level of profitability, and this is particularly one of the exciting challenges to still undertake, the demonstration of the profitability, at different levels, of such installations.

Finally, the potential selection and modification of the plant species to improve this adaption to the aforementioned degraded soil conditions and poor-quality waters would also pose significant improvements on the dry matter yields obtained, although this path is still in the very early stages of development (Danelli et al. 2020).

The last Global biorefinery status report points out the use of marginal land and the cultivation of resilient species as a solution to overcome the current limitations of lignocellulose material availability and foster the growth of the bioeconomy (Annevelink et al. 2022). In this sense, considering the inputs required for the cultivation, the plant species' resilience, the availability of marginal and degraded soils, and the potential ability to remove pollutants from soil and waters, *A. donax* L. can be considered as a convenient

species and its cultivation should be promoted, even over other species more commonly cultivated such as *Miscanthus* or switchgrass. A recent study has proven that *Arundo* provides higher efficiency for syngas production than *Miscanthus*, from exergy analysis (Manić et al. 2023), although both species are more favorable than corn stalk or municipal wastes, which are more commonly used as feedstock for methane or syngas production. The potential invasive character of this plant species is certainly a thread to consider, although the potential benefits from the cultivation, also from an environmental point of view, should not be disregarded.

5 Conclusions and outlook

5.1 Conclusions

The extensive literature published on this topic shows the interest in the use of giant reed for several purposes in a bioeconomy scenario. The abundant biomass generated by this plant, its fast-growing rate, and the low inputs needed for its cultivation has made several authors propose *Arundo* as a promising source of lignocellulosic biomass. The extensive range of applications for products obtained from its cultivation, from sugars to a wide range of chemicals, besides the traditional hand-craft products, have made policymakers refer to this plant as a high-interest crop. This non-food crop is considered to have great potential as an energy crop, especially in the Mediterranean basin, although it can also adapt to colder and wetter climatic conditions.

The biorefineries' growth potential is linked to their sustainability, considering its three aspects (environmental, social, and economic). The cascade approach is seen as the most interesting to maximize the potential of the biomass and, thus, its profitability, showing giant reed a suitable composition to follow such an approach and exploit the different fractions. Hemicellulose-derived products are usually the first compounds obtained, as it is a relatively easy compound to degrade, and it accounts for a major fraction of the raw biomass. need of a pre-treatment stage to ease the separation of the different fractions, thus maximizing the range of products to obtain and yields, has been demonstrated. These pre-treatments also induce an increase in the material's digestibility. The low recalcitrance of *Arundo* biomass allows for conducting such pretreatments with low-concentration solutions, especially acids, and mild conditions. These are suitable for the solubilization of hemicellulose and partial depolymerization of lignin and cellulose. Acids are used to catalyze such reactions in concentrations below 2%. Other options include using

ionic liquids, which can be reused several times. Microwave pre-treatment has also been proposed to pretreat the biomass rapidly while releasing sugars simultaneously, although heating in semicontinuous or continuous mode should be further explored in order to increase process scalability and profitability.

5.2 Outlook

Even if the invasive potential of *A. donax* is clear, an adequate management strategy would bring significant environmental improvements, especially in areas with soil erosion risk and affected by droughts, due to the resistance of this plant to saline or low-quality waters and soils. This strategy should not only include the adoption of the processes for maximizing the yields of bioproducts obtained at lower energy requirements but also crop management, only using marginal or degraded soils, low-quality waters, or even wastewaters to reduce the need for nitrogen fertilization. The cultivation of giant reed appears then as a potential strategy to reduce the risk of soil loss and desertification risk, especially in the Mediterranean area.

Different strategies can be employed for reed valorization depending on the intended end. However, the sugars platform seems to be one of the most promising ones, considering the wide range of bio-products that can be obtained: polymers, such as PLA, PHA, or PBS, fats for biodiesel production, bioethanol, and other chemicals used in synthesis, especially xylose and levulinic acid. After sugar production, the residual solid biomass can be fed into further processes to obtain lignin and cellulose fibers or further processed to maximize sugar production. Antioxidant compounds, biochar, bio-oils, and energy products can be obtained at the later steps of the value-chain. The high yields obtained under relatively mild conditions and the wide range of products potentially produced from *Arundo* materials make direct energy valorization (burning) a non-desirable strategy, making the refining a more efficient and sustainable approach.

Even though some authors have performed environmental analysis on the crop, the inputs required, and the performance of bioproducts obtained (mainly related to bioethanol), more studies on the environmental and economic impact of *Arundo* cultivation and its processing are still required.

The scaling-up of such infrastructures to cover the gap between demonstration plants and large-scale production ones still needs to be undertaken, as recognized in the Global Bioeconomy Summit in 2020. Thus, there is a promising field of study, framed on the green deal strategy of the EU

and the sustainable development goals, to optimize not only the technical feasibility of biorefineries but also the environmental, economic, and social performance of such installations.

Author contributions: Conceptualization, Z.O.; methodology and literature search: Z.O., L.S.; writing—original draft preparation, Z.O. and I.B.; writing—review and editing, all authors.; visualization, L.S.; supervision, Z.O., E.C. All the authors have accepted responsibility for the entire content of this submitted manuscript and approved submission.

Research funding: Zaida Ortega acknowledges the Spanish Ministry of Universities for funding the internship at QUB, funded by the grant received by Order UNI/501/2021 of May 26th 2021, coming from the European Union towards Next Generation funds (Plan de Recuperación, Transformación y Resiliencia del Gobierno de España: C21.I4.P1. Resolución del 2 de julio de 2021 de la Universidad de Las Palmas de Gran Canaria por la que se convocan Ayudas para la recualificación del sistema universitario español para 2021–2023). Luis Suárez acknowledges the funding through the Ph.D. grant program cofinanced by the Canarian Agency for Research, Innovation and Information Society of the Canary Islands Regional Council for Employment, Industry, Commerce and Knowledge (ACIISI) and by the European Social Fund (ESF) (grant number TESIS2021010008).

Conflict of interest statement: The authors declare that they have no conflicts of interest regarding this article.

References

- Abreu, M., Silva, L., Ribeiro, B., Ferreira, A., Alves, L., Paixão, S.M., Gouveia, L., Moura, P., Carvalheiro, F., Duarte, et al. (2022). Low indirect land use change (ILUC) energy crops to bioenergy and biofuels: a review. *Energies* 15: 4348.
- Accardi, D.S., Russo, P., Lauri, R., Pietrangeli, B., and di Palma, L. (2015). From soil remediation to biofuel: process simulation of bioethanol production from *Arundo donax*. *Chem. Eng. Trans.* 43: 2167–2172.
- Ahmed, M.J. (2016). Potential of *Arundo donax* L. stems as renewable precursors for activated carbons and utilization for wastewater treatments: review. *J. Taiwan Inst Chem Eng* 63: 336–343.
- Alexopoulou, E., Zanetti, F., Scordia, D., Zegada-Lizarazu, W., Christou, M., Testa, G., Cosentino, S.L., and Monti, A. (2015). Long-term yields of switchgrass, giant reed, and miscanthus in the Mediterranean basin. *Bioenergy Res.* 8: 1492–1499.
- Alshaal, T., Elhawati, N., Domokos-Szabolcsy, É., Kátai, J., Márton, L., Czákó, M., El-Ramady, H., and Fári, M.G. (2015). Giant reed (*Arundo donax* L.): a green technology for clean environment. In: Ansari, A.A., Singh Gill, S., Gill, R., Lanza, G.R., and Newman, L. (Eds.), *Phytoremediation: management of environmental contaminants*. Cham: Springer, pp. 3–20.
- Amaducci, S. and Perego, A. (2015). Field evaluation of *Arundo donax* clones for bioenergy production. *Ind. Crops Prod.* 75: 122–128.
- Andreu-Rodriguez, J., Medina, E., Ferrandez-Garcia, M.T., Ferrandez-Villena, M., Ferrandez-Garcia, C.E., Paredes, C., Bustamante, M.A., and Moreno-Caselles, J. (2013). Agricultural and industrial valorization of *Arundo donax* L. *Commun. Soil Sci. Plant Anal.* 44: 598–609.
- Angelini, L.G., Ceccarini, L., Nasso, N., and Bonari, E. (2009). Comparison of *Arundo donax* L. and *Miscanthus x giganteus* in a long-term field experiment in central Italy: analysis of productive characteristics and energy balance. *Biomass Bioenergy* 33: 635–643.
- Annevelink, B., Garcia Chavez, L., van Ree, R., and Vural Gursel, I. (2022). Global biorefinery status report 2022. IEA Bioenergy, Available at: <https://www.ieabioenergy.com/wp-content/uploads/2022/09/IEA-Bioenergy-Task-42-Global-biorefinery-status-report-2022-220712.pdf>.
- Antonetti, C., Bonari, E., Licursi, D., Di Nasso, N.N., and Galletti, A.M.R. (2015). Hydrothermal conversion of giant reed to furfural and levulinic acid: optimization of the process under microwave irradiation and investigation of distinctive agronomic parameters. *Molecules* 20: 21232–21353.
- Antonetti, C., Licursi, D., Fulignati, S., Valentini, G., and Galletti, A.M.R. (2016). New frontiers in the catalytic synthesis of levulinic acid: from sugars to raw and waste biomass as starting feedstock. *Catalysts* 6: 196.
- Ask, M., Olofsson, K., di Felice, T., Ruohonen, L., Penttilä, M., Lidén, G., and Olsson, L. (2012). Challenges in enzymatic hydrolysis and fermentation of pretreated *Arundo donax* revealed by a comparison between SHF and SSF. *Process Biochem.* 47: 1452–1459.
- Bacher, W., Sauerbeck, G., Mix-Wagner, G., and el Bassam, N. (2001). Giant reed (*Arundo donax* L.) network: improvement, productivity and biomass quality. Federal Agricultural Research Centre (FAL), Available at: https://literatur.thuenen.de/digbib_extern/zi025259.pdf.
- Badagliaccio, D., Megna, B., and Valenza, A. (2020). Induced modification of flexural toughness of natural hydraulic lime based mortars by addition of giant reed fibers. *Case Stud. Construct. Mater.* 13: e00425.
- Baldini, M., da Borso, F., Ferfua, C., Zuliani, F., and Danuso, F. (2017). Ensilage suitability and bio-methane yield of *Arundo donax* and *Miscanthus x giganteus*. *Ind. Crops Prod.* 95: 264–275.
- Baldoni, E., Reumerman, P., Parisi, C., Platt, R., González Hermoso, H., Vikla, K., Vos, J., and M'barek, R. (2021). Chemical and material driven biorefineries in the EU and beyond. Publications Office of the EU, Available at: <https://data.europa.eu/doi/10.2760/8932>.
- Barana, D., Salanti, A., Orlandi, M., Ali, D.S., and Zoia, L. (2016). Biorefinery process for the simultaneous recovery of lignin, hemicelluloses, cellulose nanocrystals and silica from rice husk and *Arundo donax*. *Ind. Crops Prod.* 86: 31–39.
- Barreca, F., Martínez Gabarrón, A., Flores Yepes, J.A., and Pastor Pérez, J.J. (2019). Innovative use of giant reed and cork residues for panels of buildings in Mediterranean area. *Resour. Conservat. Recycl.* 140: 259–266.
- Bartoli, M., Rosi, L., Giovannelli, A., Frediani, P., and Frediani, M. (2016). Production of bio-oils and bio-char from *Arundo donax* through microwave assisted pyrolysis in a multimode batch reactor. *J. Anal. Appl. Pyrolysis* 122: 479–489.
- Bernal, M.P., Grippi, D., and Clemente, R. (2021). Potential of the biomass of plants grown in trace element-contaminated soils under mediterranean climatic conditions for bioenergy production. *Agronomy* 11: 1750.
- Bernardini, J., Licursi, D., Anguillesi, I., Cinelli, P., Coltelli, M.B., Antonetti, C., Galletti, A.M.R., and Lazzeri, A. (2017). Exploitation of *Arundo donax* L. hydrolysis residue for the green synthesis of flexible polyurethane foams. *BioResources* 12: 3630–3655.

- Bonfante, A., Impagliazzo, A., Fiorentino, N., Langella, G., Mori, M., and Fagnano, M. (2017). Supporting local farming communities and crop production resilience to climate change through giant reed (*Arundo donax* L.) cultivation: an Italian case study. *Sci. Total Environ.* 601–602: 603–613.
- Bosco, S., Nassi o Di Nasso, N., Roncucci, N., Mazzoncini, M., and Bonari, E. (2016). Environmental performances of giant reed (*Arundo donax* L.) cultivated in fertile and marginal lands: a case study in the Mediterranean. *Eur. J. Agron.* 78: 20–31.
- Buss, W., Graham, M.C., Shepherd, J.G., and Mašek, O. (2016). Suitability of marginal biomass-derived biochars for soil amendment. *Sci. Total Environ.* 547: 314–322.
- Calvo, M.V., Colombo, B., Corno, L., Eisele, G., Cosentino, C., Papa, G., Scaglia, B., Pilu, R., Simmons, B., and Adani, F. (2018). Bioconversion of giant cane for integrated production of biohydrogen, carboxylic acids, and polyhydroxyalkanoates (PHAs) in a multistage biorefinery approach. *ACS Sustain. Chem. Eng.* 6: 15361–15373.
- Cano-Ruiz, J., Ruiz Fernández, J., Alonso, J., Mauri, P.V., and Lobo, M.C. (2021). Value-added products from wastewater reduce irrigation needs of *Arundo donax* energy crop. *Chemosphere* 285: 131485.
- Caparrós, S., Ariza, J., Hernanz, D., and Díaz, M.J. (2006). *Arundo donax* L. Valorization under hydrothermal and pulp processing. *Ind. Eng. Chem. Prod. Res. Dev.* 45: 2940–2948.
- Cappelli, G., Yamaç, S.S., Stella, T., Francone, C., Paleari, L., Negri, M., and Confalonieri, R. (2015). Are advantages from the partial replacement of corn with second-generation energy crops undermined by climate change? A case study for giant reed in northern Italy. *Biomass Bioenergy* 80: 85–93.
- Carnevale, M., Longo, L., Gallucci, F., and Santangelo, E. (2022). Influence of the harvest time and the airflow rate on the characteristics of the *Arundo* biochar produced in a pilot updraft reactor. *Biomass Convers. Biorefinery* 12: 2525–2539.
- Ceotto, E., Marchetti, R., and Castelli, F. (2018). Residual soil nitrate as affected by giant reed cultivation and cattle slurry fertilization. *Ital. J. Agron.* 13: 317–323.
- Chen, J., Yang, S., Alam, M.A., Wang, Z., Zhang, J., Huang, S., Zhuang, W., Xu, C., and Xu, J. (2021). Novel biorefining method for succinic acid processed from sugarcane bagasse. *Bioresour. Technol.* 324: 124615.
- Chen, Z., Jiang, D., Zhang, T., Lei, T., Zhang, H., Yang, J., Shui, X., Li, F., Zhang, Y., and Zhang, Q. (2022). Comparison of three ionic liquids pretreatment of *Arundo donax* L. For enhanced photo-fermentative hydrogen production. *Bioresour. Technol.* 343. <https://doi.org/10.1016/j.biortech.2021.126088>.
- Christou, M. (2011). Eurobioref 2011, September 19, 2011. The terrestrial biomass: formation and properties (crops and residual biomass). Centre for Renewable Energy Sources and Saving, Lecce, Available at: http://www.eurobioref.org/Summer_School/Lectures_Slides/day2/Lectures/L03_M%20Christou.pdf.pdf.
- Corneli, E., Adessi, A., Dragoni, F., Ragagnini, G., Bonari, E., and De Philippis, R. (2016). Agroindustrial residues and energy crops for the production of hydrogen and poly- β -hydroxybutyrate via photofermentation. *Bioresour. Technol.* 216: 941–947.
- Corno, L., Pilu, R., and Adani, F. (2014). *Arundo donax* L.: a non-food crop for bioenergy and bio-compound production. *Biotechnol. Adv.* 32: 1535–1549.
- Corno, L., Pilu, R., Tran, K., Tambone, F., Singh, S., Simmons, B.A., and Adani, F. (2016). Sugars production for green chemistry from 2nd generation crop (*Arundo donax* L.): a full field approach. *ChemistrySelect* 1: 2617–2623.
- Cosentino, S.L., Copani, V., D'Agosta, G.M., Sanzone, E., and Mantineo, M. (2006). First results on evaluation of *Arundo donax* L. clones collected in Southern Italy. *Ind. Crops Prod.* 23: 212–222.
- Costa, J., Barbosa, B., and Fernando, A.L. (2016). Wastewaters reuse for energy crops cultivation. *IFIP Adv. Inf. Commun. Technol.* 470: 507–514.
- Cotana, F., Cavalaglio, G., Nicolini, A., Gelosia, M., Coccia, V., Petrozzi, A., and Brinchi, L. (2014). Lignin as co-product of second generation bioethanol production from ligno-cellulosic biomass. *Energy Procedia* 45: 52–60.
- Cristaldi, A., Oliveri Conti, G., Cosentino, S.L., Mauromicale, G., Copat, C., Grasso, A., Zuccarello, P., Fiore, M., Restuccia, C., and Ferrante, M. (2020). Phytoremediation potential of *Arundo donax* (giant reed) in contaminated soil by heavy metals. *Environ. Res.* 185: 109427.
- Csurhes, S. (2016). Invasive weed risk assessment: giant reed (*Arundo donax*). Department of Agriculture and Fisheries (Biosecurity Queensland), Available at: https://www.daf.qld.gov.au/_data/assets/pdf_file/0006/59973/IPA-Giant-Reed-Risk-Assessment.pdf.
- Curt, M.D., Mauri, P.V., Sanz, M., Cano-Ruiz, J., del Monte, J.P., Aguado, P.L., and Sánchez, J. (2017). The ability of the *Arundo donax* crop to compete with weeds in central Spain over two growing cycles. *Ind. Crops Prod.* 108: 86–94.
- Dahmardeh Ghalehno, M., Madhoushi, M., Tabarsa, T., and Nazerian, M. (2011). The manufacture of particleboards using mixture of reed (surface layer) and commercial species (middle layer). *Eur. J. Wood Wood Prod.* 69: 341–344.
- Danelli, T., Cantaluppi, E., Tosca, A., Cassani, E., Landoni, M., Bosio, S., Adani, F., and Pilu, R. (2019). Influence of clonal variation on the efficiency of *Arundo donax* propagation methods. *J. Plant Growth Regul.* 38: 1449–1457.
- Danelli, T., Laura, M., Savona, M., Landoni, M., Adani, F., and Pilu, R. (2020). Genetic improvement of *Arundo donax* L.: opportunities and challenges. *Plants* 9: 1548.
- De Bari, I., Liuzzi, F., Ambrico, A., and Trupo, M. (2020). *Arundo donax* refining to second generation bioethanol and furfural. *Processes* 8: 1–15.
- Dell'Omo, P.P. and Spena, V.A. (2020). Mechanical pretreatment of lignocellulosic biomass to improve biogas production: comparison of results for giant reed and wheat straw. *Energy* 203. <https://doi.org/10.1016/j.ENERGY.2020.117798>.
- Di Fidio, N., Antonetti, C., and Raspolli Galletti, A.M. (2019). Microwave-assisted cascade exploitation of giant reed (*Arundo donax* L.) to xylose and levulinic acid catalysed by ferric chloride. *Bioresour. Technol.* 293: 122050.
- Di Fidio, N., Galletti, A.M.R., Fulignati, S., Licursi, D., Liuzzi, F., De Bari, I., and Antonetti, C. (2020). Multi-step exploitation of raw *Arundo donax* L. for the selective synthesis of second-generation sugars by chemical and biological route. *Catalysts* 10: 79.
- Di Fidio, N., Ragagnini, G., Dragoni, F., Antonetti, C., and Raspolli Galletti, A.M. (2021). Integrated cascade biorefinery processes for the production of single cell oil by *Lipomyces starkeyi* from *Arundo donax* L. hydrolysates. *Bioresour. Technol.* 325: 124635.
- Di Girolamo, G., Bertin, L., Capecci, L., Ciavatta, C., and Barbanti, L. (2014). Mild alkaline pre-treatments loosen fibre structure enhancing methane production from biomass crops and residues. *Biomass Bioenergy* 71: 318–329.
- di Girolamo, G., Grigatti, M., Barbanti, L., and Angelidaki, I. (2013). Effects of hydrothermal pre-treatments on Giant reed (*Arundo donax*) methane yield. *Bioresour. Technol.* 147: 152–159.

- Di Girolamo, G., Grigatti, M., Bertin, L., Ciavatta, C., and Barbanti, L. (2016). Enhanced substrate degradation and methane yield with maleic acid pre-treatments in biomass crops and residues. *Biomass Bioenergy* 85: 306–312.
- D'Imporzano, G., Pilu, R., Corno, L., and Adani, F. (2018). *Arundo donax* L. can substitute traditional energy crops for more efficient, environmentally-friendly production of biogas: a life cycle assessment approach. *Bioresour. Technol.* 267: 249–256.
- Dragoni, F., Nasso, N.N., Tozzini, C., Bonari, E., and Ragaglini, G. (2015a). Aboveground yield and biomass quality of giant reed (*Arundo donax* L.) as affected by harvest time and frequency. *BioEnergy Res.* 8: 1321–1331.
- Dragoni, F., Ragaglini, G., Corneli, E., Nasso, N.N., Tozzini, C., Cattani, S., and Bonari, E. (2015b). Giant reed (*Arundo donax* L.) for biogas production: land use saving and nitrogen utilisation efficiency compared with arable crops. *Ital. J. Agron.* 10: 192–201.
- European Union (2017). Invasive alien species of union concern environment. European Commission, Available at: <https://eur-lex.europa.eu/legal-content/EN/TXT/?uri=CELEX:32017R1263>.
- Eurostat (2019). Annual crop statistics. Eurostat, Available at: https://ec.europa.eu/eurostat/cache/metadata/Annexes/apro_cp_esms_an1.pdf.
- Eurostat (2020). *Integrated farm statistics manual 2020 edition*. Publications of the European Office.
- Fabbrini, F., Ludovisi, R., Alasia, O., Flexas, J., Douthe, C., Ribas Carbo, M., Robson, P., Taylor, G., Scarascia-Mugnozza, G., Keurentjes, J.J.B., et al. (2019). Characterization of phenology, physiology, morphology and biomass traits across a broad Euro-Mediterranean ecotypic panel of the lignocellulosic feedstock *Arundo donax*. *GCB Bioenergy* 11: 152–170.
- Fagnano, M., Impagliazzo, A., Mori, M., and Fiorentino, N. (2015). Agronomic and environmental impacts of giant reed (*Arundo donax* L.): results from a long-term field experiment in hilly areas subject to soil erosion. *BioEnergy Res.* 8: 415–422.
- Fazio, S. and Barbanti, L. (2014). Energy and economic assessments of bio-energy systems based on annual and perennial crops for temperate and tropical areas. *Renew. Energy* 69: 233–241.
- Fernando, A.L., Barbosa, B., Costa, J., and Papazoglou, E.G. (2016). Giant reed (*Arundo donax* L.): a multipurpose crop bridging phytoremediation with sustainable bioeconomy. In: Prasad, M.N.V. (Ed.), *Bioremediation and bioeconomy*. Amsterdam, Elsevier, pp. 77–95.
- Ferrández-García, C.E., Andreu-Rodríguez, J., Ferrández-García, M.T., Ferrández-Villena, M., and García-Ortuño, T. (2012). Panels made from giant reed bonded with non-modified starches. *BioResources* 7: 5904–5916.
- Ferrández-García, M.T., Ferrández-García, C.E., García-Ortuño, T., Ferrández-García, A., and Ferrández-Villena, M. (2019). Experimental evaluation of a new giant reed (*Arundo donax* L.) composite using citric acid as a natural binder. *Agronomy* 9: 882.
- Ferrández-García, M.T., Ferrández-García, A., García-Ortuño, T., Ferrández-García, C.E., and Ferrández-Villena, M. (2020). Assessment of the physical, mechanical and acoustic properties of *Arundo donax* L. biomass in low pressure and temperature particleboards. *Polymers* 12: 1361.
- Ferrández Villena, M., Ferrández García, C.E., García Ortuño, T., Ferrández García, A., and Ferrández García, M.T. (2020). The influence of processing and particle size on binderless particleboards made from *Arundo donax* L. rhizome. *Polymers* 12: 696.
- Ferreira, C.S.S., Seifollahi-Aghmiuni, S., Destouni, G., Ghajarnia, N., and Kalantari, Z. (2022). Soil degradation in the European Mediterranean region: processes, status and consequences. *Sci. Total Environ.* 805: 150106.
- Fiore, V., Botta, L., Scaffaro, R., Valenza, A., and Pirrotta, A. (2014a). PLA based biocomposites reinforced with *Arundo donax* fillers. *Compos. Sci. Technol.* 105: 110–117.
- Fiore, V., Scalici, T., and Valenza, A. (2014b). Characterization of a new natural fiber from *Arundo donax* L. as potential reinforcement of polymer composites. *Carbohydr. Polym.* 106: 77–83.
- Fiore, V., Piperopoulos, E., and Calabrese, L. (2019). Assessment of *Arundo donax* fibers for oil spill recovery applications. *Fibers* 7: 75.
- Forte, A., Zucaro, A., Fagnano, M., Bastianoni, S., Basosi, R., and Fierro, A. (2015). LCA of *Arundo donax* L. lignocellulosic feedstock production under Mediterranean conditions. *Biomass Bioenergy* 73: 32–47.
- Galia, A., Schiavo, B., Antonetti, C., Galletti, A.M.R., Interrante, L., Lessi, M., Scialdone, O., and Valenti, M.G. (2015). Autohydrolysis pretreatment of *Arundo donax*: a comparison between microwave-assisted batch and fast heating rate flow-through reaction systems. *Biotechnol. Biofuels* 8: 218.
- Garau, M., Castaldi, P., Diquattro, S., Pinna, M.V., Senette, C., Roggero, P.P., and Garau, G. (2021). Combining grass and legume species with compost for assisted phytostabilization of contaminated soils. *Environ. Technol. Innov.* 22: 101387.
- García-Ortuño, T., Andréu-Rodríguez, J., Ferrández-García, M.T., Ferrández-Villena, M., and Ferrández-García, C.E. (2011). Evaluation of the physical and mechanical properties of particleboard made from giant reed (*Arundo donax* L.). *BioResources* 6: 477–486.
- Gavilá, L., Constantí, M., Medina, F., Pezoa-Conte, R., Anugwom, I., and Mikkola, J.P. (2018). Lactic acid production from renewable feedstock: fractionation, hydrolysis, and fermentation. *Adv. Sustain. Syst.* 2: 1700185.
- Gazoulis, I., Kanatas, P., Papastilianou, P., Tataridas, A., Alexopoulou, E., and Travlos, I. (2021). Weed management practices to improve establishment of selected lignocellulosic crops. *Energies* 14: 2478.
- Ge, X., Burner, D.M., Xu, J., Phillips, G.C., and Sivakumar, G. (2011). Bioethanol production from dedicated energy crops and residues in Arkansas, USA. *Biotechnol. J.* 6: 66–73.
- Ge, X., Xu, F., Vasco-Correa, J., and Li, Y. (2016). Giant reed: a competitive energy crop in comparison with miscanthus. *Renew. Sustain. Energy Rev.* 54: 350–362.
- Giacobbe, S., Balan, V., Montella, S., Fagnano, M., Mori, M., and Faraco, V. (2016). Assessment of bacterial and fungal (hemi)cellulose-degrading enzymes in saccharification of ammonia fibre expansion-pretreated *Arundo donax*. *Appl. Microbiol. Biotechnol.* 100: 2213–2224.
- Hong, S.H. and Lee, E.Y. (2016). Restoration of eroded coastal sand dunes using plant and soil-conditioner mixture. *Int. Biodeterior. Biodegrad.* 113: 161–168.
- Jensen, E.F., Casler, M.D., Farrar, K., Finnan, J.M., Lord, R., Palmborg, C., Valentine, J., and Donnison, I.S. (2018). Giant reed: from production to end use. In: Alexopoulou, E. (Ed.), *Perennial grasses for bioenergy and bioproducts*. Amsterdam, Academic Press Inc. Elsevier, pp. 107–150.
- Jeon, Y.J., Xun, Z., and Rogers, P.L. (2010). Comparative evaluations of cellulosic raw materials for second generation bioethanol production. *Lett. Appl. Microbiol.* 51: 518–524.
- Jiménez-Ruiz, J., Hardion, L., Del Monte, J.P., Vila, B., and Santín-Montanyà, M.I. (2021). Monographs on invasive plants in Europe N° 4: *Arundo donax* L. *Bot. Lett.* 168: 131–151.
- Komolwanich, T., Tatijarn, P., Prasertwasu, S., Khumsupan, D., Chaisuwan, T., Luengnaruemitchai, A., and Wongkasemjit, S. (2014). Comparative potentiality of Kans grass (*Saccharum spontaneum*) and giant reed (*Arundo donax*) as lignocellulosic feedstocks for the release of monomeric sugars by microwave/chemical pretreatment. *Cellulose* 21: 1327–1340.

- Krička, T., Matin, A., Bilandžija, N., Jurišić, V., Antonović, A., Voća, N., and Grubor, M. (2017). Biomass valorisation of *Arundo donax* L., *Miscanthus × giganteus* and *Sida hermaphrodita* for biofuel production. *Int. Agrophys.* 31: 575–581.
- Lambertini, C. (2019). Why are tall-statured energy grasses of polyploid species complexes potentially invasive? A review of their genetic variation patterns and evolutionary plasticity. *Biol. Invas.* 21: 3019–3041.
- Lemons e Silva, C.F., Schirmer, M.A., Maeda, R.N., Barcelos, C.A., and Pereira, N. (2015). Potential of giant reed (*Arundo donax* L.) for second generation ethanol production. *Electron. J. Biotechnol.* 18: 10–15.
- Leong, H.Y., Chang, C.K., Khoo, K.S., Chew, K.W., Chia, S.R., Lim, J.W., Chang, J.S., and Show, P.L. (2021). Waste biorefinery towards a sustainable circular bioeconomy: a solution to global issues. *Biotechnol. Biofuels* 14: 87.
- Lewandowski, I., Scurlock, J.M.O., Lindvall, E., and Christou, M. (2003). The development and current status of perennial rhizomatous grasses as energy crops in the US and Europe. *Biomass Bioenergy* 25: 335–361.
- Licursi, D., Antonetti, C., Bernardini, J., Cinelli, P., Coltelli, M.B., Lazzeri, A., Martinelli, M., and Galletti, A.M.R. (2015). Characterization of the *Arundo donax* L. solid residue from hydrothermal conversion: comparison with technical lignins and application perspectives. *Ind. Crops Prod.* 76: 1008–1024.
- Licursi, D., Antonetti, C., Mattonai, M., Pérez-Armada, L., Rivas, S., Ribechini, E., and Raspolli Galletti, A.M. (2018). Multi-valorisation of giant reed (*Arundo donax* L.) to give levulinic acid and valuable phenolic antioxidants. *Ind. Crops Prod.* 112: 6–17.
- Liu, D., Zou, C., and Xu, M. (2019). Environmental, ecological, and economic benefits of biofuel production using a constructed wetland: a case study in China. *Int. J. Environ. Res. Publ. Health* 16: 827.
- Liu, H., Cheng, C., and Wu, H. (2021a). Sustainable utilization of wetland biomass for activated carbon production: a review on recent advances in modification and activation methods. *Sci. Total Environ.* 790: 148214.
- Liu, Q.R., Li, J., Zhao, X.F., Xu, B., Xiao, X.H., Ren, J., and Li, S.X. (2021b). Alkaloids and phenylpropanoid from rhizomes of *Arundo donax* L. *Nat. Prod. Res.* 35: 465–470.
- Liu, S., Ge, X., Liew, L.N., Liu, Z., and Li, Y. (2015). Effect of urea addition on giant reed ensilage and subsequent methane production by anaerobic digestion. *Bioresour. Technol.* 192: 682–688.
- Liu, S., Ge, X., Liu, Z., and Li, Y. (2016a). Effect of harvest date on *Arundo donax* L. (giant reed) composition, ensilage performance, and enzymatic digestibility. *Bioresour. Technol.* 205: 97–103.
- Liu, S., Xu, F., Ge, X., and Li, Y. (2016b). Comparison between ensilage and fungal pretreatment for storage of giant reed and subsequent methane production. *Bioresour. Technol.* 209: 246–253.
- Loaces, I., Schein, S., and Noya, F. (2017). Ethanol production by *Escherichia coli* from *Arundo donax* biomass under SSF, SHF or CBP process configurations and in situ production of a multifunctional glucanase and xylanase. *Bioresour. Technol.* 224: 307–313.
- López, F., García, J.C., Pérez, M.J., Zamudio, M.A.M., and Gil, G. (2010). Chemical and energetic characterization of species with a high-biomass production: fractionation of their components. *Environ. Prog. Sustain.* 29: 499–509.
- Malheiro, R., Ansolin, A., Guarnier, C., Fernandes, J., Amorim, M.T., Silva, S.M., and Mateus, R. (2021). The potential of the reed as a regenerative building material—characterisation of its durability, physical, and thermal performances. *Energies* 14: 4276.
- Manić, N., Janković, B., Stojiljković, D., Popović, M., Cvetković, S., and Mikulčić, H. (2023). Thermodynamic study on energy crops thermochemical conversion to increase the efficiency of energy production. *Thermochim. Acta* 719: 179408.
- Manniello, C., Cillis, G., Statuto, D., Di Pasquale, A., and Picuno, P. (2022a). Concrete blocks reinforced with *Arundo donax* natural fibers with different aspect ratios for application in bioarchitecture. *Appl. Sci.* 12: 2167.
- Manniello, C., Cillis, G., Statuto, D., Di Pasquale, A., and Picuno, P. (2022b). Experimental analysis on concrete blocks reinforced with *Arundo donax* fibres. *J. Agricult. Eng.* 53: 1–7.
- Mantziaris, S., Iliopoulos, C., Theodorakopoulou, I., and Petropoulou, E. (2017). Perennial energy crops vs. durum wheat in low input lands: economic analysis of a Greek case study. *Renew. Sustain. Energy Rev.* 80: 789–800.
- Martínez Gabarrón, A., Flores Yepes, J.A., Pastor Pérez, J.J., Berná Serna, J.M., Arnold, L.C., and Sánchez Medrano, F.J. (2014). Increase of the flexural strength of construction elements made with plaster (calcium sulfate dihydrate) and common reed (*Arundo donax* L.). *Construct. Build. Mater.* 66: 436–441.
- Martínez-Sanz, M., Erboz, E., Fontes, C., and López-Rubio, A. (2018). Valorization of *Arundo donax* for the production of high performance lignocellulosic films. *Carbohydr. Polym.* 199: 276–285.
- Ministerio de Agricultura Alimentación y Medioambiente (2013). Catálogo español de especies exóticas invasoras - *Arundo donax* L. Gobierno de España, Available at: https://www.miteco.gob.es/es/biodiversidad/temas/conservacion-de-especies/arundo_donax_2013_tcm30-69809.pdf.
- Ministerio de Economía Industria y Competitividad (2017). Manual sobre las Biorrefinerías en España. BioPlat, Suschem, Gobierno de España, Available at: https://www.suschem-es.org/docum/pb/2017/publicaciones/Manual_de_Biorrefinerias_en_Espana_feb_2017.pdf.
- Ministerio para la Transición Ecológica (2019). Real Decreto 216/2019, de 29 de marzo, por el que se aprueba la lista de especies exóticas invasoras preocupantes para la región ultraperiférica de las islas Canarias y por el que se modifica el Real Decreto 630/2013, de 2 de agosto, por el que se regula el Catálogo español de especies exóticas invasoras. Gobierno de España, Available at: https://www.boe.es/diario_boe/txt.php?id=BOE-A-2019-4675.
- Molino, A., Larocca, V., Valerio, V., Rimauro, J., Marino, T., Casella, P., Cerbone, A., Arcieri, G., and Viola, E. (2018). Supercritical water gasification of lignin solution produced by steam explosion process on *Arundo donax* after alkaline extraction. *Fuel* 221: 513–517.
- Monti, A., Fazio, S., and Venturi, G. (2009). Cradle-to-farm gate life cycle assessment in perennial energy crops. *Eur. J. Agron.* 31: 77–84.
- Monti, A., Zanetti, F., Scordia, D., Testa, G., and Cosentino, S.L. (2015). What to harvest when? Autumn, winter, annual and biennial harvesting of giant reed, miscanthus and switchgrass in Northern and Southern Mediterranean area. *Ind. Crops Prod.* 75: 129–134.
- Nassi o Di Nasso, N., Roncucci, N., Triana, F., Tozzini, C., and Bonari, E. (2011). Seasonal nutrient dynamics and biomass quality of giant reed (*Arundo donax* L.) and miscanthus (*Miscanthus × giganteus* Greef et Deuter) as energy crops. *Ital. J. Agron.* 6: 24.
- Neto, C.P., Seca, A., Nunes, A.M., Coimbra, M.A., Domingues, F., Evtuguin, D., Silvestre, A., and Cavaleiro, J.A.S. (1997). Variations in chemical composition and structure of macromolecular components in different morphological regions and maturity stages of *Arundo donax*. *Ind. Crops Prod.* 6: 51–58.
- Nsanganwimana, F., Marchand, L., Douay, F., and Mench, M. (2014). *Arundo donax* L., a candidate for phytomanaging water and soils contaminated by trace elements and producing plant-based feedstock. A review. *Int. J. Phytoremediation* 16: 982–1017.

- Ortega, Z., Romero, F., Paz, R., Suárez, L., Benítez, A.N., and Marrero, M.D. (2021). Valorization of invasive plants from Macaronesia as filler materials in the production of natural fiber composites by rotational molding. *Polymers* 13: 2220.
- Otter, P., Hertel, S., Ansari, J., Lara, E., Cano, R., Arias, C., Gregersen, P., Grischek, T., Benz, F., Goldmaier, A., et al. (2020). Disinfection for decentralized wastewater reuse in rural areas through wetlands and solar driven onsite chlorination. *Sci. Total Environ.* 721: 137595.
- Pansuksan, K., Sukprasert, S., and Karaket, N. (2020). Phytochemical compounds in *Arundo donax* L. rhizome and antimicrobial activities. *Pharmacognosy J.* 12: 287–292.
- Pari, L., Scarfone, A., Santangelo, E., Figorilli, S., Crognale, S., Petruccioli, M., Suardi, A., Gallucci, F., and Barontini, M. (2015). Alternative storage systems of *Arundo donax* L. and characterization of the stored biomass. *Ind. Crops Prod.* 75: 59–65.
- Pari, L., Bergonzoli, S., Cetera, P., Suardi, A., Alfano, V., Palmieri, N., Stefanoni, W., and Mattei, P. (2021). *29th European Biomass Conference and Exhibition Proceedings, 26–29 April 2021. Assessment of comminuted biomass behaviour during Arundo donax storage*. Marseille: ETA Florence Renewable Energies, pp. 306–309.
- Parisi, C. (2022). Distribution of the bio-based industry in the EU database and visualisation. European Commission, Available at: https://knowledge4policy.ec.europa.eu/visualisation/bio-based-industry-biorefineries-eu_en.
- Piccitto, A., Scordia, D., Corinzia, S.A., Cosentino, S.L., and Testa, G. (2022). Advanced biomethane production from biologically pretreated giant reed under different harvest times. *Agronomy* 12. <https://doi.org/10.3390/agronomy12030712>.
- Pilu, R., Cassani, E., Landoni, M., Badone, F.C., Passera, A., Cantaluppi, E., Corno, L., and Adani, F. (2014). Genetic characterization of an Italian Giant Reed (*Arundo donax* L.) clones collection: exploiting clonal selection. *Euphytica* 196: 169–181.
- Pinto, P.C.R., Oliveira, C., Costa, C.A., Gaspar, A., Faria, T., Ataíde, J., and Rodrigues, A.E. (2015). Kraft delignification of energy crops in view of pulp production and lignin valorization. *Ind. Crops Prod.* 71: 153–162.
- Piperopoulos, E., Khaskhoussi, A., Fiore, V., and Calabrese, L. (2021). Surface modified *Arundo donax* natural fibers for oil spill recovery. *J. Nat. Fibers* 19: 8230–8245.
- Pirozzi, D., Ausiello, A., Strazza, R., Trofa, M., Zuccaro, G., and Toscano, G. (2013). Exploitation of agricultural biomasses to produce II-generation biodiesel. *Chem. Eng. Trans.* 32: 175–180.
- Pirozzi, D., Ausiello, A., Yousuf, A., Zuccaro, G., and Toscano, G. (2014). Exploitation of oleaginous yeasts for the production of microbial oils from agricultural biomass. *Chem. Eng. Trans.* 37: 469–474.
- Pirozzi, D., Fiorentino, N., Impagliazzo, A., Sannino, F., Yousuf, A., Zuccaro, G., and Fagnano, M. (2015). Lipid production from *Arundo donax* grown under different agronomical conditions. *Renew. Energy* 77: 456–462.
- Poddar, B.J., Nakhate, S.P., Gupta, R.K., Chavan, A.R., Singh, A.K., Khardenavis, A.A., and Purohit, H.J. (2022). A comprehensive review on the pretreatment of lignocellulosic wastes for improved biogas production by anaerobic digestion. *Int. J. Environ. Sci. Technol.* 19: 3429–3456.
- Proietti, S., Moscatello, S., Fagnano, M., Fiorentino, N., Impagliazzo, A., and Battistelli, A. (2017). Chemical composition and yield of rhizome biomass of *Arundo donax* L. grown for biorefinery in the Mediterranean environment. *Biomass Bioenergy* 107: 191–197.
- Ragaglini, G., Dragoni, F., Simone, M., and Bonari, E. (2014). Suitability of giant reed (*Arundo donax* L.) for anaerobic digestion: effect of harvest time and frequency on the biomethane yield potential. *Bioresour. Technol.* 152: 107–115.
- Raposo Oliveira Garcez, L., Hofmann Gatti, T., Carlos Gonzalez, J., Cesar Franco, A., and Silva Ferreira, C. (2022). Characterization of fibers from culms and leaves of *Arundo donax* L. (Poaceae) for handmade paper production. *J. Nat. Fibers* 19: 12805–12813.
- Raspolli Galletti, A.M., Antonetti, C., Ribechini, E., Colombini, M.P., Nassi o Di Nasso, N., and Bonari, E. (2013). From giant reed to levulinic acid and gamma-valerolactone: a high yield catalytic route to valeric biofuels. *Appl. Energy* 102: 157–162.
- Reinhardt, J., Hilgert, P., and von Cossel, M. (2022). Yield performance of dedicated industrial crops on low-temperature characterized marginal agricultural land in Europe – a review. *Biofuels, Bioprod. Biorefining* 16: 609–622.
- Ribechini, E., Zanaboni, M., Raspolli Galletti, A.M., Antonetti, C., Nassi o Di Nasso, N., Bonari, E., and Colombini, M.P. (2012). Py-GC/MS characterization of a wild and a selected clone of *Arundo donax*, and of its residues after catalytic hydrothermal conversion to high added-value products. *J. Anal. Appl. Pyrolysis* 94: 223–229.
- Romero-Munar, A., Baraza, E., Cifre, J., Achir, C., and Guliás, J. (2018a). Leaf plasticity and stomatal regulation determines the ability of *Arundo donax* plantlets to cope with water stress. *Photosynthetica* 56: 698–706.
- Romero-Munar, A., Tauler, M., Guliás, J., and Baraza, E. (2018b). Nursery preconditioning of *Arundo donax* L. plantlets determines biomass harvest in the first two years. *Ind. Crops Prod.* 119: 33–40.
- Sallustio, L., Harfouche, A.L., Salvati, L., Marchetti, M., and Corona, P. (2022). Evaluating the potential of marginal lands available for sustainable cellulosic biofuel production in Italy. *Socio-Econ. Plann. Sci.* 82: 101309.
- Sánchez, E., Scordia, D., Lino, G., Arias, C., Cosentino, S.L., and Nogués, S. (2015). Salinity and water stress effects on biomass production in different *Arundo donax* L. clones. *BioEnergy Res.* 8: 1461–1479.
- Sargin Karahancer, S., Eriskin, E., Sarioglu, O., Capali, B., Saltan, M., and Terzi, S. (2016). Utilization of *Arundo donax* in hot mix asphalt as a fiber. *Construct. Build. Mater.* 125: 981–986.
- Savy, D. and Piccolo, A. (2014). Physical-chemical characteristics of lignins separated from biomasses for second-generation ethanol. *Biomass Bioenergy* 62: 58–67.
- Schmidt, T., Fernando, A.L., Monti, A., and Rettenmaier, N. (2015). Life cycle assessment of bioenergy and bio-based products from perennial grasses cultivated on marginal land in the Mediterranean region. *BioEnergy Res.* 8: 1548–1561.
- Scordia, D. and Cosentino, S.L. (2019). Perennial energy grasses: resilient crops in a changing European agriculture. *Agriculture* 9: 169.
- Scordia, D., Cosentino, S.L., Lee, J.W., and Jeffries, T.W. (2011). Dilute oxalic acid pretreatment for biorefining giant reed (*Arundo donax* L.). *Biomass Bioenergy* 35: 3018–3024.
- Scordia, D., Cosentino, S.L., Lee, J.W., and Jeffries, T.W. (2012). Bioconversion of giant reed (*Arundo donax* L.) hemicellulose hydrolysate to ethanol by *Scheffersomyces stipitis* CBS6054. *Biomass Bioenergy* 39: 296–305.
- Scordia, D., Cosentino, S.L., and Jeffries, T.W. (2013). Enzymatic hydrolysis, simultaneous saccharification and ethanol fermentation of oxalic acid pretreated giant reed (*Arundo donax* L.). *Ind. Crops Prod.* 49: 392–399.
- Shatalov, A.A. and Pereira, H. (2006). Papermaking fibers from giant reed (*Arundo donax* L.) by advanced ecologically friendly pulping and bleaching technologies. *BioResources* 1: 45–61.

- Shatalov, A.A. and Pereira, H. (2012). Xylose production from giant reed (*Arundo donax* L.): modeling and optimization of dilute acid hydrolysis. *Carbohydr. Polym.* 87: 210–217.
- Shatalov, A.A. and Pereira, H. (2013). High-grade sulfur-free cellulose fibers by pre-hydrolysis and ethanol-alkali delignification of giant reed (*Arundo donax* L.) stems. *Ind. Crops Prod.* 43: 623–630.
- Shatalov, A.A., Duarte, L.C., Carvalho, F., Duarte, J.C., Gírio, F.M., Pereira, H., and Martins, L.O. (2013). *Proceedings of the 2nd Iberoamerican Congress on Biorefineries, 10–12 April 2013: CROBIOREF: Integrated strategy for the upgrading of giant reed (Arundo donax L.) for materials and chemicals*. Jaén, Sociedad Iberoamericana para el Desarrollo de las Biorrefinerías (SIADEB) y la Universidad de Jaén, pp. 641–648.
- Shatalov, A.A., Morais, A.R.C., Duarte, L.C., and Carvalho, F. (2017). Selective single-stage xylan-to-xylose hydrolysis and its effect on enzymatic digestibility of energy crops giant reed and cardoon for bioethanol production. *Ind. Crops Prod.* 95: 104–112.
- Shilpi, S., Lamb, D., Bolan, N., Seshadri, B., Choppala, G., and Naidu, R. (2019). Waste to watt: anaerobic digestion of wastewater irrigated biomass for energy and fertiliser production. *J. Environ. Manage.* 239: 73–83.
- Shtein, I., Baruchim, P., and Lev-Yadun, S. (2021). Division of labour among culms in the clonal reed *Arundo donax* (Poaceae) is underlain by their pre-determined hydraulic structure. *Bot. J. Linnean Soc.* 195: 348–356.
- Sicilia, A., Santoro, D.F., Testa, G., Cosentino, S.L., and Lo Piero, A.R. (2020). Transcriptional response of giant reed (*Arundo donax* L.) low ecotype to long-term salt stress by unigene-based RNAseq. *Phytochemistry* 177: 112436.
- Sidana, A., Kaur, S., and Yadav, S.K. (2022). Assessment of the ability of *Meyerozyma guilliermondii* P14 to produce second-generation bioethanol from giant reed (*Arundo donax*) biomass. *Biomass Convers. Biorefinery*. <https://doi.org/10.1007/S13399-021-02211-4>.
- Singh, K., Awasthi, A., Sharma, S.K., Singh, S., and Tewari, S.K. (2018). Biomass production from neglected and underutilized tall perennial grasses on marginal lands in India: a brief review. *Energy, Ecol. Environ.* 3: 207–215.
- Siri-Prieto, G., Bustamante, M., Battaglia, M., Ernst, O., Seleiman, M.F., and Sadeghpour, A. (2021). Effects of perennial biomass yield energy grasses and fertilization on soil characteristics and nutrient balances. *Agron. J.* 113: 4292–4305.
- Solarte-Toro, J.C. and Cardona Alzate, C.A. (2021). Biorefineries as the base for accomplishing the sustainable development goals (SDGs) and the transition to bioeconomy: technical aspects, challenges and perspectives. *Bioresour. Technol.* 340: 125626.
- Solinas, S., Deligios, P.A., Sulas, L., Carboni, G., Viridis, A., and Ledda, L. (2019). A land-based approach for the environmental assessment of Mediterranean annual and perennial energy crops. *Eur. J. Agron.* 103: 63–72.
- Suárez, L., Castellano, J., Romero, F., Marrero, M.D., Benítez, A.N., and Ortega, Z. (2021). Environmental hazards of giant reed (*Arundo donax* L.) in the Macaronesia region and its characterisation as a potential source for the production of natural fibre composites. *Polymers* 13: 2101.
- Suárez, L., Ortega, Z., Romero, F., Paz, R., and Marrero, M.D. (2022). Influence of giant reed fibers on mechanical, thermal, and disintegration behavior of rotomolded PLA and PE composites. *J. Polym. Environ.* 30: 4848–4862.
- Suárez, L., Barczewski, M., Kosmela, P., Marrero, M.D., and Ortega, Z. (2023). Giant reed (*Arundo donax* L.) fiber extraction and characterization for its use in polymer composites. *J. Nat. Fibers* 20: 2131687.
- Thakur, V.K., Thakur, M.K., Raghavan, P., and Kessler, M.R. (2014). Progress in green polymer composites from lignin for multifunctional applications: a review. *ACS Sustain. Chem. Eng.* 2: 1072–1092.
- Tomàs, J., Mateu, J., Gil, L., Boira, H., and Llorens, L. (2020). *Arundo micrantha* Lam. as an alternative to *Arundo donax* L. as energy crop in saline soils irrigated with treated urban wastewaters. *Plant Biosyst.* 154: 560–567.
- Torrado, I., Bandeira, F., Shatalov, A.A., Carvalho, F., and Duarte, L.C. (2014). The impact of particle size on the dilute acid hydrolysis of giant reed biomass. *Electron. J. Energy Environ.* 2: 1–9.
- Vaidya, A.A., Collet, C., Gaugler, M., and Lloyd-Jones, G. (2019). Integrating softwood biorefinery lignin into polyhydroxybutyrate composites and application in 3D printing. *Mater. Today Commun.* 19: 286–296.
- Ventorino, V., Robertiello, A., Viscardi, S., Ambrosanio, A., Faraco, V., and Pepe, O. (2016). Bio-based chemical production from *Arundo donax* feedstock fermentation using *Coszenzea myxofaciens* BPM1. *BioResources* 11: 6566–6581.
- Ventorino, V., Robertiello, A., Cimini, D., Argenzio, O., Schiraldi, C., Montella, S., Faraco, V., Ambrosanio, A., Viscardi, S., and Pepe, O. (2017). Bio-based succinate production from *Arundo donax* hydrolysate with the new natural succinic acid-producing strain *Basfia succiniciproducens* BPP7. *BioEnergy Res.* 10: 488–498.
- Villegas Calvo, M., Colombo, B., Corno, L., Eisele, G., Cosentino, C., Papa, G., Scaglia, B., Pilu, R., Simmons, B., and Adani, F. (2018). Bioconversion of giant cane for integrated production of biohydrogen, carboxylic acids, and polyhydroxyalkanoates (PHAs) in a multistage Biorefinery Approach. *ACS Sustain. Chem. Eng.* 6: 15361–15373.
- Viola, E., Zimbardi, F., Valerio, V., and Villone, A. (2015). Effect of ripeness and drying process on sugar and ethanol production from giant reed (*Arundo donax* L.). *AIMS Bioeng.* 2: 29–39.
- Yang, J., Wang, X., Shen, B., Hu, Z., Xu, L., and Yang, S. (2020). Lignin from energy plant (*Arundo donax*): pyrolysis kinetics, mechanism and pathway evaluation. *Renew. Energy* 161: 963–971.
- Yang, L. and Li, Y. (2014). Anaerobic digestion of giant reed for methane production. *Bioresour. Technol.* 171: 233–239.
- You, T., Wang, R., Zhang, X., Ramaswamy, S., and Xu, F. (2018). Reconstruction of lignin and hemicelluloses by aqueous ethanol anti-solvents to improve the ionic liquid-acid pretreatment performance of *Arundo donax* Linn. *Biotechnol. Bioeng.* 115: 82–91.
- You, T.T., Mao, J.Z., Yuan, T.Q., Wen, J.L., and Xu, F. (2013). Structural elucidation of the lignins from stems and foliage of *Arundo donax* Linn. *J. Agric. Food Chem.* 61: 5361–5370.
- You, T.T., Zhang, L.M., and Xu, F. (2016). Progressive deconstruction of *Arundo donax* Linn. to fermentable sugars by acid catalyzed ionic liquid pretreatment. *Bioresour. Technol.* 199: 271–274.
- Zeng, P., Guo, Z., Xiao, X., Peng, C., Liao, B., Zhou, H., and Gu, J. (2022). Facilitation of *Morus alba* L. intercropped with *Sedum alfredii* H. and *Arundo donax* L. on soil contaminated with potentially toxic metals. *Chemosphere* 290: 133107.
- Zhang, D., Jiang, Q.W., Liang, D.Y., Huang, S., and Liao, J. (2021). The potential application of giant reed (*Arundo donax*) in ecological remediation. *Front. Environ. Sci.* 9: 652367.
- Zheng, H., Sun, C., Hou, X., Wu, M., Yao, Y., and Li, F. (2018). Pyrolysis of *Arundo donax* L. to produce pyrolytic vinegar and its effect on the growth of dinoflagellate *Karenia brevis*. *Bioresour. Technol.* 247: 273–281.
- Zucaro, A., Forte, A., Faugno, S., Impagiazio, A., and Fierro, A. (2018). Effects of urea-fertilization rates on the environmental performance of giant reed lignocellulosic feedstock produced for biorefinery purpose. *J. Clean. Prod.* 172: 4200–4211.

6.2. USE OF GIANT REED (ARUNDO DONAX L.) FOR POLYMER COMPOSITES OBTAINING: A MAPPING REVIEW

P1

P2

P3

P4

P5

P6

P7

P8

P9

P10



Use of giant reed (*Arundo donax* L.) for polymer composites obtaining: a mapping review

Luis Suárez¹ · Zaida Ortega¹ ·
Mateusz Barczewski² · Eoin Cunningham³

Received: 28 December 2022 / Accepted: 31 March 2023 / Published online: 19 April 2023
© The Author(s) 2023

Abstract The massive biomass availability generated by the common giant reed (*Arundo donax* L.) motivates the research for its possible industrial use for high-added-value products through a biorefinery approach. The literature demonstrates the potential of common cane to obtain different high-value compounds, such as levulinic acid, oligosaccharides, fermentable sugars, highly digestible fiber for animal feed, polyphenols, and natural fibers for composite materials, among others. *Arundo* can also provide

valuable lignocellulosic fibers with an application as composite reinforcement, which is the aim of this review. The work is split into different sections: fiber obtaining, mainly done by mechanical procedures, fiber characterization (composition, thermal degradation, "mechanical properties", and crystallinity), and properties of composites with reed fiber. Most authors refer to producing board panels with insulating properties, followed by introducing reed fibers or ground materials in thermoset resins. Few papers focus on the production of thermoplastic composites with *Arundo*, which shows the opportunity for deepening research in this area. PRISMA flowchart has been followed to perform the literature review. Different sources have been used, and retrieved results have been combined to obtain the core studies assessed in this review, evaluating the options of using *Arundo* fibers to obtain polymer composites.

Supplementary Information The online version contains supplementary material available at <https://doi.org/10.1007/s10570-023-05176-x>.

L. Suárez
Departamento de Ingeniería Mecánica, Universidad de Las Palmas de Gran Canaria, Las Palmas de Gran Canaria, Spain

Z. Ortega (✉)
Departamento de Ingeniería de Procesos, Universidad de Las Palmas de Gran Canaria, Las Palmas de Gran Canaria, Spain
e-mail: zaida.ortega@ulpgc.es

M. Barczewski
Faculty of Mechanical Engineering, Institute of Materials Technology, Poznan University of Technology, Poznan, Poland

E. Cunningham
School of Mechanical and Aerospace Engineering, Queen's University Belfast, Stranmillis Road, Belfast BT9 5AH, UK

Keywords *Arundo donax* · Giant reed · Biomass · Fibers · Composites

Introduction

Certain plant species, such as *Arundo donax* L., also known as common cane, giant reed, or reed, have spread without control in many areas of the globe. Specifically, the giant reed is among the top 100 most dangerous invasive species in the world, according to the International Union for the

Conservation of Nature (Lowe et al. 2000), due to its rapid growth, pyrophyte nature, and contribution to the spread of fires. Of particular concern is the distribution of *Arundo* in the Mediterranean or subtropical climate areas, such as Algeria, Morocco, Brazil, France, Portugal, Spain, Italy, and Australia, among others (Jiménez-Ruiz et al. 2021). Despite its rapid growth and potential invasive character, this species is not included in Europe's list of invasive alien species of Union concern (European Union 2017).

Arundo donax L. is a perennial Grass from the *Gramineae* family. Despite its uncertain origin, due to the small size and the high number of chromosomes, many authors place it in East Asia (Jensen et al. 2018). Giant reed produces flowers, although its seeds are not usually viable, at least out of Asia (Jiménez-Ruiz et al. 2021). This plant reproduces through the rhizome or by producing roots on the nodes (Corno et al. 2014), which explains its rapid spread and poor genetic diversity (Pilu et al. 2014; Sicilia et al. 2020). Figure 1 shows some specimens of *Arundo* and the main parts of the plant: leaves and culms or stems.

Culms are hollow and have 2–3 cm diameters, reaching up to 6 m in height, with stem-clasping leaves along the entire stem (Csurhes 2016). The rapid growth of this species and its quick adaption to a wide range of environmental conditions have contributed to its great spread and naturalization, especially in Mediterranean countries (Lambertini 2019; Shtein et al. 2021). This plant species provides good yields (Scordia and Cosentino 2019) even under drought or high salinity (Sánchez et al.

2015; Licursi et al. 2018; Romero-Munar et al. 2018), pointing it as a promising source of lignocellulosic feedstock.

Several studies deal with using such plants from established crops, and the EU includes the reed as a relevant energy crop (Eurostat 2020). Its high biomass production explains the vast literature about optimizing the crop for its use in biorefineries (Copani et al. 2013; Cosentino et al. 2014, 2016), especially for bioethanol production and bioenergy (Accardi et al. 2015; Jensen et al. 2018). Reed has also gained attention for obtaining some biomolecules, such as furfural or levulinic acid, among others (Raspolli Galletti et al. 2013; Antonetti et al. 2015; Di Fidio et al. 2020). Other uses of *Arundo* have been investigated, such as paper and pulp (Shatalov and Pereira 2006; Raposo Oliveira Garcez et al. 2022) or biochar production (Ahmed 2016), or an absorbent material for oil spill recovery (Fiore et al. 2019; Piperopoulos et al. 2021). Some other uses for *Arundo* are found in the restoration of traditional architecture (Malheiro et al. 2021) and as an insulation material (Barreca et al. 2019). Its cultivation is also a strategy for soil bioremediation (Alshaal et al. 2015; Fernando et al. 2016), with the additional benefit of the biomass's ulterior valorization for obtaining methane or biochar.

Compared to the extensive research on biofuels and biomolecules, little attention has been paid to obtaining reed composites. This paper aims to comprehensively review *Arundo*'s potential for its exploitation as reinforcement or filler of polymer composites, including fiber extraction procedures and fiber and derived materials characterization.

Materials and methods

This literature review has assessed several papers related to *Arundo* and sustainable materials, with particular attention to polymer composites. Those studies related to the biorefinery processes for the production of green molecules have not been considered in the preparation of this manuscript. A first bibliographic search was performed using the Scopus search engine, combining the "keywords" in Table 1 plus the term "*Arundo*". The search performed using "*Arundo* OR (giant reed)" led to 1584 publications in Scopus and 1551 in Web of Science (WoS) in



Fig. 1 **a** *Arundo donax* L. aboveground parts of the plants. **b** culms and leaves separated

Table 1 Number of papers retrieved from Scopus and WoS search

Keywords	Scopus	WoS
Composite + fiber	92	46
Polymer + composite	85	20
Composite + characterization	99	24
Polymer + characterization	174	17
Fiber + characterization	230	32
Fiber + polymer	150	21
Composite + fiber + characterization	80	21

November 2022, while combining it with the different "keywords" listed below, reduced the results, as shown below:

The data from Scopus for the above "keywords" were downloaded and combined in an Excel file. After removing duplicates (same studies appearing in the different searches), a total of 292 studies result (Excel file attached as an online resource; tab "final studies"). The next step consisted of analyzing authors' "keywords" to remove those papers that, even appearing in the literature search, were not directly related to the work topic, that is, composites production with *Arundo*. The database created is also found in the already mentioned Excel file (tabs named "author keywords" and "author keywords refined", as obtained and after the refining). Some of the studies removed from the initial list are related to soil bioremediation, genomics, biosorption processes, cultivation, and energy production, among others. Some of these are still mentioned in this manuscript to settle the framework but are not studied in detail. From the authors' "keywords" refining, a final number of 48 papers remain, with 287 "keywords". A similar process was followed with the index "keywords" (those standardized by the search engine), retrieving 851 "keywords". These last "keywords" analysis was finally discarded because most of them are very vague and include terms such as "nonhuman", "plant", or "standard", among others (tab "index keywords"). So, the retrieved documents are finally those coming from the authors' "keywords" assessment (tab "final studies refined 2" in the excel file; the blank rows from the "final studies refined" tab have been removed in this sheet to make all studies more easily accessible).

A similar process was followed with the searches in WoS. In the end, after removing the duplicates, 67

studies arose from the total 182 retrieved, which, after refining, led to 25 documents. It is interesting to note the significant differences in the documents retrieval from both sources; apparently, Scopus provides a higher number of results, and both sources need a later step of refining to remove all those studies not directly related to the scope of the literature review. After the refining processes, the results of both searches were combined, leading to the same studies already selected from Scopus.

Figure 2 shows the number of publications in the last years, with different keyword combinations (plus the term "*Arundo*", not shown in the legend for clarity). The number of yearly publications (dash-line) shows a positive trend; these series refer only to the studies finally selected for the review. The continuous line provides a clearer picture of the publications per year, as it results from all the publications retrieved from the seven categories, excluding duplicates from the different searches. The figure also shows a distribution of the main author's "keywords" in the 48 papers, finally constituting the core of this research studies. When grouping all of them by similarity, it appears evident that *Arundo* is the most repeated word, with 16%. If this term is removed, as all papers contain it either in the "keywords" or in the "title" or "abstract", and following: "mechanical properties" is the most important term, followed by fibers, composite, and characterization, with 11% each one. It should be highlighted that in the graph, mechanical characterization includes mechanical, mechanics, tensile, flexural, stiffness, etc. Similarly, "composites" includes "composite", "polymer composite", or "natural fiber composite".

It is then clear that most retrieved papers focus on composites and particleboard obtaining and their mechanical characterization. At the same time, other terms such as treatments, sustainability, or curing behavior appear only residually.

Finally, as literature searches are highly dependent on the "keywords" used in the search itself and on authors' ones, as seen in Table 1, the online tool Inciteful XYZ (Literature connector) has been used to perform a final bibliographic search. This open-source tool produces graphs with connections among different papers related to a specific field, showing the relationships between various research studies dealing with *Arundo*'s use for composites. The tool also provides the most relevant papers in

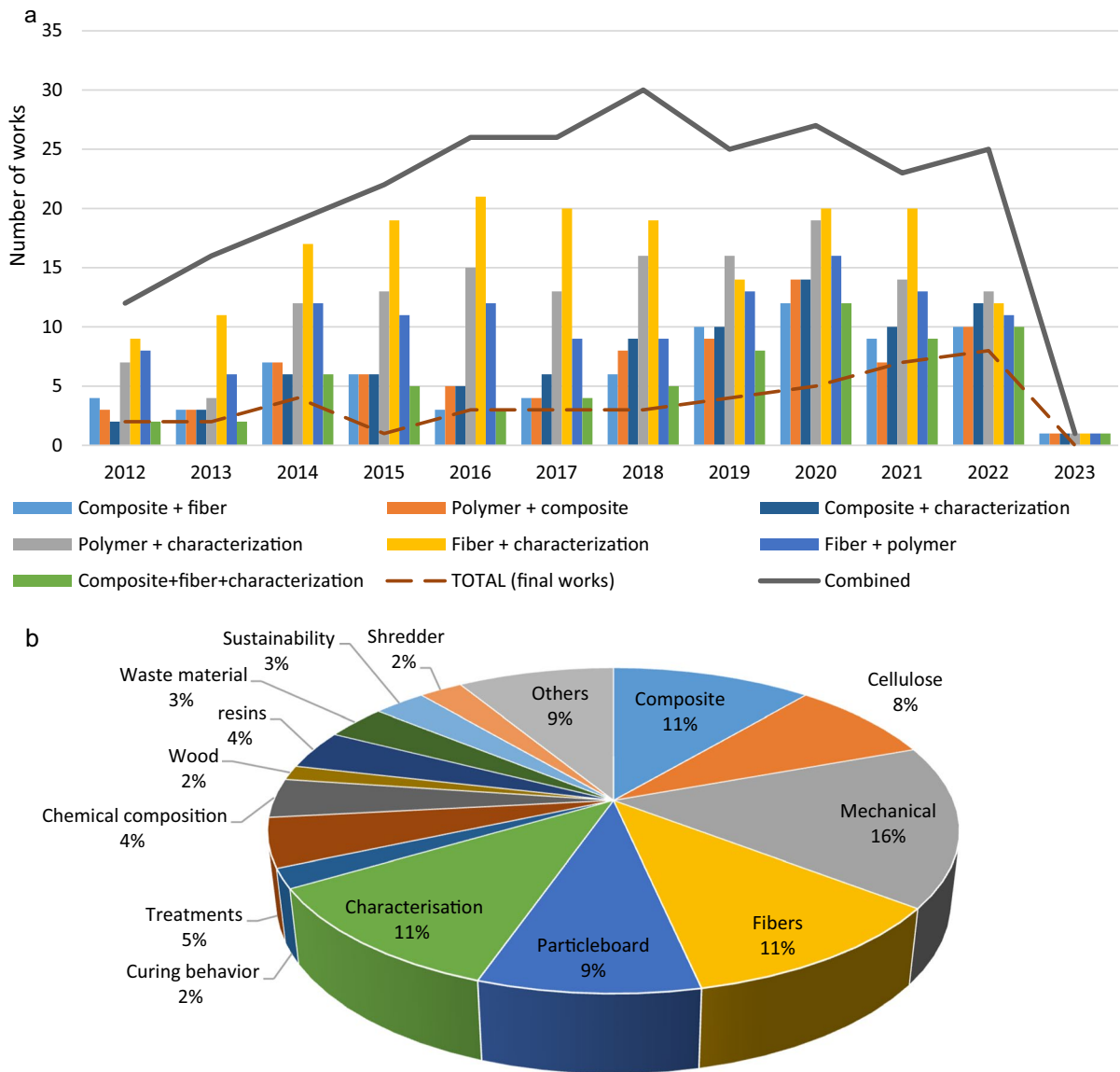


Fig. 2 **a** Evolution in the publication of papers using the words in Table 1 in the last 10 years. **b** Distribution of authors' "keywords" in the core papers of this review

the area, refining the search by the number of citations and closeness to the papers used as seeds (minimum of 5 to ensure the obtaining of relevant results), which in this case were the ones listed below:

- Characterization of a new natural fiber from *Arundo donax* L. as potential reinforcement of polymer composites: <https://doi.org/10.1016/j.carbpol.2014.02.016>
- Valorization of Invasive Plants from Macaronesia as Filler Materials in the Production of Natural Fiber Composites by Rotational Molding: <https://doi.org/10.3390/polym13132220>
- Effect of plasma treatment on the properties of *Arundo donax* L. leaf fibres and its bio-based epoxy composites: A preliminary study: <https://doi.org/10.1016/J.COMPOSITESB.2016.03.053>
- Characterization of raw and treated *Arundo donax* L. cellulosic fibers and their effect on the cur-

ing kinetics of bisphenol A-based benzoxazine: <https://doi.org/10.1016/j.ijbiomac.2020.08.179>

- Environmental Hazards of Giant Reed (*Arundo donax* L.) in the Macaronesia Region and Its Characterisation as a Potential Source for the Production of Natural Fibre Composites: <https://doi.org/10.3390/polym13132101>
- The manufacture of particleboards using mixture of reed (surface layer) and commercial species (middle layer): <https://doi.org/10.1007/s00107-010-0437-7>
- Characterization of Fibers from Culms and Leaves of *Arundo donax* L. (Poaceae) for Handmade Paper Production: <https://doi.org/10.1080/15440478.2022.2076005>

The software also provides a list of the most relevant papers in the field, ranging by PageRank (number of citations), similar papers (biased by publication data), and most important recent papers, combining the number of citations, field relevance, and publication date. This list was compared to that obtained from the Scopus and WoS searches. Again, not all references retrieved directly relate to the topic assessed but focus instead on other types of fibers. In any case, this is an interesting tool for the very first stages of research. After comparing the documents from this search with the ones obtained from WoS and Scopus, any new references were included. Finally, a total of 83 studies were referenced during the preparation of this manuscript. Figure 3 summarizes all the processes, following the flow chart established by PRISMA (Preferred Reporting Items for Systematic Reviews and Meta-Analyses).

Fibers obtained from giant reed

The methods for obtaining giant reed fibers are mechanical, chemical, or a combination of both.

Mechanical procedures are the most extended ones in the literature. Most authors process the lignocellulosic material by chopping and grinding it, using the resulting material for obtaining the composites (Fiore et al. 2014c, a; Bessa et al. 2020, 2021b). Several authors also used this approach for particleboard production (García-Ortuño et al. 2011; Ferrández-García et al. 2012; Andreu-Rodríguez et al. 2013; Ramos et al. 2018; Barreca et al. 2019; Ferrández-García

et al. 2019; Ferrández Villena et al. 2020b, a; Ferrández-García et al. 2020). Other authors focused on using bast fibers obtained with a scalpel and a brush (Fiore et al. 2014a; Scalici et al. 2016). Other authors proposed using chemical methods to get cellulosic fibers with different applications. For example, Shatalov and Pereira (2013) conducted a first hydrolysis to remove hemicellulose and lignin, producing a cellulose pulp with around 94% α -cellulose. Tarchoun et al. (2019) followed a completely chlorine-free approach to get microcrystalline cellulose with up to 80% crystallinity. Barana et al. (2016) have proposed a sequential method for obtaining lignin, hemicellulose, and cellulose nanocrystals, using a chemical procedure consisting of an alkaline treatment followed by bleaching and acid hydrolysis. These authors recovered around 50% of the cellulose, hemicellulose, and lignin. Martínez-Sanz et al. (2018) have prepared lignocellulosic films by selective removal of lignin and hemicellulose by a similar chemical method. The films, especially those obtained after hemicellulose removal, showed good mechanical and water barrier properties and high transparency, comparable to those for thermoplastic starch, making them interesting for the packaging industry.

Similarly, Pinto and collaborators (2015) have proposed pulping *Arundo* stalks in an alkali solution at a moderate temperature (160 °C) to obtain cellulose pulp. The lignin from the black liquor (about 100 g lignin/kg of dry matter) was also recovered, allowing further valorization.

Finally, Suárez et al. have developed a lab-scale procedure based on a series of rolling mills to open the reed culms and separate the fibrous material from the softer one (Suárez et al. 2021, 2022b; Ortega et al. 2021). Finer fibers with higher cellulose content (about 67%) and good "mechanical properties" (Suárez et al. 2022a) can be obtained by combining chemical soaking in a NaOH solution and mechanical processing.

Fiber characterization

Table 2 summarizes the main composition and properties of *Arundo* fibers reported in the literature for composite applications. There is a considerable dispersion of data for the chemical composition from the different published studies, which can be attributed

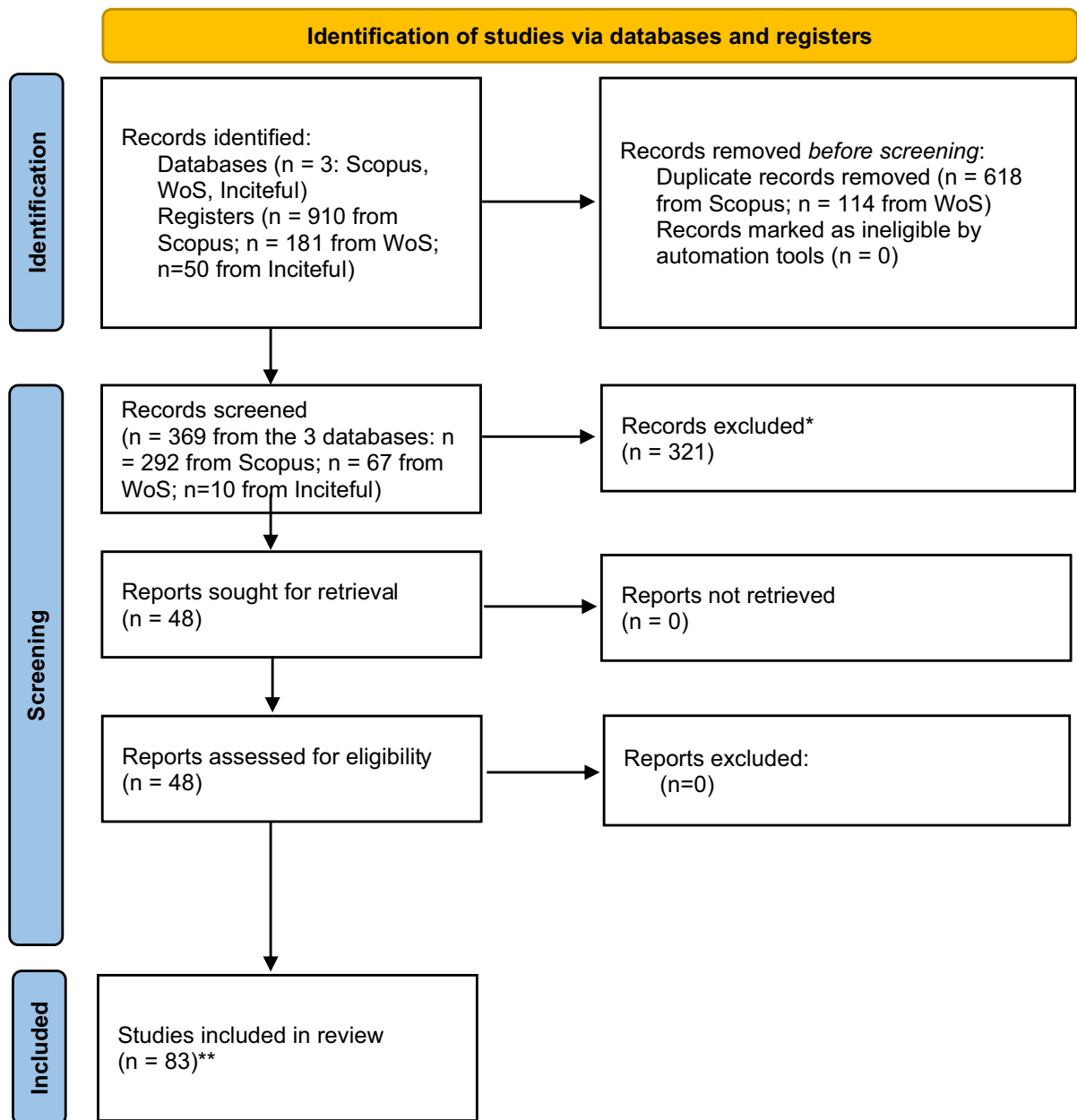


Fig. 3 Flowchart following PRISMA guidelines followed for the literature review

to the reed processing for fiber obtaining. Most studies have been performed with a mechanical procedure and show higher lignin content (17–24%) than those fibers obtained by combining a chemical and mechanical process (5.3%). Only some authors have calculated the density of the fibers, obtaining higher values for those fibers with higher cellulose content; other authors have also found a positive correlation

between the cellulose content of a fiber and its density (Charca et al. 2021; Suárez et al. 2022a). Reed fibers obtained by simple mechanical procedures show about 35–45% cellulose, while those obtained by combining chemical and mechanical operations have an increased cellulose content, almost reaching 70%. Fibers commonly used in composites show a wide range of compositions, with cellulose contents

Table 2 Properties of fibers obtained from giant reed for composites application

Material	Procedure	Composition		Density (g/cm ³)	Degradation temperature ^A (°C)	Tensile strength (MPa)	Elastic modulus (GPa)	Crystallinity index (%)	References
		Klason Lignin (%)	Cellulose (%)	Hemicellulose (%)					
Stems fibers	Rolling mill	24.1 ± 1.4	45.2 ± 3.0	35.1 ± 2.8	233.3 ± 5.7	–	–	–	Suárez et al. (2021)
	Manual decortication + scalpel	17.2	43.2	20.5	115 (275) ^B	248	9.4	–	Fiore et al. (2014b)
	Chemical soaking + mechanical	5.3 ± 0.1	67.5 ± 1.9	15.3 ± 4.6	237.8 (273) ^C	905 ± 300	45 ± 12	66.7	Suárez et al. (2022a)
	Milling	24.9 ± 0.3	38.0 ± 3.7	42.4 ± 1.3	226.9 (264) ^C	–	–	59.1	Suárez et al. (2022a)
	Milling	19.8	35.5	26.8	110 (267) ^B	–	–	49.9	Bessa et al. (2020)
Leaves fibers	Cutting	–	–	–	–	133.9 ± 0.3	3.5 ± 0.0	–	Manniello et al. (2022a)
	Combing with a metal brush	–	–	–	130 (210) ^B	174 ± 146	16 ± 12	–	Scalici et al. (2016)
	Chemical soaking	0.8 ± 0.1	68.8 ± 4.3	20.0 ± 3.8	175.9 (280) ^C	1000 ± 500	39 ± 25	73.1	Suárez et al. (2022a)

^ATemperature for 5% weight loss^BMoisture (authors report onset degradation temperature placed in brackets)^CMoisture (10% weight loss temperature in brackets)

from $\approx 40\%$ for the wheat straw to 85% for ramie or over 70% for kenaf, flax, or hemp (Henrique et al. 2015). The literature shows a clear linear relationship between cellulose content and crystallinity index for cotton (Oh et al. 2005; Kim et al. 2018; Abidi and Manike 2018), as also happening in the few papers providing these values for *Arundo* fibers.

Thermal degradation temperatures of fibers obtained from giant reed are in the same range in the different studies, with temperatures above 230 °C, which confirms their suitability for polymer composites production, including thermoplastic and thermoset matrices. These are also in the same range as other commonly used vegetal fibers, such as flax or jute (Fiore et al. 2014b), banana, abaca (Ortega et al. 2013), or hemp (Kabir et al. 2012). The dominant mechanism occurring during the thermal degradation of biomass is diffusion-based phenomena (Ornaghi et al. 2020), mainly attributed in the first stages to cellulose and hemicellulose degradation. Their mutual ratio in the total share of the cellulose fraction, the extractive low molecular weight compounds, and the moisture in the fibers directly affect the material degradation onset temperatures. It is observed in the table that some authors reported lower degradation temperatures due to humidity evaporation, which increased if considered 10% weight loss instead of 5%.

The highest differences among the various studies are observed for the "mechanical properties" of the fibers; this is attributed, again, to the different processing of the biomass. The thick bast fibers have a less homogenous surface than the thinner ones, which can significantly influence the final values obtained (as cross-sections can also have considerable variations). From Table 2, it is observed that those fibers with higher cellulose content also provide better "mechanical properties". In particular, culm reed fibers obtained by combining chemical and mechanical procedures offered a tensile strength of 900 MPa, with an elastic modulus of 45 GPa, in the range of other lignocellulose fibers commonly used in the composites sector. For instance, kenaf fibers provided tensile strength close to 600 MPa (Wang et al. 2016), jute of about 300 MPa and 13 GPa of elastic modulus (Barreto et al. 2010), flax of about 1400 MPa and 58 GPa (Zhu et al. 2013), and bamboo 140–230 MPa and 11–17 GPa (Yu et al. 2022). Values reported in the literature for the mechanical behavior of other fibers are also highly variable (Table 3) due to the assay's

sensitivity to the geometry of the single fiber (a circular section is usually assumed, although it is not always accurate) and the different testing conditions.

Table 3 summarizes some of the properties for different lignocellulose fibers to provide a clear comparison of properties. As observed, cellulose content varies from around 30% for bamboo and jute to 80% for *agave americana*, flax or sisal. *Arundo* fibers provide a cellulose content close to 70%, when extracted by the combined chemical and mechanical procedure, thus in the range of other fibers commonly used for composites obtaining, which is also observed for "mechanical properties". From this summary, the relationship between cellulose content and crystallinity index is patent. As already mentioned, there is a wide variation in such properties, which is due not only to the natural origin of the fibers, but also to their irregularities in shape and diameter. Fibers from giant reed exhibit a mechanical behavior also comparable to other lignocellulose fibers, such as jute, flax, abaca or sisal. Crystallinity index for *Arundo* fibers is close to sisal and abaca, higher than jute, banana or kenaf, although lower than flax.

The potential of *Arundo* for composite reinforcement is clear, as reported by several authors, but also when comparing the results with other widely used vegetal fibers. Lignocellulose fibers are considered, in general terms, as a sustainable alternative for composites production. However, the need of resources for their cultivation needs also to be considered; water, fertilizers and soil use together with extraction and treatment processes should be taken into account when analyzing the impact of such materials in the environment and their economic profitability. An alternative to reduce costs and environment impact is the use of vegetal residues or by-products. In this sense, various materials have been proposed in the literature, from wood dust, spent buckwheat, rice and wheat straw, or banana fibers. A different option is the use of biomass with a rapid growth and low requirements, which is the case of *Arundo donax* (Licursi et al. 2018; Scordia and Cosentino 2019). The rapid growth of this plant and its ability to proliferate even under severe droughts makes its use particularly interesting for the production of green compounds and products in the context of a biorefinery.

Arundo donax is not, for the moment, a commercial crop, although some experimental plantations have been studied, mainly in Italy. However, there is

Table 3 Summary of properties for different lignocellulose fibers

Fiber	Cellulose (%)	Density (g/cm ³)	Degradation temperature (°C)	Tensile strength (MPa)	Elastic modulus (GPa)	Diameter (μm)	Crystallinity (%)	References
<i>Agave americana</i>	61–80	1.3–1.4	210–290	640–1200	2–9	100–150	–	Charca et al. (2021), Ortega et al. (2019), Hulle et al. (2015)
<i>Arundo donax</i>	43–68	1.2–1.6	273–275	248–905	9–45	157	66.7	Fiore et al. (2014b), Suárez et al. (2022a)
Jute	33–72	1.3–1.5	218–330	300–860	13–27	–	55–58	Barreto et al. (2010), Fiore et al. (2014b), Henrique et al. (2015), Yu et al. (2022); Zhu et al. (2013)
Flax	71–81	1.4–1.5	210–282	345–1454	28–68	10–80	86.1	Fiore et al. (2014b), Henrique et al. (2015), Ortega et al. (2013), Wang et al. (2016), Zhu et al. (2013)
Sisal	66–78	1.5	302	511–635	9–22	–	72	Barreto et al. (2010), Fiore et al. (2014b), Henrique et al. (2015), Ortega et al. (2013)
Banana	60–65	1.5	270	230–1032	34–37	180	39	Barreto et al. (2010), Henrique et al. (2015), Ortega et al. (2013)

Table 3 (continued)

Fiber	Cellulose (%)	Density (g/cm ³)	Degradation temperature (°C)	Tensile strength (MPa)	Elastic modulus (GPa)	Diameter (μm)	Crystallinity (%)	References
Abaca	56–63	1.5	273	400–700	12–24	381	69	Henrique et al. (2015), Ortega et al. (2013), Yu et al. (2022)
Kenaf	61–72	1.2	–	240–627	14–53	–	41–48	Barreto et al. (2010), Wang et al. (2016), Zhu et al. (2013)

extensive literature focusing on its use as raw material due to the high biomass production rates exhibited by this plant, even when grown on exhausted or polluted soils with low quality waters. Some studies signal this plant as with great potential to reduce the soil degradation and loss, especially in the Mediterranean basin, where an extreme danger of soil loss exists (Ferreira et al. 2022). Some authors have performed a life cycle assessment to compare the environmental performance of *Arundo*, determining a better environmental behavior than other crops such as maize-wheat or sorghum (Dragoni et al. 2015; Sallustio et al. 2022). However, no studies on the environmental performance of giant reed for fiber obtained have been found during the literature review performed. In any case, the studies analysing the potential impacts of *Arundo* cultivation conclude that positive environmental and economic results can be obtained, especially when using low-quality waters and marginal soils. Considering a biorefinery scheme for the production of valuable chemical compounds (such as levulinic or lactic acid, furfural, or polyphenols), the obtaining of fibers (with high cellulose content) would be a further step in the valorization of this lignocellulose material, which would not only come from a residue, but also from a low-impact crop.

In summary, *Arundo* fibers can be used in composites production, as their performance is similar to other conventionally and commercial used fibers, with the advantage of having a potential lower impact, if a good cultivation and planning is performed. Good

management practices need to be ensured in order to contribute to the achievement of sustainable development goals (SDG) and reduce the risks associated to its potential invasive character. *Arundo* has the advantage of being highly resistant to pathogens and changing weather conditions, and is of perennial nature and distributed worldwide, which means that its production can take place through the year and is not accumulated in a particular season.

Giant reed as filler/reinforcement of composite materials

The studies about obtaining composites with giant reed are limited and mainly focus on particleboard production (García-Ortuño et al. 2011; Ferrández-García et al. 2012; Andreu-Rodríguez et al. 2013; Barreca et al. 2019; Ferrández-García et al. 2019; Ferrández Villena et al. 2020b; Ferrández-García et al. 2020). Those studies on composites production use shredded vegetal material (Fiore et al. 2014c, a; Bessa et al. 2020, 2021b), bast fibers obtained by combing with a teeth brush (Fiore et al. 2014b; Scalici et al. 2016), or rudimentary mechanical procedures (Suárez et al. 2021, 2022b; Ortega et al. 2021), as summarized in Table 2. This section shows the conditions and properties found in the literature for composites with *Arundo*-derived materials for particleboard production, thermoset, and thermoplastic composites.

Other authors have focused on using these fibers for building materials. These are not within the scope of this paper and so are only referenced here very briefly to show the potential of *Arundo* fibers for various applications. For example, Maniello et al. (2022a, 2022b) studied the influence of *Arundo* fibers aspect ratio in the mechanical behavior of concrete blocks, finding improvements in tensile strength and Young's modulus for 1% loaded blocks and a high positive correlation between fiber length and tensile modulus. Using reed in a plaster matrix also improved over 100% of the flexural strength of bricks (Martínez Gabarrón et al. 2014); flexural toughness can also be doubled with such fibers (Badagliacco et al. 2020). Similarly, Ismail and Jaeel (2014) proposed using up to 12.5% ash and giant reed fibers to replace sand in concrete mixes partially. The compressive strength increased by nearly 8% when adding 7.5% giant reed ashes and 2.5% for the same load of reed fibers. Finally, using *Arundo* fibers at 0.75% decreased the moisture susceptibility of asphalts while increasing the tensile strength ratio, obtaining an asphalt pavement that accomplishes with standards (Sargin Karahancer et al. 2016).

Particleboards obtaining

Regarding boards' production, Ghalehno et al. (2010) used ground material at 20–40% by weight in a urea–formaldehyde resin, obtaining a composite material, by compression molding, with better "mechanical properties" than the resin, although using wood fibers as core material (Table 4). Baquero Basto et al. (2018) incorporated 30–40% of ground reed fiber into a vegetable polyurethane resin, improving the rigidity and tensile strength of the resin, although with a decrease in flexural properties. Ferrández-García and collaborators (2019), on the other hand, obtained a composite material using only cane plant material and citric acid as a natural binder. The stems were ground to 2 mm, and 5–10% citric acid was added along with another 10% water; the boards were obtained by compressing the mixture at 150 °C and 1.7 to 2.5 MPa for 7 min. The boards obtained have mechanical and thermal properties good enough to be used as insulating materials in construction. These same authors also produced a composite material using urea–formaldehyde resin as a matrix and ground reed in three different sizes,

Table 4 Particleboards produced with *Arundo* and properties (MOR: modulus of rupture; MOE: modulus of elasticity)

Material	Binder*	Conditions	Properties		References
			Density (kg/m ³)	Mechanical (N/mm ²)	
Ground rhizomes	None (water, 15%)	110 °C 2.5 MPa 7–15 min	700–900	MOR: 5–15 MOE: 700–2000	Ferrández Villena et al. (2020b)
Milled culms	Starch (5 and 10%)	110 °C 2.6 MPa 15 min	800–900	MOR: 7–16 MOE: 600–2500	Ferrández-García et al. (2012)
Milled culms	Citric acid (5 and 10%)	110 °C 2.6 MPa 7 min	600–850	MOR: 2–12 MOE: 260–2440	Ferrández-García et al. (2019)
Milled culms	Urea–formaldehyde (20%)	180 °C 3.3 MPa 15 min	460–600	MOR: 3.7–10 MOE: 970–1360	Flores et al. (2011)
Milled culms	Urea–formaldehyde (8%)	120 °C 2.6–3.5 MPa 4–6 min	628–820	MOR: 10.0–17.7 MOE: 1190–3025	García-Ortuño et al. (2011; Ferrández-García et al. 2020)
Cellulose microfibrers from milled culms	Urea–formaldehyde (90–95%)	190 °C 23 MPa 7 min	642–680	MOR: 14–21 MOE: 2846–3246	Ait Benhamou et al. (2022)
Milled culms	Phenol formaldehyde (8–20%)	3; 25 MPa	–	MOE: 1200–2000; 1900–3400	Flores-Yepes et al. (2012)

*Percentages of the binder relate to the *Arundo* material

obtaining good acoustic insulation results (Ferrández-García et al. 2020). These studies have found that lignocellulosic material from *Arundo* is suitable for producing medium-density boards with applications in indoor furniture and acoustic or insulating panels.

Composites with thermoset materials

Table 5 summarizes different combinations used in the literature with *Arundo* fibers. To get a clearer idea of the results obtained, the "mechanical properties" for the best formulations prepared in each work are given as the percentage of increase (or decrease) regarding the neat matrix.

Scalici and collaborators (2016) obtained composites using a biobased epoxy resin, using fibers from leaves at 2.5 and 5% with 1 and 3 cm length, by manual lay-up and compression molding at 1 kPa and 25°C for 7 days. These authors found that plasma treatment of fibers provided a better

adhesion between the fibers and the resin, due to the appearance of functional groups (C–O–C and C–OH) which, together with the changes in morphology, provided a higher anchorage between both materials.

The obtained composites showed improved flexural modulus, regardless of the fiber size, ratio, and treatment, while strength was only enhanced for samples with treated fibers. The best properties are obtained for treated 3 cm-length fibers at 5%, with an increase of 80% in flexural modulus and 38% in flexural strength. Similar results are obtained for the composites with 2.5% fiber. It then appears that plasma treatment is more significant than the ratio of fiber used. The damping factor ($\tan \delta$) decreased for plasma-treated fiber composites, and the glass transition temperature also shifted to higher values, showing improved bending between both materials. This effect was also confirmed by SEM observation of breakage sections, where no pull-out was observed.

Table 5 Composites providing the best results when using *Arundo* and thermoset and thermoplastic resins from different studies (E: elastic modulus, σ : strength)

Matrix	Fiber	Processing	Fiber length	Ratio (w/w %)	Variation (%)		References
					Tensile	Flexural	
Epoxy	Leaves fibers	Plasma treated (150 W, 120 s)	3 cm	5%	–	E: + 80 σ : + 38	Scalici et al. (2016)
Epoxy	Ground stems	Untreated	150–300 μm	10%	E: + 40 σ : -38	E: + 15 σ : -35	Fiore et al. (2014c)
Polyester (thermoset)	Ground stems	NaOH 6% w/w, room T, 24 h, solution/fiber: 1:25 w/w	18–25 mm	$\approx 10\%$ (40%v/v)	E: + 22 σ : + 57	E: + 36 σ : + 45	Chikouche et al. (2015)
PLA	Ground stems	Injection molding; untreated fibers	300–500 μm^A	20%	E: + 40 σ : -26	E: + 45 σ : -20	Fiore et al. (2014a)
PE	Fiber bundles; rolling mill	Compression molding; untreated fibers	75–500 μm^A	40%	E: + 49 σ : -42	E: + 170 σ : 0	Suárez et al. (2021)
PP	Fiber bundles; rolling mill	Compression molding; untreated fibers	75–500 μm^A	40%	E: + 38 σ : -48	E: + 74 σ : -30	Suárez et al. (2021)
PE	Fiber bundles; rolling mill	Rotational molding; untreated ground fibers	> 250 μm^A	20%	E: 0 σ : -25	E: 0 σ : -37	Ortega et al. (2021)
PE	Fiber bundles; rolling mill	Rotational molding; untreated ground fibers	3–4 mm	10%	E: + 43 σ : -17	E: 0 σ : 0	Suárez et al. (2022b)
PLA	Fiber bundles; rolling mill	Rotational molding; untreated ground fibers	3–4 mm	10%	E: 0 σ : 0	E: + 423 σ : -42	Suárez et al. (2022b)

^AMesh size

Fiore and collaborators (2014c) also prepared epoxy-based composites with ground *Arundo* stems at 5, 10, and 15%, separating the fractions by size: lower than 150 μm , 150–300 μm , 300–500 μm , and 0.5 to 2 mm. The bigger particles were not used for high loadings (over 10%) due to the high viscosity of the mix with the resin, making it impossible to cast. These authors found an increase in voids content when increasing the amount of lignocellulosic material; particle size also seems to have this effect, although to a lower extent (an increase in length leads to a slight rise in voids content). Tensile or flexural elastic modules are unaffected by the particle size. The tensile modulus is increased significantly for composites, with a higher rise for 10% composites, while flexural modules are similar regardless of the amount of fiber used. Similarly, tensile and flexural strength is reduced when *Arundo* particles are introduced within the epoxy resin due to the lack of compatibility between both materials; the higher the filler size, the more drastic reductions. Using over 10% of fibers leads to more significant reductions in strength, related to the appearance of voids and poor interaction between the resin and the fibers. In particular, the use of 15% filler led to porosity values close to 5% (almost double than for 10%-loaded composites), which results in a reduction of tensile modulus from the 2.95 GPa for the 10% composite to 2.82 GPa, which can be considered as no significant, although also reducing the tensile strength in more than a 30% (from the 41 MPa for 10% *Arundo* composite to 30 MPa for the 15% one). Glass transition temperature or dynamic "mechanical properties" were not observed for composites compared to the neat matrix. However, the incorporation of the reed results in a slightly improved storage modulus in the rubbery state (over glass transition temperature, placed around 70 °C).

Chikouche et al. (2015) proposed using a simple NaOH treatment before introducing the fibers into a polyester matrix, varying the NaOH solution concentration from 2 to 8%. They prepared composites with 40% (in volume) of filler (about 10% in weight), finding improvements in tensile and flexural properties for all formulations. The treatment increases the mechanical behavior of the composites with increasing concentration of the soda solution, with a maximum at 6%; further increases

result in lowering of the tensile and flexural strength of the composite, while maintaining the elastic modulus. An excess of alkali result in fiber weakening, which affects the final performance of the composite. Besides, it is important to emphasize the need of residual alkali neutralization to avoid fiber or matrix degradation.

Finally, Bessa and collaborators (2020, 2021a, 2021b) studied the influence of giant reed fibers on the properties of bisphenol A aniline-based polybenzoxazine composites, including not only composites' properties but also curing kinetics. First, different pretreatments were applied to the fibers (NaOH 5%, aminopropyl-trimethoxysilane 5%, or a combination of both, for 3 h at room temperature) and then introduced in a 25% w/w in the matrix (Bessa et al. 2020). They found a maximum decrease of 10% in activation energy for the resin curing for silane-treated fibers. In later research, these authors processed the *Arundo* ground culms to isolate the microcrystalline cellulose and also introduced it in the same matrix at different ratios: 5, 10, 15, and 20% in weight. They found that introducing such fibers increased the polymer glass transition temperature. The optimum loading was 15%, which resulted in a reduction of 10% in the activation energy for the resin curing (Bessa et al. 2021a). So, introducing lignocellulosic fibers from *Arundo* seems to positively influence the cross-linking of this bisphenol A-based resin.

Regarding the mechanical behavior of such composites, these authors also studied the influence of introducing 5, 10, and 15% fibers treated with NaOH, silane, or their combination, as in their previous work (Bessa et al. 2020). They found significant increases in glass transition temperature with increased fiber content and reduced damping factor values, especially for silanized fibers (Bessa et al. 2021b). Storage modulus increased for all composites, higher for higher loadings, and more significantly for alkali-silane-treated fibers, thus demonstrating a higher compatibility between fiber and matrix. For this treatment, glass transition temperature increased in almost 30 °C (from 188 °C for the neat resin to 217 °C), while storage modulus was increased in over 100% in the glass region, increasing from the about 2 GPa for the bisphenol-A resin to almost 3.5 GPa for the 25% silane treated fiber.

Composites with thermoplastic materials

Fiore et al. (2014a) obtained a composite material with a PLA matrix, using the ground stems as reinforcement material, at a 10 and 20% ratio, by injection molding. These authors concluded that as the reed content increased, the tensile and flexural elastic modules also increased, while the tensile and flexural strength decreased. This study found that the fiber content is more significant than the fiber length in the final properties of the composite, at least for the two fractions of ground material used (150–300 μm and 300–500 μm). Reed fibers have also been introduced in polyethylene (PE) and polypropylene (PP) matrices under compression molding (Suárez et al. 2021) in ratios of up to 40% by weight. These authors found a drastic decrease in impact properties, especially for all PP composites and for PE for 30 and 40% loadings. As observed in other studies, elastic modulus rises, and tensile strength decreases when increasing the filler ratio, although without significantly affecting flexural strength for PE. The improvements for the PP matrix are more discrete, probably due to the low processing temperature used.

Finally, the literature has also explored the rotational molding of PE and PLA with *Arundo*-derived materials. Up to 20% of fibers were introduced in PE at different particle sizes: lower than 75, 75–125, 125–250, and higher than 250 μm (Ortega et al. 2021), finding decreases in tensile strength and elastic modulus for the smaller particles. Impact strength is reduced for all composites, as otherwise expected from rotomolded samples. Only the composites with larger particle size provide a similar modulus to the used PE. The specificities of this processing method, where no pressure is applied, and the lack of compatibility between the fibers and the matrix explain the poor results obtained.

Longer fibers (3–4 mm length) at 5 and 10% loadings provided no significant differences in rotomolded PE parts (except for impact strength). In contrast, impact and flexural properties are reduced for PLA-based composites (Suárez et al. 2022b). These authors have treated the fibers with a NaOH solution 1 N (40 g/l), getting fibers with increased thermal stability without any change in the "mechanical properties" of the composites. Despite the relatively poor mechanical behavior obtained for PLA composites, incorporating *Arundo* fibers results in a higher degradation

in a biodegradation assay, observed the reduction in melting and glass transition temperature after the assay. The fibers' hydrophilic character increases the composite's moisture uptake and accelerates the PLA chains' hydrolysis.

An analysis on the properties of *Arundo*-PE based composites show that tensile strength is reduced with the increase ratio of fiber, regardless the process used (compression or rotational molding). In contrast, elastic modulus tend to increase with the amount of lignocellulose fiber (Table 6). All these studies were performed by dry blending the materials in the composite before its processing (PE powder and the *Arundo* materials). That is, no melt-blending was performed, as commonly performed for injection-molded samples, for the production of compression or rotationally molded composites. Flexural properties respond more favorably to the introduction of the fibers, with lighter or no reductions in strength and higher increases in flexural modulus, reaching more than double of the value for the neat polymer. The behavior shown by giant reed composites is similar to those obtained with other lignocellulose materials. For example, rotomolded composites with 10% of agave (López-Bañuelos et al. 2012) or 10% of abaca or banana fibers (Ortega et al. 2013) shown a flexural elastic modulus of around 600 MPa (about two times higher than for neat PE). These composites also exhibited reductions of 30–50% in tensile strength, while elastic modulus was almost folded by two. Finally, regarding impact behavior, it is well-accepted that this property is greatly affected by the incorporation of any foreign material, due to the particularities of rotomolding, where no pressure is applied.

The research performed to date on giant reed have not incorporated any compatibilizer for the composites preparation, and only NaOH-treatments were applied, although not particular differences were found in the behavior of the composites, despite the increase in the thermal stability of the fibers. A deeper study on the surface modification of *Arundo* fibers, the changes in the topography of fibers, and its influence in the final behavior of the composite is an interesting path to explore in future research. *Arundo* fibers provide good features, comparable to other commercial fibers, and are obtained from a plant with a promising future due to its high growth rates, low requirements and potential as biorefinery's feedstock. The lifecycle assessment (LCA) of *Arundo* crops for

Table 6 "mechanical properties" of *Arundo*-PE composites

Processing	Fiber length	Ratio (w/w %)	Tensile strength (MPa)	Tensile modulus (MPa)	Flexural strength (MPa)	Flexural modulus (MPa)	Impact strength (kJ/m ²)	References
Rotational molding; untreated fibers	3–4 mm	0	16	380	19	620	19	Suárez et al. (2022b)
		5	13	470	18	670	15	
		10	11	490	18	800	12	
Rotational molding; 1N NaOH treated fibers	3–4 mm	0	16	380	19	620	19	
		5	13	540	18	700	15	
		10	12	500	17	740	10	
Rotational molding; untreated fibers	> 250 µm ^A	0	16	400	18	650	18	Ortega et al. (2021)
		20	12	400	13	650	8	
Compression molding; untreated fibers	75–500 µm ^A	0	16	600	19	630	16	Suárez et al. (2021)
		10	13	700	20	750	14	
		20	11	850	21	1400	12	
		30	11	850	20	1700	7	
		40	9	900	18	1700	6	
Compression molding; 1N NaOH-treated fibers	75–500 µm ^A	0	16	600	19	630	16	
		10	10	700	19	750	15	
		20	12	700	19	900	9	
		30	8	760	18	1500	6	
		40	8	800	16	1500	6	

^AMesh size

bioenergy production have shown a positive behavior, while the LCA of reed-composite materials have not yet been investigated, which gives further options for further investigation.

Potential new functionalities of giant reed as active composite fillers

Several research papers describe the possibility of valorization of the giant reed as a valuable source of biomass and fibers and underline the possibility of obtaining extracts and valuable chemical products.

The contained extracts and low-molecular-weight volatile compounds may be a source of compounds with additional impact on the polymeric matrix when using lignocellulosic products with low processing levels, resulting in new functional properties of composites manufactured with their use. To date, the possibility of getting additional functional features of composites produced with *Arundo donax* has not yet been investigated in the literature; however, the promising results of research already carried out for the plant raw material require consideration. Wang et al. (2011) demonstrated the possibility of extracting

volatile oils with allelopathic activity. The extracted allelochemicals revealed an inhibitory effect on *M. aeruginosa*, the most common toxic cyanobacterial bloom in eutrophic freshwater sources. In the case of the production of thermoplastic composites intended for outdoor exposure, the desired feature is not only the improvement of their performance but also increased resistance to weathering conditions (water absorption and resistance to UV radiation). Girotto et al. (2021) demonstrated that the leaves of *Arundo donax* contain compounds with antioxidant properties, including phenolic compounds and terpenes.

Moreover, the rhizome also includes phytochemicals with antimicrobial activity (Pansuksan et al. 2020). Considering the possibility of migration of low-molecular compounds from extracts or oils reported for other plant-based residues used as polymeric composite fillers (Barczewski et al. 2018; Van Schoors et al. 2018), one can assume that *Arundo donax* fibers could also provide antioxidant or stabilization features to the polymer matrices, increasing processing range and improving aging behavior. This is an exciting path to explore in future research on lignocellulosic-derived composites.

Conclusions

The extensive literature published on this topic shows a high interest in using giant reed for several purposes in the industrial environment. The abundant biomass generated by this plant, its fast-growing rate, and the low inputs needed for its cultivation have made several authors signal *Arundo* as a promising source of lignocellulosic biomass. Most research focuses on using this plant for a biorefinery context and producing energy or chemical products, although obtaining fibers for several uses is also proposed.

An exciting strategy to maximize the environmental and economic benefits of lignocellulosic materials used within industrial applications is the cascade process, where the different fractions of the material (simplified to cellulose, hemicellulose, and lignin) could be separated and used. One such approach involves obtaining natural fibers with high cellulose content and valorizing the remaining fractions for other purposes. Further studies are required to determine the environmental, economic, and social impacts of *Arundo* cultivation and use, as for most

natural fibers. Such studies should assess the crop performance and obtain the lignocellulosic biomass from residual materials. The lifecycle analysis of such materials should include the processing for fibers production (including their treatment) and the later composite performance (durability, recyclability, or biodegradability). In this sense, it should be highlighted that *Arundo donax* L. shows high resistance to salinity, droughts, and pathogens, which makes it possible to grow it in marginal or degraded soils and with low-quality waters. The cultivation of reed in such conditions for producing fibers (and additional products derived from a biorefinery) would imply an additional environmental benefit compared to other common plants grown for fiber-obtaining purposes, where cultivable land, fertilizers, and good-quality waters are used. However, the invasive potential character of this plant species should not be disregarded, despite the potential benefits of its cultivation. Finally, this review has shown the relevance of the extraction procedure in the cellulose content and properties of the fibers and, consequently, in composites. *Arundo*-derived materials, especially fibers, have increased tensile and flexural modules, both in thermoset and thermoplastic matrixes. Several authors have identified the need to treat the fibers, either with plasma or with chemicals, to improve the adhesion between the fiber and the matrix, reduce the number of voids and increase the "mechanical properties" (or at least not to reduce them). This work has allowed identifying the gap existing for *Arundo* fibers use in composites in the literature compared to other lignocellulosic fibers. Ground reed has been successfully used to obtain panels by compression molding and thermoset resins, while its use in thermoplastic matrices is still pretty unexplored in the literature. Besides, the antioxidant features provided by such natural materials should also be assessed in the future to improve plastic products' behavior under atmospheric conditions (UV light and humidity). Thus, there is a promising field of study framed on the green deal strategy of the EU and sustainable development goals to optimize not only the technical performance of the composites but also their environmental, economic, and social performances.

Acknowledgments Zaida Ortega acknowledges the Spanish Ministry of Universities for funding the internship at QUB, funded by the grant received by Order UNI/501/2021 of May

26th, 2021, coming from the European Union towards Next Generation funds (Plan de Recuperación, Transformación y Resiliencia del Gobierno de España: C21.I4.P1. Resolución del 2 de julio de 2021 de la Universidad de Las Palmas de Gran Canaria por la que se convocan Ayudas para la recualificación del sistema universitario español para 2021–2023). Luis Suárez also acknowledges the funding through the Ph.D. grant program co-financed by the Canarian Agency for Research, Innovation and Information Society of the Canary Islands Regional Council for Employment, Industry, Commerce and Knowledge (ACIISI) and by the European Social Fund (ESF) (Grant number TESIS2021010008).

Author contributions ZO had the idea for the article, LS, ZO, and MB performed the literature search and data analysis, ZO and LS prepared the manuscript draft, and all authors critically revised and agreed on the content of the final work.

Funding Open Access funding provided thanks to the CRUE-CSIC agreement with Springer Nature. Plan de Recuperación, Transformación y Resiliencia del Gobierno de España: C21.I4.P1. Resolución del 2 de julio de 2021 de la Universidad de Las Palmas de Gran Canaria por la que se convocan Ayudas para la recualificación del sistema universitario español para 2021–2023. Canarian Agency for Research, Innovation and Information Society of the Canary Islands Regional Council for Employment, Industry, Commerce and Knowledge (ACIISI) and the European Social Fund (ESF) (Grant number TESIS2021010008).

Declarations

Conflict of interest The authors declare no potential conflict of interest.

Ethical approval The authors confirm that the manuscript has not been submitted to any other journal for simultaneous consideration and has not been previously published.

Consent for publication All authors approved the manuscript before submission and consent.

Open Access This article is licensed under a Creative Commons Attribution 4.0 International License, which permits use, sharing, adaptation, distribution and reproduction in any medium or format, as long as you give appropriate credit to the original author(s) and the source, provide a link to the Creative Commons licence, and indicate if changes were made. The images or other third party material in this article are included in the article's Creative Commons licence, unless indicated otherwise in a credit line to the material. If material is not included in the article's Creative Commons licence and your intended use is not permitted by statutory regulation or exceeds the permitted use, you will need to obtain permission directly from the copyright holder. To view a copy of this licence, visit <http://creativecommons.org/licenses/by/4.0/>.

References

- Abidi N, Manike M (2018) X-ray diffraction and FTIR investigations of cellulose deposition during cotton fiber development. *Text Res J* 88:719–730. <https://doi.org/10.1177/0040517516688634>
- Accardi DS, Russo P, Lauri R et al (2015) From soil remediation to biofuel: process simulation of bioethanol production from *Arundo donax*. *Chem Eng Trans* 43:2167–2172. <https://doi.org/10.3303/CET1543362>
- Ahmed MJ (2016) Potential of *Arundo donax* L. stems as renewable precursors for activated carbons and utilization for wastewater treatments: review. *J Taiwan Inst Chem Eng* 63:336–343. <https://doi.org/10.1016/j.jtice.2016.03.030>
- Ait Benhamou A, Boussetta A, Kassab Z et al (2022) Application of UF adhesives containing unmodified and phosphate-modified cellulose microfibers in the manufacturing of particleboard composites. *Ind Crop Prod*. <https://doi.org/10.1016/j.indcrop.2021.114318>
- Alshaal T, Elhawati N, Domokos-Szabolcsy É, Kátai J, Márton L, Czako M, El-Ramady H, Fári MG (2015) Giant reed (*Arundo donax* L.): a green technology for clean environment. In: Ansari AA, Gill SS, Gill R, Lanza GR, Newman L (eds) *Phytoremediation: management of environmental contaminants*, volume 1. Springer International Publishing, Cham, pp 3–20. https://doi.org/10.1007/978-3-319-10395-2_1
- Andreu-Rodriguez J, Medina E, Ferrandez-Garcia MT et al (2013) Agricultural and industrial valorization of *Arundo donax* L. *Commun Soil Sci Plant Anal* 44:598–609. <https://doi.org/10.1080/00103624.2013.745363>
- Antonetti C, Bonari E, Licursi D et al (2015) Hydrothermal conversion of giant reed to furfural and levulinic acid: Optimization of the process under microwave irradiation and investigation of distinctive agronomic parameters. *Molecules* 20:21232–21353. <https://doi.org/10.3390/molecules201219760>
- Badagliacco D, Megna B, Valenza A (2020) Induced modification of flexural toughness of natural hydraulic lime based mortars by addition of giant reed fibers. *Case Stud Constr Mater*. <https://doi.org/10.1016/j.cscm.2020.E00425>
- Baquero Basto D, Monsalve Alarcón J, Sánchez Cruz M (2018) Experimental characterization of composite panels made with *Arundo donax* fibers and vegetable resin. *Sciencia et Technica* 23:119–125
- Barana D, Salanti A, Orlandi M et al (2016) Biorefinery process for the simultaneous recovery of lignin, hemicelluloses, cellulose nanocrystals and silica from rice husk and *Arundo donax*. *Ind Crops Prod* 86:31–39. <https://doi.org/10.1016/j.indcrop.2016.03.029>
- Barczewski M, Mysiukiewicz O, Kloziński A (2018) Complex modification effect of linseed cake as an agricultural waste filler used in high density polyethylene composites. *Iran Polym J* 27:677–688. <https://doi.org/10.1007/s13726-018-0644-3>
- Barreca F, Martinez Gabarron A, Flores Yepes JA, Pastor Pérez JJ (2019) Innovative use of giant reed and cork residues for panels of buildings in Mediterranean area. *Resour*

- Conserv Recycl 140:259–266. <https://doi.org/10.1016/J.RESCONREC.2018.10.005>
- Barreto ACH, Esmeraldo MA, Rosa DS et al (2010) Cardanol biocomposites reinforced with jute fiber: microstructure, biodegradability, and mechanical properties. *Polym Compos* 31:1928–1937. <https://doi.org/10.1002/pc.20990>
- Bessa W, Trache D, Derradji M et al (2020) Characterization of raw and treated *Arundo donax* L. cellulosic fibers and their effect on the curing kinetics of bisphenol A-based benzoxazine. *Int J Biol Macromol* 164:2931–2943. <https://doi.org/10.1016/J.IJBIOMAC.2020.08.179>
- Bessa W, Trache D, Derradji M et al (2021b) Effect of different chemical treatments and loadings of *Arundo donax* L. fibers on the dynamic mechanical, thermal, and morphological properties of bisphenol A aniline based polybenzoxazine composites. *Polym Compos* 42:5199–5208. <https://doi.org/10.1002/PC.26215>
- Bessa W, Tarchoun AF, Trache D, Derradji M (2021) Preparation of amino-functionalized microcrystalline cellulose from *Arundo donax* L. and its effect on the curing behavior of bisphenol A-based benzoxazine. *Thermochim Acta* 698:178882. <https://doi.org/10.1016/j.tca.2021.178882>
- Charca S, Tenazoa C, Junior HS (2021) Chemical composition of natural fibers using the measured true density. case study: Ichu fibers. *J Nat Fibers* 10(1080/15440478):1952143
- Chikouche MDL, Merrouche A, Azizi A et al (2015) Influence of alkali treatment on the mechanical properties of new cane fibre/polyester composites. *J Reinf Plast Compos* 34:1329–1339. <https://doi.org/10.1177/0731684415591093>
- Christou M, Alexopoulou E, Cosentino SL, Copani V, Nogue S, Sanchez E, Monti A, Zegada-Lizarazu W, Pari L, Scarfone A (2018) Giant reed: from production to end use. Perennial grasses for bioenergy and bioproducts. Elsevier, pp 107–151. <https://doi.org/10.1016/B978-0-12-812900-5.00004-7>
- Copani V, Cosentino SL, Testa G, Scordia D (2013) Agamic propagation of giant reed (*Arundo donax* L.) in semi-arid Mediterranean environment. *Ital J Agron* 8(1s):1. <https://doi.org/10.4081/ija.2013.s1>
- Corno L, Pilu R, Adani F (2014) *Arundo donax* L.: a non-food crop for bioenergy and bio-compound production. *Bio-technol Adv* 32:1535–1549. <https://doi.org/10.1016/j.biotechadv.2014.10.006>
- Cosentino SL, Scordia D, Sanzone E et al (2014) Response of giant reed (*Arundo donax* L.) to nitrogen fertilization and soil water availability in semi-arid Mediterranean environment. *Eur J Agron* 60:22–32. <https://doi.org/10.1016/j.eja.2014.07.003>
- Cosentino SL, Patanè C, Sanzone E et al (2016) Leaf gas exchange, water status and radiation use efficiency of giant reed (*Arundo donax* L.) in a changing soil nitrogen fertilization and soil water availability in a semi-arid Mediterranean area. *Eur J Agron* 72:56–69. <https://doi.org/10.1016/j.eja.2015.09.011>
- Csurhes S (2016) Invasive weed risk assessment: Giant reed *Arundo donax*. Queensland Government. Available at https://www.daf.qld.gov.au/_data/assets/pdf_file/0006/59973/IPA-Giant-Reed-Risk-Assessment.pdf (last accessed 24th February 2023)
- Dahmardeh Ghalehno M, Madhoushi M, Tabarsa T, Nazerian M (2010) The manufacture of particleboards using mixture of reed (surface layer) and commercial species (middle layer). *Eur J Wood Wood Prod* 69:341–344. <https://doi.org/10.1007/S00107-010-0437-7>
- Dragoni F, Ragaglini G, Corneli E et al (2015) Giant reed (*Arundo donax* L.) for biogas production: land use saving and nitrogen utilisation efficiency compared with arable crops. *Ital J Agron* 10:192–201. <https://doi.org/10.4081/ija.2015.664>
- Eurostat (2020) Integrated farm statistics manual. Publications Office of the European Union, Luxembourg. ISBN: 978–92–76–21580–6. Available at: <https://ec.europa.eu/eurostat/web/products-manuals-and-guidelines/-/ks-gq-20-009> (last access 24th February 2023)
- Fernando AL, Barbosa B, Costa J, Papazoglou EG (2016) Giant reed (*Arundo donax* L.). Bioremediation and bioeconomy. Elsevier, pp 77–95. <https://doi.org/10.1016/B978-0-12-802830-8.00004-6>
- Ferrández Villena M, Ferrández García A, García Ortuño T et al (2020a) Properties of wood particleboards containing giant reed (*Arundo donax* L.) particles. *Sustainability (switzerland)* 12:1–10. <https://doi.org/10.3390/su122410469>
- Ferrández Villena M, Ferrández Garcia CE, García Ortuño T et al (2020b) The influence of processing and particle size on binderless particleboards made from *Arundo donax* L. *Rhizome Polymers* 12:696. <https://doi.org/10.3390/polym12030696>
- Ferrández-García MT, Ferrandez-Garcia CE, Garcia-Ortuño T et al (2019) Experimental evaluation of a new giant reed (*Arundo donax* L.) composite using citric acid as a natural binder. *Agronomy* 882(9):882. <https://doi.org/10.3390/AGRONOMY9120882>
- Ferrandez-García MT, Ferrandez-Garcia A, Garcia-Ortuño T, Ferrandez-Garcia CE, Ferrandez-Villena M (2020) Assessment of the physical, mechanical and acoustic properties of *Arundo donax* L. biomass in low pressure and temperature particleboards. *Polymers* 12(6):1361. <https://doi.org/10.3390/polym12061361>
- Ferrández-García CE, Andreu-Rodríguez J, Ferrández-García MT, Ferrández-Villena M, García-Ortuño T (2012) Panels made from giant reed bonded with non-modified starches. *BioResources*. <https://doi.org/10.15376/biores.7.4.5904-5916>
- Ferreira CSS, Seifollahi-Aghmiuni S, Destouni G, Ghajarnia N, Kalantari Z (2022) Soil degradation in the European mediterranean region: processes, status and consequences. *Sci Total Environ* 805:150106. <https://doi.org/10.1016/j.scitotenv.2021.150106>
- Di Fidio N, Galletti AMR, Fulignati S et al (2020) Multi-step exploitation of raw *Arundo donax* L. For the selective synthesis of second-generation sugars by chemical and biological route. *Catalysts*. <https://doi.org/10.3390/catal10010079>
- Fiore V, Botta L, Scaffaro R et al (2014a) PLA based biocomposites reinforced with *Arundo donax* fillers. *Compos Sci Technol* 105:110–117. <https://doi.org/10.1016/j.compscitech.2014.10.005>
- Fiore V, Scalici T, Valenza A (2014b) Characterization of a new natural fiber from *Arundo donax* L. as potential

- reinforcement of polymer composites. *Carbohydr Polym* 106:77–83. <https://doi.org/10.1016/j.carbpol.2014.02.016>
- Fiore V, Scalici T, Vitale G, Valenza A (2014c) Static and dynamic mechanical properties of *Arundo donax* fillers-epoxy composites. *Mater Des* 57:456–464. <https://doi.org/10.1016/j.matdes.2014.01.025>
- Fiore V, Piperopoulos E, Calabrese L (2019) Assessment of *Arundo donax* fibers for oil spill recovery applications. *Fibers* 7:75.7-75. <https://doi.org/10.3390/FIB7090075>
- Flores JA, Pastor JJ, Martínez-Gabarrón A et al (2011) *Arundo donax* chipboard based on urea-formaldehyde resin using under 4 mm particles size meets the standard criteria for indoor use. *Ind Crops Prod* 34:1538–1542. <https://doi.org/10.1016/j.indcrop.2011.05.011>
- Flores-Yepes J-A, Pastor-Perez J-J, Gimeno-Blanes F-J, Rodríguez-Guisado I, Frutos-Fernandez M-J (2012) Full recovery of *Arundo donax* particleboard from swelling test without waterproofing additives. *BioResources*. <https://doi.org/10.15376/biores.7.4.5222-5235>
- García-Ortuño T, Andréu-Rodríguez J, Ferrández-García MT, Ferrández-Villena M, Ferrández-García CE (2010) Evaluation of the physical and mechanical properties of particleboard made from giant reed (*Arundo donax* L.). *BioResources* 6(1):477–486. <https://doi.org/10.15376/biores.6.1.477-486>
- Giroto L, Franco AC, Nunez CV et al (2021) Phytotoxicity and allelopathic potential of extracts from rhizomes and leaves of *Arundo donax*, an invasive grass in neotropical savannas. *Not Botanicæ Horti Agrobot Cluj-Napoca* 49(3):12440. <https://doi.org/10.15835/nbha49312440>
- Henrique P, Pereira F, De M et al (2015) Vegetal fibers in polymeric composites: a review. *Polímeros* 25:9–22. <https://doi.org/10.1590/0104-1428.1722>
- Hulle A, Kadole P, Katkar P (2015) Agave Americana leaf fibers. *Fibers* 3:64–75. <https://doi.org/10.3390/fib3010064>
- Ismail ZZ, Jael AJ (2014) A novel use of undesirable wild giant reed biomass to replace aggregate in concrete. *Constr Build Mater* 67:68–73. <https://doi.org/10.1016/j.conbuildmat.2013.11.064>
- Jiménez-Ruiz J, Hardion L, Del Monte JP et al (2021) Monographs on invasive plants in Europe N° 4: *Arundo donax* L. *Botany Lett* 168:131–151. <https://doi.org/10.1080/23818107.2020.1864470>
- Kabir MM, Wang H, Lau KT et al (2012) Mechanical properties of chemically-treated hemp fibre reinforced sandwich composites. *Compos B Eng* 43:159–169. <https://doi.org/10.1016/j.compositesb.2011.06.003>
- Kim HJ, Liu Y, French AD et al (2018) Comparison and validation of fourier transform infrared spectroscopic methods for monitoring secondary cell wall cellulose from cotton fibers. *Cellulose* 25:49–64. <https://doi.org/10.1007/s10570-017-1547-8>
- Lambertini C (2019) Why are tall-statured energy grasses of polyploid species complexes potentially invasive? A review of their genetic variation patterns and evolutionary plasticity. *Biol Invasions* 21:3019–3041. <https://doi.org/10.1007/S10530-019-02053-2>
- Licursi D, Antonetti C, Mattonai M et al (2018) Multi-valorisation of giant reed (*Arundo donax* L.) to give levulinic acid and valuable phenolic antioxidants. *Ind Crops Prod* 112:6–17. <https://doi.org/10.1016/j.indcrop.2017.11.007>
- López-Bañuelos RH, Moscoso FJ, Ortega-Gudiño P, Mendizabal E, Rodrigue D, González-Núñez R (2012) Rotational molding of polyethylene composites based on agave fibers. *Polym Eng Sci* 52:2489–2497
- Lowe S, Brown M, Boudejelas Poorter D (2000) 100 of the world's worst invasive alien species: a selection from the global invasive species database. In: Encyclopedia of biological invasions. the invasive species specialist group (ISSG) a specialist group of the species survival commission (SSC) of the world conservation union (IUCN), Auckland, pp 715–716
- Malheiro R, Ansolín A, Guarnier C et al (2021) The potential of the reed as a regenerative building material—characterisation of its durability, physical, and thermal performances. *Energies*. <https://doi.org/10.3390/EN14144276>
- Manniello C, Cillis G, Statuto D et al (2022) Concrete blocks reinforced with arundo donax natural fibers with different aspect ratios for application in bioarchitecture. *Appl Sci* (Switzerland). <https://doi.org/10.3390/app12042167>
- Manniello C, Cillis G, Statuto D et al (2022) Experimental analysis on concrete blocks reinforced with *Arundo donax* fibres. *J Agric Eng*. <https://doi.org/10.4081/JAE.2021.1288>
- Martínez Gabarrón A, Flores Yepes JA, Pastor Pérez JJ et al (2014) Increase of the flexural strength of construction elements made with plaster (calcium sulfate dihydrate) and common reed (*Arundo donax* L.). *Constr Build Mater* 66:436–441. <https://doi.org/10.1016/j.conbuildmat.2014.05.083>
- Martínez-Sanz M, Erboz E, Fontes C, López-Rubio A (2018) Valorization of *Arundo donax* for the production of high performance lignocellulosic films. *Carbohydr Polym* 199:276–285. <https://doi.org/10.1016/j.carbpol.2018.07.029>
- Oh SY, Dong IY, Shin Y et al (2005) Crystalline structure analysis of cellulose treated with sodium hydroxide and carbon dioxide by means of X-ray diffraction and FTIR spectroscopy. *Carbohydr Res* 340:2376–2391. <https://doi.org/10.1016/J.CARRES.2005.08.007>
- Ornaghi HL, Ornaghi FG, Neves RM et al (2020) Mechanisms involved in thermal degradation of lignocellulosic fibers: a survey based on chemical composition. *Cellulose* 27:4949–4961. <https://doi.org/10.1007/s10570-020-03132-7>
- Ortega Z, Monzón MD, Benítez AN et al (2013) Banana and abaca fiber-reinforced plastic composites obtained by rotational molding process. *Mater Manuf Process* 28:130614085148001. <https://doi.org/10.1080/10426914.2013.792431>
- Ortega Z, Castellano J, Suárez L et al (2019) Characterization of Agave Americana L. plant as potential source of fibres for composites obtaining. *SN Appl Sci* 1:987. <https://doi.org/10.1007/s42452-019-1022-2>
- Ortega Z, Romero F, Paz R et al (2021) Valorization of invasive plants from Macaronesia as filler materials in the production of natural fiber composites by rotational molding. *Polymers*. <https://doi.org/10.3390/POLYM13132220>
- Pansuksan K, Sukprasert S, Karaket N (2020) Phytochemical compounds in *Arundo donax* L. rhizome antimicrobial activities. *Pharmacognosy J* 12:287–292. <https://doi.org/10.5530/pj.2020.12.45>

- Pilu R, Cassani E, Landoni M et al (2014) Genetic characterization of an Italian giant reed (*Arundo donax* L.) clones collection: exploiting clonal selection. *Euphytica* 196:169–181. <https://doi.org/10.1007/s10681-013-1022-z>
- Pinto PCR, Oliveira C, Costa CA et al (2015) Kraft delignification of energy crops in view of pulp production and lignin valorization. *Ind Crops Prod* 71:153–162. <https://doi.org/10.1016/j.indcrop.2015.03.069>
- Piperopoulos E, Khaskhoussi A, Fiore V, Calabrese L (2021) Surface modified *Arundo donax* natural fibers for oil spill recovery. *J Nat Fibers*. <https://doi.org/10.1080/15440478.2021.1961343>
- Ramos D, Mansouri NEE, Ferrando F, Salvadó J (2018) All-lignocellulosic fiberboard from steam exploded *Arundo donax* L. *Molecules*. <https://doi.org/10.3390/MOLECULES23092088>
- Raposo Oliveira Garcez L, Hofmann Gatti T, Carlos Gonzalez J et al (2022) Characterization of fibers from culms and leaves of *Arundo donax* L. (Poaceae) for handmade paper production. *J Nat Fibers*. <https://doi.org/10.1080/15440478.2022.2076005>
- Raspolli Galletti AM, Antonetti C, Ribechini E et al (2013) From giant reed to levulinic acid and gamma-valerolactone: a high yield catalytic route to valeric biofuels. *Appl Energy* 102:157–162. <https://doi.org/10.1016/j.apenergy.2012.05.061>
- Romero-Munar A, Baraza E, Cifre J et al (2018) Leaf plasticity and stomatal regulation determines the ability of *Arundo donax* plantlets to cope with water stress. *Photosynthetica* 56:698–706. <https://doi.org/10.1007/s11099-017-0719-y>
- Sallustio L, Harfouche AL, Salvati L et al (2022) Evaluating the potential of marginal lands available for sustainable cellulosic biofuel production in Italy. *Soc-Econ Plan Sci* 82:101309. <https://doi.org/10.1016/j.seps.2022.101309>
- Sánchez E, Scordia D, Lino G et al (2015) Salinity and water stress effects on biomass production in different *Arundo donax* L. Clones *Bioenergy Res* 8:1461–1479. <https://doi.org/10.1007/s12155-015-9652-8>
- Sargin Karahancer S, Eriskin E, Sarioglu O et al (2016) Utilization of *Arundo donax* in hot mix asphalt as a fiber. *Constr Build Mater* 125:981–986. <https://doi.org/10.1016/J.CONBUILDMAT.2016.08.147>
- Scalici T, Fiore V, Valenza A (2016) Effect of plasma treatment on the properties of *Arundo donax* L. leaf fibres and its bio-based epoxy composites: a preliminary study. *Compos B Eng* 94:167–175. <https://doi.org/10.1016/j.compositesb.2016.03.053>
- Scordia D, Cosentino SL (2019) Perennial energy grasses: resilient crops in a changing European agriculture. *Agriculture (Switzerland)*. <https://doi.org/10.3390/AGRICULTURE9080169>
- Shatalov AA, Pereira H (2006) Papermaking fibers from giant reed (*Arundo donax* L.) by advanced ecologically friendly pulping and bleaching technologies. *BioResources* 1:45–61. <https://doi.org/10.15376/biores.1.1.45-61>
- Shatalov AA, Pereira H (2013) High-grade sulfur-free cellulose fibers by pre-hydrolysis and ethanol-alkali delignification of giant reed (*Arundo donax* L.) stems. *Ind Crops Prod* 43:623–630. <https://doi.org/10.1016/j.indcrop.2012.08.003>
- Shtein I, Baruchim P, Lev-Yadun S (2021) Division of labour among culms in the clonal reed *Arundo donax* (Poaceae) is underlain by their pre-determined hydraulic structure. *Bot J Linn Soc* 195:348–356. <https://doi.org/10.1093/botlinnean/boaa062>
- Sicilia A, Santoro DF, Testa G, Cosentino SL, Piero ARL (2020) Transcriptional response of giant reed (*Arundo donax* L.) low ecotype to long-term salt stress by unigene-based RNAseq. *Phytochemistry* 177:112436. <https://doi.org/10.1016/j.phytochem.2020.112436>
- Suárez L, Castellano J, Romero F et al (2021) Environmental hazards of giant reed (*Arundo donax* L.) in the Macaronesia region and its characterisation as a potential source for the production of natural fibre composites. *Polymers*. 13:2101. <https://doi.org/10.3390/POLYM13132101>
- Suárez L, Barczewski M, Kosmela P et al (2022) Giant reed (*Arundo donax* L.) fiber extraction and characterization for its use in polymer composites. *J Nat Fibers*. <https://doi.org/10.1080/15440478.2022.2131687>
- Suárez L, Ortega Z, Romero F et al (2022b) Influence of giant reed fibers on mechanical, thermal, and disintegration behavior of rotomolded PLA and PE composites. *J Polym Environ*. <https://doi.org/10.1007/s10924-022-02542-x>
- Tarchoun AF, Trache D, Klapötke TM et al (2019) Ecofriendly isolation and characterization of microcrystalline cellulose from giant reed using various acidic media. *Cellulose* 26:7635–7651. <https://doi.org/10.1007/s10570-019-02672-x>
- European Union (2017) Invasive Alien Species of Union concern. ISBN: 978–92–79–70168–9. Available at: https://environment.ec.europa.eu/topics/nature-and-biodiversity/invasive-alien-species_en (last access 24th February 2023)
- Van Schoors L, Gueguen Minerbe M, Moscardelli S et al (2018) Antioxidant properties of flax fibers in polyethylene matrix composites. *Ind Crops Prod* 126:333–339. <https://doi.org/10.1016/j.indcrop.2018.09.047>
- Wang C, Bai S, Yue X et al (2016) Relationship between chemical composition, crystallinity, orientation and tensile strength of kenaf fiber. *Fibers Polym* 17:1757–1764. <https://doi.org/10.1007/s12221-016-6703-5>
- Wang H, Wang Y, Cao W, et al. (2011) Allelopathic activity of volatile oil from giant reed on *Microcystin aeruginosa*. In: 2011 International conference on electric technology and civil engineering (ICETCE). pp 991–993
- Yu B, Cao C-F, Yuen R (2022) Progress in flame-retardant sustainable fiber/polymer composites. In: Hu T., Nabipour H., Wang X. (Eds) *Bio-Based Flame Retardants for Polymeric Materials*. pp 419–449. <https://doi.org/10.1016/B978-0-323-90771-2.00013-4>
- Zhu J, Zhu H, Njuguna J, Abhyankar H (2013) Recent development of flax fibres and their reinforced composites based on different polymeric matrices. *Materials (basel)* 6:5171–5198. <https://doi.org/10.3390/ma6115171>

Publisher's Note Springer Nature remains neutral with regard to jurisdictional claims in published maps and institutional affiliations.

6.3. GIANT REED (*ARUNDO DONAX* L.) FIBRE EXTRACTION
AND CHARACTERIZATION FOR ITS USE IN POLYMER
COMPOSITES

P1

P2

P3

P4

P5

P6

P7

P8

P9

P10

Giant Reed (*Arundo donax* L.) Fiber Extraction and Characterization for Its Use in Polymer Composites

Luis Suárez^a, Mateusz Barczewski^b, Paulina Kosmela^c, María D. Marrero^a, and Zaida Ortega^d

^aDepartamento de Ingeniería Mecánica, Universidad de Las Palmas de Gran Canaria, Las Palmas de Gran Canaria, Spain; ^bDepartment of Mechanical Engineering, Institute of Materials Technology, Faculty of Mechanical Engineering, Poznan University of Technology, Poznan, Poland; ^cDepartment of Polymer Technology, Faculty of Chemistry, Gdansk University of Technology, Gdansk, Poland; ^dDepartamento de Ingeniería de Procesos, Universidad de Las Palmas de Gran Canaria, Las Palmas de Gran Canaria, Spain

ABSTRACT

This work describes an extraction method for giant reed fibers from stems and leaves based on chemical soaking and crushing through a rolling mill. Obtained fibers, together with the shredded plant (stems + leaves), are characterized in terms of chemical composition, thermal stability, morphology, and crystallinity. Mechanical properties of fibers have also been assessed (single fiber tensile tests). The results show that the proposed method allows obtaining fibers with higher cellulose content (near 70%), good thermal stability (10% weight loss over 270°C), higher density, and better mechanical properties than other *Arundo* fibers previously reported in the literature. Fibers from leaves are thinner and show higher crystallinity than those from stems (72 μm vs. 157 μm , 73% vs. 67% crystallinity, respectively), although mechanical properties are similar for both (around 900 MPa for tensile strength and over 45 GPa for elastic modulus). Analysis of the microstructure shows that fibers consist of microfibril bundles, and the removal of a thin layer of non-cellulosic nature is clear; fibers provide a rougher, cleaner surface than shredded raw material.

摘要

本工作描述了一种从茎和叶中提取巨型芦苇纤维的方法，该方法基于化学浸泡和通过轧机破碎。获得的纤维以及切碎的植物（茎+叶）具有化学成分、热稳定性、形态和结晶度的特征。还评估了纤维的机械性能（单纤维拉伸试验）。结果表明，与文献中先前报道的其他*Arundo*纤维相比，所提出的方法可以获得纤维素含量更高（接近70%）、热稳定性好（270°C以上失重10%）、密度更高和机械性能更好的纤维。叶纤维比茎纤维更薄，结晶度更高（分别为72 μm 和157 μm ，73%和67%结晶度），但两者的机械性能相似（拉伸强度约为900 MPa，弹性模量超过45 GPa）。微观结构分析表明，纤维由超细纤维束组成，并清除了一层薄薄的非纤维素性质；纤维提供了比粉碎原料更粗糙、更清洁的表面。

KEYWORDS

Giant reed; *Arundo donax*; natural fibers; characterization

关键词


巨大的芦苇; *Arundo donax*; 天然纤维; 刻画

Introduction

Arundo donax L. is a perennial grass from the *Gramineae* family, with an uncertain origin due to its small size and the high number of chromosomes found in this species, although many authors place it in East Asia (Jensen et al. 2018). Although giant reed produces flowers, seeds are not usually viable,

CONTACT Luis Suárez  luis.suarez@ulpgc.es  Edificio de Fabricación Integrada, Parque Científico – Tecnológico de la ULPGC Campus universitario de Tafira Baja, 35017, Las Palmas de Gran Canaria, Las Palmas, Spain

This article has been corrected with minor changes. These changes do not impact the academic content of the article.

 Supplemental data for this article can be accessed online at <https://doi.org/10.1080/15440478.2022.2131687>

© 2022 The Author(s). Published with license by Taylor & Francis Group, LLC.

This is an Open Access article distributed under the terms of the Creative Commons Attribution-NonCommercial-NoDerivatives License (<http://creativecommons.org/licenses/by-nc-nd/4.0/>), which permits non-commercial re-use, distribution, and reproduction in any medium, provided the original work is properly cited, and is not altered, transformed, or built upon in any way.

and reproduction takes place through the rhizome or shoot fragmentations. Stems are hollow and have diameters around 2–3 cm, reaching up to 6 m in height, with stem-clasping leaves along the entire stem (Csurhes 2016). Giant reed is generally recognized as an interesting source of biomass due to its high productivity and low requirements (Jensen et al. 2018), as it can be grown in almost any type of soil and with a minimal amount of water (Ahmed 2016), with high thermal and pathogen resistance (Accardi et al. 2015).

This species is mainly studied as a feedstock for biorefineries, especially for ethanol and bioenergy products (Accardi et al. 2015; Jensen et al. 2018). Reed has also gained attention for obtaining other biomolecules, such as furfural or levulinic acid, among others (Antonetti et al. 2015; Di Fidio et al. 2020; Raspolli Galletti et al. 2013). Other uses of *Arundo* have been investigated, such as paper and pulp (Shatalov and Pereira 2013), biochar production (Ahmed 2016), as filler in concrete (Ismail and Jaeel 2014), or for oil spill recovery (Piperopoulos et al. 2021). Its cultivation is also proposed as a strategy for soil bioremediation (Fernando et al. 2016; Tarek et al. 2015).

Compared to the extensive research performed on biofuels and biomolecules, only a little attention has been paid to the obtaining of reed composites, mainly related to particle board production (Barreca et al. 2019; García-Ortuño et al. 2011; C. E. Ferrández-García et al. 2012; Andreu-Rodriguez et al. 2013; M. T. Ferrández-García et al. 2020; Ferrandez-Garcia et al. 2019; Ferrández Villena et al. 2020). Those studies on composite production use shredded vegetal material (Bessa et al. 2020, 2021; Fiore et al. 2014; Fiore, Scalici, and Valenza 2014) or bast fibers obtained by combining with a teeth brush (Fiore, Scalici, and Valenza 2014; Scalici, Fiore, and Valenza 2016) or rudimentary mechanical procedures (Ortega et al. 2021; Suárez et al. 2021). From the limited papers found in the literature in this field, these mainly focus on thermoset resins (Bessa et al. 2021; Chikouche et al. 2015; Fiore, Scalici, and Valenza 2014), being polylactic acid (PLA) (Fiore et al. 2014) and polyethylene (PE) used as thermoplastic matrixes (Ortega et al. 2021; Suárez et al. 2021). This paper focuses on the characterization of *Arundo* fibers, obtained from the stems and the leaves, using a combination of chemical and mechanical procedures that provide finer fibers.

Arundo is still considered one of the worst invasive plants in the world (Jiménez-Ruiz et al. 2021), and several actions take place periodically to try to control their spread in many parts of the world. This invasive character is due to its rapid and easy propagation but also to the difficulties in removing its rhizomatous root system. To achieve successful eradication, the continuous application of herbicides, such as glyphosate (Jiménez Auzmendi 2014; Martín, Carolina, and Barroso 2019), or biological/mechanical treatments (Jiménez-Ruiz et al. 2021) are needed, not even arriving to a complete eradication of the plant (Jensen et al. 2018). For example, control campaigns have been performed in Murcia (Aymerich et al. 2012) or Canary Islands (Jiménez Auzmendi 2014) in Spain, Oregon in USA (Martín, Carolina, and Barroso 2019), and Queensland in Australia (Csurhes 2016).

Consequently, a large amount of residual biomass is available in different areas with potential interest as reinforcement of composites, among other possible uses, to advance toward more efficient use of resources and a zero waste strategy.

Materials and methods

Materials preparation

Specimens of *Arundo donax* L. plants have been collected in Gran Canaria (28.081344–15.473501) and show 2–3 cm diameter and around 4–5 m height. The rhizomes were removed, and three different materials were prepared: leaves, stems, and raw material. Leaves and stems were used separately for fiber obtaining. For characterization purposes, all samples were milled in a Retsch ZM 200 mill to a particle size lower than 0.5 mm. All reagents were purchased in analytical grade from Sigma Aldrich and were used without further modification.

Fiber obtaining

Fibers from the stems were obtained after 7–10 days of soaking them in a 1 N NaOH solution and subsequent crushing of the resulting material in a lab-made mechanical device, as described in Suárez et al. (2021). Once obtained, fibers were washed in water until neutral pH and dried under room conditions for 3–4 days. Fibers were then cut to 3–5 mm length, washed again to remove fine dust, dried at 60°C in a forced air dryer device TG 200 from Retsch, and then sieved in an AS200 Control device from Retsch, using 75 and 800 µm sieves to remove fines and clustered particles.

Fibers from the leaves were also obtained after immersing the green leaves in a 1 N NaOH solution for 3 weeks, and then just by shaking them in water. Once washed, they were cut, washed again, dried, and sieved, as explained for fibers obtained from stems.

Finally, the raw material was chopped, dried at room conditions, and then processed twice in an SM 300 cutting mill from Retsch, using a 10 mm screen. The last step to prepare the shredded material was washing with water, drying with forced air and sieving.

For stems, a fiber extraction yield of around 34% is obtained (on a dry basis), while it is quite lower for leaves (8%). Figure 1 shows the aspect of the obtained materials; fibers are thinner than those obtained in other published works (Fiore, Scalici, and Valenza 2014; Ortega et al. 2021; Suárez et al. 2021).

Chemical characterization

Humidity, ash content, extractives, cellulose, hemicellulose, and lignin were determined. The lignin content was determined using the Klason method according to the ANSI/ASTM 1997a standard (American National Standard Institute 1977), which consists of hydrolysis with H₂SO₄. Acid-soluble lignin (ASL) was determined from the resulting liquor, measuring absorbance at 205 nm, using an extinction coefficient of 110 l/g·cm (Proietti et al. 2017) in a Cary 60 UV–VIS spectrophotometer from Agilent Technologies. Holocellulose content was also determined following a gravimetric method (Browning 1967), in which acetic acid and sodium chlorite were used for the sample delignification. Once this sample was obtained, the total cellulose content was obtained following ANSI/ASTM 1977b standard (American National Standard Institute 1977). Hemicellulose is calculated as holocellulose minus cellulose contents.

Extractive content was determined following NREL/TP-510-42619 (Sluiter et al. 2008), consisting of two subsequent extraction processes, with water and ethanol, respectively.

Three replicas from three different batches were used for all these tests. The results are expressed as average values ± standard deviations.

Density determination

The real density of the samples was measured in an Ultrapyc 5000 Foam gas pycnometer from Anton Paar, using nitrogen as flow gas, at a target pressure of 68.9 kPa (10.0 psi), with temperature control targeted at 20.0°C. A small cell (10 cm³) was used, running 15 scans per sample under the flow mode and setting the apparatus for fine powder.



Figure 1. Pictures of materials obtained (from left to right): (a) fibers from stems, (b) fibers from leaves, and (c) shredded material.

Fourier Transformed Infrared (FTIR) spectroscopy

FTIR spectra were obtained in a Perkin Elmer spectrum Two spectrophotometer from Perkin Elmer, under the attenuated total reflectance (ATR) mode, from 4000 to 500 cm^{-1} , at a resolution of 4 cm^{-1} , obtaining each spectrum as the average of 64 scans. Intensities in absorbance of peaks at 2900 cm^{-1} , 1420 cm^{-1} , 1375 cm^{-1} , and 893 cm^{-1} have been calculated in Perkin Elmer software to calculate the crystallinity of the samples.

Thermal characterization

Thermogravimetric tests (TGA) were conducted to determine the thermal stability of the samples. TGA was performed in a Netzsch TG 2091F1 Libra apparatus, from 20°C to 900°C at a heating rate of 10°C/min under a nitrogen atmosphere (20 ml/min), using alumina crucibles. The first derivative (DTG) curve was calculated, and values of temperature for 5%, 10%, 20%, and 50% mass loss were determined.

Morphology

Sample dimensions were obtained from optical microscopy observations performed in an Olympus B×51 microscope at 5x and reflected light. A minimum of 50 particles were measured for each sample, with at least 3 measurements per particle.

The sample's morphology was assessed using a Hitachi TM3030 Scanning Electron Microscopy (SEM). Samples were placed in copper tape and coated via electrical glow discharge of Au/Pd target in an SC7620 Mini Sputter Coater from Quorum Technologies. "Fibers" surface and section were observed at different magnifications, at 15 kV.

X-ray diffraction (XRD)

The crystallinity of the samples was obtained from diffraction patterns with Cu K α radiation ($\lambda = 1.5406 \text{ \AA}$) in a Seifert URD6 apparatus, using 30 kV and 40 mA. Diffractograms were recorded from $2\theta = 10^\circ$ to $2\theta = 40^\circ$ in 0.05 steps. The presented data were smoothed using the Savitzky-Golay function (polynomial order 2, points of window 15). Crystallinity was determined according to the following equation (Wang et al. 2016):

$$\text{Crystallinity} = \frac{(I_{002} - I_{am})}{I_{002}} \times 100\% \quad (1)$$

where I_{002} is the diffraction intensity of the cellulose I crystalline region (maximum intensity in the 2θ angle range between 20° and 23°), and I_{am} is the diffraction intensity of the amorphous cellulose region (minimum intensity in the 2θ angle range between 18° and 19°).

Mechanical properties

Single fiber tests were performed on leaves and stem fibers to determine their tensile strength and elastic modulus. Thirty fibers were tested per sample in a Dongguan Liyi Test Equipment LY-1065 tester at 1 mm/min rate and a gauge length of 30 mm, following ASTM D3379-75. "Fibers" diameter was determined as the average value of 8 measurements, performed in a micrometer, considering a circular section of the fibers.

Results and discussion

Chemical characterization

Table 1 shows the average values for the obtained fibers and shredded material composition. The composition of the shredded material is similar to *Arundo* stems found in other studies. In particular,

ashes have been found in higher content in leaves than in stems (Jensen et al. 2018; Martínez-Sanz et al. 2018), as also found for fibers obtained in this study, being the average content of ashes in stems between 1.9% and 5.5% in most studies (Chikouche et al. 2015; Davide et al. 2016; Shatalov and Pereira 2005). As expected, lignin content for raw shredded material is much higher than for processed fibers, accounting for around 35%; other authors have reported similar values for total lignin, approximately 30% (Davide et al. 2016) and Klason lignin, about 20% for the stems without leaves (Bessa et al. 2021; Suárez et al. 2021).

Total extractives for these materials are below 3.0% due to the fiber extraction or the washing of the shredded material (data not shown). As expected, the process followed for fiber obtaining removes hemicellulose in the plant and leads to a fiber with relatively high cellulose content, in the range of jute or sisal fibers, and, in any case, higher than for fibers obtained in previous works (around 45% (Fiore, Scalici, and Valenza 2014; Suárez et al. 2021)). Lignin content is higher in fibers from stems than in fibers from leaves and within the ranges found in the literature. As stems show a woody rigid structure and contain a higher amount of lignin than leaves, fibers from stems also show higher lignin content than fibers from the leaves. No significant differences in cellulose and hemicellulose content are found for both types of fibers.

Density determination

Table 1 shows the density values for the three materials studied; fibers from leaves show higher density than fibers from stems, which is also higher than from shredded material. For the same species, density measurements can be correlated to the plant's chemical composition (Charca, Tenazoa, and Junior 2021); the material with higher density has higher cellulose content and lower lignin amount. It then appears that *Arundo* fibers obtained in this research show higher density than shredded material and higher cellulose content, as seen in Table 1, due to the procedure followed for fiber extraction. Removing hemicellulose and lignin allows for a higher proportion of cellulose, resulting in a higher density of the fibers. Fiore, Scalici, and Valenza (2014) determined a density for *Arundo* fibers obtained by the mechanical procedure of 1.168 g/cm³ and cellulose content of 43.59%; fibers obtained here show around 50% more cellulose and densities around 40% higher, while shredded material shows similar composition and density than fibers obtained in that research.

FTIR spectroscopy

Figure 2 shows the average recorded spectra for the samples of shredded material, fibers from leaves, and fibers from stems. Typical bands for lignocellulosic materials can be observed, namely:

- Broad band at 3000–3700 cm⁻¹, assigned to O-H stretching.
- The double peak at 2918 and 2850 cm⁻¹, attributed mainly C-H aliphatic groups in hemicellulose (Chikouche et al. 2015), which decreases in intensity due to the fiber extraction process, is also confirmed in chemical composition assays.
- The sharp peak at 1733 cm⁻¹, related to C=O stretching in lignin and hemicellulose (Bessa et al. 2020; Scalici, Fiore, and Valenza 2016), is found for shredded material but not for fibers. This is

Table 1. Composition (in %) and density of shredded material and fiber samples (average values \pm standard deviation).

	Cellulose	Hemicellulose	Lignin			Ashes	Real density (g/cm ³)
			Klason	ASL	Total		
Shredded material	38.0 \pm 3.7	42.4 \pm 1.3	24.9 \pm 0.3	8.2 \pm 1.0	32.4 \pm 2.7	4.9 \pm 1.1	1.1727 \pm 0.0882
Fibers from stems	67.5 \pm 1.9	15.3 \pm 4.6	20.4 \pm 1.5	5.3 \pm 0.1	25.7 \pm 0.6	0.4 \pm 0.2	1.5456 \pm 0.0506
Fibers from leaves	68.8 \pm 4.3	20.0 \pm 3.8	10.5 \pm 2.0	0.8 \pm 0.1	11.2 \pm 2.2	1.8 \pm 0.5	1.6290 \pm 0.0538

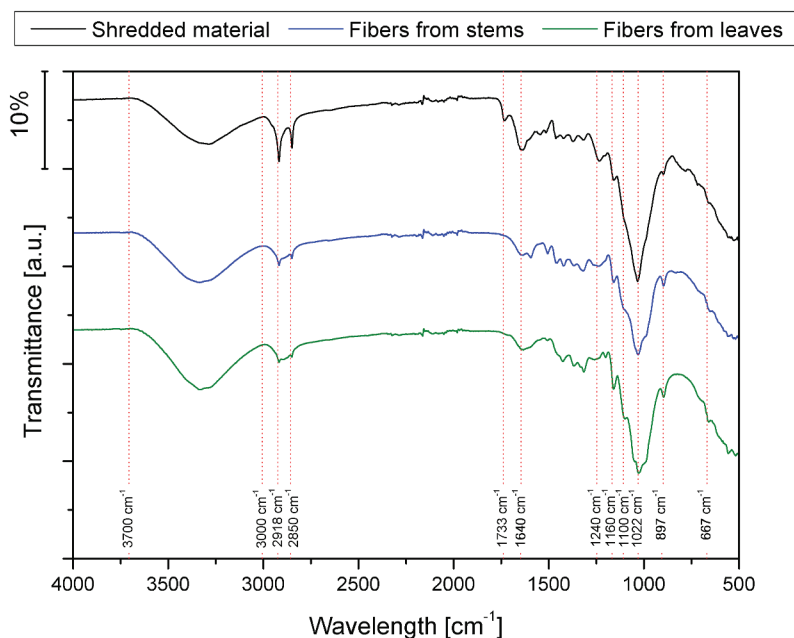


Figure 2. FTIR spectrum for different samples.

correlated with the intensity reduction at 1240 cm^{-1} , also found for fibers, attributed to C-O stretching in lignin (Fiore, Scalici, and Valenza 2014).

- The peak at 1640 cm^{-1} is reduced for fibers, as the removal of hemicellulose and lignin leads to less absorbed water (Martínez-Sanz et al. 2018).
- High-intensity peaks at 1022 cm^{-1} (C=O stretching ring vibration in cellulose) are observed for the three samples, although the relative intensity is higher for fibers than for raw material. This may suggest higher cellulose content for fibers, as observed in the quantification analysis. C-O-C asymmetric stretching at 1160 cm^{-1} also appears clearly for fibers, while it is only a light shoulder for shredded material. The precise definition of a peak at 1100 cm^{-1} may also indicate the higher presence of cellulose I crystals (Martínez-Sanz et al. 2018).

Therefore, in summary, it appears that the procedure proposed for *Arundo* fiber extraction allows obtaining a fiber of good quality to be used in composites, according to the literature, where several treatments (soda, plasma, silanization, etc.) are applied to materials from *Arundo* to improve their surface, in terms of chemical bonding. Fibers obtained only by crushing or peeling show the peak at 1740 cm^{-1} , which can be removed by performing an alkaline treatment (Suárez et al. 2021); this is also in agreement with results obtained from chemical composition tests, which show lower lignin and hemicellulose contents in samples obtained with the procedure described in this paper than for those obtained using only mechanical means.

The Total Crystallinity Index (TCI) and the Lateral Order Index (LOI) can be calculated from FTIR spectra after baseline correction and normalizing (El Oudiani, Msahli, and Sakli 2017), thus giving an approximate idea of the crystallinity of samples. The first one, TCI, is obtained by dividing the absorbance of peaks at 1375 cm^{-1} and 2900 cm^{-1} , being the value obtained proportional to the degree of crystallinity of the cellulose. The second one, LOI, is obtained by dividing absorbance at 1420 cm^{-1} by that at 893 cm^{-1} , considering this last an empirical crystallinity index and also attributed to the proportion of cellulose I (Sang Youn et al. 2005). As observed in Table 2, TCI and LOI values are higher for fiber samples than for shredded materials, thus indicating that fibers show higher crystallinity, a fact that was otherwise expected, as seen in the chemical composition of the three materials. Apparently, fibers from leaves have a higher amount of crystalline cellulose, while fibers from stems

Table 2. Approximation of crystallinity of samples by FTIR spectrum.

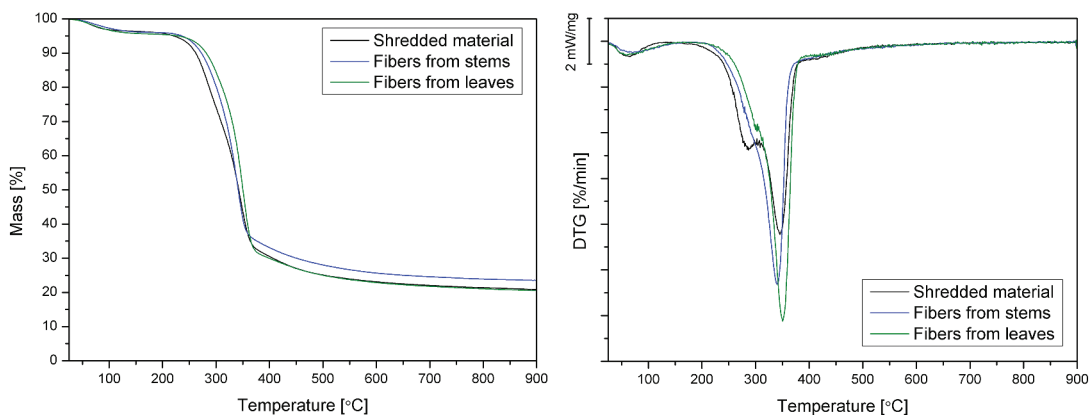
	TCI	LOI	A1620	A897	A667
Shredded material	0.279	0.503	74.817	13.830	4.710
Fibers from stems	0.515	1.026	28.483	18.463	15.140
Fibers from leaves	0.664	0.666	31.560	27.557	13.850

have a higher-order degree in the entire structure. Similar conclusions arise if areas of the bands at 1640, 897, and 667 cm^{-1} are considered (Abidi and Manike 2018). A higher area at 1640 cm^{-1} is related to higher water absorption, directly related to higher amorphous content, while more significant areas in the other two peaks are linked to higher cellulose crystallinity.

Thermal characterization

TGA curves for all considered materials show a similar course (Figure 3). However, leaf fibers seem to have higher degradation temperatures than fibers from stems, which are also more stable than shredded material. Residual biomass also has similar values for the three materials.

The most important peak found in the derivative curves is related to cellulose degradation, arising between 338°C and 350°C for these samples (pure cellulose has a maximum pyrolysis rate at 355°C (Yang et al. 2007)); fibers show a higher degradation rate at this peak than shredded material (Table 3). Besides, DTG curves also show some differences in their shape. Only for shredded material samples, the main peak has a shoulder at around 290.8°C due to the hemicellulose degradation (hemicellulose pyrolysis takes place before cellulose degradation, starting at about 220°C (Bessa et al. 2020)) (Table 3). When considering hemicellulose and cellulose pyrolysis ranges (210–315°C and 315–400°C, respectively), shredded material shows a weight loss of 27.9% in the first step and 37.1% in the second one, being the first decrease considerably lower for fiber samples (23.1% and 16.8% for stems and leaves fibers, respectively), while the α -cellulose-related step shows higher values (39.6% and 48.5%). These values are in the range of those found by other authors for *Arundo*-treated fibers, although with lower

**Figure 3.** TGA (left) and DTG (right) for stem and leaves fibers and shredded plant.**Table 3.** Temperatures for 5%, 10%, 20%, and 50% weight loss, residual mass DTG peak values.

	T_5 (°C)	T_{10} (°C)	T_{20} (°C)	T_{50} (°C)	Residual mass (%)	DTG peak		T_d (°C)
						T (°C)	Degradation rate (%/min)	
Shredded material	226.9	263.9	289.2	343.2	21.64	343.4	7.93	212
Fibers from stems	237.8	273.1	301.3	341.7	23.19	338.5	10.00	233
Fibers from leaves	175.9	280.3	311.0	350.6	20.58	349.9	11.24	237

peak temperatures (up to 340°C as the maximum value) (Bessa et al. 2020). Scalici and collaborators also obtained the first shoulder on the DTG curve at 285°C and maximum weight loss (30%) at around 340 °C for fibers obtained from leaves (Scalici, Fiore, and Valenza 2016).

Arundo materials obtained and characterized in this work show similar or even higher temperature stability than other fibers from the same species (due to the proposed extraction process) or other vegetal fibers. The onset degradation temperature is found to be around 300°C, thus confirming that it can be considered an excellent candidate to be used in composite production; weight loss starts over 270°C, in the range (or even higher) than other commonly used vegetal fibers, such as flax or jute (Fiore, Scalici, and Valenza 2014). Considering the analyzed fibers as potential reinforcement of thermoplastic composites, it is essential to define the temperature range that will allow their melt processing with polymer without degradation of the lignocellulosic structure. According to the methodology described by Bledzki et al. (Bledzki, Mamun, and Volk 2010), the starting decomposition temperature (T_d) of natural fibers is assumed to be the temperature value associated with a 1% mass loss above 150°C. This approach is due to completely removing free and bonded moisture contents in lignocellulosic fibers below the selected temperature. T_d values are additionally presented in Table 3. The reported test results agree with the spectroscopic analysis results, namely the estimated water absorption determined as the increase in absorbance intensity at 1620 cm^{-1} .

Morphology

Optical microscopy has been used to determine diameters' distribution for the three different samples; fibers obtained from the leaves are thinner ($71.6 \pm 35.1 \mu\text{m}$) than those obtained from the stems ($156.5 \pm 73.5 \mu\text{m}$). Shredded particles show the biggest size ($370.3 \pm 133.0 \mu\text{m}$). As observed in Figure 4, the shredded sample shows some thin fibers (lower than 50 μm in diameter), which were released during the mechanical shredding procedure, although these are merely testimonials. Most fibers have diameters between 50 and 150 microns, while the leaf fibers show an important percentage of fibers under 50 microns and stem fibers between 150 and 250 microns. Shredded material has a uniform distribution at bigger particle sizes (250–350 μm).

On the other hand, SEM micrographs (Figure 5) show clear differences between shredded and fiber samples. Fiber bundles of aligned microfibrils can be observed for all samples, usually happening for cellulosic fibers. These bundles are covered with a layer probably made of lignin or hemicellulose for shredded material (Khan et al. 2020). In contrast, this layer is reduced and appears broken for fiber samples (both from leaves and stems), giving a rougher aspect. This is in agreement with assays performed, which show lower hemicellulose content for fibers than for shredded material. Thinner fibers can be observed for fibers from leaves, as also determined in optical microscopy; this may be due to the higher lignin content, which bonds fibers together, as observed in SEM pictures. Fiber cell wall (Figure S1.c) has the same geometrical structure and different sizes of wall and lumen as already mentioned (Fiore, Scalici, and Valenza 2014). Cellulose is arranged in a spiral shape through the cellular wall; in some samples, elongated vascular cells and pit membranes (Lian et al. 2019) for water and nutrient exchange can also be observed (see Figure S1).

X-ray diffraction (XRD)

The XRD plots presenting X-ray diffraction patterns made for three types of fibers are shown in Figure 6. For all curves, a dominant peak at 2θ in the range of 22–23° can be noted, referred to as the crystallographic plane (002) characteristic for crystalline forms of cellulose I (Wang et al. 2016). The curves differ in peak intensities, taking the higher values for fibers and the lowest for shredded material. Additionally, the peak in the (101) crystallographic plane, also attributed to the crystalline cellulose phase (Barreto et al. 2010), is more distinct for fibers from stems. In the result of the calculations made for X-ray data according to Equation (1), the samples of natural fibers showed degrees of crystallinity at the level of 59.1%, 66.7%, and 73.1% for shredded material, fibers from stems, and leaves, respectively. Despite the changeable values concerning TCI resulting from a different

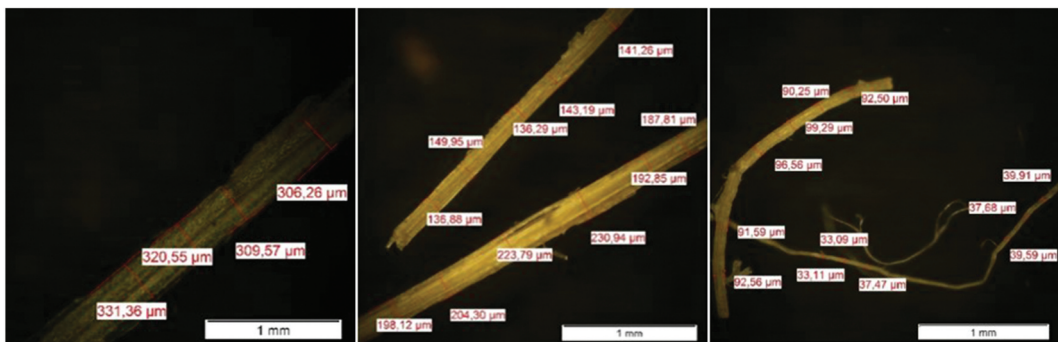
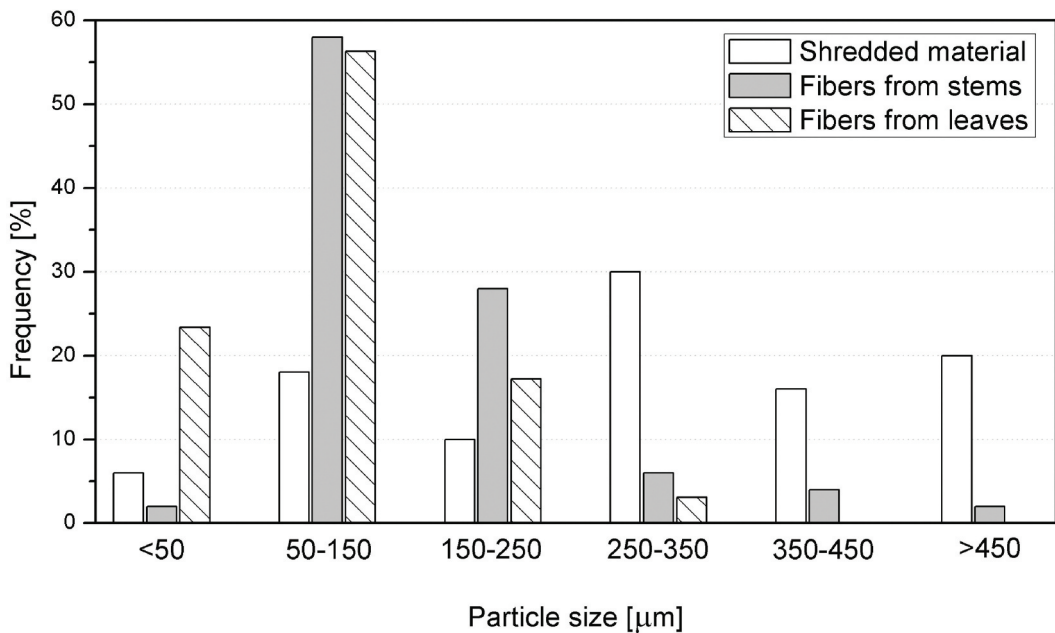


Figure 4. Particle size distribution (frequency vs. particle size, in microns) (above). Pictures from optical microscope and measurements for (a) shredded material, (b) stem fiber, and (c) leaves fiber (below).

methodology (Liu et al. 2012), the trend is comparable; the highest crystallinity characterizes fibers obtained from leaves.

Generally, the higher the cellulose content, the higher the CI. Some authors have even reported a linear correlation between these two parameters (Abidi and Manike 2018). The cellulose in the fibers obtained in this work account for over 65% of the total biomass, and CI is over 60%, while other authors report cellulose contents of 35% and 43% have revealed CI of 50% and 66%, respectively (Bessa et al. 2020; Chikouche et al. 2015). Alkali-treated fibers show higher crystallinity values, increasing up to 58.2% and 75.4%.

Mechanical properties

Single fiber tests have allowed obtaining tensile strength and elastic modulus for the two types of fibers obtained in this work; fibers from stems show an average strength of around 905 MPa, varying from 600 to 1200 MPa, and an elastic modulus close to 42 GPa (31–56 GPa). Fiore and collaborators (Fiore,

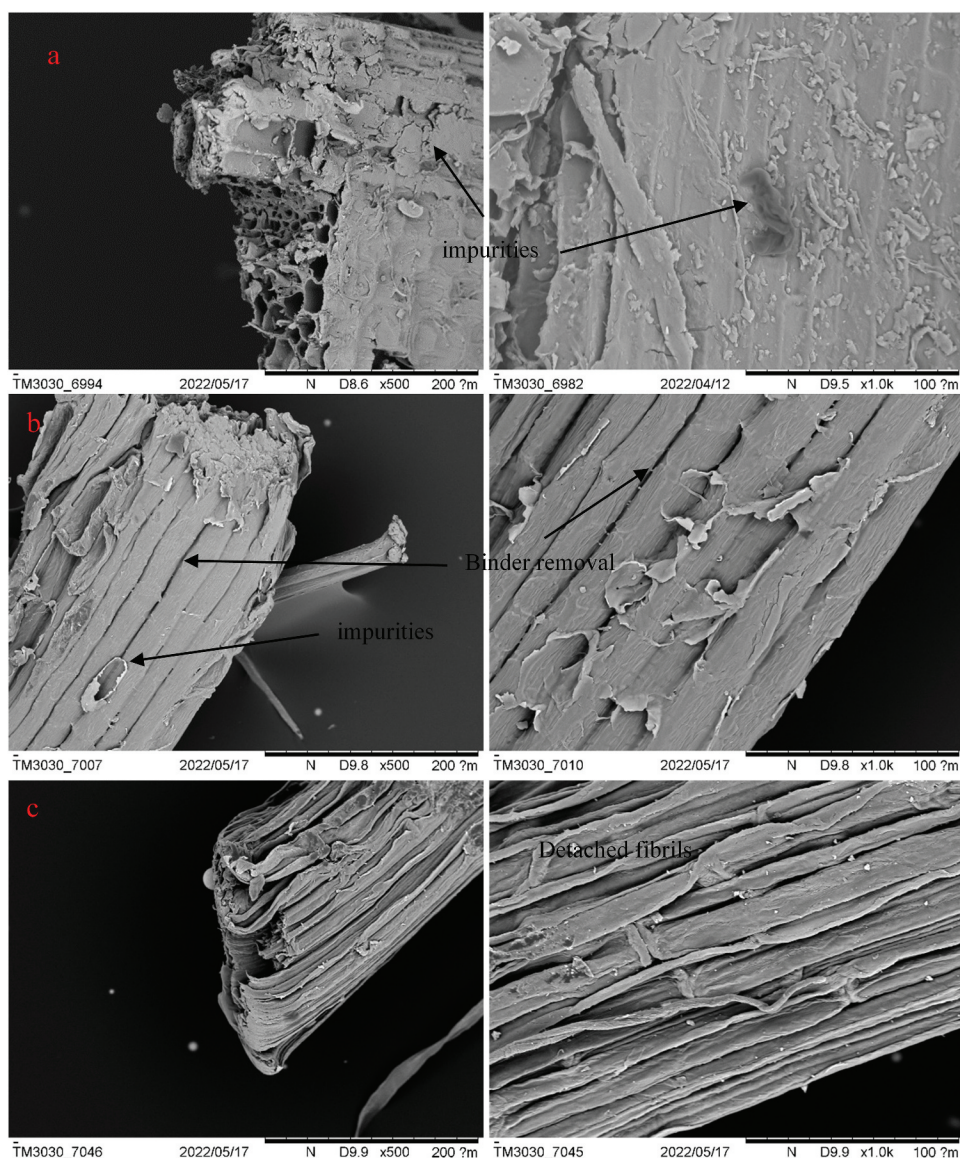


Figure 5. SEM pictures for (a) shredded material, (b) stem fiber, and (c) leaves fiber, at 500x and 1000 x magnifications.

Scalici, and Valenza 2014) reported 248 MPa and 9.4 GPa for fibers obtained from stems, which are quite lower than those shown here and those reported for other natural fibers, such as abaca (400–980 MPa; 8–20 GPa), jute (393–773 MPa; 27 GPa), flax (345–1035 MPa; 28 GPa) or bamboo (140–1000 MPa, 11–89 GPa) (Odesanya et al. 2021).

Fibers from leaves provide similar values, around 1000 MPa for tensile strength and 39 GPa for elastic modulus, although with higher dispersion of results, especially for modules. Tensile strength varied from 400 to 1500 MPa (a standard deviation of 300 MPa), while elastic modulus values from 12 to nearly 74 GPa were obtained (19 GPa deviation). This behavior for leaf fibers was also reported in (Scalici, Fiore, and Valenza 2016), although they also received lower values (173.90 ± 146.09 MPa for strength and 15.96 ± 12.17 GPa for modulus). The higher dispersion of results may be related to the increased distribution of diameters found for this material. On the other hand, as observed in SEM pictures, leaf fibers show detached microfibrils, which could explain the variability of results.

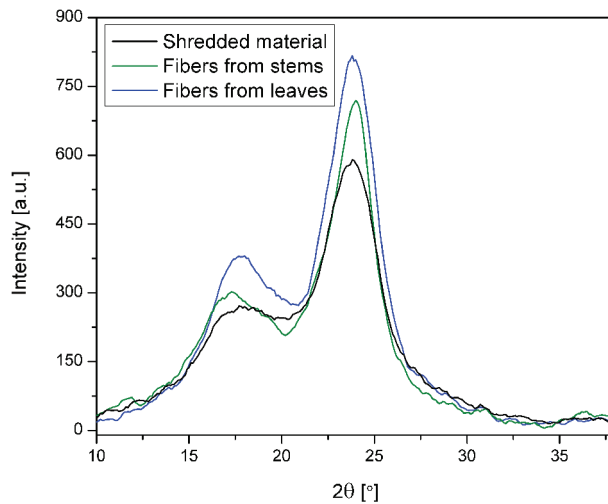


Figure 6. X-ray diffractograms for shredded material, stem fibers, and leaf fibers.

Table 4. Statistical parameters for tensile strength (in MPa) and modulus (in GPa) for *Arundo* fibers.

Tensile strength							
	Average	SD	Median	IQR	Shape parameter	Scale parameter	R^2
Stems	906	323	970	371	2.37	156.92	0.99
Leaves	961	258	962	411	4.10	1058.83	0.97
Modulus							
Stems	42	12	40	13	3.72	46.55	0.97
Leaves	39	19	35	28	1.99	43.89	0.98

Fiber's tensile strength and elastic modulus have been analyzed following a two-parameter Weibull distribution, as found in other works in the literature (Andersons et al. 2005; Fiore, Scalici, and Valenza 2014; Fiore, Valenza, and Di Bella 2011). The probability plots for these two properties can be found in the supplementary material (Figure S2). These graphs show that the data obtained fit a Weibull distribution quite well, as demonstrated by the correlation parameter in Table 4. Table 4 summarizes the statistical parameters obtained in such analysis. For a Weibull distribution, the shape parameter is related to the data variability, while the scale parameter corresponds to the 63.2%ile of the data. In this case, the results obtained are pretty close to normality, as the shape factor is in, or close to, the 2–4 range (Fiore, Valenza, and Di Bella 2011).

Conclusions

This study confirms that *Arundo donax* can be used as a source for high cellulose fibers with interesting mechanical properties and good thermal stability, suitable for thermoplastic composite production. It has been determined that fibers from leaves are thinner (diameter around 70 μm) and show higher crystallinity values (from FTIR and XRD analysis) than fibers from stems, which are thicker (around 150 μm). Thermal stability is similar for both, with an onset temperature of over 300°C. SEM pictures show the different morphology between shredded material and fibers and not much difference between fibers from stems and leaves, apart from fibrillation and lower fiber diameters. Fibers are formed by microfibril bundles and provide a rough surface due to the removal of binding agents, which may lead to a higher surface and, thus, better attachment to the polymeric matrix.

Highlights

- *Arundo donax* can be used as a source for high cellulose fibers with good mechanical properties
- Leaves fibers are thinner and more crystalline than stem fibers
- *Arundo* fibers show good thermal stability, with an onset temperature of over 300 °C
- The proposed method allows for the obtaining of fibers with good mechanical properties
- Fibers are formed by microfiber bundles and provide a rough surface

Acknowledgments

This research was funded by European Funding for Regional Development (FEDER), INTERREG MAC 2014-2020 program, providing funds for MAC Inv2Mac project (Grant number MAC2/4.6d/229). Luis Suárez also acknowledges the funding through the PhD grant program cofinanced by the Canarian Agency for Research, Innovation and Information Society of the Canary Islands Regional Council for Employment, Industry, Commerce and Knowledge (ACIISI) and by the European Social Fund (ESF) (Grant number TESIS2021010008). The authors would also like to thank Dr Katarzyna SKóczewska and MSC Sławomir Michałowski for their invaluable help and technical support in the field of XRD analysis.

Disclosure statement

No potential conflict of interest was reported by the author(s).

Funding

The work was supported by the Agencia Canaria de Investigación, Innovación y Sociedad de la Información [TESIS2021010008].

ORCID

Luis Suárez  <http://orcid.org/0000-0002-6709-1555>
 Mateusz Barczewski  <http://orcid.org/0000-0003-1451-6430>
 Paulina Kosmela  <http://orcid.org/0000-0003-4158-2679>
 María D. Marrero  <http://orcid.org/0000-0002-9396-1649>
 Zaida Ortega  <http://orcid.org/0000-0002-7112-1067>

References

- Abidi, N., and M. Manike. 2018. X-ray diffraction and FTIR investigations of cellulose deposition during cotton fiber development. *Textile Research Journal* 88 (7):719–30. doi:10.1177/0040517516688634.
- Accardi, D. S., P. Russo, R. Lauri, B. Pietrangeli, and L. Di Palma. 2015. From soil remediation to biofuel: Process simulation of bioethanol production from *Arundo donax*. *Chemical Engineering Transactions* 43:2167–72. doi:10.3303/CET1543362.
- Ahmed, M. J. 2016. Potential of *Arundo donax* L. stems as renewable precursors for activated carbons and utilization for wastewater treatments: Review. *Journal of the Taiwan Institute of Chemical Engineers* 63 (June):336–43. doi:10.1016/j.jtice.2016.03.030.
- American National Standard Institute. 1977. “ANSI/ASTM, 1977b. standard test methods for alpha-cellulose in wood D 1103-60.” Washington DC, USA.
- Andersons, J., E. Sparniņš, R. Joffe, and L. Wallström. 2005. Strength distribution of elementary flax fibres. *Composites Science and Technology* 65 (3–4):693–702. doi:10.1016/J.COMPSCITECH.2004.10.001.
- Antonetti, C., E. Bonari, D. Licursi, N. Nassio Di Nasso, and A. M. Raspolli Galletti. 2015. Hydrothermal conversion of giant reed to furfural and levulinic acid: Optimization of the process under microwave irradiation and investigation of distinctive agronomic parameters. *Molecules* 20 (12):21232–353. doi:10.3390/molecules201219760.
- Aymerich, F. R., M. A. E. Selma, I. H. García, V. M. Z. Pérez, P. F. Celdrán, R. V. López, J. M. Fernández, and J. M. Ródenas. 2012. “Seguimiento y Análisis de Las Actuaciones Para El Control Experimental de La Caña Común (*Arundo Donax*) En La Región de Murcia.” Murcia.
- Barreto, A. C. H., M. A. Esmeraldo, D. S. Rosa, P. B. A. Fechine, and S. E. Mazzetto. 2010. Cardanol biocomposites reinforced with jute fiber: Microstructure, biodegradability, and mechanical properties. *Polymer Composites* 31 (11):1928–37. doi:10.1002/PC.20990.
- Bessa, W., D. Trache, M. Derradji, H. Ambar, M. Benziane, and B. Guedouar. 2021, July. Effect of different chemical treatments and loadings of *Arundo donax* L. fibers on the dynamic mechanical, thermal, and morphological

- properties of bisphenol a aniline based polybenzoxazine composites. (pc.26215) *Polymer Composites* 42 (10):5199–208. doi: <https://doi.org/10.1002/pc.26215>.
- Bessa, W., D. Trache, M. Derradji, H. Ambar, A. F. Tarchoun, M. Benziane, and B. Guedouar. 2020. Characterization of raw and treated *Arundo donax* L. cellulosic fibers and their effect on the curing kinetics of bisphenol a-based benzoxazine. *International Journal of Biological Macromolecules* 164 (December):2931–43. doi:10.1016/j.ijbiomac.2020.08.179.
- Bledzki, A. K., A. A. Mamun, and J. Volk. 2010. Barley husk and coconut shell reinforced polypropylene composites: The effect of fibre physical, chemical and surface properties. *Composites Science and Technology* 70 (5):840–46. doi:10.1016/J.COMPSCITECH.2010.01.022.
- Browning, B. L. 1967. *Methods of wood chemistry. volumes I & II. methods of wood chemistry. volumes I & II*. New York: Interscience Publishers. Vol. 102. <http://www.biblio.com/book/methods-wood-chemistry-volume-1-browning/d/710364055>.
- Charca, S., C. Tenazoa, and H. S. Junior. 2021. Chemical composition of natural fibers using the measured true density. Case study: Ichu fibers. *Journal of Natural Fibers* 1–6. doi:10.1080/15440478.2021.1952143.
- Chikouche, M. D. L., A. Merrouche, A. Azizi, M. Rokbi, and S. Walter. 2015. Influence of alkali treatment on the mechanical properties of new cane fibre/polyester composites. *Journal of Reinforced Plastics and Composites* 34 (16):1329–39. doi:10.1177/0731684415591093.
- Csurhes, S. 2016. “Invasive weed risk assessment: Giant reed *Arundo Donax*.” https://www.daf.qld.gov.au/__data/assets/pdf_file/0006/59973/IPA-Giant-Reed-Risk-Assessment.pdf.
- Davide, B., A. Salanti, M. Orlandi, D. S. Ali, and L. Zoia. 2016. Biorefinery process for the simultaneous recovery of lignin, hemicelluloses, cellulose nanocrystals and silica from rice husk and *Arundo donax*. *Industrial Crops and Products* 86 (August):31–39. doi:10.1016/j.indcrop.2016.03.029.
- Di Fidio, N., A. M. Raspolli Galletti, S. Fulignati, D. Licursi, F. Liuzzi, I. De Bari, and C. Antonetti. 2020. Multi-step exploitation of raw *Arundo donax* L. for the selective synthesis of second-generation sugars by chemical and biological route. *Catalysts* 10 (1):79. doi:10.3390/catal10010079.
- Fernando, A. L., B. Barbosa, J. Costa, and E. G. Papazoglou. 2016 January. Giant reed (*Arundo donax* L.). *Bioremediation and Bioeconomy* 77–95. doi:10.1016/B978-0-12-802830-8.00004-6.
- Ferrández-García, C. E., J. Andreu-Rodríguez, M. T. Ferrández-García, M. Ferrández-Villena, and T. García-Ortuño. 2012. Panels made from giant reed bonded with non-modified starches. *BioResources* 7 (4):5904–16. doi:10.15376/biores.7.4.5904-5916.
- Ferrandez-Garcia, M. T., C. Eugenia Ferrandez-Garcia, T. Garcia-Ortuño, A. Ferrandez-Garcia, and M. Ferrandez-Villena. 2019. Experimental evaluation of a new giant reed (*Arundo donax* L.) composite using citric acid as a natural binder. *Agronomy* 9 (12):882. doi:10.3390/agronomy9120882.
- Ferrández-García, M. T., A. Ferrández-García, T. García-Ortuño, C. E. Ferrández-García, and M. Ferrández-Villena. 2020. Assessment of the physical, mechanical and acoustic properties of *Arundo donax* L. biomass in low pressure and temperature particleboards. *Polymers* 12 (6):1361. doi:10.3390/POLYM12061361.
- Ferrández Villena, M., C. E. F. Garcia, T. García Ortuño, A. Ferrández García, and M. T. Ferrández García. 2020. The influence of processing and particle size on binderless particleboards made from *Arundo donax* L. rhizome. *Polymers* 12 (3):696. doi:10.3390/polym12030696.
- Fiore, V., L. Botta, R. Scaffaro, A. Valenza, and A. Pirrotta. 2014. PLA based biocomposites reinforced with *Arundo donax* fillers. *Composites Science and Technology* 105 (December):110–17. doi:10.1016/j.compscitech.2014.10.005.
- Fiore, V., T. Scalici, and A. Valenza. 2014. Characterization of a new natural fiber from *Arundo donax* L. as potential reinforcement of polymer composites. *Carbohydrate Polymers* 106 (1):77–83. doi:10.1016/j.carbpol.2014.02.016.
- Fiore, V., A. Valenza, and G. Di Bella. 2011. Artichoke (*Cynara cardunculus* L.) fibres as potential reinforcement of composite structures. *Composites Science and Technology* 71 (8):1138–44. doi:10.1016/J.COMPSCITECH.2011.04.003.
- Francesco, B., A. M. Gabarron, J. A. F. Yepes, and J. J. P. Pérez. 2019. Innovative use of giant reed and cork residues for panels of buildings in Mediterranean area. *Resources, Conservation and Recycling* 140 (January):259–66. doi:10.1016/j.resconrec.2018.10.005.
- Galletti, A. M. R., C. Antonetti, E. Ribechini, M. P. Colombini, N. N. O Di Nasso, and E. Bonari. 2013. From giant reed to levulinic acid and gamma-valerolactone: A high yield catalytic route to valeric biofuels. *Applied Energy* 102 (February):157–62. doi:10.1016/j.apenergy.2012.05.061.
- García-Ortuño, T., J. Andréu-Rodríguez, M. T. Ferrández-García, M. Ferrández-Villena, and C. E. Ferrández-García. 2011. Evaluation of the physical and mechanical properties of particleboard made from giant reed (*Arundo donax* L.). *BioResources* 6 (1):477–86. doi:10.15376/biores.6.1.477-486.
- Ismail, Z. Z., and A. J. Jaël. 2014. A novel use of undesirable wild giant reed biomass to replace aggregate in concrete. *Construction and Building Materials* 67 (September):68–73. doi:10.1016/j.conbuildmat.2013.11.064.
- Javier, A.-R., E. Medina, M. T. Ferrandez-Garcia, M. Ferrandez-Villena, C. E. Ferrandez-Garcia, C. Paredes, M. A. Bustamante, and J. Moreno-Caselles. 2013. Agricultural and industrial valorization of *Arundo donax* L. *Communications in Soil Science and Plant Analysis* 44 (1–4):598–609. doi:10.1080/00103624.2013.745363.
- Jensen, E. F., M. D. Casler, K. Farrar, J. M. Finnan, R. Lord, C. Palmborg, J. Valentine, and I. S. Donnison. 2018. Giant reed: From production to end use. In *Perennial Grasses for Bioenergy and Bioproducts*, ed. E. Alexopoulou, 107–50. London: Academic Press Inc. Elsevier.
- Jiménez Auzmendi, E. 2014. Plantas Invasoras, ¿ Batalla Perdida? ¿ O No ? *Investigación, Gestión Y Técnica Forestal, En La Región de La Macaronesia* 135–55. Universidad de La Laguna. Editor: Juan Carlos Santamarta Cerezal. 2014. 978-

- 84-617-3391-0. Madrid: Colegio de Ingenieros de Montes. Accessed at: <https://mdc.ulpgc.es/utills/getfile/collection/MDC/id/177834/filename/218410.pdf>
- Jiménez-Ruiz, J., L. Hardion, J. P. Del Monte, B. Vila, and M. I. Santín-Montanyá. 2021. Monographs on invasive plants in Europe N° 4: *Arundo donax* L. *Botany Letters* 168 (1):131–51. doi:10.1080/23818107.2020.1864470.
- Khan, A., R. Vijay, D. L. Singaravelu, M. R. Sanjay, S. Siengchin, F. Verpoort, K. A. Alamry, and A. M. Asiri. 2020. Characterization of natural fibers from *Cortaderia selloana* grass (pampas) as reinforcement material for the production of the composites. *Journal of Natural Fibers*. doi:10.1080/15440478.2019.1709110.
- Lian, C., R. Liu, C. Xiufang, S. Zhang, J. Luo, S. Yang, X. Liu, and B. Fei. 2019. Characterization of the pits in parenchyma cells of the moso bamboo [*Phyllostachys edulis* (Carr.) J. Houz.] Culm. *Holzforschung* 73 (7):629–36. doi:10.1515/HF-2018-0236.
- Liu, Y., D. Thibodeaux, G. Gamble, P. Bauer, and D. VanDerveer. 2012. Comparative investigation of Fourier transform infrared (FT-IR) spectroscopy and X-ray diffraction (XRD) in the determination of cotton fiber crystallinity. *Applied Spectroscopy* 66 (8):983–86. doi:10.1366/12-06611.
- Martin, S., J. A. G. Carolina, and J. Barroso. 2019. Control of volunteer giant reed (*Arundo donax*). *Invasive Plant Science and Management* 12 (1):43–50. doi:10.1017/inp.2018.36.
- Martínez-Sanz, M., E. Erboz, C. Fontes, and A. López-Rubio. 2018. Valorization of *Arundo donax* for the production of high performance lignocellulosic films. *Carbohydrate Polymers* 199 (November):276–85. doi:10.1016/j.carbpol.2018.07.029.
- Odesanya, K. O., R. Ahmad, M. Jawaaid, S. Bingol, G. O. Adebayo, and Y. H. Wong. 2021. Natural fibre-reinforced composite for ballistic applications: A review. *Journal of Polymers and the Environment* 29 (12):3795–812. doi:10.1007/s10924-021-02169-4.
- Ortega, Z., F. Romero, R. Paz, L. Suárez, A. N. Benítez, and M. D. Marrero. 2021. Valorization of invasive plants from macaronesia as filler materials in the production of natural fiber composites by rotational molding. *Polymers* 13 (13):2220. doi:10.3390/polym13132220.
- Oudiani, A. E., S. Msahli, and F. Sakli. 2017. In-depth study of agave fiber structure using Fourier transform infrared spectroscopy. *Carbohydrate Polymers* 164 (May):242–48. doi:10.1016/J.CARBPOL.2017.01.091.
- Piperopoulos, E., A. Khaskhoussi, V. Fiore, and L. Calabrese. 2021. Surface modified *Arundo donax* natural fibers for oil spill recovery. *Journal of Natural Fibers* 1–16. doi:<https://doi.org/10.1080/15440478.2021.1961343>.
- Proietti, S., S. Moscatello, M. Fagnano, N. Fiorentino, A. Impagliazzo, and A. Battistelli. 2017. Chemical composition and yield of rhizome biomass of *Arundo donax* L. grown for biorefinery in the Mediterranean environment. *Biomass & Bioenergy* 107 (December):191–97. doi:10.1016/j.biombioe.2017.10.003.
- Sang Youn, O., D. I. Yoo, Y. Shin, H. C. Kim, H. Y. Kim, Y. S. Chung, W. H. Park, and J. H. Youk. 2005. Crystalline structure analysis of cellulose treated with sodium hydroxide and carbon dioxide by means of X-ray diffraction and FTIR spectroscopy. *Carbohydrate Research* 340 (15):2376–91. doi:10.1016/J.CARRES.2005.08.007.
- Scalici, T., V. Fiore, and A. Valenza. 2016. Effect of plasma treatment on the properties of *Arundo donax* L. leaf fibres and its bio-based epoxy composites: A preliminary study. *Composites Part B: Engineering* 94 (June):167–75. doi:10.1016/j.compositesb.2016.03.053.
- Shatalov, A. A., and H. Pereira. 2005. Kinetics of organosolv delignification of fibre crop *Arundo donax* L. *Industrial Crops and Products* 21 (2):203–10. doi:10.1016/j.indcrop.2004.04.010.
- Shatalov, A. A., and H. Pereira. 2013. High-grade sulfur-free cellulose fibers by pre-hydrolysis and ethanol-alkali delignification of giant reed (*Arundo donax* L.) stems. *Industrial Crops and Products* 43 (1):623–30. doi:10.1016/j.indcrop.2012.08.003.
- Sluiter, A., R. Ruiz, C. Scarlata, J. Sluiter, and D. And Templeton NREL/TP-510-42619 - Determination of Extractives in Biomass: Laboratory Analytical Procedure (LAP). Technical Report NREL/TP-510-42619. January 2008. Accessible on: <https://www.nrel.gov/docs/gen/fy08/42619.pdf>
- Suárez, L., J. Castellano, F. Romero, M. D. Marrero, A. N. Benítez, and Z. Ortega. 2021. Environmental hazards of giant reed (*Arundo donax* L.) in the Macaronesia region and its characterisation as a potential source for the production of natural fibre composites. *Polymers* 13 (13):2101. doi:10.3390/polym13132101.
- Tarek, A., N. Elhawat, É. Domokos-Szabolcsy, J. Káti, L. Márton, M. Czako, H. El-Ramady, and M. G. Fári. 2015. Giant reed (*Arundo donax* L.): A green technology for clean environment. *Phytoremediation: Management of Environmental Contaminants* 1:1–20. doi:10.1007/978-3-319-10395-2_1.
- Wang, C., S. Bai, X. Yue, B. Long, and L. P. Choo-Smith. 2016. Relationship between chemical composition, crystallinity, orientation and tensile strength of kenaf fiber. *Fibers and Polymers* 2016 (11):1757–64. doi:10.1007/S12221-016-6703-5.
- Yang, H., R. Yan, H. Chen, D. H. Lee, and C. Zheng. 2007. Characteristics of hemicellulose, cellulose and lignin pyrolysis. *Fuel* 86 (12–13):1781–88. doi:10.1016/j.fuel.2006.12.013.

6.4. A NEW IMAGE ANALYSIS ASSISTED SEMI-AUTOMATIC
GEOMETRICAL MEASUREMENT OF FIBRES IN
THERMOPLASTIC COMPOSITES: A CASE STUDY ON
GIANT REED FIBRES

P1

P2

P3

P4

P5

P6

P7

P8

P9

P10



Article

A New Image Analysis Assisted Semi-Automatic Geometrical Measurement of Fibers in Thermoplastic Composites: A Case Study on Giant Reed Fibers

Luis Suárez ^{1,*} , Mark Billham ², Graham Garrett ², Eoin Cunningham ³, María Dolores Marrero ¹ and Zaida Ortega ^{4,*}

- ¹ Departamento de Ingeniería Mecánica, Universidad de Las Palmas de Gran Canaria, 35017 Las Palmas de Gran Canaria, Spain; mariadolores.marrero@ulpgc.es
- ² Polymer Processing Research Centre, School of Mechanical and Aerospace Engineering, Queen's University of Belfast, Belfast BT9 5AH, UK; m.billham@qub.ac.uk (M.B.); g.s.garrett@qub.ac.uk (G.G.)
- ³ School of Mechanical and Aerospace Engineering, Queen's University Belfast, Stranmillis Road, Belfast BT9 5AH, UK; e.cunningham@qub.ac.uk
- ⁴ Departamento de Ingeniería de Procesos, Universidad de Las Palmas de Gran Canaria, 35017 Las Palmas de Gran Canaria, Spain
- * Correspondence: luis.suarez@ulpgc.es (L.S.); zaida.ortega@ulpgc.es (Z.O.)

Abstract: This work describes a systematic method for the analysis of the attrition and residual morphology of natural fibers during the compounding process by twin-screw extrusion. There are several methods for the assessment of fiber lengths and morphology, although they are usually based on the use of non-affordable apparatus or time-consuming methods. In this research, the variation of morphological features such as the length, diameter and aspect ratio of natural fibers were analyzed by affordable optical scanning methods and open-source software. This article presents the different steps to perform image acquisition, refining and measurement in an automated way, achieving statistically representative results, with thousands of fibers analyzed per scanned sample. The use of this technique for the measurement of giant reed fibers in polyethylene (PE) and polylactide (PLA)-based composite materials has proved that there are no significant differences in the output fiber morphology of the compound, regardless of the fiber feed sizes, extruder scale, or the polymer used as matrix. The ratio of fiber introduced for the production of composites also did not significantly affect the final fiber size. The greatest reduction in size was obtained in the first kneading zone during compounding. Pelletizing or injection molding did not significantly modify the fiber size distribution.

Keywords: aspect ratio; composites; fibers; measurement; morphology; open source; low-cost technique



Citation: Suárez, L.; Billham, M.; Garrett, G.; Cunningham, E.; Marrero, M.D.; Ortega, Z. A New Image Analysis Assisted Semi-Automatic Geometrical Measurement of Fibers in Thermoplastic Composites: A Case Study on Giant Reed Fibers. *J. Compos. Sci.* **2023**, *7*, 326. <https://doi.org/10.3390/jcs7080326>

Academic Editor: Fabrizio Sarasini

Received: 30 June 2023

Revised: 2 August 2023

Accepted: 7 August 2023

Published: 9 August 2023



Copyright: © 2023 by the authors. Licensee MDPI, Basel, Switzerland. This article is an open access article distributed under the terms and conditions of the Creative Commons Attribution (CC BY) license (<https://creativecommons.org/licenses/by/4.0/>).

1. Introduction

When natural fibers are used to produce biocomposites, they can be present in different formats, such as: particles, short or long fibers, continuous or discontinuous, aligned (uni-, bi- or multi-directionally) or randomly distributed, as well as forming woven fabrics or non-woven mats [1]. The morphology, orientation and distribution of the fibers are key issues that determine the processability and performance of the composites. The processability of composites based on short fibers and particles is usually easier and cheaper, while composites based on long fibers and fabrics are often more challenging to process, although they can also achieve better mechanical performance [2]. Therefore, fiber morphology, as well as distribution and integration within the matrix, has a decisive influence on the processability, mechanical properties, tribological behavior and general performance of the composites [3–5].

Compounding extrusion is a common process for the preparation of thermoplastic-based composites with random-oriented chopped fiber reinforcement and particles. This is

a pre-process for the preparation of materials for ulterior processing (injection, compression or rotational molding). During the compounding process, one or more polymers are intimately blended with additives and fillers, such as short fibers, by using twin-screw extruders. Some of the key properties in the performance of extruded fiber compounds, in addition to the inherent fiber strength and the quality of the bonding interface within the matrix, are the length, diameter and aspect ratio of the fibers [4]. Fiber lengths in extruded thermoplastic compounds are usually in the order of a few millimeters, becoming even less than 1 mm after injection molding processes [6]. In terms of diameters, most lignocellulosic fibers for biocomposite production have diameters lower than a few hundred microns [7], dimensions which are reduced by attrition of the bundles during processing [5].

The physical degradation of lignocellulosic fibers during the compounding process is affected by parameters such as the feed and shear rate, as well as the rotation speed and geometric configuration of the screws [8]. The residual fiber morphology (length, diameter and aspect ratio) in molded parts is affected by several factors during compounding process, from the polymer matrix selection and the type of filler—which affect the processing temperature, viscosity and shear rate of the compound—to the fiber content or the screw profile, among others. Along the entire process, the fibers are subjected to severe stresses, which cause the breakage of fibers [4,5]; these stresses are due to hydrodynamic effects, fiber-fiber interactions and fiber-equipment interaction [9].

This work describes a systematic method for the analysis of the residual morphology of short fibers during and after compounding processes (molding stage). A wide variety of measurement approaches have been documented in the literature for the dimensional analysis of fibers in composite processing, but no standard has been accepted [10]. The methods found in bibliography range from time-consuming manual techniques [11], where fiber detection is done manually by clicking on the endpoints of the fibers; to fully automated systems, usually not affordable in terms of economic costs, incorporating automation in sample preparation and object detection, as well as analysis tools based on artificial intelligence (AI) and deep learning algorithms [12]. According to some authors, there are no “absolute” length values from one system to another, and a 20% variance is typically accepted as valid [12].

Most methods are based on the removal of the polymer matrix (destructive methods) and consist of four main steps:

- Separation of the fibers from the matrix by pyrolysis [9] or chemical dilution [8,13]
- Dispersion of the fibers on a surface (2D) or in a liquid or gaseous medium (3D) [14]
- Image acquisition by microscopy, laser diffraction or high-resolution scanning [14]
- Fiber detection: manually [15] or with the support of automated systems [10]

Non-destructive methods are mainly based on micro-CT [16] and advanced automated software for fiber identification, such as MorFi [12,17] or Ellix [18]. However, this method remains challenging [10,19] due to the variation in fiber widths and their intersections [15,20].

As an alternative to the rough hand-measuring methods and expensive automated equipment, this article presents a new approach based on affordable optical scanning methods (as also proposed in other works [21,22]), and the open-source software ImageJ2 [23]. This measurement method provides a statistically significant number of measurements at each sampling (thousands of data points per sample) and has been tested for the study of giant reed (*Arundo donax* L.) fibers during processing. From raw materials (fibers of two different lengths) to injection-molded samples (using two different extruders for compounding preparation), the method also assesses the variations found during the compounding stage throughout the twin-screw extruders. Some authors indicate that the viscosity of the polymer melt can affect the fiber's attrition [5], and so two different matrices (PLA and HDPE), and four different fiber loadings (from 5 to 40%), have been analyzed. The proposed method combines elements from other techniques and aims to minimize the manual input to achieve highly reproducible measurements in a cost-effective way, in contrast with other research, which focus on expensive equipment, time consuming methods or measurement of a low number of objects, usually not exceeding 300 values [9,24,25].

2. Materials and Methods

Fibers from a giant reed were extracted from *Arundo donax* L. culms, as described elsewhere [26], and cut to nominally 1.5 and 3 mm average length, to assess the influence of fiber length in the feeding.

Two different polymer matrices were used in the research: high density polyethylene (HDPE, grade HD6081, from Total (Feluy, Belgium)) and polylactide (PLA, grade Luminy L105, from Corbion Polymers (Gorinchem, The Netherlands)). HDPE has a melt flow index (MFI) of 8 g/10 min (190 °C/2.16 kg) and a density of 960 kg/m³, while PLA has an MFI of 30 g/10 min (190 °C/2.16 kg) and a density of 1240 kg/m³, according to the manufacturers' datasheets. These two matrices were selected to determine if their different properties influenced the fiber performance during the different steps of processing.

The compounding was prepared using two different extruders, to assess the effect of two similar configurations of the screw—although at different barrel size and L/D ratio—in the fibers' shortening (ThermoScientific Process11 (Karlsruhe, Germany) and Collin ZK25 (Maitenbeth, Germany), with the screw configurations shown in Table 1). In addition, samples from various locations throughout the first extruder were taken to analyze the evolution of fiber morphology and dimensions along the compounding process (Figure 1).

Table 1. Configuration of the twin-screw extruders used in the research.

Apparatus	Diameter (mm)	L/D Ratio	Screw Speed (rpm)	Screw Configuration
ThermoScientific Process11	11	40/1	100	
Collin ZK25	25	30/1	250	



Figure 1. Samples taken along the Process11 extruder.

Finally, the influence of the ratio of fiber used was also determined, by preparing compounds at 5, 10, 20 and 40% fiber loadings (in weight). The compound was injection molded in an Arburg 320S injection molding machine. The following temperature profile, from back to nozzle, was used: 175-180-185-185-190 °C, for HDPE; for PLA, the temperature profile was 190-195-200-205-210 °C, keeping a back pressure of 100 bar, a flow rate of

70 cm³/s and a holding pressure of 250 bar. The mold temperature was kept at 30 °C in both cases.

The procedure for the measurement of the fibers is summarized in the following steps, detailed in Section 2.1 below:

1. Sample preparation
2. Image acquisition
3. Pre-processing and segmentation
4. Object detection and measurement
5. Statistical analysis

2.1. Description of the Developed Methodology

2.1.1. Sample Preparation

After the preparation of the compound, thin films of approximately 200 microns thick were prepared by compressing the samples (approximately 1 g) in a hot press at 200 °C in between anti-adherent foils. The film specimen was obtained from pellets, extruded filaments and injection-molded parts fragments, depending on the processing step under study. In order to spread the fibers and obtain more accurate readings, the prepared films are folded together with a neat polymer film, melted and pressed again, in that way dispersing the fibers (Figure 2). A specimen prepared in this way is big enough to be statistically significant, as it contains several thousand fibers [22]. Compression of the composite materials is conducted by gradually applying pressure (increasing the pressure by 5 bar every 10 s up to 30 bar, obtaining a sample film thickness of about 200 microns) once the matrix is completely melted, to avoid or reduce the shear effects that can influence the shortening or separation of the fibers. Rheological and thermal analysis of the materials were considered to set temperature processing.

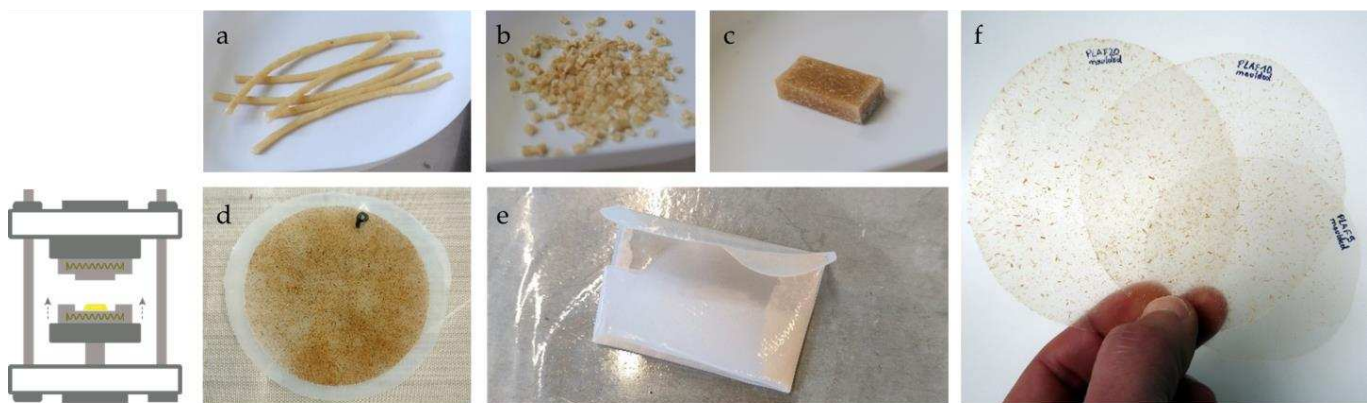


Figure 2. Sample preparation: from (a) extruded filament, (b) pellets or (c) molded part. (d,e) Sample film folded together with polymer film to enhance fiber dispersion. (f) Specimens ready for image analysis.

2.1.2. Image Acquisition

An image with thousands of fibers is captured using a flatbed document scanner (Canon CanoScan LiDE 400 (Tokyo, Japan)) at a high-resolution of 4800 dpi (dots per inch) [27]. This optical resolution corresponds to 5.29 microns per pixel, which is 2 to 10 times smaller than the diameter of commonly used natural fibers such as cotton, flax or hemp; that is, approximately less than half the fibers' diameter. A blue piece of paper was used as a background to enhance the contrast with the fibers (yellowish) and facilitate identification (Figure 3a).

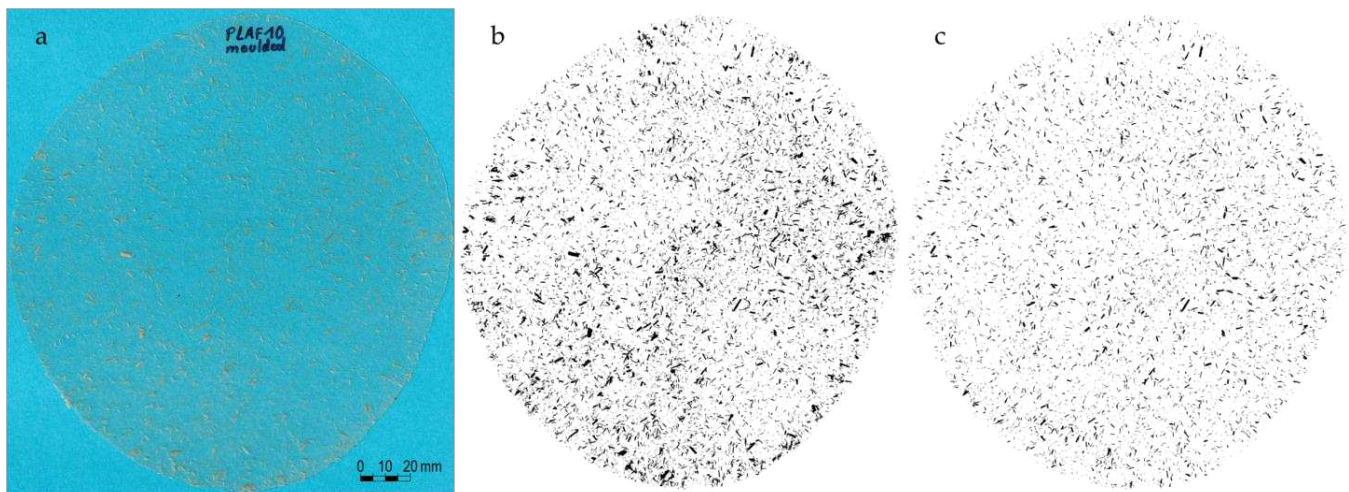


Figure 3. Image processing for fiber measurement: (a) scanned image; (b) image after binary segmentation; (c) image after shape filtering.

2.1.3. Pre-Processing and Segmentation

The objective of this stage is to convert the scanned color bitmap image into a binary (black and white) image. This consists of dividing the digital image into several segments where the objects of interest, namely the fibers, are separated from the background by a process of thresholding or binarization (Figure 3b). This task is performed using the photo-editing software Adobe Photoshop 24.7. For this purpose, an action script has been recorded with the necessary instructions to automate the processing (Figure 4). The binarization process is conducted through a selection based on the color range, the creation of a uniform color fill layer, the refinement of the mask edges and the conversion of the image to indexed color mode. Before running the binary segmentation, a selection is made on the working area of the image to avoid any possible shadows captured during the scanning process along the edge of the sample.

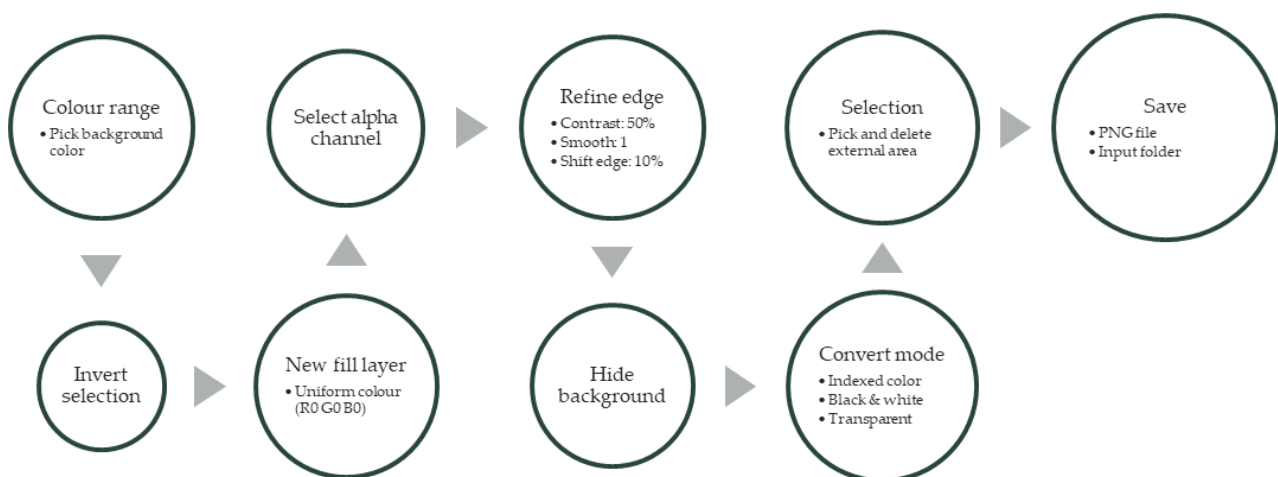


Figure 4. Photoshop action script for image segmentation.

Adobe Photoshop is used not only for its potential and versatility in image editing, but also for its ability to manage massive files. In this way, the original file (.JPG), with a size of about 200 or 300 MB, is transformed into a black and white picture with a reduced size of only 1 or 2 MB, which is much faster and easier to process in ImageJ (analysis program). Alternatively, it would be possible to run the proposed method using exclusively open-source software if smaller images are processed, consequently with a lower number

of fibers per sample. In that case the segmentation could be done directly by the ImageJ program used for the dimensional analysis, but several samples should be processed to reach a statistically significant data set.

Although the steps included in the action script for masking and selection can be adjusted and customized for each image, when working with batches of samples with the same background color and the same thermoplastic matrix, it is not necessary to modify these settings for each image, as the process is fully automated by executing the pre-programmed script.

2.1.4. Object Detection and Measurement

After image segmentation, ImageJ (FIJI) is used for morphological analysis and fiber measurement. ImageJ (Bethesda, Maryland, WA, USA) [23] is a Java-based image-processing program widely used in several areas of scientific research.

A procedure has been developed for fully-automatic fiber recognition based on some shape filtering criteria (Figure 5). After filtering, the selected objects are added to the ROI manager to later obtain a table with measurement results. Every binary object found in the picture is morphologically analyzed in terms of its feret diameters (maximum and minimum), aspect ratio, convexity and solidity [28]. The maximum feret diameter (L) determines the length of the fiber, while the minimum feret diameter (D) determines the thickness of the fiber. Aspect ratio is calculated as the length divided by the thickness. Other methods, based on “geodesic diameter” and “geodesic radius”, were also evaluated for fiber length and diameter calculations [10], but these were rejected as the dimensions were often overestimated.

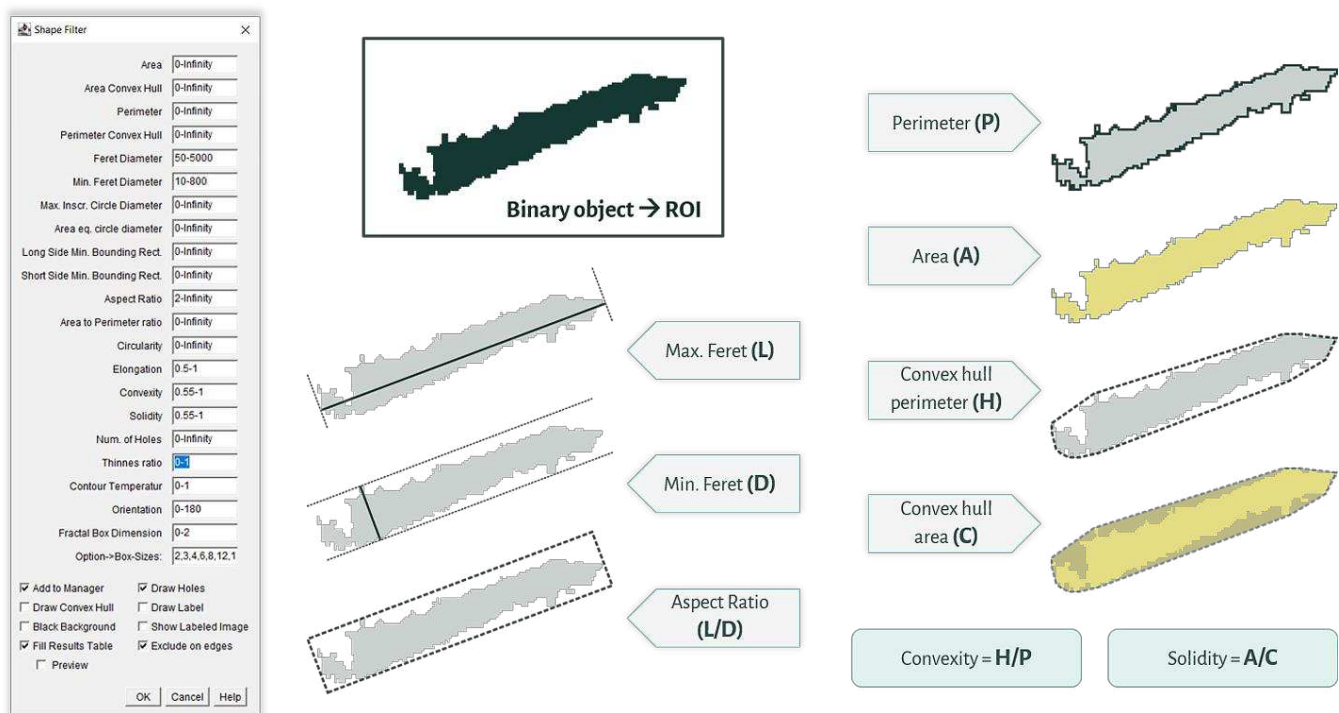


Figure 5. Shape filtering criteria.

The aim of the shape filtering is to identify individual fibers by avoiding or rejecting objects found on the binary image, such as bubbles, clusters, intersecting fibers and fine particles. By convention, particles with a length smaller than 200 μm are considered as ‘fine’ elements and not fibers [29]. After this step, a new picture of isolated fibers with no or little curvature is obtained (Figure 3c).

The admissible ranges for all morphological parameters are set in the “Shape filter” plugin for individual fiber recognition. Similar to the segmentation stage, all instructions

are recorded in an ImageJ macro for automatic image processing. In this way, the file with the binary image (after segmentation) is read from an input folder and the filtered image is saved into an output folder (Figure S1). The measurement data results are saved in a CSV file for further analysis.

The adjustment of the morphological filtering parameters is performed by an iterative process and direct visualization of the results until the desired screening threshold is reached; that is, eliminating possible bubbles, clusters or intersecting fibers and fine particles. This is done by overlaying the filtered binary images on the scanned bitmap image, varying the selection ranges at each step until an image containing only individualized fibers is obtained. Although this task is initially tedious in the definition of the methodology, once the filter ranges are delimited, these settings can be applied for all fiber-reinforced composites of similar characteristics. However, it is also possible to vary the values of the ranges if, for example, the diameters or lengths of the analyzed fibers are larger or smaller.

2.1.5. Statistical Analysis

The statistical analysis is done using Jamovi 2.3.26, a free and open-source statistical platform. Measurement data are analyzed to obtain average and deviation values, as well as frequency distribution (tables and graphs) of the length, diameter and aspect ratio of the fibers at each stage of processing. The capability of importing a large amount of data into the statistical analysis software is useful to compare variations from one stage to another; i.e., from fed fibers to extruded compound, granulation or injection molding.

3. Results and Discussion

This section shows the results obtained from the above-described methodology for the case study selected; that is, the processing of giant reed fibers with two different matrices, in two different kinds of processing equipment, with two different starting fiber lengths and in different weight loadings.

3.1. Fibers Shortening along the Extruder

Samples at different zones of the Process 11 extruder, from hopper to die, were collected during the compounding process. The compounded material was taken out by opening the barrel of the twin-extruder after reaching a stable production rate.

After sample film preparation by platen press and measurement of the fibers according to the described method, it was found that:

- The greatest reduction in fiber length and diameter occurs from the first zone of the extrusion process, where more than 85% of the fibers for HDPE and 90% for the PLA compound become shortened to less than 1 mm in length (Figure 6).
- There is not much variation along the rest of the screw, either in length or diameter.
- The processing leads to a narrower size distribution, that is, despite the most important reduction in length occurring in zone 1, fibers continue suffering further attrition, obtaining at the end of the process a composite with similar fiber length to those from zone one, but with lower variability. This effect was also observed by Hubbe and Grigsby [4].

At this point it is worth noting that although mean values and variance are widely used in the literature for the morphological characterization of fibers, as they allow a quick nominal size classification, they can be influenced and biased by a non-symmetrical distribution of the data [18]. For a more accurate analysis, distribution charts allow the reduction of the estimation error throughout the process. This explains the apparent increase in fiber diameter and length from zone 1 to zone 2; if fiber distribution is compared, and not only average values, it was found that the size reduction is obtained mainly in Section 1, remaining mostly unchanged along the remaining zones in the extruder.

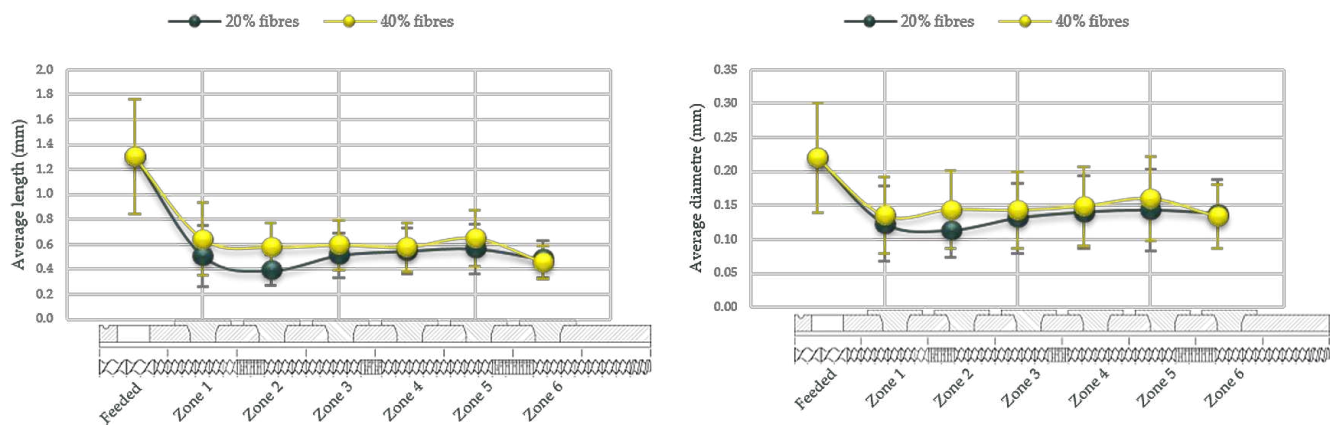


Figure 6. Fiber length and diameter evolution in HDPE-based composites produced in Process 11 twin-screw extruder (20% and 40% filler ratio).

3.2. Influence of Extruder Size

When comparing the production of identical compounding formulations produced by the two different extruders used in the study, it was found that:

- Fiber attrition is slightly higher in the larger extruder (ZK25), which has a more aggressive screw configuration (Figure 7). For PLA composites with 20% lignocellulosic filler, the average fiber length is reduced by more than a quarter after extrusion, while for the smaller extruder the fiber shortening is only about a third.
- The injection molding process seems not to significantly affect the residual fiber morphology. That is, both composites provided the same fiber length and diameter in the final part, regardless of the extruder in which the compound was prepared.

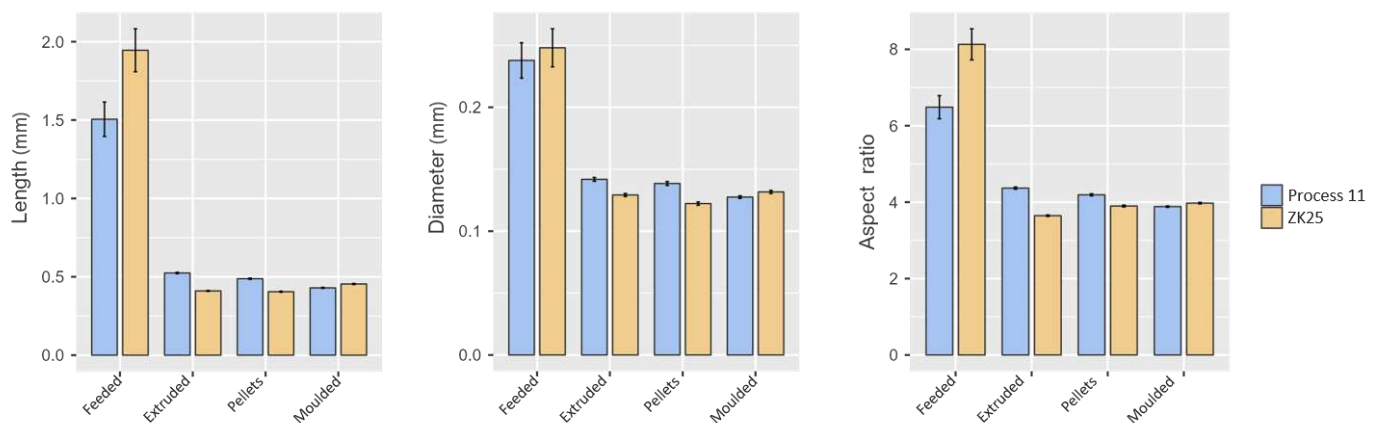


Figure 7. Variation in length, diameter and aspect ratio of fibers for the same composite formulation (PLA + 20% fibers), produced on Process 11 and ZK25 extruders.

3.3. Influence of Fiber Length in the Feeding

Despite using fibers that were twice as long for the extruder feed, the average fiber dimensions in the manufactured compound remains the same. The fiber size distribution (lengths and diameters) is practically identical at the end of the compounding process (Figure 8), regardless of the size of the input fibers. Only a small, non-significant difference is observed in the aspect ratio. The average value obtained for this morphological characteristic is slightly higher for composites produced from shorter fibers after extrusion and pelletizing.

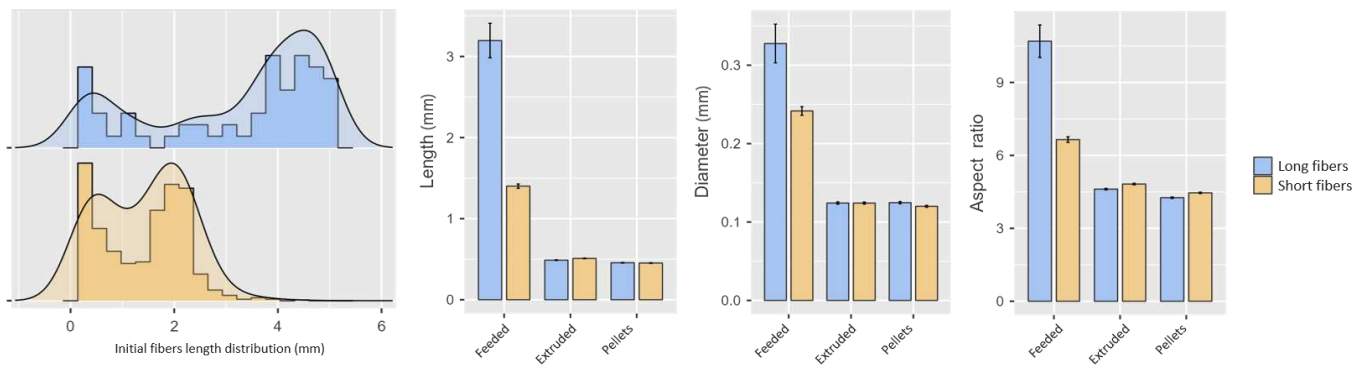


Figure 8. Variation of fiber dimensions for the same composite formulation (HDPE + 20% fibers), produced by ZK25 extruder, when fed fibers of different initial nominal sizes.

3.4. Influence of Polymer Matrix

Regarding the effect of the thermoplastic resin on fiber attrition, only a slightly lower incidence of processing on the diameter or thickness of the fiber bundles is observed when PLA is used as the matrix (Figure 9). This might be due to the lower viscosity of the polymer (with an MFI about three times that for HDPE); the higher flow of material might then reduce the fiber attrition.

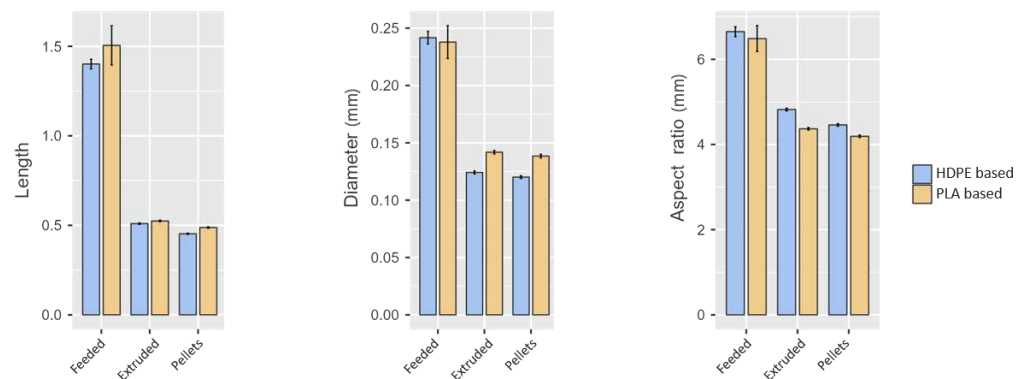


Figure 9. Fiber size changes for HDPE and PLA composites reinforced with 20% fiber. Compounding produced by ZK25 extruder.

3.5. Influence of Filler Ratio

Having used fiber contents of 5, 10, 20 and 40% by weight, no significant differences were found when varying the filler ratio on the residual size of the fibers present in the composite material. Figure 10 shows the results obtained for the composites at 5 and 20%.

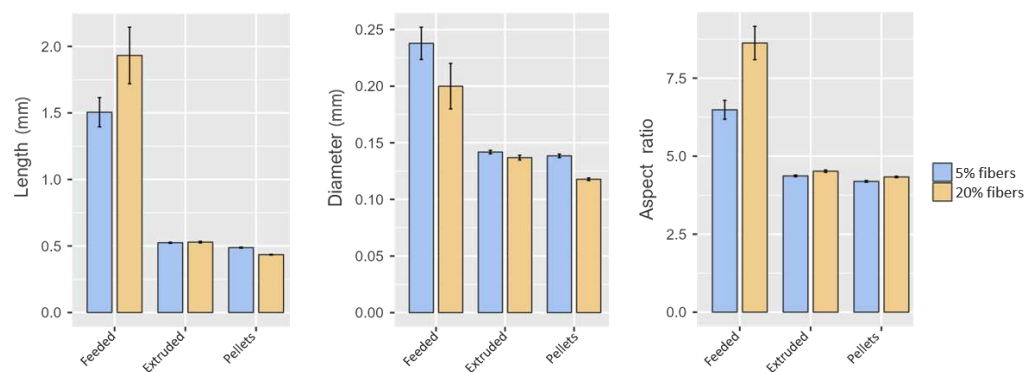


Figure 10. Fiber size changes in the HDPE composites reinforced with 5 and 20% fiber. Compounding produced by ZK25 extruder.

3.6. Method Validation

In order to validate the proposed methodology, the results obtained have been compared against those obtained by manual measurement. For this purpose, a scanned sample has been divided into sectors in order to have a manageable image for the hand-measurement procedure, thus containing only a few hundred fibers instead of thousands. The same sub-sample was analysed using the semi-automatic method and by hand, using the manual measurement tools provided by ImageJ. In the first instance, it was found that the number of objects (fibres) detected by the automatic procedure is four times the number of fibres that were identified manually. This difference is mainly due to the ability of automatic filtering to detect small particles that are difficult to pick out when fibres are selected by hand. By setting a shape criterion that fixes the minimum length for filtering at the smallest of the manually detected fibre lengths, the results obtained by both procedures are quite similar, as shown in Table 2.

Table 2. Comparative results between semi-automatic and manual measuring methods.

		95% Confidence Interval								
	Measurement Method	N	Mean	Lower	Upper	Median	SD	Variance	Minimum	Maximum
Length	manual	105	0.781	0.725	0.837	0.672	0.288	0.083	0.353	1.858
	semi-automatic	239	0.621	0.589	0.652	0.547	0.245	0.06	0.35	1.878
Diameter	manual	105	0.161	0.15	0.171	0.15	0.053	0.003	0.068	0.373
	semi-automatic	239	0.174	0.161	0.188	0.137	0.107	0.011	0.035	0.634
Aspect ratio	manual	105	5.022	4.726	5.318	4.864	1.529	2.338	2.414	10.12
	semi-automatic	239	4.161	3.945	4.377	3.845	1.692	2.863	2.01	12.491

Note: The CI of the mean assumes sample means follow a t-distribution with $N - 1$ degrees of freedom.

The subsample analysed shows the residual fibre morphology in the extruded PLA compound with 5% fibre by weight. It was found that length and aspect ratio of the fibers, when the mean values are taken into account, shows a variation of 20% from one method to the other, which is within the typical variance [12]; the differences in mean diameter are only about 10%.

However, more representative than these mean values are the data distributions. As shown in Figure 11, the frequencies and distribution plots obtained by the proposed method correlate consistently with the manual measurement, both for the length and diameter or aspect ratio of the fibers. It is patent from this figure that the distribution of length and diameter (and therefore, aspect ratio) are very similar between both methods. As already mentioned, the semi-automatic procedure measures smaller particles that are discarded during the manual procedure, explaining the lower mean and median values found, particularly for lengths. On the other hand, the time needed for the processing of samples should be highlighted; the semi-automatic procedure only took less than 1 min to provide the results on 239 measurements, while the manual operation needed over 1 h to obtain only half of the results. When considering the time needed to obtain a significant number of measured elements, as shown for the entire sample (some thousands), versus the ones measured in this sub-sample (only about 100), it is clear that manual measurement might not provide optimal results. That is, the proposed method seems to slightly bias the fiber length to shorter lengths compared to the manual procedure, but nonetheless this method is considered as providing more significant results, due to the bigger size of the sample and the consideration of most elements in the image, not only those easier to measure by hand.

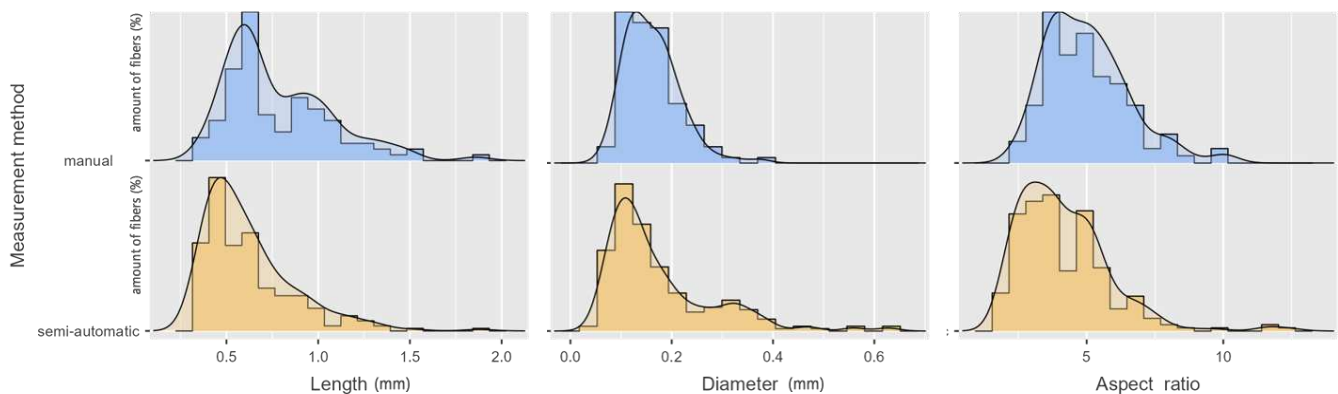


Figure 11. Frequency distribution plots for length, diameter and aspect ratio of fibers by manual vs. semi-automatic method.

4. Conclusions

From the presented methodology, the following conclusions can be highlighted:

- An alternative and affordable method for morphometric analysis of fibers during compounding processes, based on conventional optical scanner and open-source software, has been developed and validated. The present methodology, based on film pressing and optical scanning image analysis, is valid for thermoplastic composites using uncolored or natural matrices that allow visual identification of the dispersed phase of the composite.
- The use of Adobe Photoshop for image segmentation allows handling of large samples to speed up the analysis process in ImageJ, obtaining good measurement reliability and a statistically significant number of measurements per sample. However, this software could be avoided if analyzing smaller images or if intending to obtain a lower number of measurements.
- The “Shape filter” plugin has been proved for individual fiber recognition by using ImageJ.

After the application of the proposed methodology to the case study of giant reed fibers in different scenarios (starting fiber length, two different matrices, four different fiber loadings, two different twin-screw compoundingers) it can be concluded that:

- The greatest reduction in fiber length occurs from the first kneading zone of the extrusion process, where more than 85% of the fibers for HDPE and 90% for the PLA compound result shortened to less than 1 mm in length.
- The fiber size distributions are remarkably similar at the end of the compounding process, regardless of the size of the input fibers or the type of polymer matrix.
- The average aspect ratio is reduced to less than 10 for all the compound formulations that were produced.
- The injection molding process does not significantly affect the morphology of the fibers; that is, neither their length nor their diameter is affected during the process.
- Results obtained agree with the observations made in other research. Further, the results obtained with the proposed methodology have been compared against those obtained by hand to validate the measurements, finding that the proposed method yields slightly lower fiber lengths than the manual procedure, although still under the accepted 20% variance, while diameters are within the same range.
- The semi-automatic method proposed allows for the measurement of a high number of fibers, yielding more representative results, as smaller particles are not disregarded, and due to the higher number of samples analyzed in just a fraction of the time consumed during the manual process.

Supplementary Materials: The following supporting information can be downloaded at: <https://www.mdpi.com/article/10.3390/jcs7080326/s1>, Figure S1: ImageJ macro for automated fiber recognition and measurement.

Author Contributions: Conceptualization, L.S.; methodology, L.S. and Z.O.; validation, L.S.; formal analysis, L.S. and Z.O.; investigation, all authors; data curation, L.S.; writing—original draft preparation, L.S. and Z.O.; writing—review and editing, L.S., Z.O., E.C., G.G. and M.B.; visualization, L.S.; funding management: M.D.M.; supervision, Z.O. All authors have read and agreed to the published version of the manuscript.

Funding: Luis Suárez acknowledges funding through the Ph.D. grant program co-financed by the Canarian Agency for Research, Innovation and Information Society of the Canary Islands Regional Council for Employment, Industry, Commerce and Knowledge (ACIISI), and by the European Social Fund (ESF) (Grant number TESIS2021010008). Zaida Ortega also acknowledges the Spanish Ministry of Universities for funding the internship at QUB, through the grant received by Order UNI/501/2021 of 26 May 2021, coming from the European Union towards Next Generation funds (Plan de Recuperación, Transformación y Resiliencia del Gobierno de España: C21.I4.P1. Resolución del 2 de julio de 2021 de la Universidad de Las Palmas de Gran Canaria por la que se convocan Ayudas para la recualificación del sistema universitario español para 2021–2023).

Data Availability Statement: Data are available from the authors upon reasonable request.

Acknowledgments: Inv2Mac project (European Funding for Regional Development (FEDER), INTERREG MAC 2014–2020 program; grant number MAC2/4.6d/229).

Conflicts of Interest: The authors declare no conflict of interest. The funders had no role in the design of the study; in the collection, analysis, or interpretation of data; in the writing of the manuscript; nor in the decision to publish the results.

References

1. Ismail, S.O.; Akpan, E.; Dhakal, H.N. Review on natural plant fibres and their hybrid composites for structural applications: Recent trends and future perspectives. *Compos. Part C Open Access* **2022**, *9*, 100322. [\[CrossRef\]](#)
2. Visweswarajah, S.B.; Selezneva, M.; Lessard, L.; Hubert, P. Mechanical characterisation and modelling of randomly oriented strand architecture and their hybrids—A general review. *J. Reinf. Plast. Compos.* **2018**, *37*, 548–580. [\[CrossRef\]](#)
3. Bourmaud, A.; Mayer-Laigle, C.; Baley, C.; Beaugrand, J. About the frontier between filling and reinforcement by fine flax particles in plant fibre composites. *Ind. Crops Prod.* **2019**, *141*, 111774. [\[CrossRef\]](#)
4. Hubbe, M.; Grigsby, W. From nanocellulose to wood particles: A review of particle size vs. the properties of plastic composites reinforced with cellulose-based entities. *BioResources* **2020**, *15*, 2030–2081. [\[CrossRef\]](#)
5. Bourmaud, A.; Shah, D.U.; Beaugrand, J.; Dhakal, H.N. Property changes in plant fibres during the processing of bio-based composites. *Ind. Crops Prod.* **2020**, *154*, 112705. [\[CrossRef\]](#)
6. Mallick, P.K. Thermoplastics and thermoplastic–matrix composites for lightweight automotive structures. In *Materials, Design and Manufacturing for Lightweight Vehicles*; Woodhead Publishing: Sawston, UK, 2020; pp. 187–228. ISBN 9780128187128.
7. Zwawi, M. A review on natural fiber bio-composites, surface modifications and applications. *Molecules* **2021**, *26*, 404. [\[CrossRef\]](#)
8. Dickson, A.; Teuber, L.; Gaugler, M.; Sandquist, D. Effect of processing conditions on wood and glass fiber length attrition during twin screw composite compounding. *J. Appl. Polym. Sci.* **2020**, *137*, 48551. [\[CrossRef\]](#)
9. Goris, S.; Back, T.; Yanev, A.; Brands, D.; Drummer, D.; Osswald, T.A. A novel fiber length measurement technique for discontinuous fiber-reinforced composites: A comparative study with existing methods. *Polym. Compos.* **2018**, *39*, 4058–4070. [\[CrossRef\]](#)
10. Di Giuseppe, E.; Castellani, R.; Dobosz, S.; Malvestio, J.; Berzin, F.; Beaugrand, J.; Delisée, C.; Vergnes, B.; Budtova, T. Reliability evaluation of automated analysis, 2D scanner, and micro-tomography methods for measuring fiber dimensions in polymer-lignocellulosic fiber composites. *Compos. Part A Appl. Sci. Manuf.* **2016**, *90*, 320–329. [\[CrossRef\]](#)
11. Gamon, G.; Evon, P.; Rigal, L. Twin-screw extrusion impact on natural fibre morphology and material properties in poly(lactic acid) based biocomposites. *Ind. Crops Prod.* **2013**, *46*, 173–185. [\[CrossRef\]](#)
12. Beaugrand, J.; Berzin, F. Lignocellulosic fiber reinforced composites: Influence of compounding conditions on defibrization and mechanical properties. *J. Appl. Polym. Sci.* **2013**, *128*, 1227–1238. [\[CrossRef\]](#)
13. Ruppel, A.; Wolff, S.; Oldemeier, J.P.; Schöppner, V.; Heim, H.-P. Influence of Processing Glass-Fiber Filled Plastics on Different Twin-Screw Extruders and Varying Screw Designs on Fiber Length and Particle Distribution. *Polymers* **2022**, *14*, 3113. [\[CrossRef\]](#)
14. Padovani, J.; Legland, D.; Pernes, M.; Gallos, A.; Thomachot-Schneider, C.; Shah, D.U.; Bourmaud, A.; Beaugrand, J. Beating of hemp bast fibres: An examination of a hydro-mechanical treatment on chemical, structural, and nanomechanical property evolutions. *Cellulose* **2019**, *26*, 5665–5683. [\[CrossRef\]](#)

15. Berton, M.; Cellere, A.; Lucchetta, G. A new procedure for the analysis of fibre breakage after processing of fibre-reinforced thermoplastics. *Int. J. Mater. Form.* **2010**, *3*, 671–674. [[CrossRef](#)]
16. Alemdar, A.; Zhang, H.; Sain, M.; Cescutti, G.; Müssig, J. Determination of fiber size distributions of injection moulded polypropylene/natural fibers using X-ray microtomography. *Adv. Eng. Mater.* **2008**, *10*, 126–130. [[CrossRef](#)]
17. Berzin, F.; Vergnes, B.; Beaugrand, J. Evolution of lignocellulosic fibre lengths along the screw profile during twin screw compounding with polycaprolactone. *Compos. Part A Appl. Sci. Manuf.* **2014**, *59*, 30–36. [[CrossRef](#)]
18. Le Moigne, N.; Van Den Oever, M.; Budtova, T.; Le, N.; Van Den Oever, M.; Budtova, T. A statistical analysis of fibre size and shape distribution after compounding in composites reinforced by natural fibres. *Compos. Part A* **2011**, *42*, 1542–1550. [[CrossRef](#)]
19. Berzin, F.; Beaugrand, J.; Dobosz, S.; Budtova, T.; Vergnes, B. Lignocellulosic fiber breakage in a molten polymer. Part 3. Modeling of the dimensional change of the fibers during compounding by twin screw extrusion. *Compos. Part A Appl. Sci. Manuf.* **2017**, *101*, 422–431. [[CrossRef](#)]
20. Wang, S.; Yata-gawa, T.; Suzuki, H.; Ohtake, Y. Image Based Measurement of Individual Fiber Lengths for Randomly Oriented Short Fiber Composites. *J. Nondestruct. Eval.* **2022**, *41*, 1–16. [[CrossRef](#)]
21. Albrecht, K.; Osswald, T.; Baur, E.; Meier, T.; Wartzack, S.; Müssig, J. Fibre Length Reduction in Natural Fibre-Reinforced Polymers during Compounding and Injection Moulding—Experiments Versus Numerical Prediction of Fibre Breakage. *J. Compos. Sci.* **2018**, *2*, 20. [[CrossRef](#)]
22. Terada, M.; Yamanaka, A.; Kimoto, Y.; Shimamoto, D.; Hotta, Y.; Ishikawa, T. Evaluation of measurement method for carbon fiber length using an optical image scanner. *Adv. Compos. Mater.* **2018**, *27*, 605–614. [[CrossRef](#)]
23. Schindelin, J.; Arganda-Carreras, I.; Frise, E.; Kaynig, V.; Longair, M.; Pietzsch, T.; Preibisch, S.; Rueden, C.; Saalfeld, S.; Schmid, B.; et al. Fiji: An open-source platform for biological-image analysis. *Nat. Methods* **2012**, *9*, 676–682. [[CrossRef](#)] [[PubMed](#)]
24. Sadik, Z.; Ablouh, E.; Sadik, M.; Benmoussa, K.; Idrissi-Saba, H.; Kaddami, H.; Arrakhiz, F.Z. Use of 2D image analysis method for measurement of short fibers orientation in polymer composites. *Eng. Solid Mech.* **2020**, *8*, 233–244. [[CrossRef](#)]
25. Terenzi, A.; Kenny, J.M.; Barbosa, S.E. Natural fiber suspensions in thermoplastic polymers. I. Analysis of fiber damage during processing. *J. Appl. Polym. Sci.* **2007**, *103*, 2501–2506. [[CrossRef](#)]
26. Suárez, L.; Barczewski, M.; Kosmela, P.; Marrero, M.D.; Ortega, Z. Giant Reed (*Arundo donax* L.) Fiber Extraction and Characterization for Its Use in Polymer Composites. *J. Nat. Fibers* **2023**, *20*, 2131687. [[CrossRef](#)]
27. Domenek, S.; Berzin, F.; Ducruet, V.; Plessis, C.; Dhakal, H.; Richaud, E.; Beaugrand, J. Extrusion and injection moulding induced degradation of date palm fibre—Polypropylene composites. *Polym. Degrad. Stab.* **2021**, *190*, 109641. [[CrossRef](#)]
28. Chinga-Carrasco, G.; Solheim, O.; Lenes, M.; Larsen, Å. A method for estimating the fibre length in fibre-PLA composites. *J. Microsc.* **2013**, *250*, 15–20. [[CrossRef](#)]
29. Ferreira, P.J.; Matos, S.; Figueiredo, M.M. Size characterization of fibres and fines in hardwood kraft pulps. *Part. Part. Syst. Charact.* **1999**, *16*, 20–24. [[CrossRef](#)]

Disclaimer/Publisher’s Note: The statements, opinions and data contained in all publications are solely those of the individual author(s) and contributor(s) and not of MDPI and/or the editor(s). MDPI and/or the editor(s) disclaim responsibility for any injury to people or property resulting from any ideas, methods, instructions or products referred to in the content.

6.5. INFLUENCE OF GIANT REED (*ARUNDO DONAX* L.)
CULMS PROCESSING PROCEDURE ON
PHYSICOCHEMICAL, RHEOLOGICAL, AND
THERMOMECHANICAL PROPERTIES OF POLYETHYLENE
COMPOSITES

P1

P2

P3

P4

P5

P6

P7

P8

P9

P10

Influence of Giant Reed (*Arundo Donax* L.) Culms Processing Procedure on Physicochemical, Rheological, and Thermomechanical Properties of Polyethylene Composites

Luis Suárez ^a, Paul R. Hanna^b, Zaida Ortega ^c, Mateusz Barczewski ^d, Paulina Kosmela ^e, Bronagh Millar ^b, and Eoin Cunningham ^f

^aDepartamento de Ingeniería Mecánica, Universidad de Las Palmas de Gran Canaria, Las Palmas, Spain; ^bPolymer Processing Research Centre, Queen's University of Belfast, Belfast, UK; ^cDepartamento de Ingeniería de Procesos, Universidad de Las Palmas de Gran Canaria, Las Palmas, Spain; ^dInstitute of Materials Technology, Faculty of Mechanical Engineering, Poznan University of Technology, Poznań, Poland; ^eDepartment of Polymer Technology, Gdansk University of Technology, Gdańsk, Poland; ^fSchool of Mechanical and Aerospace Engineering, Queen's University Belfast, Belfast, UK

ABSTRACT



Giant reed (*Arundo donax* L.) is a plant species with a high growth rate and low requirements, which makes it particularly interesting for the production of different bioproducts, including natural fibers. This work assesses the use of fibers obtained from reed culms as reinforcement for a high-density polyethylene (HDPE) matrix. Two different lignocellulosic materials were used: i) shredded culms and ii) fibers obtained by culms processing, which have not been reported yet in literature as fillers for thermoplastic materials. A good stress transfer for the fibrous composites was observed, with significant increases in mechanical properties; composites with 20% fiber provided a tensile elastic modulus of almost 1900 MPa (78% increase versus neat HDPE) and a flexural one of 1500 MPa (100% increase), with an improvement of 15% in impact strength. On the other hand, composites with 20% shredded biomass increased by 50% the tensile elastic modulus (reaching 1560 MPa) and the flexural one (up to 1500 MPa), without significant changes in impact strength. The type of filler is more than its ratio; composites containing fibers resulted in a higher performance than the ones with shredded materials due to the higher aspect ratio of fibers.


KEYWORDS

Arundo donax; giant reed; biomass; fibers; composites; HDPE; characterization; injection molding

关键词

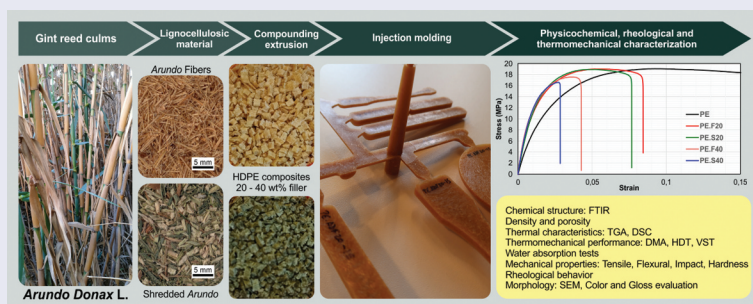
Arundo donax; 巨大的芦苇; 生物量; 纤维; 复合材料; HDPE; 刻画; 注射成型

CONTACT Zaida Ortega  zaida.ortega@ulpgc.es  Departamento de Ingeniería de Procesos, Universidad de Las Palmas de Gran Canaria, Las Palmas, Spain

 Supplemental data for this article can be accessed online at <https://doi.org/10.1080/15440478.2023.2296909>

© 2024 The Author(s). Published with license by Taylor & Francis Group, LLC.

This is an Open Access article distributed under the terms of the Creative Commons Attribution License (<http://creativecommons.org/licenses/by/4.0/>), which permits unrestricted use, distribution, and reproduction in any medium, provided the original work is properly cited. The terms on which this article has been published allow the posting of the Accepted Manuscript in a repository by the author(s) or with their consent.



摘要

巨型芦苇 (*Arundo donax* L.) 是一种生长速率高、要求低的植物, 这使得它对生产包括天然纤维在内的不同生物产品特别感兴趣。这项工作评估了从芦苇秆中获得的纤维作为高密度聚乙烯 (HDPE) 基体的增强材料的用途。使用了两种不同的木质纤维素材料: i) 切碎的秆和ii) 通过秆加工获得的纤维。这些纤维在文献中尚未被报道为热塑性材料的填料。观察到纤维复合材料具有良好的应力传递, 机械性能显著提高; 含20%纤维的复合材料的拉伸弹性模量几乎为1900MPa (与纯HDPE相比增加了78%), 弯曲弹性模量为1500MPa (增加了100%), 冲击强度提高了15%。另一方面, 具有20%切碎生物质的复合材料的拉伸弹性模量 (达到1560MPa) 和弯曲弹性模量 (高达1500MPa) 增加了50%, 而冲击强度没有显著变化。填料的种类多于其配比; 含有纤维的复合材料由于纤维的高纵横比而比含有切碎材料的复合材料具有更高的性能。

Introduction

Arundo donax L. is a perennial Grass from the *Gramineae* family, probably with East Asia origin (Jensen et al. 2018). This plant shows a high growth rate and produces an impressive amount of biomass, which currently has very limited use. Several works have demonstrated the potential of this plant for the biorefinery industry (Copani et al. 2013; Cosentino et al. 2014, 2016; Jensen et al. 2018; Licursi et al. 2015, 2018; Ortega et al. 2023) and it is considered as an energy crop because of its potential to produce bioethanol, bioenergy, or green products following a biorefineries scheme. The use of a cascade biorefinery process is an exciting strategy to maximize the environmental and economic benefits of lignocellulosic materials used within industrial applications; in this approach, the different fractions of the material could be separated for their further use. One interesting product that can be obtained from such industries are cellulose fibers for composites obtaining, while also exploiting the remaining fractions for the obtaining of other products, such as sugars for a later fermentation, antioxidants or bio-char (Ortega et al. 2023).

Some authors have proposed using giant reed as a raw material to obtain natural fibers, although not many publications study the manufacturing of composites using fibers. Most literature related to composites production from *Arundo* focuses on particleboard production (Andreu-Rodriguez et al. 2013; Barreca et al. 2019; Ferrández Villena et al. 2020; Ferrandez-Garcia et al. 2019; Ferrandez-Garcia et al. 2020; Ferrández-García et al. 2012; García-Ortuño et al. 2011). In such works, the lignocellulosic material is ground and blended in up to 40% by weight with a thermoset resin or natural binders, such as citric acid (Baquero Basto, Monsalve Alarcón, and Sánchez Cruz 2018; Dahmardeh Ghalehno et al. 2010; Ferrandez-Garcia et al. 2019; Ferrandez-García et al. 2020); the medium-density boards obtained show properties within the range of other materials used as insulating material in the construction or furniture sector.

As explained in a previous review paper from authors (Suárez et al. 2023,) three methods are mainly used for reed processing: grinding (Bessa et al. 2020, 2021; Fiore et al. 2014, 2014) rudimentary

scraping to obtain bast fibers (Fiore et al. 2014; Ortega et al. 2021; Scalici, Fiore, and Valenza 2016; Suárez et al. 2021, 2022) or the combination of a chemical soaking and mechanical scraping to get thinner and stiffer fibers (Suárez et al. 2023). Purely chemical methods have also been explored in the literature for the separation of microcrystalline cellulose (Shatalov and Pereira 2013)(p) (Barana et al. 2016; Tarchoun et al. 2019). From the studies reported in the literature, it can be concluded that the initial preparation of the filler derived from this plant and the applied mechanical and chemical modification procedure significantly affect the properties of composites produced. For example, acid hydrolysis allows for the removal of hemicellulose and the obtaining of a pulp with high cellulose content (Shatalov and Pereira 2013; Tarchoun et al. 2019) while the use of alkali results in the removal of lignin and the obtaining of a material with about 50% cellulose (Barana et al. 2016; Martínez-Sanz et al. 2018). The procedure applied for obtaining the fibers in this research work combines a chemical and a mechanical approach (Suárez et al. 2023) for the obtaining of fibers with high aspect ratio and high cellulose content, close to 70%.

Epoxy-based composites have been studied at different fiber loadings; for example, the addition of 10% in weight of bast fibers showed improved tensile modulus of the epoxy matrix, while tensile and flexural strength were reduced due to a low compatibility between the lignocellulosic material and the resin. To overcome this, plasma treatment has been applied to the fibers (Scalici, Fiore, and Valenza 2016) and it has been found that 5% loading increased the flexural modulus by up to 80% and flexural strength by almost 40%. The lack of compatibility between both materials not only prevents the transmission of the applied force between both materials but also results in voids formation, which reduce the effective area of the test part. Apart from plasma, an alkaline treatment based on NaOH or the silanization (Bessa et al. 2020) of fibers has been proposed for their use in unsaturated polyester or bisphenol-based matrices. For polyester, composites at 40% loading (in volume) were prepared, resulting in an improvement of tensile and flexural properties (Chikouche et al. 2015).

Some studies have also been performed using thermoplastic materials as a matrix. For example, PLA-composites with up to 20% of *Arundo* ground culms were prepared by injection molding, with tensile and flexural elastic moduli rising with the increased content of lignocellulosic material, while the strength was reduced in both tests. Further studies using *Arundo* to produce polymer composites by injection molding have not been found in the literature, therefore demonstrating the novelty of this work. The present paper shows the results obtained for composites with 20% and 40% *Arundo* fibers, which have only been obtained with this plant by compression molding (Suárez et al. 2021). In this work, polyethylene (PE) and polypropylene (PP) were used as matrices, resulting in an increase in elastic modulus and a decrease in tensile and flexural strength. Rotationally-molded composites with *Arundo* resulted in similar behavior, although a lower rate of filler was used due to the process sensitivity to the introduction of non-polymeric materials (Suárez et al. 2022). In addition, the literature reviewed typically used ground material or bast fibers obtained from rudimentary procedures, with lower cellulose content and mechanical properties than the fibers used in this research.

In this paper, the properties of composites obtained with shredded culms and fibers obtained by combined chemical and mechanical methods are assessed. Giant reed fibers used in this research show a high cellulose content (around 68%, in the range of flax or hemp (Henrique et al. 2015) with a crystallinity index over 65%, and thermal degradation temperature above 230°C, similar to other commonly used fibers in the composites sector, such as jute, abaca, or hemp (Fiore, Scalici, and Valenza 2014; Kabir et al. 2012; Ortega et al. 2013). The shredded material also shows good thermal stability for its processing into a HDPE matrix (Suárez et al. 2023). From the energy point of view, it is beneficial to produce composites based on the less processed plant raw materials. Therefore, this research work aims at contributing to the achievement of the EU-green deal strategy objectives and the sustainable development goals, by the obtaining of composites with good performance and an expected improved environmental character due to the partial substitution of a polymer matrix with a renewable material of lignocellulose origin. Other authors have reported some few results on the use of giant reed materials in thermoplastic processes, although with a different starting material. To the best of authors knowledge, no references in literature have used the two lignocellulose materials

reported in this work: fibers obtained from a chemo-mechanical procedure of giant reed culms, with high cellulose content, and shredded material from the entire aerial parts of the reed, with lower cellulose and higher hemicellulose contents. A comprehensive correlation assessment between the method of obtaining the giant reed-based fillers and the processing, physicochemical, thermal, and thermomechanical properties of injection-molded thermoplastic composites manufactured with their use was presented.

Materials and methods

Materials

High-density polyethylene (HDPE), grade HD6081 from Total was used. This polymer exhibits a melt flow index (MFI) of 8 g/10 min (190°C/2.16 kg) and a density of 960 kg/m³, according to the manufacturer's datasheet.

Fibers and shredded material from *Arundo* culms were prepared as explained in previous work (Suárez et al. 2023). In short, shredded material was prepared by grinding the aerial parts of the plant (culms and leaves) and washing them with water. Fibers were obtained after soaking culms in a 1N NaOH solution for around 1 week (3 l of solution per kg of biomass), with further processing by a series of rolling mills to separate the fibers from the softer material. Finally, fibers were cut to approximately 3 mm in length.

The composites are named after the type of lignocellulosic material used and its content (in weight %); for example, PE.F20 stands for composites with 20% of fibers, while PE.S20 refers to composites with 20% of shredded material. Table 1 lists the samples' full names and information about their composition.

Composites preparation

The materials used were dried overnight before compounding: lignocellulosic fibers at 105°C and HDPE at 60°C. Composites were prepared in a ThermoScientific Process11 twin screw-extruder (configuration shown in Figure 1), with the following temperature profile: 170-175-175-185-185-175-165-165°C (from hopper to die). The screw speed at 100 rpm.

Before injection molding, the materials were dried at 60°C overnight with dry air (dewpoint of −40°C). ISO mechanical test specimens were manufactured using an Arburg 320S injection molding machine. The following temperature profile, from back to nozzle, was used: 175-180-185-185-190°C, while mold temperature was 30°C, and cooling time was 15 s. The back pressure was 5 MPa, the holding pressure was 50 MPa and the dosage volume of 50 cm³. Switchover pressure was recorded for every molding and averaged for the various composites.

Characterization

Different characterization tests were performed on the pellets and the injection-molded parts. For the pellets, chemical structure, melt flow index, and thermal analysis (thermogravimetry and differential scanning calorimetry) were assessed. For molded parts, density, water absorption, mechanical testing,

Table 1. Materials prepared and their markings.

Short name	Formulation
PE	HDPE
PE.S20	HDPE +20% shredded <i>Arundo</i>
PE.S40	HDPE +40% shredded <i>Arundo</i>
PE.F20	HDPE +20% <i>Arundo</i> fiber
PE.F40	HDPE +40% <i>Arundo</i> fiber

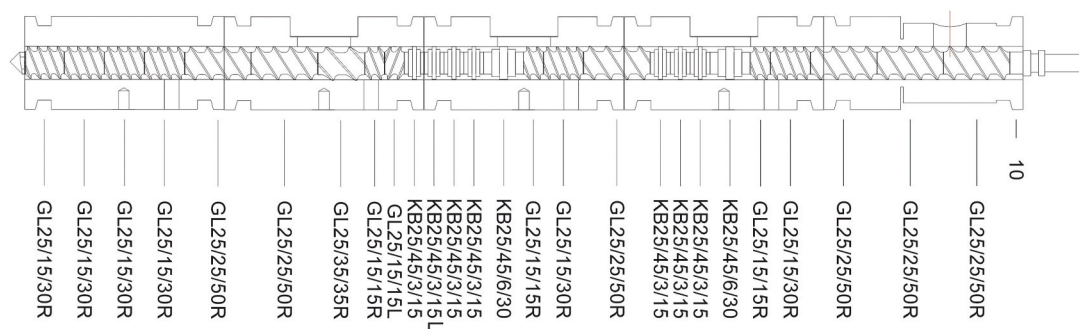


Figure 1. Extruder screw configuration with three different mixing and kneading zones.

dynamic mechanical analysis, rheological behavior, heat deflection and Vicat softening temperatures (HDT and VST), and microscopic structure were analyzed.

Fourier Transform Infrared (FTIR) spectra were obtained in a Spectrum 100 spectrophotometer from Perkin Elmer, under Attenuated Total Reflectance (ATR) mode with a zinc selenide single bounce crystal, recording 64 scans per spectra at a resolution of 4 cm^{-1} , in the wavelengths between 4000 and 600 cm^{-1} .

The Melt Flow Index (MFI) of composite materials was obtained following ISO 1133, in a 7053 apparatus from Kayeness Inc (Dynisco Company), using a load of 2.16 kg and a temperature of 190°C .

Thermogravimetric analysis (TGA) was performed in a Netzsch TG 209F1 Libra device, using alumina crucibles and samples nominally of $10 \pm 0.2\text{ mg}$, under nitrogen atmosphere. The tests were conducted at a heating rate of $10^\circ\text{C}/\text{min}$, from 30°C to 900°C .

Heat deflection temperature (HDT) was obtained for injection-molded samples according to ISO 75 standard (heating rate of $120^\circ\text{C}/\text{h}$ and 1.8 MPa load). Vicat softening temperature (VST) was measured following ISO 306 B50 standard, at a heating rate of $50^\circ\text{C}/\text{h}$ and a loading of 50 N. For both tests TPC/3 TOP VST/HDT apparatus was used. For each series, at least three measurements were made to average the results.

The thermal behavior of materials was determined by differential scanning calorimetry (DSC). The analyses were conducted in a Perkin Elmer DSC 6 device under nitrogen atmosphere and aluminum sealed crucibles. Samples nominally of $10 \pm 0.2\text{ mg}$ were prepared for these tests. The measurements were performed from 30°C to 200°C at $10^\circ\text{C}/\text{min}$, with two heating cycles. The temperatures for melting at both heating cycles (T_{m1} and T_{m2} , respectively) and crystallization (T_c) from the cooling step were determined. Three replicas were performed for each material sample, and results are expressed as average values, also providing standard deviations. Finally, the melting and crystallization enthalpies (ΔH_{m1} , ΔH_{m2} , and ΔH_c) were also calculated and employed to obtain the degree of crystallinity (χ):

$$\chi = \frac{1}{1 - m_f} \cdot \frac{\Delta H_m}{\Delta H_0} \cdot 100 \quad (1)$$

where ΔH_0 is the enthalpy for a HDPE crystalline sample (293 J/g) (Balasuriya, Ye, and Mai 2003,) and m_f is the mass rate of the lignocellulose (20% and 40% for composites).

The density of the prepared materials was measured following the Archimedes principle, as specified in ISO 1183 standard, using methanol medium at room temperature, in a LA620P precision balance from Sartorius AG Germany. Five measurements were performed per sample, giving the results as average value and standard deviation. The theoretical density of each formulation was calculated following the rule of mixtures (equation 2):

$$\rho_C = \rho_f \cdot V_f + \rho_m \cdot (1 - V_f) \quad (2)$$

Where V_f is the mass ratio of the lignocellulosic material, and ρ_c , ρ_f , and ρ_m , the density of the composite (theoretical), fiber and matrix. These values were further used to calculate the composite porosity (P) (equation 3), by comparing the theoretical and experimental values obtained:

$$P(\%) = \frac{\rho_{theo} - \rho_{exp}}{\rho_{theo}} \cdot 100 \quad (3)$$

Water absorption was carried out according to ISO 62:2008, immersing the specimens in deionized water and weighing them periodically until achieving a constant mass. The water absorption (W) was calculated using the following equation:

$$W(\%) = \frac{W_t - W_0}{W_0} \cdot 100 \quad (4)$$

where W_0 is the initial mass of the sample, W_t the mass of the sample at t time. Three replicates per sample were assessed.

The kinetics of water uptake can be obtained using Fick's law:

$$D = \pi \cdot \left(\frac{k \cdot h}{4 \cdot W_m} \right)^2 \quad (5)$$

Where D is the diffusion coefficient (m (Copani et al. 2013)/s), h is the thickness of the original sample, W_m is the maximum moisture absorbed by the sample and k is the initial slope of the curve of water uptake versus $t^{1/2}$, as described by equation 6 (Bazan et al. 2020):

$$k = \frac{W_2 - W_1}{\sqrt{t_2} - \sqrt{t_1}} \quad (6)$$

If the moisture uptake for each measurement taken is compared with the maximum water uptake of each sample, the parameters n , associated with the diffusion mode, and k , related to the interaction between the material and the water, can be calculated as (George, Bhagawan, and Thomas 1998):

$$\frac{W_t}{W_m} = k \cdot t^n \quad (7)$$

The mechanical properties of composites (tensile, flexural, impact, and hardness) were determined as follows: i) tensile properties: ISO 527-2:2012, at a rate of 10 mm/min for ultimate tensile strength and 2 mm/min for elastic modulus, ii) flexural properties: ISO 178:2019, with 64 mm between cantilevers, determining the elastic modulus and flexural strength, at the same rates defined for tensile tests. These tests were made in a LS5 universal testing machine (Lloyd), with a cell load of 500 N for modulus and of 5 kN for strength, with 5 replicates per test. iii) Charpy impact tests: UNE-EN ISO 179-1/1eA:2019, with a 7.5 J pendulum and an impact rate of 3.7 m/s in a Ceast Resil impactor P/N 6958.000, using notched samples. Ten replicates were used for this assay. iv) Hardness: ISO 2039 standard, conducting the tests in a KB Prüftechnik device (ball indentation hardness test), with a minimum of 7 measurements per each material series. Results for all properties are given as average values and standard deviation (SD).

Thermomechanical properties of the different materials were evaluated by Dynamic Mechanical Thermal Analysis (DMTA) in a Triton 2000 device, from Triton Technology, under single cantilever bending method. A strain of 10 μ m was applied at 1 Hz frequency, in the temperature range between -100°C and 100°C , at a heating of $2^\circ\text{C}/\text{min}$.

Rheological behavior was assessed using an AR G2 oscillatory rheometer from TA instruments, using 25 mm diameter parallel plates. The experiments were performed at 190°C , with 2.5 mm gap and in a nitrogen atmosphere. Preliminary tests were performed using the strain sweep mode, in order to ensure later experiments are performed in the linear viscoelastic (LVE) region. In these tests, strain

was varied between 0.1% and 5%. Angular frequency sweeps were performed at 0.5% strain, in the LVE region, in the range of 0.01 to 100 rad/s.

The analysis of rheological evaluation was supplemented with experiments conducted using a capillary rheometer Dynisco LCR 7000, at 190°C, as for oscillatory measurements. This test, performed with a capillary die with a diameter of $D = 2$ mm and $L/D = 20$, allowed determining the effect of the lignocellulosic materials on the rheological properties of the HDPE matrix. The high value of L/D made the Bagley correction to be. T changes in the rheological behavior were analyzed by means of the apparent shear stress; the dependence between the apparent melt viscosity (η) and the apparent shear rate ($\dot{\gamma}$) (in double logarithmic scale) allow to describe the viscosity curves in the non-Newtonian range a the power-law (Gai and Cao 2013) (equation 8):

$$\eta = K(\dot{\gamma})^{n-1} \quad (8)$$

Where K is the consistency coefficient, and n is the power law index (Djellali et al. 2015).

Scanning electron microscopy (SEM) observations were performed over the samples surface and fractured sections of tensile specimens, with the aim of determining the distribution of the filler in the matrix and describe an interaction between filler and matrix. SEM observations were performed in a Hitachi FlexSEM 1000, at different magnifications and an accelerating voltage of 5 kV, over previously gold-sputtered samples.

The color of the samples was assessed by optical spectroscopy, using a HunterLab Miniscan MS/S-4000S spectrophotometer, following the procedure specified by the International Commission on Illumination (CIE) $L^*a^*b^*$ coordinates. According to this system, L^* is related to the color lightness (black: $L^* = 0$, white: $L^* = 100$), a^* refers to green(−) and red(+), and, finally, b^* measures blue(−) and yellow(+) The measurements were done by placing the samples in a specially designed light trap chamber. The total color difference parameter (ΔE^*) is defined as (Chorobiński, Skowroński, and Bieliński 2019):

$$\Delta E^* = [(\Delta L^*)^2 + (\Delta a^*)^2 + (\Delta b^*)^2]^{0.5} \quad (9)$$

Finally, the measurement of the gloss of the surface of samples was performed using the TestAn DT 268 glossmeter, according to ISO 2813: 2001 at an angle of 20, 60, and 85° of the apertures of the image of the light source and the receiver. The presented results are mean values taken from 20 measurements.

Results

Chemical structure – FTIR

Figure 2a, b shows the FTIR spectra for the different materials used in this work: i) *Arundo* fibers and shredded *Arundo* plants (Figure 2a), II) PE, iii) 20% composites, and iv) 40% composites (Figure 2b). As already analyzed in previous work (Suárez et al. 2023,) the shredded material shows peaks associated to hemicellulose and lignin, which disappear or are reduced for fiber samples, due to the extraction procedure which was followed. Composites for both types of materials show almost overlapped spectra, closer to PE for the lower loadings. Composites with 40% of lignocellulosic material start showing some of the characteristic bands of such materials, namely around $3600\text{--}3000\text{ cm}^{-1}$, related to O-H stretching, and $1200\text{--}850\text{ cm}^{-1}$, characteristic of C=O bonds in cellulosic compounds.

The double peak at 2916 and 2848 cm^{-1} are related to C-H bonds (symmetric and asymmetric vibrations) from the polyethylene chain, although is also present in the lignocellulosic materials (with less intensity) and attributed to hemicellulose so more intense for shredded material than for the fiber. The peaks at 1472 and 729 cm^{-1} are related to C-H stretching in HDPE, and so are also found for the composites. It can be observed that the introduction of the lignocellulosic materials modifies the signal of neat HDPE, with the appearance of bands due to the giant reed materials. Other authors have

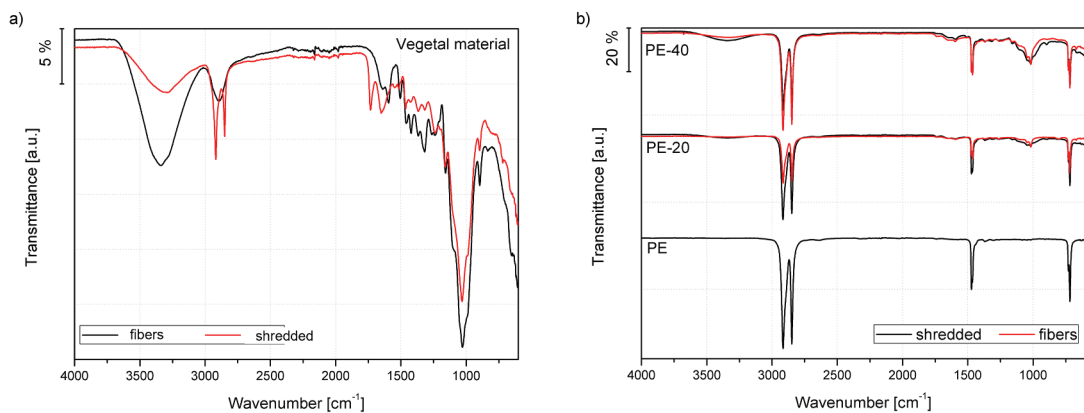


Figure 2. FTIR spectra of the fillers (a) and injection molded samples (b).

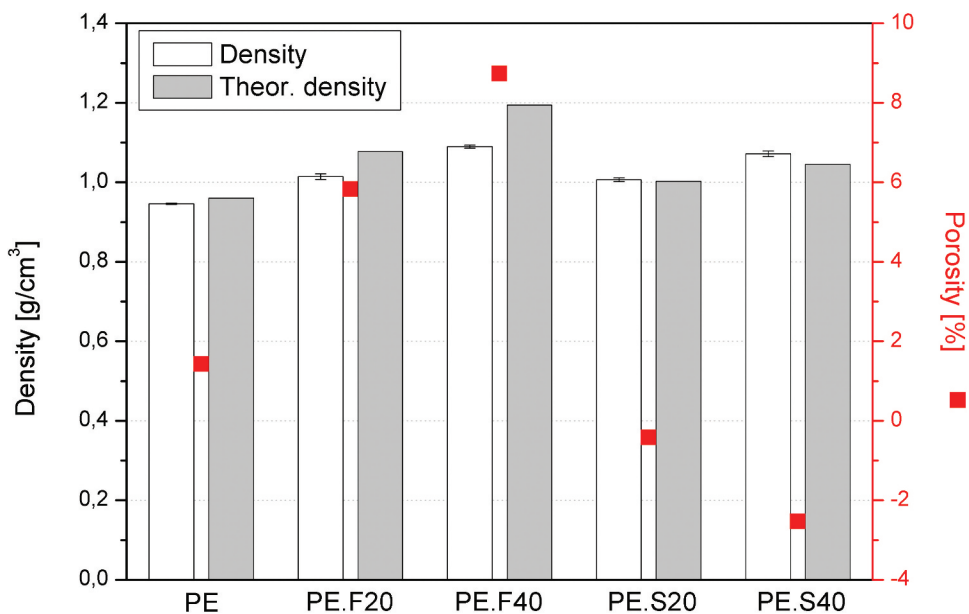


Figure 3. The porosity of PE-arundo composites based on measured and theoretical density.

reported similar modifications, especially for high filler loadings (Hejna et al. 2020; Mendes et al. 2021).

Density and porosity assessment

Figure 3 shows the values for theoretical and experimental densities of the composites and the porosity calculated by comparing them. Density values increase with the increasing content of lignocellulosic material in the composite. If comparing the density values obtained in the methanol assay and the theoretical ones (Equation 2), the porosity values could be obtained (Equation 3). It can be seen that the values for theoretical and experimental density for composites with shredded materials are pretty similar, so the porosity values can be considered zero. The values obtained were -0.5 and -2.5% for 20% and 40% composites, possibly due to some overpacking during injection molding or the standard deviation of the measurements taken. Porosity values for composites with fibers are 5.8 and 8.7%, for

20% and 40% fiber content, respectively, which can still be considered acceptable, especially for such high lignocellulosic contents.

Thermal behavior

Thermogravimetry

Figure 4 shows the thermogravimetric (TG) and derivative (DTG) curves obtained for the polyethylene and its composites. The thermal stability for 20% and 40% composites is similar, regardless of the type of lignocellulose material used. The residual mass at the end of the assay is also found in similar proportions for both sets of composites and are due to the inorganic compounds in the biomass, i.e., about 20% (Suárez et al. 2023). From DTG, the most significant peak is related to the PE decomposition, taking place at about 460°C, while for composites, there is also a smaller one, between 220°C and 360°C, due to the cellulose degradation. For composite materials with shredded *Arundo*, as also observed for the material itself, a small shoulder at about 290°C is found due to hemicellulose pyrolysis. A similar behavior is described in the literature for composites with lignocellulose-derived fillers. All composites are thermally stable until reaching about 240°C, 50°C above the processing temperature, which indicates a temperature-wide processability window for such materials (Mazzanti, Mollica, and El Kissi 2016). For instance, 5% weight loss happens at about 420°C for neat PE, about 290°C for 20% composites, and 270°C for 40% ones. Similar results are found in literature, with degradation starting at 214°C for hemp fibers at 40% in a polypropylene matrix or 262°C for 30 wt.% wood fibers-filled HDPE composites (Monteiro et al. 2012). There is a direct correlation between the amount of lignocellulosic material introduced and the weight loss, as also observed in Figure 4a. Some authors have proposed using TG and DTG curves to calculate the proportion of filler in the composite experimentally; following the procedure set by Nabinejad et al (Nabinejad et al. 2023) less than 10% difference between the theoretical and the experimental ratios are found: 21.7% and 20.9% for 20% composites (fiber and shredded, respectively), and 42.8% and 39.1% for 40%.

Differential scanning calorimetry

For polyethylene samples, the melting temperature is around 133°C, finding a slight increase for 20% composites. Melting and crystallization peaks are not altered because of the lignocellulose materials introduction, and no differences between the first and second heating cycles could be observed, neither in temperatures of the phase transitions nor in crystallinity values (Table 2). Other authors have reported similar behavior for HDPE-based composites: negligible difference in melting temperatures, although with reductions in enthalpies (Andrzejewski et al. 2020; Dolça et al. 2022).

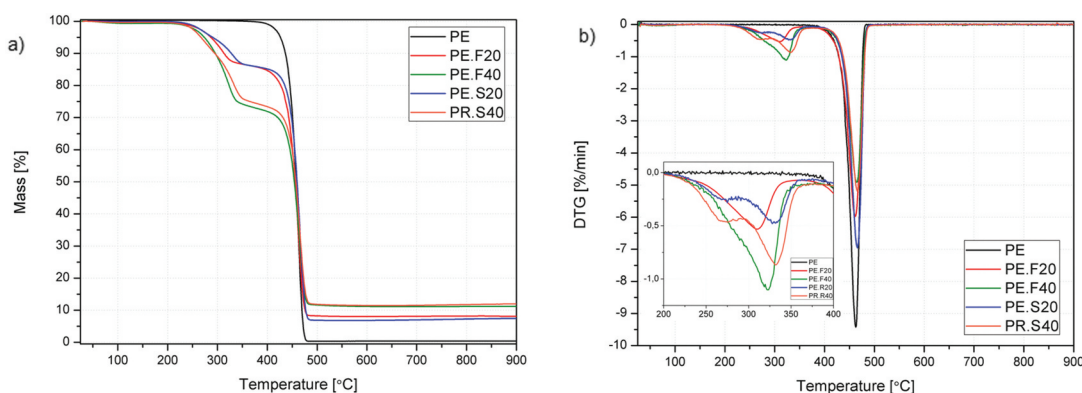


Figure 4. a) TG curve for the different materials and b) DTG curve.

Table 2. Thermal parameters for HDPE and its composites from DSC tests.

Material	T _{m1} [°C]	T _{m2} [°C]	T _c [°C]	ΔH _{m1} [J/g]	ΔH _{m2} [J/g]	ΔH _c [J/g]	χ ₁ [%]	χ ₂ [%]
HDPE	132.7 ± 0.3	135.3 ± 0.9	112.9 ± 0.0	175.4 ± 13.5	172.6 ± 8.2	193.3 ± 21.2	59.9 ± 4.6	58.9 ± 2.8
PE.F20	136.9 ± 0.4	134.7 ± 1.0	111.5 ± 0.0	118.7 ± 12.9	125.8 ± 11.2	135.8 ± 9.3	50.6 ± 5.5	53.7 ± 4.8
PE.F40	132.7 ± 0.4	133.9 ± 0.7	113.1 ± 0.7	108.6 ± 22.8	109.5 ± 18.4	108.4 ± 12.12	61.8 ± 13.0	62.3 ± 10.5
PE.S20	137.2 ± 0.6	136.2 ± 1.4	111.1 ± 0.7	119.4 ± 0.4	128.4 ± 3.1	140.8 ± 4.0	50.9 ± 0.2	54.8 ± 1.3
PE.S40	133.0 ± 0.9	135.0 ± 1.9	112.1 ± 1.4	76.4 ± 17.1	79.8 ± 15.7	82.5 ± 15.3	43.5 ± 9.7	45.5 ± 8.9

The crystallinity seems to decrease with the incorporation of the lignocellulosic material, except for 40% fiber composites, which shows a value close to that of neat PE (although it also gives a higher deviation). The high content of such fibers could counteract the reduction of crystallinity due to the incorporation of the lignocellulosic material, with relatively high crystallinity (close to 70% (Suárez et al. 2023)). Besides, cellulose can act as an active nucleation center (Dolça et al. 2022) and fibers contain over 65% of cellulose, according to previous research conducted. The geometry of the fillers can also influence their effect on crystallization; usually, smaller particles lead to higher crystallinity (Dolza et al. 2021).

On the contrary, incorporating lignocellulosic materials into the HDPE matrix can hinder the crystallization process, especially at lower loadings, due to the restrained mobility of the polymer chains (Fendler et al. 2007). An increase in melting temperature for 20% composites has been observed for bamboo-HDPE composites at the same loadings, with a reduction in melting enthalpy also and, thus, in crystallinity (Mohanty and Nayak 2010; Wang et al. 2014). There is no clear trend in the literature about the effect of lignocellulosic fillers in HDPE: some authors found reductions in crystallinity (Fendler et al. 2007,) while others have found increases (Jaramillo et al. 2021). No significant changes have been also reported (Mendes et al. 2021,) usually getting crystallinity values typically close to 50% for composites with natural fillers (Andrzejewski et al. 2020) (see supplementary figure S1).

Thermomechanical behavior

The introduction of lignocellulosic materials can effectively increase the range of application of the neat HDPE, as both parameters measured, heat deflection temperature (HDT) and Vicat softening temperature (VST), increased (Table 3). It was found that higher ratios of biomass led to higher thermomechanical stability of composites. The filler type showed a lower influence on the HDT or the VST than the percentage of filler used. Despite slight differences higher statically assessed thermomechanical stability values were noted for *Arundo* fibers composites compared to *Arundo* shredded filler. This effect was noticeable in the samples subjected to point loading and three-point bending. The values of HDT and VST correlate with the changes of mechanical properties (hardness and flexural elasticity modulus described later in Section 3.5), and described in the literature for polyethylene-based composites (Schellenberg 1997). It results from better dispersion of fibers in the polymer matrix and higher reinforcing efficiency associated with the increased shape factor of fibrous filler (aspect ratio about 4 for fibers, with fiber lengths about 0.8 mm; particle size for shredded filler is around 0.45 mm). Based on the DSC analysis, the increase in resistance to static load in the high-temperature range should not be associated to the change in the crystallinity. The HDPE composites

Table 3. Heat deflection (HDT) and Vicat softening temperatures (VST).

Material	HDT [°C]	VST [°C]
HDPE	41.00 ± 1.03	72.32 ± 1.34
PE.F20	57.27 ± 1.03	81.30 ± 0.80
PE.F40	72.88 ± 1.31	85.75 ± 1.64
PE.S20	55.31 ± 1.60	78.93 ± 0.22
PE.S40	67.51 ± 3.80	83.40 ± 0.93

produced exhibit a HDT close to PP or PET, with increases of about 50% regarding the neat HDPE. The dynamic mechanical analysis also observes this improved thermal resistance (section 3.6).

Water absorption tests

Figure 5a clearly shows that higher lignocellulosic loadings result in higher water absorption. In contrast, HDPE water absorption is almost negligible. Each point is the average value of three measurements. Moisture uptake equilibrates at a maximum of 2% for 20% composites but is increased by over 400% for 40% loadings, reaching up to 9% after the 28 days of the assay. As the materials used in this work are hydrophilic, an increase in water uptake for the composites was expected. The parts' thickness was measured at the beginning and the end of the assay to determine their swelling. This parameter follows a similar trend to water uptake, i.e., higher loadings increased swelling. Composites with fibers show higher swelling values than composites with shredded *Arundo*, following the same trend as water uptake. This increased water uptake by fibers is surprising, as a lesser hydrophilic character was expected due to the higher cellulose and lower hemicellulose contents of fibers compared to shredded material [22]. However, the morphology of the materials also plays an important role; fibers are thinner and have a higher aspect ratio than shredded material, and so have a higher area exposed, which might explain this behavior. This observation correlates with the porosity values obtained by comparing theoretical and experimental densities, the composites with higher porosity exhibited higher water uptake due to a larger number of entry points where water molecules could ingress, as well as having a higher internal free volume in which the hydrophilic cellulosic content could swell. The aspect of the formation of the polymeric skin layer on injection molded samples, depending on the nature of the flow of filled molten composite during forming, cannot also be omitted (Najafi, Tajvidi, and Chaharmahli 2006; Salasinska et al. 2016).

Mechanical properties could be modified by the hydration of the fibers and their swelling, which could partially debond the fiber from the matrix, thus reducing the stress transfer between both phases. However, Bazan et al (Bazan et al. 2020), performed these studies with coconut and flax fibers, and despite the increase in water uptake and the swelling observed, no change in the mechanical properties of the composite was found, probably because of the high stability of the HDPE matrix.

From the data obtained, Fick's diffusion coefficient can be calculated using Equations (5-7). Figure 5b shows the representation of W_t/W_m versus time on a logarithmic scale, from which the parameter n is calculated. It can be seen that the data are linear in nature, except for neat PE, where the absorption values are so low that some data points were removed to get approximate values for such parameters (Table 4). The parameter n indicates the type of diffusion behavior that is taking place;

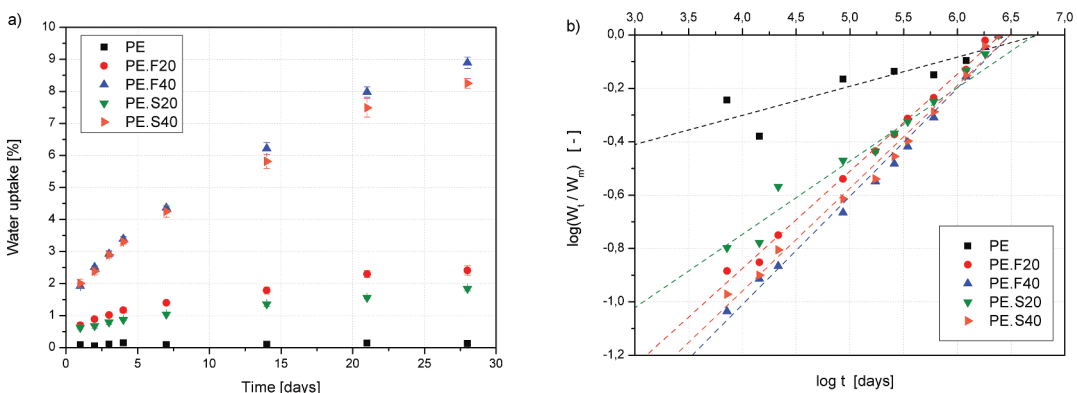


Figure 5. Results of moisture absorption. a) water uptake vs. time, b) calculation of Fick's law parameters ($\log W_t/W_m$ versus \log time).

Table 4. Water uptake parameters of PE and its composites.

Material	D (m ² /s)	k (%/s ^{0.5})	n	Swelling (%)	Sorption (g/g)	Permeability (m ² /s)
PE	3.62·10 ⁻¹⁵	3.53·10 ⁻⁵	0.11	1.1	0.001	4.523·10 ⁻¹⁸
PE.F20	3.22·10 ⁻¹³	1.61·10 ⁻³	0.36	3.3	0.024	7.758·10 ⁻¹⁵
PE.F40	2.32·10 ⁻¹³	4.98·10 ⁻³	0.41	8.3	0.089	2.064·10 ⁻¹⁴
PE.S20	3.56·10 ⁻¹³	1.10·10 ⁻³	0.30	2.3	0.018	6.548·10 ⁻¹⁵
PE.S40	3.46·10 ⁻¹³	4.88·10 ⁻³	0.39	6.6	0.083	2.855·10 ⁻¹⁴

a value equal to 0.5 means a Fickian diffusion, while a value of 0.5–1.0 indicates an anomalous diffusion. In this case, it is observed that diffusion approaches the behavior predicted by Fick's law, with values ranging from 0.30 to 0.41, except for the neat HDPE. Other authors have found a similar behavior for pineapple leaf fibers (George, Bhagawan, and Thomas 1998) or wood flour (Bazan et al. 2020). Diffusion coefficients found for *Arundo* composites are higher than for neat PE and are of the same order for all composites. They are also in a similar range to other values found in the literature: 4·10⁻¹³ m (Copani et al. 2013)/s for composites containing 40% rice hulls (Wang, Sain, and Cooper 2006,) or 3.6·10⁻¹⁴ m (Copani et al. 2013)/s for composites with 30% pineapple fiber (George, Bhagawan, and Thomas 1998,) both in a PE matrix. Lower lignocellulose loadings lead to lower diffusion coefficients; for example, diffusion coefficients around 3·10⁻¹² m (Copani et al. 2013)/s are obtained for 12% wood, flax, or coconut fibers in HDPE-based composites, increased up to 6·10⁻¹² m (Copani et al. 2013)/s for the same percentage of basalt fibers (Bazan et al. 2020).

Some authors point out that moisture absorption in natural fiber composites is affected both by diffusion and percolation and so propose other parameters for the study of water uptake. George et al (George, Bhagawan, and Thomas 1998). calculated the sorption of water as the relationship between the mass of water absorbed by the sample and the weight of the sample itself and then introduced the permeability, obtained by the combination of sorption and diffusion ($P=D \times S$).

Sorption and permeability coefficients increased with the content of lignocellulose in the composite, as also observed in the literature (George, Bhagawan, and Thomas 1998,) with values in the same range as those obtained by George et al. for pineapple fibers. Permeability for HDPE is about 1000 times lower than for composites due to the excellent barrier properties and hydrophobic character of this polymer.

Mechanical properties: tensile, flexural, impact, and hardness tests

As summarized in Table 5, 20% composites had the same tensile strength as neat HDPE, while 40% loadings led to a decrease of 8% and 14% for fiber and shredded material, respectively. This decrease could be related to the increased porosity of the composite, in the case of fiber material, and the reduced stress transfer between the matrix and the *Arundo*-derived materials. This may be due to a reduced compatibility between the fibers and the matrix or the formation of agglomerates. Therefore, for 20% composites, where tensile strength is not reduced, this suggests a sign of good adhesion between fiber and matrix and evidence of a good stress transfer between them (Fendler et al. 2007; Qiu, Endo, and Hirotsu 2004).

On the contrary, flexural strength increased for all composite samples, with no significant difference for the composites containing 20% of either fibers or shredded materials, where an increase in strength of about 15% was observed compared to neat HDPE. The most significant improvements are found for tensile and flexural modulus. The composites with fibers provided the highest module, almost a twofold increase regarding the modulus of HDPE. This property appears to be more affected by the type of filler used than for the filler ratio, as no significant difference was found between 20% and 40% fiber or between 20% and 40% shredded material. However, the flexural modulus shows a different trend. In this case, the amount of filler is more significant than its type, finding similar values for 20% composites (again, with an improvement of 100% regarding the HDPE values). Finally, only composites with shredded materials do not show increased impact resistance, with 20% providing

Table 5. Average values (\pm standard deviations) for mechanical properties of the materials (for neat HDPE, the assay was stopped at 200% elongation prior to the breaking point of the samples).

Material	Impact		Tensile properties			Flexural properties			DMA		Hardness	
	Strength [kJ/m ²] (Copani et al. 2013)		Strength [MPa]	Modulus [MPa]	ϵ_b [%]	Strength [MPa]	Modulus [MPa]	E'[:10 (García-Ortuño et al. 2011)Pa]	B'[:10 (Ferrández-García et al. 2012)Pa ⁻¹ % ⁻¹]		Ball indentation hardness [MPa]	
HDPE	6.37 \pm 0.12 ^a		18.99 \pm 0.07 ^b	1058 \pm 16	>200*	26.54 \pm 0.10	753 \pm 56 ^g	1.402	<0.004		44.0 \pm 0.5	
PE.F20	7.47 \pm 0.19		19.05 \pm 0.11 ^b	1881 \pm 45 ^{c,d}	9.12	30.47 \pm 0.23 ^f	1538 \pm 77 ^h	1.734	0.633		52.0 \pm 1.2	
PE.F40	7.08 \pm 0.14		17.46 \pm 0.14	2022 \pm 98 ^c	3.81	30.67 \pm 0.22 ^f	1270 \pm 125	1.928	1.361		59.6 \pm 2.7	
PE.S20	6.13 \pm 0.13 ^a		19.05 \pm 0.10 ^b	1560 \pm 108 ^e	7.01	30.53 \pm 0.22 ^f	1469 \pm 23 ^h	1.659	0.860		49.9 \pm 1.9	
PE.S40	5.47 \pm 0.18		16.36 \pm 0.32	1675 \pm 119 ^{d,e}	2.70	28.98 \pm 0.23	767 \pm 73 ^g	1.782	2.081		57.3 \pm 1.1	

Tukey tests for comparison of properties of the different series of materials have been used at a 95% confidence level. Those materials with the same superscript letter show no statistical difference for the property.

similar behavior to PE, while 40% loadings reduce the impact strength. Composites with fibers exhibited an increase in impact strength of 17 and 11% for 20% and 40% fibers.

Other authors have reported that the incorporation of 12% of flax fiber has produced no changes in the tensile strength of a PE matrix and an increase of about 100% in elastic modulus; for flexural properties, this same composite provided an increase of about 75% flexural strength and almost doubled the flexural modulus and also led to a moderate increase, of about 10%, in impact strength (Bazan et al. 2020). Several works report a decrease in the mechanical performance of natural fiber composites and propose using compatibilizers, such as maleated polyethylene (MAPE), to increase the tensile strength of the resulting material (Jaramillo et al. 2021). For example, introducing MAPE in composites with 20% of hemp, jute, or flax provided similar or slightly higher tensile strength values than neat HDPE, 2-folding the elastic modulus (Dolza et al. 2021). The composites obtained with *Arundo*-derived materials have provided, in general terms, an improved mechanical behavior compared to the neat PE, already folding by two the elastic modulus of the polymer, thus demonstrating the good potential of these materials, particularly fibers, for composites obtaining; a similar trend was observed for bamboo fibers, which had a reinforcing effect for 20% loadings, increasing flexural strength and tensile and flexural modulus with increasing loadings of fibers, up to 30% (Mohanty and Nayak 2010). Mohanty and Nayak have also found a decrease in properties with further increases in the fiber content, which they relate to the incompatibility of fibers with the matrix; the incorporation of a 2% MAPE led to more significant improvements in mechanical properties, especially in modulus and flexural strength, which were improved by 100% in comparison to the composites at the same loading without the compatibilizer. In contrast, Lei et al. did not find any improvement by using MAPE or carboxylated polyethylene for 30% wood flour HDPE composites, which reduced tensile strength by over 30% and impact strength by more than 50% (Lei et al. 2007).

Table 5 also summarizes the results of ball indentation hardness of injection-molded polyethylene and its composites. The addition of both types of filler improved the hardness of the composites compared to neat HDPE. Taking into account the low tendency of HDPE to heterogeneous nucleation and the presented DSC results, it can be said that the effect of increasing the hardness results from the distribution of rigid filler structures in the boundary layer and not from a change in the degree of crystallinity of the polymer. Considering the changes in the chemical structure of *Arundo* fibers compared to shredded plant parts, the higher values of the series containing fibers are understandable.

A slight increase in hardness was found for composites. Neat HDPE exhibited a hardness of 60.0 Shore D, which increased to 62.5 for 20% composites and 65.0 for 40% composites. For this property, the ratio of filler is more significant than its type, as for the flexural testing. Similar values were obtained for 20% coir, flax, or coffee husks HDPE composites (Ayyanar et al. 2022; Chimeni-Yomeni et al. 0000; Jaramillo et al. 2021); lignocellulosic materials show a higher hardness than PE, which explains this trend.

Thermomechanical performance – DMA

The analysis of storage modulus (E'), loss modulus (E''), and damping factor ($\tan\delta$) with temperature allows evaluating the changes in the mechanical properties due to the addition of fibers and shredded material to the HDPE matrix (Figure 6). DMA is an essential test for the evaluation of the mechanical properties of materials due to its sensitiveness to structural changes, including the interfacial bond between the fibers or fillers and the matrix (Correa-Aguirre et al. 2020).

The DMA storage moduli (Figure 6a) is indicative of the elastic behavior of the materials. All composites provide higher storage modulus than neat HDPE, meaning that the lignocellulosic material stiffens the matrix along the temperature range studied. The materials containing fibers show higher values of storage modulus than those made with shredded material, which means that these composites are stiffer, as also found in tensile and flexural tests. The starting value of the storage modulus is similar for all samples and tends to increase for composites while remaining constant for PE in the rubbery plateau area. The storage modulus decreases in an expected constant way, as also

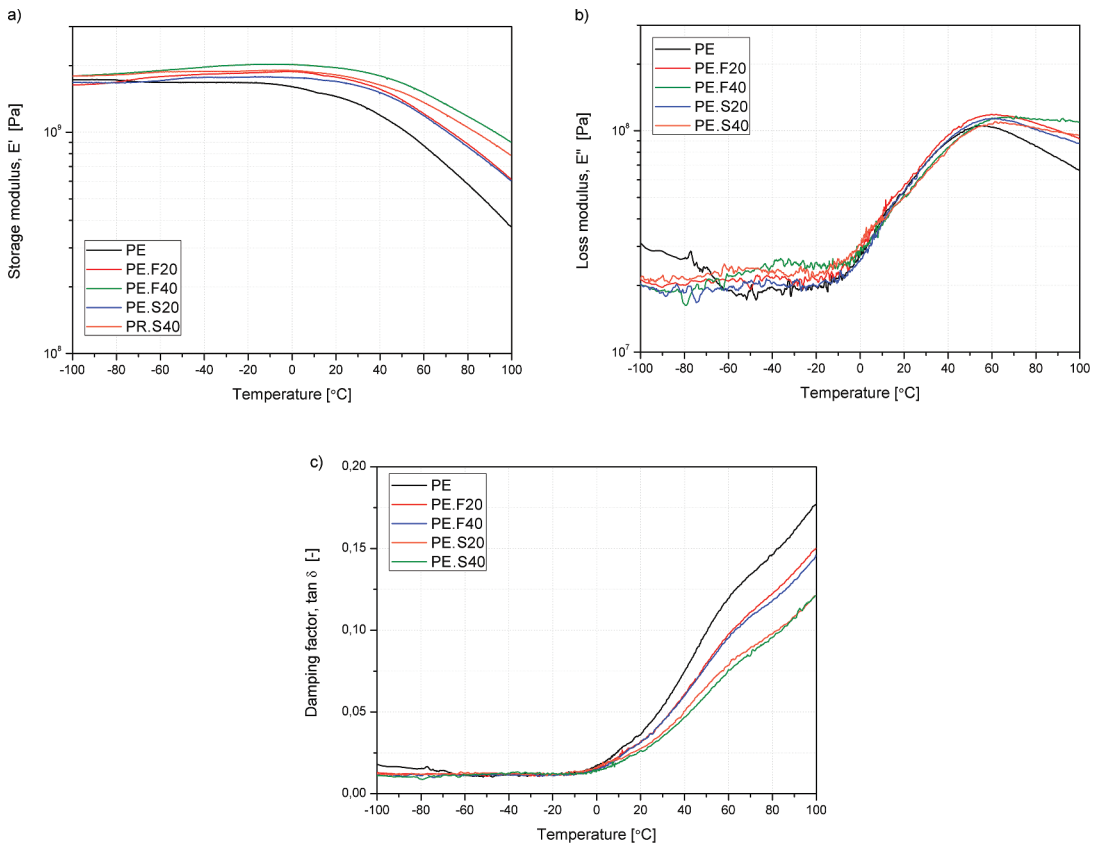


Figure 6. Variation of a) storage modulus, b) loss modulus and c) $\tan \delta$ with temperature from DMA.

found in other works (Andrzejewski et al. 2020; Zhang et al. 2002). This decrease takes place at higher temperatures with the increase in lignocellulosic content.

The storage modulus for the HDPE decreased with temperature, while for composites there was a slight increase up to about 0°C, and then it started to decrease abruptly. HDPE composites with 20% microcellulose fibers, using 2% of MAPE as compatibilizer, led to an increase of 45% storage elastic modulus at −20°C (Fendler et al. 2007,) while for 20% hemp the increase reached 30% and 100%, again using MAPE as compatibilizer (Dolza et al. 2021,) at 0°C and 75°C. These authors have not provided results without the use of MAPE, so results are not directly comparable. Correo-Aguirre et al (Correo-Aguirre et al. 2020). observed an increase of 18% in storage modulus when using 20% of bagasse fibers in a PP matrix. The increased stiffness can be related to hindering HDPE polymer chain movements due to the introduction of fibers and shows that the composites have an increased capacity to store energy compared to the matrix. These results agree with the data obtained from impact tests, where higher values were also obtained for composites and are also observed in the reduced values of $\tan \delta$. For 20% *Arundo* fibers composite, the storage modulus increased by 11%, 16%, and 19% at −20°C, 0°C, and 75°C, and 21%, 25%, and 36% for 40% fibers. As observed in the graph, the shredded material also increases the storage modulus, although to lower values, namely 6, 9, and 17% for 20%, and 13, 17 and 29% for 40%, at the same temperatures.

For loss modulus, the PE maximum value is found at 57°C, corresponding to the α -transition, generally observed in the range from 20°C to 70°C (Molefi, Luyt, and Krupa 2010) or even 100°C (Hejna et al. 2020); this transition is related to chain movements in the crystalline region of the polymer. For the composites, this transition is slightly shifted to higher temperature values,

approaching 70°C for composites with 40% fibers. Composites with fibers show higher peak temperatures than shredded material. The shift of this transition toward higher temperatures and its increase indicates a more resistant structure in the composites and it is also related to the reduction in the polymer chain mobility. The β -transition for HDPE, usually related to segmental motions in the amorphous region, takes place at about 0°C; however, some authors have reported that this transition is usually absent (Mohanty and Nayak 2010,) as is also happening in this study.

Bhattacharjee and Bajwa (Bhattacharjee and Bajwa 2018) observed a 40% increase in storage modulus for HDPE loaded with wood flour, as well as an increase in tensile and flexural properties. The use of seaweed in a HDPE leads to an increase of the storage modulus of about 10%, which increases with the seaweeds content, up to 30% (Ferrero et al. 2015). The introduction of 30% of banana fiber in HDPE, with a 3% of MAPE as compatibilizer, leads to similar results: around 30% increase in storage modulus, maximum temperature from E'' plot shift from 57°C to 63°C and a slight decrease in $\tan \delta$ (0.18 to 0.16) (Satapathy and Kothapalli 2018). Lei et al. found an increase in both storage and loss modulus when using bagasse or pine flour in a recycled HDPE matrix, for a 30% loading (Lei et al. 2007). At 23°C, storage modulus increased from 1.55 GPa for HDPE to 2.29 GPa and 2.23 GPa for bagasse and pine, respectively, while loss modulus varied from the initial 0.15 GPa to 0.19 and 0.18 GPa, respectively. These authors did not get further improvements by using compatibilizers such as MAPE or carboxylated polyethylene. All *Arundo* composites show lower loss modulus than pure PE, which means that the incorporation of the lignocellulosic materials provides higher elastic recovery. γ -transitions occur for HDPE at temperatures lower than the ones used in the study, and so are not visible, although they might correspond to the small peak seen around -70°C (Molefi, Luyt, and Krupa 2010,) also visible in storage modulus as a short descending step for PE.

The glass transition temperature (T_g) in highly crystalline polymers, as it is the case of HDPE, is difficult to identify; this is in line with the results obtained in this research. The glass transition occurs when the chains in the amorphous regions begin a coordinated large-scale motion. Therefore, this transition is not observable in the highly crystalline HDPE, although an intense peak for α -transition is usually observed. DSC has provided crystallinity values over 45% for all samples, reaching up to 60%, which may explain that T_g is not visible in these assays, so the plots do not show this characteristic peak. The $\tan \delta$ plot shows an inflection in the curves at 50–60°C, corresponding to α -transition, also observed in E'' plots as a maximum.

The $\tan \delta$ is the ratio of the loss to the storage modules; therefore, the damping factor is useful to assess the relative contributions of the viscous and elastic components in viscoelastic materials. Again this curve does not show the β -transition, although a slight inflexion in the curves is seen at about 10°C; this could be attributed to the glass-rubber transition of the amorphous phase (Barczewski et al. 2018). The increased stiffness found for composites implies a reduction in damping properties, compared to the neat PE, as seen from the $\tan \delta$ plot. The composites with higher stiffness revealed lower values of damping factor, as also observed by other authors (Barczewski et al. 2018). The thermomechanical behavior of the materials is apparently more influenced by the amount of lignocellulosic material than by its type. Good fiber-matrix adhesion limits the mobility of polymer chains and thus reduce the damping factor, with a simultaneous increase of T_g (Scalici, Fiore, and Valenza 2016); obtained results would then suggest that fibers are well bonded to the matrix.

From the DMA results the brittleness (B) of the different materials can be calculated, using equation 8, proposed by Brostow et al (Brostow, Hagg Lobland, and Khoja 2015):

$$B = \frac{1}{\varepsilon_b \cdot E'} \quad (10)$$

Where E' is the storage modulus from DMA at 1.0 Hz and ε_b the elongation at break, both at room temperature.

The brittleness values obtained at 25°C for the different formulations are found in Table 5. According to these authors, lower brittleness values imply higher dimensional stability of the

material under repetitive loading. So, 20% composites would be more stable than 40% ones, and fibers are more stable than shredded material. Another factor that can be calculated from DMA analysis is the adhesion factor (A in equation 9), as described by Kubat et al (Kubát, Rigdahl, and Welandar 1990,) and considering that the behavior of the composite is due to the properties of the matrix, the filler and the interphase, and resulting in (Hejna et al. 2020):

$$A = \frac{1}{1 - x_F} \cdot \frac{\tan \delta_C}{\tan \delta_{PE}} - 1 \quad (11)$$

Where x_F is the ratio of the filler in the composite (in volume).

Lower values of A indicate higher interfacial adhesion (Jyoti et al. 2016); an increase in A is associated with higher damping and a higher loss of energy or viscoelastic behavior, and higher energy dissipation due to chain movements inside the composite (Karaduman et al. 2014). Hejna et al (Hejna et al. 2020). explain that a high porosity or insufficient interfacial adhesion favors these movements. As this factor depends on the damping factor, it also varies with temperature. It can be seen that at higher loadings, higher values of the adhesion factor are observed, and therefore there is lower adherence between the lignocellulosic material and the matrix. The values for this parameter are similar regardless of the type of lignocellulosic material introduced. The negative values of the adhesion factor obtained are due to the simplification of the calculations and the removal of the interphase region (Hejna et al. 2020; Mysiukiewicz et al. 2020). The lower and more stable values are obtained at temperatures over 15°C, meaning that the lignocellulosic materials do not provide as much positive effect below room temperature.

Several authors propose using the entanglement factor as an approximation to the intensity of the interaction between matrix and filler/reinforcement, together with the efficiency factor (Andrzejewski et al. 2020; Jyoti et al. 2016; Pandey et al. 2016; Panwar and Pal 2017). The entanglement factor is usually calculated at several temperatures to evaluate the potential differences in such interactions due to different service conditions. The entanglement factor (N) is calculated as:

$$N = \frac{E'}{RT} \quad (12)$$

Where E' is the storage modulus at a certain temperature (T , in K) and R is the universal gas constant.

The reinforcement efficiency (r) also gives an idea of the filler/matrix interaction:

$$E'_c = E'_m \cdot (1 + r \cdot V_f) \quad (13)$$

Where E'_c and E'_m are the storage modulus of the composite and the matrix, respectively, and V_f the percentage of the filler (by volume).

It is interesting to note that lower values of the entanglement factor are found for 20% composites up to approximately -70°C, possibly corresponding to the end of γ -transition of the HDPE (Khanna et al. 1985) (Figure 7b). From that moment, the difference in storage modulus is increasing with the temperature, getting the lowest value for the neat HDPE. A clear difference between the composites with fibers and with shredded material is observed for this factor, as also found in tensile and flexural tests. The efficiency factor increases abruptly after approximately 15°C. This was also observed in the storage modulus versus temperature plot, where the composites provided higher values of E' than the neat HDPE. These findings are in good agreement with the static mechanical results, where higher mechanical performance was obtained for fibers, particularly at 20%.

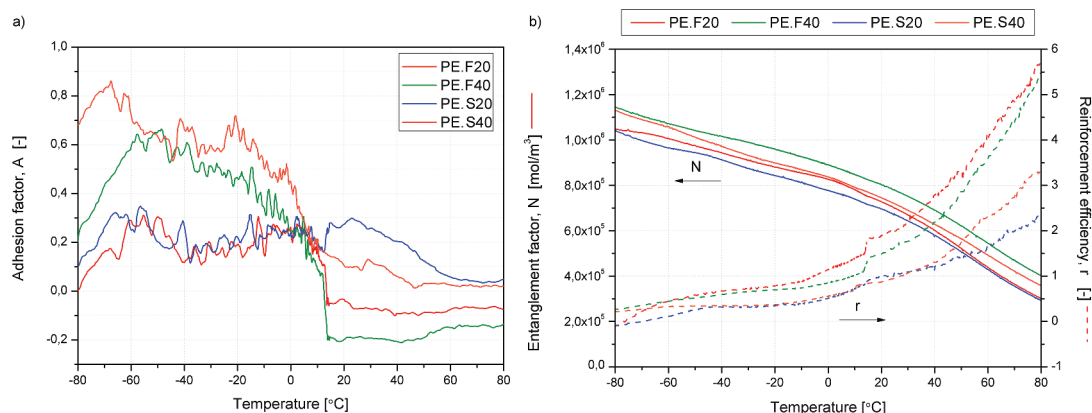


Figure 7. a) adhesion factor calculated for the composites, b) entanglement factor (left axis) and reinforcement efficiency (right axis).

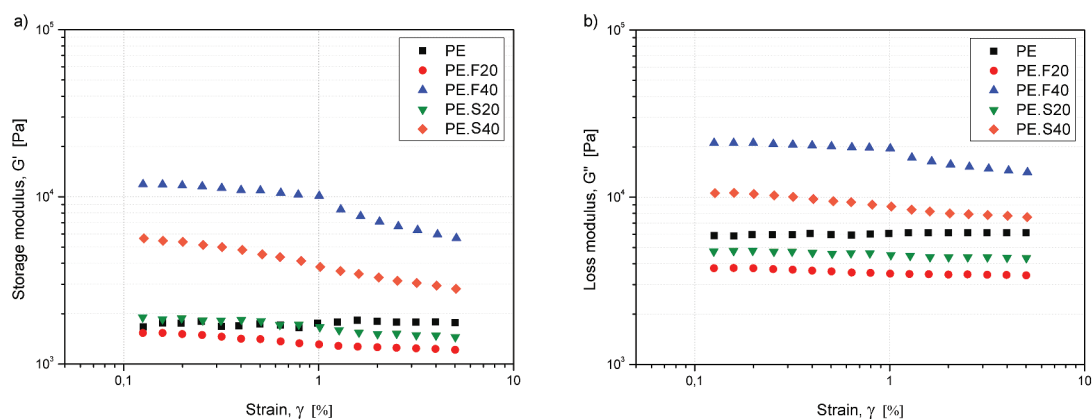


Figure 8. Results of strain-sweep rheological experiments: a) storage modulus, b) loss modulus.

Rheological behavior

Oscillatory rheometry

Figure 8 shows the storage and loss modulus (G' and G'') versus strain (γ), obtained during strain sweep assays. It can be observed that the introduction of 20% lignocellulosic filler of both types to HDPE does not cause significant modifications of the storage and loss moduli, while both increase for 40% composites. HDPE and composites at 20% exhibit a linear viscoelastic (LVE) region in the studied range (0.1–5% strain), while 40% loadings show a shorter LVE area, with a short step around 1% strain, although this is not considered particularly significant. The frequency sweep tests were performed at 0.5% strain, thus in the LVE for all materials. It is well known that incorporating fillers into polymer matrices usually produces a shortening of this LVE region; this is connected with the creation of the spatial structure of restricted rigid filler domains (Adebayo et al. 2021; Berzin et al. 2019). 0.5% strain is a commonly used value for PE-based materials and oscillation mode assays. For this strain, the value of G' for HDPE is 1.7 kPa, similar to 20% composites as observed in the graph (1.4 and 1.8 kPa for fibers and shredded material, respectively), while this increased significantly for 40% composites, increasing by almost 300% for shredded material (reaching up to 4.5 kPa) and by 800% for fibers (arriving almost to 11 kPa).

Figure 9 shows, in logarithmic scale, the results of frequency sweep tests, in the oscillation mode, versus angular frequency (ω). At lower ω all composites provide higher values of both moduli than the

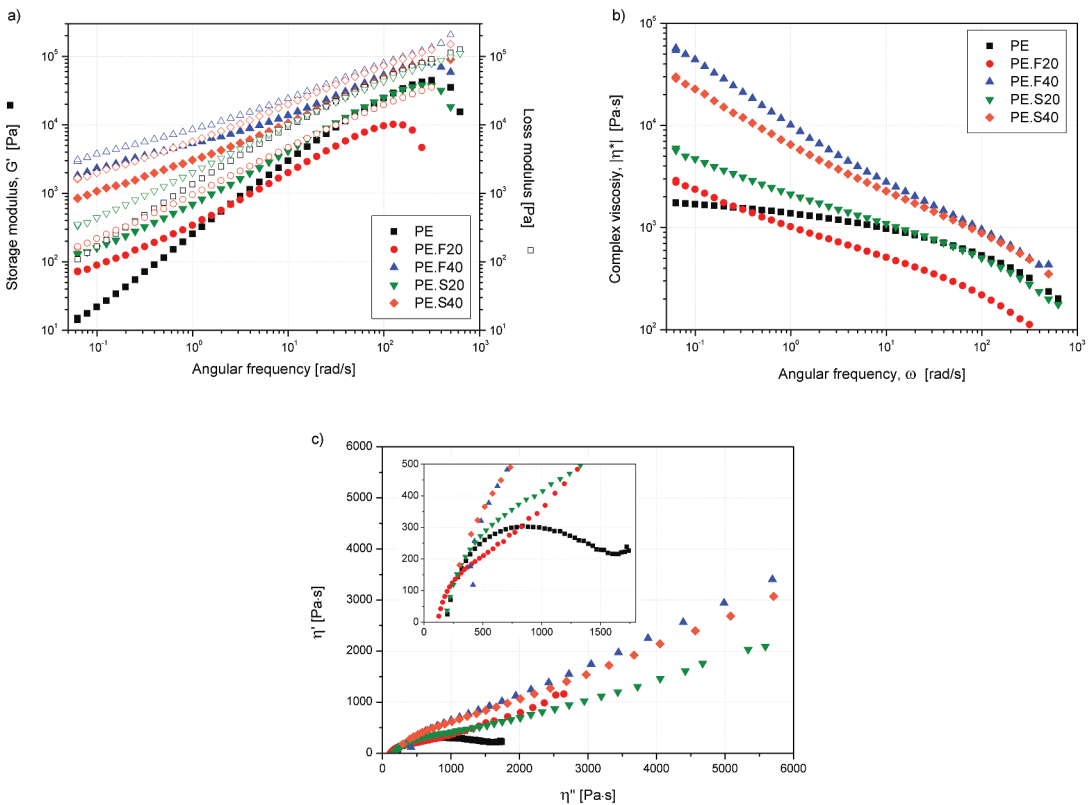


Figure 9. Results of frequency-sweep rheological experiments: a) storage and loss modulus, b) complex viscosity, c) Cole-Cole plot.

neat polyethylene, although at higher frequencies, the trend changes, and only 40% loadings show higher moduli than PE, as observed by Patti et al. for PP composites (Patti et al. 2021). The values of G'' are higher than those of G' for all composites, which means the viscous part is dominant over all of the studied range; both curves follow a linear trend in a similar pattern for each material. The increase in moduli is evident in the low-frequency range (0.1–10 rad/s), as the curves tend to overlap at high frequencies, likely due to the fibers aligning at higher frequencies.

No flow point is obtained for any of the composite materials with 40% loadings, that is, the storage and loss modulus do not cross-over each other in the studied region. The increase of both modules shows the reinforcing effect of the lignocellulosic materials, with a predominant viscous character of the rheological behavior. This effect suggests that the obtained composite materials, despite the higher resistance to flow of the filled bulk, will not be characterized with limited processability.

Figure 9b shows the complex viscosity ($|\eta^*|$) for the materials tested. A Newtonian plateau is observed for neat HDPE at frequencies under 10 rad/s, which does not occur for composites, which are more shear thinning in nature, as observed in other works also (Hejna et al. 2020). Complex viscosity is higher for the 40% composites, but is reduced for 20% fiber composites, especially for shear rates over 1 rad/s. The use of shredded material at this loading only increases the viscosity at low ω values, which would again suggest fiber alignment and overlapping at high ω . The lack of plateau observed for composites could indicate the formation of agglomerates of the lignocellulosic materials in the samples (Barczewski et al. 2022; Berzin et al. 2019). The greater viscosity increase in low ω range results from increased physical impact of the fibrous *Arundo* filler characterized with higher aspect ratio. Other works have shown a moderate increase of viscosity for up to 30% loadings of wood-derived materials, with abrupt increases for 40% composites, which result in a more difficult processing of such

composites (Adebayo et al. 2021; Koohestani et al. 2019). The viscosity curves for all materials show shear thinning behavior or pseudoplasticity, meaning they become less viscous at increasing angular frequencies. As also found in the literature, at high frequencies the effect of the interaction between particles becomes less prominent than the matrix contributions and thus the viscosity values for composites tend to approach that of the matrix (Adebayo et al. 2021; Ogah, Afiukwa, and Nduji 2014).

The real and imaginary parts of the complex viscosity allow the evaluation of the compatibility of polymer blends or composite materials (Aid et al. 2019; Mysiukiewicz et al. 2020). This method, known as Cole-Cole plot (Figure 8c), states that miscible homogeneous blends provide semi-circle-shaped smooth curves, while deviations from this Maxwellian fluid ideality reflect a poor distribution or miscibility of the phases studied. For this study, it is seen that PE has a relatively smooth course, close to a semicircle, as also do 20% composites, at least to a certain value. Forty percent composites show a higher deviation from the ideal plot, especially at higher viscosity values, where the curves tend to form a straight line, thus indicating agglomerations of the filler, as found in other works (Mysiukiewicz et al. 2020; Stanciu et al. 2020).

Finally, the flow tests were performed to determine the zero-shear viscosity (η_0), using the Carreau-Yasuda regression. As for all the parameters studied, the values for η_0 increase with the biomass loading, i.e. 1579 Pa·s (PE), 2529 Pa·s (PE.F20), 37970 Pa·s (PE.F40), 5156 Pa·s (PE.S20), 13250 Pa·s (PE.S40). Those results are in agreement with the MFI values and with data reported in the literature (Adebayo et al. 2021; Berzin et al. 2019; Mohanty and Nayak 2010) and with the increases recorded in switchover pressure during injection molding: the higher lignocellulose content resulted in lower MFI, or higher viscosity of the material (Figure 9). The composites with shredded material have a higher viscosity and lower density than those with fibers. Figure 10 shows the mean MFI values obtained for the different materials, and the modification of zero-shear stress and switch pressure during processing compared to the values obtained for neat HDPE.

Capillary rheometry

The effect of two different lignocellulosic fillers incorporated with 20% and 40% on rheological behavior during capillary flow was additionally investigated. The results are presented as changes of shear viscosity (η) in the function of apparent shear rate ($\dot{\gamma}_A$) in Figure 11. The addition of the filler increased the shear

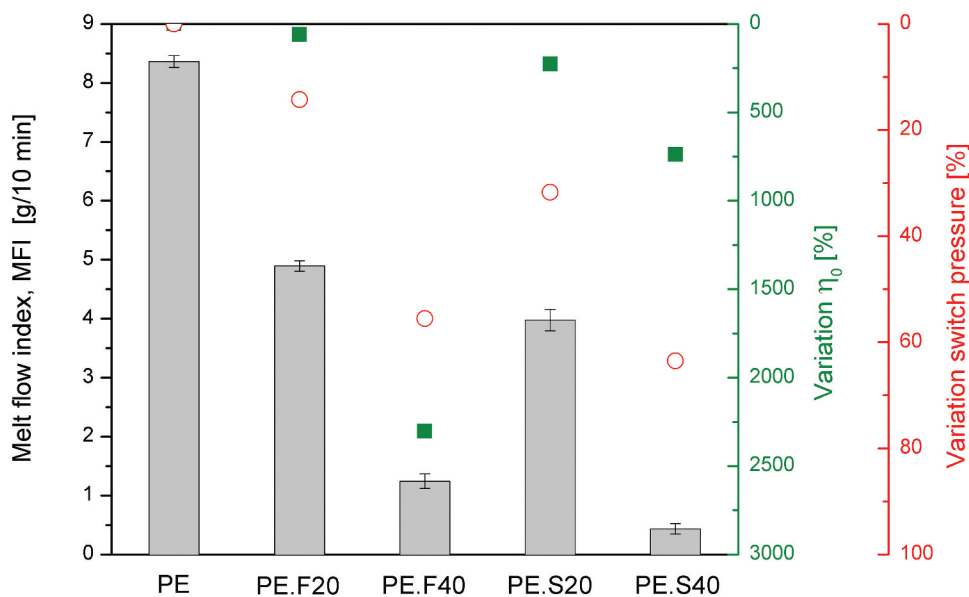


Figure 10. MFI and variation of zero-shear stress and switchover pressure for the different materials.

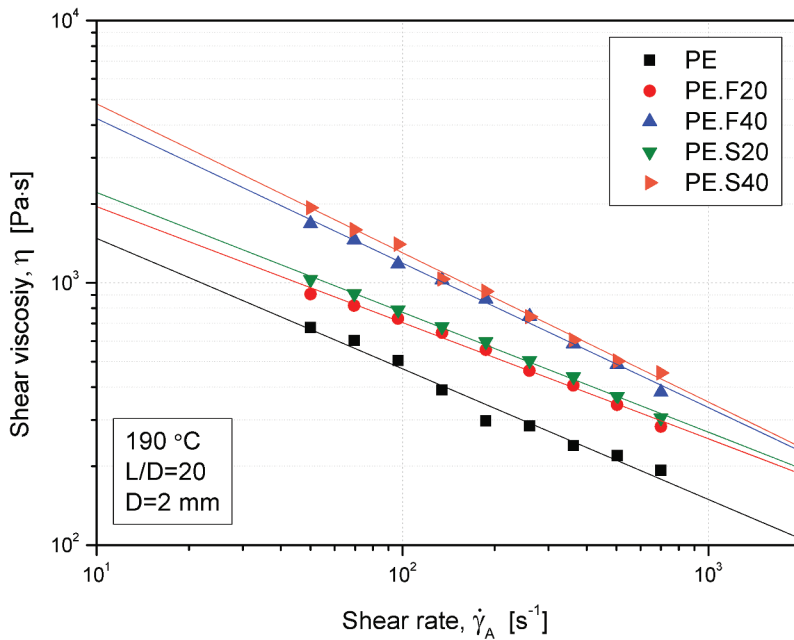


Figure 11. Shear viscosity vs. shear rate curves obtained by capillary rheology.

viscosity compared to unmodified polyethylene. This phenomenon is characteristic of polymer composites and was also noted for other materials modified with lignocellulosic fillers (Kuan et al. 2003; Lewandowski et al. 2016). *Arundo* fiber composites were characterized by slightly lower viscosities compared to shredded-filled series, as was also observed in oscillatory tests. The slight differences most likely resulted from the tendency of the fibrous material to orient in the flow direction during capillary flow, which resulted in a lower flow resistance than for composites filled with irregularly particle-shaped filler with a low aspect ratio.

The determination of the power law index (n) according to Equation (8), allows to describe the nature of fluid as Newtonian ($n = 1$), non-Newtonian shear-thinning ($0 < 1$), or shear thickening ($n > 1$) (Smitthipong, Tantatherdtam, and Chollakup 2015). The analyzed composites show, similarly to the unmodified polymer, shear-thinning behavior. The decrease in the value of the power law index noted for series with the highest share of filler in polymeric bulk is typical to the behavior of polymer composites (Ares et al. 2010,) as described in the literature. In the case of the unmodified high-density polyethylene, the n value is lower than for composites containing 20 wt% of the filler. This effect is rather not due to a change in the non-Newtonian nature of the flow but to the higher likeness of non-filled high-density polyethylene to the stick-slip phenomenon (Barczewski et al. 2017,) which results in a lower degree of fitting of the model curve to experimental data, as shown in Table 6. The consistency factor K increased with the filler content, resulting from increased resistance to the flow of polymeric melts with dispersed rigid lignocellulosic structures (Sewda and Maiti 2010). Moreover, this parameter is higher for composites containing shredded

Table 6. Power law model parameters for PE and PE composites.

Material	K [Pa·s ^{n}]	n [-]	R^2 [-]
PE	4,654	0.502	0.981
PE.F20	5,420	0.557	0.989
PE.F40	15,035	0.449	0.996
PE.S20	6,328	0.543	0.997
PE.S40	17,867	0.431	0.994

Arundo than for those with the fibrous filler; the explanation for this phenomenon may be the increased interaction between the irregularly shaped filler particles during the capillary flow and the increased interaction behavior of its constituents.

Structure evaluation

Figure 12 shows a representative image from SEM observation of the test samples surface for each formulation. The surface for neat HDPE is smooth and without marks, while the composites show a rougher surface, with some lignocellulosic material close to the surface, leading to flow marks and shrinks. As explained in section 3.9, this different roughness explains the changes in gloss observed for composites versus the pure matrix.

From the fracture section of the samples after the tensile tests, it can be observed (Figure 13) that fibers are not aligned in a particular direction but are rather found well dispersed in the matrix, without any preferent orientation. On the other hand, some pull-out can be seen, more relevant for the composites at higher loadings. For the same ratio of filler, more pull-out was found for materials with shredded reed. This is in agreement with the observation on the adhesion factor and the reinforcing efficiency; fibrous composites show better adhesion and higher efficiency than those with shredded lignocellulose materials, also explaining the better mechanical performance of such series of materials.

In Figure 13a SEM images, the cross-sections of samples with 20% and 40% fiber can be observed. In the 20% one, no signs of evident pull-out are observed, while this is evident for the 40% composite, where some voids appear as a consequence of insufficient adhesion between fiber and matrix. The slight reduction in tensile strength found for this series of composites (regarding neat HDPE) might be explained by the debonding of part of the fibers. On the other hand, Figure 13c shows a section of a PE.F20 sample at a higher magnification, where it is patterning that all fibers are not strongly bonded to the matrix. Although an increase in elastic modulus is found for composites, the good stress transfer between fiber and matrix (requiring a good adhesion between phases) is evidenced by the increase in tensile strength, which wasn't obtained for these composites and is also happening in the literature. Some compatibilizers would be needed to increase the compatibility between both phases; however, special attention should be paid to the selection and application of such treatment. Most of them focus on the use of coupling agents, such as maleated polyethylene; not all authors have found

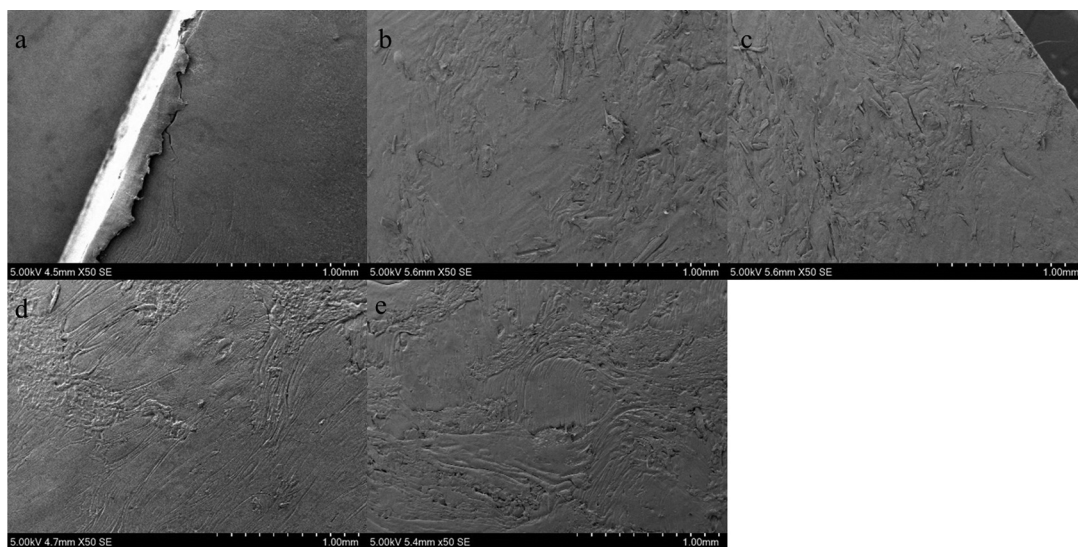


Figure 12. SEM images of the surface of the different parts, obtained at 50× magnification: a) PE, b) PE.F20, c) PE.F40, d) PE.R20, e) PE.R40.

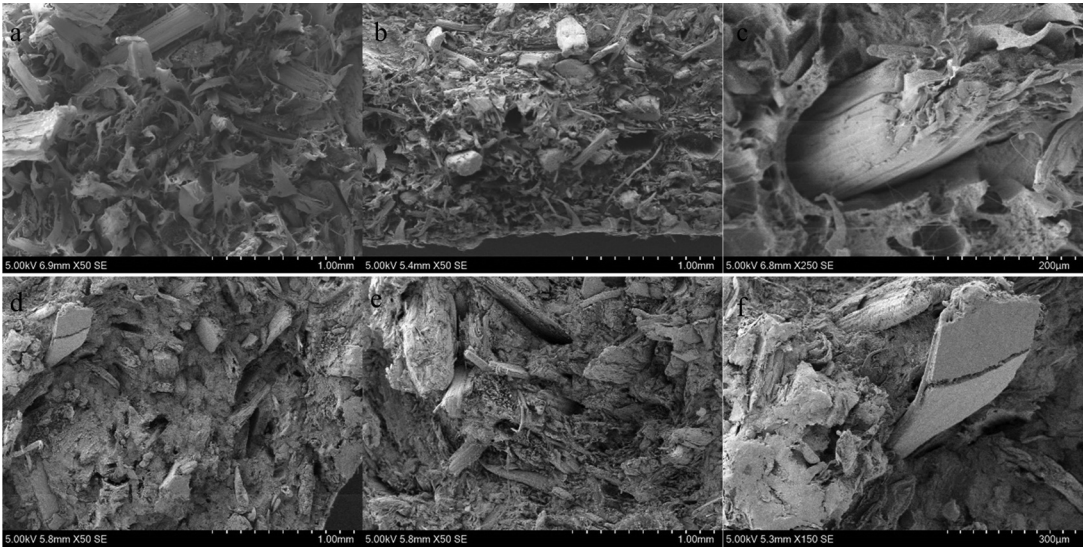


Figure 13. Cross-section micrographies for the different parts, obtained at different magnifications: a) PE.F20 and b) PE.F40 at 50 \times , c) PE.F20 at 250 \times ; d) PE.R20 and e) PE.R40 at 50 \times , f) PE.R20 at 150 \times .

improvements in mechanical performance, despite the expected better adhesion, as explained in sections 3.5 and 3.6. Similar observations are made for silanized fillers, this last releasing an important amount of volatile compounds. A balance between technical performance of the composite and environmental behavior should be reached. Similar observations can be made regarding the composites with shredded materials, although finding, in this case, a higher number of voids (Figure 13d,e); that is, the adhesion between the HDPE matrix and the filler is lower than for the case of fibers, which is in line with the observations made from static and dynamic mechanical testing. Finally, it is also evidenced for these composites that the filler consists of less homogeneous materials, with fibers and fiber bundles (Figure 13f).

Color and gloss evaluation

The results from color and gloss evaluation are summarized in Table 7. The decrease in the L^* parameter is related to the darkening of the samples. From these values, and as observed in Figure 14, composites with fiber are lighter and tend more yellow than those with shredded material, which are darker and greener. Despite the different values for the L^* , a^* , and b^* parameters obtained for all composites, the color changes in the neat PE are similar for all samples. Regarding gloss, it can be observed that fiber composites at both loadings provide a matted surface with lower gloss than composites with shredded materials. At the same time, the gloss of composite shredded materials decreased with the increased content of filler. The lower gloss is due to the rougher surface obtained for composites.

Table 7. Parameters for color and gloss evaluation.

Material	Color				Gloss		
	L^*	a^*	b^*	ΔE	20°	60°	85°
PE	72.47 ± 0.13	-0.91 ± 0.03	-0.31 ± 0.12	–	27.38 ± 3.46	69.03 ± 5.06	84.72 ± 2.17
PE.F20	56.26 ± 0.86	12.37 ± 0.45	23.67 ± 0.91	31.845	0.98 ± 0.17	7.83 ± 1.12	8.46 ± 2.74
PE.F40	58.37 ± 1.34	12.00 ± 0.69	26.16 ± 1.37	32.651	1.06 ± 0.54	7.63 ± 2.93	17.42 ± 5.51
PE.S20	41.61 ± 1.24	5.32 ± 0.30	18.77 ± 0.62	36.810	7.13 ± 0.99	32.39 ± 3.15	53.89 ± 2.91
PE.S40	49.33 ± 1.48	4.44 ± 0.24	15.61 ± 1.00	28.593	3.01 ± 0.95	18.16 ± 4.21	35.51 ± 7.33

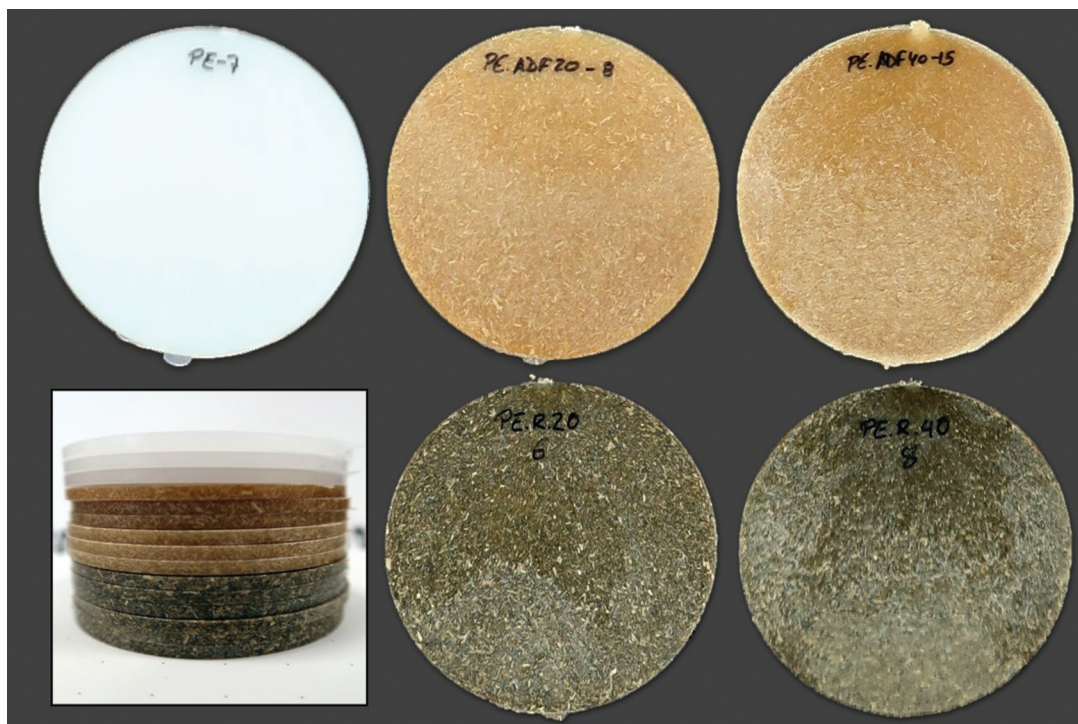


Figure 14. Photography of injection-molded samples of the various formulations.

Conclusions

The obtaining of composite materials containing giant reed is still rather incipient in the literature, contrary to other lignocellulose fibers, or to other uses given to this plant species. Most literature about *Arundo donax* L. is related to the obtaining of green products, such as ethanol or levulinic acid. In this work, two different *Arundo donax* L. derived materials have been used for obtaining composites at 20% and 40% weight loadings, obtaining a material with a good processability window (higher degradation temperature than the processing one required: degradation starts at 240°C, which is 50°C above the processing temperature).

The viscosity of the composites increases with the amount of filler used, finding a more viscous material for the composites with the fibrous material in contrast to the shredded material, due to the higher aspect ratio of the filler. The increased viscosity is well correlated with the reductions in MFI and the higher values of switch over pressure during the injection molding of the composites.

The FTIR analysis does not evidence any particular chemical interaction between filler and matrix; the formation of chemical bonds between both phases would require a compatibilizer and might reduce the pull-out of fibers in the mechanical testing, thus, to higher mechanical properties.

In any case, a good stress transfer is observed for the composites, particularly for those containing reed in the form of fibers, even though any compatibilizer was introduced in the process. The tensile and flexural strength was not reduced, and elastic modules in both assays were increased significantly. So, composites with 20% fiber exhibit a tensile strength of about 19 MPa and an elastic modulus of 1.9 GPa, which is almost twice that of the neat matrix, while flexural strength of this series is increased by a 15% (reaching 30 MPa) and elastic modulus is also increase by over 100%, getting over 1500 MPa. The increased porosity found for composites has not reduced the mechanical properties of the composite, which is a further indicator of the good behavior of the *Arundo*-derived materials in the HDPE matrix. In any case, porosity values

are considered low, finding the maximum value of 8.7% for 40% fiber composites; this can be related to a good processing of the materials and also to the good thermal stability of the material: as it is not degraded during processing, no decomposition products, in the form of vapor or gases, are generated. Finally, only those composites with fiber increased the impact resistance of the matrix, which might be related to better adhesion of the fiber to the matrix, as also found in SEM observations and DMA assays. Impact strength is increased by 20% for fibrous composites, while the composites with 20% shredded material provided comparable values to the HDPE; only the series with 40% shredded material shows a slight decrease of about 10% for this property.

The TGA assays have allowed confirming that the ratio of each filler used corresponds to the blend prepared at the compounding stage, apart from confirming that the material is thermally stable for about 50°C above the required processing temperature. Neither the melting point nor the crystallinity of the matrix is affected by incorporating the lignocellulose materials, as commonly accepted in literature for HDPE-based composites; melting takes place at about 135°C. However, the heat deflection and Vicat softening temperatures are significantly increased as a consequence of biomass incorporation; in particular, HDT is almost increased by 100% for the 40% fiber composites (41°C for neat HDPE vs. 73°C for this composite), while VST rises from 72°C for the matrix to 86°C for this same material. This increase might be an indicator of the good stability of injection-molded composites for their use under temperature-changing conditions, such as outdoor applications. In any case, the aging performance and stability of such materials under UV and humidity cycles should be assessed prior to anticipating a good behavior under such circumstances. The content of polyphenols and other antioxidant compounds in biomass would provide additional benefits to consider. These tests, together with the analysis of recyclability and the study of lifecycle of composites would allow establishing the techno-environmental benefits of using such materials in contrast to the neat matrix or to other composites obtained with natural fibers. The use of a lignocellulosic filler coming from a residue would *a priori* result in an improved environmental behavior, although this point is being confirmed in the near future by conducting a proper LCA.

Despite their different composition, a significant increase in water uptake for the composites was observed, without significant differences due to the type of filler. Swelling is more significant for the composites with higher loading, reaching values up to 8% for PE.F40 samples. The values obtained for diffusion coefficients are similar to those obtained in literature for other composites with lignocellulose fibers, in the range of $2.3\text{--}3.6 \cdot 10^{-13}$ m (Copani et al. 2013)/s, in the range of 100 times higher than for neat HDPE polymer, of hydrophobic nature.

Finally, introducing the biomass in the HDPE matrix results in changes in the aesthetics of the part; while composites with fibers tend to get a yellowish color, those with shredded reeds show a greener aspect. The different flow behavior of both composites explains the higher surface roughness observed in SEM for the fiber composites, which results in a matte appearance, regardless of the fiber ratio used. For the composites with 20% of the shredded material, a thin layer of PE is likely to be formed on the outer surface of the part, producing a smoother surface with higher gloss, which is also reduced for the higher-loaded samples.

Therefore, the potential of giant reed as raw material to produce fibers and fillers has been demonstrated, allowing to obtain a composite with good aesthetics, thermal stability, and mechanical performance. Further experiments are being conducted to determine other properties of the composites and finish their characterization; in particular, the resistance to oxidation/aging under humid environment and UV light, the thermal and acoustic insulating character, and the environmental behavior, including an analysis of the recyclability of the material, are being undertaken.

Highlights

- HDPE-based composites with up to 40% biomass from *Arundo donax* were produced.
- Addition of 20 wt% *Arundo* improve elastic and flexural modulus.
- Thermal stability is increased due to the incorporation of *Arundo* biomass.
- Fibrous filler provided better adhesion and properties than particle-shaped one.

Acknowledgments

Luis Suárez: Ph.D. grant program co-financed by the Canarian Agency for Research, Innovation and Information Society of the Canary Islands Regional Council for Employment, Industry, Commerce and Knowledge (ACIISI) and by the European Social Fund (ESF) (Grant number TESIS2021010008).

Disclosure statement

No potential conflict of interest was reported by the author(s).

Funding

The work was supported by the Agencia Canaria de Investigación, Innovación y Sociedad de la Información [TESIS2021010008]; Spanish Ministry of Universities [Next Generation funds (Order UNI/501/2021)].

ORCID

Luis Suárez  <http://orcid.org/0000-0002-6709-1555>
 Zaida Ortega  <http://orcid.org/0000-0002-7112-1067>
 Mateusz Barczewski  <http://orcid.org/0000-0003-1451-6430>
 Paulina Kosmela  <http://orcid.org/0000-0003-4158-2679>
 Bronagh Millar  <http://orcid.org/0000-0003-3961-0087>
 Eoin Cunningham  <http://orcid.org/0000-0003-2555-7705>

Author contributions

Conceptualization: Zaida Ortega; Methodology: Zaida Ortega, Luis Suárez, Mateusz Barczewski, Paul R. Hanna; Formal analysis: Luis Suárez, Paul R. Hanna, Zaida Ortega, Mateusz Barczewski, Paulina Kosmela, Bronagh Millar, Eoin Cunningham; Investigation: Luis Suárez, Paul R. Hanna, Zaida Ortega, Mateusz Barczewski, Paulina Kosmela, Bronagh Millar, Eoin Cunningham; Supervision: Zaida Ortega; Visualization: Luis Suárez, Mateusz Barczewski; Writing – original draft: Luis Suárez, Zaida Ortega, Mateusz Barczewski; Writing – review & editing: all authors.

References

- Adebayo, G. O., A. Hassan, R. Yahya, F. Okieimen, and N. M. Sarih. 2021. "Dynamic Rheological Properties of Spotted Mangrove/high-Density Polyethylene Composites." *Journal of Thermoplastic Composite Materials* 34 (9): 1273–1285. <https://doi.org/10.1177/0892705719870587>.
- Aid, S., A. Eddhahak, S. Khelladi, Z. Ortega, S. Chaabani, and A. Tcharkhtchi. 2019. "On the Miscibility of PVDF/PMMA Polymer Blends: Thermodynamics, Experimental and Numerical Investigations." *Polymer Testing* 73:222–231. <https://doi.org/10.1016/j.polymertesting.2018.11.036>.
- Andreu-Rodriguez, J., E. Medina, M. T. Ferrandez-Garcia, M. Ferrandez-Villena, C. E. Ferrandez-Garcia, C. Paredes, M. A. Bustamante, et al. 2013. "Agricultural and Industrial Valorization of *Arundo donax* L." *Communications in Soil Science and Plant Analysis* 44 (1–4): 598–609. <https://doi.org/10.1080/00103624.2013.745363>.
- Andrzejewski, J., B. Gapiński, A. Islam, and M. Szostak. 2020. "The Influence of the Hybridization Process on the Mechanical and Thermal Properties of Polyoxymethylene (POM) Composites with the Use of a Novel Sustainable Reinforcing System Based on Biocarbon and Basalt Fiber (BC/BF)." *Materials* 13 (16): 3496. <https://doi.org/10.3390/MA13163496>.

- Andrzejewski, J., A. Krawczak, K. Wesoły, and M. Szostak. 2020. "Rotational Molding of Biocomposites with Addition of Buckwheat Husk Filler. Structure-Property Correlation Assessment for Materials Based on Polyethylene (PE) and Poly(lactic Acid) PLA." *Composites Part B Engineering* 202:108410. <https://doi.org/10.1016/j.compositesb.2020.108410>.
- Ares, A. R. Bouza, S. G. Pardo, M. J. Abad, and L. Barral. 2010. "'Rheological, Mechanical and Thermal Behaviour of Wood Polymer Composites Based on Recycled Polypropylene'." *Journal of Polymers and the Environment* 18: 318–325. doi:10.1007/s10924-010-0208-x.
- Ayyanar, C. B., M. D. Dharshini, K. Marimuthu, S. Akhil, T. Mugilan, C. Bharathiraj, S. Mavinkere Rangappa, et al. 2022. "Design, Fabrication, and Characterization of Natural Fillers Loaded HDPE Composites for Domestic Applications." *Polymer Composites* 43 (8): 5168–5178. <https://doi.org/10.1002/pc.26806>.
- Balasuriya, P. W., L. Ye, and Y. W. Mai. 2003. "Morphology and Mechanical Properties of Reconstituted Wood Board Waste-Polyethylene Composites." *Composite Interfaces* 10 (2/3): 319–341. <https://doi.org/10.1163/156855403765826946>.
- Baquero Basto, D., J. Monsalve Alarcón, and M. Sánchez Cruz. 2018. "Experimental Characterization of Composite Panels Made with Arundo Donax Fibers and Vegetable Resin." *Sciencia et Technica* 23:119–125. <https://www.redalyc.org/journal/849/84956661017/84956661017.pdf>.
- Barana, D., A. Salanti, M. Orlandi, D. S. Ali, and L. Zoia. 2016. "Biorefinery Process for the Simultaneous Recovery of Lignin, Hemicelluloses, Cellulose Nanocrystals and Silica from Rice Husk and Arundo Donax." *Industrial Crops and Products* 86:31–39. <https://doi.org/10.1016/j.indcrop.2016.03.029>.
- Barczewski, M., A. Hejna, J. Aniśko, J. Andrzejewski, A. Piasecki, O. Mysiukiewicz, M. Bąk, et al. 2022. "Rotational Molding of Polylactide (PLA) Composites Filled with Copper Slag as a Waste Filler from Metallurgical Industry." *Polymer Testing* 106:107449. <https://doi.org/10.1016/j.POLYMERTESTING.2021.107449>.
- Barczewski, M., K. Lewandowski, M. Schmidt, and M. Szostak. 2017. "Melt fracture and rheology of linear low density polyethylene - calcium carbonate composites." *Polymer Engineering & Science* 57 (9): 998–1004. <https://doi.org/10.1002/pen.24477>.
- Barczewski, M., D. Matykievicz, O. Mysiukiewicz, and P. Maciejewski. 2018. "Evaluation of Polypropylene Hybrid Composites Containing Glass Fiber and Basalt Powder." *Journal of Polymer Engineering* 38 (3): 281–289. <https://doi.org/10.1515/polyeng-2017-0019>.
- Barreca, F., A. Martinez Gabarron, J. A. Flores Yepes, and J. J. Pastor Pérez. 2019. "Innovative Use of Giant Reed and Cork Residues for Panels of Buildings in Mediterranean Area." *Resources, Conservation and Recycling* 140:259–266. <https://doi.org/10.1016/J.RESCONREC.2018.10.005>.
- Bazan, P., D. Mierziński, R. Bogucki, and S. Kuciel. 2020. "Bio-Based Polyethylene Composites with Natural Fiber: Mechanical, Thermal, and Ageing Properties." *Materials* 13 (11): 2595. <https://doi.org/10.3390/ma13112595>.
- Berzin, F., T. Amornsakchai, A. Lemaitre, R. Castellani, and B. Vergnes. 2019. "Influence of Fiber Content on Rheological and Mechanical Properties of Pineapple Leaf Fibers-Polypropylene Composites Prepared by Twin-Screw Extrusion." *Polymer Composites* 40 (12): 4519–4529. <https://doi.org/10.1002/pc.25308>.
- Bessa, W., D. Trache, M. Derradji, H. Ambar, M. Benziane, and B. Guedouar. 2021. "Effect of Different Chemical Treatments and Loadings of Arundo Donax L. Fibers on the Dynamic Mechanical, Thermal, and Morphological Properties of Bisphenol a Aniline Based Polybenzoxazine Composites." *Polymer Composites* 42 (10): 5199–5208. <https://doi.org/10.1002/PC.26215>.
- Bessa, W., D. Trache, M. Derradji, H. Ambar, A. F. Tarchoun, M. Benziane, B. Guedouar, et al. 2020. "Characterization of Raw and Treated Arundo Donax L. Cellulosic Fibers and Their Effect on the Curing Kinetics of Bisphenol A-Based Benzoxazine." *International Journal of Biological Macromolecules* 164:2931–2943. <https://doi.org/10.1016/J.IJBIOMAC.2020.08.179>.
- Bhattacharjee, S., and D. S. Bajwa. 2018. "Degradation in the Mechanical and Thermo-Mechanical Properties of Natural Fiber Filled Polymer Composites Due to Recycling." *Construction and Building Materials* 172:1–9. <https://doi.org/10.1016/j.conbuildmat.2018.03.010>.
- Brostow, W., H. E. Hagg Lobland, and S. Khoja. 2015. "Brittleness and Toughness of Polymers and Other Materials." *Materials Letters* 159:478–480. <https://doi.org/10.1016/j.matlet.2015.07.047>.
- Chikouche, M. D. L., A. Merrouche, A. Azizi, M. Rokbi, and S. Walter. 2015. "Influence of Alkali Treatment on the Mechanical Properties of New Cane Fibre/Polyester Composites." *Journal of Reinforced Plastics and Composites* 34 (16): 1329–1339. <https://doi.org/10.1177/0731684415591093>.
- Chimeni-Yomeni, D., A. Fazli, C. Dubois, and D. Rodrigue. "Low Density Polyethylene Composites Based on Flax Fibers Modified by a Combination of Coupling Agent." *Polymer Engineering & Science*, <https://doi.org/10.1002/pen.26126>. n/a(n/a)
- Chorobiński, M., Ł. Skowroński, and M. Bieliński. 2019. "Metodyka wyznaczania wybranych charakterystyk barwienia polietylenu z wykorzystaniem systemu CIELab." *Polimery* 64 (10): 690–696. <https://doi.org/10.14314/polimery.2019.10.6>.
- Copani, V., S. L. Cosentino, G. Testa, and D. Scordia. 2013. "Agamic Propagation of Giant Reed (Arundo Donax L.) in Semi-Arid Mediterranean Environment." *Italian Journal of Agronomy* 8 (4): 18–24.

- Correa-Aguirre, J. P., F. Luna-Vera, C. Caicedo, B. Vera-Mondragón, and M. A. Hidalgo-Salazar. 2020. "The Effects of Reprocessing and Fiber Treatments on the Properties of Polypropylene-Sugarcane Bagasse Biocomposites." *Polymers* 12 (7): 1440. <https://doi.org/10.3390/POLYM12071440>.
- Cosentino, S. L., C. Patanè, E. Sanzone, G. Testa, and D. Scordia. 2016. "Leaf gas exchange, water status and radiation use efficiency of giant reed (*Arundo donax* L.) in a changing soil nitrogen fertilization and soil water availability in a semi-arid Mediterranean area." *The European Journal of Agronomy* 72:56–69. <https://doi.org/10.1016/j.eja.2015.09.011>.
- Cosentino, S. L., D. Scordia, E. Sanzone, G. Testa, and V. Copani. 2014. "Response of Giant Reed (*Arundo Donax* L.) to Nitrogen Fertilization and Soil Water Availability in Semi-Arid Mediterranean Environment." *The European Journal of Agronomy* 60:22–32. <https://doi.org/10.1016/j.eja.2014.07.003>.
- Dahmardeh Ghalehno, M., M. Madhoushi, T. Tabarsa, and M. Nazerian. 2010. "The Manufacture of Particleboards Using Mixture of Reed (Surface Layer) and Commercial Species (Middle Layer)." *European Journal of Wood and Wood Products* 69 (3): 341–344. <https://doi.org/10.1007/S00107-010-0437-7>.
- Djellali, S., T. Sadoun, N. Haddaoui, and A. Bergeret. 2015. "Viscosity and Viscoelasticity Measurements of Low Density Polyethylene/Poly(lactic Acid) Blends." *Polymer Bulletin* 72 (5): 1177–1195. <https://doi.org/10.1007/s00289-015-1331-6>.
- Dolça, C. E. Fages, E. Gongga, D. Garcia-Sanoguera, R. Balart, and L. Quiles-Carrillo. 2022. "The Effect of Varying the Amount of Short Hemp Fibers on Mechanical and Thermal Properties of Wood–Plastic Composites from Biobased Polyethylene Processed by Injection Molding." *Polymers* 14 (1): 138. doi:10.3390/polym14010138.
- Dolza, C., E. Fages, E. Gongga, J. Gomez-Caturla, R. Balart, and L. Quiles-Carrillo. 2021. "Development and Characterization of Environmentally Friendly Wood Plastic Composites from Biobased Polyethylene and Short Natural Fibers Processed by Injection Moulding." *Polymers* 13 (11): 1692. <https://doi.org/10.3390/polym13111692>.
- Fendler, A., M. P. Villanueva, E. Gimenez, and J. M. Lagarón. 2007. "Characterization of the Barrier Properties of Composites of HDPE and Purified Cellulose Fibers." *Cellulose* 14 (5): 427–438. <https://doi.org/10.1007/s10570-007-9136-x>.
- Ferrández-García, C. E., J. Andreu-Rodríguez, M. T. Ferrández-García, M. Ferrández-Villena, and T. García-Ortuño. 2012. "Panels Made from Giant Reed Bonded with Non-Modified Starches." *BioResources* 7 (4): 5904–5916. <https://doi.org/10.15376/biores.7.4.5904-5916>.
- Ferrández-García, M. T., C. E. Ferrández-García, T. García-Ortuño, A. Ferrández-García, and M. Ferrández-Villena. 2019. "Experimental Evaluation of a New Giant Reed (*Arundo Donax* L.) Composite Using Citric Acid as a Natural Binder." *Agronomy* 9 (12): 882. <https://doi.org/10.3390/AGRONOMY9120882>.
- Ferrández-García, M. T., A. Ferrández-García, T. García-Ortuño, C. E. Ferrández-García, and M. Ferrández-Villena. 2020. "Assessment of the Physical, Mechanical and Acoustic Properties of *Arundo Donax* L. Biomass in Low Pressure and Temperature Particleboards." *Polymers* 12 (6): 1361. <https://doi.org/10.3390/POLYM12061361>.
- Ferrández Villena, M., C. E. Ferrández García, T. García Ortuño, A. Ferrández García, and M. T. Ferrández García. 2020. "The Influence of Processing and Particle Size on Binderless Particleboards Made from *Arundo Donax* L. Rhizome." *Polymers* 12 (3): 696. <https://doi.org/10.3390/polym12030696>.
- Ferrero, B., V. Fombuena, O. Fenollar, T. Boronat, and R. Balart. 2015. "Development of Natural Fiber-Reinforced Plastics (NFRP) Based on Biobased Polyethylene and Waste Fibers from *Posidonia Oceanica* Seaweed." *Polymer Composites* 36 (8): 1378–1385. <https://doi.org/10.1002/pc.23042>.
- Fiore, V., L. Botta, R. Scaffaro, A. Valenza, and A. Pirrotta. 2014. "PLA Based Biocomposites Reinforced with *Arundo Donax* Fillers." *Composites Science and Technology* 105:110–117. <https://doi.org/10.1016/j.compscitech.2014.10.005>.
- Fiore, V., T. Scalici, and A. Valenza. 2014. "Characterization of a New Natural Fiber from *Arundo Donax* L. as Potential Reinforcement of Polymer Composites." *Carbohydrate Polymers* 106 (1): 77–83. <https://doi.org/10.1016/j.carbpol.2014.02.016>.
- Fiore, V., T. Scalici, G. Vitale, and A. Valenza. 2014. "Static and Dynamic Mechanical Properties of *Arundo Donax* Fillers-Epoxy Composites." *Materials & Design* 57:456–464. <https://doi.org/10.1016/j.matdes.2014.01.025>.
- Gai, J. G., and Y. Cao. 2013. "Structure Memory Effects and Rheological Behaviors of Polyethylenes in Processing Temperature Window." *Journal of Applied Polymer Science* 129 (1): 354–361. <https://doi.org/10.1002/app.38754>.
- García-Ortuño, T., J. Andréu-Rodríguez, M. T. Ferrández-García, M. Ferrández-Villena, and C. E. Ferrández-García. 2011. "Evaluation of the Physical and Mechanical Properties of Particleboard Made from Giant Reed (*Arundo Donax* L.)." *BioResources* 6 (1): 477–486. <https://doi.org/10.15376/biores.6.1.477-486>.
- George, J., S. S. Bhagawan, and S. Thomas. 1998. "Effects of Environment on the Properties of Low-Density Polyethylene Composites Reinforced with Pineapple-Leaf Fibre." *Composites Science and Technology* 58 (9): 1471–1485. [https://doi.org/10.1016/S0266-3538\(97\)00161-9](https://doi.org/10.1016/S0266-3538(97)00161-9).
- Hejna, A., M. Barczewski, J. Andrzejewski, P. Kosmela, A. Piasecki, M. Szostak, T. Kuang, et al. 2020. "Rotational Molding of Linear Low-Density Polyethylene Composites Filled with Wheat Bran." *Polymers* 12 (5): 1004. <https://doi.org/10.3390/POLYM12051004>.
- Henrique, P., F. Pereira, M. De, F. Rosa, M. Odila, H. Cioffi, D. R. Mulinari, et al. 2015. "Vegetal Fibers in Polymeric Composites: A Review." *Polímeros* 25 (1): 9–22. <https://doi.org/10.1590/0104-1428.1722>.

- Jaramillo, L. Y., M. Vásquez-Rendón, S. Upegui, J. C. Posada, and M. Romero-Sáez. 2021. "Polyethylene-Coffee Husk Eco-Composites for Production of Value-Added Consumer Products." *Sustainable Environment Research* 31 (1): 34. <https://doi.org/10.1186/s42834-021-00107-6>.
- Jensen, E. F., M. D. Casler, K. Farrar, J. M. Finnan, R. Lord, C. Palmborg, Valentine J, and Donnison IS 2018. "Giant Reed: From Production to End Use." In *Perennial Grasses for Bioenergy and Bioproducts*, edited by E. Alexopoulou, 107–150. Amsterdam: Academic Press Inc. Elsevier.
- Jyoti, J., B. P. Singh, A. K. Arya, and S. R. Dhakate. 2016. "Dynamic Mechanical Properties of Multiwall Carbon Nanotube Reinforced ABS Composites and Their Correlation with Entanglement Density, Adhesion, Reinforcement and C Factor." *RSC Advances* 6 (5): 3997–4006. <https://doi.org/10.1039/C5RA25561A>.
- Kabir, M. M., H. Wang, K. T. Lau, F. Cardona, and T. Aravinthan. 2012. "Mechanical Properties of Chemically-Treated Hemp Fibre Reinforced Sandwich Composites." *Composites Part B Engineering* 43 (2): 159–169. <https://doi.org/10.1016/j.compositesb.2011.06.003>.
- Karaduman, Y., M. M. A. Sayeed, L. Onal, and A. Rawal. 2014. "Viscoelastic Properties of Surface Modified Jute Fiber/ Polypropylene Nonwoven Composites." *Composites Part B Engineering* 67:111–118. <https://doi.org/10.1016/j.compositesb.2014.06.019>.
- Khanna, Y. P., E. A. Turi, T. J. Taylor, V. V. Vickroy, and R. F. Abbott. 1985. "Dynamic Mechanical Relaxations in Polyethylene." *Macromolecules* 18 (6): 1302–1309. <https://doi.org/10.1021/ma00148a045>.
- Koohestani, B., A. K. Darban, P. Mokhtari, E. Yilmaz, and E. Darezereshki. 2019. "Comparison of Different Natural Fiber Treatments: A Literature Review." *International Journal of Environmental Science and Technology* 16 (3): 629–642. <https://doi.org/10.1007/s13762-018-1890-9>.
- Kuan, H. C., J. M. Huang, C. C. M. Ma, and F. Y. Wang. 2003. "Processability, Morphology and Mechanical Properties of Wood Flour Reinforced High Density Polyethylene Composites." *Plastics, Rubber & Composites* 32 (3): 122–126. <https://doi.org/10.1179/146580103225001363>.
- Kubát, J., M. Rigdahl, and M. Welandér. 1990. "Characterization of Interfacial Interactions in High Density Polyethylene Filled with Glass Spheres Using Dynamic-Mechanical Analysis." *Journal of Applied Polymer Science* 39 (7): 1527–1539. <https://doi.org/10.1002/app.1990.070390711>.
- Lei, Y., Q. Wu, F. Yao, and Y. Xu. 2007. "Preparation and Properties of Recycled HDPE/Natural Fiber Composites." *Composites Part A: Applied Science and Manufacturing* 38 (7): 1664–1674. <https://doi.org/10.1016/j.compositesa.2007.02.001>.
- Lewandowski, K., K. Piszczek, S. Zajchowski, and J. Mirowski. 2016. "Rheological Properties of Wood Polymer Composites at High Shear Rates." *Polymer Testing* 51:58–62. <https://doi.org/10.1016/j.polymertesting.2016.02.004>.
- Licursi, D., C. Antonetti, J. Bernardini, P. Cinelli, M. B. Coltelli, A. Lazzeri, M. Martinelli, et al. 2015. "Characterization of the Arundo Donax L. Solid Residue from Hydrothermal Conversion: Comparison with Technical Lignins and Application Perspectives." *Industrial Crops and Products* 76:1008–1024. <https://doi.org/10.1016/j.indcrop.2015.08.007>.
- Licursi, D., C. Antonetti, M. Mattonai, L. Pérez-Armada, S. Rivas, E. Ribechini, A. M. Raspolli Galletti, et al. 2018. "Multi-Valorisation of Giant Reed (Arundo Donax L.) to Give Levulinic Acid and Valuable Phenolic Antioxidants." *Industrial Crops and Products* 112:6–17. <https://doi.org/10.1016/j.indcrop.2017.11.007>.
- Martínez-Sanz, M., E. Erboz, C. Fontes, and A. López-Rubio. 2018. "Valorization of Arundo Donax for the Production of High Performance Lignocellulosic Films." *Carbohydrate Polymers* 199:276–285. <https://doi.org/10.1016/j.carbpol.2018.07.029>.
- Mazzanti, V., F. Mollica, and N. El Kissi. 2016. "Rheological and Mechanical Characterization of Polypropylene-Based Wood Plastic Composites." *Polymer Composites* 37 (12): 3460–3473. <https://doi.org/10.1002/pc.23546>.
- Mendes, J. F., J. T. Martins, A. Manrich, B. R. Luchesi, A. P. S. Dantas, R. M. Vanderlei, P. C. Claro, et al. 2021. "Thermo-Physical and Mechanical Characteristics of Composites Based on High-Density Polyethylene (HDPE) E Spent Coffee Grounds (SCG)." *Journal of Polymers and the Environment* 29 (9): 2888–2900. <https://doi.org/10.1007/s10924-021-02090-w>.
- Mohanty, S., and S. K. Nayak. 2010. "Short Bamboo Fiber-Reinforced HDPE Composites: Influence of Fiber Content and Modification on Strength of the Composite." *Journal of Reinforced Plastics and Composites* 29 (14): 2199–2210. <https://doi.org/10.1177/0731684409345618>.
- Molefi, J. A., A. S. Luyt, and I. Krupa. 2010. "Comparison of the Influence of Copper Micro- and Nano-Particles on the Mechanical Properties of Polyethylene/Copper Composites." *Journal of Materials Science* 45 (1): 82–88. <https://doi.org/10.1007/s10853-009-3894-9>.
- Monteiro, S. N., V. Calado, R. J. S. Rodriguez, and F. M. Margem. 2012. "Thermogravimetric Behavior of Natural Fibers Reinforced Polymer Composites—An Overview." *Materials Science and Engineering: A* 557:17–28. <https://doi.org/10.1016/j.msea.2012.05.109>.
- Mysiukiewicz, O., P. Kosmela, M. Barczewski, and H. A. Hejna. 2020. "Mechanical, Thermal and Rheological Properties of Polyethylene-Based Composites Filled with Micrometric Aluminum Powder." *Materials* 13 (5): 1242. <https://doi.org/10.3390/ma13051242>.
- Nabinejad, O. D. Suján, M. E. Rahman, and I. J. Davies. 2015. "Determination of Filler Content for Natural Filler Polymer Composite by Thermogravimetric Analysis." *Journal of Thermal Analysis and Calorimetry* 122: 227–233. doi:10.1007/s10973-015-4681-2.

- Najafi, S. K., M. Tajvidi, and M. Chaharmahli. 2006. "Long-Term Water Uptake Behavior of Lignocellulosic-High Density Polyethylene Composites." *Journal of Applied Polymer Science* 102 (4): 3907–3911. <https://doi.org/10.1002/app.24172>.
- Ogah, A. O., J. N. Afiukwa, and A. A. Nduji. 2014. "Characterization and Comparison of Rheological Properties of Agro Fiber Filled High-Density Polyethylene Bio-Composites." *OJPChem* 4 (01): 12–19. <https://doi.org/10.4236/ojpchem.2014.41002>.
- Ortega, Z., I. Bolaji, L. Suárez, and E. Cunningham. 2023. "A Review of the Use of Giant Reed (*Arundo Donax* L.) in the Biorefineries Context". *Reviews in Chemical Engineering*. <https://doi.org/10.1515/revce-2022-0069>.
- Ortega, Z., M. D. Monzón, A. N. Benítez, M. Kearns, M. McCourt, and P. R. Hornsby. 2013. "Banana and Abaca Fiber-Reinforced Plastic Composites Obtained by Rotational Molding Process." *Materials and Manufacturing Processes* 28 (8): 130614085148001. <https://doi.org/10.1080/10426914.2013.792431>.
- Ortega, Z., F. Romero, R. Paz, L. Suárez, A. N. Benítez, and M. D. Marrero. 2021. "Valorization of Invasive Plants from Macaronesia as Filler Materials in the Production of Natural Fiber Composites by Rotational Molding." *Polymers* 13 (13): 2220. <https://doi.org/10.3390/POLYM13132220>.
- Pandey, A. K., R. Kumar, V. S. Kachhavah, and K. K. Kar. 2016. "Mechanical and Thermal Behaviours of Graphite Flake-Reinforced Acrylonitrile–Butadiene–Styrene Composites and Their Correlation with Entanglement Density, Adhesion, Reinforcement and C Factor." *RSC Advances* 6 (56): 50559–50571. <https://doi.org/10.1039/C6RA09236E>.
- Panwar, V., and K. Pal. 2017. "An Optimal Reduction Technique for rGo/ABS Composites Having High-End Dynamic Properties Based on Cole-Cole Plot, Degree of Entanglement and C-Factor." *Composites Part B Engineering* 114:46–57. <https://doi.org/10.1016/j.compositesb.2017.01.066>.
- Patti, A., L. Nele, M. Zarrelli, L. Graziosi, and D. Acierno. 2021. "A Comparative Analysis on the Processing Aspects of Basalt and Glass Fibers Reinforced Composites." *Fibers and Polymers* 22 (5): 1449–1459. <https://doi.org/10.1007/s12221-021-0184-x>.
- Qiu, W., T. Endo, and T. Hirotsu. 2004. "Interfacial Interactions of a Novel Mechanochemical Composite of Cellulose with Maleated Polypropylene." *Journal of Applied Polymer Science* 94 (3): 1326–1335. <https://doi.org/10.1002/app.21123>.
- Salasinska, K., M. Polka, M. Gloc, and J. Ryszkowska. 2016. "Natural Fiber Composites: The Effect of the Kind and Content of Filler on the Dimensional and Fire Stability of Polyolefin-Based Composites." *Polimery* 61 (4): 255–265. <https://doi.org/10.14314/polimery.2016.255>.
- Satapathy, S., and R. V. S. Kothapalli. 2018. "Mechanical, Dynamic Mechanical and Thermal Properties of Banana Fiber/Recycled High Density Polyethylene Biocomposites Filled with Flyash Cenospheres." *Journal of Polymers and the Environment* 26 (1): 200–213. <https://doi.org/10.1007/s10924-017-0938-0>.
- Scalici, T., V. Fiore, and A. Valenza. 2016. "Effect of Plasma Treatment on the Properties of *Arundo Donax* L. Leaf Fibres and Its Bio-Based Epoxy Composites: A Preliminary Study." *Composites Part B Engineering* 94:167–175. <https://doi.org/10.1016/j.compositesb.2016.03.053>.
- Schellenberg, J. 1997. "Blends of High-Density Polyethylene with Homogeneous Long-Chain Branched Polyethylenes." *Advances in Polymer Technology* 16 (2): 135–145. [https://doi.org/10.1002/\(SICI\)1098-2329\(199722\)16:2<135:AID-ADV6>3.0.CO;2-V](https://doi.org/10.1002/(SICI)1098-2329(199722)16:2<135:AID-ADV6>3.0.CO;2-V).
- Sewda, K., and S. N. Maiti. 2010. "Effect of Teak Wood Flour on Melt Rheological Behaviour of High Density Polyethylene." *Polymer-Plastics Technology and Engineering* 49 (4): 418–425. <https://doi.org/10.1080/03602550903413839>.
- Shatalov, A. A., and H. Pereira. 2013. "High-Grade Sulfur-Free Cellulose Fibers by Pre-Hydrolysis and Ethanol-Alkali Delignification of Giant Reed (*Arundo Donax* L.) Stems." *Industrial Crops and Products* 43 (1): 623–630. <https://doi.org/10.1016/j.indcrop.2012.08.003>.
- Smitthipong, W., R. Tantatherdtam, and R. Chollakup. 2015. "Effect of Pineapple Leaf Fiber-Reinforced Thermoplastic Starch/Poly(lactic Acid) Green Composite: Mechanical, Viscosity, and Water Resistance Properties." *Journal of Thermoplastic Composite Materials* 28 (5): 717–729. <https://doi.org/10.1177/0892705713489701>.
- Stanciu, M. D., H. Teodorescu Draghicescu, F. Tamas, and O. M. Terciu. 2020. "Mechanical and Rheological Behaviour of Composites Reinforced with Natural Fibres." *Polymers* 12 (6): 1402. <https://doi.org/10.3390/polym12061402>.
- Suárez, L., M. Barczewski, P. Kosmela, M. D. Marrero, and Z. Ortega. 2023. "Giant Reed (*Arundo Donax* L.) Fiber Extraction and Characterization for Its Use in Polymer Composites." *Journal of Natural Fibers* 20 (1). <https://doi.org/10.1080/15440478.2022.2131687>.
- Suárez, L., J. Castellano, F. Romero, M. D. Marrero, A. N. Benítez, and Z. Ortega. 2021. "Environmental Hazards of Giant Reed (*Arundo Donax* L.) in the Macaronesia Region and Its Characterisation as a Potential Source for the Production of Natural Fibre Composites." *Polymers* 2021 13 (13): 2101. <https://doi.org/10.3390/polym13132101>.
- Suárez, L., Z. Ortega, M. Barczewski, and E. Cunningham. 2023. "Use of Giant Reed (*Arundo Donax* L.) for Polymer Composites Obtaining: A Mapping Review." *Cellulose* 30 (8): 4793–4812. Published online 2023. <https://doi.org/10.1007/s10570-023-05176-x>.
- Suárez, L., Z. Ortega, F. Romero, R. Paz, and M. D. Marrero. "Influence of Giant Reed Fibers on Mechanical, Thermal, and Disintegration Behavior of Rotomolded PLA and PE Composites." *Journal of Polymers and the Environment* 30 (11): 4848–4862. <https://doi.org/10.1007/s10924-022-02542-x>.

- Tarchoun, A. F., D. Trache, T. M. Klapötke, M. Derradji, and W. Bessa. 2019. "Ecofriendly Isolation and Characterization of Microcrystalline Cellulose from Giant Reed Using Various Acidic Media." *Cellulose* 26 (13–14): 7635–7651. <https://doi.org/10.1007/s10570-019-02672-x>.
- Wang, K., F. Addiego, A. Laachachi, B. Kaouache, N. Bahlouli, V. Toniazzo, and D. Ruch. 2014. "Dynamic Behavior and Flame Retardancy of HDPE/Hemp Short Fiber Composites: Effect of Coupling Agent and Fiber Loading." *Composite Structures* 113:74–82. <https://doi.org/10.1016/j.compstruct.2014.03.009>.
- Wang, W., M. Sain, and P. A. Cooper. 2006. "Study of Moisture Absorption in Natural Fiber Plastic Composites." *Composites Science and Technology* 66 (3): 379–386. <https://doi.org/10.1016/j.compscitech.2005.07.027>.
- Zhang, F., T. Endo, W. Qiu, L. Yang, and T. Hirotsu. 2002. "Preparation and Mechanical Properties of Composite of Fibrous Cellulose and Maleated Polyethylene." *Journal of Applied Polymer Science* 84 (11): 1971–1980. <https://doi.org/10.1002/app.10428>.

6.6. RELATIONSHIP BETWEEN THE SHAPE OF GIANT REED-BASED FILLERS AND THERMAL PROPERTIES OF POLYETHYLENE COMPOSITES: STRUCTURAL RELATED THERMAL EXPANSION AND DIFFUSIVITY STUDIES

P1

P2

P3

P4

P5

P6

P7

P8

P9

P10



Relationship Between the Shape of Giant Reed-Based Fillers and Thermal Properties of Polyethylene Composites: Structural Related Thermal Expansion and Diffusivity Studies

Mateusz Barczewski¹ · Luis Suárez² · Patryk Mietliński¹ · Arkadiusz Kloziński³ · Zaida Ortega⁴

Received: 30 October 2023 / Accepted: 16 June 2024 / Published online: 10 July 2024
© The Author(s) 2024

Abstract

This paper describes the effect of two different fillers derived from giant reed (*Arundo donax* L.), namely fibers and shredded aerial parts of the plant, on the thermal properties of polyethylene-based composites, as the analysis of dimensional stability of lignocellulose-based composites, and its relationship with their thermal diffusivity, has not yet been assessed in the literature. It has been found that the introduction of such materials resulted in a significant reduction of the coefficient of thermal expansion, particularly more important in the case of fibers, due to their higher aspect ratio; in particular, this coefficient is reduced to less than half for fibrous composites (from $1.6 \cdot 10^{-4} \text{ K}^{-1}$ to $6.1 \cdot 10^{-5} \text{ K}^{-1}$ or $3.5 \cdot 10^{-5} \text{ K}^{-1}$ for 20 and 40% loadings). This parameter also influences the thermal diffusivity of the final parts; the diffusivity of composites increases with the ratio of lignocellulosic filler used, particularly when using fibers, due to a better orientation of these fibers than the shredded material, which does not exhibit a fibrous shape. Composites with 20% share of the filler exhibited a thermal diffusivity increased by about 15% compared to neat polyethylene, while 40% loadings resulted in a 25% and 60% increase for ground and fibrous materials, respectively. These results provide additional features to lignocellulose-composites characterization, providing properties not usually mentioned in the literature to expand the knowledge about such composite materials beyond mechanical properties, providing a broader range of properties to offer a wider application area of such composites.

Statement of Novelty

Arundo donax L. is of great interest to biorefineries due to its fast growth and resistance to adverse environmental conditions. Most research on this plant species focuses on obtaining energy products or valuable chemicals, while very few are related to composite production, particularly on thermoplastic materials. The work found in the literature so far does not provide insights into the relationships between the types of filler (and their aspect ratio) and their thermal properties. Therefore, this work expands the knowledge on the thermal behavior of lignocellulose-polymer composites, supplementing the research, usually focused only on mechanical properties, in their characterization by correlative analysis of thermal influenced dimensional change with structure and thermal diffusivity. Determining the coefficient of thermal expansion (CTE) is a relevant parameter to assess the possibilities of using a material at high or low temperatures and evaluate the dimensional stability of a product during its service lifetime. On the other hand, thermal diffusivity brings together the capacity of a material to store thermal energy and distribute it throughout the material; that is, it relates heat capacity and thermal conductivity, which are also essential in using materials in market applications. Therefore, the work not only

✉ Mateusz Barczewski
mateusz.barczewski@put.poznan.pl

✉ Zaida Ortega
zaida.ortega@ulpgc.es

¹ Division of Metrology and Measurement Systems,
Institute of Mechanical Technology, Poznan University of
Technology, Piotrowo 3, Poznań 61-138, Poland

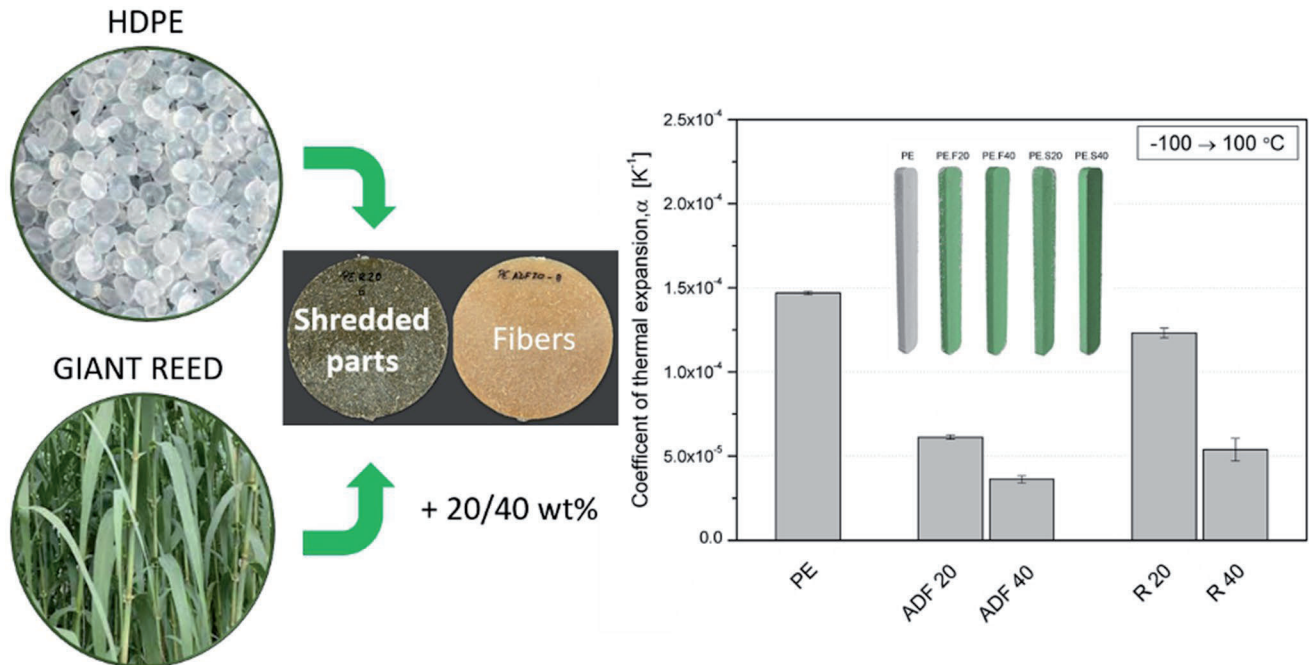
² Departamento de Ingeniería Mecánica, Universidad de Las
Palmas de Gran Canaria, Edificio de Ingenierías, Campus
universitario de Tafira Baja, Las Palmas 35017, Spain

³ Institute of Chemical Technology and Engineering, Poznan
University of Technology, Berdychowo 4, Poznań
60-965, Poland

⁴ Departamento de Ingeniería de Procesos, Universidad de Las
Palmas de Gran Canaria, Edificio de Ingenierías, Campus
universitario de Tafira Baja, Las Palmas 35017, Spain

provides the results of thermal diffusivity and CTE of thermoplastic-reed composites but also correlates both parameters as a way to widen the range of application of plant-based composites in areas where dimensional stability (i.e., low thermal expansion) is required.

Graphical Abstract



Keywords Giant reed · Natural filler · Thermal diffusivity · Thermal expansion · Polyethylene

Introduction

A pivotal focus on environmental responsibility and recycling principles has gained prominence in the quest for sustainable composite materials. Initiatives driven by a shared commitment to environmental stewardship have marked notable progress in utilizing plant-based fillers and the development of composites with reduced polymer content [1]. As researchers worldwide intensify efforts towards innovative solutions for the introduction of waste streams, this paper contributes to the scientific discourse by exploring the thermal behavior of polymer composites containing lignocellulose fibers as a way to widen the knowledge about such materials and increase their uptake in commercial applications. Such composites are commonly referred to as natural fiber composites (NFC) or wood polymer composites (WPC) [2–4]. Besides the often used long natural fibers, mainly in the implementation with thermoset polymers [5, 6], many studies focused on composites reinforced with plant particle-shaped fillers or short fibers [1, 7, 8]. Current research activities increasingly focus on attempts to completely valorize plant parts and give each waste-based filler

a dedicated function depending on its specific physicochemical, mechanical, or chemical characteristics [4, 9].

Apart from the understanding of the effect of lignocellulose fibers within polymer matrices in the mechanical behavior or durability of materials, the determination of the coefficient of thermal expansion (CTE) is a relevant parameter to determine the possibilities of using a material at high or low temperatures, as the dimensional change resulting from the thermal expansion phenomenon can be undesirable. On the other hand, thermal diffusivity is related to the capacity of a material to store thermal energy and distribute it throughout the material; that is, it relates heat capacity and thermal conductivity. It is then advisable to correlate thermal expansion in detail with the ability to accumulate and distribute heat due to the high requirements for polymeric and composite products regarding dimensional stability during exploitation. In most cases of injection-molded products, minimizing the thermal expansivity of final products is crucial [10]. This phenomenon is related to the polymer structure's heterogeneity and phase transitions [11]. As shown in previous studies, the crystallinity and the introduction of fillers result in significant changes in the thermal expansion of products made of thermoplastic polymers

[11–13]. The most effective and straightforward method for obtaining good dimensional stability in a polymeric composite is introducing a filler with high-temperature conductivity [14]. While the relationships between the role of the filler orientation in the polymer matrix and the interfacial bonding have been described for inorganic fillers [15, 16], these studies are strongly limited in the case of composites with plant-based fillers. The influence of the shape factor of natural plant fillers on the mechanical properties and structure of composites based on thermoplastic polymers has been studied previously [17, 18]; however, the correlations between their thermal properties and temperature-assessed dimensional stability should still be explained, considering broad aspects of natural fillers' structure.

Biodiversification and the diversity of plant structure, influenced by species characteristics and environmental conditions accompanying growth, is often a significant objection to using plant-derived fillers [19–21]. It is advisable to correlate the chemical composition of plant-based fillers with the final properties of their composites and consider the impact of grinding processes and their shape [22]. Therefore, it becomes purposeful and justified to conduct research in the field of pre-testing the broadest possible range of composites reinforced with natural-based fillers to define the crucial aspects determining their role in modifying polymeric composites' thermal behavior.

Giant reed (*Arundo donax* L.) is considered a promising crop for obtaining bioenergy and bioproducts, including natural fibers for composites production [23–27], following a biorefinery scheme. The interest in using this plant relies on its fast growth and resistance to adverse environmental conditions, such as water scarcity or poor quality. Most research on this plant species focuses on the obtaining of energy products (ethanol or biogas) or valuable chemicals (levulinic acid or oligosaccharides), while very few are related to the obtaining of composites, particularly on thermoplastic materials [27–32]. This plant can be grown in marginal or polluted lands, with low-quality waters and low fertilizers or pesticides use, which could imply a vital step within the establishment of an industrial crop to produce valuable products without replacing food crops or using valuable inputs (water, land) for their growing, thus contributing to the achievement of the sustainable development goals (SDG). This research work compares the behavior of the neat matrix (high-density polyethylene, HDPE) with composites loaded at 20 and 40% in weight of two different fillers: fibers obtained from the culms of the giant reed through a chemo-mechanical process and ground stems and leaves, as a more inexpensive material with almost no processing, as described in our previous works [32, 33]. This work allows expanding the knowledge on the thermal behavior of polymer composites containing lignocellulose

fibers, and particularly, it constitutes a supplement realized research in the manufacturing and characterizing *Arundo donax*-based composites by correlative analysis of thermal influenced dimensional change with structure and thermal diffusivity.

Materials and Methods

Materials and Sample Preparation

A high-density polyethylene (HDPE) purchased from Total (Antwerpen, Belgium) with the trade name HD6081 was used as a polymeric matrix. This HDPE is characterized by a 0.960 g/cm³ density and 8 g/10 min (190 °C/2.16 kg) melt flow index (MFI).

Natural fillers used for manufacturing the composites were produced from the same plant part, i.e., *Arundo donax* L. culms (from Gran Canaria island, Spain). The fillers used are fibers and shredded material. Shredded filler was obtained by grinding aerial plant parts (leaves, culms) and washing them with water. Fibers were obtained after soaking culms in a NaOH (from Sigma Aldrich, Missouri, USA) solution for around one week, with further processing by a series of rolling mills to separate the fibers from the softer material. A full description of the manufacturing procedure was previously given [33].

The samples were named appropriately in the work regarding their material composition and filler concentration, as follows: PE for unmodified polyethylene, PE.F20 and PE.F40 for composites with 20 and 40 wt% fibers, and PE.S20 and PE.S40 for composites with shredded *Arundo*.

Lignocellulosic fibers were dried overnight at 105 °C before compounding, while HDPE was dried overnight at 60 °C before melt processing. Composites were melt-mixed in a ThermoScientific Process11 (Massachusetts, USA) co-rotating twin-screw extruder with a temperature profile set up 170–175–175–185–185–175–165–165 °C and screw rotation speed of 100 rpm, cooled in a water bath and pelletized. Samples were formed by injection molding through an Arburg 320 S hydraulic injection molding machine (Lossburg, Germany). Prior to processing, pellets were dried at 60 °C overnight with dry air (dewpoint of –40 °C). From the back to the nozzle, the following temperature profile was used: 175–180–185–185–190 °C, while the mold temperature was 30 °C, and the cooling time was 15 s. The back pressure was 5 MPa, and the holding pressure was 50 MPa. The aspect ratio of both fillers was determined by optical means [34] for the injection molded composites; it was found to be about 1 for composites with shredded material and over 4 for those with fibers, with sizes of 0.65 mm length for the fibers and 0.23 mm for the shredded material [35].

Methods

The composite samples' structure was examined using a measuring X-ray tomography, model v|tome|x s240 (Waygate Technologies / GE Sensing & Inspection Technologies GmbH, Pennsylvania, USA). Micro-computed tomography (μ CT) was used to evaluate the filler distribution in injection-molded samples and their porosity. The following parameters were used during the measurements: X microfocus x-ray tube (voltage 150 kV/current 200 μ A), exposure time of 150 ms per picture, and voxel size of 123 μ m.

The thermal diffusivity analysis was performed using a modified Ångström method with a Maximus (Poznan, Poland) apparatus. Previous works by Prociak, Jakubowska, and collaborators [36, 37] described the experimental setup in detail. In short, this method is characterized by a convenient preparation of samples and short analysis time; one end of the sample is heated, and the temperature of the sample at two points is measured using resistance temperature detectors [36], as shown in Fig. 1.

During investigations, the micro heater was charged with 23 V to heat the samples for 400 s. Thermal diffusivity (D) is

dependent on thermal conductivity (λ), specific heat capacity at constant pressure (c_p), and density (ρ) [37], defined by the following formula:

$$D = \frac{\lambda}{c_p \cdot \rho} \quad (1)$$

The specific heat capacity determination was realized according to the DIN 51,007 standard with differential scanning calorimetry (DSC) measurements, conducted using a Netzsch DSC 214 Nevio apparatus (Selb, Germany) with aluminum crucibles and 20 ± 0.1 mg samples under nitrogen flow. All samples were heated with a constant heating rate of 10 $^{\circ}$ C/min from -50 to 200 $^{\circ}$ C and held molten for five minutes. For the test, sapphire references have been used.

Thermal expansion analyses were performed on the Netzsch TMA 402 F1 Hyperion apparatus (Selb, Germany). The measurements were carried out in a heating cycle with a 2 $^{\circ}$ C/min heating rate with a flow of 100 ml/min protective argon atmosphere. The measurements were conducted in the temperature range of -100 to 100 $^{\circ}$ C, with an applied force of 0.01 N. The test results were analyzed using the Netzsch Proteus software. Due to changes in the linear coefficient of thermal expansion (CTE) in the tested temperature range, this coefficient was determined for the entire range and sub-ranges, respectively -100 – 25 $^{\circ}$ C and 25 – 100 $^{\circ}$ C. These ranges were selected considering the potential applicability of composites in different service conditions, i.e., under room temperature or frozen environments and over room temperature, considering sectors such as packaging or urban furniture.

Results and Discussion

Figures 2 and 3 show the structural analysis results of 3D computed tomography of tested materials. Figure 2a shows the distribution of fibers in the volume of the injection molded samples, while Fig. 2b presents a void distribution. In the case of both fillers used, for 20 wt%, uneven filling of the volume of the composite product with a visible skin layer is visible. A more heterogeneous structure was noted for the fibrous filler (PE.F), which may be related to the more directional arrangement of the filler particles in the core of the sample. This effect is also observable in Fig. 3f. Complete measurement data associated with the presence of pores in the structure of the samples are presented in Fig. 3a–e. The observed points allowed for determining the size and volume of pores observed for a selected sample from each series. The calculated porosity in the samples was as follows: PE 0.09%; PE.F20 0.29%; PE.F40 0.86%; PE.S20 0.36%; PE.S40 1.26%. Composite series containing



Fig. 1 Experimental setup for the measurement of thermal diffusivity

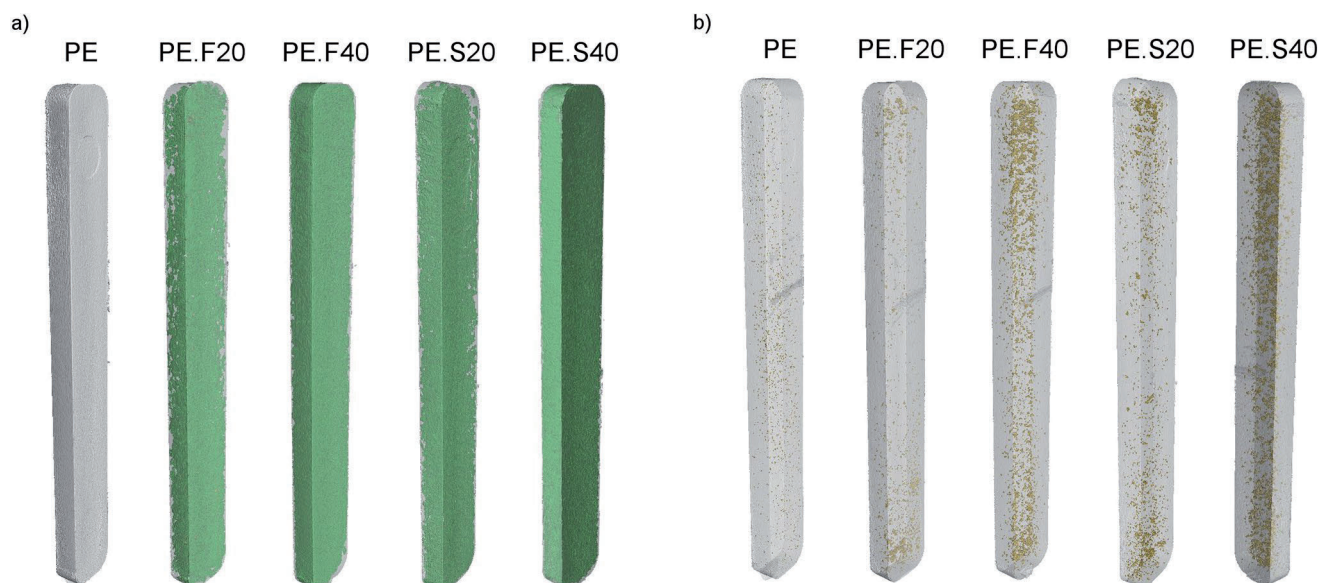


Fig. 2 3D computed tomography images presenting filler arrangement (a); porosity (b)

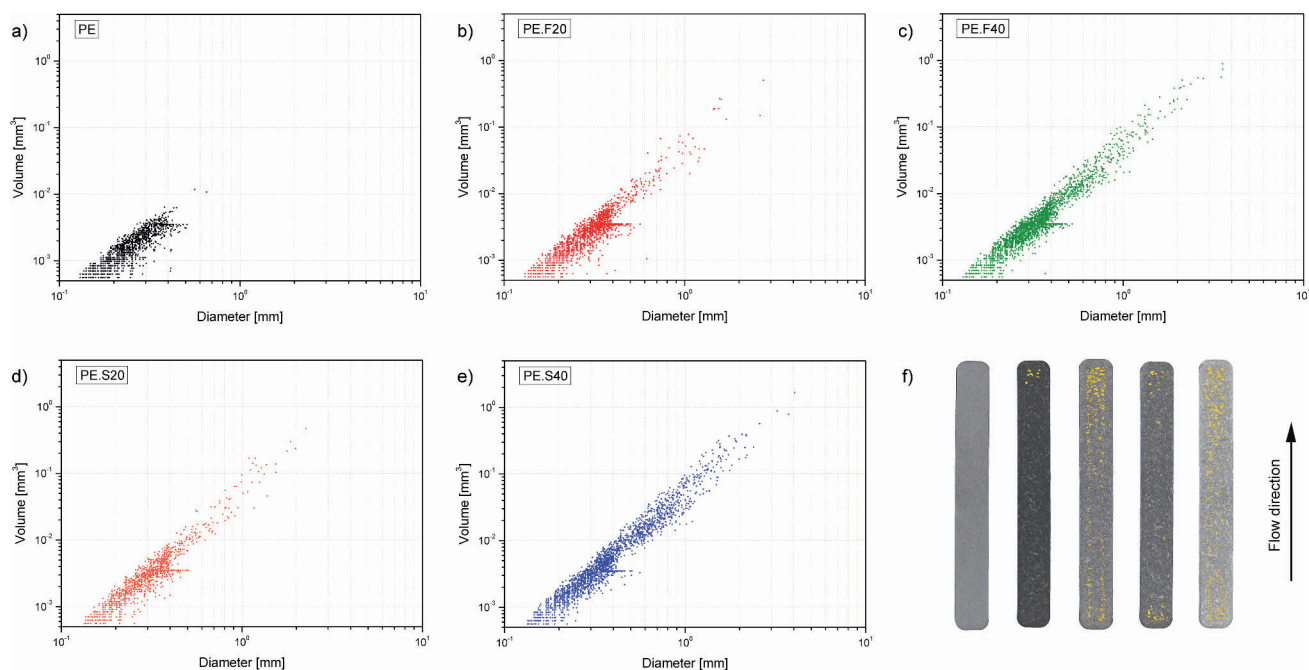


Fig. 3 Characterization of injection molded samples porosity distribution

shredded irregular particles are more porous than fiber-filled composites because of the fillers' larger specific surface area [38].

The results of TMA measurements in the form of changes in length (dL/L_0) and average values of the coefficient of thermal expansion determined in three temperature ranges (-100–25; 25–100; -100–100 °C) are shown in Fig. 4. The courses of changes in the elongation of the samples unambiguously indicate a much more favorable effect of fibrous fillers on the dimensional stability of the

specimens subjected to temperature changes. For 20 wt% R-filled composites, the shape of the $dL/L_0(T)$ curve is similar to that of unmodified PE, and the average values for these materials series in all three ranges are comparable. In the case of composites filled with fibers, a change in the course of the curve and a significant limitation of α can be noted, which is probably related to the formation of a network of physical interactions between the fibers dispersed in the matrix, which significantly restricts their mobility caused by changes of polymer thermal expansion. The

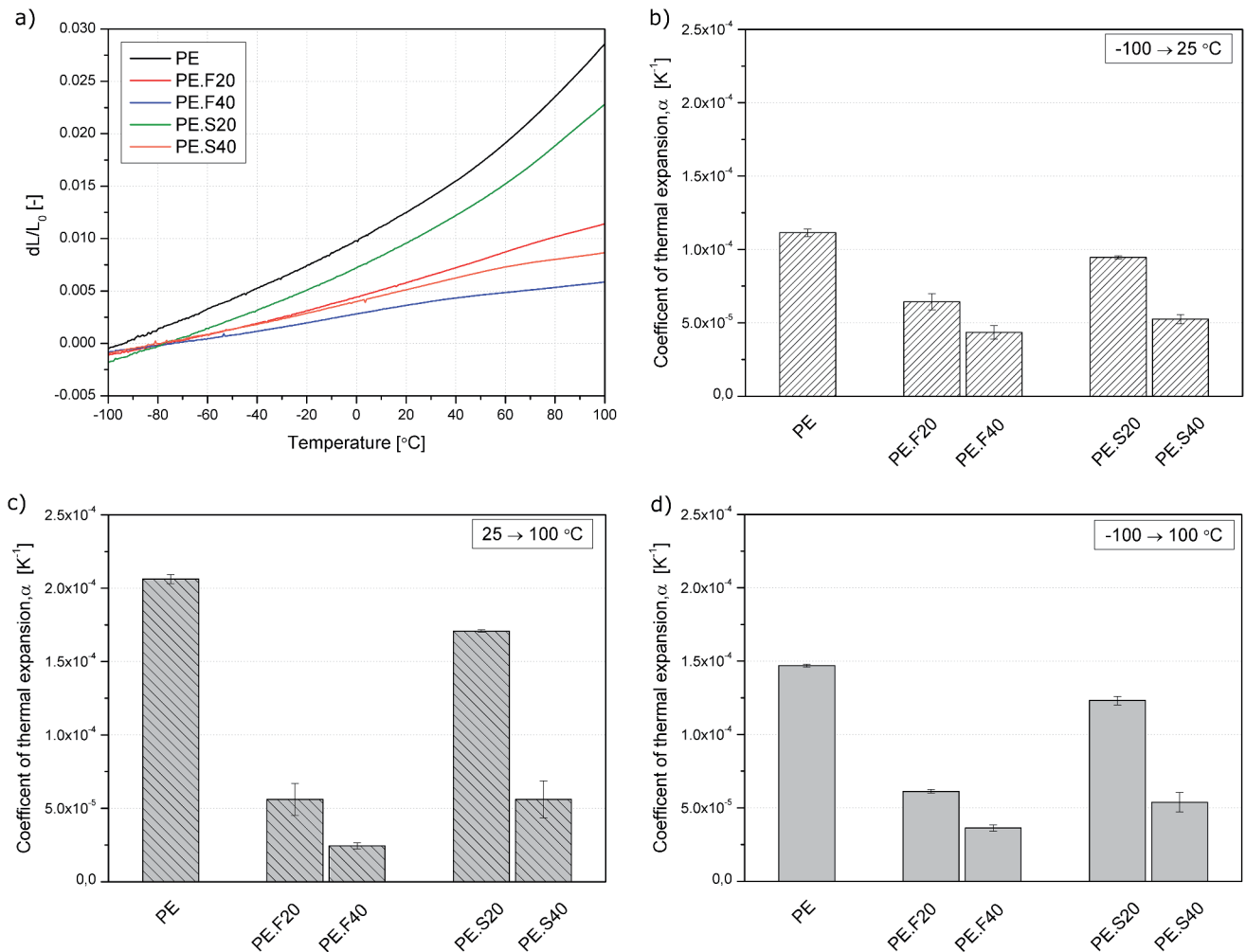


Fig. 4 Course of samples dimension change (a), and mean values of coefficient of thermal expansion in the temperature ranges of -100–25 $^{\circ}\text{C}$ (b), 25–100 $^{\circ}\text{C}$ (c), -100–100 $^{\circ}\text{C}$ (d)

sample containing 40 wt% shredded reed shows comparable average α values to PE.F20 in the 25 to 100 $^{\circ}\text{C}$ range. In the range most important from the perspective of using PE composites (-100 to 25 $^{\circ}\text{C}$), the most beneficial results were obtained for the sample containing 40 wt% *Arundo* fibers. The obtained research results are related to the partial orientation of the fillers with an increased shape coefficient and greater consistency for creating 3D steric hindrances in the sample volume, as found in previous work of authors [32], where the materials containing fibers showed higher values of storage modulus than those made with shredded material in the whole range of temperature studied (-100 to 100 $^{\circ}\text{C}$). This increased stiffness is related to the hindering of polymer chain movements due to the introduction of fibers, as also shown here for CTE. Besides, the orientation of fibers was demonstrated in capillary rheometry testing.

In addition to the arrangement of the fillers and their mutual interactions, the interphase volume surrounding the filler dispersed in the polymeric matrix plays a vital role, as

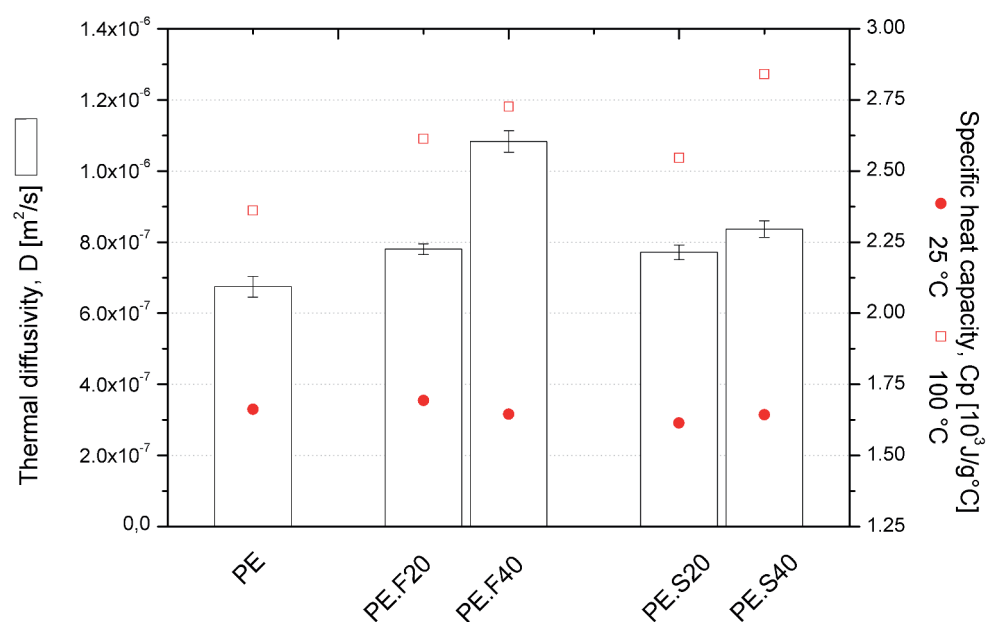
demonstrated in the work of Tripathi and Dey [39]. A reduction of CTE is expected with increased interfacial adhesion between filler and matrix. A lower porosity in the injection molded samples was obtained for fibrous composites, and higher interfacial interactions also occur in such composites, demonstrated by higher mechanical properties [32]. Yang et al. [12] confirmed an additional reduction of thermal expansion of PP-wood flour composite by increasing interfacial interactions with the introduction of maleic anhydride grafted polypropylene (MAPP). Increased adhesion at the interface of PE-fiber composites, resulting from an increase in the shape factor of fillers, causes a more prominent limitation of the mobility of macromolecules and, consequently, a decrease in the coefficient of thermal expansion. These results are in agreement with our earlier work [32], in which the calculated values of adhesion factor based on DMA indicated a reduction in interactions in the temperature range of HDPE β -relaxation [40] above 0 $^{\circ}\text{C}$ for composites containing shredded part plants and better interfacial adhesion in

composites with fibrous fillers. For the automotive industry, the coefficient of thermal expansion should be lower than $5 \cdot 10^{-5} \text{ K}^{-1}$; composites at 40% loading accomplish this limit, and it is almost reached for 20% fibrous composites, meaning these composites might find an application in the manufacturing of internal door panels [10], at least for internal covering.

Measuring the thermal diffusivity of the material by the Ångström method allows for obtaining information about the sample's ability to conduct heat relative to heat storage. Figure 5 presents the mean values of thermal diffusivity and specific heat capacity of injection molded polyethylene and composite samples. Thermal diffusivity gradually rises for composite samples with increasing filler content, with a more distinct effect observed for the PE.F40 series. Increasing the share of lignocellulosic filler translated into increased pore content, resulting in reduced thermal conductivity, as also found by Prisco [41]. Thermal diffusivity was found to decrease with increased content of banana fiber in a PP matrix, while no specific trend is seen for Cp. In this work by Paul et al. [42], the density increases with the fiber loading, although porosity values were not measured. This might explain the opposite behavior found; a higher porosity of composites would result in reduced thermal conductivity and diffusivity. Considering Eq. (1), based on the results D, it can be concluded that the probably dominant effect was replacing a significant part of the polymer by volume with the natural filler, which decreased specific heat. The introduction of the oriented filler with an increased aspect ratio (fibers) probably increased the contact surface of the oriented fiber fillers in the flow direction, which resulted in a change in thermophysical parameters and a more pronounced impact of this filler on D. The results are

contrary to those presented by Kalaprasad et al., [43] who found that sisal fibers had a marginal effect on the change in thermal resistance, while in the same temperature range test used in the Ångström method, LDPE-sisal composites were characterized by reduced thermal diffusivity. The difference in the conducted tests resulted mainly from the method of sample preparation, forced significant orientation in the case of work results, and the lack of porosity resulting from process features. Changes in thermal diffusivity are related to the free path in the material; the presence of porosity and other structural defects will change this parameter. The presence of pores in the considered case probably caused a decrease in the thermal conductivity of composites, while the orientation of natural fibers significantly influences changes in the thermal conductivity of composites with matrixes of thermoplastic polymers. [43] In the case of monodirectional aligned fibers, the thermal conductivity in the fiber direction is independent of the fiber content. Randomly oriented fibers, as observed in injection-molded specimens, will rather reveal a behavior close to the case of discussed materials evaluated in a perpendicular direction to natural fiber alignment. According to results presented by Tazi et al., [44] the addition of lignocellulosic fillers leads to a decrease in the specific heat capacity of the polymer composites, that is, these fillers provide thermal insulating behavior, as this property is directly related to the possibility of changing the temperature of the heated material by the same amount of heat. Similarly, the specific heat capacity values measured by differential scanning calorimetry at 25 °C, i.e., the initial temperature of the measurement D by the Ångström method, for composite materials, are slightly lower than those of unmodified PE. However, a different tendency can be noted when analyzing the values at 100 °C,

Fig. 5 Thermal diffusivity by Ångström method and specific heat capacity of PE and its composites



the maximum temperature of the range used in dilatometric measurements. ADR- and R-filled composites are characterized by an increase in C_p compared to the PE series. However, increasing the filler share resulted in an additional increase in this value.

Conclusions

This research work has shown the effect of lignocellulose fillers on the thermal properties of polyethylene-based composites, finding that the aspect ratio of the filler plays a significant role in such properties. The orientation of the fibers during the processing by injection molding allows for a reduced porosity of the final samples despite their higher aspect ratio compared to the shredded material. This phenomenon of preferential orientation of the fibers would also imply a higher surface contact between the polymer and the filler, resulting in a greater extent of modification of the thermal properties of the composite. Therefore, the dimensional stability of the composites with fiber is improved in all the studied ranges, with this improvement being even higher for the range from 25 to 100 °C. The higher thermal diffusivity found for composites with fibers compared to shredded particles, particularly for high loading of the lignocellulose material, is also related to the orientation of the fibers during the processing.

Acknowledgements The results presented in this paper were partially funded with grants for education allocated by the Ministry of Science and Higher Education in Poland executed under the subject of No 0613/SBAD/4820. Luis Suárez acknowledges the funding through the Ph.D. grant program co-financed by the Canarian Agency for Research, Innovation and Information Society of the Canary Islands Regional Council for Employment, Industry, Commerce and Knowledge (ACIISI) and by the European Social Fund (ESF) (Grant number TESIS2021010008).

Author Contribution M.B., Z.O. the study conception and design; L.S. material preparation; M.B., P.M., A.K., Z.O., L.S. data collection, and analysis; M.B., Z.O. the first draft of the manuscript writing and edition; M.B., Z.O. review process. All authors read and approved the final manuscript.

Funding Open Access funding provided thanks to the CRUE-CSIC agreement with Springer Nature.

Data Availability The data that support the findings of this study are available upon reasonable request.

Declarations

Generative AI in Scientific Writing The authors declare that they did not use generative AI systems while preparing and writing the manuscript.

Competing Interests The authors declare that they have no known

competing financial interests or personal relationships that could have appeared to influence the work reported in this paper.

Open Access This article is licensed under a Creative Commons Attribution 4.0 International License, which permits use, sharing, adaptation, distribution and reproduction in any medium or format, as long as you give appropriate credit to the original author(s) and the source, provide a link to the Creative Commons licence, and indicate if changes were made. The images or other third party material in this article are included in the article's Creative Commons licence, unless indicated otherwise in a credit line to the material. If material is not included in the article's Creative Commons licence and your intended use is not permitted by statutory regulation or exceeds the permitted use, you will need to obtain permission directly from the copyright holder. To view a copy of this licence, visit <http://creativecommons.org/licenses/by/4.0/>.

References

- Sanjay, M.R., Madhu, P., Jawaidd, M., Senthamaraiannan, P., Senthil, S., Pradeep, S.: Characterization and properties of natural fiber polymer composites: A comprehensive review, (2018)
- Lewandowski, K., Piszczek, K., Skórczewska, K., Mirowski, J., Zajchowski, S., Wilczewski, S.: Rheological properties of wood polymer composites at high shear rates – evaluation of additional pressure losses as a result of inlet effects. *Compos. Part. Appl. Sci. Manuf.* **154** (2022). <https://doi.org/10.1016/j.compositesa.2022.106804>
- Salasinska, K., Osica, A., Ryszkowska, J.: The use of tree leaves as reinforcement in composites with recycled PE-HD matrix. *Polimery.* **57**, 646–655 (2012). <https://doi.org/10.14314/polimery.2012.646>
- Partanen, A., Carus, M.: Wood and natural fiber composites current trend in consumer goods and automotive parts. *Reinf. Plast.* **60**, 170–173 (2016). <https://doi.org/10.1016/j.repl.2016.01.004>
- Djehader, D., Redjel, B.: Water Absorption Behavior and Its Effect on Charpy Impact Test of Jute Yarn Reinforced Polyester Composites. *Compos. Theory Pract.* 65–71 (2022)
- Matykievicz, D., Mysiukiewicz, O.: Epoxy composites reinforced with natural fillers such as flax fiber and linseed cakes (Rapid communication). *Polimery/Polymers.* **65**, 828–832 (2020). <https://doi.org/10.14314/polimery.2020.11.11>
- Formela, K., Hejna, A., Piszczek, Ł., Saeb, M.R., Colom, X.: Processing and structure–property relationships of natural rubber/wheat bran biocomposites. *Cellulose.* **23**, 3157–3175 (2016). <https://doi.org/10.1007/s10570-016-1020-0>
- Rangappa, S.M., Siengchin, S., Parameswaranpillai, J., Jawaidd, M., Ozbakkaloglu, T.: Lignocellulosic fiber reinforced composites: Progress, performance, properties, applications, and future perspectives. *Polym. Compos.* **43**, 645–691 (2022). <https://doi.org/10.1002/pc.26413>
- Formela, K., Kurańska, M., Barczewski, M.: Recent advances in development of Waste-based polymer materials: A review. *Polym. (Basel).* **14**, 1050 (2022). <https://doi.org/10.3390/polym14051050>
- Park, H.S., Dang, X.P., Roderburg, A., Nau, B.: Development of plastic front side panels for green cars. *CIRP J. Manuf. Sci. Technol.* **6**, 44–52 (2013). <https://doi.org/10.1016/j.cirpj.2012.08.002>
- Shangguan, Y., Chen, F., Yang, J., Jia, E., Zheng, Q.: A new approach to fabricate polypropylene alloy with excellent low-temperature toughness and balanced toughness-rigidity through unmatched thermal expansion coefficients between components. *Polym. (Guildf).* **112**, 318–324 (2017). <https://doi.org/10.1016/j.polymer.2017.02.022>

12. Yang, H.S., Wolcott, M.P., Kim, H.S., Kim, H.J.: Thermal properties of lignocellulosic filler-thermoplastic polymer bio-composites. *J. Therm. Anal. Calorim.* **82**, 157–160 (2005). <https://doi.org/10.1007/s10973-005-0857-5>
13. van Dorp, E.R., Möglinger, B., Hausnerova, B.: Thermal expansion of semi-crystalline polymers: Anisotropic thermal strain and crystallite orientation. *Polym. (Guildf)*. **191**, 1–21 (2020). <https://doi.org/10.1016/j.polymer.2020.122249>
14. Chen, X., Zhao, W., Zhang, Y., Shi, G., He, Y., Cui, Z., Fu, P., Pang, X., Zhang, X., Liu, M.: Concurrent enhancement of dimensional stability and thermal conductivity of thermoplastic polyamide 12T/Boron nitride composites by constructing oriented structure. *Compos. Commun.* **33**, 101193 (2022). <https://doi.org/10.1016/j.coco.2022.101193>
15. Huang, R., Xu, X., Lee, S., Zhang, Y., Kim, B.J., Wu, Q.: High Density Polyethylene composites Reinforced with Hybrid Inorganic fillers: Morphology, mechanical and thermal expansion performance. *Mater. (Basel)*. **6**, 4122–4138 (2013). <https://doi.org/10.3390/ma6094122>
16. Raghava, R.S.: Thermal expansion of organic and inorganic matrix composites: A review of theoretical and experimental studies. *Polym. Compos.* **9**, 1–11 (1988). <https://doi.org/10.1002/pc.750090102>
17. Shaikh, H., Allothman, O.Y., Alshammari, B.A., Jawaid, M.: Dynamic and thermo-mechanical properties of polypropylene reinforced with date palm nano filler. *J. King Saud Univ. - Sci.* **35**, 102561 (2023). <https://doi.org/10.1016/j.jksus.2023.102561>
18. Friedrich, D.: Thermoplastic moulding of wood-polymer composites (WPC): A review and research proposal on thermo-physical and geometric design options using hot-pressing. *Eur. J. Wood Wood Prod.* **80**, 7–21 (2022). <https://doi.org/10.1007/s00107-021-01767-2>
19. Wróbel-Kwiatkowska, M., Starzycki, M., Zebrowski, J., Oszmiański, J., Szopa, J.: Lignin deficiency in transgenic flax resulted in plants with improved mechanical properties. *J. Biotechnol.* **128**, 919–934 (2007). <https://doi.org/10.1016/j.jbiotec.2006.12.030>
20. Krutul, D., Antczak, A., Klosinska, T., Drozddek, M., Radomski, A., Zawadzki, J.: The chemical composition of poplar wood in relation to the species and age of trees. *Ann. WULS Wood Technol.* **105**, 125–132 (2019). <https://doi.org/10.5604/01.3001.0013.7728>
21. Liu, M., Fernando, D., Daniel, G., Madsen, B., Meyer, A.S., Ale, M.T., Thygesen, A.: Effect of harvest time and field retting duration on the chemical composition, morphology and mechanical properties of hemp fibers. *Ind. Crops Prod.* **69**, 29–39 (2015). <https://doi.org/10.1016/j.indcrop.2015.02.010>
22. Soccalingame, L., Bourmaud, A., Perrin, D., Bénézet, J.-C., Bergeret, A.: Reprocessing of wood flour reinforced polypropylene composites: Impact of particle size and coupling agent on composite and particle properties. *Polym. Degrad. Stab.* **113**, 72–85 (2015). <https://doi.org/10.1016/j.polymdegradstab.2015.01.020>
23. Barana, D., Salanti, A., Orlandi, M., Ali, D.S., Zoia, L.: Biorefinery process for the simultaneous recovery of lignin, hemicelluloses, cellulose nanocrystals and silica from rice husk and *Arundo donax*. *Ind. Crops Prod.* **86**, 31–39 (2016). <https://doi.org/10.1016/j.indcrop.2016.03.029>
24. Ortega, Z., Bolaji, I., Suárez, L., Cunningham, E.: A review of the use of giant reed (*Arundo donax* L.) in the biorefineries context. *Rev. Chem. Eng.* **0** (2023). <https://doi.org/10.1515/revce-2022-0069>
25. Licursi, D., Antonetti, C., Mattonai, M., Pérez-Armada, L., Rivas, S., Ribechini, E., Raspolli Galletti, A.M.: Multi-valorisation of giant reed (*Arundo Donax* L.) to give levulinic acid and valuable phenolic antioxidants. *Ind. Crops Prod.* **112**, 6–17 (2018). <https://doi.org/10.1016/j.indcrop.2017.11.007>
26. Shatalov, A.A., Pereira, H.: High-grade sulfur-free cellulose fibers by pre-hydrolysis and ethanol-alkali delignification of giant reed (*Arundo donax* L.) stems. *Ind. Crops Prod.* **43**, 623–630 (2013). <https://doi.org/10.1016/j.indcrop.2012.08.003>
27. Suárez, L., Ortega, Z., Barczewski, M., Cunningham, E.: Use of giant reed (*Arundo donax* L.) for polymer composites obtaining: A mapping review. *Cellulose*. **30**, 4793–4812 (2023). <https://doi.org/10.1007/s10570-023-05176-x>
28. Fiore, V., Scalici, T., Valenza, A.: Characterization of a new natural fiber from *Arundo donax* L. as potential reinforcement of polymer composites. *Carbohydr. Polym.* **106**, 77–83 (2014). <https://doi.org/10.1016/j.carbpol.2014.02.016>
29. Ortega, Z., Romero, F., Paz, R., Suárez, L., Benítez, A.N., Marrero, M.D.: Valorization of invasive plants from Macaronesia as Filler materials in the production of Natural Fiber composites by Rotational Molding. *Polym. (Basel)*. **13**, 2220 (2021). <https://doi.org/10.3390/polym13132220>
30. Fiore, V., Botta, L., Scaffaro, R., Valenza, A., Pirrotta, A.: PLA based biocomposites reinforced with *Arundo donax* fillers. *Compos. Sci. Technol.* **105**, 110–117 (2014). <https://doi.org/10.1016/j.compscitech.2014.10.005>
31. Suárez, L., Ortega, Z., Romero, F., Paz, R., Marrero, M.D.: Influence of Giant Reed fibers on mechanical, thermal, and Disintegration Behavior of Rotomolded PLA and PE composites. *J. Polym. Environ.* **30**, 4848–4862 (2022). <https://doi.org/10.1007/s10924-022-02542-x>
32. Suárez, L., Hanna, P.R., Ortega, Z., Barczewski, M., Kosmela, P., Millar, B., Cunningham, E.: Influence of Giant Reed (*Arundo Donax* L.) Culms Processing Procedure on Physicochemical, Rheological, and Thermomechanical properties of Polyethylene composites. *J. Nat. Fibers*. **21** (2024). <https://doi.org/10.1080/15440478.2023.2296909>
33. Suárez, L., Barczewski, M., Kosmela, P., Marrero, M.D., Ortega, Z.: Giant Reed (*Arundo donax* L.) Fiber extraction and characterization for its use in Polymer composites. *J. Nat. Fibers*. **20**, 1–14 (2023). <https://doi.org/10.1080/15440478.2022.2131687>
34. Suárez, L., Billham, M., Garrett, G., Cunningham, E., Marrero, M.D., Ortega, Z.: A new image analysis assisted semi-automatic geometrical measurement of fibers in Thermoplastic composites: A Case Study on Giant Reed fibers. *J. Compos. Sci.* **7**, 326 (2023). <https://doi.org/10.3390/jcs7080326>
35. Suárez, L., Ni Mhuirí, A., Millar, B., McCourt, M., Cunningham, E., Ortega, Z.: Recyclability Assessment of Lignocellulosic Fiber composites: Reprocessing of Giant Reed/HDPE composites by Compression Molding. In: Hamrol, A., Grabowska, M., Hinz, M. (eds.) *Manufacturing 2024*. Springer Nature (2024)
36. Prociak, A., Sterzyński, T., Pielichowski, J.: Thermal diffusivity of polyurethane foams measured by the modified Angstrom method. *Polym. Eng. Sci.* **39**, 1689–1695 (1999). <https://doi.org/10.1002/pen.11563>
37. Jakubowska, P., Sterzyński, T.: Thermal diffusivity of polyolefin composites highly filled with calcium carbonate. *Polimery/Polymers*. **57**, 271–275 (2012). <https://doi.org/10.14314/polimery.2012.271>
38. Kumari, R., Ito, H., Takatani, M., Uchiyama, M., Okamoto, T.: Fundamental studies on wood/cellulose-plastic composites: Effects of composition and cellulose dimension on the properties of cellulose/PP composite. *J. Wood Sci.* **53**, 470–480 (2007). <https://doi.org/10.1007/s10086-007-0889-5>
39. Tripathi, D., Dey, T.K.: Thermal conductivity, coefficient of linear thermal expansion and mechanical properties of LDPE/Ni composites. *Indian J. Phys.* **87**, 435–445 (2013). <https://doi.org/10.1007/s12648-013-0256-x>
40. Khanna, Y.P., Turi, E.A., Taylor, T.J., Vickroy, V.V., Abbott, R.F.: Dynamic mechanical relaxations in polyethylene.

- Macromolecules. **18**, 1302–1309 (1985). <https://doi.org/10.1021/ma00148a045>
41. Prisco, U.: Thermal conductivity of flat-pressed wood plastic composites at different temperatures and filler content. *Sci. Eng. Compos. Mater.* **21**, 197–204 (2014). <https://doi.org/10.1515/secm-2013-0013>
42. Annie Paul, S., Boudenne, A., Ibos, L., Candau, Y., Joseph, K., Thomas, S.: Effect of fiber loading and chemical treatments on thermophysical properties of banana fiber/polypropylene commingled composite materials. *Compos. Part. Appl. Sci. Manuf.* **39**, 1582–1588 (2008). <https://doi.org/10.1016/j.compositesa.2008.06.004>
43. Kalaprasad, G., Pradeep, P., Mathew, G., Pavithran, C., Thomas, S.: Thermal conductivity and thermal diffusivity analyses of low-density polyethylene composites reinforced with sisal, glass and intimately mixed sisal/glass fibres. *Compos. Sci. Technol.* **60**, 2967–2977 (2000). [https://doi.org/10.1016/S0266-3538\(00\)00162-7](https://doi.org/10.1016/S0266-3538(00)00162-7)
44. Tazi, M., Sukiman, M.S., Erchiqui, F., Imad, A., Kanit, T.: Effect of wood fillers on the viscoelastic and thermophysical properties of HDPE-wood composite. *Int. J. Polym. Sci.* **2016** (2016). <https://doi.org/10.1155/2016/9032525>

Publisher's Note Springer Nature remains neutral with regard to jurisdictional claims in published maps and institutional affiliations.

P1

P2

P3

P4

P5

P6

6.7. RECYCLABILITY ASSESSMENT OF LIGNOCELLULOSIC
FIBRE COMPOSITES: REPROCESSING OF GIANT
REED/HDPE COMPOSITES BY COMPRESSION MOULDING

P7

P8

P9

P10



Recyclability Assessment of Lignocellulosic Fiber Composites: Reprocessing of Giant Reed/HDPE Composites by Compression Molding

Luis Suárez¹ , Aoife Ní Mhuirí², Bronagh Millar³, Mark McCourt³,
Eoin Cunningham² , and Zaida Ortega⁴

¹ Departamento de Ingeniería Mecánica, Universidad de Las Palmas de Gran Canaria, Las Palmas de Gran Canaria, Spain
luis.suarez@ulpgc.es

² School of Mechanical and Aerospace Engineering, Queen's University Belfast, Stranmillis Road, Belfast, UK

³ Polymer Processing Research Centre, School of Mechanical and Aerospace Engineering, Queen's University of Belfast, Belfast, UK

⁴ Departamento de Ingeniería de Procesos, Universidad de Las Palmas de Gran Canaria, Las Palmas de Gran Canaria, Spain
zaida.ortega@ulpgc.es

Abstract. This study verified the possibility of recycling polyethylene-based composites with up to 40% of lignocellulosic reinforcement after 5 cycles of compression molding, milling and extrusion. Two forms of filler from the same plant species, *Arundo donax* L., were studied, namely, fibers and shredded aerial parts of the plant. The properties of composites were assessed at each processing step, finding that the reprocessing affects to more extend the particulate filler than the fibrous one; the lower particle size resulted in lowered tensile properties. However, despite the fiber size reduction, as aspect ratio is not drastically diminished, the better dispersion of the fibers in the matrix counteracts the negative effects of their shorter size. Impact properties are improved with the recycling, possibly due to the increased homogeneity of the samples, which is also translated into a higher density (and lower porosity). The thermomechanical stability of the fiber composites is higher than for the shredded ones. The reduction in size of the fillers is reflected in the lowered viscosity obtained after the reprocessing. The fibers continue stiffening the matrix after the 5 reprocessing cycles, where the milled material acts more as a filler, reducing tensile properties, although showing a good flexural behavior.

Keywords: Lignocellulose · Natural Fiber Composite · Recycling · Compression Molding

1 Introduction

It is undeniable that composite materials possess unique features and properties that are unachievable using simple, uncombined materials. Although these composites allow for a wider range of uses and improved lifespan of products, they can be difficult to dispose of sustainably or recycle depending on the materials the composite is made from. In an age where being eco-friendly is becoming more and more of a priority, materials that can be recycled are a better option for manufacturing and construction. This has led to works claiming increased sustainability or renewability of natural fiber composites, although these materials' recyclability, biodegradation, or carbon footprint determination have not yet been fully assessed [1, 2]. Of particular concern is the breakage of the fibers during the reprocessing, which leads to reduced aspect ratio [3–5] and a decrease in mechanical properties, usually after 5–7 cycles [2]. Natural Fibers (NF) are one of the most-used green fillers in polymer matrices. In general terms, using natural fibers improves mechanical properties and reduces weight, while also providing interesting acoustic and thermal insulation feature. Besides, vegetal fibers are a renewable material and are considered eco-friendly materials.

Some of these fibers are cultivated for the obtaining of the fibers, as for example flax or hemp [3], while others are obtained from side-streams or wastes from other crops, as in the case of banana fibers [6, 7], tomato crop by-products [8], coffee wastes [9], or spent grain from brewery [10], among many others. Another environmental favorable option is the use of plants with a fast growth and low inputs requirements; one of such plants is *Arundo donax* L., also known as giant reed. This plant grows rapidly and contains high proportions of cellulose [11]. Because of these factors, but also due to its potential invasive character, *Arundo donax* derived materials have been the subject of research as potential fillers or functional additives in composites [11–17], but has also been proposed as feedstock of biorefinery processes [18–20].

As found in the literature, more work is needed on the potential to recycle NF composites [2, 21]. The aforementioned reduction in fiber length and aspect ratio has a huge impact on the properties of the materials, usually leading to reduced mechanical performance. Ideally, the recycled materials would maintain the properties of the original material so they could be recycled repeatedly and still perform to the same standard as the originals. However, because the material is being shredded and extruded several times, it is likely that properties such as tensile strength and viscosity will decrease due to the thermal degradation of the materials or a decrease in the aspect ratio of the fibers as they are broken during the shredding and pelletizing processes. In applications such as injection molding, the decrease in fiber length could be beneficial as the viscosity should also decrease. Depending on the plant fibers, composition and plastic chosen, the effects of recycling can vary. Besides, the consecutive thermal cycles and the shear stress induced during compounding could also lead to a degradation of the polymer matrix to certain extent, which would also result in a deterioration of the composite behavior. For instance, some composites such as polypropylene with flax can go up to seven cycles without exhibiting significant change in elastic modulus or tensile strength [3], while HDPE/kraft pulp composites result in a drastic reduction of mechanical performance, even with the use of additives based on maleic anhydride at high molecular weight [22]. In the same line, although some other works have pointed out the need to using antioxidants

and stabilizers to reduce the negative effect of reprocessing, not only in the fillers but also in the matrix itself [23]. A further advantage of using lignocellulose wastes is the fact that these materials can still contain some phenolic compounds with antioxidant activity, thus being capable to reduce the negative effects of thermo-oxidation during reprocessing [10].

1.1 Research Problem

This work assesses the possibility of recycling composites made of (HDPE) and giant reed fibers (*Arundo donax* L.) in up to 40% in weight. The composites were produced by melt-compounding in a twin-screw extruder and compression molded. Then, after testing, they were ground, and reprocessed again by twin-screw and compression, repeating this reprocessing for 5 times. Although the fibers from *Arundo* have been characterized and tested as reinforcement or filler of composite matrices, there hasn't been any significant research into the reprocessing of such composites and the impact of recycling in the final properties of the materials. The behavior of the composites at each reprocessing was assessed against fiber length, diameter and aspect ratio.

2 Material and Methods

2.1 Materials and Sample Preparation

High-density polyethylene (HDPE), grade HD6081 from Total was used as matrix. This polymer is characterized by a melt flow index (MFI) of 8 g/10 min (190 °C/2.16 kg) and a density of 960 kg/m³, according to the manufacturer's datasheet.

Two different *Arundo* derived materials were used, at 20 and 40 wt% loading: shredded material, obtained by grinding the aerial parts of the plant, and fibers obtained from culms, as described in a previous work of authors [11]. The composites are named after the type of vegetal material used and its content (in weight %); followed by a number to indicate the reprocessing cycle; so, PE.S20-0 refers to composites with 20% shredded material after extrusion and compression molding (original material), while PE.S20-1 stands for this same material after the first recycling step.

2.2 Methods

Processing and Reprocessing

The materials used were dried overnight before compounding: lignocellulosic fibers at 105 °C and HDPE at 60 °C. Composites were prepared in a Thermo Scientific Haake Rheomex PTW 16 OS twin screw extruder, with a L/D relationship of 25, with screw rotation speed of 300 rpm and the following temperature profile (from hopper to nozzle): 170-175-170-165-160-60 °C. Once the compounding was extruded, it was processed in a Collin P 200 platen press in a square plate mold, which were later die cut to obtain the test samples. The processing temperature was 190 °C, the material was kept at 10 bar for 2 min, and then at 25 bar for the cooling stage. Once the samples were tested, they were ground in an Alpine Augsburg chipping device, model RO 16/8, working at 1400 rpm,

and reprocessed by extrusion and compression molding, using the same parameters already mentioned, repeating this procedure 5 times.

Composites Characterization

Fourier transform infrared spectroscopy (FTIR) was performed in a Perkin Elmer Spectrum 100, under attenuated total reflectance mode. The wavelength was set in the 4000–640 cm^{-1} range, scanning each sample 64 times at a resolution of 4 cm^{-1} .

Density of the composites was determined following the procedure described at ISO1183 standard, based on the Archimedes principle, using methanol, measuring 5 replicates. Porosity was obtained comparing the theoretical density, considering the density of the HDPE and the fillers (1.5456 g/cm^3 for the fibers and 1.1727 g/cm^3 for the shredded material) [11] with the experimental one.

Melt flow index (MFI) was calculated for the pellets produced at each stage, under the protocol established at ISO1133, in a Kayeness Galaxy device, model 7053, at 190 °C, with a mass of 2.16 kg.

Mechanical testing was conducted on die cut samples from the compression molded plates, tensile and flexural testing were performed in a Lloyd LS5 apparatus, using 5 replicas per type of material, following ISO 527 standard for tensile testing and ISO 178 for flexural assays. For tensile, the gauge length was settled at 60 mm and a strain rate of 1 mm/min was used; for flexural, the strain rate was set at 2 mm/min, with a node span of 64 mm, the test stopped when deformation reached 17 mm. Impact strength was determined in a Ceast Resil impact tester, under Charpy mode on unnotched bars, as for ISO 179 standard, using a pendulum of 7.5 J, a span of 62 mm and an impact rate of 3.7 m/s. 10 replicas were used to determine impact resistance.

Thermomechanical properties of the different materials were evaluated by Dynamic Mechanical Thermal Analysis in a Tritec 2000 device (Triton Technology), at single cantilever bending method. A strain of 50 μm was applied at 1 Hz frequency, in the temperature range from –80 to 80 °C, at a heating of 2 °C/min (ISO 6721).

Another parameter calculated from DMA analysis is the adhesion factor (A), as described by Kubát et al. [24], and simplified according to Hejna et al. [25]:

$$A = \frac{1}{1 - x_F} \cdot \frac{\tan\delta_C}{\tan\delta_{PE}} - 1 \quad (1)$$

where x_F is the ratio of the filler in the composite (in volume).

Lower values of A indicate higher interfacial adhesion, while high values of this factor are related to higher viscoelastic character and higher energy dissipation due to chain movements inside the composite [26], or to high porosity or insufficient adhesion between polymer and filler [25].

Finally, the entanglement factor (N) and the reinforcement efficiency (r) have also been proposed by several authors as a way to determine the intensity of the interaction between the matrix and the filler [26–29]. The entanglement factor is usually calculated at several temperatures to evaluate the potential differences in such interactions due to different service conditions, according to Eq. 2:

$$N = \frac{E'}{RT} \quad (2)$$

where E' is the storage modulus at T temperature (in K), R the universal gas constant.

Finally, the reinforcement efficiency is obtained from the relationship between the storage modulus of the composite and the matrix:

$$E'_c = E'_m \cdot (1 + r \cdot V_f) \quad (3)$$

where E'_c and E'_m are the storage modulus of the composite and the matrix, respectively, and V_f the percentage of the filler (by volume).

Rheological behavior was assessed in an AR G2 oscillatory rheometer (TA instruments), using 25 mm diameter parallel plates. The experiments were performed at 190 °C under nitrogen with 2.5 mm gap. Preliminary tests were performed in the strain sweep mode to ensure later experiments took place in the linear viscoelastic region. In these tests, strain was varied between 0.1 and 5%. Angular frequency sweeps were performed at 0.5% strain, in the LVE region, in the range of 0.01 to 100 rad/s.

Finally, the fillers morphology was also assessed in the different stages, by obtaining a thin layer of the composite, via platen press. Once the film is obtained, it is scanned with a high-resolution optical scanner and the image is analyzed using ImageJ. This way, thousands of elements (fibers or particles) can be measured, obtaining a representative value for their geometrical parameters [5].

3 Results and Discussion

3.1 FTIR Analysis

Figure 1a shows the FTIR spectra for the different materials used in this work, only for cycles 1 and 5, and 40% loadings, to have a clear image. Composites for both type of lignocellulose filler show a similar curve, with more intense bands for 40% loaded composites in the areas of 3600–3000 cm^{-1} , related to O-H stretching, and 1200–850 cm^{-1} , characteristic of C = O, both associated to cellulosic compounds. These bands are more intense for composites based on fibers, due to their higher cellulose content [11]. Apart from this, not particular bands are observed, meaning no intense bonds are formed between matrix and filler, or these being overlapped with the HDPE typical fingerprint. Furthermore, when zooming (Fig. 1b) into the interest area for the calculation of the carbonyl index (i.e., between 1800 and 1450 cm^{-1}), the appearance of bands at about 1720 cm^{-1} is not observed for any of the materials, thus indicating that the reprocessing is not apparently producing any oxidation in the polymer. The composites containing the shredded plant exhibits some absorbance in this area, though, which is attributed to the ketone and carbonyl groups in lignin, pectins and waxes, naturally present in this material and mostly removed by the fiber extraction process.

3.2 Mechanical Behavior

Table 1 summarizes the mechanical properties of the different series of composites and cycle processing. As observed, and as expected, there are no differences in the behavior of the neat HDPE as a consequence of the reprocessing (p -value > 0.1). In contrast, for the composites two different trends are observed, depending on the type of filler

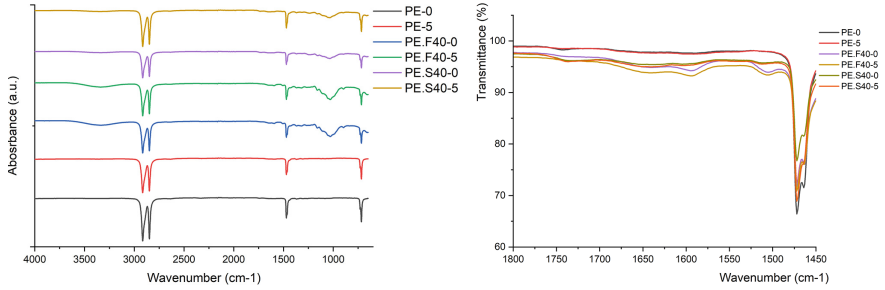


Fig. 1. FTIR spectra for a) neat HDPE and 40% composites in cycles 0 and 5 between 4000 and 500 cm^{-1} , and b) FTIR spectra zoomed between 1800 and 1450 cm^{-1} .

Table 1. Different properties for the different materials and processing cycle (E: elastic modulus, σ : ultimate stress, ϵ : deformation; MFI: melt flow index; η_0 : zero-shear viscosity)

Material	Cycle	Impact strength (kJ/m ²)	Tensile					Density (kg/m ³)	Porosity (%)	MFI (g/10 min)	η (Pa·s)
			E (MPa)	σ (MPa)	ε _{break}	ε _{max stress}					
PE	0	6.2 ± 1.9	747.9 ± 82.9	21.0 ± 1.6	2.309 ± 0.243	0.073 ± 0.041	0.949±0.008	1.1±0.9	8.4±0.2	1579	
	1	5.8 ± 2.0	875.3 ± 39.0	20.4 ± 0.1	2.167 ± 0.246	0.090 ± 0.006	0.932±0.014	2.9±1.7	8.0±0.1	1372	
	2	5.4 ± 2.3	810.1 ± 55.9	19.6 ± 0.6	2.138 ± 0.213	0.090 ± 0.003	0.946±0.004	1.5±0.5	8.5±0.1		
	3	5.8 ± 2.2	860.0 ± 23.4	20.2 ± 0.2	2.148 ± 0.138	0.091 ± 0.004	0.942±0.006	1.9±0.7	8.3±0.1	1324	
	4	5.9 ± 2.1	832.8 ± 26.1	19.8 ± 0.3	2.131 ± 0.211	0.093 ± 0.007	0.946±0.006	1.4±0.7	8.4±0.1		
	5	5.8 ± 2.0	829.9 ± 34.2	20.1 ± 0.2	2.252 ± 0.220	0.091 ± 0.002	0.949±0.009	1.2±1.1	8.5±0.1	1492	
PE.F20	0	7.3 ± 1.2	926.6 ± 72.9	16.5 ± 0.5	0.060 ± 0.006	0.048 ± 0.004	0.990±0.01	4.7±0.9	4.7±0.2	2529	
	1	8.6 ± 2.2	734.7 ± 35.5	14.5 ± 0.4	0.092 ± 0.013	0.061 ± 0.003	0.999±0.011	3.8±0.6	5.7±0.1	4370	
	2	9.4 ± 2.4	754.7 ± 15.9	14.5 ± 0.2	0.091 ± 0.006	0.062 ± 0.003	0.988±0.022	4.9±2.1	3.5±0.4		
	3	10.5 ± 1.3	793.7 ± 34.3	14.8 ± 0.6	0.087 ± 0.011	0.058 ± 0.003	1.008±0.017	3.0±1.4	3.2±0	14340	
	4	9.8 ± 1.9	839.5 ± 11.0	15.2 ± 0.3	0.090 ± 0.012	0.057 ± 0.002	1.008±0.005	2.9±0.4	3.4±0.2		
	5	9.3 ± 1.9	841.2 ± 16.9	15.1 ± 0.4	0.101 ± 0.020	0.058 ± 0.005	1.012±0.01	2.6±0.9	3.7±0.5	11210	
PE.F40	0	6.0 ± 0.8	834.0 ± 88.2	12.1 ± 0.8	0.037 ± 0.006	0.026 ± 0.004	1.052±0.015	7.0±1.4	0.4±0.1	37970	
	1	6.6 ± 1.1	1096.7 ± 81.0	13.1 ± 0.6	0.040 ± 0.011	0.026 ± 0.004	1.070±0.009	5.4±0.9	1.8±0.2	38510	
	2	5.9 ± 1.2	1079.0 ± 15.7	13.3 ± 0.7	0.042 ± 0.010	0.026 ± 0.004	1.076±0.006	4.9±0.6	1.2±0.3		
	3	7.3 ± 1.8	1039.7 ± 57.3	13.4 ± 0.3	0.049 ± 0.009	0.026 ± 0.004	1.076±0.012	4.9±1.2	1.4±0.2	61400	
	4	6.1 ± 0.6	1121.0 ± 43.9	13.2 ± 0.0	0.044 ± 0.022	0.025 ± 0.004	1.084±0.01	4.2±45.5	1.2±0.4		
	5	6.3 ± 0.5	1112.6 ± 62.2	13.7 ± 0.5	0.046 ± 0.008	0.029 ± 0.003	1.080±0.006	4.5±45	1.5±0.1	55790	
PE.S20	0	6.4 ± 0.8	996.8 ± 46.7	15.6 ± 1.0	0.040 ± 0.008	0.036 ± 0.006	<0.794	>30 %	1.7±0.1	5156	
	1	8.2 ± 0.9	657.5 ± 37.7	12.1 ± 0.3	0.147 ± 0.231	0.037 ± 0.006	1.009±0.009	10.8±0.8	2.4±0.0	5315	
	2	8.5 ± 1.1	704.7 ± 25.5	12.5 ± 0.6	0.049 ± 0.007	0.038 ± 0.003	0.994±0.04	12.2±3.5	2.5±0.1		
	3	8.4 ± 1.4	668.0 ± 30.5	11.8 ± 0.4	0.041 ± 0.005	0.036 ± 0.006	1.009±0.008	10.8±0.7	2.7±0.2	4742	
	4	7.1 ± 2.1	671.9 ± 35.0	11.6 ± 0.2	0.146 ± 0.236	0.033 ± 0.002	0.945±0.02	16.5±47.7	2.8±0.2		
	5	9.3 ± 1.9	657.5 ± 25.9	11.8 ± 0.3	0.045 ± 0.006	0.036 ± 0.002	0.957±0.025	15.5±46.5	2.9±0.1	3566	
PE.S40	0	6.4 ± 0.5	1061.0 ± 62.7	15.1 ± 1.2	0.037 ± 0.009	0.033 ± 0.007	0.861±0.042	23.9±3.7	0.9±0.0	13250	
	1	5.1 ± 0.9	670.7 ± 145.1	10.2 ± 0.8	0.029 ± 0.006	0.027 ± 0.005	0.946±0.045	16.4±3.9	1.3±0.1	13810	
	2	5.9 ± 1.0	690.8 ± 54.3	9.7 ± 0.8	0.037 ± 0.005	0.028 ± 0.002	1.012±0.024	10.5±2.1	1.2±0.0		
	3	5.9 ± 0.9	798.3 ± 96.6	10.0 ± 0.7	0.027 ± 0.006	0.023 ± 0.003	1.007±0.021	11±1.9	1.3±0.0	21570	
	4	6.4 ± 1.2	815.3 ± 66.5	10.4 ± 1.1	0.029 ± 0.007	0.024 ± 0.003	1.003±0.046	11.4±2	1.5±0.1		
	5	6.1 ± 1.4	771.2 ± 104.7	10.0 ± 0.9	0.032 ± 0.003	0.026 ± 0.003	0.989±0.037	12.6±5.5	1.5±0.0	9894	

used. For 20% fibrous composites, there are no significant differences either in tensile modulus or maximum stress, except between cycle 0 and 1; after first reprocessing,

the fiber length (and aspect ratio) is reduced, thus explaining the lowered mechanical properties. On the other hand, despite this reduction in aspect ratio is also observed for F40, it is counteracted by the higher dispersion of the fibers within the matrix; the more homogeneous material produced after the reprocessing delivers a material with better mechanical properties. For the shredded materials, the lower particle size obtained after the first reprocessing is the responsible for the reduction in properties, as also concluded from DMA analysis; in this case, as the lignocellulose is in particle form, the possible higher uniformity of the material is not counteracting the low particle size, this acting as points for stress concentration and reducing the modulus and the tensile strength. Therefore, the fibrous composites at high loadings benefit from the reprocessing, while the remaining materials show a reduction of approximately 15% for F20 (both for modulus and ultimate stress) and 30% for materials with the shredded *Arundo*. Contrarily, the increased uniformity of the material, despite the size reduction of the fillers, might improve the impact resistance of the composites. The composites at 20% improve the impact strength, while those at 40% do not modify significantly the behavior of the matrix (p-values for the comparisons PE vs. composites at 20% <0.02 , and >0.9 for PE vs. 40% composites). Previous research of authors with these same fillers provided a similar behavior, although with significant improvements in elastic modulus, both at tensile and flexural testing [30]. This difference is due to the processing; in that case, the composites were molded by injection molding, which not only implies the use of higher pressure but also a preferential orientation of the fibers due to the flow occurring to fill in the cavity.

As observed in Fig. 2, the aspect ratio of the fibers is reduced after the reprocessing, while for shredded materials it keeps relatively unchanged, at lower values. Besides, this material is not defined by an aspect ratio itself, as it consists more in an irregular shaped filler (aspect ratio close to 1), while fibers exhibit an aspect ratio of approximately 6 at the feeding, which is reduced to 4 in the first reprocessing [5], arriving up to 3 in the last cycle. The particle size for shredded material is reduced in 24% after processing, while fiber length is reduced from 1.5 mm to 0.5 mm, with diameter reducing from 0.23 to 0.14 mm after the first extrusion cycle [5]. This difference in size and aspect ratio explains the lower tensile properties of the shredded composites compared to the fibrous ones. Aspect ratio for the fibers in the composite is reduced from 4.4 for cycle 0 to approximately 3.5 for the remaining cycles, tending to increase in the final cycles (not statistically significant), due to a further decrease in fibers diameter; the most significant decrease (p-value < 0.001) is found from stage 0 to 1.

The stiffening character of both fillers is observed in the increased elastic modulus and in the lower deformation at which the maximum stress takes place for cycle 0 (Fig. 3); despite the reduction in the modulus and strength observed after the reprocessing, the strain at break is not modified in general terms. For instance, strain at ultimate stress (for tensile tests) is 0.070 for neat HDPE, 0.049 for PE.F20, 0.036 for PE.F40 and 0.034 for particulate composites. Similar results are obtained for flexural testing, with strain at break not significantly modified due to reprocessing but decreased for the composites compared to the polymer. The stress at 3.5% deformation is similar for all samples, despite their filler content or processing cycle, approximately happening at 22 MPa. The tensile and flexural stress is reduced for all composites compared to the matrix,

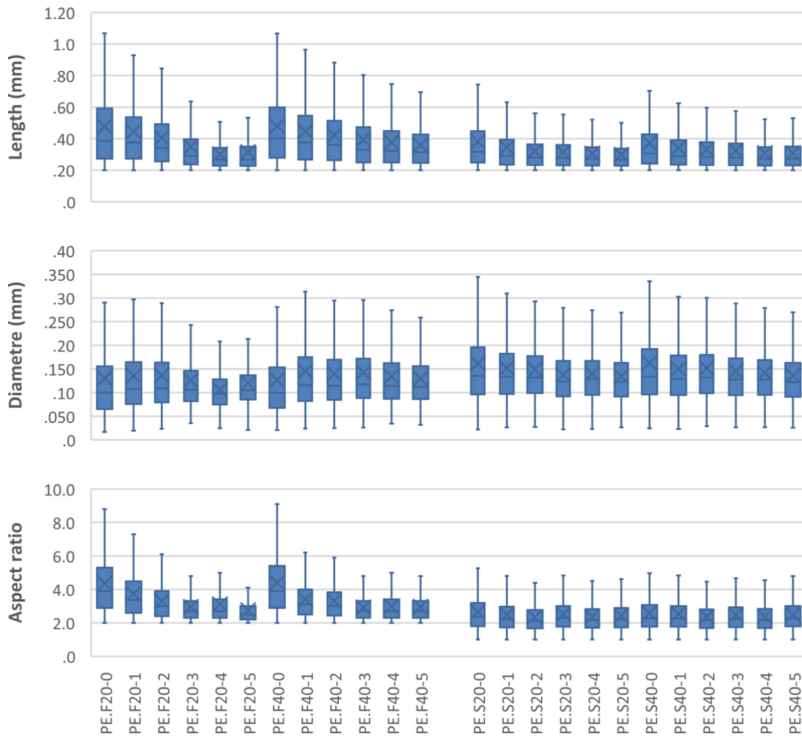


Fig. 2. Variation of geometrical features from cycles 0 to 5 for fibrous composites: a) length, b) diameter, and c) Aspect ratio.

due to a reduced adhesion between the lignocellulose and the polyethylene, acting the filler as a concentrator of stress. Only the neat PE show a significant decrease in the flexural modulus (p-value: 0.017). The remaining series show no statistical difference due to the reprocessing (p-values: 0.854, 0.995, 0.114, 0.959 for F20, F40, R20 and R40, respectively).

Similar observations are made for ultimate flexural strength, with no differences due to the reprocessing in any case (p-values close to 1 for all series). However, flexural ultimate strength is reduced due to the lignocellulosic fillers, particularly in fibrous shape.

The increased stiffness of the material is aligned with the reduced values for strain at which ultimate stress take place, which is reduced from 0.094 to 0.07 and 0.05 for 20 and 40% composites, respectively; furthermore, the stress at which 3.5% strain takes place is also increased for composites, increasing slightly for all composites series compared to neat PE. The shredded material seems benefiting in more extent the elastic modulus than the fibers.

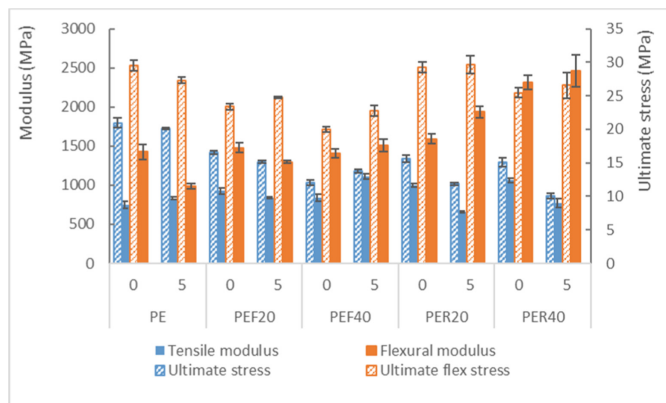


Fig. 3. Mechanical properties (tensile and flexural elastic modulus and ultimate stress) for the different materials in cycles 0 and 5

3.3 Thermomechanical Behavior. Matrix – Filler Interactions

As observed in the mechanical testing, no difference is found for the polyethylene as a consequence of reprocessing; this also is found for F20 series, while for F40 the storage modulus (E') shows a trend to increase slightly with the processing. An opposite trend is found for the series with shredded Arundo: the samples with the material extruded only once shows a significantly higher storage modulus than the remaining cycles (Fig. 4a). What is also interesting is to note that for all composite materials the curves as smoother with the reprocessing, due to the higher uniformity of the materials (Figs. 4b and 4c). All composites with fibers provide higher storage modulus than neat HDPE, meaning that the lignocellulosic material stiffens the matrix, while those with shredded reed biomass exhibit lower E' than PE, until room temperature. The difference is more notable for the reprocessed materials (Fig. 4c), as also found in mechanical testing. The starting value of the storage modulus for cycle zero is in a similar range for all materials, being considerable higher for fibrous composites and lower for shredded material in cycle 5. The storage modulus decreases in an expected constant way, as also found in other works [31]. This decrease occurs at higher temperatures with the increase in lignocellulose ratio. The decrease in E' is more abrupt for neat HDPE than for composites in any processing cycle, even arriving to obtain slightly higher values for the shredded composites at temperatures over 20°C. This means that the biomass is providing a higher thermomechanical stability to the polymer. The damping factor ($\tan \delta$) shows an inflection in the curves at 50–60 °C, corresponding to α -transition, also observed in E'' plots as a maximum. Another slight inflexion in the curves happens at 0–10 °C, more visible for the reprocessed material, being attributed to the glass-rubber transition of the amorphous phase in PE [32].

The reinforcement efficiency (r) calculated shows that fibers stiffen the matrix in more extent than shredded materials (Fig. 4d), starting this reinforcement at lower temperatures. The entanglement factor (N) for PE and PE.F20 is very close; as this parameter also gives an indication of the efficient adhesion between fiber and matrix, fibrous composites seem providing better behavior than shredded samples, as also found for the

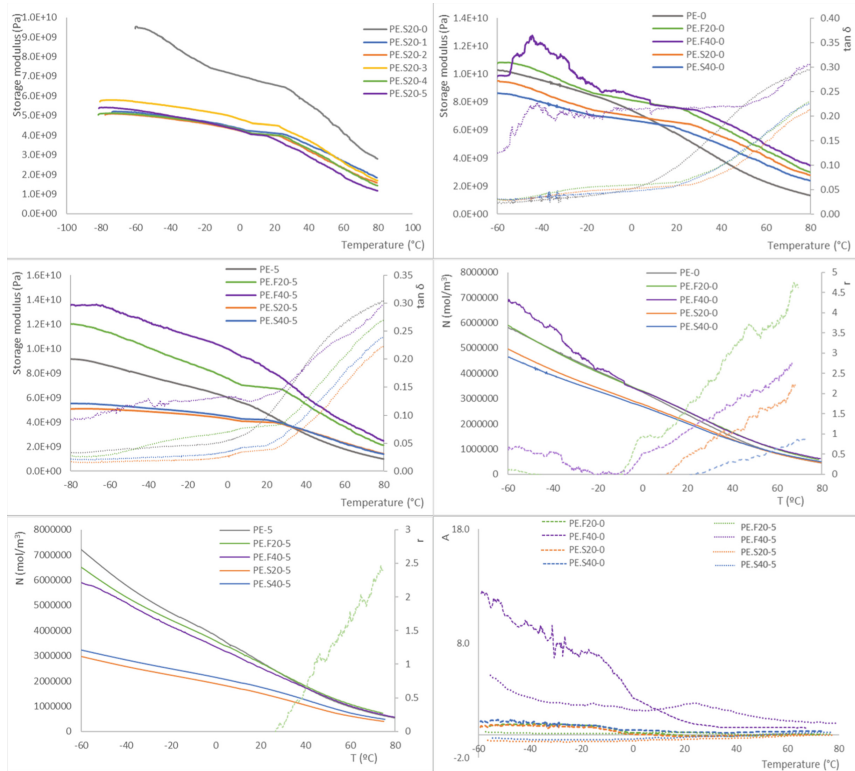


Fig. 4. Results of DMA: a) storage modulus vs. temperature for PE.S20 reprocessing, b) comparison of storage modulus for cycle 0 for all materials, c) storage modulus for all materials in cycle 5, d) entanglement factor and reinforcement efficiency for cycle 0, e) entanglement factor and reinforcement efficiency for cycle 5, f) adhesion factor for cycles 0 and 5.

efficiency and adhesion factor (Figs. 4e and 4f). The reprocessing makes the difference in entanglement clearer for the composites series; only F20 seems providing a positive value of the reinforcement efficiency.

As for mechanical properties, the reprocessing affects negatively the shredded material composites, with a reduction in tensile properties; for fibers, despite the size decrease, aspect ratio is still relatively high (being still be considered as fibers), and the higher homogeneity counteracts the size reduction. The beneficial effect of the reprocessing in the homogeneity of F40 series can be clearly seen when plotting the adhesion factor versus temperature for cycles 0 and 5 (Fig. 4f); not only the parameter A is reduced, but also the curve is more stable along the studied temperature range.

3.4 Rheological Behavior

Rheological analysis provides information about the viscosity of a polymer (or a blend) but can also provide indirect information about the changes occurred in the macromolecular structure of the polymer [33, 34] because of the processing. In the first cycle, the

different flow behavior due to the incorporation of the biomass is observed, particularly at low angular frequencies (Fig. 5a, continuous lines). Composites at 20% loading show a similar behavior, despite their different geometrical features, while significant differences are observed for the composites at 40%. Fibrous composites show a higher viscosity than the ones with shredded material, possibly due to the formation of agglomerates of the fibers, due to their higher aspect ratio. The viscosity curves for all materials show shear thinning behavior or pseudoplasticity, except for PE, which shows the typical Newtonian plateau; composites reduce their viscosity at increasing angular frequencies. When shear stress increases, the effect of the interaction between the particles loses significance and the viscosity values tend to approach those of the matrix [34, 35]. Figure 5a also shows the viscosity curves obtained for parts after reprocessing them 5 times (dash lines). The composites with shredded reed show a decrease in viscosity and, particularly, the samples with 20% shredded material show a behavior very close to that of the neat HDPE. The course of the curves remains unaltered for the fibrous composites. There is no evidence of important modifications in the rheological behavior of the materials, thus confirming the FTIR observations, that is, no oxidation or crosslinking is happening in the matrix due to the reprocessing. The reduction of viscosity observed for composites with shredded material is due to the reduction of the particle size resulting from the successive grindings and melt-mixing; this phenomenon is not observed (or happens to lower extent) for fibrous composites. This is likely to happen due to a more intimate blend of fibers and matrix, as observed by the lower adhesion factor obtained from DMA, which is translated into a better dispersion in the matrix, which counteracts the reduction in length and aspect ratio, which also results in an increase in E' .

When analyzing the storage (G') and loss modulus (G'') versus angular frequency (Fig. 5b) it is observed that loss modulus is higher than storage one, thus meaning that all the samples have a predominant viscous character. This also happens for recycled composites. However, the difference between these curves is reduced with the increasing ratio of filler, and also being lower for composites with fiber than for those with shredded vegetal material, related to a stiffening effect occurred because of the fibers. As also happening for the viscosity curves, the differences between the different series are reduced at higher angular frequencies. While fibrous composites show a tendency to an increase in storage modulus with reprocessing, as said because of a better homogeneity of the composites and an increased stiffness, those containing shredded material exhibit a lower storage modulus after the reprocessing due to the reduction of the particles size, which also leads to a lower viscosity. The viscous character of the materials is not affected by the reprocessing, that is, the curves of loss modulus are overlapped for the different cycles for each material.

Finally, the flow tests were performed to determine the zero-shear viscosity (η_0), using the Carreau-Yasuda regression. As for all the parameters studied, the values for η_0 increase with the biomass loading are shown in Table 1. The same trend already described for the viscosity at higher shear rates is observed here, that is, the fibrous composites tend to increase viscosity, while the composites with shredded materials show a decrease in that parameter. Those results are in agreement with the MFI values; the MFI for neat HDPE varies from 8.0 to 8.5 for all the processing stages, that is, the fluidity of the matrix is not significantly affected by the material's reprocessing. However, when it

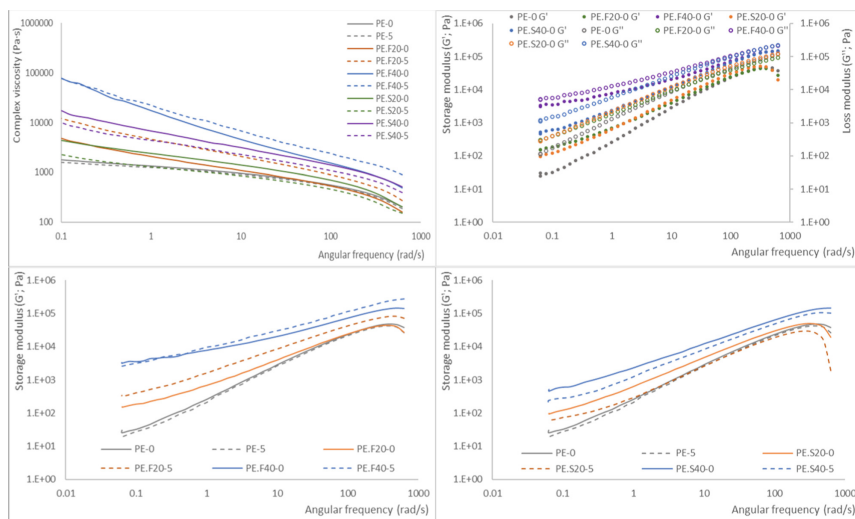


Fig. 5. Results of frequency-sweep rheological experiments: a) complex viscosity for cycles 1 and 5 b) storage and loss modulus for cycle 0, c) storage modulus for fiber composites in cycles 0 and 5, d) storage modulus for shredded reed composites in cycles 0 and 5.

comes to composites, significant modifications are found. In first place, and as expected, the values decrease with the increased content of filler, regardless of this geometry, that is, the composites 40% loaded composites show a lower melt flow index than 20% ones, also lower than HDPE. Regarding the influence of reprocessing in the fluidity of the material, there is a general trend to an increase in the fluidity from the original prepared pellet to the first reprocessing, followed by a later drop in the next cycle. After the second cycle, the MFI remains unchanged. This might be explained by the lack of changes observed for the matrix, and by the fact that the lignocellulose size is mainly reduced in the first processing, being almost unaltered for successive reprocessing. So, the increase in the MFI might be due to the particle size reduction, while the later drop and stability might be related to an incipient crosslinking happening in the matrix or to a better interaction between filler and matrix, as a consequence of the better distribution of the filler and the intimate mix achieved by the reprocessing via twin-screw compounding. This might be confirmed by the reduction in porosity achieved along the different processing cycles, particularly after the second processing: a higher degree of mixing results in lower air bubbles trapped within the blend, and thus, in an increased density (reduced porosity).

4 Conclusions

This study concludes that recycling polyethylene-based composites with lignocellulosic reinforcement is feasible, and the choice of filler type and its processing significantly influence the material properties, with potential trade-offs between tensile and flexural behavior. The effect of filler type (particles vs. fibers) was observed, noting that the reprocessing impacted particulate filler more significantly than fibrous filler.

It was found that lower particle size resulted in decreased tensile properties and lowered viscosity. Despite fiber size reduction, the maintained aspect ratio contributed to better dispersion in the matrix, mitigating negative effects, as also happening by the better homogeneity due to the reprocessing. Finally, a higher thermomechanical stability in fiber composites compared to shredded ones has been noticed.

Acknowledgements. Luis Suárez: Canarian Agency for Research, Innovation and Information Society of the Canary Islands Regional Council for Employment, Industry, Commerce and Knowledge (ACIISI) and by the European Social Fund (Grant TESIS2021010008).

Zaida Ortega: Spanish Ministry of Universities, Order UNI/501/2021 of May 26th, 2021. Next Generation funds from European Union (Plan de Recuperación, Transformación y Resiliencia del Gobierno de España: C21.I4.P1).

References

1. Suárez, L., Castellano, J., Díaz, S., Tcharkhtchi, A., Ortega, Z.: Are natural-based composites sustainable? *Polymers* **13**, 2326 (2021). <https://doi.org/10.3390/polym13142326>
2. Zhao, X., et al.: Recycling of natural fiber composites: challenges and opportunities. *Resour. Conserv. Recycl.* **177** (2022). <https://doi.org/10.1016/j.resconrec.2021.105962>
3. Barteau, G., et al.: Recycling of wood-reinforced poly-(propylene) composites: a numerical and experimental approach. *Ind. Crops. Prod.* **167** (2021)
4. Albrecht, K., Osswald, T., Baur, E., Meier, T., Wartzack, S., Müssig, J.: Fibre length reduction in natural fibre-reinforced polymers during compounding and injection moulding—experiments versus numerical prediction of fibre breakage. *J. Compos. Sci.* **2**(20) (2018)
5. Suárez, L., Billham, M., Garrett, G., Cunningham, E., Marrero, M., Ortega, Z.: A new image analysis assisted semi-automatic geometrical measurement of fibers in thermoplastic composites: a case study on giant reed fibers. *J. Compos. Sci.* **7**(326) (2023)
6. Ortega, Z., Benítez, A.N., Monzón, M.D., Hernández, P.M., Angulo, I., Marrero, M.D.: Study of banana fiber as reinforcement of polyethylene samples made by compression and injection molding. *J. Biobased Mater. Bioenergy* (2010). <https://doi.org/10.1166/jbmb.2010.1075>
7. Monzón, M.D., et al.: Experimental analysis and simulation of novel technical textile reinforced composite of banana fibre. *Materials* **12** (2019). <https://doi.org/10.3390/ma12071134>
8. Bourmaud, A., et al.: A circular approach for the valorization of tomato by-product in biodegradable injected materials for horticulture sector. *Polymers* **15** (2023)
9. Hejna, A., Barczewski, M., Kosmela, P., Mysiukiewicz, O.: Comparative analysis of the coffee and cocoa industry by-products on the performance of polyethylene-based composites. *Waste Biomass Valori.* **14**, 2691–2706 (2023). <https://doi.org/10.1007/s12649-023-02041-7>
10. Hejna, A., Maré, M., Kowalkowska-Zedler, D., Pładzyk, A., Barczewski, M.: Insights into the thermo-mechanical treatment of brewers' spent grain as a potential filler for polymer composites. *Polymers* **13** (2021). <https://doi.org/10.3390/polym13060879>
11. Suárez, L., Barczewski, M., Kosmela, P., Marrero, M., Ortega, Z.: Giant reed (*Arundo Donax* L.) fiber extraction and characterization for its use in polymer composites. *J. Nat. Fibers* **20**(1) (2023)
12. Suárez, L., Ortega, Z., Barczewski, M., Cunningham, E.: Use of giant reed (*Arundo Donax* L.) for polymer composites obtaining: a mapping review. *Cellulose* (2023)

13. Gulihonenahali Rajkumar, A., Hemath, M., Kurki Nagaraja, B., Neerakallu, S., Thiagamani, S.M.K., Asrofi, M.: An artificial neural network prediction on physical, mechanical, and thermal characteristics of giant reed fiber reinforced polyethylene terephthalate composite. *J. Ind. Text.* (2021). <https://doi.org/10.1177/15280837211064804>
14. Suárez, L., Ortega, Z., Romero, F., Paz, R., Marrero, M.D.: Influence of giant reed fibers on mechanical, thermal, and disintegration behavior of rotomolded PLA and PE composites. *J. Polym. Environ.* **30**, 4848–4862 (2022). <https://doi.org/10.1007/s10924-022-02542-x>
15. Suárez, L., Castellano, J., Romero, F., Marrero, M.D., Benítez, A.N., Ortega, Z.: Environmental hazards of giant reed (*Arundo Donax* L.) in the macaronesia region and its characterisation as a potential source for the production of natural fibre composites. *Polymers* **13** (2021)
16. Baquero Basto, D., Monsalve Alarcón, J., Sánchez Cruz, M., Alarcón, J.M., Sánchez Cruz, M.: Experimental characterization of composite panels made with *Arundo Donax* Fibers and vegetable resin. *Scientia et Technica Año XXII* **23**, 119–125 (2018)
17. Fiore, V., Scalici, T., Valenza, A.: Characterization of new natural fiber from *Arundo Donax* L as potential reinforcement of polymer composites. *Carbohydr. Polym.* **106**, 77–83 (2014)
18. Suárez, L., Ortega, Z., Barczewski, M., Cunningham, E.: Use of giant reed (*Arundo Donax* L.) for polymer composites obtaining: a mapping review. *Cellulose* **30**, 4793–4812 (2023)
19. Ortega, Z., Bolaji, I., Suárez, L., Cunningham, E.: A review of the use of giant reed (*Arundo Donax* L.) in the biorefineries context. *Rev. Chem. Eng.* (2023)
20. Nazli, R.I., Tansi, V., Öztürk, H.H., Kusvuran, A.: *Miscanthus*, switchgrass, giant reed, and bulbous canary grass as potential bioenergy crops in a semi-arid mediterranean environment. *Ind. Crops. Prod.* **125**(9–23) (2018). <https://doi.org/10.1016/j.INDCROP.2018.08.090>
21. Soroudi, A., Jakubowicz, I.: Recycling of bioplastics, their blends and biocomposites: a review. *Eur. Polym. J.* **49**, 2839–2858 (2013). <https://doi.org/10.1016/j.eurpolymj.2013.07.025>
22. Fonseca-Valero, C., Ochoa-Mendoza, A., Arranz, J., González, C.: Mechanical recycling and composition effects on the properties and structure of hardwood cellulose-reinforced high density polyethylene eco-composites. *Compos. Part A Appl. Sci. Manuf.* **69**, 94–104 (2015)
23. Wang, H., Zhang, J., Fu, H., Wang, W., Wang, Q.: Effect of an antioxidant on the life cycle of wood flour/polypolypropylene composites. *J. For. Res.* **31**, 1435–1443 (2020)
24. Kubát, J., Rigdahl, M., Weland, M.: Characterization of interfacial interactions in high density polyethylene filled with glass spheres using dynamic-mechanical analysis. *J. Appl. Polym. Sci.* **39**, 1527–1539 (1990). <https://doi.org/10.1002/app.1990.070390711>
25. Hejna, A., et al.: Rotational molding of linear low-density polyethylene composites filled with wheat bran. *Polymers* **12**(1004) (2020). <https://doi.org/10.3390/polym12051004>
26. Jyoti, J., Singh, B.P., Arya, A.K., Dhakate, S.R.: Dynamic mechanical properties of multiwall carbon nanotube reinforced ABS composites and their correlation with entanglement density, adhesion, reinforcement and C factor. *RSC Adv.* **6**, 3997–4006 (2016)
27. Andrzejewski, J., Gapiński, B., Islam, A., Szostak, M.: The influence of the hybridization process on the mechanical and thermal properties of polyoxymethylene (POM) composites with the use of a novel sustainable reinforcing system based on biocarbon and basalt fiber (BC/BF). *Materials* **13**(3496) (2020). <https://doi.org/10.3390/ma13163496>
28. Panwar, V., Pal, K.: An optimal reduction technique for RGO/ABS composites having high-end dynamic properties based on cole-cole plot, degree of entanglement and c-factor. *Compos. B Eng.* **114**, 46–57 (2017). <https://doi.org/10.1016/j.compositesb.2017.01.066>
29. Mysiukiewicz, O., Kosmela, P., Barczewski, M., Hejna, A.: Mechanical, thermal and rheological properties of polyethylene-based composites filled with micrometric aluminum powder. *Materials* **13**(1242) (2020). <https://doi.org/10.3390/ma13051242>
30. Suárez, L., et al.: Influence of giant reed (*Arundo Donax* L.) culms processing procedure on physicochemical, rheological, and thermomechanical properties of polyethylene composites. *J. Nat. Fibers* **21**(1) (2024)

31. Zhang, F., Endo, T., Qiu, W., Yang, L., Hirotsu, T.: Preparation and mechanical properties of composite of fibrous cellulose and maleated polyethylene. *J. Appl. Polym. Sci.* **84** (2002)
32. Barczewski, M., Matykiewicz, D., Mysiukiewicz, O., Maciejewski, P.: Evaluation of polypropylene hybrid composites containing glass fiber and basalt powder. *Jf. Polym. Eng.* **38** (2018)
33. Drabek, J., Zatloukal, M.: Evaluation of thermally induced degradation of branched polypropylene by using rheology and different constitutive equations. *Polymers* **8**(317) (2016)
34. Ogah, A.O., Afiukwa, J.N., Nduji, A.A.: Characterization and comparison of rheological properties of agro fiber filled high-density polyethylene bio-composites. *Open J. Polym. Chem.* **04**, 12–19 (2014). <https://doi.org/10.4236/ojpchem.2014.41002>
35. Adebayo, G.O., Hassan, A., Yahya, R., Okieimen, F., Sarih, N.M.: Dynamic rheological properties of spotted mangrove/high-density polyethylene composites. *J. Thermoplast. Compos. Mater.* **34**, 1273–1285 (2021). <https://doi.org/10.1177/0892705719870587>

P1

P2

P3

P4

P5

P6

P7

6.8. RECYCLING OF HDPE-GIANT REED COMPOSITES: PROCESSABILITY AND PERFORMANCE

P8

P9

P10

Research Article

Luis Suárez*, Mateusz Barczewski, Mark Billham, Andrzej Miklaszewski, Patryk Mietliński, and Zaida Ortega*

Recycling of HDPE-giant reed composites: Processability and performance

<https://doi.org/10.1515/gps-2024-0229>

received October 28, 2024; accepted January 30, 2025

Abstract: Giant reed (*Arundo donax*), a plant species with potential for obtaining lignocellulosic fibres, was validated as reinforcement in thermoplastic composites with good processability, thermo-mechanical performance, and aesthetics. This study evaluates the impact of closed-loop recycling of high-density polyethylene (HDPE)-based composites with up to 40% of reed fillers: fibres and shredded plants, on their processing and application properties. *Arundo* fillers do not significantly impact the processing stability and performance of recycled composites and can improve some aspects. Minor chemical composition differences were observed, highlighting oxidation resistance. All formulations keep their viscous character and reduce the melt flow index slightly, benefiting reprocessing due to the absence of degradation-prone coupling agents. The composites remain thermally stable up to 230°C, with only slight weight loss at 160°C due to lignocellulosic filler degradation. Fillers lead to longer oxidation induction time compared to neat HDPE. Reprocessed moulded materials show higher stiffness and improved ultimate tensile and flexural strength, but lower impact resistance due to shorter filler

length. Smaller fillers and improved matrix distribution also reduce water uptake. Fibrous fillers reduce the aspect ratio, making composites with shredded reed more similar to reed fibres, which are costlier to produce. Shortening of the reprocessed fibrous filler is associated with increased crystallinity in composite materials.

Keywords: giant reed, natural fibres, composites, recycling, reprocessing

1 Introduction

Increased global awareness of using sustainable resources to reduce the carbon footprint of the manufacturing industry has driven the search for new bio-based materials. Recycling and reuse strategies have also promoted advances in the recovery and upcycling of these materials. In the field of polymers and composites processing, besides the development of novel materials formulated from renewable sources and the move away from overexploitation of fossil resources, the introduction of natural fibres, such as the lignocellulosic ones, has also reduced the amount of plastic in various applications. The use of natural fibres for composite production not only allows a reduction in the consumption of polymeric matrices but also promotes the development of advanced materials with improved attributes such as better specific properties, thermal or acoustic insulation, and low cost [1,2]. Moreover, fillers derived from plant resources, besides promoting the biodegradation of polymeric compounds [3,4], represent a great opportunity for the development of more sustainable recycling strategies compared to those based on fillers of synthetic origin, such as glass or carbon fibres [5].

Giant reed (*Arundo donax* L.) is a versatile plant species that has attracted great interest due to its potential applications in green biorefineries and sustainable materials. Its high biomass yield, adaptability to different environments and low cultivation requirements make it an attractive candidate for the production of biofuels, biochemicals, and other value-added products [6,7]. This plant

* **Corresponding author: Luis Suárez**, Departamento de Ingeniería Mecánica, Universidad de Las Palmas de Gran Canaria, Edificio de Ingenierías, Campus universitario de Tafira Baja, 35017, Las Palmas, Spain, e-mail: luis.suarez@ulpgc.es

* **Corresponding author: Zaida Ortega**, Departamento de Ingeniería de Procesos, Universidad de Las Palmas de Gran Canaria, Edificio de Ingenierías, Campus universitario de Tafira Baja, 35017, Las Palmas, Spain, e-mail: zaida.ortega@ulpgc.es

Mateusz Barczewski: Poznan University of Technology, Institute of Mechanical Technology, Piotrowo 3, 61-138, Poznań, Poland

Mark Billham: AMIC-PPRC, Queen's University of Belfast, Ashby Building, BT9 5AH, Belfast, Northern Ireland, United Kingdom

Andrzej Miklaszewski: Poznan University of Technology, Institute of Materials Science and Engineering, Jana Pawla II 24, 61-139, Poznan, Poland

Patryk Mietliński: Poznan University of Technology, Institute of Mechanical Technology, Division of Metrology and Measurement Systems, Piotrowo 3, 61-138, Poznan, Poland

species, native to East Asia and widespread in subtropical and warm temperate climates around the world, can be used to produce biofuels such as biogas and bio-ethanol through biological fermentation, as well as bioenergy through direct biomass combustion [8,9]. Its high biomass production and low input requirements make it a competitive energy crop compared to other lignocellulosic feedstock [10,11]. The plant can be processed to obtain various high-value compounds, including levulinic acid, oligosaccharides, fermentable sugars, and polyphenols, demonstrating its potential for green chemistry applications [6,12]. Its biomass can also be used for producing wooden building materials such as bricks or particleboards, enhancing its role in sustainable construction [7,13–15]. In addition, its role in phytoremediation and environmental management further underscores its potential in advancing sustainable development goals. Giant reed is capable of growing in contaminated soils and improving soil fertility by accumulating pollutants in its biomass [16,17] and can be used to remove pollutants from wastewater [18], thereby improving water quality and contributing to environmental sustainability.

On the other hand, polyolefins, a class of polymers derived from olefinic hydrocarbons, or alkenes, whose discovery dates back to the 1930s, have grown exponentially since then and revolutionized the global plastics industry. These materials have transformed modern life and are still the subject of intense research and development because of their diverse applications. Due to their versatility, low cost, and mechanical properties, polyolefins have consolidated their position as the most widely manufactured and used plastic worldwide. This family of thermoplastics, including polyethylene (PE) and polypropylene (PP), make up the majority of the global plastics market, with their use and production continually increasing, reaching the global output of nearly 220 million tons/year [19]. In fact, polyolefins accounted for almost half of the demand from plastic converters in Europe in 2021 [20]. Its use in a variety of applications, including food packaging, industrial products, consumer goods, structural plastics, and medical applications, has made its recyclability a critical issue, primarily due to its extensive use in short-term applications such as packaging [21]. PE, in particular, leads the plastics industry with a market share of over 31% [4] and stands out for its versatility to be used as a matrix in the production of composites due to its excellent properties and wide range of applications. Characteristics such as toughness, near-zero moisture absorption, chemical inertness, low coefficient of friction, ease of processing, and unique electrical properties make it an ideal candidate for use in composite materials, where it can serve as a robust matrix that enhances the overall performance of the composite [22]. Moreover, PE is

not only the most commonly used thermoplastic in the polymers and composites industry but also offers great potential for continuous closed-loop recycling. Research has shown that high-density polyethylene (HDPE) can be reprocessed several times while maintaining compatible performance characteristics, thus mitigating the impacts of plastic waste [23,24].

The addition of a large variety of plant-based fillers such as jute [25], hemp [26], sugarcane bagasse [27], spent coffee grounds [28], peanut shells [29], palm [30], banana [31], or sisal fibres [32] into an HDPE matrix has been widely studied as a way to produce more sustainable materials. This strategy of obtaining biocomposites usually improves the mechanical properties of HDPE, including significant increases in stiffness and elasticity and reduces thermal stability. Good interfacial adhesion between fibres and the HDPE matrix is crucial for enhancing mechanical performance. Treatments such as mercerization, chemical functionalization, and the use of compatibilizers like maleic anhydride grafted PE have been studied [33]. However, there is still a gap in the study of the recyclability of these materials, the literature found on the effects of their reprocessing remains limited [34,35]. Not surprisingly, the properties of recycled polyolefin-based natural fibre composites (NFCs), including their viscosity, average molecular mass, crystallinity, and fibre dimensions, are significantly affected by thermo-mechanical reprocessing. Minimizing thermal degradation, oxidation, aesthetics, or mechanical performance deterioration of such materials requires careful consideration of various recycling parameters, including screw rotational speed, throughput rate, and barrel temperature profile among others [36].

In the previous work, giant reed has proven to be a promising plant species for obtaining high value-added fibres [37]. Its potential application as a reinforcing material in PE-based composites has also been reported [38,39]. These composites have excellent thermal stability allowing a wide processing window, interesting mechanical performance with efficient stress transfer and good aesthetics. The present work explores these materials in depth to analyze the effects of thermo-mechanical closed-loop recycling and to determine the changes in processability and in-use performance parameters upon reprocessing.

2 Materials and methods

2.1 Materials

NFC, based on a HDPE matrix and lignocellulosic fillers from giant reed (*Arundo donax* L.), were prepared by

twin-screw extrusion compounding, as described in a previous work [38]. The polymer used was HDPE grade HD6081 from Total Petrochemicals, with a melt flow index (MFI) of 8 g/10 min (190°C/2.16 kg) and a density of 960 kg·m⁻³, according to the producer's specifications. Besides, two different forms of Arundo-derived materials were used as reinforcement phase of the composites, namely, fibres (F), extracted from the stems of giant reeds, and shredded material (S), obtained by grinding aerial parts (stems and leaves) of the same plant species. Reed fibres were obtained after 1 week of soaking in an alkaline solution and further processing using a roller press. Once the fibre bundles were extracted from the stems, they were washed in water to neutral pH, dried, cut to a length of 3–5 mm, and sieved to remove fines and clustered particles. The procedure for preparing the shredded material consisted of chopping and drying the collected plants, shredding them with a laboratory rotary mill, washing the shredded material, drying, and sieving [37]. The fibres were cut to approximately 3 mm length, showing a diameter of $157 \pm 74 \mu\text{m}$, while shredded material shows an average particle size of $370 \pm 133 \mu\text{m}$ [37,40,41]; fibre length is reduced to $781 \pm 288 \mu\text{m}$ after compounding obtaining [38,40,42].

The composite materials were named according to the type and amount of lignocellulosic filler (in% by weight): PE.F20 and PE.F40 correspond to composites with 20% and 40% Arundo fibres respectively, while PE.S20 and PE.S40 refer to composites produced with 20% and 40% Arundo shredded material. Before recycling, the physicochemical, rheological, and thermomechanical properties of the compounds, produced by the ThermoScientific Process11 twin-screw extruder with temperatures from 170°C to 185°C, with the profile shown in the previous work [38], and the test specimens, subsequently moulded by an Arburg 320S injection moulding machine, were determined [38].

2.2 Recycling process

The original moulded parts (cycle 0) were ground at 1,400 rpm in an Alpine Augsburg shredder machine (model RO 16/8) and then reprocessed up to five times (cycles 1 to 5) using a ThermoScientific Haake Rheomex PTW 16 OS twin-

screw extruder to evaluate the effect of mechanical recycling on performance of the HDPE-Arundo composites. Reprocessing was performed with a screw rotation speed of 300 rpm and the following hopper-to-nozzle temperature profile: 170-175-170-165-165-160-160°C. The used extruder has an *L/D* ratio of 25 and a screw profile with three kneading zones as shown in Figure 1.

The same process was repeated separately for the four Arundo composite formulations (PE.F20, PE.F40, PE.S20, and PE.S40) as well as for the neat HDPE polymer (PE). After completing the five thermo-mechanical reprocessing cycles, the materials were remoulded again using an Arburg 320S injection-moulding machine (cycle 6). The nomenclature used to designate materials after this reprocessing step includes the suffix -r at the end of the name of each formulation, thus PE-r, PE.F20-r, PE.F40-r, etc.

The manufacturing parameters used for injection moulding were as follows: temperature profile (from hopper to nozzle) set at 175-180-185-185-190°C, mould temperature at 30°C, cooling time of 15 s, back pressure of 5 MPa, holding pressure of 50 MPa, and dosing volume of 50 cm³. Switchover pressure was recorded for each moulding and averaged for the different composites. Materials were dried at 60°C (–40°C dew point) overnight before processing.

2.3 Characterization

The recycled materials were subjected to several characterization tests, both on pellets and injection-moulded specimens. Prior to the moulding process, the compounds were analyzed chemically, thermally, and rheologically using Fourier transform infrared (FTIR) spectroscopy, thermogravimetry (TGA), differential scanning calorimetry (DSC), MFI, and oscillatory and capillary rheometry. In addition, the effects of the recycling process on the morphology (length, diameter, and aspect ratio) of the reinforcing particles as well as on the density and porosity of the composite materials were assessed using microcomputed tomography and optical microscopy. The injection-moulded samples were also evaluated for a number of other attributes, including hygroscopicity, changes in appearance (colour and gloss), wide-angle



Figure 1: Screw profile configuration.

X-ray scattering (WAXS), mechanical behaviour (hardness, tensile, flexural, and impact strength), dynamic mechanical thermal analysis (DMTA), heat deflection temperature (HDT), Vicat softening temperature (VST), thermal diffusivity, and thermal expansion.

FTIR spectra were obtained using a Spectrum 100 spectrophotometer from Perkin Elmer, under attenuated total reflectance mode with a zinc selenide single bounce crystal. Each spectrum was recorded with 64 scans at a resolution of 4 cm^{-1} , covering wavelengths between 4,000 and 600 cm^{-1} .

Rheological behaviour was assessed using both oscillatory and capillary rheometry. For realization tests in the oscillatory mode, the AR G2 rheometer from TA Instruments, with parallel plates of 25 mm diameter, was used. The oscillatory tests were conducted in a nitrogen environment at 190°C , and with a 2.5 mm gap. The strain sweep mode was used for preliminary testing so that subsequent experiments take place in the linear viscoelastic (LVE) region. The range of strain in these tests was 0.1–5%. In the LVE region, angular frequency sweeps between 0.01 and $100\text{ rad}\cdot\text{s}^{-1}$ were carried out at 0.5% strain. Dynisco LCR 7000 rheometer was used for capillary tests. A capillary die of 2 mm diameter (D) and $L/D = 20$ was applied. The presented results were subjected to the Rabinowitsch correction, while the Bagley correction was omitted due to the use of a die with a high L/D ratio. The applied temperature for the capillary test was 190°C . Furthermore, MFI of each material was determined according to ISO 1133 on a Kayeness Inc. 7053 apparatus (Dynisco Company) using a load of 2.16 kg and a temperature of 190°C .

The thermal properties of the materials were obtained by DSC and thermogravimetric analysis using a Perkin Elmer DSC 4000 apparatus and a Perkin Elmer TGA 4000 device, respectively. Nominal samples of $10 \pm 0.2\text{ mg}$ were prepared using sealed aluminium crucibles under a nitrogen atmosphere for DSC analysis. Thermogravimetric experiments were performed between 30°C and 900°C by heating the samples at $10^\circ\text{C}\cdot\text{min}^{-1}$ in open alumina crucibles, while DSC measurements were performed from 30°C to 200°C at the same heating rate and with two heating cycles. Melting temperatures were determined for both cycles (T_{m1} and T_{m2} , respectively) and crystallization temperatures (T_c) for the cooling step. Finally, the enthalpies of melting and crystallization (H_{m1} , H_{m2} , and H_c) were also calculated and used to obtain the degree of crystallinity (χ), as from Eq. 1:

$$\chi = \frac{1}{1 - m_f} \cdot \frac{\Delta H_m}{\Delta H_0} \cdot 100 \quad (1)$$

DSC was also applied to determine the oxidation induction time (OIT) according to the standard ISO 11357-6. For this purpose, the samples were heated from 30°C to 220°C (heating rate $20^\circ\text{C}\cdot\text{min}^{-1}$) under nitrogen flow and then

kept at 220°C for 5 min in nitrogen; the gas was then switched to oxygen, and the time required for sample oxidation was measured.

WAXS tests were carried out with Pan-analytical Empyrean, Almelo (Netherlands) equipment with the copper anode ($\text{Cu-K}\alpha - 1.54\text{ \AA}$, 45 kV, and 40 mA) in the Bragg–Brentano reflection mode configuration. The measurement parameters were adjusted to $3\text{--}60^\circ 2\theta$, with a 45 s per step 0.05° . Applying the deconvolution procedure using the Lorentzian function allows the separation of the amorphous and crystalline components from the obtained diffraction patterns. The crystallinity has been calculated according to Eq. 2 [43]:

$$X_{\text{WAXD}} = \frac{A_{\text{cr}}}{A_{\text{cr}} + A_{\text{am}}} \cdot 100\% \quad (2)$$

where A_{cr} is the sum of the area of scattering from the crystalline phase and A_{am} is the sum of the area of amorphous scattering of tested PE-based samples.

For injection-moulded specimens, HDT was determined according to ISO 75 (heating rate of $120^\circ\text{C}\cdot\text{h}^{-1}$ and load of 1.8 MPa). The VST was measured at a load of 50 N and a heating rate of $50^\circ\text{C}\cdot\text{h}^{-1}$ according to ISO 306 B50. The TPC/3 TOP VST/HDT device was used for both tests, with a minimum of three measurements for each series to average the results.

A modified Ångström method was used with a Maximus instrument (Poznan, Poland) to analyze the thermal diffusivity, following a procedure outlined by [44]. The samples were heated at 400 s using a 23 V charge on the microheater during the experiment. Thermal diffusivity (D) is determined by Eq. 3, which involves thermal conductivity (λ), density (ρ), and specific heat capacity at constant pressure (c_p) [45].

$$D = \frac{\lambda}{c_p \cdot \rho} \quad (3)$$

Thermal expansion tests were conducted using the Netzsch Hyperion TMA 402 F1 device, heating at $2^\circ\text{C}\cdot\text{min}^{-1}$ with $100\text{ mL}\cdot\text{min}^{-1}$ argon flow. Measurements covered -100°C to 100°C , split into -100°C to 25°C and 25°C to 100°C , applying 0.01 N force. Analysis was done with Netzsch Proteus software.

The variation in filler morphology was assessed before and after recycling of the composites using the method described in a previous publication [40]. Images were taken with a high-resolution flatbed scanner, Canon CanoScan LiDE 400, at 4,800 dpi and analyzed with ImageJ software to determine the length, diameter, and aspect ratio of the lignocellulosic fibres and particles.

The impact of recycling on the filler distribution and porosity of the injection-moulded samples were evaluated

using X-ray tomography, model v|tome|x s240 (Waygate Technologies/GE Sensing & Inspection Technologies GmbH), with the following specific settings: 150 kV voltage and 200 μ A current for the Microfocus X-ray tube, 150 ms exposure time per image, and 123 μ m voxel size.

The density of the materials was measured according to ISO 1183 using Archimedes' principle. This was done using a methanol medium at room temperature on a Sartorius AG precision balance. Each sample was subjected to five measurements to obtain a mean value and standard deviation.

The water absorption test, as per ISO 62, involved soaking the samples in deionized water at 23°C and measuring their weight until a stable mass was achieved. The water absorption (W) was calculated using Eq. 4 on three replicas of each sample.

$$W(\%) = \frac{W_t - W_0}{W_0} \cdot 100 \quad (4)$$

Fick's law was used to determine the rate at which water is absorbed, also calculating the diffusion coefficient:

$$D = \pi \cdot \left(\frac{k \cdot h}{4 \cdot W_m} \right)^2 \quad (5)$$

In the aforementioned formula, D represents the diffusion coefficient, h is the original sample thickness, W_m is the maximum moisture absorbed, and k is the initial slope of the water uptake curve versus $t^{1/2}$:

$$k = \frac{W_1 - W_2}{\sqrt{t_2} - \sqrt{t_1}} \quad (6)$$

Tensile and flexural tests were carried out using a Lloyd LS5 universal testing machine according to ISO 527 and ISO 178 standards, with five replicas for each material and test type. In both cases, the tests were done at a strain rate of 2 mm·min⁻¹ to determine the elastic moduli and 10 mm·min⁻¹ to evaluate the ultimate strengths. Impact strength was measured on notched specimens using a Ceast Resil impact machine in Charpy mode per ISO 179-1/1eA:2023, with a 7.5 J pendulum, 62 mm span, and 3.7 m·s⁻¹ impact speed, with 10 specimens tested. Ball indentation hardness was measured according to the ISO 2039 standard using a KB Prüftechnik device, with at least seven measurements per material series and a load of 132 N. Average values and standard deviation are provided for all properties.

DMTA was used to assess the thermo-mechanical properties of each material using a Triton 2000 device (Triton Technology). The evaluation was conducted under the single cantilever bending method, applying a strain of 10 μ m at 1 Hz frequency and a heating rate of 2°C·min⁻¹ over the temperature range of -100°C to 100°C. From the

DMTA results, the brittleness (B) and the adhesion factor (A) of the different materials by using Eqs. 7 and 8 as proposed by Brostow et al. [46] and Kubát et al. [47], respectively, were calculated.

$$B = \frac{1}{\varepsilon_b \cdot E'} \quad (7)$$

where ε_b is the elongation at break and E' is the storage modulus, both at room temperature.

$$A = \frac{1}{1 - \chi_F} \cdot \frac{\tan \delta_C}{\tan \delta_{PE}} - 1 \quad (8)$$

In Eq. 8, χ_F is the volume proportion of the filler in the composite, and $\tan \delta_C$ and $\tan \delta_{PE}$ are the damping factors of the composite and the matrix.

The entanglement factor (N) and reinforcement efficiency (r) were also assessed to measure the strength of the filler-matrix interaction. The entanglement factor (N) is calculated as follows:

$$N = \frac{E'}{R \cdot T} \quad (9)$$

In this case, R is the universal gas constant and E' is the storage modulus at a specific temperature (T), in Kelvin.

Finally, the reinforcement efficiency (r) is determined from the ratio between the storage modulus of the composite (E'_c) and the matrix (E'_m), taking into account the volume fraction of the filler (V_f):

$$E'_c = E'_m (1 + r \cdot V_f) \quad (10)$$

Changes in the aesthetic appearance of the materials after reprocessing were evaluated by optical spectroscopy, using a HunterLab Miniscan MS/S-4000S spectrophotometer for colour measurement ($L^*a^*b^*$ coordinates), and a Test An DT 268 glossmeter for determination of gloss according to ISO 2813 at measuring angles of 20°, 60°, and 85°. The total colour difference parameter (ΔE^*) is determined as shown in Eq. 11:

$$\Delta E^* = [(\Delta L^*)^2 + (\Delta a^*)^2 + (\Delta b^*)^2]^{0.5} \quad (11)$$

3 Results and discussion

3.1 Chemical structure and composition

Reprocessing of polyolefins and polyolefin-based composites is associated with the formation of various functional groups that indicate oxidative degradation. FTIR analysis has revealed increases in absorption bands corresponding to carboxylic acids, ketones, aldehydes, alcohols, and

ethers. These peaks suggest ongoing oxidation and breakdown of the polymer matrix and reinforcing fibres, particularly evident after multiple cycles [36,48]. The intensity and presence of specific peaks in the spectra can change substantially after several reprocessing cycles. For instance, the increase in absorption bands associated with oxidative degradation can show more significant oxidation levels in composites with repeated processing. Such oxidation profiles can be quantified by measuring peak heights and areas as indicators of degradation [49].

Figure 2 shows the changes observed in the FTIR spectra for the original and recycled materials. The peak patterns are very similar, with only minor variations among the different formulations of composites, both before and after recycling. Comparable results were reported by Bhattacharjee and Bajwa after six recycling cycles on HDPE composites filled with 30% wood flour [50] and by Fonseca-Valero *et al.* for five-cycle reprocessed HDPE-matrix composites with 48 wt% of cellulose fibres [49]. The broad band attributed to the O–H groups in the range of $3,600\text{--}3,000\text{ cm}^{-1}$, which was originally more intense in composite materials with 40% lignocellulosic fillers, completely disappears in all formulations after reprocessing. Meanwhile, the C–H peaks characteristic of HDPE-based composites, wavenumbers around $2,920$, $2,850$, $1,470$, and 720 cm^{-1} , are still present even after the reprocessing cycles. This is consistent with the literature, where several studies have demonstrated the oxidation resistance of HDPE [23].

On the other hand, the vibration band peak in the double bond region (above $1,500\text{ cm}^{-1}$) also disappears after recycling. The same trend is observed for the peaks in the fingerprint region from $1,400$ to 750 cm^{-1} . The high-intensity peak at $1,016\text{ cm}^{-1}$, which shows the C–O group of cellulose in the original composites, does not

completely disappear, but its signal is greatly attenuated after reprocessing.

This flattening of fingerprint characteristic absorption bands originating from the lignocellulosic filler may be related to a more homogeneous composite structure. Macromolecules of polyolefins subjected to multiple processing are shortened, which causes a decrease in the polymer viscosity [51]. The proposed analysis method is based on measurements performed for the injected surface of the samples. Due to the shortening of the fibre length and changes in the rheological properties, the surface of the injection moulded reprocessed sample reveals a homogeneous polymer skin layer without filler inclusions. It should be emphasized, however, that in the case of none of the analyzed samples, the appearance of additional absorption bands was noted in the range of the formation of carbonyl groups ($1,600\text{--}1,800\text{ cm}^{-1}$), thus meaning that no changes related to intensive degradation changes of PE matrix have aroused [52].

3.2 Rheological behaviour

3.2.1 MFI

From a rheological perspective, the processing stability of thermoplastic compounds can be assessed by examining changes in MFI [24] and, consequently, by observing fluctuations in V/P switchover pressure (changeover from the velocity to pressure control) during injection moulding [53]. The MFI of polymers tends to increase with recycling, indicating changes in molecular weight and flow behaviour. This increase may be attributed to chain scissions,

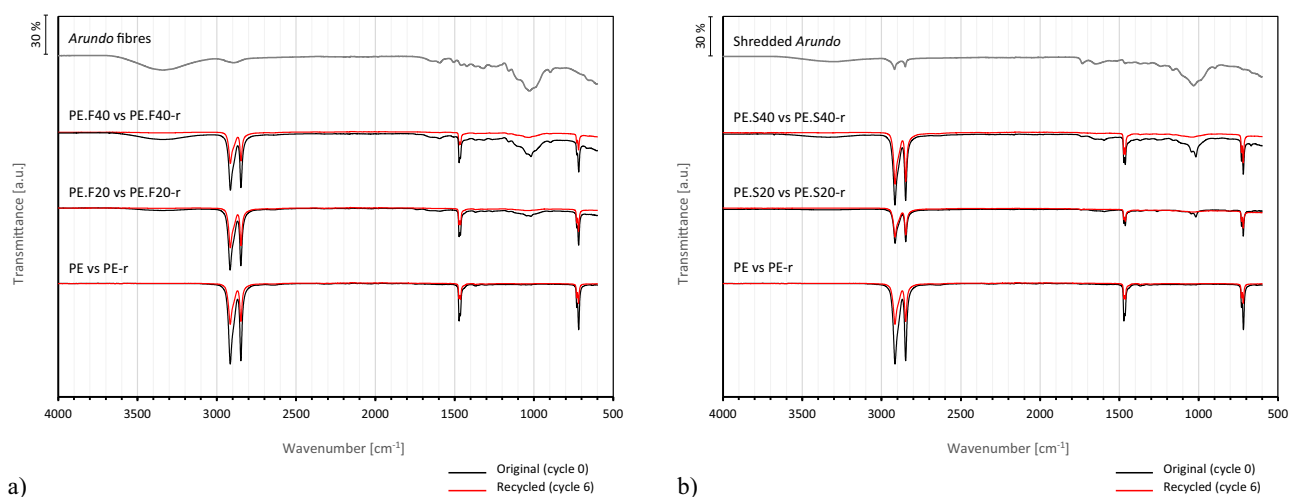


Figure 2: FTIR spectra of original (cycle 0) versus recycled composite (cycle 6) with (a) fibre and (b) shredded fillers.

in which polymer chains are broken down into shorter lengths, which can lead to increased susceptibility to oxidation. From the injection moulding side, it is worth highlighting that a steady feed in the plasticizing process is necessary to ensure product quality in terms of homogeneity, operational stability, and production speed. While continuous reprocessing of high- or low-density PE results in more difficult injection moulding due to a progressive decrease in MFI [54], the incorporation of *Arundo* fillers into the thermoplastic matrix not only does not increase the difficulty of processing but also seems to make it somewhat easier. Thus, after the reprocessing cycles, all material series show a slightly higher MFI, which is more noticeable in the biocomposites with shredded reed filler, as shown in Figure 3. Similar behaviour was observed by Fonseca-Valero et al. [49], which they attributed to the cellulose fibre degrading as a result of shear stresses, compression, and elongation on the melt during reprocessing. The size reduction of the lignocellulosic fillers, which was confirmed by microscopic observation and measurement, as described later, contributed to this behaviour.

Therefore, when comparing pure HDPE with PE.F40-r series, the required moulding pressure is only about 40% higher after recycling due to an increase in the melt flow rate and homogenization of the material blend. Any composite formulation resembles the behaviour of the PE matrix in this respect and shows no noticeable signs of deterioration.

Several studies on natural fibre-reinforced polyolefin composites have found an increase in viscosity as a result of chemical treatments to improve the matrix-reinforcement interface [55]; also lubrication effects produced by

coupling agents have been reported [56]. However, it has also been concluded that these effects largely disappear with recycling cycles [57]. The lack of binding additives or treatments in the HDPE-*Arundo* compounding favoured a slight improvement rather than a worsening of processability throughout the closed-loop recycling.

3.2.2 Oscillatory and capillary rheometry

The rheological properties, which directly influence the moulding process, are assessed by rheological curves obtained by oscillatory (Figure 4) and capillary rheometry (Figure 5).

Different behaviours were observed depending on the geometry of the measuring system, which resulted from the characteristic flow properties of filled polymeric systems. From oscillatory rheology tests, it can be seen that fibrous composites tend to increase viscosity, while composites with shredded material show a lower impact on complex viscosity, which can be related to the lower ability of this filler to create a 3D physical network of hindered particles in composite melt compared to fibres. In all samples, a predominant viscous character is evidenced by a higher loss moduli compared to storage one. Fibrous composites tend to increase the storage modulus with reprocessing along the angular frequency analyzed, while the series with shredded materials show the opposite behaviour. In any case, the differences between the curves before and after recycling decrease with increasing filler and are lower for fibrous composites than shredded plant material. Finally, no significant changes in the rheological behaviour of the pure PE were observed, supporting the

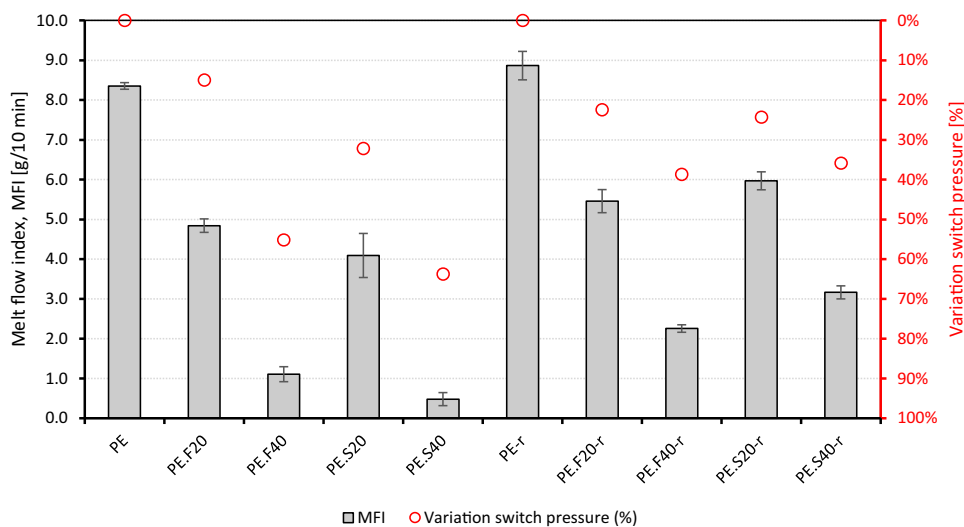


Figure 3: MFI and switchover pressure variation for the different materials.

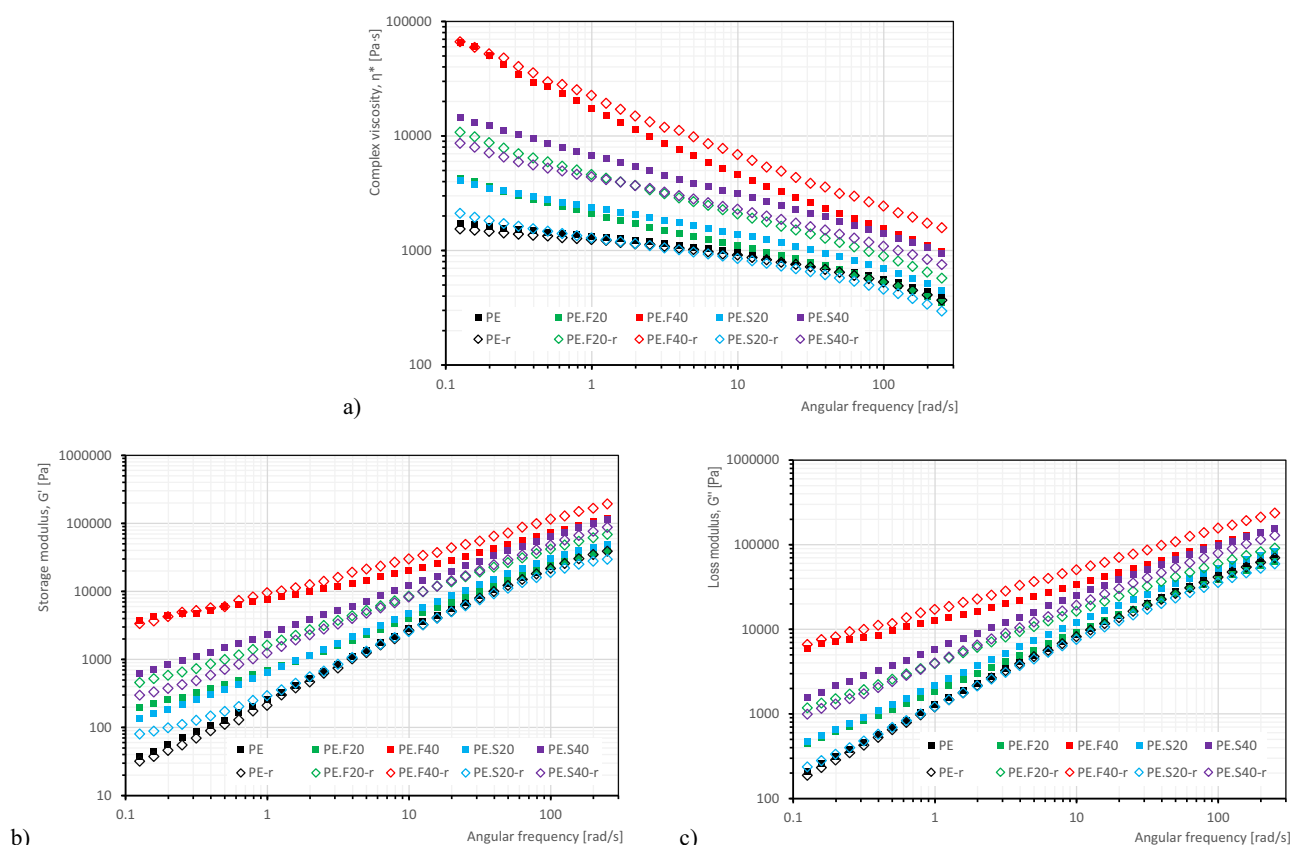


Figure 4: Oscillatory rheology results: (a) complex viscosity, (b) storage modulus, and (c) loss modulus.

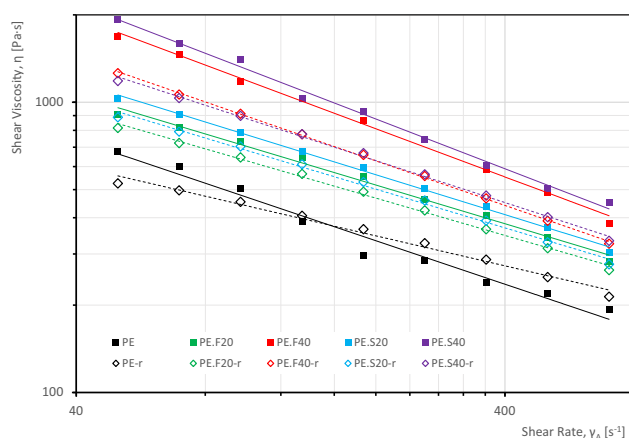


Figure 5: Capillary rheology results: Shear viscosity vs shear rate.

FTIR observations by showing that the matrix does not undergo oxidation or cross-linking as a result of reprocessing.

In addition, from capillary rheology tests (Figure 5), it was found that both before and after reprocessing, the fibrous composite materials were characterized by slightly lower viscosities compared to the shredded ones. This may be because the fibres can align more easily in the direction of flow [58,59]. Finally, the flow resistance of the composites

with 40% filler after recycling is almost identical regardless of the type of filler.

3.3 Thermal behaviour

3.3.1 TGA

The thermogravimetric analysis (Figure 6) shows that all compounds remain thermally stable, even after recycling, up to approximately 40°C above the processing temperature, despite a small weight loss (lower than 2%) upon reaching 160°C, which is only noticeable in the 40% loaded composites, and probably due to an initial degradation of the lignocellulosic fillers after multiple reprocessing. Similarly to the original composites, the thermal stability of the recycled compounds varies depending on the loading percentage, regardless of the type of filler, with the first degradation peak (from derivative thermogravimetry [DTG]) occurring around 350°C. The PE.F40-r and PE.S40-r formulations undergo a faster degradation, resulting in a mass loss of around 25% at this initial peak, related to the biomass degradation; however, the composites with 20%

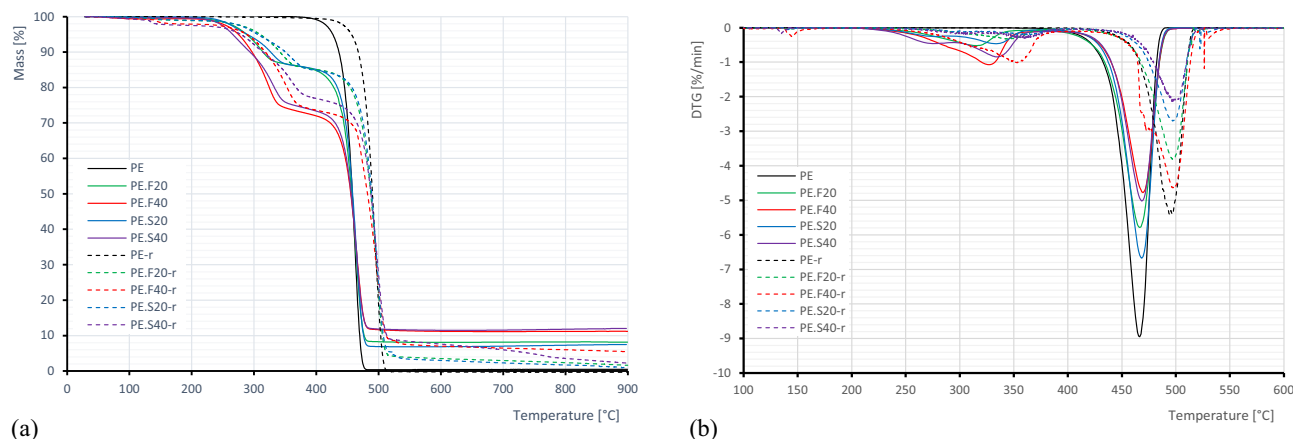


Figure 6: (a) TG and (b) DTG curves pre- and post-recycling processes.

lignocellulosic material degrade at a much slower rate; this is following the same trend observed in the nonrecycled materials. Thus, the increase in the amount of plant filler correlates with a higher weight loss due to thermal degradation of said filler, as expected. In any case, the most significant peak occurs when the decomposition temperature of the HDPE matrix is reached. After the recycling cycles, this point is delayed by about 30°C for all materials due to the removal of volatile or labile compounds during the previous processing [50,56,60]. Regarding the residual mass after reaching 900°C, also the composite with 40% fibres is the only one in which the amount of inorganic compounds present after carbonization exceeds 5% of the initial mass.

3.3.2 DSC

Based on DSC results, it can be seen that the recycling process minimally affects the temperatures of the phase transitions. When analyzing the thermal behaviour before and after reprocessing, it is noted that there are no major

variations in melting temperatures, with T_{m2} in the range of 134.6–135.6°C for all materials, and only a minimal rise in crystallization temperatures, less than 5°C for recycled ones, as shown in Table 1. These findings align with previous research on HDPE-based composites, indicating that neither the presence of lignocellulosic materials nor reprocessing cycles significantly influence melting and crystallization temperatures [61,62].

On the other hand, it has been observed that neat HDPE experiences a decrease in the enthalpies of melting and crystallization after going through reprocessing cycles, whereas the lignocellulosic-filled materials exhibit a noticeable increase of 20–40% in energy flow compared to the original composites. The composite materials also show a slight increase in their degree of crystallinity, which can be attributed to the reduction in particle size and its nucleation effect, as described by Chen and Yan [63]. These authors correlate the nucleation ability of lignocellulosic fibres in HDPE-based composites (without any coupling agent) not only with their topography, surface energy, wettability, and chemical composition but also with the presence of

Table 1: DSC test results for all materials before and after reprocessing

Material	T_{m1} (°C)	T_{m2} (°C)	T_c (°C)	ΔH_{m1} (J·g ⁻¹)	ΔH_{m2} (J·g ⁻¹)	ΔH_c (J·g ⁻¹)	χ_1 (%)	χ_2 (%)	OIT (min)
PE	132.7	135.3	112.9	175.4	172.6	193.3	59.9	58.9	36.8
PE.F20	136.9	134.7	111.5	118.7	125.8	135.8	50.6	53.7	51.3
PE.F40	132.7	133.9	113.1	108.6	109.5	108.4	61.8	62.3	76.1
PE.S20	137.2	136.2	111.1	119.4	128.4	140.8	50.9	54.8	45.4
PE.S40	133.0	135.0	112.1	76.4	79.8	82.5	43.5	45.4	27.1
PE-r	134.6	135.6	116.5	142.7	164.6	165.2	48.7	56.2	7.9
PE.F20-r	135.6	135.5	114.1	156.5	156.4	164.1	66.8	66.7	19.3
PE.F40-r	136.8	135.6	113.5	134.2	152.5	155.2	76.3	86.8	29.4
PE.S20-r	133.9	135.0	114.5	139.3	165.2	172.5	59.4	70.5	18.1
PE.S40-r	136.4	134.6	117.0	101.9	96.6	95.7	58.0	55.0	11.8

fibres of very short length (1.15 ± 0.86 mm), in the same size range used in the present work.

3.3.3 OIT

The reprocessing of polymer composites can have profound effects on their oxidation stability. Thermal processing can cause oxidation of polymers, which can be accelerated by factors such as high processing temperatures and extended residence times in the extruder [64]. Prolonged exposure to high temperatures near decomposition points can result in the formation of decomposition products that further alter material properties. Thus, degradation resulting from repeated exposure can lead to weaker bonds and unsaturated structures, which negatively impact the composites' mechanical properties and thermal stability [50]. During the first processing cycle, the reed fibre increased the oxidation time of the polymeric compounds (Table 1), even duplicating it in the case of 40% loading with respect to neat PE. After recycling, a drastic reduction in OIT was observed for all materials. However, the formulation with a higher *Arundo* fibre content managed to counteract this effect by only 20% compared to the virgin polymer matrix. Therefore, the *Arundo*-derived fillers are providing interesting stabilizing features to the PE matrix, due to their content in phenolic groups, mainly coming from lignin; other researchers have recently proposed the use of postconsumption coffee or tea solids or spent brewery grains as a way to valorize these residues while becoming a source of antioxidant stabilizing the polymer [60,65,66].

3.3.4 Thermal diffusivity

Few studies have been found in the literature on the parameters of thermal diffusivity and how it relates to the dimensional stability of lignocellulosic composites [67]. For some applications, however, it may be very interesting to analyze the heat transfer rate through the material. Figure 7 shows the mean values and standard deviation of the thermal diffusivity of PE and reed composites in injection moulded parts with the original materials and after several thermo-mechanical processing cycles. After the first cycle, only the PE.F40 series showed a significant increase in heat transfer rate, while after reprocessing, all lignocellulosic composites show an increase in their thermal diffusivity.

3.3.5 Thermal expansion

The results of the thermomechanical analysis (TMA) show the changes in length (dL/L_0) and thermal expansion coefficients (α) of the different materials before and after reprocessing, determined in three temperature ranges (-100°C to 25°C ; 25°C to 100°C ; -100°C to 100°C). Figure 8a shows that the introduction of lignocellulosic reinforcement contributes to the higher dimensional stability of the original composites over the entire analyzed temperature range compared to the PE matrix. The decrease in thermal expansion is more significant in fibrous composites and particularly in those reinforced with 40% *Arundo* fibres. This seems to be related to the formation of a network of physical interactions between the dispersed fibres

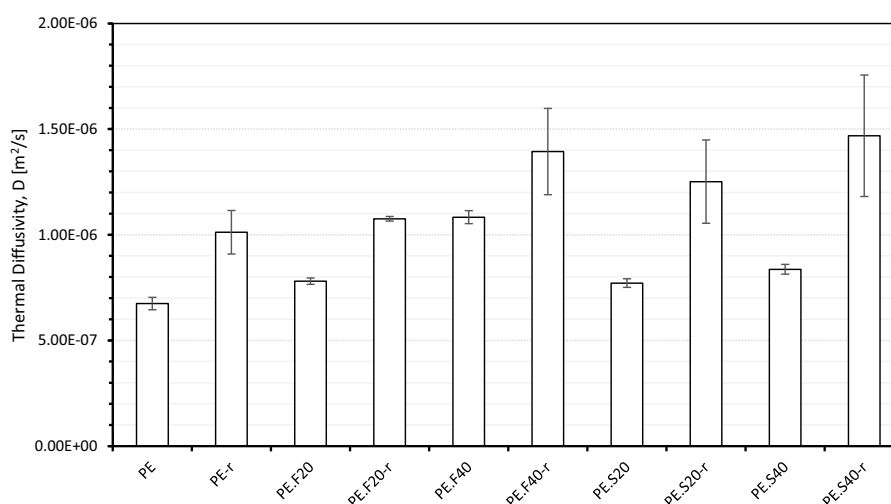


Figure 7: Thermal diffusivity of PE-Arundo composites.

within the matrix that significantly restricts their mobility and greater consistency to create 3D steric hindrances in the sample volume, as described in the previous work [67].

Regarding the recycling effect on the variation of relative length change, reprocessing leads to a slight increase in the dimensional variation of the composites with temperature due to the shortening of the fillers and consequently, a lower restriction in the mobility of the polymer matrix. However, the material with 20% shredded reed shows an opposite behaviour above -16°C . Thus, over the entire temperature range, this formulation (PE.S20-r) shows an almost identical trend to the composites with 20% fibrous filler after reprocessing (PE.F20-r). This is in agreement with the results of the morphological analysis of the composites with a lower proportion of fillers, as well as with the thermo-mechanical performance of both formulations loaded at 20% after recycling. The higher shortening rate of fibres after multiple extrusions leads to an equivalent performance to that of composites made from shredded reed. From this perspective, it can be concluded that the use of shredded reed as reinforcement in low-load composite materials is a more cost-effective option when reprocessing

is considered, taking into account the more economical and sustainable nature of its production process [37].

In terms of thermal expansion coefficients, only neat HDPE and the 20% shredded series show a significant reduction in α over the entire temperature range. If we limit the analysis to the most likely temperature range for conventional use (-100°C to 25°C), PE-r shows a reduction in α of 13%, while PE.S20-r reduces this factor by 35%, as shown in Figure 8b. The other formulations keep similar expansion coefficients in this interval even after recycling and expand to a greater extent when the temperature is increased beyond 25°C .

3.4 Mechanical and thermo-mechanical performance

3.4.1 Deflection and softening temperatures

It was found that thermo-mechanical performance evaluated in static load conditions and non-isothermal conditions, such as HDT and VST, were significantly affected by successive reprocessing, as shown in Table 2. Both

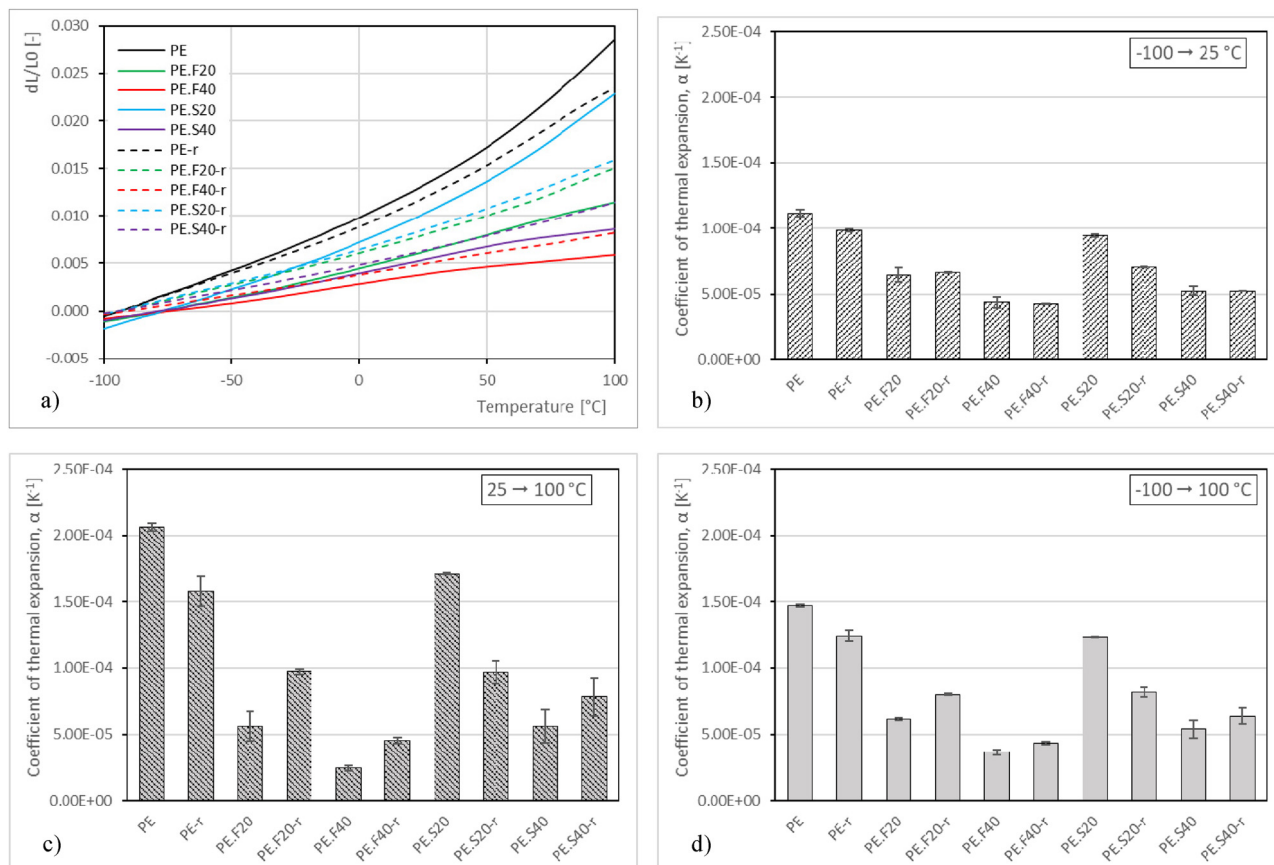


Figure 8: TMA results: (a) changes in length and average coefficients of thermal expansion within temperature intervals of (b) -100°C to 25°C , (c) 25°C to 100°C , and (d) -100°C to 100°C .

Table 2: Average values (\pm standard deviations) for mechanical and thermo-mechanical properties of HDPE matrix and Arundo composites before and after closed-loop reprocessing

Material	HDT (°C)	VST (°C)	Ball indentation hardness (N·mm ⁻²)	Impact strength (kJ·m ⁻²)	Tensile properties		Flexural properties		DMTA	
					Ultimate strength (MPa)	Elastic modulus (MPa)	Ultimate strength (MPa)	Elastic modulus (MPa)	E' (10 ⁹ Pa)	B (10 ⁻⁹ Pa ⁻¹ ·s ⁻¹)
PE	41.0 ± 1.3	72.3 ± 1.6	44.0 ± 0.5	6.4 ± 0.1	19.0 ± 0.1	1,058.5 ± 16.9	26.5 ± 0.1	753.1 ± 56.1	1.402	<0.04
PE.F20	57.3 ± 1.3	81.3 ± 1.6	52.0 ± 1.3	7.5 ± 0.2	19.0 ± 0.1	1,881.6 ± 45.1	30.5 ± 0.2	1,538.2 ± 77.9	1.734	0.63
PE.F40	72.9 ± 1.6	85.8 ± 3.0	59.6 ± 2.9	7.1 ± 0.1	17.5 ± 0.1	2,022.8 ± 98.1	30.6 ± 0.2	1,270.7 ± 125.7	1.928	1.36
PE.S20	55.3 ± 2.0	78.9 ± 0.3	49.9 ± 2.0	6.1 ± 0.1	19.0 ± 0.1	1,490.9 ± 28.7	30.6 ± 0.3	1,469.7 ± 23.4	1.659	0.86
PE.S40	67.5 ± 4.7	83.4 ± 1.9	57.3 ± 1.2	5.5 ± 0.2	16.4 ± 0.3	1,675.3 ± 119.4	28.9 ± 0.3	767.8 ± 73.9	1.782	2.08
PE-r	42.4 ± 1.3	72.5 ± 1.2	35.7 ± 0.5	6.5 ± 0.5	21.7 ± 0.1	1,399.5 ± 29.7	31.3 ± 0.4	931.4 ± 43.1	1.874	<0.04
PE.F20-r	52.2 ± 0.4	75.2 ± 1.0	39.1 ± 0.9	6.3 ± 0.0	19.4 ± 0.0	2,003.5 ± 53.3	33.0 ± 0.3	2,088.2 ± 51.9	2.458	0.23
PE.F40-r	66.0 ± 0.2	76.3 ± 1.0	44.3 ± 0.5	5.7 ± 0.1	18.3 ± 0.1	2,919.9 ± 121.8	35.1 ± 0.2	2,935.5 ± 77.3	2.598	0.88
PE.S20-r	50.1 ± 1.0	74.7 ± 1.1	38.8 ± 0.9	4.8 ± 0.1	19.2 ± 0.2	1,914.8 ± 58.9	33.8 ± 0.2	1,778.1 ± 48.6	2.161	0.36
PE.S40-r	59.1 ± 0.1	76.6 ± 1.7	43.4 ± 0.9	4.9 ± 0.1	18.0 ± 0.1	2,542.2 ± 54.8	34.8 ± 0.5	2,359.9 ± 155.1	2.434	0.89

Tukey tests were used to compare the properties of the different material groups with a 95% confidence level. *P*-values for the pairwise comparison of each property are reported in the Supplementary Material section (Tables S1–S8).

properties are reduced after recycling for all series, starting to deform under load at lower temperatures (between 4.2°C and 9.4°C below), with the effect being more noticeable in composites with higher lignocellulosic filler loadings. This effect is consistent with the results reported by Bhattacharjee and Bajwa [50], where a similar trend in the evolution of thermo-mechanical properties after six reprocessing cycles of HDPE-based composites was found, but contrasts with the results of the same authors regarding the effects of continuous recycling on the remaining stiffness properties: tensile modulus, flexural modulus, and storage modulus.

3.4.2 Mechanical properties

Figure 9 shows an overview of the variation in the mechanical properties of the original and reprocessed materials. If we look at the stiffness under quasi-static tensile and bending tests at room temperature, increases of up to 50% and 200%, respectively, are observed for the PE.S40-r series. Similar rigidity gains, even at higher absolute values, are achieved for composites with 40% fibres. Meanwhile, recycled materials with lower biomass content are also moderately stiffer (up to 30% in flexural modulus). Ultimate tensile and flexural strength results are as well slightly above the initial values for all series, with all variations

being statistically significant as a function of both the type and the amount of filler following analysis of variance and Tukey's post hoc tests (Supplementary Material). The stiffening in recycled composites is mainly due to the predominance of cross-linking reactions in the polymer matrix structure [68] since no improvement in phase bonding was observed as a result of thermo-mechanical reprocessing following the adhesion factor (A) calculated from the DMTA tests.

The increased cellulose filler content contributes to the stiffening of the polymeric material in the original composites with both types of fillers as a result of the distribution of stiff filler structures in the boundary layer [38]. The recycling process leads to a further increase of this property for all series due to the increase in the rigidity of the matrix. It is observed that the elastic modulus for the original material is more dependent on the type of filler, while this trend changes for the recycled materials. This is presumably a consequence of the smaller size of the rigid particles and the lower aspect ratio of the fibres, which explains the reduced difference in the elastic modulus between fibres and shredded samples series. Therefore, the aspect ratio has a more pronounced impact on stiffness than the type of filler. Regarding the impact strength, the results of the prior research indicating that a higher MFI lowers the toughness of composites [69] are supported by the correlation between increased flowability and lower impact

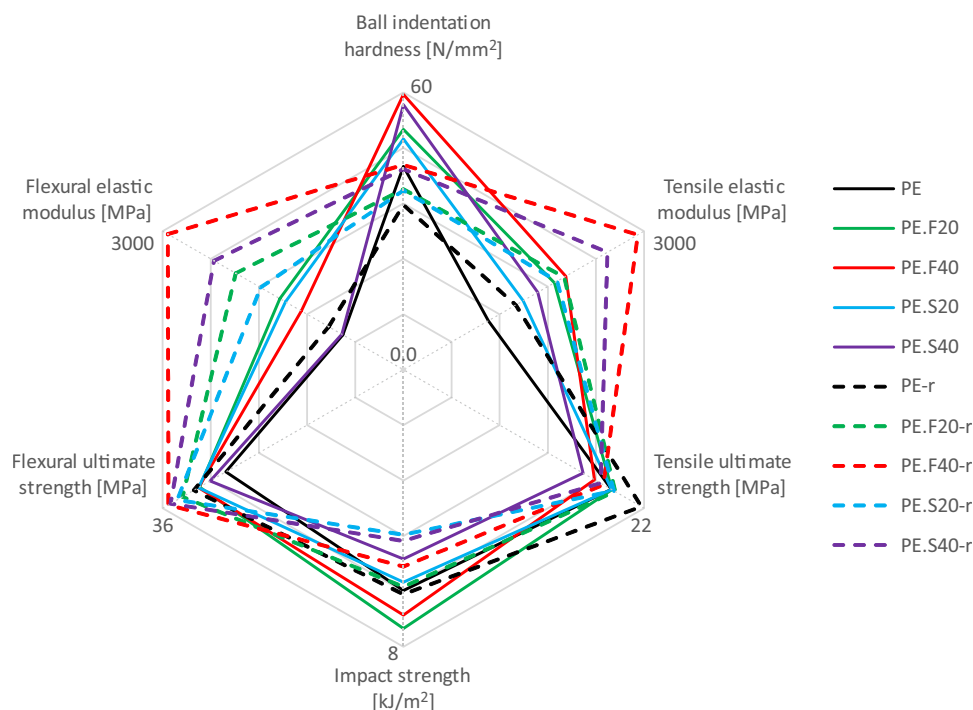


Figure 9: Overall results on the mechanical properties of the original and reprocessed materials.

resistance after reprocessing. As in the first injection moulding, composites with fibrous fillers have higher impact strength than those with shredded material after reprocessing.

3.4.3 DMTA

DMTA provides valuable information on the viscoelastic behaviour of thermoplastic composites at different temperatures and loading rates. By measuring dynamic parameters such as storage modulus (E'), loss modulus (E''), and

damping factor ($\tan \delta$), which are temperature dependent and reveal insights into the interfacial bonding between the fillers and polymer matrix, it is possible to emphasize the rheological behaviour of NFC in terms of energy dissipation under cyclic load [70].

During the first moulding (cycle 0), it was found that all composite series produced higher storage modulus than neat HDPE, meaning that plant fillers stiffen the matrix over the studied temperature window [38]. After the reprocessing (cycle 6), the composites, as well as the PE matrix, undergo an even greater rise in storage moduli that reach average values 64% higher than those of the original

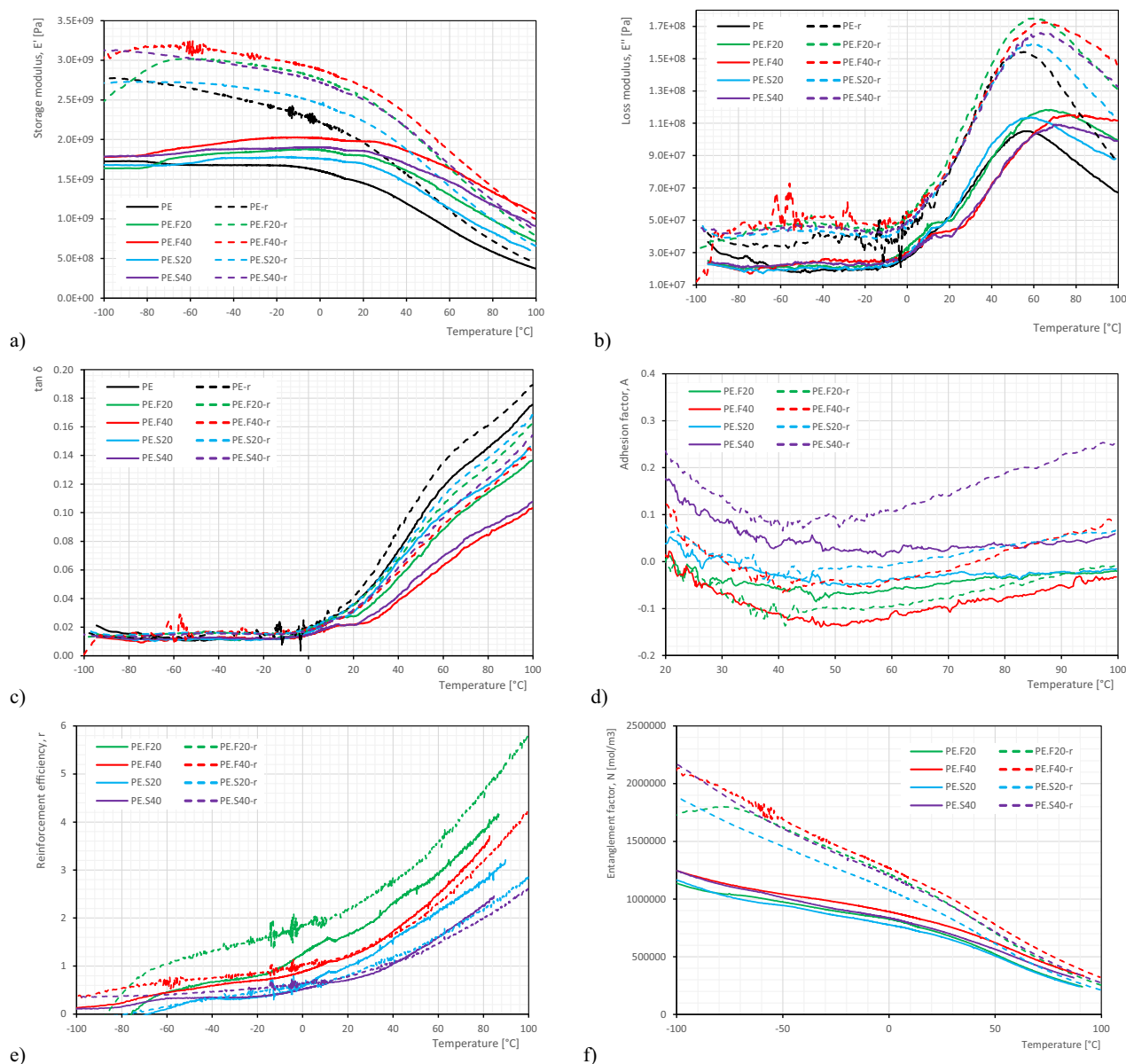


Figure 10: Variation of (a) storage modulus, (b) loss modulus, (c) loss factor, (d) adhesion factor, (e) entanglement factor, and (f) reinforcement efficiency from DMTA.

materials at -60°C , increased by 49% at -20°C and 37% above at 20°C (Figure 10a). It is worth noting that, compared to the initial processing stage, after recycling, the type of filler is more decisive in the evolution of storage modulus than the loading amount for the range of temperatures studied. The defibrillation and entanglement of the reed fibres within the matrix favour stress transmission largely than the irregularly shaped particles of the shredded filler.

Both the recycled *Arundo* composites and HDPE matrix show higher loss moduli than the original materials (Figure 10b), which means that reprocessing provides a lower elastic recovery and a more predominantly viscous behaviour, as observed in the rheological analysis. Maximum loss modulus values occur at about 60°C for all recycled series, with the higher loading composites shifting this value about 7°C lower compared to the first processing cycle. This temperature represents the α -relaxation, associated with an interlamellar shear process of HDPE, which is usually in the range from 20°C to 70°C [71]. This peak in E'' curve corresponds to the transformation from the rigid phase to the viscous state and represents the highest service temperature for composite applications, which is consistent with the results observed from the HDT and VST tests.

The α -transition is also observed as an inflection in the curves in $\tan \delta$ plots (Figure 10c). Loss factor curves show another inflection point between 0°C and 10°C , which can be attributed to the slippage or relaxation of the crystalline regions in PE, rather than the glass transition of the amorphous regions [72,73]. Although no significant variation of loss factor was observed in the temperature range from -100°C to this inflection point, all series show an increase in $\tan \delta$ beyond it. This trend is opposite to that found by Ramzy [74] when recycling hemp and sisal reinforced PP composites and indicates a deterioration in fatigue performance of HDPE-*Arundo* composites after recycling.

The brittleness (B) of the different formulations at 25°C is reduced by about 60% for all composites, except for the PE.F40-r series, which only improves this mechanical property by about a third as shown in Table 2. The main reason for this different behaviour is the lower increase in ductility for materials with 40% fibre content after thermo-mechanical processing. The elongation at break (ϵ_b) of the PE.F40-r series is only 15% higher than that of PE.F40, while the other composites can achieve elongations 70–90% longer compared to the original materials. The relative increase of the entanglement factor together with the higher stiffness of the fibres, in a higher weight ratio, might explain the lower change in the stretchability of these samples despite the reduction in the fibre size.

The adhesion of reinforcing materials in NFC depends on the affinity between the phases. It is well known that polyolefins have a nonpolar and hydrophobic character, and a difference in polarity with respect to plant fibres causes a deterioration of mechanical properties of composites [75]. Since lower values of A indicate higher interfacial adhesion [76], it can be deduced from Figure 10c that this condition is only met when reprocessing 20% fibre material. The remaining reed composites seem to show weaker adhesion after reprocessing. This could be due to thermo-oxidative degradation of cellulose fillers over multiple reprocessing cycles as demonstrated by Fonseca-Valero et al. [49].

Entanglement factor (n) and reinforcement efficiency (r) have been also used to assess the degree of intertwining of fibres within the matrix and how effectively the plant fillers enhance the composite's strength. As with the original material, fibre composites with lower loading have the highest intertwining factor after the closed-loop recycling process (Figure 10e), which could be related to the more brittle character described earlier. In terms of reinforcement efficiency, the better mechanical performance of the fibrous composites is once again confirmed, being the 20% the only series providing a clear positive change after reprocessing in reinforcement efficiency, while the entanglement factor increases for all composites due to the higher homogeneity achieved.

3.5 Morphological analysis

3.5.1 WAXS

Figure 11 shows X-ray diffraction patterns of the PE and its composites obtained by injection moulding before (black line) and after six reprocessing cycles (red line). In the case of all WAXS patterns, characteristics for PE reflections at 21.4° , 23.8° , 29.3° , and 36.2° are observed, which correspond to crystal planes (110), (200), (210), and (020) results from the orthorhombic characteristic of crystalline structure developed in the polymer [77,78]. In the case of pure PE, additional diffraction reflection is observed in the plane (010) at 19.4° , corresponding to the developed monoclinic phase [78]. Taking into account the diffractometric characteristics of the used filler described in our earlier work [37], the change in the shape of the WAXS pattern of composite samples is justified. In the case of shredded and fibrous reed-based fillers, broad diffractometric peaks with a maximum at $2\theta = 22\text{--}23^{\circ}$ are observed at (002) crystallographic plane originated from cellulose I [79] and (101), attributed

to crystalline cellulose phase [80]. In the case of composite materials, the maximum intensity of the diffraction peaks was limited; the higher the filler content, the lower it was. This effect was more pronounced for the shredded material. The sixfold reprocessing increased the intensity of the observed diffractometric peaks for all the given materials. Figure 12 presents the crystallinity values calculated according to Eq. 2. The introduction of lignocellulose fillers reduced the crystallinity of the original materials. These results are in line with those reported by Sewda and Maiti [81]. However, it should be considered that the external layer of the materials formed was studied at very high cooling and shear rates, which may influence the crystalline structure at the sample surface due to the effects of frozen-in molecular elongation and lamellae orientation [82]. Moreover, solidification conditions different from

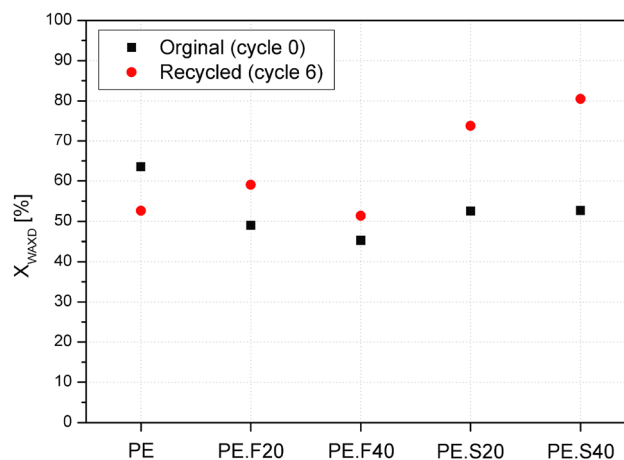


Figure 12: WAXS-based crystallinity of PE and its composites before and after reprocessing.

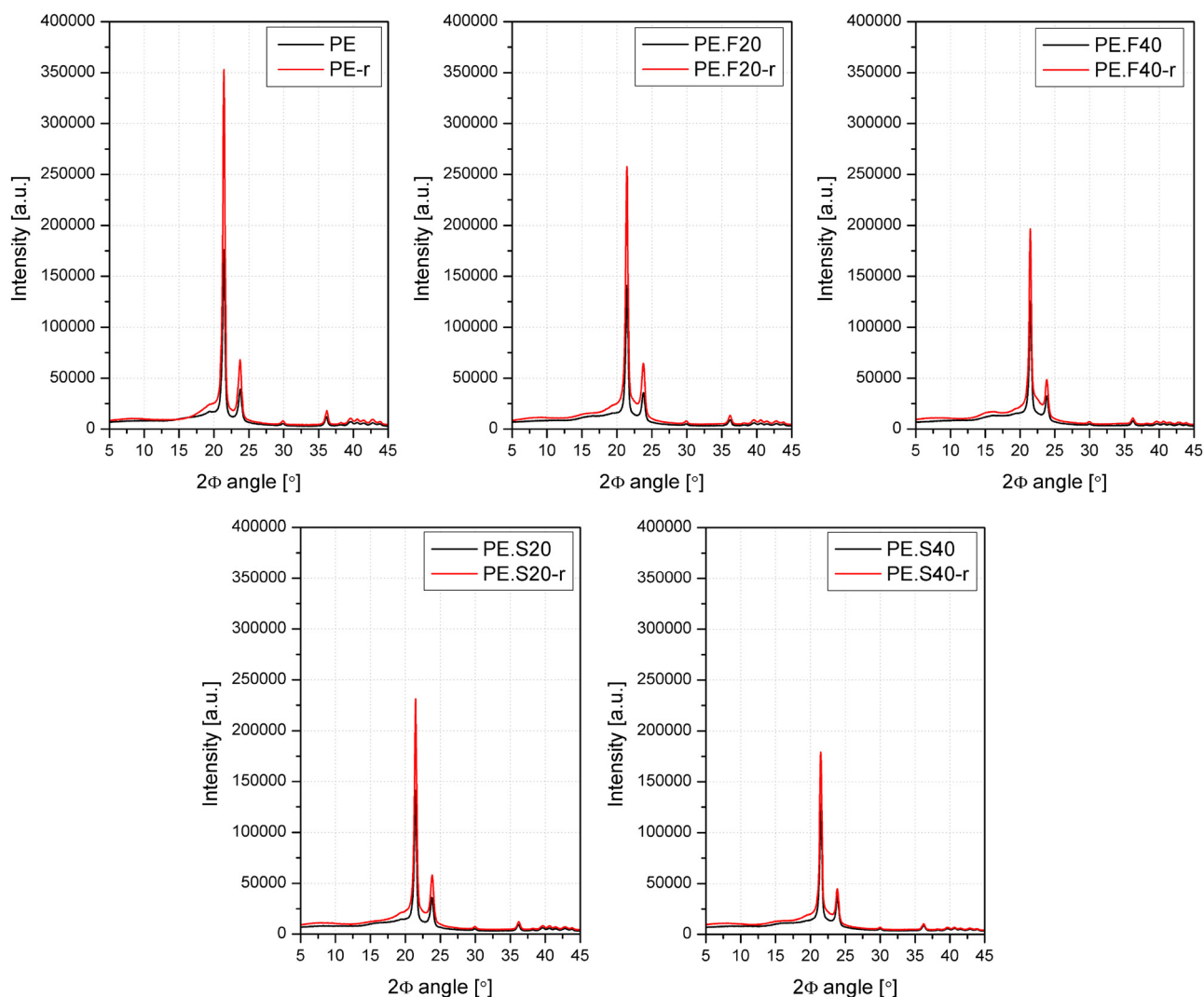


Figure 11: WAXS patterns of original (cycle 0) and recycled (cycle 6) PE and its composites.

those in the case of samples tested by DSC may provide differences in the values determined by those analytical techniques. Considering the determined crystallinity based on diffractometric analysis results (Figure 12), an opposite trend can be observed in the case of pure PE and composites in the change of the degree of crystallinity induced by reprocessing, which is in line with the DSC results from the first heating. In the case of PE, reprocessing probably caused an intensive chain scission phenomenon, leading to the shortening of macromolecules and, due to degradative changes, an increase in the share of amorphous domains. The phenomenon of partial shortening of main PE chains probably also took place in the case of reed-filled materials. However, in this case, the effect of increasing crystallinity is observed. It suggests that macromolecules with lower molecular weight were more susceptible to heterogeneous nucleation caused by dispersed polymeric matrix fillers.

3.5.2 Particle size assessment

Filler size and distribution are some of the most influential parameters on both the mechanical performance, water uptake and thermal behaviour of short fibre-reinforced polymer composites. Figure 13 shows how the aspect ratio of *Arundo* fibres decreases after reprocessing, while for shredded reed it remains largely unchanged at lower values. The variation in aspect ratio is a consequence of shortening of the fibre length due to mechanical reprocessing; this is reduced, on average, by a quarter of its initial length. A similar length variation was reported by Lila et al. after five cycles of extrusion and injection moulding on bagasse fibre-reinforced PP [83]. The diameter of the fibrous filler remains practically unchanged at around 125 microns, as an average value. Benoit, in her study on

long-term closed-loop recycling of HDPE/flax composites, found that fibre breakage occurs primarily during the first cycles [57]. After a few reprocessing cycles, there is no significant variation in either length or aspect ratio, although a decrease in standard deviation is noted, indicating that the distribution tends to become smaller with recycling.

On the other hand, the shredded filler undergoes size changes of the same order of magnitude in both length and diameter. For this reason, the aspect ratio of the irregularly shaped particles remains practically unchanged. The lower reinforcement efficiency and impact strength of the recycled shredded composites in comparison to the fibrous ones can be explained by this difference in fillers size and aspect ratio, as for the first injection moulding.

3.5.3 Density and porosity

The increased fibre content in PE-based composites generally results in higher density due to the mass contribution of the lignocellulosic fibres. However, it is reasonable to expect that the effective density might drop in comparison to the original composite if the plant fillers deteriorate during reprocessing. This effect could be accentuated in cases where the surface and interfacial areas become compromised, resulting in weaker bonds. Thus, according to some studies found in the literature, reprocessing can lead to a reduction in the overall density of HDPE-based composites due to the degradation of raw materials, especially when the reinforcing cellulose fillers lose their structural integrity and decrease in crystallinity over successive processing cycles [68,84].

In this case, as expected due to the density of the fillers, the more the lignocellulosic material in the composite, the higher the density measured. However, when comparing

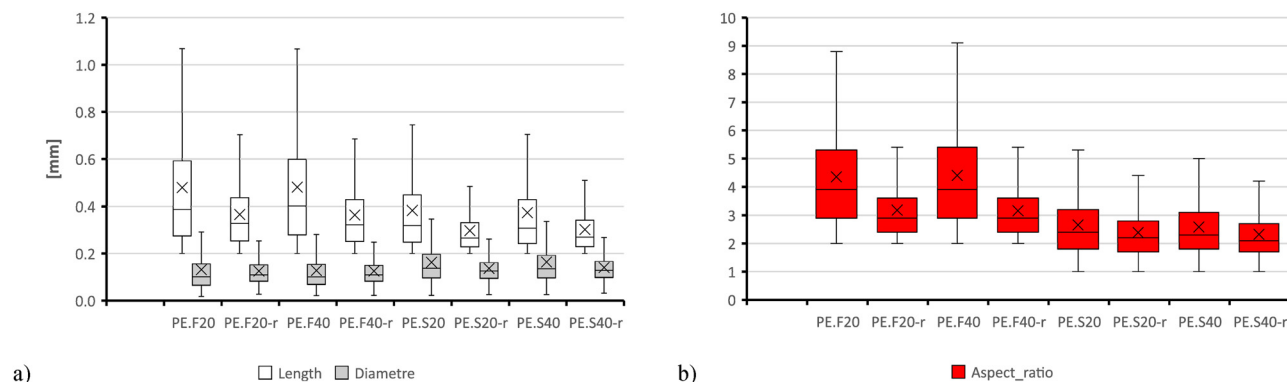


Figure 13: Variations in (a) length and diameter and (b) aspect ratio of filler particles due to reprocessing.

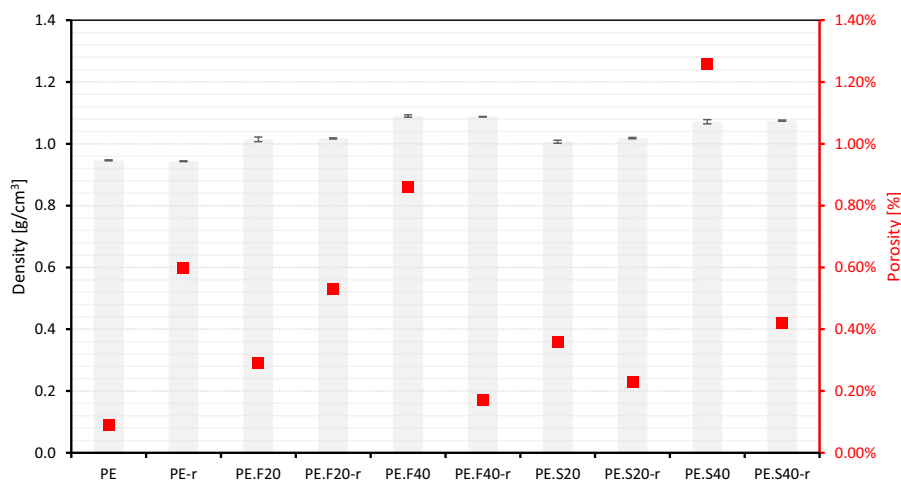


Figure 14: Average density and porosity of original vs recycled materials.

the density of injection-moulded samples in cycle 0 and cycle 6, almost identical specific weights were measured before and after recycling each material formulation, for both fibres and shredded reed fillers. This is consistent with the density progression reported on long-term closed-loop recycling of HDPE/flax composites, in which negligible fluctuations of density were also observed [57]. It should be mentioned that, in the present work, the original and reprocessed materials were moulded using the same injection process parameters. Therefore, the lower MFI in the recycled composites might have influenced the compactness of the samples.

An increase in porosity due to the breakdown of fibre structures, which could create gaps in the matrix, is another possible effect of composites reprocessing. The presence of voids not only affects the mechanical attributes

but also the physical properties such as density or hygroscopicity. The porosity in Figure 14 is determined by X-ray tomography on injection-moulded samples (80 mm long, 10 mm wide, and 4 mm thick). The most significant variations in the amount of trapped air voids were observed for the 40% filler samples, with a reduction in the pore volume of nearly 0.8% after five cycles of extrusion reprocessing and subsequent injection moulding of the composites (Figure 15).

3.6 Water absorption

Despite the hydrophobic nature of HDPE, which generally saturates to less than 1% without significant swelling, NFC



Figure 15: 3D computed tomography images presenting pores distribution.

based on this type of thermoplastic matrix may present a high level of water uptake influenced by the presence of pores, gaps between the polymer and the reinforcing phase, or micro-cracks affecting the water permeability within the matrix/filler [27,62].

By adding plant fibres to the polymer matrix, the water absorption capacity of NFC is significantly increased. This is mainly due to the hydrophilic nature of lignocellulosic fibres, which makes these materials more susceptible to swelling and dimensional instability. On the other hand, reprocessing significantly influences the water absorption properties of composite materials, particularly those reinforced with natural fibres. Some research works indicate that with each successive reprocessing cycle, the water absorption rate and capacity of composites tend to decrease [85]. For instance, a study on mechanical recycling of biobased PE-agave fibre composites found a reduction of approximately 11% in maximum water absorption capacity between the first and fourth cycles [86]. The smaller size of the fibres and their better dispersion within the matrix as the number of cycles increases are responsible for this decrease, as they improve the encapsulation of the filler and reduce the voids between the two phases of the composite.

Figure 16 shows the water absorption during 4 weeks of immersion in distilled water at room temperature for moulded parts made from the different studied materials in cycle 0 and cycle 6. Maximum water absorption typically occurs over long periods; González-Aguilar reported a time of 1,000–1,200 h for saturation of PE biocomposites with up to 50% agave fibres [86]. Apart from neat HDPE, which has negligible absorption rates, the composites with the lowest

amounts of filler, PE.F20-r, and PE.S20-r, were the first to reach the equilibrium point with a saturation level of around 1% after barely 2 weeks, which is 55% and 41% less than before reprocessing, respectively. Meanwhile, the PE.S40-r series is the one that shows the greatest decrease in the water uptake, going from a maximum absorption of over 8% after a month of soaking for the original material to only 3.3%. The fibrous composite with the highest loading amount, on the other hand, also reduces its absorption capacity, but only by one-third compared to the initial value.

Table 3 shows the variation of other parameters related to the hygroscopicity and kinetics of water absorption, such as the Fick diffusion coefficient, swelling, sorption, or permeability. Regarding the swelling of the samples at the end of the test, the trend is similar to that found for water uptake. The composite with 40% reed fibre shows the greatest thickening variation before and after recycling. Except for this sample series, the reduction in swelling is about half compared to the original material.

All samples followed a Fickian-type behaviour with diffusion coefficients in the recycled materials slightly higher than those obtained in the first injection moulding. Water sorption shows the ratio between the mass of water absorbed by the sample and the weight of the sample itself, considering both diffusion and percolation mechanisms. It was found that water sorption capacity depends mainly on the amount of *Arundo* filler. While there is no difference after recycling between composites with 20% fibre or shredded composite, in those with 40% reed, fibre composites show the highest sorption level. Regarding the permeability, obtained by the combination of sorption and

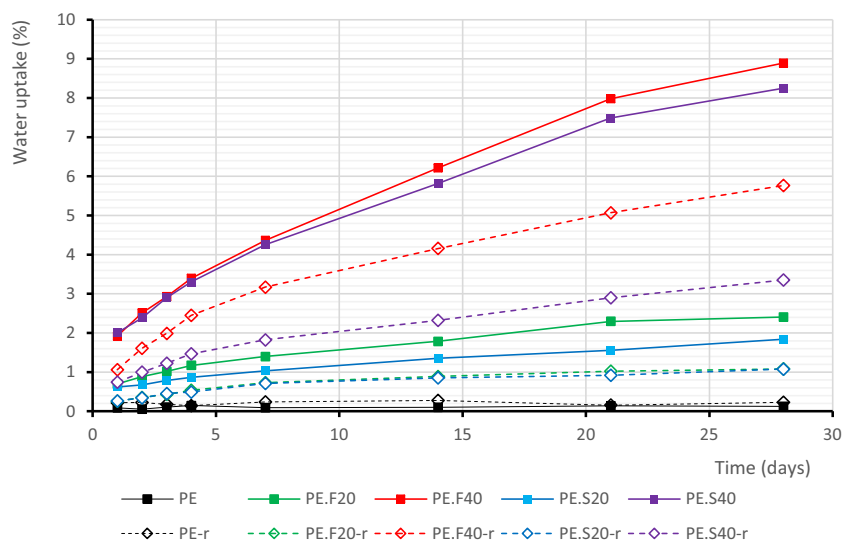


Figure 16: Evolution of water uptake vs time for the original and the reprocessed materials.

Table 3: Variation of water uptake parameters

Material	k (%/s ^{0.5})	D (m ² ·s ⁻¹)	n	Swelling (%)	Sorption (g·g ⁻¹)	Permeability (m ² ·s ⁻¹)
PE	3.53×10^{-5}	2.62×10^{-13}	0.12	1.1	0.001	3.44×10^{-16}
PE.F20	1.61×10^{-3}	3.56×10^{-13}	0.36	3.3	0.024	8.52×10^{-15}
PE.F40	4.98×10^{-3}	2.70×10^{-13}	0.40	8.3	0.089	2.40×10^{-14}
PE.S20	1.10×10^{-3}	2.84×10^{-13}	0.29	2.3	0.018	5.22×10^{-15}
PE.S40	4.88×10^{-3}	2.90×10^{-13}	0.38	6.6	0.083	2.39×10^{-14}
PE-r	1.10×10^{-4}	2.91×10^{-13}	0.06	0.5	0.002	6.82×10^{-16}
PE.F20-r	8.09×10^{-4}	4.40×10^{-13}	0.33	1.4	0.011	4.76×10^{-15}
PE.F40-r	3.86×10^{-3}	3.50×10^{-13}	0.42	5.5	0.058	2.02×10^{-14}
PE.S20-r	6.29×10^{-4}	2.70×10^{-13}	0.25	1.2	0.011	2.92×10^{-15}
PE.S40-r	2.19×10^{-3}	3.36×10^{-13}	0.41	3.0	0.034	1.13×10^{-14}

diffusion attributes, it is interesting to note that despite a worsening of this property for the HDPE matrix, all composites show a reduction in permeability after the closed-loop reprocessing. These results are comparable to those reported by Jubinville when analyzing HDPE-based composites reinforced with hemp hurd. In this study, it was found that beyond 15% loading, the absorption kinetics of the cellulosic phase becomes more important than that of the matrix. Composites with 50% hemp showed the highest diffusion and permeability coefficients due to the incapacity of the matrix to efficiently encapsulate the hydrophilic material and contain moisture penetration [62].

3.7 Colour and gloss evaluation

Reprocessing often leads to significant changes in the visual appearance of NFC. For instance, a gradual shift from original colours to yellowish or darker can occur due to thermal degradation and oxidation processes during recycling.

An overview of the colour and gloss assessment is shown in Table 4. Taking as reference the colour of the original moulded samples (cycle 0), noticeable colour changes were appreciated for all reprocessed series, resulting in a less vibrant and more muted colour appearance, in line with the trend reported by other biocomposites recycling studies in the literature [86,87]. A decrease in the parameter ΔL^* (lightness) is related to the darkening of the samples, while negative values of Δa^* (red/green coordinate) indicate a trend from red to greener colours and Δb^* (yellow/blue coordinate) below zero denotes a shift from yellow to blue hues. Although both composites and recycled HDPE show total colour differences (ΔE) of comparable magnitude, PE-r series mainly varies in shade, keeping hues with similar values to those of the original material. The most significant change colour coordinates occur in the shredded *Arundo* composites, which change from a more yellowish hue in the original compounding to a more bluish colour after reprocessing.

Gloss is the visual perception of direct light reflected from a surface that is associated with perceived brightness.

Table 4: Colour and gloss changes

Material	Colour							Gloss		
	L^*	a^*	b^*	ΔL^* ⁽¹⁾	Δa^* ⁽¹⁾	Δb^* ⁽¹⁾	ΔE ⁽¹⁾	20°	60°	85°
PE	72.47 ± 0.13	-0.91 ± 0.03	-0.31 ± 0.12	—	—	—	—	27.4 ± 3.5	69.0 ± 5.2	84.7 ± 2.2
PE.F20	56.26 ± 0.88	12.37 ± 0.46	23.67 ± 0.94	-16.21	13.28	23.98	31.845	1.0 ± 0.2	7.8 ± 1.1	8.5 ± 2.8
PE.F40	58.37 ± 1.42	12.00 ± 0.71	26.16 ± 1.40	-14.10	12.91	26.47	32.651	1.1 ± 0.5	7.6 ± 3.0	17.4 ± 5.6
PE.S20	41.61 ± 1.27	5.32 ± 0.30	18.77 ± 0.64	-30.86	6.23	19.08	36.810	7.1 ± 1.0	32.4 ± 3.2	53.9 ± 3.0
PE.S40	49.33 ± 1.52	4.44 ± 0.25	15.61 ± 1.02	-23.14	5.36	15.92	28.593	3.0 ± 1.0	18.2 ± 4.3	35.5 ± 7.5
PE-r	62.32 ± 0.11	-1.18 ± 0.03	-0.12 ± 0.07	-10.15	-0.27	0.19	10.154	31.7 ± 1.7	74.6 ± 2.3	89.1 ± 2.8
PE.F20-r	45.27 ± 0.61	10.08 ± 0.40	20.12 ± 0.70	-11.00	-2.29	-3.55	11.778	2.6 ± 0.6	17.1 ± 1.5	25.7 ± 3.9
PE.F40-r	49.92 ± 1.33	10.56 ± 0.52	19.71 ± 1.30	-8.45	-1.44	-6.45	10.725	0.9 ± 0.4	7.3 ± 3.4	13.5 ± 5.9
PE.S20-r	36.24 ± 1.30	2.45 ± 0.42	10.04 ± 0.66	-5.37	-2.87	-8.73	10.648	2.5 ± 0.3	17.5 ± 1.0	26.5 ± 5.6
PE.S40-r	38.25 ± 3.08	2.31 ± 0.42	8.55 ± 0.88	-11.08	-2.13	-7.06	13.308	1.9 ± 0.7	14.1 ± 1.0	24.4 ± 8.0

⁽¹⁾ Differences in colour calculated with respect to neat HDPE in cycle 0 and with respect to unrecycled equivalents in cycle 6.

High reflectance surfaces are referred to as glossy; while semi-gloss or matt surfaces are less reflective. Considering the variety of gloss found among the different samples, the standard measurement at 60° was complemented by measurements at an angle of 20° for high gloss surfaces (values above 70 GU) and at 85° for matt surfaces (values below 10 GU). In the first moulding, it was observed that the fibre composites provided a matt surface with lower gloss than the shredded reed ones. And among the latter, the gloss decreased with the increasing filler content. The most noticeable variation observed after recycling was in the PE.F20-r series, with a marked increase in gloss. This is possibly caused by the smoother surface produced by the reduction in fibre size and a more uniform distribution of the filler. For shredded composites, a rougher surface finish after the final injection moulding results in a decrease in reflectivity. Mechanical attrition of irregularly shaped particles during reprocessing may contribute to this change. As the particles break down, the surface texture of the composite changes, which may scatter light more diffusely rather than reflect it in a specular manner.

4 Conclusions

Despite small losses in thermo-mechanical properties, the study reveals that HDPE-Arundo composites exhibit a worthy level of sustainability, with some improvements in processability and mechanical performance after closed-loop recycling using co-rotating twin-screw extrusion. These characteristics allow for reuse and reprocessing, prolonging the durability of such resources.

FTIR spectroscopy reveals minor variations in chemical composition between the original and the recycled materials. HDPE-based composites show resistance to oxidation, as seen in the persistence of C–H peaks, while some C–O groups in the fingerprint region, related to cellulose, weaken after recycling.

Adding Arundo fillers to the HDPE matrix does not hinder processing and may even improve it. After five-cycle reprocessing, all materials tend to increase their MFI slightly, most noticeably for biocomposites with shredded reed fillers. After that, the most loaded fibrous compound only need 40% higher moulding pressure than pure HDPE. The lack of adhesion promoters in the compounding phase seems to favour a trend towards improving processability and some aspects of mechanical performance rather than degrading the materials throughout the recycling process. Oscillatory rheology revealed that fibrous composites increase complex

viscosity, while shredded ones decrease it. All formulations keep their viscous character, with higher loss moduli than storage moduli. Capillary rheology confirmed that the flow resistance mainly depends on the filler amount, regardless of type.

Thermogravimetric analysis proved thermal stability up to 40°C above processing temperature by injection moulding. Melting temperatures remain consistent around 135°C, while crystallization temperatures slightly increase by less than 5°C for recycled formulations. Arundo-filled materials show an increase in the enthalpies of fusion and crystallization of between 20% and 40% and a small increase in crystallinity. Despite the initial contribution of reed fillers to the OIT, multiple reprocessing led to a drop in OIT for all materials by more than half compared to the PE matrix, except for the PE.F20-r series, which manages to contain it at only 20% less.

HDT and VST decrease after recycling up to a maximum of 9°C, especially in composites with higher lignocellulose loading. On the contrary, reprocessed materials rise their stiffness, in both flexural and tensile elastic moduli, because of the cross-linking reactions typical of PE, and without any enhancements in the inter-phase adhesion being observed. Impact strength is negatively affected by the shortening of the filler length, which results in a one-quarter reduction in aspect ratio after reprocessing in the case of reed fibres. However, tensile and flexural strength increase by up to 10% and 20%, respectively, due to improved fibre intertwining highlighted by entanglement factor and reinforcement efficiency. PE.S40-r was the series that showed the greatest increase in mechanical properties after reprocessing, approaching in performance that of the comparatively more expensive 40% reed fibres composite. All reprocessed materials become tougher, while neat HDPE and 40% filled composites also significantly increase their resilience.

DMTA study found that plant fillers stiffen the HDPE matrix even more after reprocessing, resulting in a higher storage modulus where the type of filler is more crucial than the filler load. The recycled materials exhibit higher loss moduli, suggesting a shift towards more viscous behaviour. An inflection point in the loss factor above 0°C points to a worsening of fatigue performance after recycling. Brittleness at room temperature is decreased by 60% in most composites, extending the elongation at break up to 90% beyond the original values, with the exception of the PE.F40-r series, which becomes slightly less ductile than the others.

No significant changes in the density and porosity of the recycled composites were observed. However, lower water absorption was confirmed, possibly due to smaller

fillers and more uniform distribution after reprocessing, reducing interphase voids in the composite through improved filler encapsulation. Finally, colour and gloss assessments showed noticeable changes in visual appearance for all reprocessed series, resulting in less vibrant colours and shredded composites having lower gloss than fibre composites.

Acknowledgments: Luis Suárez: Ph.D. grant program co-financed by the Canarian Agency for Research, Innovation and Information Society of the Canary Islands Regional Council for Employment, Industry, Commerce and Knowledge (ACIISI) and by the European Social Fund (ESF) (Grant number TESIS2021010008). LICEM project (EIS 2021 33), funded by Consejería de Economía, Conocimiento y Empleo, Gobierno de Canarias, through FEDER funds (Canarias Avanza con Europa).

Funding information: The authors state no funding involved.

Author contributions: Luis Suárez: methodology, formal analysis, investigation, visualization, and writing – original draft preparation; Mateusz Barczewski: conceptualization, methodology, investigation, formal analysis, and writing – reviewing and editing; Mark Billham: investigation, resources, and writing – reviewing and editing; Andrzej Miklaszewski: investigation and writing – reviewing and editing; Patryk Mietliński: investigation; Zaida Ortega: conceptualization, methodology, investigation, resources, writing – reviewing and editing, and supervision. All authors read and approved the final manuscript.

Conflict of interest: The authors state no conflict of interest.

Data availability statement: The datasets generated during and/or analysed during the current study are available from the corresponding author on reasonable request.

References

- [1] Kumar R, Ul Haq MI, Raina A, Anand A. Industrial applications of natural fibre-reinforced polymer composites—challenges and opportunities. *Int J Sustain Eng*. 2019;12(3):212–20.
- [2] Praveena BA, Buradi A, Santhosh N, Vasu VK, Hatgundi J, Huliya D. Study on characterization of mechanical, thermal properties, machinability and biodegradability of natural fiber reinforced polymer composites and its Applications, recent developments and future potentials: A comprehensive review. *Mater Today Proc*. 2022;52:1255–9.
- [3] Rajeshkumar L, Kumar PS, Ramesh M, Sanjay MR, Siengchin S. Assessment of biodegradation of lignocellulosic fiber-based composites – A systematic review. *Int J Biol Macromol*. 2023;253:127237.
- [4] Usman MA, Momohjimoh I, Gimba ASB. Effect of groundnut shell powder on the mechanical properties of recycled polyethylene and its biodegradability. *J Min Mater Charact Eng*. 2016;4(3):228–40.
- [5] Zhao X, Copenhaver K, Wang L, Korey M, Gardner DJ, Li K, et al. Recycling of natural fiber composites: Challenges and opportunities. *Resour Conserv Recycl*. 2022;177:105962.
- [6] Ortega Z, Bolaji I, Suárez L, Cunningham E. A review of the use of giant reed (*Arundo donax* L.) in the biorefineries context. *Rev Chem Eng*. 2024;40(3):305–28.
- [7] Suárez L, Ortega Z, Barczewski M, Cunningham E. Use of giant reed (*Arundo donax* L.) for polymer composites obtaining: a mapping review. *Cellulose*. 2023;30(8):4793–812.
- [8] Corno L, Pilu R, Adani F. *Arundo donax* L.: A non-food crop for bioenergy and bio-compound production. *Biotechnol Adv*. 2014;32(8):1535–49.
- [9] Fernando AL, Barbosa B, Costa J, Papazoglou EG. Giant reed (*Arundo donax* L.): A multipurpose crop bridging phytoremediation with sustainable bioeconomy. *Bioremediation and Bioeconomy*. Elsevier; 2016. p. 77–95. doi: 10.1016/B978-0-12-802830-8.00004-6.
- [10] Coppa E, Astolfi S, Beni C, Carnevale M, Colarossi D, Gallucci F, et al. Evaluating the potential use of Cu-contaminated soils for giant reed (*Arundo donax*, L.) cultivation as a biomass crop. *Env Sci Pollut Res*. 2020;27(8):8662–72.
- [11] Bonfante A, Impagliazzo A, Fiorentino N, Langella G, Mori M, Fagnano M. Supporting local farming communities and crop production resilience to climate change through giant reed (*Arundo donax* L.) cultivation: An Italian case study. *Sci Total Env*. 2017;601–602:603–13.
- [12] Di Fidio N, Antonetti C, Galletti AMR. Microwave-assisted cascade exploitation of giant reed (*Arundo donax* L.) to xylose and levulinic acid catalysed by ferric chloride. *Bioresour Technol*. 2019;293:122050.
- [13] Barreca F, Martinez Gabarron A, Flores Yepes JA, Pastor Pérez JJ. Innovative use of giant reed and cork residues for panels of buildings in Mediterranean area. *Resour Conserv Recycl*. 2019;140:259–66.
- [14] Ferrandez-Villena M, Ferrandez-Garcia A, Garcia-Ortuno T, Ferrandez-Garcia CE, Ferrandez Garcia MT. Properties of wood particleboards containing giant reed (*Arundo donax* L.) particles. *Sustainability*. 2020;12(24):1–10.
- [15] Manniello C, Cillis G, Statuto D, Di Pasquale A, Picuno P. Experimental analysis on concrete blocks reinforced with *Arundo donax* fibres. *J Agric Eng*. 2022;53(1). doi: 10.4081/jae.2021.1288.
- [16] Alshaal T, Elhawati N, Domokos-Szabolcsy É, Kátai J, Márton L, Czákó M, et al. Giant reed (*Arundo Donax* L.): A green technology for clean environment. In *Phytoremediation: Management of environmental contaminants*. Vol. 1, Cham: Springer; 2015. p. 1–20. doi: 10.1007/978-3-319-10395-2_1.
- [17] Galletti S, Cianchetta S, Righini H, Roberti R. A Lignin-Rich Extract of Giant Reed (*Arundo donax* L.) as a Possible Tool to Manage Soilborne Pathogens in Horticulture: A Preliminary Study on a Model Pathosystem. *Horticulturae*. 2022;8(7):589.
- [18] Mavrogianopoulos G, Vogli V, Kyritsis S. Use of wastewater as a nutrient solution in a closed gravel hydroponic culture of giant reed (*Arundo donax*). *Bioresour Technol*. 2002;82(2):103–7.

- [19] Dai L, Lata S, Cobb K, Zou R, Lei H, Chen P, et al. Recent advances in polyolefinic plastic pyrolysis to produce fuels and chemicals. *J Anal Appl Pyrolysis*. 2024;180:106551.
- [20] Janssens V. *Plastics – the Facts* 2022. *Plast Eur*. 2022;81. <https://plasticseurope.org/knowledge-hub/plastics-the-facts-2022>.
- [21] Faust K, Denifl P, Hapke M. Recent advances in catalytic chemical recycling of polyolefins. *ChemCatChem*. 2023;15(13):e202300310.
- [22] Khanam PN, AlMaadeed MAA. Processing and characterization of polyethylene-based composites. *Ad Manuf: Polym Compos Sci*. 2015;1(2):63–79.
- [23] Douiri L, Jdidi H, Kordoghli S, El Hajj Sleiman G, Béreaux Y. Degradation indicators in multiple recycling processing loops of impact polypropylene and high density polyethylene. *Polym Degrad Stab*. 2024;219:110617.
- [24] Benoit N, González-Núñez R, Rodrigue D. High density polyethylene degradation followed by closed-loop recycling. *Prog Rubber, Plast Recycl Technol*. 2017;33(1):17–37.
- [25] Dugvekar M, Dixit S. High density polyethylene composites reinforced by jute fibers and rice stalk dust: A mechanical study. *Mater Today Proc*. 2021;47:5966–9.
- [26] Bolka S, Slapnik J, Rudolf R, Bobovnik R, Mešl M. Thermal and mechanical properties of biocomposites based on green PE-HD and hemp fibers. *Contemp Mater*. 2017;8(1):80–90.
- [27] Cestari SP, Albitres G, Mendes LC, Altstädt V, Gabriel JB, Avila G, et al. Advanced properties of composites of recycled high-density polyethylene and microfibers of sugarcane bagasse. *J Compos Mater*. 2018;52(7):867–76.
- [28] Mendes JF, Martins JT, Manrich A, Luchesi BR, Dantas A, Vanderlei RM, et al. Thermo-physical and mechanical characteristics of composites based on high-density polyethylene (HDPE) e spent coffee grounds (SCG). *J Polym Env*. 2021;29(9):2888–900.
- [29] García E, Louvier-Hernández JF, Cervantes-Vallejo FJ, Flores-Martínez M, Hernández R, Alcaraz-Caracheo LA, et al. Mechanical, dynamic and tribological characterization of HDPE/peanut shell composites. *Polym Test*. 2021;98:107075.
- [30] Laftah WA, Majid RA, Ibrahim AN. Preparation and characterization of bio-film composite based on high density polyethylene and oil palm trunk fiber. *Polym Polym Compos*. 2022;30:096739112210959. doi: 10.1177/09673911221095988.
- [31] Satapathy S, Kothapalli RVS. Mechanical, dynamic mechanical and thermal properties of banana fiber/recycled high density polyethylene biocomposites filled with flyash cenospheres. *J Polym Env*. 2018;26(1):200–13.
- [32] Li Y, Hu C, Yu Y. Interfacial studies of sisal fiber reinforced high density polyethylene (HDPE) composites. *Compos Part A Appl Sci Manuf*. 2008;39(4):570–8.
- [33] Colom X, Carrasco F, Pagès P, Canavate J. Effects of different treatments on the interface of HDPE/lignocellulosic fiber composites. *Compos Sci Technol*. 2003;63(2):161–9.
- [34] Suárez L, Castellano J, Díaz S, Tcharkhtchi A, Ortega Z. Are natural-based composites sustainable? *Polym (Basel)*. 2021;13(14):2326.
- [35] Aziz T, Haq F, Farid A, Kiran M, Faisal S, Ullah A, et al. Challenges associated with cellulose composite material: Facet engineering and prospective. *Env Res*. 2023;223:115429.
- [36] Ismail H, Ilyas SSM. *Recycled polymer blends and composites*. Cham: Springer; 2023. doi: 10.1007/978-3-031-37046-5.
- [37] Suárez L, Barczewski M, Kosmela P, Marrero MD, Ortega Z. Giant reed (*Arundo donax* L.) fiber extraction and characterization for its use in polymer composites. *J Nat Fibers*. 2023;20(1):1–14.
- [38] Suárez L, Hanna PR, Ortega Z, Barczewski M, Kosmela P, Millar B, et al. Influence of giant reed (*Arundo donax* L.) culms processing procedure on physicochemical, rheological, and thermomechanical properties of polyethylene composites. *J Nat Fibers*. 2024;21(1). doi: 10.1080/15440478.2023.2296909.
- [39] Suárez L, Castellano J, Romero F, Marrero MD, Benítez AN, Ortega Z. Environmental hazards of giant reed (*Arundo donax* L.) in the macaronesia region and its characterisation as a potential source for the production of natural fibre composites. *Polym (Basel)*. 2021;13(13). doi: 10.3390/polym13132101.
- [40] Suárez L, Billham M, Garrett G, Cunningham E, Marrero MD, Ortega Z. A new image analysis assisted semi-automatic geometrical measurement of fibers in thermoplastic composites: a case study on giant reed fibers. *J Compos Sci*. 2023;7(8):326.
- [41] Suárez L, Billham M, Garrett G, Cunningham E, Marrero MD, Ortega Z. A new approach for semi-automatic measurement and morphological analysis of fibres throughout thermoplastic compounding process: a case study on giant reed fibers. In 6th International Conference on Natural Fibers 2023. *Nature Inspired Sustainable Solutions*; 2023. p. 100–2.
- [42] Suárez L, Ní Mhuirí A, Millar B, McCourt M, Cunningham E, Ortega Z. Recyclability assessment of lignocellulosic fiber composites: reprocessing of giant reed/HDPE composites by compression molding. In: Hamrol A, Grabowska M, Hinz M, editors. *Manufacturing 2024*. Cham: Springer; 2024. p. 198–212. doi: 10.1007/978-3-031-56474-1_15.
- [43] Tarani E, Arvanitidis I, Christofilos D, Bikiaris DN, Chrissafis K, Vourlias G. Calculation of the degree of crystallinity of HDPE/GNPs nanocomposites by using various experimental techniques: a comparative study. *J Mater Sci*. 2023;58(4):1621–39.
- [44] Prociak A, Sterzyński T, Pielichowski J. Thermal diffusivity of polyurethane foams measured by the modified Angstrom method. *Polym Eng Sci*. 1999;39(9):1689–95.
- [45] Jakubowska P, Sterzyński T. Thermal diffusivity of polyolefin composites highly filled with calcium carbonate. *Polimery*. 2012;57(4):271–5.
- [46] Brostow W, Hagg Lobland HE, Khoja S. Brittleness and toughness of polymers and other materials. *Mater Lett*. 2015;159:478–80.
- [47] Kubát J, Rigdahl M, Welander M. Characterization of interfacial interactions in high density polyethylene filled with glass spheres using dynamic-mechanical analysis. *J Appl Polym Sci*. 1990;39(7):1527–39.
- [48] Podara C, Termine S, Modestou M, Semitekolos D, Tsirogianis C, Karamitrou M, et al. Recent trends of recycling and upcycling of polymers and composites: a comprehensive review. *Recycling*. 2024;9(3):37.
- [49] Fonseca-Valero C, Ochoa-Mendoza A, Arranz-Andrés J, González-Sánchez C. Mechanical recycling and composition effects on the properties and structure of hardwood cellulose-reinforced high density polyethylene eco-composites. *Compos Part A Appl Sci Manuf*. 2015;69:94–104.
- [50] Bhattacharjee S, Bajwa DS. Degradation in the mechanical and thermo-mechanical properties of natural fiber filled polymer composites due to recycling. *Constr Build Mater*. 2018;172:1–9.
- [51] Spicker C, Rudolph N, Kühnert I, Aumtate C. The use of rheological behavior to monitor the processing and service life properties of recycled polypropylene. *Food Packag Shelf Life*. 2019;19:174–83.
- [52] Barbeş L, Rădulescu C, Stihl C. ATR-FTIR spectrometry characterisation of polymeric materials. *Rom Rep Phys*. 2014;66(3):765–77.

- [53] Huang PW, Peng HS. Number of times recycled and its effect on the recyclability, fluidity and tensile properties of polypropylene injection molded parts. *Sustainability*. 2021;13(19):11085.
- [54] Yin S, Tuladhar R, Shi F, Shanks RA, Combe M, Collister T. Mechanical reprocessing of polyolefin waste: A review. *Polym Eng Sci*. 2015;55(12):2899–909.
- [55] González-Sánchez C, Fonseca-Valero C, Ochoa-Mendoza A, Garriga-Meco A, Rodríguez-Hurtado E. Rheological behavior of original and recycled cellulose-polyolefin composite materials. *Compos Part A Appl Sci Manuf*. 2011;42(9):1075–83.
- [56] Correa-Aguirre JP, Luna-Vera F, Caicedo C, Vera-Mondragón B, Hidalgo-Salazar MA. The effects of reprocessing and fiber treatments on the properties of polypropylene-sugarcane bagasse biocomposites. *Polym (Basel)*. 2020;12(7). doi: 10.3390/POLYM12071440.
- [57] Benoit N, González-Núñez R, Rodrigue D. Long-term closed-loop recycling of high-density polyethylene/flax composites. *Prog Rubber, Plast Recycl Technol*. 2018;34(4):171–99.
- [58] Thomasset J, Carreau PJ, Sanschagrin B, Ausias G. Rheological properties of long glass fiber filled polypropylene. *J Nonnewton Fluid Mech*. 2005;125(1):25–34.
- [59] Le Moigne N, Van Den Oever M, Budtova T. Dynamic and capillary shear rheology of natural fiber-reinforced composites. *Polym Eng Sci*. 2013;53(12):2582–93.
- [60] Barczewski M, Ortega Z, Piskowski P, Aniśko J, Kosmela P, Szulc J. A case study on the rotomolding behavior of black tea waste and bio-based high-density polyethylene composites: Do active compounds in the filler degrade during processing? *Compos Part C Open Access*. 2024;13:100437.
- [61] Cestari SP, Mendes LC, Altstädt V, Lopes LMA. Upcycling polymers and natural fibers waste – properties of a potential building material. *Recycling*. 2016;1(1):205–18.
- [62] Jubinville D, Chen G, Mekonnen TH. Simulated thermo-mechanical recycling of high-density polyethylene for the fabrication of hemp hurd plastic composites. *Polym Degrad Stab*. 2023;211:110342.
- [63] Chen J, Yan N. Crystallization behavior of organo-nanoclay treated and untreated kraft fiber-HDPE composites. *Compos Part B Eng*. 2013;54(1):180–7.
- [64] Dorigato A. Recycling of polymer blends. *Adv Ind Eng Polym Res*. 2021;4(2):53–69.
- [65] Hejna A, Barczewski M, Kosmela P, Aniśko J, Szulc J, Skórczewska K, et al. More than just a beer – Brewers' spent grain, spent hops, and spent yeast as potential functional fillers for polymer composites. *Waste Manag*. 2024;180:23–35.
- [66] Song W, Yang Y, Cheng X, Jiang M, Zhang R, Militky J, et al. Utilization of spent coffee grounds as fillers to prepare polypropylene composites for food packaging applications. *Microsc Res Tech*. 2023;86(11):1475–83.
- [67] Barczewski M, Suárez L, Mietliński P, Kłodziński A, Ortega Z. Relationship between the shape of giant reed-based fillers and thermal properties of polyethylene composites: structural related thermal expansion and diffusivity studies. *Waste Biomass Valoriz*. 2024;15:1–10.
- [68] Mendes AA, Cunha AM, Bernardo CA. Study of the degradation mechanisms of polyethylene during reprocessing. *Polym Degrad Stab*. 2011;96(6):1125–33.
- [69] Lu JZ, Wu Q, Negulescu II, Chen Y. The influences of fiber feature and polymer melt index on mechanical properties of sugarcane fiber/polymer composites. *J Appl Polym Sci*. 2006;102(6):5607–19.
- [70] Stanciu MD, Draghicescu HT, Tamas F, Terciu OM. Mechanical and rheological behaviour of composites reinforced with natural fibres. *Polymers*. 2020;12(6):1402.
- [71] Molefi JA, Luyt AS, Krupa I. Comparison of the influence of copper micro- and nano-particles on the mechanical properties of polyethylene/copper composites. *J Mater Sci*. 2010;45(1):82–8.
- [72] Barczewski M, Matykiewicz D, Mysiukiewicz O, Maciejewski P. Evaluation of polypropylene hybrid composites containing glass fiber and basalt powder. *J Polym Eng*. 2018;38(3):281–9.
- [73] Lozano-Sánchez LM, Bagudanch I, Sustaita AO, Iturbe-Ek J, Elizalde LE, García-Romeu ML, et al. Single-point incremental forming of two biocompatible polymers: an insight into their thermal and structural properties. *Polym (Basel)*. 2018;10(4):391.
- [74] Ramzy A. Recycling aspects of natural fibre reinforced polypropylene composites. Clausthal: Clausthal University of Technology; 2018.
- [75] de Carvalho MS, Azevedo JB, Barbosa JDV. Effect of the melt flow index of an HDPE matrix on the properties of composites with wood particles. *Polym Test*. 2020;90:106678.
- [76] Jyoti J, Singh BP, Arya AK, Dhakate SR. Dynamic mechanical properties of multiwall carbon nanotube reinforced ABS composites and their correlation with entanglement density, adhesion, reinforcement and C factor. *RSC Adv*. 2016;6(5):3997–4006.
- [77] Liu Y, Li H, Ji Z, Kashimura Y, Tang Q, Furukawa K, et al. Molecular structure, crystallinity and morphology of polyethylene/polypropylene blends studied by raman mapping, scanning electron microscopy, wide angle X-ray diffraction, and differential scanning calorimetry. *Polym J*. 2006;38(11):1127–36.
- [78] Wu X, Pu L, Xu Y, Shi J, Liu X, Zhong Z, et al. Deformation of high density polyethylene by dynamic equal-channel-angular pressing. *RSC Adv*. 2018;8(40):22583–91.
- [79] Wang C, Bai S, Yue X, Long B, Choo-Smith LP. Relationship between chemical composition, crystallinity, orientation and tensile strength of kenaf fiber. *Fibers Polym*. 2016;17(11):1757–64.
- [80] Barreto ACH, Esmeraldo MA, Rosa DS, Fachine PBA, Mazzetto SE. Cardanol biocomposites reinforced with jute fiber: Microstructure, biodegradability, and mechanical properties. *Polym Compos*. 2010;31(11):1928–37.
- [81] Sewda K, Maiti SN. Crystallization and melting behavior of HDPE in HDPE/teak wood flour composites and their correlation with mechanical properties. *J Appl Polym Sci*. 2010;118(4):2264–75.
- [82] Li J, Yang S, Turng LS, Zheng W, Jiang S. Comparative study of crystallization and lamellae orientation of isotactic polypropylene by rapid heat cycle molding and conventional injection molding. *E-Polymers*. 2017;17(1):71–81.
- [83] Lila MK, Singhal A, Banwait SS, Singh I. A recyclability study of bagasse fiber reinforced polypropylene composites. *Polym Degrad Stab*. 2018;152:272–9.
- [84] Åkesson D, Fuchs T, Stöss M, Root A, Stenvall E, Skrifvars M. Recycling of wood fiber-reinforced HDPE by multiple reprocessing. *J Appl Polym Sci*. 2016;133(35):43877.
- [85] Shahi P, Behraves AH, Daryabari SY, Lotfi M. Experimental investigation on reprocessing of extruded wood flour/HDPE composites. *Polym Compos*. 2012;33(5):753–63.
- [86] González-Aguilar SE, Robledo-Ortiz JR, Arellano M, Martín del Campo AS, Rodrigue D, Pérez-Fonseca AA. Mechanical recycling of biobased polyethylene-agave fiber composites. *J Thermoplast Compos Mater*. 2024;2024:1–21.
- [87] Burgstaller C, Renner K. Recycling of wood-plastic composites – a reprocessing study. *Macromol*. 2023;3(4):754–65.

P1

P2

P3

P4

P5

P6

P7

P8

6.9. INFLUENCE OF GIANT REED FIBRES ON MECHANICAL,
THERMAL, AND DISINTEGRATION BEHAVIOUR OF
ROTOMOLDED PLA AND PE COMPOSITES

P9

P10



Influence of Giant Reed Fibers on Mechanical, Thermal, and Disintegration Behavior of Rotomolded PLA and PE Composites

Luis Suárez¹ · Zaida Ortega² · Francisco Romero¹ · Rubén Paz¹ · María D. Marrero¹

Accepted: 28 July 2022 / Published online: 1 September 2022
© The Author(s) 2022

Abstract

This paper assesses the modifications in the properties of rotomolded polyethylene (PE) and polylactic acid (PLA) composites obtained with 5 and 10% giant reed fibers, mainly focusing on the alterations due to a bio-disintegration process. Thermal properties (melting temperature and crystallinity degree), morphology (via optical and scanning electron microscopy), and chemical changes (by Fourier Transformed Infrared spectroscopy) were studied. Composites with untreated and NaOH-treated fibers were obtained, finding that this treatment does not improve the mechanical performance of composites due to increased porosity. The introduction of natural fibers into a PE matrix does not significantly modify the thermal and bio-disintegration properties of the rotomolded material. Regarding mechanical properties, PE-composites show increased tensile modulus and reduced impact and tensile strength than the matrix. On the other hand, PLA composites show lower impact and flexural strength than neat PLA, remaining the rest of the mechanical properties unchanged regardless of the fibers' addition. The incorporation of *Arundo* fibers modifies to a great extent the thermal and degradation behavior of the PLA matrix.

Keywords Rotational molding · Characterization · Bio-disintegration · PLA · PE · Giant reed

Introduction

Rotational molding is a well-established technology that produces hollow parts with good surface quality and mechanical properties. The range of available materials is not as comprehensive as for other polymer processing technologies. For this reason, several authors have focused on using materials adapted to rotomolding specificities. Polyethylene (PE) accounts for more than 90% of the rotomolding market [1], while polylactic acid (PLA) is the second most used one [2–6] due to its recyclability, biodegradability, and good properties. Some studies with other materials, such as PE/PLA blends [6], polycaprolactone (PCL) [7], or recycled materials, can be found in the literature. For recycled materials, the use of up to 35% of cable waste in a PE matrix has been proposed [8]. The parts made with fully recycled plastic residues have also been studied, showing low mechanical

properties due to the difficulty of obtaining PE pure fractions from post-consumer plastics [9]. Copper slag has been introduced into a PLA matrix up to 20%, bringing a composite material stiffer and harder than the polymer itself [10]. Finally, some attempts to recycle PLA fractions have been performed [11, 12], paying particular attention to the degradation that may arise in the polymer due to reprocessing.

On the other hand, the literature shows limited rotomolding studies using fillers or reinforcements from natural fibers or waste materials. Regarding natural fibers, Torres and Aragon found that the introduction of up to 10% in weight (w/w) of cabuya and sisal fiber noticeably reduced the impact properties of the composite without any improvement in tensile properties [13], while Wang et al. reported no modification of these properties for 10% w/w flax composites [14]. Ortega et al. produced composites with 5% w/w of banana and abaca fibers with significant improvements in mechanical properties, except for impact strength [15]. Cisneros-López et al. have also found no statistical differences in mechanical properties for composites containing up to 10% w/w of agave fibers in a PLA matrix, while higher loadings of fibers result in an important decrease in mechanical performance [16]. Hejna et al. obtained composites with up to 20% w/w of wheat bran, although only those with up

✉ Zaida Ortega
zaida.ortega@ulpgc.es

¹ Departamento de Ingeniería Mecánica, Universidad de Las Palmas de Gran Canaria, 35017 Las Palmas, Spain

² Departamento de Ingeniería de Procesos, Universidad de Las Palmas de Gran Canaria, 35017 Las Palmas, Spain

to 5% content did not show significant loss of mechanical properties [1]. Buckwheat husks have been used up to 30% w/w for composites production, although with substantial reductions in mechanical properties [17]. The use of compatibilizers, such as maleated PLA or glycidyl methacrylate grafted PLA, increases the amount of fiber used up to 20% (w/w) [18, 19]. However, this implies a further step of processing and, thus, higher cost. 10% loading (in weight) is commonly used for rotational molding [20].

Some authors have pointed out that the voids found in rotomolded parts are responsible for the reduction in mechanical properties of composites [16]. The lack of continuity in the matrix hinders the formation of the crystals. The deficient contact between the fiber and the matrix avoids a good stress transfer between both components. Particle size distribution has also been proven to significantly affect the properties of rotomolded parts [18–20] and the amount of filler introduced into a PE or PLA matrix [17, 21].

This paper focuses on using fibers obtained from *Arundo donax* L. stems as fillers of rotationally molded PE or PLA matrixes. This species, also known as common reed or giant reed, is a rhizomatous grass with a quick growth rate, which makes it especially interesting due to the high amount of biomass available. Different high-added value products can be obtained from this plant in a biorefineries context: fibers [22–24], bioethanol [25, 26], xylose [27], levulinic acid [28, 29] or bio-polymers [30, 31]. Different works in literature propose its use as raw material for oil spill recovery [32], soil remediation [33], or paper obtaining [34]. Rajkumar and collaborators have proposed using PET as the matrix of composites with peeled stems [35]. Similarly, several authors have used the shredded plant to produce panels using natural binders, such as citric acid, with applications in acoustic and thermal insulation [36, 37].

Some authors have proposed obtaining fibers from reed and using them for composites, especially by compression molding. For example, Fiore et al. have obtained reed-PLA composites with higher modulus than the matrix [38], while Suárez et al. proposed using these fibers in PE and PP matrixes [24] with significant increases in elastic modulus. Monsalve Alarcón and collaborators [39] obtained composites with a PU-natural resin with improved stiffness. Other authors have explored *Arundo*'s use as epoxy fillers reinforcement [40, 41], providing higher tensile moduli and lower strength. Finally, Ortega et al. have produced rotationally molded PE-composites with this filler, with a drop in mechanical properties [21].

On the other hand, the impact of polymers on the environment is undeniable due to their abuse and long lifecycle. In recent years, biodegradable plastics' presence in consumer products, mainly in packaging, has been widely increased to overcome this problem. It is essential to differentiate between bio-degradation and bio-disintegration,

as these terms are often confused. Degradation refers to the modification of macromolecules due to their release from the primary chemical chain, and it is often associated with a decrease in performance. However, it is usually preferred to refer to it as the decrease in molecular weight. The term biodegradation refers to the degradation process performed by living cells and not by enzymes isolated from them. So, the degradation tests usually performed in literature, especially in the bio-materials field, which assess the modifications of a material due to enzyme action, cannot be considered biodegradation assays. Finally, disintegration relates to the breakage of a sample into smaller parts than the original size [42].

Plastics biodegradation is greatly affected by the nature of the material (chemical structure and functional groups, crystallinity, molecular weight, additives), the type of organism involved in the process (bacteria, fungi, algae), and the conditions (temperature, humidity, pH) in which the process takes place [43]. PLA has often been classified as a biodegradable material, although this process only takes place under a compost environment, that is, in the presence of appropriate microorganisms and elevated temperature [44]. For these authors, the main factors affecting the PLA biodegradation process are polymer molecular weight (the higher the weight, the slower the degradation) and the L/D monomer ratio (higher crystallinity leads to lower degradation). Abiotic degradation can take place if the material is immersed in hot water and is considered crucial for biodegradation of PLA, as it leads to ester links hydrolysis [44, 45].

Most literature about PLA biodegradation focuses on processes performed at thermophilic conditions (around 58 °C) [46–48]. However, some authors suggest using mesophilic conditions (37 °C) [49], as most municipal waste treatment plants operate in these conditions and also because these are usually more stable and have lower energy requirements.

This paper deals with the assessment of the properties of composite parts obtained by rotational molding, using two different matrixes: PE and PLA and giant reed (*Arundo donax*) fibers at 5 and 10 wt % loading. Mechanical behavior, morphology, and bio-disintegration of composite materials have been assessed. Bio-disintegration assays have been performed following the procedure in UNE-EN 20200:2015, which simulates composting processes under controlled conditions for 12 weeks. This is an important step in the analysis scheme to assess the compostability of plastic materials. The procedure consists, in short, of studying the differences found in plastics before and after subjecting them to the action of natural microbes found in compost. Although the use of natural fibers for composites obtaining has been widely studied in the literature, not much research has been conducted on the bio-disintegration behavior of such materials. So, the main aim of this paper is to determine if the introduction of cellulosic fibers into the polymer matrixes

modifies its susceptibility to the microorganisms' action and, thus, its disintegration.

Materials and Methods

Materials

A general-purpose PE from Matrix (Revolve N-461, Northampton, UK), in powder form, was used as matrix. The polylactic acid (PLA) matrix used was from Corbion (Luminy L105, with 99% L-isomer), also in powder form.

The fibers were obtained at Universidad de Las Palmas de Gran Canaria (ULPGC), following previously described processes [24]. In short, the extraction process consisted of a mechanical step of subsequent crushing of the stems. Once obtained and dried, fibers were cut to 3–4 mm in length. Part of these fibers was treated to improve thermal stability using a 1 N NaOH solution and a solid/liquid relation of 25 g/l. The treatment lasted 1 h at room temperature and ended with various washings with de-ionized water until reaching neutral pH. Untreated fibers showed an average diameter of $132 \pm 33 \mu\text{m}$, while for treated ones, this was $92 \pm 21 \mu\text{m}$.

Methods

Composites Production

Arundo fibers were dried overnight in an oven at 105 °C, while PE was dried at 40 °C overnight and PLA at 100 °C for 4 h. Composites were prepared by dry blending of the matrix with the fibers (at 5 and 10% weight) in a V-shape mixer and then introduced in a lab-made rotomolding device, as described previously [21], using a rotation rate of 2.30 rpm in the primary axis and 9.14 rpm in the secondary axis (speed ratio of 1/4). The internal air temperature in the mold was monitored with a thermocouple introduced via the venting hole located in the middle of one side of the cube. The heating stage stopped when the internal temperature reached 180 °C for PE and 185 °C for PLA, although due to thermal inertia, interior air temperature reached slightly higher values. The mold was cooled by forced air while keeping the mold rotation until reaching 50 °C. Average heating times were 22 min for PE and 32 for PLA, regardless of the incorporation of fibers. Contrarily, cooling times varied for PE samples; cooling was faster for 10% loadings than for 5% and pure PE (process cycles are found in supplementary materials (Fig. S1)). Cubic parts of 120 mm side and 3–4 mm thickness were obtained (Fig. 1), and test bars were machined from them, following ISO 3167:2014 standard for the dimensions of the test bars for tensile tests, ISO 178:2019 standards for flexural tests, and ISO 180:2019 standards for Izod-impact tests.

The samples obtained have been named with the matrix used (PE, PLA) followed by the type of fiber (AD: *Arundo donax*, ADt: *Arundo donax* treated) and the ratio of fiber (5, 10).

Fibers are well distributed in all composite parts obtained, although some clustering can be observed for 10% treated fibers, especially on the inner surface of the cubes (Fig. 1b, d–f). Untreated fiber does not seem to degrade during the processing, as the composites obtained do not show big bubbles, dark color, or characteristic odor. Some authors have experienced processing issues when using other fibers in rotomolded parts. For example, 10% hemp fiber composites did not even show enough consolidation unless using treated fibers [50]. However, in this research, *Arundo* fibers were successfully incorporated into the matrix, not forming fiber balls inside the part due to the mold rotation.

Bio-disintegration and thermal behavior were assessed for neat matrix and composites with 10% fibers.

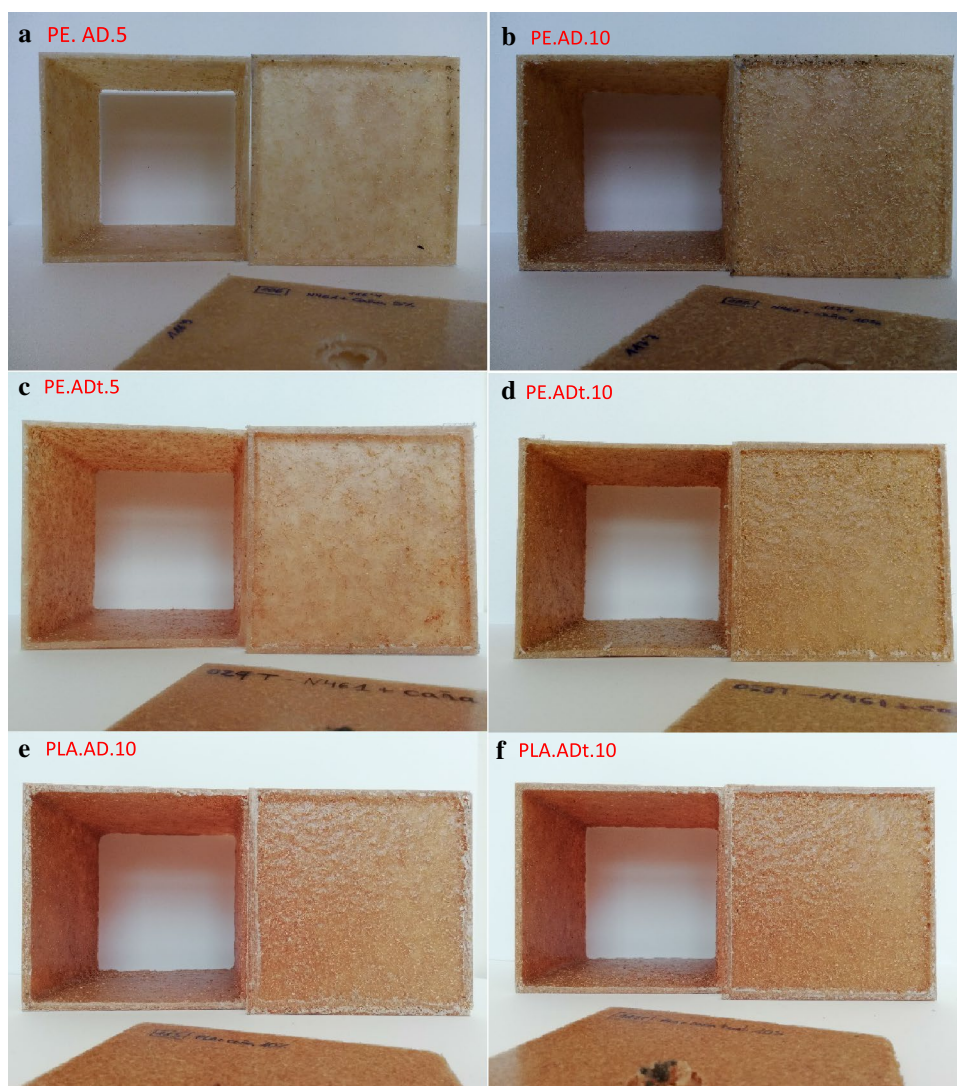
Mechanical Testing

Composite samples were tested to determine their tensile properties according to ISO 527–2:2012, at a rate of 10 mm/min, determining the elastic modulus and ultimate tensile strength. Flexural properties were measured according to ISO 178:2019 at the same rate, with a distance between cantilevers of 64 mm, determining the elastic modulus and flexural strength. Tensile and flexural tests were performed in a universal testing machine from Dongguan Liyi Test Equipment Co. Ltd. (LY-1065). A PCE-FG1k load cell of 200 kg maximum capacity from PCE Instrument) was used for the flexural tests, and a YZC-516 with 500 kg maximum capacity from Guang CE for the tensile essays. Impact tests were performed on unnotched samples, following UNE-EN ISO 180:2019, using a 5.5 J pendulum and an impact rate of 3.5 m/s. The energy absorbed by the part on Izod configuration was determined in an Izod and Charpy impact tester model LY-XJJD 50 from Dongguan Liyi Test Equipment Co. Ltd.

Bio-disintegration Assays

Disintegrability of the materials was determined by an assay performed in simulated composting conditions, following the protocol established in EN 14806:2005. A synthetic biowaste was prepared by mixing vegetal residues, rabbit feed (commercial product based on alfalfa and vegetable flours, with proteins and cellulose content of 15% and 20%, respectively), mature compost, volumizing agent (wood chips), urea and water (up to 55% of the final weight). This biowaste was placed in boxes (45 × 62 × 18 cm) with holes on the lower part and sides, set at 6.5 cm from the bottom.

Fig. 1 Pictures of composite parts obtained. PE composites with **a** 5% untreated fibers in PE, **b** 10% untreated fibers in PE, **c** 5% treated fibers in PE, and **d** 10% treated fibers. PLA composites with **e** 10% untreated fiber in PLA and **f** 10% treated fiber in PLA



A 5 cm—layer of expanded clay is placed on the bottom of the boxes to ensure ventilation and drainage.

The boxes are manually aerated weekly for the first four weeks and then every two weeks. pH, weight, and humidity levels were assessed weekly during the entire process, while temperatures were checked daily. Once dried and weighted, each sample was placed in the synthetic waste with enough distance not to touch either the walls of the box or other sample and then entirely covered with more synthetic waste. The overall duration of the assay was 12 weeks.

At the end of the test, the samples were recovered, washed with water, and oven-dried at 105 °C, obtaining the disintegration degree as follows:

$$\text{Disintegration degree (\%)} = \frac{m_f - m_o}{m_o} \cdot 100$$

where m_f is the dry mass of each test bar at the end of the assay and m_o is the initial mass of this same bar.

Microscopic Observations

After the tensile test, the surface of obtained parts and cross-section of test samples were observed under an optical microscope and SEM. An Olympus BX51 microscope was used for optical microscopy to assess the differences found in the parts' surfaces.

The surface microstructure of samples was also assessed before and after the disintegration assay. A Hitachi TM3030 tabletop scanning electron microscope (SEM) under different magnifications, working at 15 kV, was used for this purpose. Test bars were sputtered with a thin Au/Pd layer in an SC 760 apparatus from Quorum Technologies for 120 s and 18 mA under an argon atmosphere. For the assays after the bio-disintegration assay, PE samples were obtained by

cutting a layer of the test bars. For PLA, this was not possible due to the material fragility. These samples were then obtained just by pressing the samples with fingers.

Thermal Behavior

Differential scanning calorimetry (DSC) was performed on all samples in a Perkin Elmer DSC 4000 apparatus. The measurements were performed at 10 °C/min, from 30 to 200 °C, with two heating cycles. Melting temperature for both heatings (T_{m1} and T_{m2} , respectively) and crystallization temperature (T_c) from the cooling step were determined, together with melting and crystallization enthalpies (ΔH_{m1} , ΔH_{m2} , and ΔH_{cc}). Cold crystallization temperature (T_{cc}) was not observed for the studied samples. For PLA samples, glass transition temperature (T_g) was also calculated. Enthalpies were used for crystallinity degree (χ) calculation, using the following expression:

$$\chi = \frac{1}{1 - m_f} \cdot \frac{\Delta H_m - \Delta H_{cc}}{\Delta H_0} \cdot 100$$

where ΔH_0 is the enthalpy for 100% crystalline sample (93.7 J/g for PLA and 293 J/g for PE) [17], and m_f is the mass fraction of the fiber (10% for composites). Three assays were performed for each sample, and results are given as average values and standard deviations.

Infrared Spectroscopy (FTIR)

Fourier infrared spectra of the samples were recorded in the range of 400–4000 cm^{-1} in a Perkin Elmer Spectrum Two spectrometer, in the attenuated total reflection mode (ATR), with a resolution of 4 cm^{-1} . Different intensity ratios were

calculated for each polymer matrix to determine the extension of the sample changes. Three spectra were obtained for each sample, accumulating 60 scans per spectrum.

Results

Evolution of Bio-disintegration Recipients

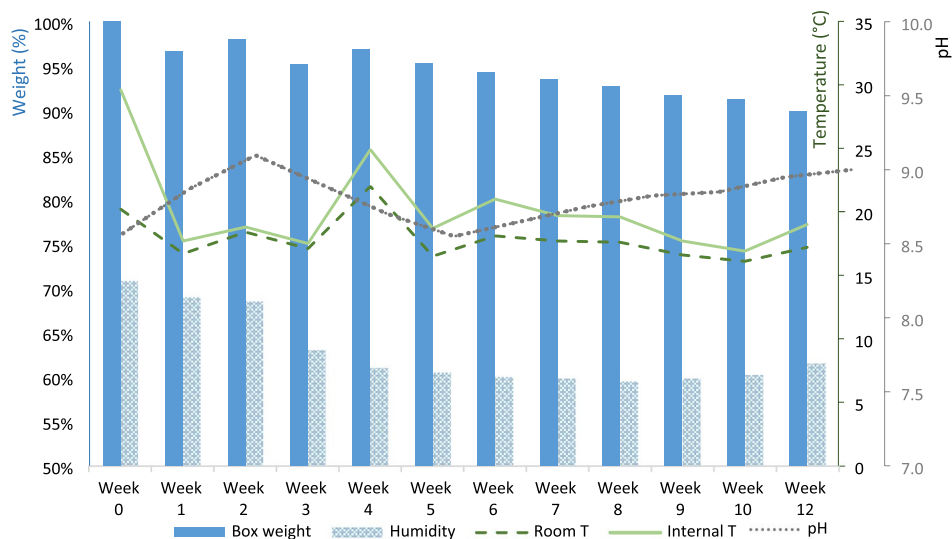
The variation of the magnitudes measured during the entire assay is drawn in Fig. 2: the weight of the disintegration boxes (in %), temperature, and humidity values.

It is clearly observed that the weight is reduced gradually, due mainly to the reduction in the humidity of the synthetic biowaste, as also observed in the figure. Initial pH was 8.31, which increased during the first weeks, coinciding with the release of ammonia odor, which was later disappearing, as expected. The maximum pH value was 9.1 in week 4. No signs of mold or other alterations were observed during the process.

The graph also shows that the biowaste temperature is progressively decreasing due to the low biological activity. In any case, the temperature inside the disintegration boxes was higher than the room temperature, and condensation could be observed on the recipients' walls, thus indicating the existence of biological activity inside them. Room temperature was quite variable in the period of the year where the assay took place (March–May). Some more mature compost and vegetable residues were added to the biowaste to increase the microbial activity and overcome this instability, although this did not have much effect (this is the reason for the weight increase in week 4).

At the end of the assay, the biowaste did not have any specific odor, and its color was notably darker. Photographs

Fig. 2 Evolution of weight and humidity in the disintegration boxes (left axis), together with temperature and pH (right axis)



of the samples were taken for visual comparison and also observed in an optical microscope. Some samples (PLA composites) were broken when recovered.

Recovered samples were dried and weighted to determine the extent of the disintegration as the weight loss percentage. Figure 3 shows that the PE samples have almost no change, while weight loss of up to 1.4% for PLA composites was obtained. 100% PLA samples do not show a significant disintegration, while adding natural fibers seems to increase this behavior slightly. It should be pointed out that, to verify that the assay was correctly prepared and that biological activity existed, a commercial biodegradable material (Bioplast 300, based on starch) was introduced as reference material, and this reached almost 40% in weight reduction. As already mentioned, PLA is considered compostable in thermophilic conditions, which is, at around 60 °C, which explains the low values of weight loss obtained in this study. Other authors working in compost piles at similar temperatures have also got similar weight losses [51]. The crystallinity of the PLA also plays a vital role in the disintegration and degradation behavior. As shown later, the grade used in this research showed high crystallinity (around 50%), which could also explain the relatively low degradation. The PLA grade used contains 99% of L-isomer, also influencing the degradation; the higher D—enantiomer content, the higher degradation rates, and the lower crystallinity (also increasing degradation kinetics) [48].

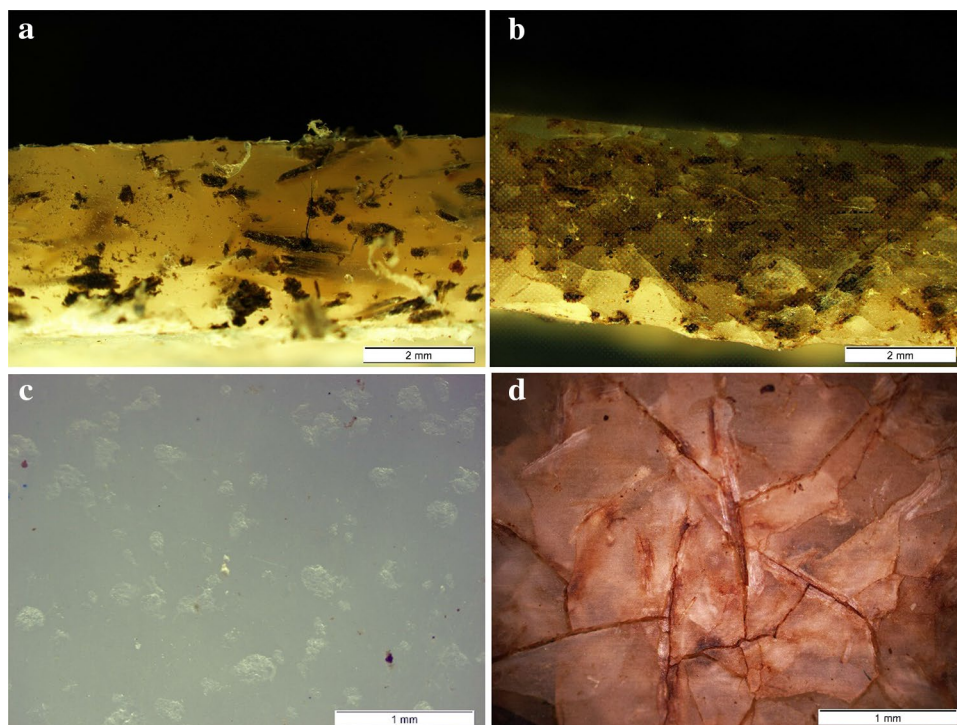
The increase in the hydrophilicity of the composite is needed for PLA degradation; for that reason, the

introduction of vegetal fibers could help in the PLA hydrolysis reactions [51, 52]. For this reason, the humidity absorption of samples before and after the process was measured (Table 1). As observed, humidity absorption of samples before the process is almost null (maximum around 1% for PLA composites), while this increased to close to 20% for PLA-treated *Arundo* composites. PE composites increase their hydrophilicity after the disintegration assay, reaching around 5% of moisture absorption. Before bio-disintegration, the hydrophilicity of PE and PLA composites is higher than for neat polymers, regardless of whether the fiber has been or not treated; due to the nature of the polymer, PLA materials show higher moisture absorption than PE-based ones. However, the PLA parts with treated fibers show significantly higher hydrophilicity than untreated ones after the essay,

Table 1 Average values (\pm standard deviations) for disintegration degree and moisture absorption

Material	Disintegration degree (%)	Moisture absorption (%)	
		Before	After
PE	0.11 ± 0.03	0.09 ± 0.03	0.86 ± 0.31
PE.AD 10	-0.58 ± 0.07	0.90 ± 0.10	4.66 ± 0.23
PE.ADt 10	-0.72 ± 0.04	0.90 ± 0.06	5.88 ± 0.30
PLA	-0.30 ± 0.10	0.68 ± 0.03	4.03 ± 0.55
PLA.AD 10	-0.89 ± 0.07	1.27 ± 0.04	12.63 ± 0.45
PLA.ADt 10	-1.40 ± 0.28	1.32 ± 0.04	19.11 ± 0.88

Fig. 3 Optical microscope pictures taken after the disintegration assay. Lateral view of composites: **a** 10% *Arundo* in PE matrix, **b** 10% *Arundo* in PLA matrix, **c** Surface of PLA, **d** Surface of 10% *Arundo* PLA



which correlates with the higher disintegration degree. The moisture absorption of PE composites increases after the essay and is significantly higher than for PE, but fiber treatment does not show any statistical difference.

Regarding the extent of the disintegration, PE materials do not show differences among the three series of materials tested; that is, no breakdown happens for this matrix. The increase in hydrophilicity is then only due to the presence of fibers in the matrix. On the other hand, the introduction of giant reed fibers within the PLA matrix increases the biodegradation ability of the material, especially for NaOH-treated fibers. Dong et al. [53] have found a similar behavior for PLA/coir composites obtained by compression molding; parts with treated fibers provide higher disintegration rates in soil burial assay. These authors attribute this behavior to the release of residual NaOH and its interaction with the polymer chain. This paper also points out that a fiber ratio over 10% does not lead to further increases in biodegradability kinetics. The increase in weight loss for PLA composites compared to neat PLA can be due to their higher hydrophilicity and the higher porosity obtained for these composites, which increases the surface exposed to water and the biota in the synthetic waste.

Mechanical Properties

Table 2 shows a summary of results obtained for the different properties assessed. The composite density is lower than the density obtained for the polymer parts. The fiber treatment does not significantly affect the density of the composite, being more relevant the amount of fiber in the material. Other authors have reported a higher density of the composite for treated fiber composites than for untreated ones [21, 54]. As fibers used in this research have similar composition [24] to those obtained by Fiore and collaborators [23], the density determined by these authors (1.168 g/cm³) can be assumed. Comparing composites' theoretical

density (density of the polymer and density of the filler multiplied by the ratios of each component) with the actual one (obtained by volume and weight measuring of the samples), calculating the porosity of the different materials. Higher fiber loadings result in higher porosity values. Besides, the use of treated fibers also led to an increase in porosity due to the formation of fiber agglomerations and poorer distribution, although this does not seem to affect the mechanical properties of the composite. This higher porosity, also observed in microscopy, is responsible for the relatively low mechanical properties determined.

Neither for PE nor for PLA composites did the NaOH treatment performed on the fibers seem to affect the mechanical properties of the composites, contrary to what was expected, being more significant the amount of fiber used, as also happened for density.

For PE, the impact strength is only significantly reduced for composites with 10% fibers, with no significant difference due to the fiber treatment. 5% PE composites show no statistical differences for this property for untreated and treated fibers. Longer fibers can provide better impact properties, as the energy needed for fiber pull-out is higher due to the longer distance required for this to happen [55] (assuming fiber does not break). However, in rotational molding, particle size distribution is a critical aspect for obtaining a well-consolidated part [54]; besides, long fibers result in entanglements, poor distribution, and the fibers not incorporated into the polymer matrix [50, 56]. The low impact properties found in this research have been previously reported in the literature for rotomolded composites [15, 16, 57] and can be explained by the low adhesion between the matrix and the fiber. Ortega et al. have obtained composites with up to 20% of size-classified *Arundo* fibers in a rotomolded PE matrix, also finding significant drops in impact strength [21]. Some authors have proposed using compatibilizers based on maleic anhydride to increase this adhesion and thus the composite efficiency [55]. The production of parts with different

Table 2 Average values (\pm standard deviations) for mechanical properties of the materials

Material	Density (g/cm ³)	Impact Strength (kJ/m ²)	Tensile properties		Flexural properties		Porosity (%)
			Strength (MPa)	Modulus (MPa)	Strength (MPa)	Modulus (MPa)	
PE	0.901 \pm 0.023	19.0 \pm 3.8 ^d	16.1 \pm 0.3	381.5 \pm 59.4	18.7 \pm 2.1 ^l	623.7 \pm 75.2 ⁿ	3.6
PE.AD 5	0.855 \pm 0.013 ^a	15.4 \pm 3.4 ^d	13.4 \pm 0.4 ^g	467.7 \pm 33.8 ^j	18.2 \pm 1.4 ^l	662.8 \pm 112.5 ⁿ	6.5
PE.AD 10	0.809 \pm 0.031 ^b	11.8 \pm 4.7 ^e	11.4 \pm 0.8 ^h	489.0 \pm 32.9 ^j	18.3 \pm 0.7 ^l	791.6 \pm 115.2 ⁿ	12.8
PE.ADt 5	0.838 \pm 0.340 ^a	14.7 \pm 3.4 ^d	13.4 \pm 1.4 ^g	544.7 \pm 81.4 ^j	18.1 \pm 1.1 ^l	690.1 \pm 105.7 ⁿ	8.3
PE.ADt 10	0.804 \pm 0.170 ^b	9.8 \pm 1.8 ^e	11.8 \pm 0.8 ^h	502.6 \pm 81.4 ^j	17.3 \pm 1.0 ^l	737.9 \pm 125.9 ⁿ	13.3
PLA	1.212 \pm 0.024	21.1 \pm 5.0	17.3 \pm 5.6 ⁱ	865.4 \pm 161.5 ^k	57.7 \pm 4.5	3862.1 \pm 412.1 ^o	2.3
PLA.AD 10	1.088 \pm 0.024 ^c	4.0 \pm 1.4 ^f	20.1 \pm 2.7 ⁱ	874.0 \pm 179.0 ^k	33.7 \pm 2.6 ^m	3148.3 \pm 280.0 ^o	10.1
PLA.ADt 10	1.079 \pm 0.037 ^c	3.7 \pm 0.7 ^f	18.5 \pm 2.8 ⁱ	774.8 \pm 108.4 ^k	33.4 \pm 6.3 ^m	3007.3 \pm 690.2 ^o	10.6

Tukey tests for comparison of properties of the different series of materials have been used at a 95% confidence level.

Those materials with the same superscript letter show no statistical difference for the property.

layers, at least one of them the neat polymer, has also been proposed as a strategy to reduce the drop in impact properties [8, 15]. However, this requires higher processing times, makes the process more complicated, and reduces the fiber ratio in the final part.

Tensile strength is diminished for all samples, being this loss more important for higher percentages of fibers. Other works working with lignocellulosic materials in rotational molding have also found lower tensile strength with increased fiber content [1, 20, 21, 58]; tensile strength drops by 50% when working with as low as 5% of hemp fibers [50]. This reduction may be due to the increased porosity of samples with the fiber introduction and the fiber agglomeration, which limits stress transfer between the fibers and the matrix.

Tensile elastic modulus slightly increases for the PE-composites, with no difference in this case due to the fiber content. It is accepted that the introduction of fibers will increase tensile modules due to their higher rigidity [55]. In any case, the particularities of the rotational molding process, where no pressure is applied, result in lower increases for this property than in other procedures, such as injection or compression molding [16]. Using compatibilizers based on maleic anhydride results in higher tensile modulus [55].

Finally, no significant changes in flexural properties are found among neat PE and composites, despite the ratio of fiber used. Other studies have found no differences in these properties when using 10% bamboo [57] or agave fibers [55].

For PLA, the impact strength is greatly reduced due to fibers, reaching around 20% of the values found for the polymer, for composites with treated and untreated fibers. This drop, together with the reduction to almost half in flexural strength, can be attributed to the increased porosity of the samples and the pull-out of the fibers from the matrix, as already explained for PE. Incorporating *Arundo* fibers in the PLA matrix has not modified the tensile properties of PLA. Similarly, agave fibers have not significantly changed tensile properties in PLA [16]. In contrast, using buckwheat husk in lower proportions has led to a drastic decrease in tensile strength [17] at comparable porosity values. This difference in behavior may be due to the format of the material used in both studies (fibers here and particles in that study), as it is well known that the morphology of the filler affects the reinforcing effect.

Microscopic Observations

Optical microscope pictures allowed observing some porosity and voids in the parts, even before the disintegration process. Good distribution of fibers is found along the surface and through the wall thickness of the specimens (Fig. 3). The only change observed in PE parts is the darkening of the fibers, while for PLA ones, many cracks appear in the surface

and cross-section of the parts. Pure PLA parts show some more roughness on the surface after the assay, although no cracks are visible (pictures of the samples before the assay are found in supplementary material (Fig. S2)). The swelling of fibers during the process may have forced the cracks to appear by size increase or by the water effect in the PLA and the beginning of hydrolysis.

The cracks appearing in PLA composite (Fig. 3b, d) parts were visible to the naked eye when recovering the parts from the synthetic compost. Some of them were even broken after the process, thus showing the extent of the degradation that occurred, even for the low weight loss observed in the assay and previously discussed.

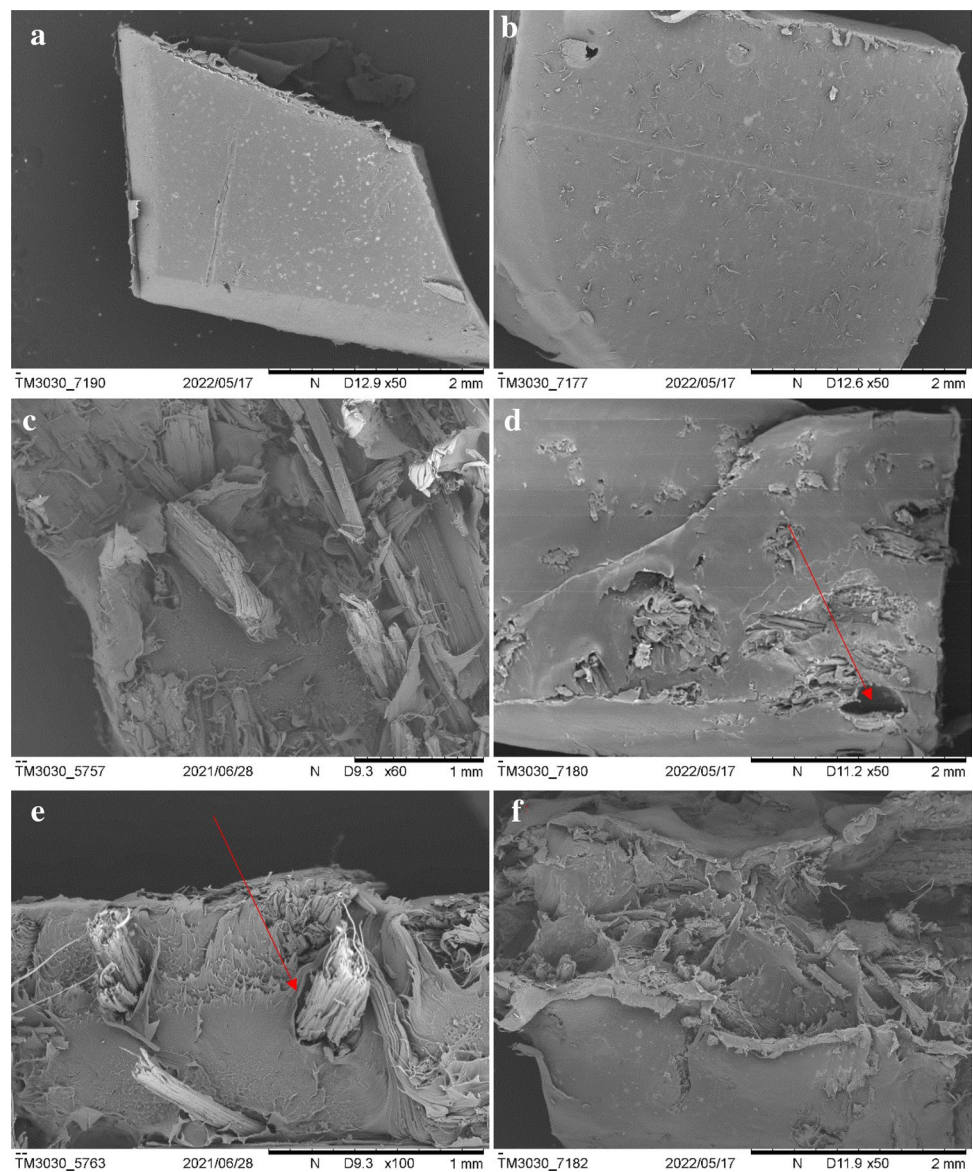
SEM micrographs for PE and PLA samples (Figs. 4, 5, respectively) show a smooth surface, almost free of porosity, while some voids can be observed for composites. For both matrixes, fibers appear randomly distributed and with poor adhesion with the matrix, as pull-out and separation between fiber and matrix are observed, thus explaining the relatively poor mechanical properties of the prepared composite. As already mentioned, no differences were found in SEM observations due to the bio-disintegration assay for this matrix. For PLA, however, the material appears fragmented, with many cracks on all surfaces of PLA-composite parts, as also observed in the optical microscope.

DSC

Typical DSC curves and results are obtained for all composites before and after the disintegration assay, as observed in Table 3 for PE samples and Table 4 for PLA ones. For polyethylene samples, the melting temperature is around 129 °C, with no difference due to the fiber content. No difference in temperatures due to the bio-disintegration assay was found, indicating, once again, that the biological process does not modify these materials. Melting and crystallization peaks are not altered, and enthalpies are only slightly reduced due to fiber introduction. Finally, no differences between the first and second heating cycles were observed, neither in temperatures nor in crystallinity values (values not shown in Table 2). Crystallinity seems to decrease in the assay because of the differences in melting enthalpies, which are also lower. This apparent reduction in crystallinity might be confirmed by other techniques, such as X-ray diffraction. Other authors have reported similar behavior for PE composites: no significant differences in thermal properties when adding foreign materials and crystallinity levels of around 40% due to the rapid crystallization of PE [17].

For PLA samples (Table 4), glass transition (58 °C) and melting temperatures (170 °C) are placed within the ranges indicated by the product datasheet and are also similar to other PLA-based materials. T_g increases with the introduction of *Arundo* fibers due to hindering PLA chains' mobility

Fig. 4 SEM micrographs for PE samples. Left pictures correspond to samples before disintegration assay, right ones, after. **a, b** PE, **c, d** PE + 10% *Arundo* fibers, **e, f** PE + 10% treated *Arundo* fibers

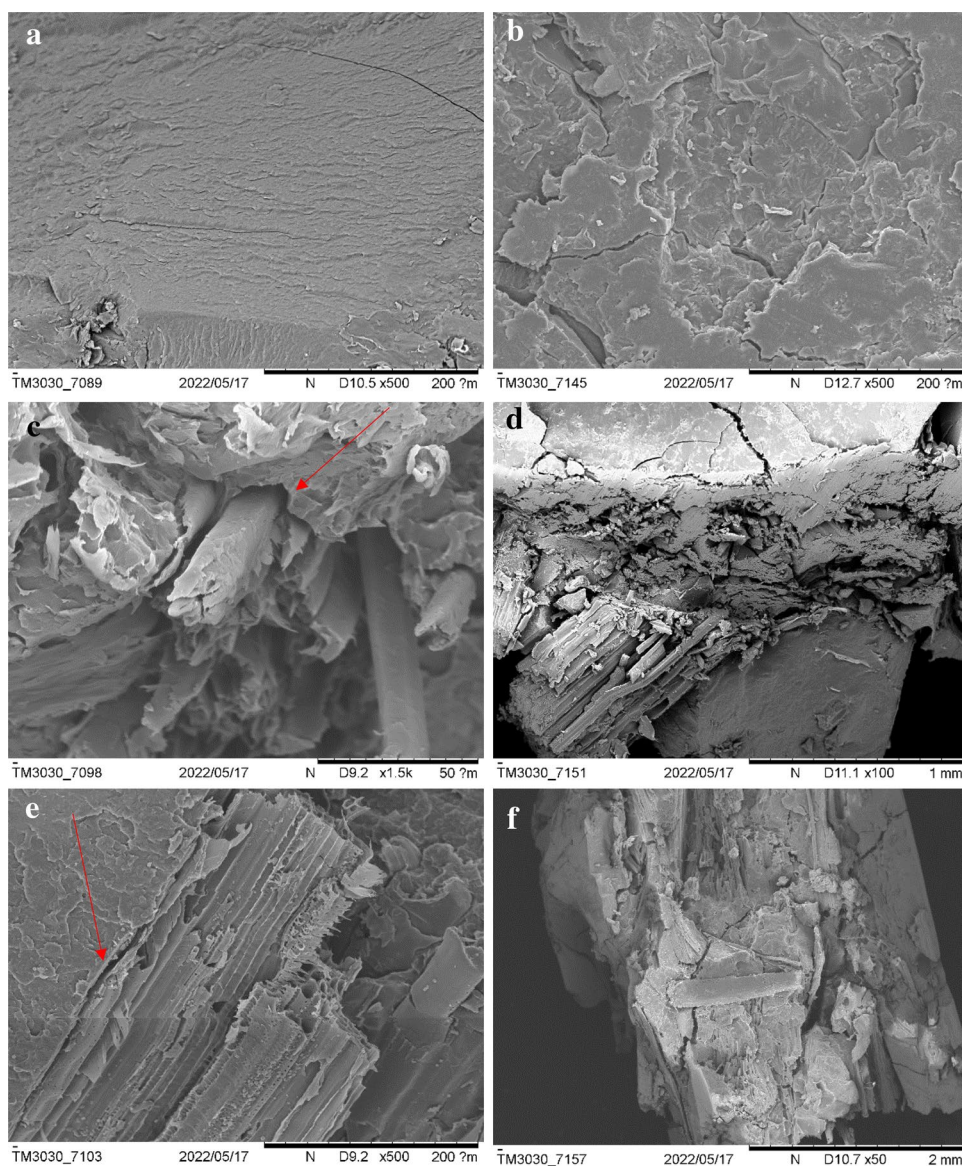


[16]. This is also observed here for T_m , which may indicate that the PLA matrix did not suffer any degradation during the processing. No cold crystallization is observed, probably because a high crystallinity level can be obtained from the process, due to the long cycle time, especially in the cooling stage. Other authors [17] found lower crystallinity values in this same process, although with a different PLA grade, also observing increases in this parameter with the introduction of lignocellulosic materials and finding a cold crystallization band. A crystallization peak in the cooling stage is observed for all samples, contrary to what was observed by Andrzejewski et al. in their mentioned work. However, other authors obtaining high crystallinity levels for the neat PLA have also observed a decrease in crystallinity when introducing foreign materials [59], thus showing the dependence of crystallinity levels with the PLA grade and the filler/

reinforcement used. Greco et al. [4] have demonstrated that rotomolded PLA after aging for 60 days at room temperature does not show any cold crystallization peak, which is in line with observations in this study, where DSC was performed not immediately after parts obtaining. So, *Arundo* fibers may act in this paper not as a nucleating agent but as hindering the crystallization naturally occurring for this material.

Once more, PLA samples show significant changes in the thermal behavior because of the assay. The melting and glass transition temperature decreased in the samples after the biological assay. This may indicate a reduction of the average molecular weight of the polymer and, thus, that the assay affects (degrades to some extent) the matrix. The composites show higher reductions than the neat PLA samples, which means that the introduction of fibers positively impacts the material's disintegration. This is probably due to the higher

Fig. 5 SEM micrographs for PLA samples. Left pictures correspond to samples before disintegration assay, right ones, after. **a, b** PLA, **c, d** PLA + 10% Arundo fibers, **e, f** PLA + 10% treated Arundo fibers



water absorption found for composite samples, as moisture has been determined as a determinant factor in the biodegradation process.

Table 3 Thermal parameters for PE samples from DSC assays

Material	T _{m1} (°C)	T _{m2} (°C)	T _c (°C)	χ ₁ (%)
Before the disintegration assay				
PE	129.0 ± 0.5	127.0 ± 0.1	109.9 ± 0.2	41.4 ± 0.8
PE.AD	129.6 ± 0.4	128.4 ± 0.3	108.2 ± 0.2	34.3 ± 5.3
PE.ADt	129.1 ± 0.1	127.2 ± 0.0	109.7 ± 0.0	38.1 ± 5.6
After the disintegration assay				
PE	129.3 ± 0.9	128.5 ± 0.8	108.5 ± 0.7	30.6 ± 2.5
PE.AD	129.7 ± 0.1	126.8 ± 0.0	109.9 ± 0.0	37.9 ± 0.5
PE.ADt	131.3 ± 1.2	128.3 ± 0.6	108.5 ± 0.8	31.7 ± 3.2

The second heating curve for samples after the disintegration assay shows a double melting peak, not appearing in the first heating. This can be explained by the first thermal heating, where the PLA thin crystals' are able to melt and recrystallize at low heating rates, the existence of more than one crystal structure, or the presence of different lamella morphologies [38]. This ability to crystallize can be seen in the second heating cycle, which continues showing high crystallinity levels.

FTIR

FTIR spectra for PE samples show no variations among the fingerprint of pure PE or composites (Fig. 6), thus meaning the polymer fully covers the fibers. The main differences are a wide band (low intensity) between 3600

and 3000 cm^{-1} and the appearance of small bands between 1200 and 900 cm^{-1} , which are attributed to the presence of fibers. For samples after the disintegration assay, these differences are even less noticeable. If the spectra before and after the assay are compared, no differences are found, thus evidencing, once again, the low effect of the assay on the properties of the composite. Some works studying the aging of PE point out the appearance of some peaks in the FTIR spectra related to carbonyl, peroxides, and unsaturated groups at around 1700 , 1200 , and 900 cm^{-1} [60], while differences in the intensities at 2920 , 1465 and 717 cm^{-1} are indicative of degradation [61]. The evaluations performed in this work have not found any of these

bands for PE, meaning none of these groups are present in the samples, or at least not in a noticeable proportion.

On the other hand, for PLA samples, no difference is observed with the introduction of fibers in the matrix (Fig. 7). At the same time, some evident changes can be seen when comparing the spectra before and after the disintegration assay, as peaks for fiber overlap those of PLA and because polymer mostly covers the fibers. So, no evident interaction between the fibers and the matrix is observed, as otherwise observed in SEM micrographs. These spectra show the typical bands for PLA, that is, carbonyl ($\text{C}=\text{O}$) stretch in lactide (1747 cm^{-1}), CH_3 bend (1465 cm^{-1} , 1381 cm^{-1} , and 1127 cm^{-1}), $\text{C}-\text{O}$ stretch (1180 , 1078 and 1043 cm^{-1}). Bands at 866 and 756 cm^{-1} are related,

Table 4 Thermal parameters for PLA samples from DSC assays

Material	T_{m1} ($^{\circ}\text{C}$)	T_{m2} ($^{\circ}\text{C}$)	T_c ($^{\circ}\text{C}$)	χ_1 (%)	χ_2 (%)	T_g ($^{\circ}\text{C}$)
Before the disintegration assay						
PLA	170.4 ± 1.4	167.3 ± 3.0	109.0 ± 0.4	61.9 ± 5.5	52.1 ± 10.8	58.1 ± 0.7
PLA.AD	174.5 ± 2.7	172.9 ± 4.5	108.4 ± 1.6	45.6 ± 3.0	41.5 ± 8.8	67.7 ± 1.2
PLA.ADt	175.7 ± 0.4	175.2 ± 0.1	110.1 ± 0.1	40.2 ± 2.4	36.4 ± 0.2	68.9 ± 0.1
After the disintegration assay						
PLA	168.5 ± 1.8	163.1 ± 2.5	107.2 ± 3.6	57.7 ± 12.3	48.0 ± 9.0	59.1 ± 2.8
PLA.AD	170.3 ± 1.4	164.4 ± 0.7	109.9 ± 0.2	48.7 ± 2.5	48.9 ± 3.0	62.9 ± 0.4
PLA.ADt	168.2 ± 0.1	159.2 ± 4.7	107.4 ± 2.0	59.9 ± 6.9	55.7 ± 8.6	63.6 ± 3.0

Fig. 6 FTIR spectra for PE samples before the disintegration assay (left) and after (right)

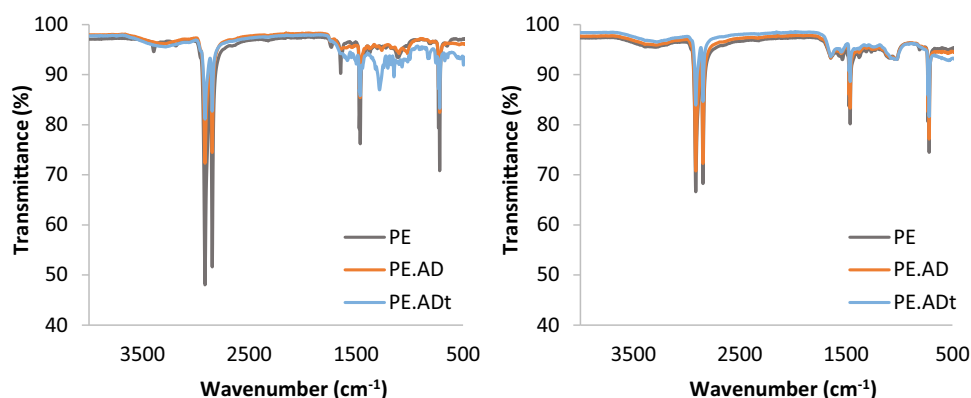
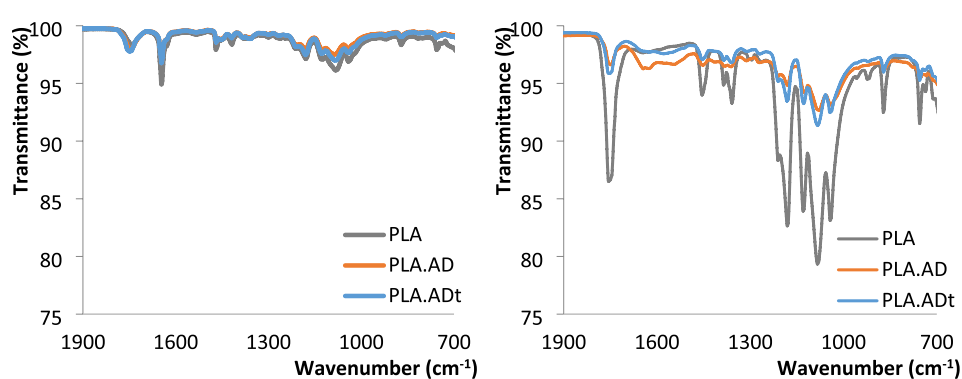


Fig. 7 FTIR spectra for PLA samples before the disintegration assay (left) and after (right)



respectively, to the amorphous and crystalline phases of PLA [11, 62]. Gorrasi et al. also propose using the band at 920 cm^{-1} as an indicator of crystallinity [48].

To determine the degradation extent, the bands related to carbonyl groups and ester groups are of particular interest because the degradation of the matrix can lead to the formation of anhydrides, carbonyl, and carboxyl groups. Some ratios are calculated with the absorption values for these bands, using the band for $-\text{CH}_3$ to normalize results [11, 52]. Table 5 shows the absorption values for these bands and the ratios obtained by dividing them by this at 1465 cm^{-1} . Ratios 1–3 (related to disintegration) show a significant increase in the comparisons before and after the disintegration assay, showing the extent of the modifications in the materials. For R4, related to the sample crystallinity, no trend is observed, which otherwise correlates with the DSC results on this parameter; this same observation is made when comparing the peaks at 922 cm^{-1} . On the other hand, higher ratios are also observed for composites than for neat PLA, as these refer to carboxyl and ester groups, also present in fibers.

Conclusion

Arundo donax fibers from stems have been introduced into rotomolded PE and PLA matrixes following a simple dry blending method, obtaining acceptable porosity levels and good fiber distribution. The impact properties are greatly affected by introducing 10% of fibers for both matrixes. PE composites show similar flexural behavior to pure PE, with a decrease of around 15% in tensile strength and an increase of over 20% in elastic modulus. PLA composites show similar properties to neat PLA, except for a significant decrease (around 40%) in flexural strength. The relatively poor mechanical behavior of the composites can be explained by the presence of voids and the poor adhesion between fiber and matrix, as found in SEM observations. NaOH fiber treatment does not affect the composite's mechanical or thermal properties.

Regarding the bio-disintegration assays, PE is almost unaffected, as no changes in FTIR spectra, calorimetric behavior, or morphology features are found. The composite after the assay seems to be slightly more hydrophilic and has less crystallinity. On the other hand, modifications to PLA-based materials are visible just after recovering the samples from the synthetic residue prepared. For these parts, many cracks are observed, especially for composite samples. The degradation is confirmed in DSC assays, with a reduction in glass transition and melting temperatures. FTIR analysis also shows the degradation of the matrix, with the increase in the intensity of bands related to carbonyl and ester groups; some ratios calculated for these peaks and normalized show the extent of the modifications achieved. The treated fiber composites show higher values for these ratios, which the presence of residual alkali solution may explain.

The weight loss of the samples during the bio-disintegration assay is almost null for the PE samples, being also quite low for the PLA samples. This can be explained by the low temperature used in the process and the characteristics of the PLA grade used in this work, with high crystallinity and L-isomer.

The greater extent of modification found for PLA composites compared to neat PLA can be explained by the higher water absorption due to the natural fibers' addition, which is an essential step for PLA degradation. Further assays should be performed to determine the changes in the polymer matrix, for example, if PLA has reduced its average molecular weight. Besides, the crystallinity of samples using X-ray diffraction could also help understand how the incorporation of fibers affects the crystallinity of these composites and if this is modified during the bio-disintegration process. Finally, micro-CT could also be performed before and after the assay to determine changes in porosity.

This paper shows the extent of the modifications that occurred in lignocellulosic fibers/PLA composites in a low-temperature disintegration process, as a first approach to determining the biodegradability of these materials.

Supplementary Information The online version contains supplementary material available at <https://doi.org/10.1007/s10924-022-02542-x>.

Table 5 Absorption ratios for characteristic bands in PLA degradation

Material	R1 = 1747/1465	R2 = 1183/1465	R3 = 1085/1465	R4 = 756/866
Before the disintegration assay				
PLA	0.679	1.244	0.849	1.119
PLA.AD	1.043	1.252	0.925	0.970
PLA.ADt	2.064	2.503	2.108	1.030
After the disintegration assay				
PLA	2.702	4.030	3.324	1.124
PLA.AD	1.597	2.727	1.961	1.128
PLA.ADt	1.947	3.159	2.510	1.132

Author Contributions ZO, LS and MDM performed the study conception and design. Material preparation, data collection and analysis were performed by LS, FR, RP and ZO. ZO wrote the first draft of the manuscript, and all authors commented on its previous versions. All authors read and approved the final manuscript.

Funding Open Access funding provided thanks to the CRUE-CSIC agreement with Springer Nature. European Funding for Regional Development (FEDER) funded this research through the INTERREG MAC 2014–2020 program, providing funds for MAC Inv2Mac project (Grant number MAC2/4.6d/229). Luis Suárez also acknowledges the funding through the Ph.D. grant program cofinanced by the Canarian Agency for Research, Innovation and Information Society of the Canary Islands Regional Council for Employment, Industry, Commerce and Knowledge (ACIISI) and by the European Social Fund (ESF) (Grant number TESIS2021010008).

Data Availability The datasets generated or analyzed during the current study are available from the corresponding author upon reasonable request.

Declarations

Conflict of interest The authors report there are no competing interests to declare.

Open Access This article is licensed under a Creative Commons Attribution 4.0 International License, which permits use, sharing, adaptation, distribution and reproduction in any medium or format, as long as you give appropriate credit to the original author(s) and the source, provide a link to the Creative Commons licence, and indicate if changes were made. The images or other third party material in this article are included in the article's Creative Commons licence, unless indicated otherwise in a credit line to the material. If material is not included in the article's Creative Commons licence and your intended use is not permitted by statutory regulation or exceeds the permitted use, you will need to obtain permission directly from the copyright holder. To view a copy of this licence, visit <http://creativecommons.org/licenses/by/4.0/>.

References

- Hejna A, Barczewski M, Andrzejewski J et al (2020) Rotational molding of linear low-density polyethylene composites filled with wheat bran. *Polymers* (Basel) 12:1004. <https://doi.org/10.3390/POLYM12051004>
- Greco A, Maffezzoli A (2016) Rotational moulding of poly-lactic acid. *AIP Conf Proc* 1779:060007. <https://doi.org/10.1063/1.4965528>
- Greco A, Maffezzoli A (2017) Rotational molding of poly(lactic acid): effect of polymer grade and granulometry. *Adv Polym Technol* 36:477–482. <https://doi.org/10.1002/ADV.21630>
- Greco A, Ferrari F, Maffezzoli A (2019) Processing of super tough plasticized PLA by rotational molding. *Adv Polym Technol* 2019:1–8. <https://doi.org/10.1155/2019/3835829>
- González-López ME, Pérez-Fonseca AA, Manríquez-González R et al (2019) Effect of surface treatment on the physical and mechanical properties of injection molded poly(lactic acid)-coir fiber biocomposites. *Polym Compos* 40:2132–2141. <https://doi.org/10.1002/pc.24997>
- Ruiz-Silva E, Rodríguez-Ortega M, Rosales-Rivera LC et al (2021) Rotational molding of poly(Lactic Acid)/polyethylene blends: effects of the mixing strategy on the physical and mechanical properties. *Polymers* 13:217. <https://doi.org/10.3390/POLYM13020217>
- Vignali A, Iannace S, Falcone G (2019) Lightweight poly(ϵ -Caprolactone) composites with surface modified hollow glass microspheres for use in rotational molding: thermal, rheological and mechanical properties. *Polymers* 11:624. <https://doi.org/10.3390/POLYM11040624>
- Díaz S, Ortega Z, McCourt M et al (2018) Recycling of polymeric fraction of cable waste by rotational moulding. *Waste Manag* 76:199–206. <https://doi.org/10.1016/J.WASMAN.2018.03.020>
- Pick L, Hanna PR, Gorman L (2022) Assessment of processability and properties of raw post-consumer waste polyethylene in the rotational moulding process. *J Polym Eng* 42:374–383. <https://doi.org/10.1515/POLYENG-2021-0212/MACHINEREA-DABLECITATION/RIS>
- Barczewski M, Hejna A, Aniśko J et al (2022) Rotational molding of polylactide (PLA) composites filled with copper slag as a waste filler from metallurgical industry. *Polym Test* 106:107449. <https://doi.org/10.1016/J.POLYMERTESTING.2021.107449>
- Aniśko J, Barczewski M, Mietliński P et al (2022) Valorization of disposable polylactide (PLA) cups by rotational molding technology: the influence of pre-processing grinding and thermal treatment. *Polym Test* 107:107481. <https://doi.org/10.1016/j.polymertesting.2022.107481>
- Cisneros-López EO, Pal AK, Rodríguez AU et al (2020) Recycled poly(lactic acid)-based 3D printed sustainable biocomposites: a comparative study with injection molding. *Mater Today Sustain*. <https://doi.org/10.1016/j.mtsust.2019.100027>
- Torres FG, Aragon CL (2006) Final product testing of rotational moulded natural fibre-reinforced polyethylene. *Polym Test* 25:568–577. <https://doi.org/10.1016/j.polymertesting.2006.03.010>
- Wang B, Panigrahi S, Tabil L, Crerar W (2007) Pre-treatment of flax fibers for use in rotationally molded biocomposites. *J Reinf Plast Compos* 26:447–463. <https://doi.org/10.1177/0731684406072526>
- Ortega Z, Monzón MD, Benítez AN et al (2013) Banana and abaca fiber-reinforced plastic composites obtained by rotational molding process. *Mater Manuf Process* 28:879–883. <https://doi.org/10.1080/10426914.2013.792431>
- Cisneros-López EO, Pérez-Fonseca AA, González-García Y et al (2018) Polylactic acid-agave fiber biocomposites produced by rotational molding: a comparative study with compression molding. *Adv Polym Technol* 37:2528–2540. <https://doi.org/10.1002/adv.21928>
- Andrzejewski J, Krawczak A, Wesoly K, Szostak M (2020) Rotational molding of biocomposites with addition of buckwheat husk filler. Structure-property correlation assessment for materials based on polyethylene (PE) and poly(lactic acid) PLA. *Compos Part B Eng* 202:108410. <https://doi.org/10.1016/j.compositesb.2020.108410>
- González-López ME, Pérez-Fonseca AA, Cisneros-López EO et al (2019) Effect of maleated PLA on the properties of rotomolded PLA-agave fiber biocomposites. *J Polym Environ* 27:61–73. <https://doi.org/10.1007/s10924-018-1308-2>
- Robledo-Ortiz JR, González-López ME, Martín del Campo AS et al (2021) Fiber-matrix interface improvement via glycidyl methacrylate compatibilization for rotomolded poly(lactic acid)/agave fiber biocomposites. *J Compos Mater* 55:201–212. <https://doi.org/10.1177/0021998320946821>
- León LDVE, Escocio VA, Visconte LLY et al (2020) Rotomolding and polyethylene composites with rotomolded lignocellulosic materials: a review. *J Reinf Plast Compos* 39:459–472. <https://doi.org/10.1177/0731684420916529>

21. Ortega Z, Romero F, Paz R et al (2021) Valorization of invasive plants from macaronesia as filler materials in the production of natural fiber composites by rotational molding. *Polymers (Basel)* 13:2220. <https://doi.org/10.3390/polym13132220>
22. Shatalov AA, Pereira H (2013) High-grade sulfur-free cellulose fibers by pre-hydrolysis and ethanol-alkali delignification of giant reed (*Arundo donax* L.) stems. *Ind Crops Prod* 43:623–630. <https://doi.org/10.1016/j.indcrop.2012.08.003>
23. Fiore V, Scalici T, Valenza A (2014) Characterization of a new natural fiber from *Arundo donax* L. as potential reinforcement of polymer composites. *Carbohydr Polym* 106:77–83. <https://doi.org/10.1016/j.carbpol.2014.02.016>
24. Suárez L, Castellano J, Romero F et al (2021) Environmental hazards of giant reed (*Arundo donax* L.) in the macaronesia region and its characterisation as a potential source for the production of natural fibre composites. *Polymers (Basel)*. <https://doi.org/10.3390/polym13132101>
25. Shatalov AA, Duarte LC, Carvalheiro F et al (2013) CROP-BIOREF: Integrated strategy for the upgrading of giant reed (*Arundo donax* L.) for materials and chemicals. *Proc 2nd Iber-oam Congr Biorefineries* 2013:641–648
26. Brusca S, Cosentino SL, Famoso F et al (2018) Second generation bioethanol production from *Arundo donax* biomass: an optimization method. *Energy Procedia*. Elsevier Ltd, Amsterdam
27. Shatalov AA, Pereira H (2012) Xylose production from giant reed (*Arundo donax* L.): modeling and optimization of dilute acid hydrolysis. *Carbohydr Polym* 87:210–217. <https://doi.org/10.1016/j.carbpol.2011.07.041>
28. Licursi D, Antonetti C, Mattonai M et al (2018) Multi-valorisation of giant reed (*Arundo Donax* L.) to give levulinic acid and valuable phenolic antioxidants. *Ind Crops Prod* 112:6–17. <https://doi.org/10.1016/j.indcrop.2017.11.007>
29. Antonetti C, Bonari E, Licursi D et al (2015) Hydrothermal conversion of giant reed to furfural and levulinic acid: optimization of the process under microwave irradiation and investigation of distinctive agronomic parameters. *Molecules* 20:21232–21353. <https://doi.org/10.3390/molecules201219760>
30. Calvo MV, Colombo B, Corno L et al (2018) Bioconversion of giant cane for integrated production of biohydrogen, carboxylic acids, and polyhydroxyalkanoates (PHAs) in a multistage biorefinery approach. *ACS Sustain Chem Eng* 6:15361–15373. <https://doi.org/10.1021/ACSUSCHEMENG.8B03794>
31. Ventorino V, Robertiello A, Cimini D et al (2017) Bio-based succinate production from *Arundo donax* hydrolysate with the new natural succinic acid-producing strain *Basfia succiniciproducens* BPP7. *BioEnergy Res* 10:488–498. <https://doi.org/10.1007/s12155-017-9814-y>
32. Piperopoulos E, Khaskhoussi A, Fiore V, Calabrese L (2021) Surface modified *Arundo donax* natural fibers for oil spill recovery. *J Nat Fibers*. <https://doi.org/10.1080/15440478.2021.1961343>
33. Cano-Ruiz J, Ruiz Galea M, Amorós MC et al (2020) Assessing *Arundo donax* L. in vitro-tolerance for phytoremediation purposes. *Chemosphere* 252:126576. <https://doi.org/10.1016/J.CHEMOSPHERE.2020.126576>
34. Raposo Oliveira Garcez L, Hofmann Gatti T, Carlos Gonzalez J et al (2022) Characterization of fibers from culms and leaves of *Arundo donax* L. (Poaceae) for handmade paper production. *J Nat Fibers*. <https://doi.org/10.1080/15440478.2022.2076005>
35. Gulihonenahali Rajkumar A, Hemath M, Kurki Nagaraja B et al (2021) An artificial neural network prediction on physical, mechanical, and thermal characteristics of giant reed fiber reinforced polyethylene terephthalate composite. *J Ind Text*. <https://doi.org/10.1177/15280837211064804>
36. Dahmardeh Ghalehno M, Madhoushi M, Tabarsa T, Nazerian M (2010) The manufacture of particleboards using mixture of reed (surface layer) and commercial species (middle layer). *Eur J Wood Wood Prod* 69(69):341–344. <https://doi.org/10.1007/S00107-010-0437-7>
37. Ferrandez-García MT, Ferrandez-García A, García-Ortuño T et al (2020) Assessment of the physical, mechanical and acoustic properties of *Arundo donax* L. biomass in low pressure and temperature particleboards. *Polymers* 12:1361. <https://doi.org/10.3390/POLYM12061361>
38. Fiore V, Botta L, Scaffaro R et al (2014) PLA based biocomposites reinforced with *Arundo donax* fillers. *Compos Sci Technol* 105:110–117. <https://doi.org/10.1016/j.compscitech.2014.10.005>
39. Monsalve Alarcón J, Sánchez Cruz M, Baquero Bastos D (2018) Evaluation of the physical and mechanical properties of caña brava (*Arundo donax*) reinforced panels. *INGE CUC* 14:66–74. <https://doi.org/10.17981/ingecuc.14.1.2018.06>
40. Fiore V, Scalici T, Vitale G, Valenza A (2014) Static and dynamic mechanical properties of *Arundo donax* fillers-epoxy composites. *Mater Des* 57:456–464. <https://doi.org/10.1016/j.matdes.2014.01.025>
41. Scalici T, Fiore V, Valenza A (2016) Effect of plasma treatment on the properties of *Arundo donax* L. leaf fibres and its bio-based epoxy composites: a preliminary study. *Compos Part B Eng* 94:167–175. <https://doi.org/10.1016/j.compositesb.2016.03.053>
42. Comité Técnico CTN 53 (2008) UNE-CEN/TR 15351 IN: plásticos. Guía terminológica en el campo de los plásticos y polímeros degradables y biodegradables
43. Shah AA, Hasan F, Hameed A, Ahmed S (2008) Biological degradation of plastics: a comprehensive review. *Biotechnol Adv* 26:246–265. <https://doi.org/10.1016/j.biotechadv.2007.12.005>
44. Husárová L, Pekařová S, Stloukal P et al (2014) Identification of important abiotic and biotic factors in the biodegradation of poly(l-lactic acid). *Int J Biol Macromol* 71:155–162. <https://doi.org/10.1016/J.IJBIOMAC.2014.04.050>
45. Agarwal M, Koelling KW, Chalmers JJ (1998) Characterization of the degradation of polylactic acid polymer in a solid substrate environment. *Biotechnol Prog* 14:517–526. <https://doi.org/10.1021/BP980015P>
46. Ruggero F, Belardi S, Carretti E et al (2022) Rigid and film bioplastics degradation under suboptimal composting conditions: a kinetic study. *Waste Manag Res* 40:1311–1321. <https://doi.org/10.1177/0734242X211063731>
47. Boonmee C, Kositanont C, Leejarkpai T (2022) Degradation behavior of biodegradable plastics in thermophilic landfill soil and wastewater sludge conditions. *Environ Res Eng Manag* 78:57–69. <https://doi.org/10.5755/J01.EREM.78.1.29502>
48. Gorrasi G, Pantani R (2013) Effect of PLA grades and morphologies on hydrolytic degradation at composting temperature: assessment of structural modification and kinetic parameters. *Polym Degrad Stab* 98:1006–1014. <https://doi.org/10.1016/J.POLYMDEGRADSTAB.2013.02.005>
49. Cucina M, De Nisi P, Trombino L et al (2021) Degradation of bioplastics in organic waste by mesophilic anaerobic digestion, composting and soil incubation. *Waste Manag* 134:67–77. <https://doi.org/10.1016/J.WASMAN.2021.08.016>
50. Oliveira MAS, Pickering KL, Sunny T, Lin RJT (2021) Treatment of hemp fibres for use in rotational moulding. *J Polym Res* 28:3. <https://doi.org/10.1007/s10965-021-02414-3>
51. Bayerl T, Geith M, Somashekar AA, Bhattacharyya D (2014) Influence of fibre architecture on the biodegradability of FLAX/PLA composites. *Int Biodeterior Biodegrad* 96:18–25. <https://doi.org/10.1016/j.ibiod.2014.08.005>
52. Moliner C, Finocchio E, Arato E et al (2020) Influence of the degradation medium on water uptake, morphology, and chemical structure of poly(lactic acid)-sisal bio-composites. *Materials (Basel)* 13:3974. <https://doi.org/10.3390/ma13183974>

53. Dong Y, Ghataura A, Takagi H et al (2014) Polylactic acid (PLA) biocomposites reinforced with coir fibres: evaluation of mechanical performance and multifunctional properties. *Compos Part A Appl Sci Manuf* 63:76–84. <https://doi.org/10.1016/j.compositesa.2014.04.003>
54. Hanana FE, Rodrigue D (2021) Effect of particle size, fiber content, and surface treatment on the mechanical properties of maple-reinforced LLDPE produced by rotational molding. *Polym Polym Compos* 29:343–353. <https://doi.org/10.1177/0967391120916602>
55. Cisneros-López EO, González-López ME, Pérez-Fonseca AA et al (2017) Effect of fiber content and surface treatment on the mechanical properties of natural fiber composites produced by rotomolding. *Compos Interfaces* 24:35–53. <https://doi.org/10.1080/09276440.2016.1184556>
56. Monzón MD, Ortega Z, Benítez AN et al (2012) Developments towards a more sustainable rotational moulding process. *ECCM 2012 Compos Venice Proc 15th Euro Conf Compos Mater* 2012:1–8
57. Abhilash SS, Singaravelu DL (2020) Effect of fiber content on mechanical and morphological properties of bamboo fiber-reinforced linear low-density polyethylene processed by rotational molding. *Trans Indian Inst Met* 73:1549–1554. <https://doi.org/10.1007/s12666-020-01922-y>
58. Höfler G, Lin RJT, Jayaraman K (2018) Rotational moulding and mechanical characterisation of halloysite reinforced polyethylenes. *J Polym Res*. <https://doi.org/10.1007/s10965-018-1525-3>
59. Huda MS, Drzal LT, Mohanty AK, Misra M (2007) The effect of silane treated- and untreated-talc on the mechanical and physico-mechanical properties of poly(lactic acid)/newspaper fibers/talc hybrid composites. *Compos Part B Eng* 38:367–379. <https://doi.org/10.1016/J.COMPOSITESB.2006.06.010>
60. Fritz M, Lauschke T, Schlebrowski T et al (2022) Photoaging phenomena of biodegradable polybutylene succinate and conventional low density polyethylene by artificial weathering – a comparative surface study. *Appl Surf Sci* 590:153058. <https://doi.org/10.1016/J.APSUSC.2022.153058>
61. Huang C, Liao Y, Zou Z et al (2022) Novel strategy to interpret the degradation behaviors and mechanisms of bio- and non-degradable plastics. *J Clean Prod* 355:131757. <https://doi.org/10.1016/J.JCLEPRO.2022.131757>
62. Arrieta MP, López J, Rayón E, Jiménez A (2014) Disintegrability under composting conditions of plasticized PLA–PHB blends. *Polym Degrad Stab* 108:307–318. <https://doi.org/10.1016/J.POLYMDEGRADSTAB.2014.01.034>

Publisher's Note Springer Nature remains neutral with regard to jurisdictional claims in published maps and institutional affiliations.

6.10. GIANT REED (*ARUNDO DONAX* L.) ENHANCED
POLYLACTIC ACID COMPOSITES: PROCESSING,
CHARACTERIZATION, AND PERFORMANCE OF
INJECTION MOULDED AND WATER DEGRADED SAMPLES

P1

P2

P3

P4

P5

P6

P7

P8

P9

P10

Giant reed (*Arundo donax* L.) enhanced polylactic acid composites: processing, characterization, and performance of injection moulded and water degraded samples.

Luis Suárez^{1*}, Mateusz Barczewski², Patryk Mietliński³, Andrzej Miklaszewski⁴, Paul Hanna⁵, Zaida Ortega⁶

¹ Departamento de Ingeniería Mecánica, Universidad de Las Palmas de Gran Canaria, Campus universitario de Tafira Baja, 35017, Las Palmas, Spain

² Poznan University of Technology, Institute of Materials Technology, Piotrowo 3, 61-138 Poznań, Poland

³ Poznan University of Technology, Institute of Mechanical Technology, Piotrowo 3, 61-138 Poznań, Poland

⁴ Poznan University of Technology, Institute of Materials Engineering, Jana Pawła II 24, 61-138 Poznań, Poland

⁵ AMIC Sustainable Polymers and Composites, Queen's University of Belfast, Ashby Building, BT9 5AH, Belfast, Northern Ireland, United Kingdom

⁶ Departamento de Ingeniería de Procesos, Universidad de Las Palmas de Gran Canaria, Campus universitario de Tafira Baja, 35017, Las Palmas, Spain

* Corresponding author: luis.suarez@ulpgc.es

ABSTRACT

Keywords:

Arundo Donax

polylactic acid

water absorption

mechanical performance

This study explores the incorporation of renewable resources from *Arundo Donax* plant into a polylactic acid (PLA) matrix to enhance mechanical properties and promote ecological sustainability. By utilizing lignocellulosic fillers obtained from this fast-growing plant species, with high biomass yield and low input requirements, this approach aims to reduce plastic waste and contribute to a circular economy. Two types of fillers, stem fibres and shredded plant particles, were introduced into the biopolymer matrix, assessing their performance in water contact applications, with a focus on how increased hydrophilicity from filler affects material properties. Characterization tests, including rheological analysis, TGA, DSC, WAXS, and DMTA, were conducted on extruded pellets and moulded samples to evaluate their structure, properties, and performance. Results indicate that *Arundo* fillers minimally alters the chemical structure of the composites, while rheological behaviour is significantly influenced by the filler type and loading. Thermal degradation varies slightly with filler content, maintaining stability suitable for injection moulding. Mechanical performance is optimized with 10% and 20% filler content, enhancing stiffness and impact strength, while higher fibre content (40%) leads to increased brittleness. The study highlights the critical impact of the filler type on moisture absorption. Water saturation significantly reduces tensile strength, while some properties partially recover upon re-drying, underscoring the resilience of PLA/*Arundo* composites under moderate loads despite the challenges of wet conditions. This research emphasizes the complex interplay between filler characteristics, composite structure, and their effects on mechanical properties, crucial for evaluating the suitability of PLA composites in various applications.

1. Introduction

The increasing global concern regarding the environmental impact of conventional plastics has urged the shift towards biopolymers and sustainable materials. Plastics, though versatile and essential in various industries and daily life, have raised significant environmental issues due to their non-biodegradable nature, contributing to pollution and ecosystem disruption [1,2]. As the accumulation of plastic waste increases, the need for biodegradable alternatives becomes urgent, together with an increase in the recycling capabilities. Research indicates that approximately 79 % of plastic waste ends up in landfills or the ocean, posing significant risks to both terrestrial and aquatic ecosystems [3,4]. This plastic crisis has raised awareness about the environmental repercussions of conventional plastics, primarily their resistance to degradation and the resulting pollution, pushing researchers and policymakers to seek sustainable alternatives [3,5–7]. The global production levels of conventional plastics continue to rise, complicating waste management efforts and environmental sustainability [6,8]. The commitment to finding renewable biodegradable or compostable plastics, such as polylactic acid (PLA) and polyhydroxyalkanoates (PHAs), arises from the recognition that these materials can potentially reduce the ecological footprint of human activities [9–11]. Ongoing studies are exploring various bioplastic materials derived from renewable resources and designed to biodegrade effectively, making it clear that the transition to bioplastics is an essential response to the environmental crisis posed by conventional plastics for single use applications [9,12–15]. The shift to biopolymers like PLA represents a critical step in addressing the challenges posed by plastic waste accumulation [5,16], taking advantage of their potential biodegradability and contributing to reduce the dependence on fossil fuels, leading to a more sustainable material economy [2,17]. Furthermore, biopolymers exhibit diverse physical and mechanical properties, opening exciting new paths for their use in applications earlier dominated by conventional plastics.

In this context, the incorporation of natural fibres, particularly lignocellulosic fibres, into biopolymers is an area of growing interest due to the synergistic benefits provided by such composites. Lignocellulosic fibres are abundant, renewable, and often biodegradable, making them ideal candidates for reinforcing biopolymer matrices. By blending natural fibres with biopolymers, the resultant composites show enhanced mechanical properties, improved thermal stability, and reduced environmental footprints compared to their synthetic counterparts [1,18,19]. For instance, the inclusion of fibres derived from *Arundo donax* L., a fast-growing species, can significantly enhance the strength and stiffness of biopolymer composites, aligning with sustainability goals without compromising performance [20–23]. These composites have garnered attention for applications in the automotive, packaging, and construction sectors, thereby contributing to a circular economy where materials are utilized and recycled efficiently [17,18].

Focusing specifically on *Arundo donax*, the giant reed shows exceptional potential as a reinforcement of polylactic acid (PLA) composites. This species is characterized by its rapid growth rate and ability to thrive in marginal conditions and boasts a rich

lignocellulosic composition that can be leveraged in the production of high-value biocomposites [1,23,24]. Studies illustrate that composites reinforced with reed fibres achieve considerable mechanical improvements, making them suitable for various load-bearing applications [20,25–29]. Research by Fiore et al. indicates that reed-PLA composites exhibit enhanced tensile strength and modulus, critical parameters for their acceptance in industrial applications [19]. Moreover, the use of giant reed in composite formulations contributes to the valorisation of agricultural waste, effectively diverting biomass from landfills and promoting resource efficiency [1,24,28].

In addition to mechanical properties, the ecological advantages of using *Arundo donax* in biocomposite formulations cannot be disregarded. With its capacity to sequester carbon and adapt to varying soil conditions, giant reed offers an environmentally friendly biomass solution for composite production [17,24,29]. Its ability to grow rapidly in adverse environments makes it attractive for biofuel production, while its lignocellulosic composition lends itself well to fibre extraction. Besides, the cascade-approach biorefinery approach can be applied to *Arundo donax* in order to ease the extraction of various high-value products such as sugars, fibres, and polyphenols, enhancing its economic viability as a raw material for composite applications [1,17,22,30,31]. This multi-faceted usage thus contributes to both biological sustainability and economic resilience within the biopolymer industry.

The growth rates and adaptability of giant reed in conditions unsuitable for food crops underscore its value as a renewable resource in the context of climate change and resource scarcity, contributing also to the strategies against soil losses [1,22,24,32,33]. While challenges such as invasion of natural habitats exist, due to its rapid growth, a responsible management of this species can unlock a pathway to sustainable industrial applications that mitigate environmental impact and promote resource circularity [22,34–38]. By harnessing the potential of *Arundo donax* as a reinforcing fibre within PLA composites, researchers and industries can contribute significantly to the shift towards more sustainable materials and practices.

In this work, two different fractions from giant reed have been used: fibres extracted by chemo-mechanical means from culms and shredded aerial parts of the plant, as explained in previous works [28,30]. Composites ranging from 5 to 40 % have been produced and comprehensively characterized in order to determine their performance and how the incorporation of these lignocellulosic fractions modifies those of the neat PLA matrix. An analysis of the variation of the properties of the composites as a consequence of their water soaking and re-drying has also been performed, as a way to determine their performance in service conditions involving water contact applications, such as in food packaging. The aim of these tests was to assess the potential degradation of the materials arising from the increased hydrophilicity of the composites due to the addition of lignocellulose fillers.

2. Materials and methods

2.1. Materials

Natural fibre composites, based on a biobased polylactic acid (PLA) matrix and lignocellulosic fillers from giant reed (*Arundo Donax* L.), were prepared by twin-screw extrusion compounding and subsequently processed by injection moulding. The polymer used was a high flow Poly(L-lactic acid) homopolymer, Luminy L105® from TotalEnergies Corbion, in pellet form, with melt flow index (MFI) of 30 g/10 min (190°C/2.16 kg), density of 1.24 g/cm³, and stereochemical purity $\geq 99\%$ (L-isomer) according to the producer's specifications.

Fibres and shreds of *Arundo Donax* were prepared as described in a previous research work [30]. In brief, the aerial parts of the plant—culms and leaves—were ground and then washed with water to create the shredded material. On the other hand, after soaking the reed culms in a 1N NaOH solution for approximately a week (3 litres of solution per kilogram of biomass), the *Arundo* fibres were extracted from the softer biomass using a series of rolling mills. The fibres were trimmed to a length of about 3 millimetres and both types of fillers, fibres and shredded reeds, were sieved to use only the fractions retained by sieves with a mesh size between 75 μm and 1500 μm in compound preparation.

Compounds with 5, 10, 20 and 40 % by weight of filler were prepared. The different formulations are identified based on the type of lignocellulosic material used and its weight percentage. For instance, PLA.F20 denotes composites containing 20 % reed fibres, whereas PLA.S20 indicates composites with 20 % shredded *Arundo*. Samples tested after water saturation are denoted with the suffix WA, specifying -wet for those tested under water-soaked conditions and -dry for those reconditioned following drying after water uptake.

2.2. Compounding and injection moulding processes

A twin screw-extruder, ThermoScientific Process11, with 40:1 L/D ratio, 11 mm diameter and screws configuration comprising three different kneading zones as shown in Figure 1, was used to prepare the compounds. The temperature profile was 160-170-170-180-180-170-165-165°C from hopper to die, and the rotation speed was set at 200 rpm. Prior to compounding, the *Arundo* fillers and PLA were dried overnight at 105°C and 60°C, respectively.

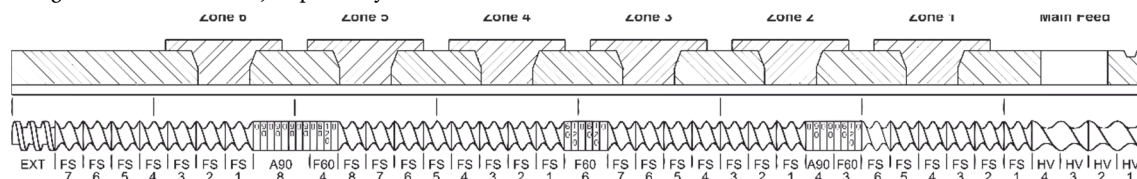


Figure 1. Twin-screw extruder configuration.

An Arburg 320S injection-moulding machine was used to mould 76 x 76 x 1.2 mm square samples (Figure 2). Moisture was removed from the granulated composites overnight at 70°C (- 40°C dew point), prior to injection moulding, using an air dryer. The mould temperature was set at 30°C, and the processing temperature profile was 190-195-200-205-210°C from the hopper to the nozzle. The switchover pressure of moulded parts was measured and the average was calculated for each moulded material. The holding pressure was set at 35 MPa for 6 seconds and the cooling time stage was 35 seconds.



Figure 2. Extruded compound (PLA.F20 and PLA.S20) and injection moulded plates (all formulations).

2.3. Characterization

The extruded pellets and moulded composites were subjected to different characterisation tests to determine their structure and chemical composition, injection-moulding processability, physico-chemical properties and mechanical and thermo-mechanical performance.

Chemical composition was assessed by Fourier Transform Infrared Spectroscopy (FTIR). FTIR spectra were recorded in the wavelength range of 4000 to 600 cm^{-1} using a Perkin Elmer Spectrum 100 spectrophotometer in Attenuated Total Reflectance (ATR) mode using a zinc selenide single bounce crystal. Each spectrum was obtained by 64 scans at 4 cm^{-1} resolution.

Rheological behaviour of PLA-based composites was analysed using an Anton Paar MCR 301 oscillatory rheometer, equipped with 25 mm diameter parallel plates and a 1.5 mm gap. The measurements were conducted at 190°C. Preliminary tests were performed using the strain sweep mode, in order to ensure later experiments are located in the linear viscoelastic (LVE) region. Angular frequency sweeps were performed at 0.02 % strain, in the LVE region, in the 0.5 to 500 rad/s range. To supplement the rheological analysis results, a Kayeness Inc. 7053 apparatus (Dynisco Company) was used to determine the Melt Flow Index (MFI) on composite pellets at 190°C temperature, in accordance with ISO 1133, by applying 2.16 kg load.

The thermal behaviour was evaluated in terms of thermogravimetric analysis (TGA) and differential scanning calorimetry (DSC). TGA was carried out in a nitrogen atmosphere using alumina crucibles and samples that were nominally 10 ± 0.2 mg in a Netzsch TG 209 F1 Libra device. The tests were carried out between 30°C and 900°C at a heating rate of 10°C/min. Meanwhile, DSC analyses were carried out in a Perkin Elmer DSC 6 device under a nitrogen atmosphere and sealed aluminium crucibles. For these tests, nominally 10 ± 0.2 mg samples were prepared. The measurements were taken during two heating cycles, from 30°C to 200°C, at a rate of 10°C/min. The melting (T_{m1} , T_{m2}) and crystallization (T_c) temperatures at both heating and cooling stages were ascertained. Lastly, the degree of crystallinity (χ) was determined by using the melting and crystallization enthalpies (ΔH_{m1} , ΔH_{m2} , and ΔH_c), according to equation 1:

$$\chi = \frac{1}{1-m_f} \cdot \frac{\Delta H_m}{\Delta H_0} \cdot 100 \quad (1)$$

where m_f is the lignocellulosic filler mass rate, ΔH_m is the variation in melting enthalpies and ΔH_0 is the enthalpy for a 100 % crystalline PLA sample (93.1 J/g) [39].

The crystalline structure was also evaluated by wide-angle X-Ray scattering (WAXS). The Pan-analytical Empyrean Almelo apparatus was used to perform WAXS tests using the Bragg–Brentano reflection mode configuration and a copper anode (Cu-K α —1.54 Å, 45 kV, and 40 mA). With 45 seconds for each step of 0.05°, the measurement parameters were set to 3–60° 2 theta.

The injection moulded square plates were laser cut to obtain standardised specimens for mechanical and thermo-mechanical testing. Tensile and flexural tests were performed on a Lloyd LS5 universal testing machine, using a 500N capacity load cell. Tensile properties were assessed following ISO 527-2 standard on ISO 20753 – Type A13 specimens, applying strain rates of 0.25 mm/min for elastic modulus calculation and 1 mm/min for ultimate tensile strength. Bending tests were performed in accordance with ISO 178, using 60 x 25 mm rectangular specimens, 22 mm span between bearings and 1 mm/min strain rate. For the Charpy impact assays they were used notched specimens (ISO 179-1 – Type 2), a 7.5 J pendulum and an impact speed of 3.7 m/s, on a Ceast Resil P/N 6958.000 testing machine, in accordance with ISO 179-1/1eA. Finally, hardness was determined according to ISO 2039 using a KB Prüftechnik ball indentation hardness tester, 132 N load, and a minimum of 7 measurements per material series. The results of all mechanical properties are given as mean values and standard deviation (SD). Tensile and flexural testing were also performed on re-dried samples, after water saturation (as explained later), in order to assess the variation of properties arising from water uptake.

Dynamic Mechanical Thermal Analysis (DMTA) was performed in a Triton 2000 device from Triton Technology to assess the thermomechanical characteristics of the different materials. These tests were performed using a single cantilever bending method in the temperature range of - 50°C to 120°C, with a heating rate of 2°C/min, and a strain of 10 μm was applied at a frequency of 1 Hz. In addition to the glass transition temperature (T_g), storage modulus (E'), loss modulus (E''), and damping factor ($\tan \delta$), the qualitative

indicator of brittleness (B) of the composite materials were determined from the DMTA results as suggested by Brostow [40], using the elongation at break determined by tensile test (ε_b) and the storage modulus (E'), both at room temperature.

$$B = \frac{1}{\varepsilon_b \cdot E'} \quad (2)$$

DMTA results were also used to assess the bond interface between the polymeric matrix and the filler, and to determine their reinforcing efficiency. Analyses were performed on injection-moulded samples, on water-soaked ones (after moisture uptake determination, as explained later) and on re-dried samples. In such an approach, the variation in thermomechanical properties due to humidity can be determined. DMTA can reflect the potential degradation of the PLA matrix or the plastization due to water uptake on humid samples, and, at the same time, a partially reversed adjustment in properties due to the re-establishment of the original PLA structure for the re-dried samples, albeit possibly with some permanent changes due to degradation processes that might have occurred during water exposure.

The C-factor, also known as the effectiveness coefficient, is a measure of how well the filler enhances the mechanical properties of the composite compared to its pure matrix. It was calculated as proposed by Tan et al. [41], from the relation between the ratios of storage moduli in the glassy region (40°C) and the rubbery region (75°C) of the composite to the matrix polymer (Equation 3). This parameter reflects the efficiency of the *Arundo* filler in reinforcing the PLA. A lower C-factor indicates a more efficient reinforcement, suggesting that the filler is effectively contributing to the overall strength and stiffness of the composite.

$$C = \frac{(E'g/E'r)_{\text{composite}}}{(E'g/E'r)_{\text{matrix}}} \quad (3)$$

The quality of the filler distribution within the polymeric matrix is evaluated by the damping reduction (DR) value, which is calculated as follows:

$$DR(\%) = \frac{(\tan \delta)_m - (\tan \delta)_c}{(\tan \delta)_m} \times 100 \quad (4)$$

The adhesion factor (A) is a measure of the strength and quality of the bond between the filler and the matrix. This parameter is determined according to Kubat et al. [42] from the ratio of the damping factor of the composite ($\tan \delta_c$) to that of the pure PLA polymer ($\tan \delta_m$), as well as the corresponding filler volume fraction (V_f). A lower adhesion factor value in natural fibre composites generally indicates stronger adhesion and better compatibility between the fibres and the matrix. This translates to a higher degree of interaction between the two phases, leading to improved mechanical properties and reduced water absorption.

$$A = \frac{1}{1-V_f} \cdot \frac{\tan \delta_c}{\tan \delta_m} - 1 \quad (5)$$

X-ray tomography, model V|tome|x s240 (Waygate Technologies / GE Sensing & Inspection Technologies GmbH), was used to evaluate the injection-moulded samples for filler and porosity distribution. The scanning parameters were as follows: voltage 110 kV, current 100 mA for the Microfocus X-ray tube, exposure time 350 ms per image, and voxel size 26 μm .

Archimedes' principle was used to measure the materials' density in accordance with ISO 1183. This was carried out on a Sartorius AG precision balance with a methanol medium at room temperature. Five measurements were made of each sample in order to determine its mean and standard deviation.

The hygroscopic behaviour was assessed according ISO 62 standard to determine the water absorption properties of the different formulations. The samples were soaked in deionized water at 23°C and their weight was recorded until a stable mass was reached. Equation 6 was used to determine the water absorption (W) on three replicates of each series.

$$W(\%) = \frac{W_t - W_0}{W_0} \cdot 100 \quad (6)$$

The diffusion coefficient and the rate of water absorption were calculated using Fick's law:

$$D = \pi \cdot \left(\frac{k \cdot h}{4 \cdot W_m} \right)^2 \quad (7)$$

In this formula, D stands for the diffusion coefficient, h is the original sample thickness, W_m is the maximum amount of moisture absorbed, and k is water uptake curve's initial slope against $t^{1/2}$:

$$k = \frac{W_1 - W_2}{\sqrt{t_2} - \sqrt{t_1}} \quad (8)$$

The contact angle test was performed to assess the changes in hydrophilicity of composites by using an Ossila contact angle goniometer (Sheffield, UK) equipped with a 25 μL glass syringe to dispense droplets of distilled water. Contact angle data are presented as an average angle based on at least three measurements.

Surface topography was assessed by contact profilometer using a Surface Roughness Tester SJ-201P, from Mitutoyo. Ten measurements, distributed on both sides of the moulded plates, were taken on each sample to determine the mean value and standard deviation of the arithmetic mean roughness (R_a) and the maximum height of the profile (R_y).

Using a HunterLab Miniscan MS/ S-4000S spectrophotometer for colour measurement ($L^*a^*b^*$ coordinates) and a Test An DT 268 glossmeter for gloss determination in accordance with ISO 2813 at measuring angles of 20°, 60°, and 85°, the aesthetic appearance of the various formulations was assessed. The total colour difference parameter (ΔE^*) was determined according to equation 9:

$$\Delta E^* = [(\Delta L^*)^2 + (\Delta a^*)^2 + (\Delta b^*)^2]^{0.5} \quad (9)$$

3. Results and discussion

3.1. Chemical structure and composition

Fourier transform infrared (FTIR) spectroscopy

The FTIR spectra shown in Figure 3 provide information on the chemical composition of the studied materials. The spectrum of pure polylactic acid reveals a prominent peak around 1750 cm^{-1} , indicating the carbonyl ($\text{C}=\text{O}$) stretching vibration, which is characteristic of the ester groups in PLA. Besides this, other bands typically observed in PLA are also present, such as those corresponding to C-O stretching at 1083 cm^{-1} , along with other peaks related to C-H bending and stretching [43]. Regarding the composites, the lignocellulosic fillers hardly change the overall shape of the spectrum, contributing only small peaks related to hydroxyl ($-\text{OH}$) groups (around 3000 cm^{-1}), C-H stretching (around 2900 cm^{-1}) and C-O stretching (around $1000\text{--}1100\text{ cm}^{-1}$). As previously examined in earlier research [28], the shredded filler displays peaks linked to hemicellulose and lignin, which diminish or vanish for reed fibres due to the extraction method employed. In any case, the spectra of composites for both material types appear to be nearly overlapping, resembling PLA closely.

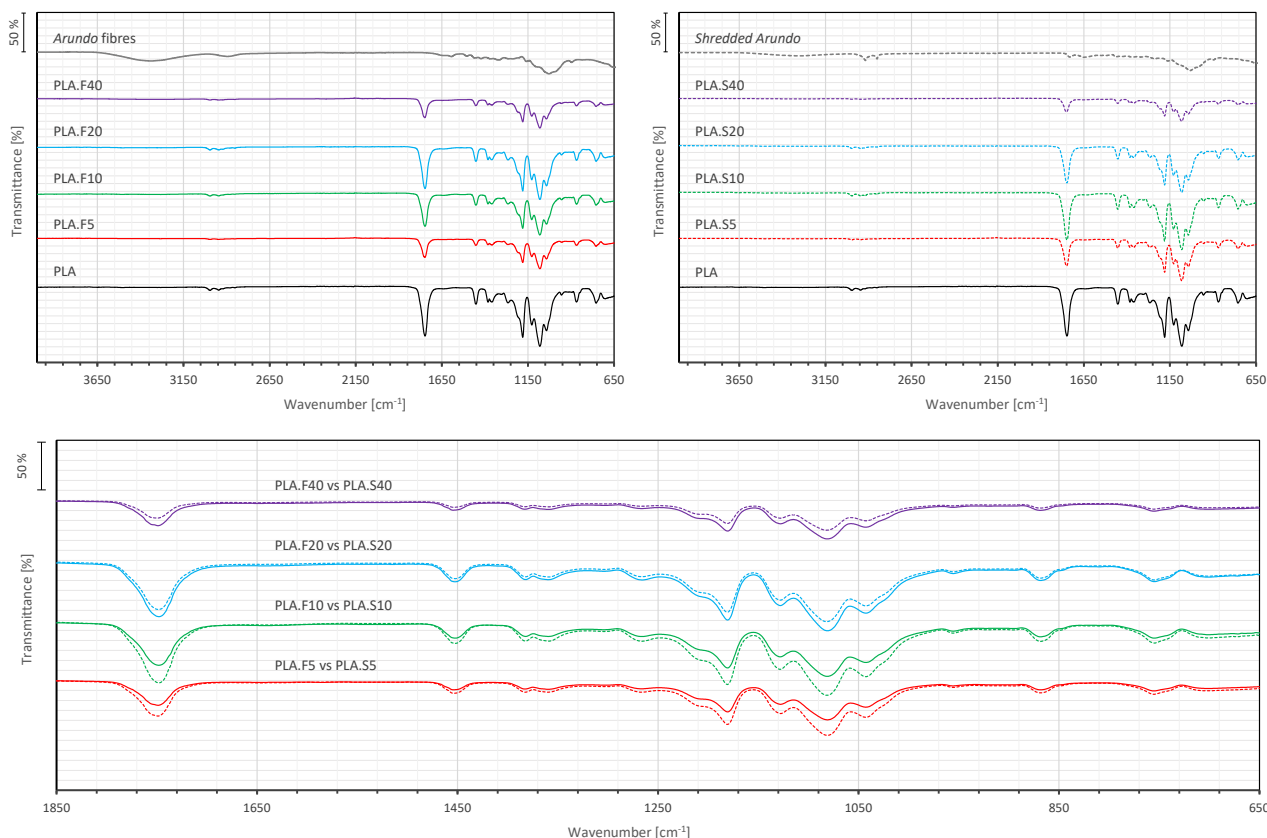


Figure 3. FTIR spectra for PLA composites based on reed fibres (solid lines) and shredded Arundo plants (dashed lines).

3.2. Rheological behaviour

The rheological behaviour of PLA and its composites has garnered extensive attention due to its critical role in processing and the performance characteristics of the materials. Neat PLA exhibits non-Newtonian shear-thinning behaviour, where complex viscosity decreases with increasing shear rates [44,45], as also observed in composite formulations in this study. This behaviour is indicative of increased polymer mobility, as it is generally accepted that the interactions between the filler and the polymer influence the flow behaviour of the polymer matrix.

All materials exhibited dominant viscous behaviour during the strain sweep test (Figure 4). At the same time, significantly higher storage modulus values were observed for composites containing shredded *Arundo* than for *Arundo* fibres, which may result from the larger filler fraction and their heterogeneous structure. The ability to form physically hindered 3D structures of the filler was more pronounced for composites containing filler with only shredded origin, as confirmed by the significantly lower LVE range values observed for these material series.

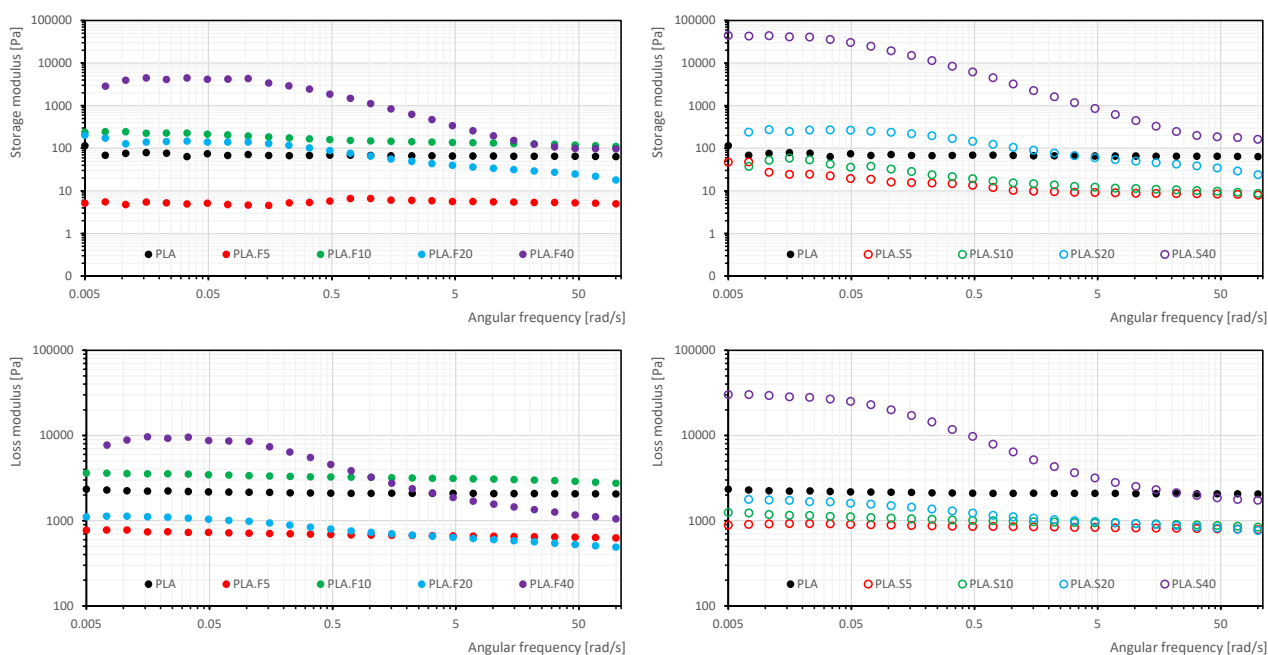


Figure 4. Storage and loss modulus for composites series under oscillatory rheometry: a) storage modulus for fibrous composites; b) storage modulus for shredded *Arundo* composites; c) loss modulus for fibrous composites; d) loss modulus for shredded *Arundo* composites.

The results of the frequency sweep experiment (Figure 5) show that only in the case of composites containing 40 wt.% of both fillers within the applied strain and angular frequency ranges did the rheological percolation threshold exceed, resulting in the absence of a plateau at low angular frequency values. All materials exhibited characteristics of non-Newtonian shear-thinning fluids. At the same time, unusual behaviour was observed for composites containing up to 20 wt.% of filler. No gradual increase in viscosity was observed with increasing filler content. In the case of shredded *Arundo*, all composites containing up to 20 wt.% of filler exhibited lower complex viscosity values than the reference PLA. In the case of fibre-filler-containing composites, this phenomenon was observed for 5 and 20 wt.% fibrous composites. This phenomenon may result from degradation of the polymer matrix, including hydrolytic degradation caused by residual moisture in the filler, occurring during the processing. For the highest filler concentrations (40 wt.%), the effect of lowering the polymer matrix viscosity was compensated by the high content of dispersed bulk fillers in the molten composite.

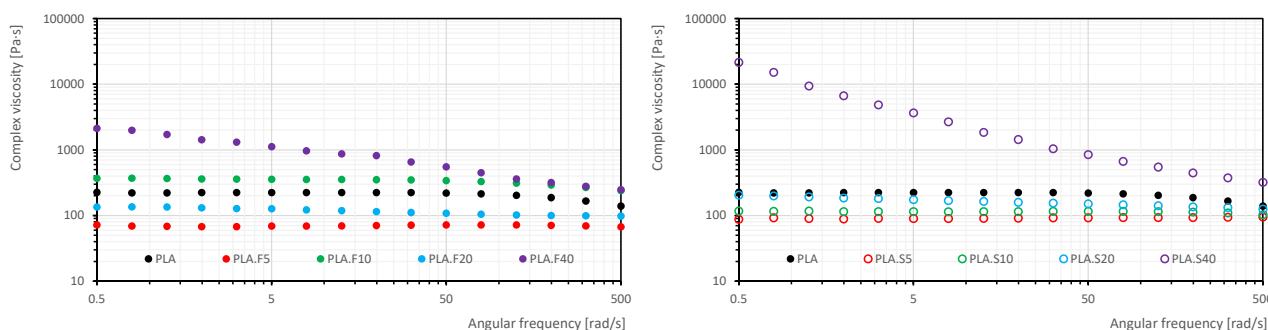


Figure 5. Complex viscosity curves for PLA composites: a) composites with *Arundo* fibres, b) composites with *Arundo* particles.

This non-uniform behaviour cannot be explained by a single factor but it is rather the reflection of fibres/particles interactions, their size and shape, the formation of network structures, shear-thinning behaviour, and the viscoelastic nature of the matrix [46–48], highlighting the complex interplay among these factors.

Seen the uneven viscous behaviour of the different composites series, several measurements were conducted, varying temperature, strain (always in the LVE) and distance between plates, in order to determine whether it was an expected trend or measurement artifacts, which sometimes lead to underestimate true shear rate or overestimate viscosity, as this phenomenon is well-known in rheometry, particularly for suspensions and polymer blends, and is often exacerbated by smooth geometries or edge fracture at high shear [49] (data not shown). However, the trend followed in all cases was similar to the one shown here.

Melt flow index

Complementary to the oscillatory rheology analysis, the melt flow index of the different material formulations prepared by twin-screw extrusion was determined. The MFI and viscosity are inversely related; a high MFI value means that the material flows easily under the test conditions, indicating a lower resistance to flow (lower viscosity). Therefore, the material is easier to process in injection moulding and extrusion, as it flows readily into moulds or through dies. However, a material with too high MFI might lack the desired strength or dimensional stability in the final product. Figure 6 shows that, in line with the viscosity results explained above, formulations with lower filler content show slightly higher MFI values or close to those found in the pure polymer, while the 40 % filler content

drastically reduces the MFI of the composites, even more markedly for shredded biomass filler. As a consequence, for the PLA.F40 and especially PLA.S40 series, a significant increase in the switchover pressure during the injection moulding process is required to achieve proper mould filling, related to the higher viscosities of these series (Figure 5). The increased pressure recorded for the shredded-*Arundo* filled composite series may be related to the particle shape of the filler, which cannot align with the polymer melt flow, as happening easier for the fibrous composites.

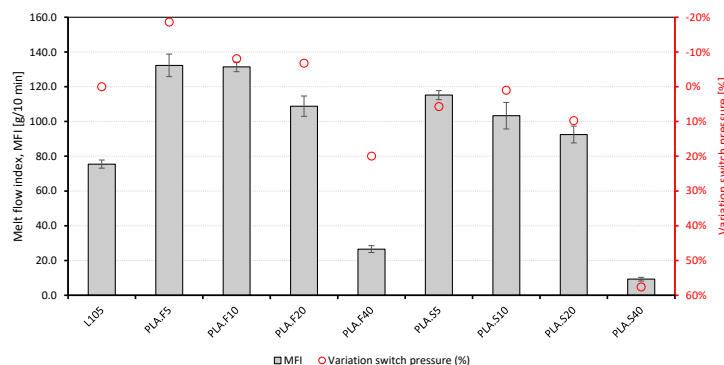


Figure 6. Melt flow index and relative variation in switchover pressure compared to neat PLA processing.

3.3. Thermal behaviour

Thermogravimetry (TGA)

The results of the thermogravimetric analysis, consisting of TG and DTG curves, are shown in Figure 7. The thermal degradation profile of the *Arundo* composites is characterized by one sharp peak between 317°C and 365°C observed in the DTG curve, whose variation is mainly affected by cellulose deterioration. The incorporation of plant fillers into the PLA matrix causes a shift in degradation peak temperature, ranging from 19°C below that of neat polymer for composites with 5 % fillers up to 66°C lower for those with higher biomass content. The key factor in the thermal deterioration is the filler ratio rather than the type of filler used in the composite. Although an improvement in the thermal stability of the fibrous series may be expected due to the alkaline treatment used to extract the fibres and the consequent removal of hemicellulose [30,50], no clear pattern can be discerned in this regard. Nevertheless, both fibre composites and shredded biomass composites show thermal stability suitable for the injection moulding process, being characterised by a degradation onset temperature above 300°C, which is far from the PLA recommended processing temperature, which is 220°C according to the manufacturer's data sheet. Similar findings are reported in the literature, where the maximum degradation rate of PLA reinforced with 30 % coir fibres occurs at 336°C [50], or at 358°C for a biocomposite with 20 % by weight of hemp [51]. Only the series with 40% *Arundo* fillers shows a small shoulder in the TG curves at 160°C, resulting in a mass loss of about 2%, which may be related to the desorption of physisorbed water in the lignocellulose, only visible for the higher ratios of biomass. Similarly, these batches are the only ones in which a significant residual mass close to 10 % is found at the end of the test, related to ashes (inorganic compounds) in the biomass. From DTG curves, it can be observed that only one main degradation peak is found for composites up to 20%, meaning that the polymer and the fillers degrade within the same temperature range. Again, for 40 % composites, a distinct behaviour is found, where a first peak related to cellulose compounds degradation at around 330°C is observed, followed by another one at about 360-370°C. For these series, shredded materials degrade about 10°C earlier than fibrous ones, which is related to the higher hemicellulose content of those particles.

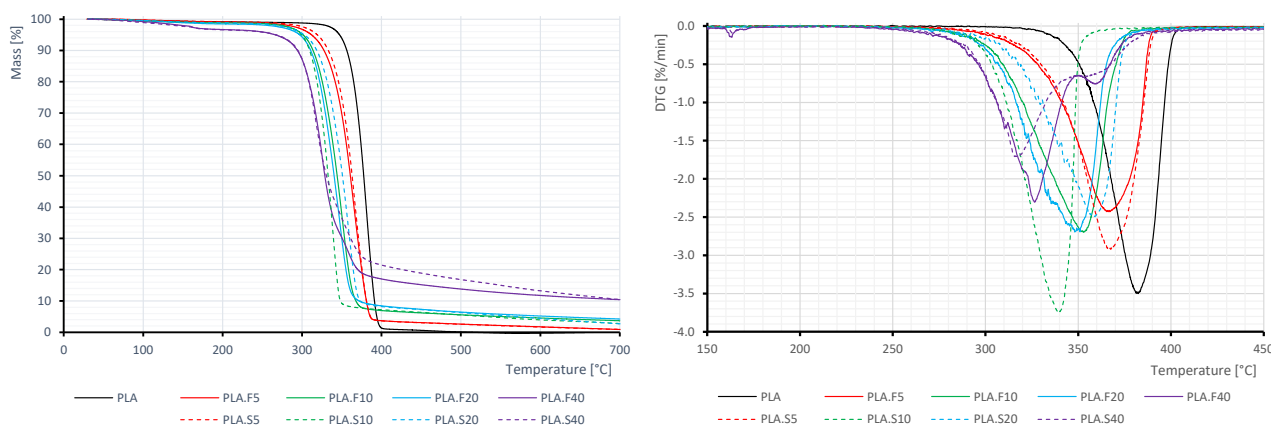


Figure 7. Thermal stability of PLA and PLA/*Arundo* composites: a) TG curves and b) DTG curves.

Differential scanning calorimetry (DSC)

Table 1 and Figure 8 show the DSC thermal parameters and related thermograms for PLA-based biocomposites and neat PLA, respectively. The addition of reed fillers has no significant effect on either T_m or T_g values. Melting and glass transition temperatures barely vary from 173°C and 66°C for all formulations. This behaviour is similar to that obtained in PLA composites where other plant or

animal fibres have been used [52–54]. Comparison of thermograms from the first and second heating shows that during the second heating, the glass transition and the exothermic cold crystallisation peak are significantly reduced; this is due to the considerably lower cooling rate under controlled conditions during the measurement, which allows for the phenomenon of crystallization from the melt in the composites. The double peaks in the melting endotherm, observed in the shredded reed composites and the PLA.F40 formulation during the second heating, are attributed to the melting of crystallites with varying sizes and morphologies, and/or order quality from the cellulosic filler, as reported by Karagöz for walnut/PLA composites [55]. The decrease in crystallization temperature for all composite materials evidenced that the plant fillers act as nucleating agents for the poly-L-lactide (PLLA) matrix, altering the mobility of the polymer chains and improving the crystallization behaviour [19,56]. In general terms, the incorporation of reed fibres or shredded biomass increased the degree of crystallinity, particularly for the 20 % and 40 % filler series, where it is almost doubled with respect to the neat PLA. It is also observed that neat PLA exhibits cold crystallization at 97.4°C, which disappears for the second heating in all composite samples. Other authors have reported a similar behaviour, with a decrease in crystallization temperature for composites, with the filler increasing the ratio of disordered alpha phase in PLA, more related to the amount of the filler than to its size [19]. This lack of cold crystallization in the second heating explains the high levels of crystallinity index calculated from melting enthalpies, while the first heating cycle refers to the injection-moulded material, which shows that it is mostly amorphous, as also found from WAXD analysis. The fibres appear to hinder the crystallization of the matrix during processing, as also do the shredded filler, although to a lesser extent. For both cases, an increase in the ratio of biomass results in higher crystallinity indexes.

Table 1. Thermal findings for PLA and its composites from DSC tests.

Material	T _g [°C]	T _{cc} [°C]	T _{m1} [°C]	T _{m2} [°C]	T _s [°C]	ΔH _{m1} [J/g]	ΔH _{m2} [J/g]	χ ₁ [%]	χ ₂ [%]
PLA	66.6	97.4	173.6	172.4	95.4	43.0	44.1	18.3	26.9
PLA.F5	64.7	89.7	173.8	173.6	102.7	30.8	33.0	9.9	36.3
PLA.F10	66.4	93.3	174.4	173.4	100.6	31.3	32.1	9.9	30.3
PLA.F20	66.0	88.5	173.8	174.4	108.1	28.4	29.1	10.8	39.1
PLA.F40	64.8	89.2	165.1	170.8	106.9	23.1	27.2	11.6	48.6
PLA.S5	64.6	91.5	172.2	170.7	100.8	40.2	44.5	11.6	50.4
PLA.S10	66.6	93.8	176.1	173.6	99.1	34.7	34.9	11.8	30.7
PLA.S20	65.1	89.0	170.6	169.7	100.9	33.6	39.0	15.8	52.3
PLA.S40	64.3	88.3	164.9	172.1	107.8	25.2	28.4	15.8	50.8

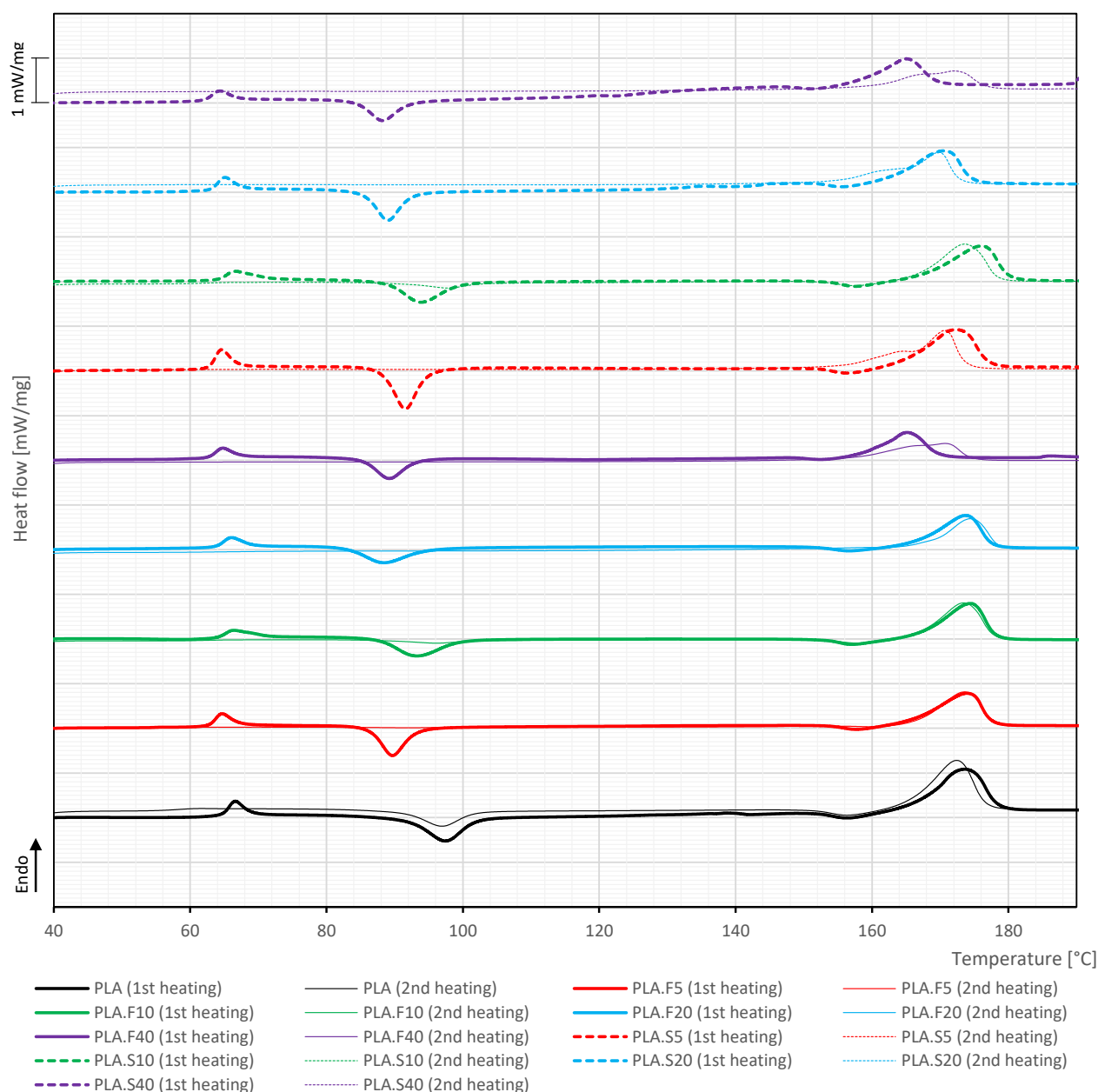


Figure 8. DSC thermograms, showing the first and second heating scan, in bold and fine lines respectively.

Wide-angle X-Ray scattering (WAXS)

Both the pure PLA and all *Arundo* composites show a predominantly amorphous structure, a consequence of the rapid cooling of the material during the injection moulding process. The diffraction patterns displayed in Figure 9 show a characteristic broad peak at 16.4° (2θ), corresponding to the amorphous region of the matrix polymer and cellulose, followed by a shoulder that evolves into a second peak with increasing filler ratio. The first distinctive peak, along with the prominent peak at 22° (2θ), were also observed in the raw fillers, both in fibres and shredded *Arundo* [30], denoting their semi-crystalline nature and high cellulose content. The second reflection peak is assigned to the crystallographic plane (002) of cellulose I [57], and as expected, its intensity is higher in the PLA.F40 and PLA.S40 series due to the significant volume fraction of cellulosic filler.

The X-ray diffraction measurements are in agreement with other investigations in which the microcrystalline structure of cellulose fillers are blended with PLA matrices and undergoes fast cooling during composite preparation [58,59]. It should be noted that the alkaline retting process used to obtain the reed fibres does not produce significant changes in the crystalline structure of the composites. This observation aligns with the findings of Le Maoigne et al. throughout flax composites [59], where the low NaOH concentration does not induce structural modifications in the cellulose I-cellulose II transition either.

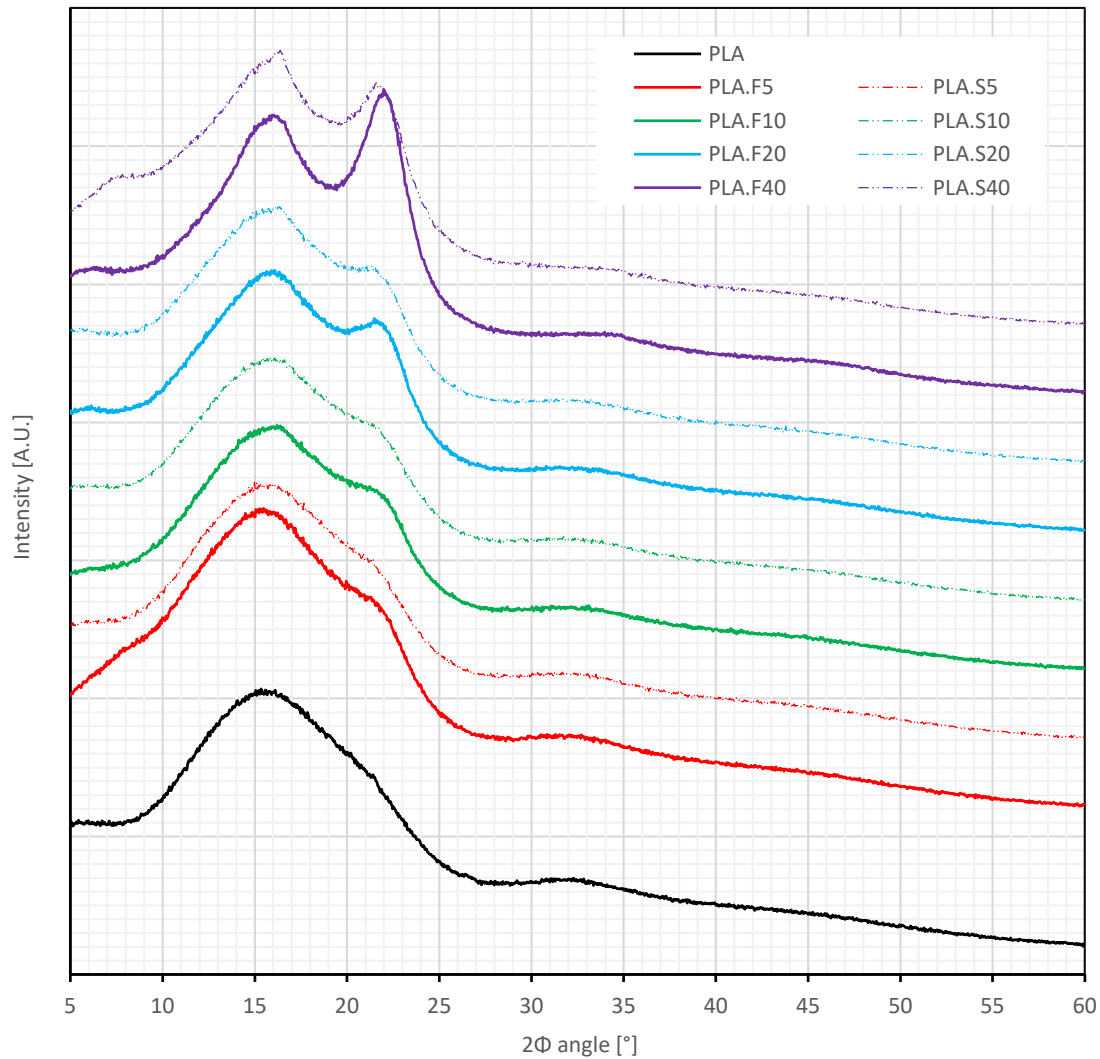


Figure 9. Diffraction pattern for PLA and PLA/*Arundo* composites.

3.4. Mechanical and thermo-mechanical performance

Mechanical static tests

From the point of view of its performance under tensile and flexural loads (Table 2), the PLA composites with 10 % or 20 % fibres and 10 % shredded biomass do not compromise the mechanical properties of the polymer matrix in terms of stiffness and ultimate stress. Both fibrous formulations also slightly increase the impact strength of the material, without significant changes in hardness compared to reference PLA. The decrease in hardness for PLA.S10 is not as drastic though. The materials with the highest fibre content (PLA.F40) offer superior stiffness and impact strength compared to neat PLA, but are limited by the extent of the permissible deformation before it breaks down, both in terms of bending and tensile strength. While the elastic modulus in both types of tests shows a fairly linear correlation with filler content, maximum strain becomes the limiting factor in composites with 5 % and 40 % filler. This may be attributed to the disruption of the PLA matrix resulting from the fillers, with 5% not being sufficient to produce any reinforcement due to an insufficient matrix-fibre interaction [60] and 40% being too much biomass, as previously reported, which forms agglomerations and decreases the matrix continuity [61]. The increase in flexural and tensile strength for 10 and 20 % fibrous composites are a sign of a good adhesion between the PLA and the fibres, as this increase evidences a good stress transfer between both materials and confirmation of high reinforcing efficiency of this filler [62–64]. On the contrary, the tensile strength of composites with shredded particles shows no significant differences for composites with only 10% filler, likely due to the aspect ratio of the fillers and a higher tendency for agglomeration of the fillers to their shape [65–68].

Table 2. Average values (\pm standard deviations) for mechanical properties of injection-moulded materials.

Material	Ball indentation hardness [N/mm ²]	Impact strength [kJ/m ²]	Tensile properties			Flexural properties		
			Tensile strength [MPa]	Elastic modulus [MPa]	Elongation at break [%]	Flexural strength [MPa]	Elastic modulus [MPa]	Strain at flexural strength [%]
PLA	118.6 \pm 3.4	7.0 \pm 0.1	48.6 \pm 5.3	2315.0 \pm 147.0	2.3 \pm 0.3	98.2 \pm 0.6	3273.6 \pm 88.6	4.0 \pm 0.1
PLA.F5	101.8 \pm 7.9	7.0 \pm 0.1	31.5 \pm 3.4	1975.7 \pm 83.1	1.6 \pm 0.1	65.6 \pm 1.1	3550.3 \pm 133.4	1.9 \pm 0.0
PLA.F10	104.7 \pm 2.4	7.8 \pm 0.2	48.1 \pm 0.7	2266.5 \pm 133.1	2.4 \pm 0.1	94.4 \pm 1.7	3653.0 \pm 49.4	3.3 \pm 0.1
PLA.F20	104.1 \pm 4.2	8.0 \pm 0.7	49.0 \pm 2.3	2442.0 \pm 188.4	2.2 \pm 0.1	93.3 \pm 1.5	4070.5 \pm 312.4	2.9 \pm 0.1
PLA.F40	118.6 \pm 2.4	9.4 \pm 0.2	38.8 \pm 2.4	2978.4 \pm 155.9	1.3 \pm 0.1	83.5 \pm 1.6	6759.3 \pm 92.8	1.5 \pm 0.0
PLA.S5	107.6 \pm 3.4	7.4 \pm 0.1	36.8 \pm 1.4	2307.5 \pm 67.1	1.8 \pm 0.1	66.4 \pm 0.7	3709.9 \pm 182.6	2.0 \pm 0.0
PLA.S10	111.1 \pm 2.9	6.7 \pm 0.1	45.6 \pm 1.0	2250.4 \pm 171.8	2.4 \pm 0.0	91.2 \pm 0.6	3490.3 \pm 118.9	3.5 \pm 0.0
PLA.S20	107.4 \pm 6.4	7.3 \pm 0.2	26.0 \pm 2.3	2360.1 \pm 125.3	1.2 \pm 0.1	49.8 \pm 1.0	3920.5 \pm 180.5	1.4 \pm 0.0
PLA.S40	111.9 \pm 7.6	8.1 \pm 0.1	31.6 \pm 2.1	2917.9 \pm 143.0	1.2 \pm 0.1	72.0 \pm 0.4	6206.2 \pm 78.4	1.4 \pm 0.0

The overall mechanical performance of the manufactured samples is beneficial, especially for the 10% and 20% filled composites, as confirmed by the stress–strain curves (Figure 10), which also show an improved elastic modulus for the 40% series. In particular, PLA.F10 and PLA.F20 exhibit curves that are almost overlapped with those of PLA, both for tensile and flexural testing.

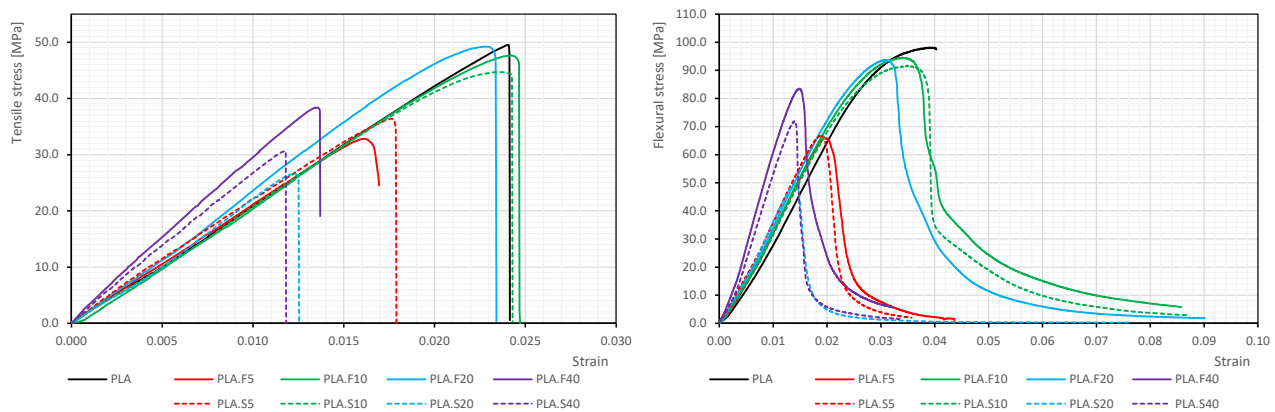


Figure 10. Stress-strain curves obtained from a) tensile and b) flexural tests for all series.

Dynamic Mechanical Thermal Analysis (DMTA)

By observing the relationship between storage moduli and loss moduli, it is found that all composite materials show markedly elastic behaviour (DMTA plots are shown as supplementary material). While a higher filler content would be expected to improve the PLA composite's elastic behaviour (higher E' values), some exceptions are observed for PLA.F5, PLA.F20, and PLA.S10 in the glassy region. One explanation for this propensity for a lower storage modulus might be that the filler agglomerates and functions as a weak point in the material, or it spreads out the PLA chains because it doesn't interact with them [69].

In the glass transition region (PLA α -relaxation), the $\tan \delta$ maxima show an almost proportional reduction in the damping factor as the filler content increases. This means that the viscous energy dissipation mechanisms will have less influence on the final material properties as the amount of polymeric matrix is replaced by stiffer lignocellulosic filler material, regardless of whether it is fibrous filler or shredded biomass. The second rubbery plateau evidences the higher stiffness of the composites with 40 % filler. The inflection point, present at around 80°C in both composites and pure PLA, also determines the onset of the cold crystallization process.

Table 3. DMTA results and related parameters for moulded, water-saturated (WA-wet) and reconditioned (WA-dry) samples. E' (storage modulus), E'' (loss modulus), tan δ (damping factor), ϵ_b (elongation at break), B (brittleness), t_g (glass transition temperature), DR (damping reduction), A (adhesion factor) and C-Factor (effectiveness coefficient).

Material	Performance at room temperature (25°C)					t_g [°C]	tan δ peak	DR ⁽¹⁾ [%]	A	C-Factor
	E' [10 ⁹ Pa]	E'' [10 ⁹ Pa]	tan δ	ϵ_b [%]	B [10 ⁹ Pa ⁻¹ % ⁻¹]					
PLA	14.235	0.246	0.017	2.3	0.030	66.4	2.463	-	-	-
PLA-WA_wet	10.366	0.190	0.018	-	-	66.4	1.614	34.5	-	-
PLA-WA_dry	10.938	0.235	0.021	2.2	0.042	69.6	2.299	6.6	-	-
PLA.F5	11.214	0.162	0.014	1.6	0.056	65.8	2.261	8.2	0.03	0.67
PLA.F5-WA_wet	9.364	0.287	0.031	-	-	61.4	1.147	53.4	0.81	0.75
PLA.F5-WA_dry	12.000	0.272	0.023	1.0	0.085	65.2	1.843	25.1	0.28	1.19
PLA.F10	16.140	0.232	0.014	2.4	0.026	66.1	1.788	27.4	0.06	0.63
PLA.F10-WA_wet	9.452	0.290	0.031	-	-	65.3	1.028	58.3	0.81	0.67
PLA.F10-WA_dry	12.545	0.280	0.022	1.6	0.051	69.6	1.689	31.4	0.22	0.78
PLA.F20	11.848	0.200	0.017	2.2	0.038	66.7	1.704	30.8	0.20	0.45
PLA.F20-WA_wet	8.518	0.307	0.036	-	-	65.6	0.891	63.8	1.32	0.29
PLA.F20-WA_dry	10.970	0.216	0.020	1.5	0.060	69.1	1.446	41.3	0.17	0.56
PLA.F40	26.452	0.497	0.019	1.3	0.028	65.1	0.947	61.5	0.93	0.10
PLA.F40-WA_wet	9.471	0.505	0.053	-	-	60.8	0.672	72.7	3.40	0.05
PLA.F40-WA_dry	17.623	0.478	0.027	1.0	0.057	65.5	0.935	62.0	1.38	0.15
PLA.S5	17.579	0.378	0.021	1.8	0.032	65.8	2.215	10.0	0.38	0.90
PLA.S5-WA_wet	13.937	0.299	0.021	-	-	60.6	1.223	50.3	0.52	0.51
PLA.S5-WA_dry	13.207	0.270	0.020	1.1	0.066	64.8	1.868	24.1	0.15	1.10
PLA.S10	12.641	0.183	0.014	2.4	0.034	66.8	1.935	21.4	0.03	0.65
PLA.S10-WA_wet	11.534	0.350	0.030	-	-	64.7	1.075	56.3	1.06	0.79
PLA.S10-WA_dry	7.813	0.200	0.026	1.7	0.078	69.5	1.460	40.7	0.93	0.53
PLA.S20	19.382	0.337	0.017	1.2	0.043	64.2	1.471	40.3	0.52	0.51
PLA.S20-WA_wet	8.829	0.322	0.036	-	-	68.6	0.961	61.0	1.29	0.29
PLA.S20-WA_dry	11.878	0.294	0.025	0.7	0.113	68.8	1.394	43.4	0.62	0.48
PLA.S40	23.660	0.519	0.022	1.2	0.037	65.3	0.987	59.9	1.43	0.13
PLA.S40-WA_wet	11.972	0.481	0.040	-	-	61.4	0.664	73.0	3.08	0.04
PLA.S40-WA_dry	18.390	0.465	0.025	1.0	0.056	63.6	0.886	64.0	1.35	0.12

⁽¹⁾ Damping reduction compared to neat moulded PLA.

Key findings from DMTA results shown in Table 3 relate to the interface and relationship between the filler material and the polymer matrix. When compared to the pure PLA matrix, the C-factor indicates how well the *Arundo* filler improves the mechanical qualities of the material. A lower C-factor indicates a more pronounced impact of the filler on thermomechanical properties change, suggesting that the filler is effectively contributing to the overall strength and stiffness of the composite. As shown in Table 3, increasing the amount of fibre or shredded reed significantly improves the efficiency of the filler, following a good linear fit, and demonstrating a strong correlation between the efficiency of the reinforcement and the filler ratio of the composite, particularly at high temperatures (75°C, above the softening temperature).

Finally, to assess the bond quality between the natural fibres and the surrounding matrix material, the adhesion factor (A) was calculated. Despite the high reinforcement efficiency found in 40 % filler composites at moderate-high temperatures, the highest A value (calculated below the softening temperature, at 40°C) was determined for these series as well, meaning the adhesion between both materials is less efficient. This behaviour is consistent with that observed in static mechanical tests, where the greatest tensile and flexural strength are found for 10 % and 20 % filler composites, and not for those with 40 % ratio, where the ultimate strength weakens. This analysis demonstrates the interest of incorporating *Arundo*-derived materials into the PLA matrix as a way to widen the range of applications and overcome the limitations of this biopolymer related to its behaviour at moderate temperatures.

3.5. Physical properties and hygroscopicity

Density and porosity

The density of the two types of fillers used in the preparation of PLA-based formulations was determined in a previous work. Using the gas pycnometer, a specific gravity of 1.546 g/cm³ was found for *Arundo* fibres, while the measured value for the shredded fibre was significantly lower at 1.173 g/cm³ due to the lower amount of cellulose in the composition [28]. Figure 11 shows the density of the injection-moulded samples and compares it with the theoretical density calculated from the combined densities and ratios of the different phases of the composite (PLA: 1.24 g/cm³). It was found that while the measured and calculated values for the fibrous series are comparable, the values for the shredded series are inversely proportional. From this finding, it can be concluded that the switchover pressure applied during the injection moulding process played a significant role in the compaction of the composite material. This probably resulted in the elimination of internal voids in the structure of this type of filler.

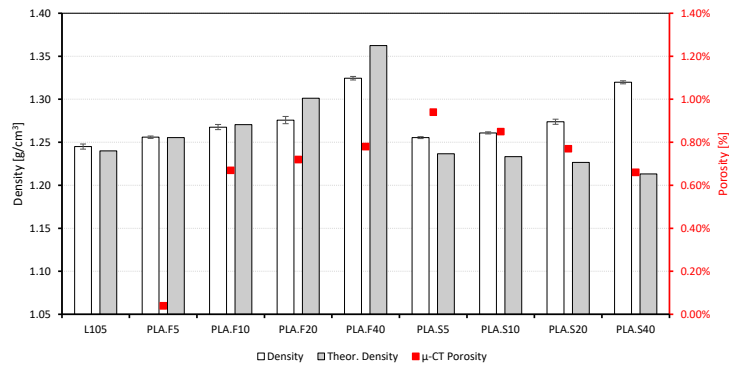


Figure 11. Average density vs theoretical density and porosity measured by computed tomography.

The utilisation of microCT for the observation of the integrity and internal composition of the moulded samples facilitated the determination of an acceptable isotropic and homogeneous distribution of the filler particles within the matrix (Figure 12). Nonetheless, it was observed some accumulation of the solid phase at the far end of the mould cavity, a phenomenon that was more pronounced in the composites with low loading levels. Regarding porosity, an acceptable level and distribution were also confirmed. However, it is noteworthy that the PLA.F5 sample demonstrated an exceptionally low porosity.

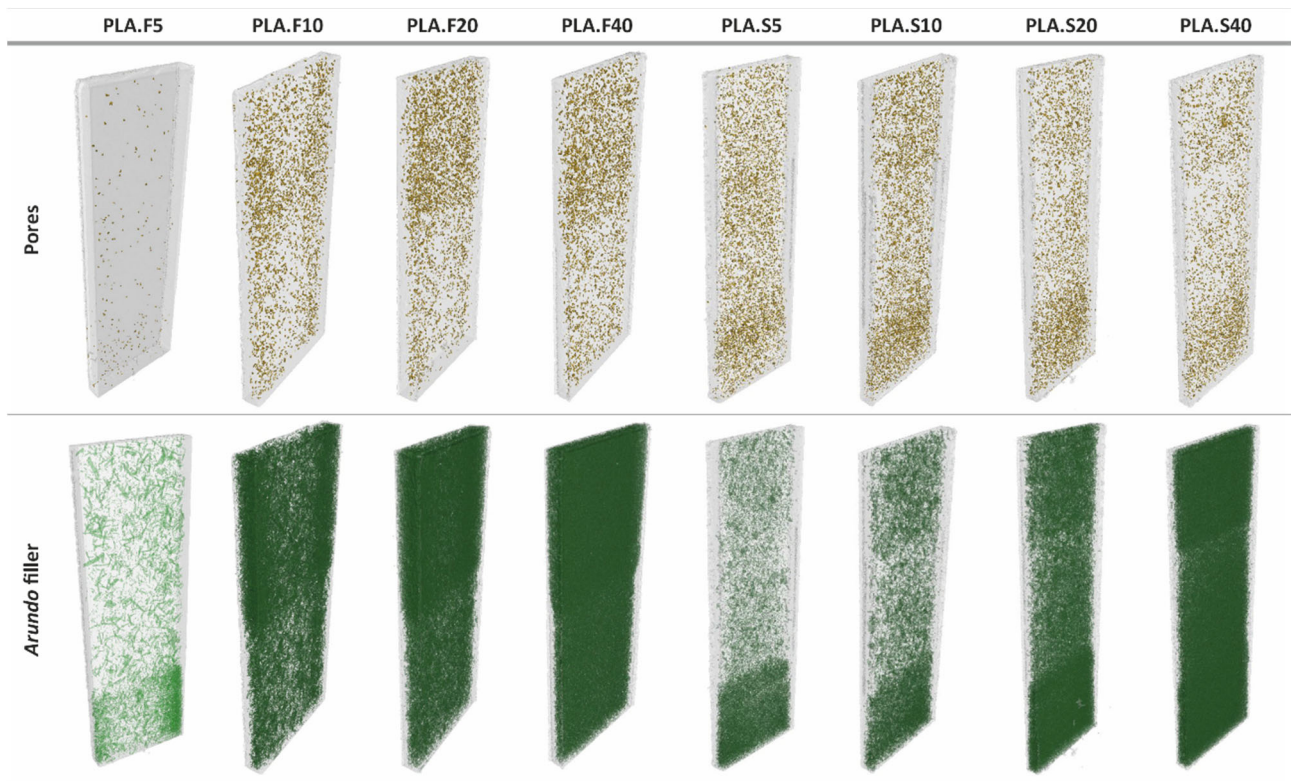


Figure 12. 3D computed tomography images presenting pores and filler distribution.

Water absorption

Moisture absorption and swelling are key challenges for PLA composites reinforced with natural fibres and cellulosic fillers, affecting their mechanical performance and durability. Numerous internal factors, such as composite characteristics, fibre loading and alignment, matrix type, fibre-matrix interaction, surface area, voids, lumen size, humidity, immersing medium temperature, and surface conditions, affect how much water is absorbed by natural fibre composites. [70]. The hydrophilic nature of natural fibres, particularly the -OH groups of cellulose and hemicellulose, enhances water absorption through hydrogen bonding [71]. On the other hand, the amorphous regions allow water to penetrate and break hydrogen bonds, while crystalline areas restrict water diffusion [72]. Fillers from plant biomass, such as the reed fillers studied, are hygroscopic, leading to increased moisture absorption in PLA composites compared to pure PLA [70,73]. Water uptake can degrade the mechanical properties and accelerate the ageing of the composite, which can be beneficial in a context of material biodegradation and waste reduction, but can also lead to a premature end of life of the products, depending on their application and usage conditions.

As expected, Figure 13 clearly shows that a higher lignocellulosic loading results in higher water absorption. Compared to the 0.7 % water absorption achieved by PLA after 4 weeks of soaking, the fibre composites reach a maximum of about 14 %, 6.3 %, 4.4 % and 3.2 % absorption depending on their content of 40, 20, 10 and 5 per cent of reed fibres. This is in line with other work where PLA composites loaded with similar fillers, such as hemp or coconut fibres, were investigated [74,75]. It should be noted that, when the filler

consists of shredded biomass, these values are significantly reduced (to almost half for 5 % filler) when comparing each series with its fibrous counterpart. The needle-like morphology of the fibres, together with a higher aspect ratio than the shredded filler, could explain this behaviour, as well as the slightly higher porosity for shredded composites compared to fibrous ones. Thus, a larger exposed surface area of the reinforcement phase would facilitate moisture penetration into the composite (Figure 13).

Swelling occurs as fibres absorb water, causing expansion mainly perpendicular to the fibre direction and sometimes shrinkage along the fibre axis, leading to internal stresses and potential damage at the fibre-matrix interface. Thickness swelling usually increases with the natural filler content and is more pronounced when the biomass is more hydrophilic. The swelling measured in the *Arundo* samples after soaking follows a similar trend to that observed for moisture absorption, it increases as the reed fibre content rises, but with smaller and less proportional variation when using shredded fillers (Table 4).

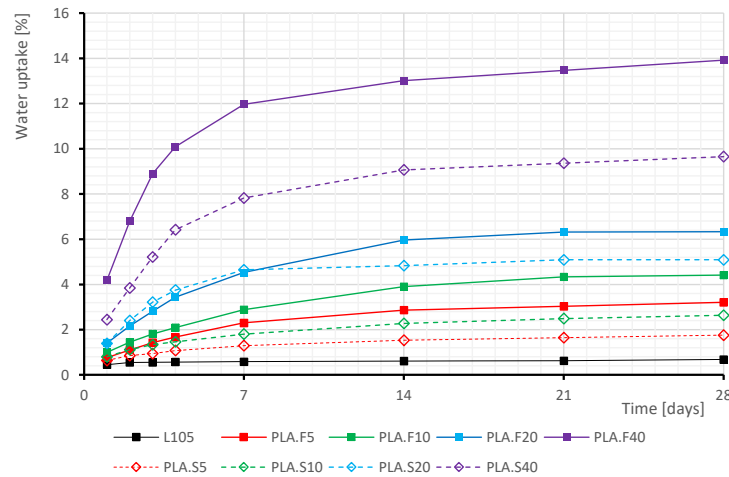


Figure 13. Evolution of water uptake vs time.

Table 4 displays the changes in additional hygroscopicity and water absorption kinetics parameters, including swelling, sorption, permeability, and the Fick diffusion coefficient. The majority of the samples exhibited Fickian behaviour, with diffusion coefficients (D) rising in direct proportion to the filler ratio and porosity. Fibrous composites exhibit higher values of swelling than particle-shaped ones, due to the higher surface area of fibres compared to particles, because of their higher aspect ratio. When both diffusion and percolation mechanisms are taken into account, water sorption illustrates the relationship between the mass of water absorbed by the sample and its own weight. The water sorption capacity was found to be more significant for fibrous composites and was again primarily dependent on the amount of *Arundo* filler.

Table 4. Variation of water uptake parameters and contact angle.

Material	D (m ² /s)	Swelling (%)	Sorption (g/g)	Permeability (m ² /s)	Contact angle (°)
L105	$2.98 \cdot 10^{-13}$	0.1	0.007	$2.02 \cdot 10^{-15}$	74.2 ± 3.4
PLA.F5	$3.82 \cdot 10^{-13}$	1.4	0.032	$1.23 \cdot 10^{-14}$	74.5 ± 3.8
PLA.F10	$2.67 \cdot 10^{-13}$	5.0	0.044	$1.18 \cdot 10^{-14}$	78.6 ± 2.1
PLA.F20	$3.43 \cdot 10^{-13}$	5.7	0.063	$2.17 \cdot 10^{-14}$	78.6 ± 2.1
PLA.F40	$4.16 \cdot 10^{-13}$	6.1	0.139	$5.79 \cdot 10^{-14}$	81.5 ± 6.3
PLA.S5	$2.46 \cdot 10^{-13}$	-0.9	0.018	$4.32 \cdot 10^{-15}$	73.6 ± 1.2
PLA.S10	$2.57 \cdot 10^{-13}$	3.7	0.026	$6.76 \cdot 10^{-15}$	74.7 ± 6.8
PLA.S20	$4.69 \cdot 10^{-13}$	4.0	0.051	$2.39 \cdot 10^{-14}$	78.3 ± 3.9
PLA.S40	$3.77 \cdot 10^{-13}$	3.7	0.097	$3.64 \cdot 10^{-14}$	79.1 ± 2.8

Surface roughness and wettability

The water contact angle (WCA) is another key factor influencing water uptake. Thus, a lower contact angle indicates better wettability of the composite by water, which results in higher absorption. Contrary to what might be expected, it was observed that wettability in PLA-*Arundo* composites decreased slightly as the amount of filler increased (Table 4). While natural fibres are hydrophilic, the addition of certain fillers can increase the contact angle, making the surface more hydrophobic (water-repelling). This effect is often observed when the filler particles create a rougher surface [76] or when the filler material itself is hydrophobic. From the measurement of the surface profiles and roughness parameters, using a stylus profilometer, a linear increase in both arithmetic mean roughness (R_a) and maximum height of the profile (R_y) was determined (Table 5). R_a represents the average deviation of the surface profile from the mean line, while R_y provides information about the vertical distance between the highest peak and the lowest valley within the entire measurement length, highlighting extreme variations. The increases in both parameters correlate with the filler weight of the composite for either fibrous or shredded fillers. This finding is consistent with similar behaviours found in the literature, and also with the WCA; for instance, Alrawi et al. highlighted the influence of surface roughness on the hydrophilicity of PLA/MMT-TiO₂ bionanocomposites,

finding that increasing the loading of montmorillonite (MMT) significantly enhanced surface roughness, which correlated with an increase in WCA [77].

Kotan and Tutak explored the relationship between coating morphology and WCA, revealing that a smoother surface from a PLA coating led to lower water contact angles compared to rougher counterparts, implying that surface smoothness can facilitate water adhesion [78]. Therefore, they found that textured surfaces typically exhibit increased contact angles unless they are highly hydrophilic. Furthermore, a recent study by Bomfim et al. explored how modifications in microstructural features, including surface roughness, affected the interactions with water, providing insights into relationships between composition, morphologies, and wettability. They reported a decline in wettability with increased porosity and roughness, which corroborates previous findings across various PLA studies [79].

3.6. Aesthetic assessment

The visual appearance of the moulded PLA/*Arundo* composites was evaluated by comparative analysis of colour, opacity and gloss (Table 5). The colour of the resulting composites is heavily dependent on the inherent hues of the natural fillers used. Thus, the reed fibres series show a lighter yellowish colour due to bleaching during alkaline retting of the *Arundo* stems, while those prepared with shredded biomass have a darker colour with less yellow hue as they contain untreated material from whole plant specimens, stems and leaves. The decrease in the parameter ΔL^* (lightness) denotes the darkening of the samples as the filler ratio increases, while lower values of Δa^* (red/green coordinate), observed in PLA.Sx series, indicate a trend from red to greener colours and lower Δb^* (yellow/blue coordinate) means a shift from yellow to blue hues. When comparing the different materials to each other, the total colour difference is noticeable in all cases, except in the comparison between the PLA.S10 and PLA.S20 series, where the difference ($\Delta E \leq 1$) can be considered imperceptible.

The amorphous structure obtained by rapid cooling of the polymer during the moulding process produces transparent PLA samples. Meanwhile, the incorporation of reed fibres causes a progressive increase in opacity that is nearly proportional to the amount of filler. Whereas the PLA.F20 series still provides some translucency, when using shredded filler, the darker pigmentation of this type of filler results in total opacity for the same loading rate. On the other hand, while pure PLA parts show a high gloss surface finish (gloss measurement above 70 GU), this parameter is reduced as the amount of filler in the composite increases. Using the 60° measurement angle, standard for semi-gloss surfaces, a progressive evolution towards more matte finishes is observed as the *Arundo* filler increases. The loss of gloss is associated with an increase in surface roughness, which, as mentioned above, affects not only the visual appearance but also the wettability of the samples.

Table 5. Colour, opacity, gloss and roughness measurements.

Material	Colour							Opacity [%]	Gloss	Roughness	
	L*	a*	b*	$\Delta L^{* (1)}$	$\Delta a^{* (1)}$	$\Delta b^{* (1)}$	$\Delta E^{(1)}$		60°	Ra	Ry
PLA	88.44 ± 0.13	-1.06 ± 0.02	1.13 ± 0.08	-	-	-	-	2.4	79.62 ± 1.65	0.27 ± 0.09	1.66 ± 0.41
PLA-WA-dry	88.13 ± 0.05	-1.03 ± 0.02	1.02 ± 0.03	-0.31	0.03	-0.11	0.326	3.2	-	-	-
PLA.F5	63.77 ± 0.44	4.60 ± 0.29	39.55 ± 0.36	-24.67	5.65	38.42	46.01	23.1	55.60 ± 1.81	0.60 ± 0.17	5.04 ± 1.28
PLA.F5-WA-dry	65.95 ± 1.09	6.94 ± 0.34	28.53 ± 0.89	-22.49	7.99	27.40	36.339	86.0	-	-	-
PLA.F10	54.93 ± 0.63	11.54 ± 0.39	43.22 ± 0.35	-33.51	12.60	42.09	55.26	43.3	43.74 ± 1.16	1.05 ± 0.36	7.40 ± 1.74
PLA.F10-WA-dry	63.85 ± 0.57	7.53 ± 0.30	25.68 ± 0.59	-24.59	8.58	24.55	35.791	95.5	-	-	-
PLA.F20	44.30 ± 0.44	16.97 ± 0.22	34.33 ± 0.76	-44.14	18.03	33.20	58.10	73.2	33.12 ± 1.29	1.19 ± 0.30	8.62 ± 1.77
PLA.F20-WA-dry	60.04 ± 1.20	8.03 ± 0.65	24.10 ± 1.10	-28.39	9.09	22.97	37.637	99.6	-	-	-
PLA.F40	46.64 ± 0.20	13.68 ± 0.21	29.09 ± 0.47	-41.80	14.73	27.96	52.41	97.6	17.28 ± 0.84	1.48 ± 0.26	12.81 ± 1.88
PLA.F40-WA-dry	66.56 ± 0.60	5.72 ± 0.21	23.33 ± 1.06	-21.88	6.78	22.20	31.897	99.9	-	-	-
PLA.S5	36.89 ± 0.64	9.97 ± 0.10	31.58 ± 1.05	-51.55	11.02	30.45	60.88	37.6	47.60 ± 2.03	0.49 ± 0.14	3.85 ± 1.07
PLA.S5-WA-dry	42.17 ± 0.65	6.96 ± 0.32	23.36 ± 1.42	-46.27	8.02	22.23	51.957	72.1	-	-	-
PLA.S10	22.28 ± 0.77	4.39 ± 0.16	11.05 ± 0.58	-66.16	5.45	9.92	67.12	89.0	37.10 ± 0.74	0.77 ± 0.29	6.39 ± 2.97
PLA.S10-WA-dry	38.67 ± 0.71	2.79 ± 0.11	16.95 ± 0.48	-49.77	3.85	15.83	52.366	98.1	-	-	-
PLA.S20	22.64 ± 0.45	2.37 ± 0.10	6.30 ± 0.42	-65.79	3.42	5.17	66.09	98.9	29.64 ± 0.68	0.94 ± 0.19	7.38 ± 1.61
PLA.S20-WA-dry	45.51 ± 0.24	2.25 ± 0.09	17.42 ± 0.48	-42.93	3.31	16.29	46.039	99.7	-	-	-
PLA.S40	31.27 ± 1.97	2.31 ± 0.24	7.75 ± 0.62	-57.17	3.37	6.62	57.65	99.1	20.26 ± 1.42	1.38 ± 0.44	10.18 ± 2.82
PLA.S40-WA-dry	47.44 ± 1.47	2.65 ± 0.29	14.13 ± 0.64	-41.00	3.70	13.01	43.169	100.0	-	-	-

⁽¹⁾ Differences in colour calculated with respect to neat moulded PLA.

3.7. Effect of water soaking on mechanical and thermomechanical properties

This section summarizes the findings of the changes observed in the PLA composites due to their saturation with water. It is well-known that moisture absorption plays a crucial role in the behaviour of PLA-lignocellulose composites. PLA is hydrophobic, while lignocellulosic materials are inherently hydrophilic, leading to increased water absorption when the composites are subjected to humid conditions. This water absorption can cause plasticization effects, reducing the glass transition temperature (T_g) and subsequently increasing the mobility of the polymer chains within the composite matrix, thus altering viscoelastic and mechanical properties [80–82].

Furthermore, it has been reported that water can lead to the formation of microcracks, which might also impact DMA results by altering storage and loss moduli [80,82].

Additionally, the exposure to humidity can modify the interfacial adhesion between the PLA matrix and the lignocellulosic fibres. This can lead to differences in the stress-strain responses of the samples upon re-drying, as the loss of moisture may cause the fillers to swell and re-adhere differently within the polymer matrix [28], resulting in partial debonding. However, Bazan et al. performed these studies with coconut and flax fibres, and despite the increase in water uptake and the swelling observed, no change in the mechanical properties of the composite was found, probably because of the high stability of the HDPE matrix [83]. Due to the hydrolytic degradation route of PLA, these assays might provide interesting insights into such composites when subjected to humid environments, such as packaging, construction, or agricultural applications [84–87].

From tensile and flexural testing (Figure 14), it was observed that the most significant differences in mechanical performance of composites are observed in the ultimate tensile strength, which is reduced by around half after degradation in water. This result is in line with the findings of similar studies on the effect of water ageing on the mechanical performance of Kenaf/PLA biocomposites, where reductions of up to 49.86 % were reported [88]. In terms of elastic moduli, although they also decrease, the drops are not as dramatic. Thus, the stiffness is only slightly affected in the re-dried specimens, except for the flexural stress, particularly in the case of composites with 40 % filler content. The most significant effect on ultimate tensile strain occurs in the series with low and medium filler content. Meanwhile, when subjected to bending stresses, the maximum strain reached by the water-degraded parts remains close to the initial values.

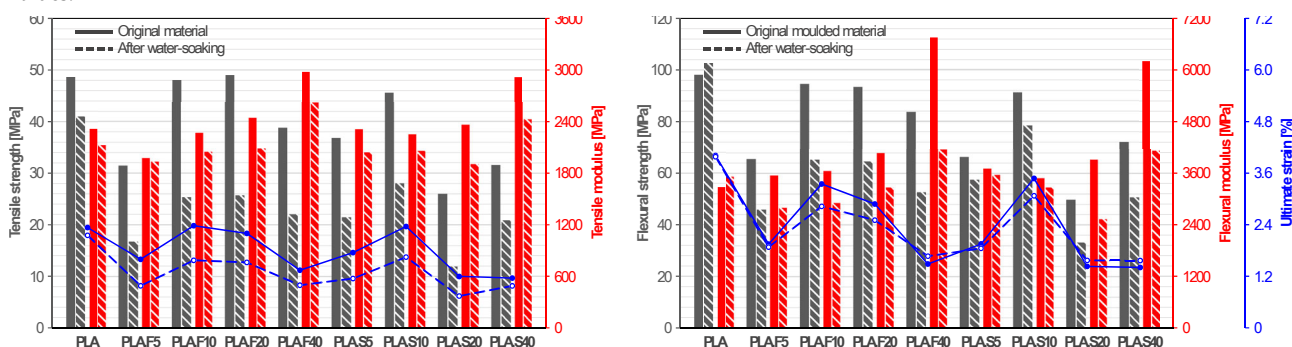


Figure 14. a) Tensile and b) flexural properties for original (solid lines and bars) and water-saturated (dashed lines and bars) materials.

From DMTA, noticeable differences for untreated, humid, and re-dried samples of PLA-lignocellulose composites are likely due to the interplay of moisture absorption affecting physical properties, the mechanical integrity and behaviour influenced by fibre-matrix interaction, and changes in polymer chain mobility under varying conditions. Hydrolytic degradation mechanisms are likely to be accelerated due to the biomass incorporation, as previously found in degradation testing [89,90]. This was confirmed by the lower viscosity determined for all sample series (data not shown). From the dynamic mechanical analysis of the moulded, water-saturated and re-dried samples, the storage modulus (Figure S1), loss modulus (Figure S2) and $\tan \delta$ (Figure S3) plots were obtained and are shown in the supplementary material. In addition, the key results from these tests are summarised in Table 3.

Looking at the storage modulus curves, as expected, it is shown that the stiffer materials are those that have not been subjected to wet degradation. After water immersion and reconditioning, the PLA.S10 and PLA.S20 series exhibit the most pronounced drop in stiffness, with reductions in elastic energy storage of nearly 40%. In contrast, the PLA.F5 series recovers its full stiffness after drying, and the PLA.F20 series achieves a behaviour comparable to that of the original sample. When analysing the tests on wet specimens, the influence of water uptake on the integrity and performance of the samples below their freezing point (0°C) can be clearly discerned. Once room temperature is reached and the absorbed water is in a liquid state, the storage modulus of the composites (above 5 % filler) is about half of that achieved after re-drying. From the $\tan \delta$ plots, the damping reductions and the shift in glass transition temperature experienced by the material under the three conditions of use studied can be ascertained. The reduction of the damping factor in the glassy region of the soaked and dried samples, compared to neat moulded PLA, varies with the amount of filler, from 24-25 % for the lowest filler ratio to 62-64 % for the highest ratio composites. Regarding the glass transition temperature, determined from the peak of $\tan \delta$, small variations of up to 4.7°C above are observed for PLA.S20, albeit with no discernible trend or pattern.

The composites' brittleness values, calculated from the elongation at break and storage modulus at room temperature, show that all reconditioned formulations become more brittle due to moisture absorption. Meanwhile, the higher C-factor in water-degraded fibrous materials indicates less effective reinforcement, which is related to the higher moisture uptake of this series with a higher aspect ratio filler. This is probably due to the debonding at the fibre-matrix interface that occurs after swelling (water absorption) and subsequent shrinkage (drying) of the fibres and a possible filler pull-out [83,91].

In summary, it was observed that, in the transition from wet to dried samples, a partially recovery of properties was obtained, which means that the original PLA structure tends to re-establish, although not entirely; some permanent changes are found due to degradation processes that might have occurred during water exposure [82,84]. The mechanical and thermo-mechanical responses found in PLA-*Arundo* composites, under water degradation conditions, suggest a versatile material capable of being employed in various industries, including packaging, automotive, construction, agriculture and consumer products. The overall performance of all materials tested after water-soaking and re-drying is far from catastrophic failure in the short term and demonstrates their viability to withstand medium loads even after saturation with water.

From an aesthetic point of view, water-degraded composites are lighter in colour and tend to yellow when using shredded biomass fillers (Figure 15). The increase in opacity for all formulations is especially noticeable in composites with lower filler content. The shift towards lighter colour and higher opacity in the water-soaked composites is usually due to changes in the matrix phase or in the bonding interface, as a result of increased crystallinity or the presence of microvoids caused by degradation in water, respectively [92].

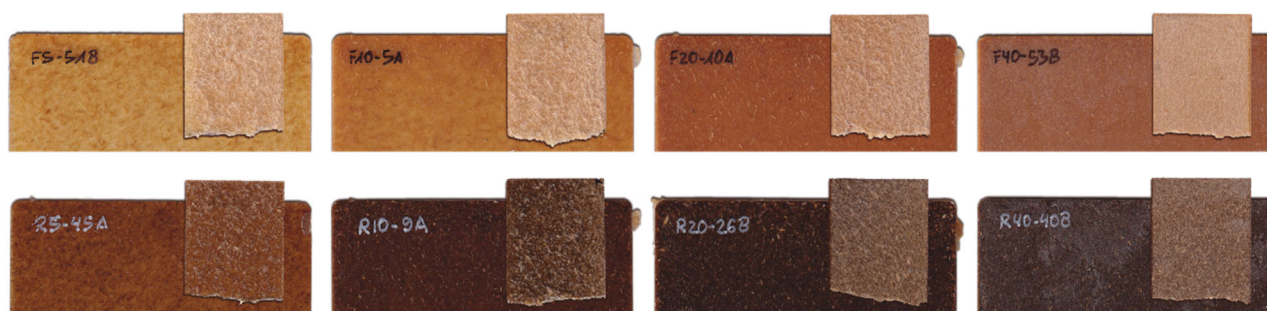


Figure 15. Injection moulded and water-degraded composite samples.

4. Conclusions

The urgent need to address the environmental challenges posed by conventional plastics has catalysed a shift towards biopolymers and sustainable materials. The incorporation of renewable resources like *Arundo Donax* plant fillers into biopolymer composites, particularly PLA, enhances their mechanical properties while promoting ecological sustainability. This path not only mitigates plastic waste but also contributes to a circular economy by effectively utilizing agricultural by-products and reducing environmental footprints. This study successfully explored the use of two different types of lignocellulosic fillers from giant reed, namely stem fibres and shredded plant specimens, in a PLA matrix, assessing their performance, particularly in water contact applications, and evaluating how these materials' properties change due to increased hydrophilicity resulting from filler incorporation.

FTIR spectra show that adding *Arundo* fillers has little effect on the chemical structure of composite materials, which remain similar to neat PLA. However, the rheological behaviour changes significantly depending on the type and amount of filler used; low fibre loading improves flow, while high loading creates jamming effects. Oscillatory rheometry might not be the most accurate technique to evaluate the rheological behaviour of these composites, due to the size of the fillers (both particles and fibres) and the low viscosity of the matrix. MFI analysis indicates that 40 % filler significantly reduces flowability, which affects processing. Additionally, thermal analyses show that the lignocellulosic content has a slight influence on the degradation temperatures, maintaining thermal stability, suitable for injection moulding, with the onset of degradation above 300°C.

Composites made with 10 % and 20 % reed fibre and 10 % shredded biomass show the best mechanical performance, matching the tensile and flexural strength of the PLA matrix, improving stiffness and impact resistance while slightly reducing hardness. Using higher ratios of fibre (40 %) boosts stiffness and impact strength but reduces deformability due to weaker adhesion and brittleness, which lowers ultimate strength. MicroCT imaging showed uniform filler distribution and generally low porosity. Higher lignocellulosic loading, especially with fibres, leads to higher water absorption, while increased surface roughness due to higher filler content reduces wettability.

The investigation found that water exposure significantly reduced the tensile strength of giant reed composites by about half, although changes in elastic moduli were less severe. Although some properties were partially recovered when the samples were reconditioned from wet to dry state, some permanent changes occurred evidencing some hydrolytic degradation. In summary, the responses of PLA-*Arundo* composites suggest that they can be effective in various industries and withstand medium loads even after being saturated with water. Future studies should explore long-term aging and cyclic wetting and drying effects for a comprehensive understanding of material performance.

5. Author Contribution

Luis Suárez: Methodology, Formal analysis, Investigation, Visualization, Writing – Original draft preparation; **Mateusz Barczewski:** Conceptualization, Methodology, Investigation, Formal analysis, Writing – Reviewing and Editing; **Paul Hanna:** Investigation, Resources, Writing – Reviewing and Editing; **Patryk Mietliński:** Investigation; **Andrzej Miklaszewski:** Investigation; **Zaida Ortega:** Conceptualization, Methodology, Investigation, Resources, Writing – Reviewing and Editing, Supervision. All authors read and approved the final manuscript.

6. Declarations

Competing Interests. The authors declare that they have no known competing financial interests or personal relationships that could have appeared to influence the work reported in this paper.

Generative AI in Scientific Writing. The authors declare that they did not use generative AI systems while preparing and writing the manuscript.

7. Acknowledgments/funding

Luis Suárez: Ph.D. grant program co-financed by the Canarian Agency for Research, Innovation and Information Society of the Canary Islands Regional Council for Employment, Industry, Commerce and Knowledge (ACIISI) and by the European Social Fund (ESF) (Grant number TESIS2021010008).

8. References

- [1] Suárez L, Ortega Z, Barczewski M, Cunningham E. Use of giant reed (*Arundo donax* L.) for polymer composites obtaining: a mapping review. *Cellulose* 2023;30:4793–812. <https://doi.org/10.1007/s10570-023-05176-x>.
- [2] Baysal A, Yayla P, Süleyman TÜRKMEN H, Türkmen HS. A review on engineering biocomposites and natural fiber-reinforced materials. *J Sustain Constr Mater Technol* 2022;7:231–249. <https://doi.org/10.47481/jscmt.1136018>.
- [3] Geyer R, Jambeck JR, Law KL, R Geyer JJKL. Production, use, and fate of all plastics ever made 2017;3:25–9. https://doi.org/10.1126/SCIADV.1700782/SUPPL_FILE/1700782_SM.PDF.
- [4] Peng C, Wang J, Liu X, Wang L. Differences in the Plasticspheres of Biodegradable and Non-biodegradable Plastics: A Mini Review. *Front Microbiol* 2022;13:849147. <https://doi.org/10.3389/FMICB.2022.849147/BIBTEX>.
- [5] Dussud C, Hudec C, George M, Fabre P, Higgs P, Bruzard S, et al. Colonization of Non-biodegradable and Biodegradable Plastics by Marine Microorganisms. *Front Microbiol* 2018;9:388586. <https://doi.org/10.3389/FMICB.2018.01571/BIBTEX>.
- [6] Amaro TMMMTMM, Rosa D, Comi G, Iacumin L. Prospects for the Use of Whey for Polyhydroxyalkanoate (PHA) Production. *Front Microbiol* 2019;10:443843. <https://doi.org/10.3389/FMICB.2019.00992/XML/NLM>.
- [7] Reinold S, Herrera A, Stile N, Salii F, Hernández-González C, Martínez I, et al. An annual study on plastic accumulation in surface water and sediment cores from the coastline of Tenerife (Canary Island, Spain). *Mar Pollut Bull* 2021;173:113072. <https://doi.org/10.1016/J.MARPOLBUL.2021.113072>.
- [8] Delina M, Taryudi, Amin MF, Hussaan AM, Trismidianto, Arifin FI, et al. The Development of Remotely Operated Underwater Vehicle for Plastic Waste Detection with Raspberry Pi. *J Phys Conf Ser* 2024;2866:012048. <https://doi.org/10.1088/1742-6596/2866/1/012048>.
- [9] Tramoy R, Gasperi J, Dris R, Colasse L, Fisson C, Sananes S, et al. Assessment of the Plastic Inputs From the Seine Basin to the Sea Using Statistical and Field Approaches. *Front Mar Sci* 2019;6:446860. <https://doi.org/10.3389/FMARS.2019.00151/BIBTEX>.
- [10] Venkateswar Reddy M, Kotamraju A, Venkata Mohan S, Reddy MV, Kotamraju A, Mohan SV, et al. Bacterial synthesis of polyhydroxyalkanoates using dark fermentation effluents: Comparison between pure and enriched mixed cultures. *Eng Life Sci* 2015;15:646–654. <https://doi.org/10.1002/ELSC.201500016>.
- [11] Fouad D, Farag M, Fouad D, Farag M. Design for Sustainability with Biodegradable Composites. *IntechOpen*; 2019. <https://doi.org/10.5772/INTECHOPEN.88425>.
- [12] Wang H, Xiong Y, Goh GD, Lin L, Dang QA, Park HE. Enhanced Degradability, Mechanical Properties, and Flame Retardation of Poly(Lactic Acid) Composite with New Zealand Jade (Pounamu) Particles. *Polym (Basel)* 2023;15:3270. <https://doi.org/10.3390/POLYM15153270>.
- [13] Frank C, Emmerstorfer-Augustin A, Rath T, Trimmel G, Nachtnebel M, Stelzer F. Bio-Polyester/Rubber Compounds: Fabrication, Characterization, and Biodegradation. *Polym (Basel)* 2023;15:2593. <https://doi.org/10.3390/POLYM15122593>.
- [14] Coltelli MB, Bertolini A, Aliotta L, Gigante V, Vannozzi A, Lazzeri A. Chain extension of poly(Lactic acid) (pla)-based blends and composites containing bran with biobased compounds for controlling their processability and recyclability. *Polymers (Basel)* 2021;13:3050. <https://doi.org/10.3390/polym13183050>.
- [15] Hejna A, Barczewski M, Kosmela P, Aniśko J, Szulc J, Skórczewska K, et al. More than just a beer – Brewers' spent grain, spent hops, and spent yeast as potential functional fillers for polymer composites. *Waste Manag* 2024;180:23–35. <https://doi.org/10.1016/J.WASMAN.2024.03.023>.
- [16] Benson NU, Bassey DE, Palanisami T. COVID pollution: impact of COVID-19 pandemic on global plastic waste footprint. *Heliyon* n.d.;7:6343.
- [17] Krička T, Matin A, Bilandžija N, Jurišić V, Antonović A, Voča N, et al. Biomass valorisation of *Arundo donax* L., *Miscanthus × giganteus* and *Sida hermaphrodita* for biofuel production. *Int Agrophysics* 2017;31:575–81. <https://doi.org/10.1515/ntag-2016-0085>.
- [18] Aaliya B, Sunooj KV, Lackner M. Biopolymer composites: a review. *Int J Biobased Plast* 2021;3:40–84. <https://doi.org/10.1080/24759651.2021.1881214>.
- [19] Fiore V, Botta L, Scaffaro R, Valenza A, Pirrotta A. PLA based biocomposites reinforced with *Arundo donax* fillers. *Compos Sci Technol* 2014;105:110–7. <https://doi.org/10.1016/j.compscitech.2014.10.005>.
- [20] Fiore V, Scalici T, Valenza A. Characterization of a new natural fiber from *Arundo donax* L. as potential reinforcement of polymer composites. *Carbohydr Polym* 2014;106:77–83. <https://doi.org/10.1016/j.carbpol.2014.02.016>.
- [21] Lu M, Pei FF, Song XK, Guo Z. Study on the Purification Effects of Constructed Wetland Plants in TP Disposal in Living Wastewater. *Appl Mech Mater* 2012;137:357–361. <https://doi.org/10.4028/WWW.SCIENTIFIC.NET/AMM.137.357>.
- [22] Ortega Z, Bolaji I, Suárez L, Cunningham E. A review of the use of giant reed (*Arundo donax* L.) in the biorefineries context. *Rev Chem Eng* 2023;0:305–28. <https://doi.org/10.1515/revce-2022-0069>.
- [23] Danelli T, Laura M, Savona M, Landoni M, Adani F, Pili R. Genetic Improvement of *Arundo donax* L.: Opportunities and Challenges. *Plants* 2020;9:1584. <https://doi.org/10.3390/PLANTS9111584>.
- [24] Amarone N, Iovane G, Marranzini D, Sessa R, Guedes MC, Faggiano B. *Arundo donax* L. as sustainable building material. *Sustain Build* 2023;6:2. <https://doi.org/10.1051/SBUILD/2023005>.
- [25] Sanyang ML, Sapuan SM, Jawaid M, Ishak MR, Sahari J. Recent developments in sugar palm (*Arenga pinnata*) based biocomposites and their potential industrial applications: A review. *Renew Sustain Energy Rev* 2016;54:533–549. <https://doi.org/10.1016/J.RSER.2015.10.037>.
- [26] Barreca F, Martínez Gabarrón A, Flores Yepes JA, Pastor Pérez JJ. Innovative use of giant reed and cork residues for panels of buildings in Mediterranean area. *Resour Conserv Recycl* 2019;140:259–66. <https://doi.org/10.1016/j.resconrec.2018.10.005>.
- [27] García-Ortuño T, Andréu-Rodríguez J, Ferrández-García MT, Ferrández-Villena M, Ferrández-García CE. Evaluation of the physical and mechanical properties of particleboard made from giant reed (*Arundo donax* L.). *BioResources* 2011;6:477–86. <https://doi.org/10.15376/biores.6.1.477-486>.
- [28] Suárez L, Hanna PR, Ortega Z, Barczewski M, Kosmela P, Millar B, et al. Influence of giant reed (*Arundo donax* L.) culms processing procedure on physicochemical, rheological, and thermomechanical properties of polyethylene composites. *J Nat Fibers* 2023;21. <https://doi.org/10.1080/15440478.2023.2296909>.
- [29] Coppola G, Gaudio MT, Lopresto CG, Calabro V, Curcio S, Chakraborty S. Bioplastic from Renewable Biomass: A Facile Solution for a Greener Environment. *Earth Syst Env* n.d.;5:231–251.
- [30] Suárez L, Barczewski M, Kosmela P, Marrero MD, Ortega Z. Giant Reed (*Arundo donax* L.) Fiber Extraction and Characterization for Its Use in Polymer Composites. *J Nat Fibers* 2023;20:1–14. <https://doi.org/10.1080/15440478.2022.2131687>.
- [31] Di Fidio N, Ragagnini G, Dragoni F, Antonetti C, Raspolli Galletti AM, Fidio N, et al. Integrated cascade biorefinery processes for the production of single cell oil by *Lipomyces starkeyi* from *Arundo donax* L. hydrolysates. *Bioresour Technol* 2021;325:124635. <https://doi.org/10.1016/J.BIORTECH.2020.124635>.
- [32] Danelli T, Sepulcri A, Masetti G, Colombo F, Sangiorgio S, Cassani E, et al. *Arundo donax* L. Biomass production in a polluted area: Effects of two harvest timings on heavy metals uptake. *Appl Sci* 2021;11:1–16. <https://doi.org/10.3390/APP11031147>.
- [33] Scordia D, Corinzia SA, Cosentino SL, Testa G. Soil water availability on biomass yield and water indicators of diverse warm-season perennial grasses in dryness conditions. *Ind Crop Prod* 2022;180:114744. <https://doi.org/10.1016/J.INDCROP.2022.114744>.
- [34] Muthuvelu KS, Rajarathinam R, Kanagaraj LP, Ranganathan RV, Dhanasekaran K, Manickam NK. Evaluation and characterization of novel sources of sustainable lignocellulosic residues for bioethanol production using ultrasound-assisted alkaline pre-treatment. *Waste Manag* 2019;87:368–374. <https://doi.org/10.1016/J.WASMAN.2019.02.015>.

- [35] Nsanganwimana F, Marchand L, Douay F, Mench M, Arundo donax L., a Candidate for Phytomanaging Water and Soils Contaminated by Trace Elements and Producing Plant-Based Feedstock. A Review. *Int J Phytoremediation* 2014;16:982–1017. <https://doi.org/10.1080/15226514.2013.810580>.
- [36] De Luca AI, Molari G, Seddaiu G, Toscano A, Bombino G, Ledda L, et al. Multidisciplinary and innovative methodologies for sustainable management in agricultural systems. *Environ Eng Manag J* 2015;14:1571–1581. <https://doi.org/10.1016/j.progpolymsci.2008.05.004>.
- [37] Cristiani P, Goglio A, Marzorati S, Fest-Santini S, Schievano A. Biochar-Terracotta Conductive Composites: New Design for Bioelectrochemical Systems. *Front Energy Res* 2020;8:581106. <https://doi.org/10.3389/FENRG.2020.581106/BIBTEX>.
- [38] Fernando AL, Barbosa B, Costa J, Papazoglou EG. Giant Reed (*Arundo donax* L.). *Bioremediation and Bioeconomy* 2016;77–95. <https://doi.org/10.1016/B978-0-12-802830-8.00004-6>.
- [39] Lim LT, Auras R, Rubino M. Processing technologies for poly(lactic acid). *Prog Polym Sci* 2008;33:820–52. <https://doi.org/10.1016/j.progpolymsci.2008.05.004>.
- [40] Brostow W, Hagg Lobland HE, Khoja S. Brittleness and toughness of polymers and other materials. *Mater Lett* 2015;159:478–80. <https://doi.org/10.1016/J.MATLET.2015.07.047>.
- [41] Tan JK, Kitano T, Hatakeyama T. Crystallization of carbon fibre reinforced polypropylene. *J Mater Sci* 1990;25:3380–4. <https://doi.org/10.1007/BF00587701/METRICS>.
- [42] Kubát J, Rigdahl M, Welander M. Characterization of interfacial interactions in high density polyethylene filled with glass spheres using dynamic-mechanical analysis. *J Appl Polym Sci* 1990;39:1527–39. <https://doi.org/10.1002/APP.1990.070390711>.
- [43] Liu W, Dong Y, Liu D, Bai Y, Lu X. Polylactic Acid (PLA)/Cellulose Nanowhiskers (CNWs) Composite Nanofibers: Microstructural and Properties Analysis. *J Compos Sci* 2018, Vol 2, Page 4 2018;2:4. <https://doi.org/10.3390/JCS2010004>.
- [44] Zhang DW, Li YJ, Feng YH, Qu JP, He HZ, Xu BP. Effect of initial fiber length on the rheological properties of sisal fiber/poly(lactic acid) composites. *Polym Compos* 2011;32:1218–1224. <https://doi.org/10.1002/PC.21141>.
- [45] Barczewski M, Hejna A, Aniśko J, Andrzejewski J, Piasecki A, Mysiukiewicz O, et al. Rotational molding of polylactide (PLA) composites filled with copper slag as a waste filler from metallurgical industry. *Polym Test* 2022;106:107449. <https://doi.org/10.1016/J.POLYMERTESTING.2021.107449>.
- [46] Feng YHY-H, Li YJY-JYJ, Xu BPB-P, Zhang DWD-WDW, Qu J-PJP, He HZH-ZHZ. Effect of fiber morphology on rheological properties of plant fiber reinforced poly(butylene succinate) composites. *Compos Part B Eng* 2013;44:193–199. <https://doi.org/10.1016/J.COMPOSITESB.2012.05.051>.
- [47] Mazzanti V, Mollica F. In-Process Measurements of Flow Characteristics of Wood Plastic Composites. *J Polym Environ* 2017;25:1044–50. <https://doi.org/10.1007/s10924-016-0876-2>.
- [48] Li DZ, Jia XC, Lu XP, Zhai SJ. Study on Rheological Properties of Polylactic Acid Retardant System. *Appl Mech Mater* 2014;488–489:293–296. <https://doi.org/10.4028/WWW.SCIENTIFIC.NET/AMM.488-489.293>.
- [49] Olivas A, Helsel MA, Martys N, Ferraris CC, George WL, Ferron R. Rheological measurement of suspensions without slippage: experimental and model. Gaithersburg, MD: 2016. <https://doi.org/10.6028/NIST.TN.1946>.
- [50] Dong Y, Ghataura A, Takagi H, Haroosh HJ, Nakagaito AN, Lau KT. Polylactic acid (PLA) biocomposites reinforced with coir fibres: Evaluation of mechanical performance and multifunctional properties. *Compos Part A Appl Sci Manuf* 2014;63:76–84. <https://doi.org/10.1016/j.compositesa.2014.04.003>.
- [51] Hedthong R, Kittikorn T, Damsongsee P, Kadea S, Khanoonkon N, Witayakran S, et al. Investigation of physico-chemical degradation through weathering acceleration of hemp/PLA biocomposite: thermal analysis. *J Therm Anal Calorim* 2023;148:2429–42. <https://doi.org/10.1007/S10973-022-11891-7/FIGURES/12>.
- [52] Szczepanik E, Szatkowski P, Molik E, Pielichowska K. The Effect of Natural Plant and Animal Fibres on PLA Composites Degradation Process. *Appl Sci* 2024, Vol 14, Page 5600 2024;14:5600. <https://doi.org/10.3390/AP14135600>.
- [53] Awad S, Siakeng R, Khalaf EM, Mahmoud MH, Fouad H, Jawaid M, et al. Evaluation of characterisation efficiency of natural fibre-reinforced polylactic acid biocomposites for 3D printing applications. *Sustain Mater Technol* 2023;36:e00620. <https://doi.org/10.1016/J.SUSMAT.2023.E00620>.
- [54] Cheng S, Lau K tak, Liu T, Zhao Y, Lam PM, Yin Y. Mechanical and thermal properties of chicken feather fiber/PLA green composites. *Compos Part B Eng* 2009;40:650–4. <https://doi.org/10.1016/J.COMPOSITESB.2009.04.011>.
- [55] Karagöz İ. Production and characterization of sustainable biocompatible PLA/walnut shell composite materials. *Polym Bull* 2024;81:11517–37. <https://doi.org/10.1007/S00289-024-05247-4/FIGURES/11>.
- [56] Nurazzi NM, Abdullah N, Norraahim MNF, Kamarudin SH, Ahmad S, Shazleen SS, et al. Thermogravimetric Analysis (TGA) and Differential Scanning Calorimetry (DSC) of PLA/Cellulose Composites. *Poly(lactic Acid)-Based Nanocellulose Cellul. Compos.*, CRC Press; 2022, p. 145–64. <https://doi.org/10.1201/9781003160458-7>.
- [57] Yuan L, Wan J, Ma Y, Wang Y, Huang M, Chen Y. The content of different hydrogen bond models and crystal structure of eucalyptus fibers during beating. *BioResources* 2013;8:717–34. <https://doi.org/10.15376/biores.8.1.717-734>.
- [58] Aji P M, Oksman K, Sain M. Mechanical properties of biodegradable composites from poly lactic acid (PLA) and microcrystalline cellulose (MCC). *J Appl Polym Sci* 2005;97:2014–25. <https://doi.org/10.1002/app.21779>.
- [59] Le Moigne N, Longerey M, Taulemesse JM, Bénét JC, Bergeret A. Study of the interface in natural fibres reinforced poly(lactic acid) biocomposites modified by optimized organosilane treatments. *Ind Crops Prod* 2014;52:481–94. <https://doi.org/10.1016/j.indcrop.2013.11.022>.
- [60] Gao Y, Qu W, Liu Y, Hu H, Cochran E, Bai X. Agricultural residue-derived lignin as the filler of polylactic acid composites and the effect of lignin purity on the composite performance. *J Appl Polym Sci* 2019;136. <https://doi.org/10.1002/app.47915>.
- [61] Ayyappan V, Rangappa SM, Tengsuthiawat J, Fiore V, Siengchin S. Investigation of thermo-mechanical and viscoelastic properties of <sc>3D</sc>-printed *Morinda citrifolia* particle reinforced poly(lactic acid) composites. *Polym Compos* 2024;45:5372–85. <https://doi.org/10.1002/pc.28133>.
- [62] Fendler A, Villanueva MP, Gimenez E, Lagarón JM. Characterization of the barrier properties of composites of HDPE and purified cellulose fibers. *Cellulose* 2007;14:427–38. <https://doi.org/10.1007/s10570-007-9136-x>.
- [63] Qiu W, Endo T, Hirotsu T. Interfacial interactions of a novel mechanochemical composite of cellulose with maleated polypropylene. *J Appl Polym Sci* 2004;94:1326–35. <https://doi.org/10.1002/app.21123>.
- [64] Moreno G, Ramirez K, Esquivel M, Jimenez G. Biocomposite Films of Polylactic Acid Reinforced with Microcrystalline Cellulose from Pineapple Leaf Fibers. *J Renew Mater* 2019;7:9–20. <https://doi.org/10.32604/jrm.2019.00017>.
- [65] Aliotta L, Gigante V, Coltell M-BB, Cinelli P, Lazzeri A, Seggiani M. Thermo-Mechanical Properties of PLA/Short Flax Fiber Biocomposites. *Appl Sci* 2019;9:3797. <https://doi.org/10.3390/app9183797>.
- [66] Suárez L, Billham M, Garrett G, Cunningham E, Marrero MD, Ortega Z. A New Image Analysis Assisted Semi-Automatic Geometrical Measurement of Fibers in Thermoplastic Composites: A Case Study on Giant Reed Fibers. *J Compos Sci* 2023;7:326. <https://doi.org/10.3390/jcs7080326>.
- [67] Wang X, Li S-CS-C, Xiang D-WD-W, Gao M, Zuo H-MH-M, Li D-S, et al. Flexural Properties and Failure Mechanisms of Short-Carbon-Fiber-Reinforced Polylactic Acid Composite Modified with MXene and GO. *Materials (Basel)* 2024;17:1389. <https://doi.org/10.3390/ma17061389>.
- [68] Tábi T, Égerházi AZ, Tamás P, Czifágy T, Kovács JG. Investigation of injection moulded poly(lactic acid) reinforced with long basalt fibres. *Compos Part A Appl Sci Manuf* 2014;64:99–106. <https://doi.org/10.1016/j.compositesa.2014.05.001>.
- [69] Cristea M, Ionita D, Iftime MM. Dynamic Mechanical Analysis Investigations of PLA-Based Renewable Materials: How Are They Useful? *Mater* 2020, Vol 13, Page 5302 2020;13:5302. <https://doi.org/10.3390/MA13225302>.
- [70] Mohammed M, Jawad AJ afar M, Mohammed AM, Oleivi JK, Adam T, Osman AF, et al. Challenges and advancement in water absorption of natural fiber-reinforced polymer composites. *Polym Test* 2023;124:108083. <https://doi.org/10.1016/J.POLYMERTESTING.2023.108083>.
- [71] Manaila E, Craciun G, Ighigeanu D. Water Absorption Kinetics in Natural Rubber Composites Reinforced with Natural Fibers Processed by Electron Beam Irradiation. *Polym* 2020, Vol 12, Page 2437 2020;12:2437. <https://doi.org/10.3390/POLYM12112437>.
- [72] Moudood A, Rahman A, Öchsner A, Islam M, Francucci G. Flax fiber and its composites: An overview of water and moisture absorption impact on their performance. *J Reinf Plast Compos* 2019;38:323–39. <https://doi.org/10.1177/0731684418818893>.
- [73] Azka MA, Sapuan SM, Abral H, Zainudin ES, Aziz FA. An examination of recent research of water absorption behavior of natural fiber reinforced polylactic acid (PLA) composites: A review. *Int J Biol Macromol* 2024;268:131845. <https://doi.org/10.1016/J.IJBIOMAC.2024.131845>.
- [74] Siva R, Sundar Reddy Nemali S, Kishore Kunchapu S, Gokul K, Arun Kumar T. Comparison of Mechanical Properties and Water Absorption Test on Injection Molding and Extrusion - Injection Molding Thermoplastic Hemp Fiber Composite. *Mater Today Proc* 2021;47:4382–6.

- <https://doi.org/10.1016/J.MATPR.2021.05.189>.
- [75] González-López ME, Pérez-Fonseca AA, Manríquez-González R, Arellano M, Rodrigue D, Robledo-Ortiz JR. Effect of surface treatment on the physical and mechanical properties of injection molded poly(lactic acid)-coir fiber biocomposites. *Polym Compos* 2019;40:2132–41. <https://doi.org/10.1002/pc.24997>.
- [76] Atmakuri A, Palevicius A, Siddabathula M, Vilkauskas A, Janusas G. Analysis of Mechanical and Wettability Properties of Natural Fiber-Reinforced Epoxy Hybrid Composites. *Polym* 2020, Vol 12, Page 2827 2020;12:2827. <https://doi.org/10.3390/POLYM12122827>.
- [77] Alrawi LI, Noriman NZ, Alomar MK, Alakrach AM, Dahham OS, Hamzah R, et al. PLA/MMT-TiO₂ Bionanocomposites: Chemical Structure and Surface Wettability. *Defect Diffus Forum* 2020;398:136–9. <https://doi.org/10.4028/WWW.SCIENTIFIC.NET/DDF.398.136>.
- [78] Kotan S, Tutak D. Production of a Polylactic Acid-Based, Chitosan- and TiO₂-Modified Biodegradable Antimicrobial Coating Material and Investigation of Its Physical Properties. *J Appl Polym Sci* 2025. <https://doi.org/10.1002/APP.57168>.
- [79] de Bomfim ASC, de Oliveira DM, Benini KCC de C, Cioffi MOH, Voorwald HJC, Rodrigue D. Effect of Spent Coffee Grounds on the Crystallinity and Viscoelastic Behavior of Polylactic Acid Composites. *Polym* 2023, Vol 15, Page 2719 2023;15:2719. <https://doi.org/10.3390/POLYM15122719>.
- [80] Yu T, Sun F, Lu M, Li Y. Water absorption and hygrothermal aging behavior of short ramie fiber-reinforced poly(lactic acid) composites. *Polym Compos* 2018;39:1098–104. <https://doi.org/10.1002/PC.24038>;JOURNAL:JOURNAL:15480569;PAGE:STRING:ARTICLE/CHAPTER.
- [81] Muthuraj R, Misra M, Mohanty AK. Hydrolytic degradation of biodegradable polyesters under simulated environmental conditions. *J Appl Polym Sci* 2015;132:42189. <https://doi.org/10.1002/APP.42189>;WGROU:STRING:PUBLICATION.
- [82] Musioł M, Šišková O, Peptu C, Christova D, Goetjes V, Zarges J-C, et al. Differentiation between Hydrolytic and Thermo-Oxidative Degradation of Poly(lactic acid) and Poly(lactic acid)/Starch Composites in Warm and Humid Environments. *Mater* 2024, Vol 17, Page 3683 2024;17:3683. <https://doi.org/10.3390/MA17153683>.
- [83] Bazan P, Mierzwiński D, Bogucki R, Kuciel S. Bio-based polyethylene composites with natural fiber: Mechanical, thermal, and ageing properties. *Materials* (Basel) 2020;13:2595. <https://doi.org/10.3390/ma13112595>.
- [84] Cruz Fabian DR, Durpekova S, Dusankova M, Cisar J, Drohsler P, Elich O, et al. Renewable Poly(Lactic Acid)/Lignocellulose Biocomposites for the Enhancement of the Water Retention Capacity of the Soil. *Polymers* (Basel) 2023;15:2243. <https://doi.org/10.3390/POLYM15102243/S1>.
- [85] Rangappa SM, Siengchin S, Parameswaranpillai J, Jawaid M, Ozbakkaloglu T. Lignocellulosic fiber reinforced composites: Progress, performance, properties, applications, and future perspectives. *Polym Compos* 2022;43:645–91. <https://doi.org/10.1002/PC.26413>.
- [86] Siakeng R, Jawaid M, Ariffin H, Sapuan SM, Asim M, Saba N. Natural fiber reinforced polylactic acid composites: A review. *Polym Compos* 2019;40:446–63. <https://doi.org/10.1002/PC.24747>.
- [87] Abbasi D, Jafari M, Bahrani P, Hemmati F, Mohammadi-Roshandeh J. Foamability of all-green polylactide/rice straw pulp biocomposites through continuous extrusion process: Effects of pulping and reactive compatibilization. *Can J Chem Eng* 2024;103:206–19. <https://doi.org/10.1002/CJCE.25361>;CTYPE:STRING:JOURNAL.
- [88] Manral A, Radhakrishnan S, Dwivedi SP, Sharma B, Gupta P, Chaudhary V. Effect of water ageing on mechanical performance of Kenaf/PLA biocomposites. *Biomass Convers Biorefinery* 2024;15:6113–30. <https://doi.org/10.1007/S13399-024-05471-Y>;FIGURES/17.
- [89] Suárez L, Ortega Z, Romero F, Paz R, Marrero MD. Influence of Giant Reed Fibers on Mechanical, Thermal, and Disintegration Behavior of Rotomolded PLA and PE Composites. *J Polym Environ* 2022;30:4848–62. <https://doi.org/10.1007/s10924-022-02542-x>.
- [90] Li YC, Wang S, Qian S, Liu Z, Weng Y, Zhang Y. Depolymerization and Re/Upycling of Biodegradable PLA Plastics. *ACS Omega* 2024;9:13509–21. <https://doi.org/10.1021/ACSOMEGA.3C08674>/ASSET/IMAGES/LARGE/AO3C08674_0009.JPEG.
- [91] Oksman K. Improved interaction between wood and synthetic polymers in wood/polymer composites. *Wood Sci Technol* 1996;30:197–205. <https://doi.org/10.1007/BF00231633>.
- [92] Vitiello L, Carroccio SC, Ambrogio V, Podda E, Filippone G, Salzano de Luna M. Degradation kinetics of PLA/hemp biocomposites: Tradeoff between nucleating action and pro-hydrolytic effect of natural fibers. *Compos Sci Technol* 2024;257:110806. <https://doi.org/10.1016/J.COMPSCITECH.2024.110806>.

Supplementary material

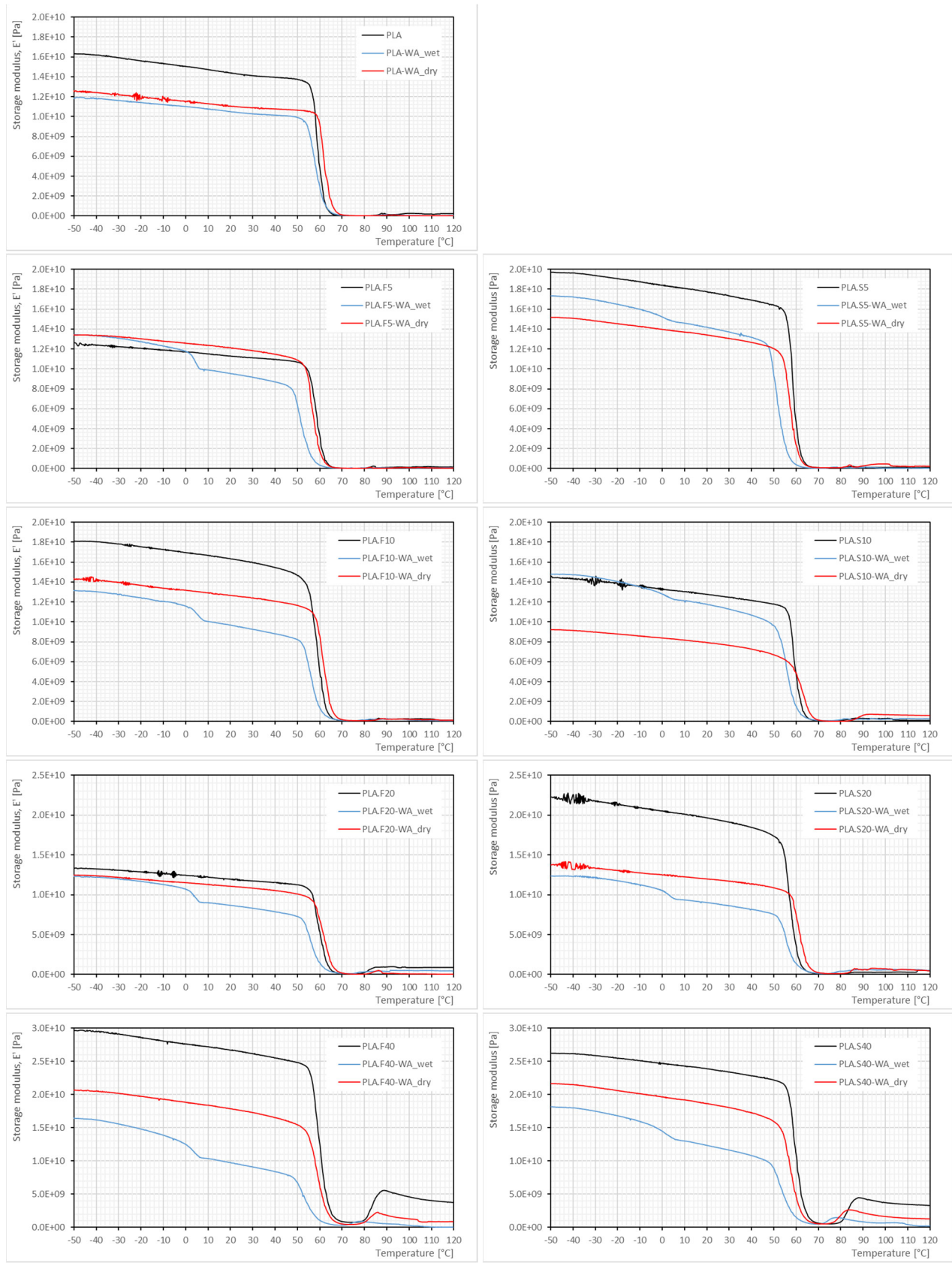


Figure S1. Storage modulus (E') of moulded, water-saturated and re-dried samples of each material formulation.

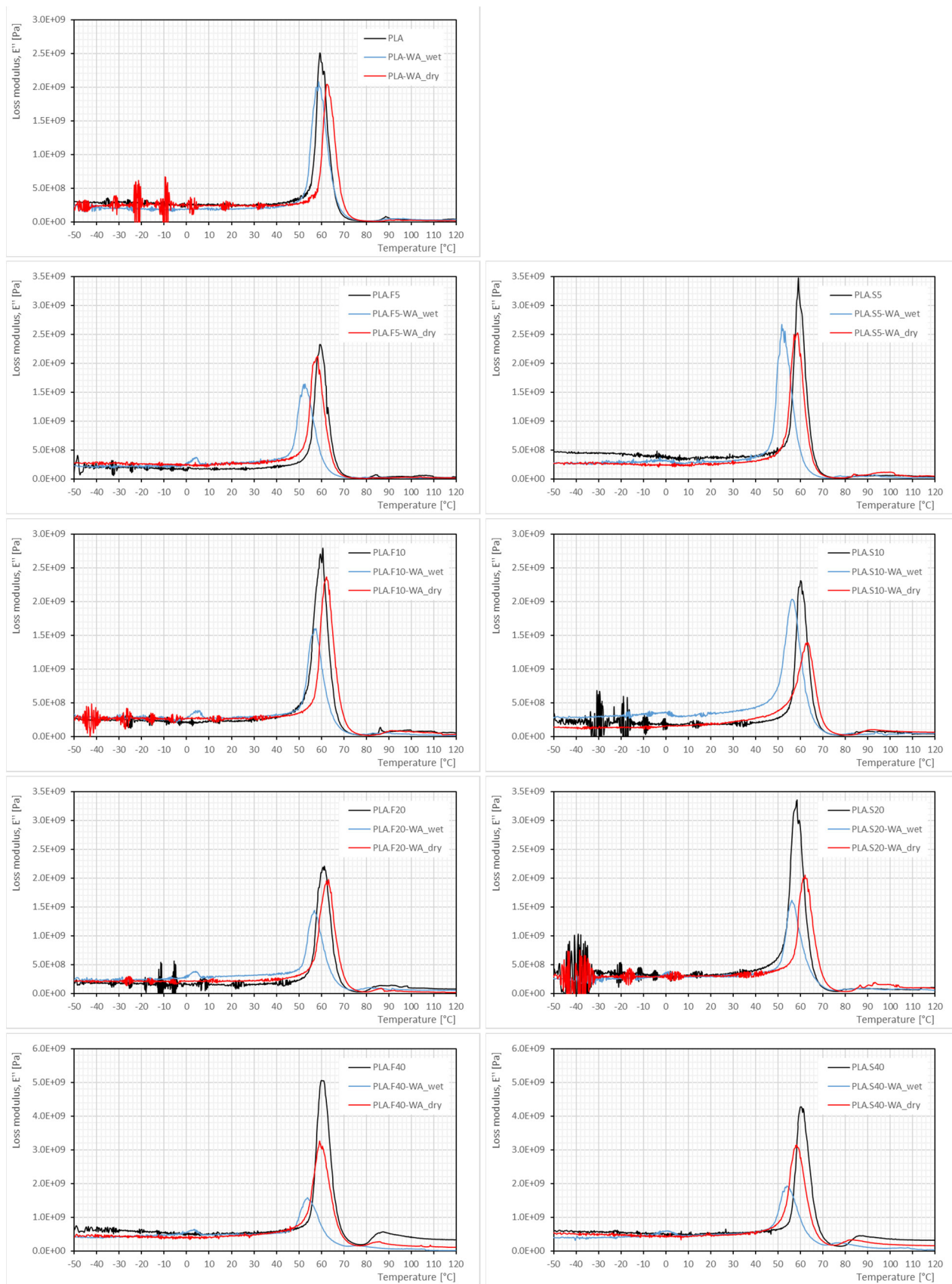


Figure S2. Loss modulus (E'') of moulded, water-saturated and re-dried samples of each material formulation.



Figure S3. Tan δ of moulded, water-saturated and re-dried samples of each material formulation.

7. OUTLOOK

7.1. CONCLUSIONS

- This thesis presents the first in-depth analysis of *Arundo donax* composites with HDPE and PLA matrices processed via injection moulding, rotational moulding and compression moulding, which includes not only their mechanical, thermal or rheological analysis, but also their recyclability and biodegradability assessment.
- *Arundo donax* has been demonstrated as a promising sustainable reinforcement for polymer composites. Giant reed is a fast-growing, renewable, and widely available biomass, especially in regions like the Canary Islands and other arid regions, due to its low requirements and good adaptability. The work performed contributes new data to support the use of invasive plant biomass in the circular bioeconomy.
- A specific methodology has been proposed to obtain high aspect ratio good quality fibres from giant reed, based on a chemo-mechanical procedure. This process yields giant reed fibres account with a high cellulose content (up to 70 %), favourable thermal stability (>230 °C), and competitive mechanical properties (tensile strength ~900 MPa, modulus ~45 GPa), comparable to commercial natural fibres such as jute or flax.
- It has been proved that fibre morphology and processing play a critical role in composite performance. Rheological behaviour, thermal stability, crystallinity, and interfacial adhesion are all influenced by filler morphology and content.
- From the analysis of fibre lengths during processing and reprocessing, it was found that the mechanical processing (twin-screw extrusion) significantly reduces the fibre length during compounding, especially in the first kneading zones of extrusion. Despite this, processed fibres maintain sufficient aspect ratios to act as effective reinforcements, even after several cycles of reprocessing.
- Fibre-based composites consistently outperform those using shredded plant material, particularly in stiffness and thermal properties, due to their better thermal stability because of the reduced hemicellulose content and also to their high aspect ratio.
- HDPE-based *Arundo* composites show improved mechanical and thermal properties compared to the neat matrix. For instance, tensile modulus increased by up to 78 % with 20 % fibre loading. Similarly, composites exhibited better dimensional and thermal stability, evidenced by increased HDT and decreased thermal expansion coefficients. These enhancements suggest applications in technical packaging, automotive interiors, and structural panels.
- *Arundo*-HDPE composites are recyclable with minimal performance loss. Fibrous HDPE composites retained over 80 % of their original tensile strength after multiple recycling cycles. These showed increased stiffness and maintained thermal stability

after five cycles of reprocessing. The use of *Arundo* may contribute antioxidant properties, improving oxidation resistance and enabling closed-loop recycling scenarios.

- *Arundo*-PLA composites offer fully biobased, biodegradable alternatives. Injection-moulded composites with 10 – 20 % fibre content showed optimal balance between stiffness and toughness.
- Biodisintegration of giant reed composites under composting conditions was faster and more effective than neat PLA, especially under home composting settings, due to the higher water absorption of composites, which favours the hydrolytic degradation route of the biopolymer.
- Water absorption is higher for fibre-filled PLA, due to the higher surface area of the fibres compared to the shredded particles. Water absorption results in reduced mechanical performance, although this can partially recover after re-drying.
- Composite performance depends on filler type, content, and processing; fibre-filled composites generally outperformed particle-filled ones due to higher aspect ratios and better stress transfer. This does not preclude the use of shredded *Arundo* as a reinforcement phase in polymer composites, as it provides acceptable mechanical performance that could be considered as a more cost-effective and less resource-intensive alternative for certain applications.
- Finally, the industrial potential of the produced composites results evidence from the performance they exhibit, although further studies are still needed. Applications might include packaging, agriculture, consumer goods, and construction materials. For instance, complete life cycle assessments (LCA) should be performed to accurately determine the potential benefit of obtained composites. Some other areas of exploration are the industrial-scale recycling, and the durability of composites under UV or saline environments.

7.2. FUTURE RESEARCH LINES

As a result of the work conducted to date, some new paths arise to continue developing the work. Different possibilities can be followed to maximize the use of this natural resource, *Arundo donax* L., as a source of renewable eco-friendly material:

- Preparation of composites with biobased materials, such as PHA/PHB or PBS. An exploration of these materials into film extrusion, blow moulding and thermoforming systems should be conducted, aiming at producing materials for packaging applications.
- Modification of the fibres and derived-biomass from reed, in order to enhance the compatibility of the polymer matrix and the biomass and obtain tailored performance to the applications. In this point, it is interesting to clarify that no modifications were conducted in this work in order to reduce the environmental footprint of the composites, due to the huge amount of water required for such modifications. However, a comprehensive LCA should be accomplished to establish the actual benefits on the use of such biomass into the composites sector.
- Complete the analysis of the performance of the composites by analysing their acoustic properties and their behaviour under fire events, factors which are crucial for the use of such materials into design, furniture and greening of interior spaces, following the principles of Kansei engineering.
- Explore further alternatives to the use of the biomass, such as the separation of lignin to produce the so-called transparent wood or fire-retardant additives.
- Establishment of an integrated cascade approach for maximizing the use of the biomass derived from the reed, including the potential production of bioplastics from the carbohydrates (sugar and starch) present in the plant naturally.
- Expand the extent of the recyclability assays to ensure its viability at long cycle times. This should include the study of the aging behaviour of the composites compared to the neat matrices; the incorporation of the raw reed, with extractives and polyphenols could provide a stabilizing effect on the composite against reprocessing and also against UV radiation.
- Complete and deep ageing testing on obtained composites, both with the HDPE and the PLA matrices, under UV-radiation and hydrothermal cycles, in order to define the durability of the composites under service conditions. Of particular interest would be the analysis of the degradation behaviour of the composites under saline atmosphere, as well as the biodegradation analysis of PLA composites in marine environments.
- Settle a value chain across the valorisation of *Arundo*-derived biomass, which considers the environmental, social and economic impacts from the entire processing, from harvesting to end of life of products, establishing a range of different applications.



ULPGC
Universidad de
Las Palmas de
Gran Canaria

Escuela de
Doctorado